SECTION 4. PHOTOCHEMICAL DATA

Table of Contents

Tables

Figures

4.1 Format and Error Estimates

In Table 4-1 we present a list of photochemical reactions considered to be of stratospheric interest. The absorption cross sections of O_2 and O_3 largely determine the extent of penetration of solar radiation into the stratosphere and troposphere. Some comments and references to these cross sections are presented in the text, but only a sample of the data is listed here. (See, for example, WMO Report No. 11 [1]; WMO Report No. 16 [851]) The photodissociation of NO in the O_2 Schumann-Runge band spectral range is another important process requiring special treatment and is not discussed in this evaluation (see, for example, Frederick and Hudson [250]; Allen and Frederick [12]; WMO Report No. 11 [1], and Minschwaner and Siskind [531]).

For some other species having highly structured spectra, such as CS_2 and SO_2, some comments are given in the text, but the photochemical data are not presented. The species CH_2O, NO_2, NO_3, ClO, BrO, and OClO also have complicated spectra, but in view of their importance for atmospheric chemistry a sample of the data is presented in the evaluation; for more detailed information on their high-resolution spectra and temperature dependence, the reader is referred to the original literature.

Table 4-2 gives recommended reliability factors for some of the more important photochemical reactions. These factors represent the combined uncertainty in cross sections and quantum yields, taking into consideration the atmospherically important wavelength regions, and they refer to the total dissociation rate regardless of product identity. The exception is $O(^1D)$ production from photolysis of O_3: the reliability factor applies to the quantum yield at the indicated wavelengths.

The error estimates are not rigorous numbers resulting from a detailed error propagation analysis of statistical manipulations of the different sets of literature values; they merely represent a consensus among the panel members as to the reliability of the data for atmospheric photodissociation calculations, taking into account the difficulty of the measurements, the agreement among the results reported by various groups, etc.

The absorption cross sections are defined by the following expression of Beer's Law:

$$I = I_o \exp(-\sigma n l),$$

where I_o and I are the incident and transmitted light intensity, respectively; σ is the absorption cross section in cm^2 $molecule^{-1}$; n is the concentration in molecule cm^{-3}; and l is the pathlength in cm. The cross sections are room temperature values at the specific wavelengths listed in the table, and the expected photodissociation quantum yields are unity, unless otherwise stated.

4.2 Halocarbon Absorption Cross Sections and Quantum Yields

The primary process in the photodissociation of chlorinated hydrocarbons is well established: absorption of ultraviolet radiation in the lowest frequency band is interpreted as an $n–\sigma^*$ transition involving excitation to a repulsive electronic state (antibonding in C–Cl), which dissociates by breaking the carbon-chlorine bond (Majer and Simons [468]). As expected, chlorofluoromethanes, which are a particular type of chlorinated hydrocarbons, behave in this fashion (Sandorfy [706]). Hence, quantum yield for photodissociation is expected to be unity for these compounds. There are several studies that show specifically that this is the case for CF_2Cl_2, $CFCl_3$, and CCl_4. These studies, which were reviewed in CODATA [177], also indicate that at shorter wavelengths, two halogen atoms can be released simultaneously in the primary process.

4.3 Web Access to Recommended Data in Text and Graphical Formats

The tables of recommended cross sections from this evaluation can be downloaded from the spectral atlas of the Max-Planck Institute for Chemistry at: http://www.atmosphere.mpg.de/enid/2295

Table 4-1. Photochemical Reactions

O_x Photochemistry

A1. $O_2 + h\nu \rightarrow O + O$

A2. $O_3 + h\nu \rightarrow O_2 + O$

$O_3 + h\nu \rightarrow O_2 + O(^1D)$

HO_x Photochemistry

B1. $HO_2 + h\nu \rightarrow$ products

B2. $H_2O + h\nu \rightarrow H + OH$

B3. $H_2O_2 + h\nu \rightarrow OH + OH$

NO_x Photochemistry

C1. $NO_2 + h\nu \rightarrow NO + O$

C2. $NO_3 + h\nu \rightarrow NO_2 + O$

$NO_3 + h\nu \rightarrow NO + O_2$

C3. $N_2O + h\nu \rightarrow N_2 + O(^1D)$

C4. $N_2O_4 + h\nu \rightarrow$ products

C5. $N_2O_5 + h\nu \rightarrow$ products

$NH_3 + h\nu \rightarrow NH_2 + H$ (1)

C6. $HONO + h\nu \rightarrow OH + NO$

C7. $HNO_3 + h\nu \rightarrow OH + NO_2$

C8. $HO_2NO_2 + h\nu \rightarrow$ products

Organic Photochemistry

$CO + h\nu \rightarrow C + O$ (1)

$CO_2 + h\nu \rightarrow CO + O$ (1)

$CH_4 + h\nu \rightarrow$ products (2)

D1. $CH_2O + h\nu \rightarrow$ products

D2. $CH_3CHO + h\nu \rightarrow$ products

D3. $C_2H_5CHO\ h\nu \rightarrow$ products

D4. $CH_3O_2 + h\nu \rightarrow$ products

D5. $C_2H_5O_2 + h\nu \rightarrow$ products

D6. $CH_3C(O)O_2 + h\nu \rightarrow$ products

D7. $CH_3OOH + h\nu \rightarrow$ products

D8. $HOCH_2OOH + h\nu \rightarrow$ products

D9 $CH_3C(O)O_2NO_2 + h\nu \rightarrow$ products

D10. $C_2H_5C(O)O_2NO_2 + h\nu \rightarrow$ products

D11. CH_2=CHCHO + $h\nu \rightarrow$ products

D12. $CH_2C(CH_3)CHO + h\nu \rightarrow$ products

D13. $CH_3C(O)CH=CH_2 + h\nu \rightarrow$ products

D14. $HOCH_2CHO + h\nu \rightarrow$ products

D15. $CH_3C(O)CH_3 + h\nu \rightarrow$ products

D16. $CH_3C(O)CH_2OH + h\nu \rightarrow$ products

D17. CHOCHO + $h\nu \rightarrow$ products

D18. $CH_3C(O)C(O)H + h\nu \rightarrow$ products

D19. $HC(O)OH + h\nu \rightarrow$ products

$(HC(O)OH)_2 + h\nu \rightarrow$ products

D20. $CH_3C(O)OH + h\nu \rightarrow$ products

D21. $CH_3C(O)OOH + h\nu \rightarrow$ products

D22. $C_2H_5C(O)OH + h\nu \rightarrow$ products

D23. $CH_3C(O)C(O)OH + h\nu \rightarrow$ products

D24. $HC(O)OCH_3 + h\nu \rightarrow$ products

D25. $HC(O)OC_2H_5 + h\nu \rightarrow$ products

D26. $HCN + h\nu \rightarrow$ products

D27. $CH_3CN + h\nu \rightarrow$ products

FO_x Photochemistry

E1. $HF + h\nu \rightarrow H + F$

E2. $FO_2 + h\nu \rightarrow$ products

E3. $F_2O + h\nu \rightarrow$ products

E4. $F_2O_2 + h\nu \rightarrow$ products

E5. $FNO + h\nu \rightarrow F + NO$

E6. $CF_4 + h\nu \rightarrow$ products

E7. $C_2F_6 + h\nu \rightarrow$ products

E8. $CF_2O + h\nu \rightarrow$ products

E9. $COHF + h\nu \rightarrow$ products

E10. $CF_3OH + h\nu \rightarrow$ products

E11. $CF_3OOCF_3 + h\nu \rightarrow$ products

E12. $CF_3OCF_3 + h\nu \rightarrow$ products

E13. $CF_3CHO + h\nu \rightarrow$ products

E14. $CF_3C(O)F + h\nu \rightarrow$ products

E15. $CF_3C(O)Cl + h\nu \rightarrow$ products

E16. $CF_3C(O)O_2NO_2 + h\nu \rightarrow$ products

E17. $CF_3CH_2CHO + h\nu \rightarrow$ products

E18. $CF_3C(O)OH + h\nu \rightarrow$ products

E19. $CH_3C(O)F + h\nu \rightarrow$ products

E20. $CH_2=CHCF_3 + h\nu \rightarrow$ products

E21. $CH_2=CFCF_3 + h\nu \rightarrow$ products

E22. $CF_2=CF_2 + h\nu \rightarrow$ products

E23. $CF_2=CFCF_3 + h\nu \rightarrow$ products

ClO_x Photochemistry

F1. $Cl_2 + h\nu \rightarrow Cl + Cl$

F2. $ClO + h\nu \rightarrow Cl + O$

F3. $ClOO + h\nu \rightarrow$ products

F4. $OClO + h\nu \rightarrow O + ClO$

F5. $ClO_3 + h\nu \rightarrow$ products

F6. $Cl_2O + h\nu \rightarrow$ products

F7. $ClOOCl + h\nu \rightarrow$ products

F8. $ClClO_2 + h\nu \rightarrow$ products

F9. $Cl_2O_3 + h\nu \rightarrow$ products

F10. $Cl_2O_4 + h\nu \rightarrow$ products

F11. $Cl_2O_6 + h\nu \rightarrow$ products

F12. $Cl_2O_7 + h\nu \rightarrow$ products

F13. $HCl + h\nu \rightarrow H + Cl$

$DCl + h\nu \rightarrow$ products

F14. $HOCl + h\nu \rightarrow$ products

F15. $ClNO + h\nu \rightarrow Cl + NO$

F16. $ClNO_2 + h\nu \rightarrow$ products

F17. $ClONO + h\nu \rightarrow$ products

F18. $ClONO_2 + h\nu \rightarrow$ products

F19. $CCl_4 + h\nu \rightarrow$ products

F20. $CH_3OCl + h\nu \rightarrow$ products

F21. $CHCl_3 + h\nu \rightarrow$ products

F22. $CH_2Cl_2 + h\nu \rightarrow$ products

F23. $CH_3Cl + h\nu \rightarrow$ products
F24. $CH_3CCl_3 + h\nu \rightarrow$ products
F25. $CH_3CH_2Cl + h\nu \rightarrow$ products
F26. $CH_3CHClCH_3 + h\nu \rightarrow$ products
F27. $CH_2ClCH_2Cl + h\nu \rightarrow$ products
F28. $CH_2ClCH_2CH_2Cl + h\nu \rightarrow$ products
F29. $CH_2Cl(CH_2)_2CH_2Cl + h\nu \rightarrow$ products
F30. $CCl_2O + h\nu \rightarrow$ products
F31. $COHCl + h\nu \rightarrow$ products
F32. $CClFO + h\nu \rightarrow$ products
F33. $CFCl_3$ (CFC-11) + $h\nu \rightarrow$ products
F34. CF_2Cl_2 (CFC-12) + $h\nu \rightarrow$ products
F35. CF_3Cl (CFC-13) + $h\nu \rightarrow$ products
F36. $CF_2ClCFCl_2$ (CFC-113) + $h\nu \rightarrow$ products
F37. CF_2ClCF_2Cl (CFC-114) + $h\nu \rightarrow$ products
F38. CF_3CF_2Cl (CFC-115)+ $h\nu \rightarrow$ products
F39. $CHFCl_2$ (HCFC-21) + $h\nu \rightarrow$ products
F40. CHF_2Cl (HCFC-22) + $h\nu \rightarrow$ products
F41. CH_2FCl (HCFC-31) + $h\nu \rightarrow$ products
F42. CF_3CHCl_2 (HCFC-123) + $h\nu \rightarrow$ products
F43. CF_3CHFCl (HCFC-124) + $h\nu \rightarrow$ products
F44. CF_3CH_2Cl (HCFC-133) + $h\nu \rightarrow$ products
F45. CH_3CFCl_2 (HCFC-141b) + $h\nu \rightarrow$ products
F46. CH_3CF_2Cl (HCFC-142b) + $h\nu \rightarrow$ products
F47. $CH_2ClCHO + h\nu \rightarrow$ products
F48. $CHCl_2CHO + h\nu \rightarrow$ products
F49. $CF_2ClCHO + h\nu \rightarrow$ products
F50. $CFCl_2CHO + h\nu \rightarrow$ products
F51. $CCl_3CHO + h\nu \rightarrow$ products
F52. $CH_3C(O)Cl + h\nu \rightarrow$ products
F53. $CH_2ClC(O)Cl + h\nu \rightarrow$ products
F54. $CHCl_2C(O)Cl + h\nu \rightarrow$ products
F55. $CCl_3C(O)Cl + h\nu \rightarrow$ products
F56. $CF_3CF_2CHCl_2$ (HCFC-225ca) + $h\nu \rightarrow$ products
F57. CF_2ClCF_2CHFCl (HCFC-225cb) + $h\nu \rightarrow$ products
F58. $CH_3C(O)CH_2Cl + h\nu \rightarrow$ products

BrO_x Photochemistry

G1. $Br_2 + h\nu \rightarrow$ products
G2. $HBr + h\nu \rightarrow$ products
G3. $BrO + h\nu \rightarrow$ products
G4. $OBrO + h\nu \rightarrow$ products
G5. $Br_2O + h\nu \rightarrow$ products
G6. $HOBr + h\nu \rightarrow$ products
G7. $BrNO + h\nu \rightarrow$ products
G8. $BrNO + h\nu \rightarrow$ products
G9. $BrONO_2 + h\nu \rightarrow$ products
G10. $BrCl + h\nu \rightarrow Br + Cl$
G11. $BrOCl + h\nu \rightarrow$ products
G12. $CH_3Br + h\nu \rightarrow$ products
G13. $CH_2Br_2 + h\nu \rightarrow$ Products
G14. $CHBr_3 + h\nu \rightarrow$ Products
G15. $CH_2BrCH_2Br + h\nu \rightarrow$ Products
G16. $C_2H_5Br + h\nu \rightarrow$ Products
G17. $COBr_2 + h\nu \rightarrow$ products
G18. $COHBr + h\nu \rightarrow$ products
G19. CH_2ClBr (Halon-1011) + $h\nu \rightarrow$ Products
G20. $CHClBr_2$ (Halon-1012) + $h\nu \rightarrow$ Products
G21. $CHCl_2Br$ (Halon-1021) + $h\nu \rightarrow$ Products
G22. CCl_3Br (Halon-1031) + $h\nu \rightarrow$ Products
G23. CHF_2Br (Halon-1201) + $h\nu \rightarrow$ Products
G24. CF_2Br_2 (Halon-1202) + $h\nu \rightarrow$ Products
G25. CF_2ClBr (Halon-1211) + $h\nu \rightarrow$ Products
G26. CF_3Br (Halon-1301) + $h\nu \rightarrow$ Products
G27. $CH_2=CHBr + h\nu \rightarrow$ Products
G28. $CHBr=CF_2 + h\nu \rightarrow$ Products
G29. $CFBr=CF_2 + h\nu \rightarrow$ Products
G30. $CH_2=CBrCF_3 + h\nu \rightarrow$ Products
G31. CF_3CH_2Br (Halon-2301) + $h\nu \rightarrow$ Products
G32. $CF_3CHClBr$ (Halon-2311) + $h\nu \rightarrow$ Products
G33. CF_3CHFBr (Halon-2401) + $h\nu \rightarrow$ Products
G34. CF_2BrCF_2Br (Halon-2402) + $h\nu \rightarrow$ Products
G35. CF_3CF_2Br (Halon-2501) + $h\nu \rightarrow$ Products
G36. $CH_3CH_2CH_2Br + h\nu \rightarrow$ Products
G37. $CH_3CHBrCH_3 + h\nu \rightarrow$ Products
G38. $CH_3C(O)CH_2Br + h\nu \rightarrow$ products

IO_x Photochemistry

H1. $I_2 + h\nu \rightarrow 2\ I$
H2. $IO + h\nu \rightarrow I + O(^3P), O(^1D)$
H3. $OIO + h\nu \rightarrow$ products
H4. $HI + h\nu \rightarrow$ products
H5. $HOI + h\nu \rightarrow OH + I$
H6. $ICl + h\nu \rightarrow I + Cl$
H7. $IBr + h\nu \rightarrow I + Br$
H8. $INO + h\nu \rightarrow I + NO$
H9. $IONO + h\nu \rightarrow I + NO_2$
H10. $IONO_2 + h\nu \rightarrow$ products
H11. $CH_3I + h\nu \rightarrow CH_3 + I$
H12. $CH_2I_2 + h\nu \rightarrow CH_2I + I$
H13. $C_2H_5I + h\nu \rightarrow C_2H_5 + I$
H14. $CH_3CHI_2 + h\nu \rightarrow$ Products
H15. $CH_3CH_2CH_2I + h\nu \rightarrow$ Products
H16. $CH_3CHICH_3 + h\nu \rightarrow$ Products
H17. $C_4H_9I + h\nu \rightarrow C_4H_9 + I$
H18. $(CH_3)_2CHCH_2I + h\nu \rightarrow (CH_3)_2CCH_2 + I$
H19. $(CH_3)_3CI + h\nu \rightarrow (CH_3)_3C + I$
H20. $C_5H_{11}I + h\nu \rightarrow C_5H_{11} + I$
H21. $CF_3I + h\nu \rightarrow CF_3 + I$
H22. $CF_2I_2 + h\nu \rightarrow$ products
H23. $C_2F_5I + h\nu \rightarrow C_2F_5 + I$
H24. $C_3F_7I + h\nu \rightarrow C_3F_7 + I$
H25. $C_4F_9I + h\nu \rightarrow C_4F_9 + I$
H26. $C_6F_{13}I + h\nu \rightarrow C_6F_{13} + I$
H27. $CH_2ICl + h\nu \rightarrow CH_2Cl + I$
H28. $CH_2BrI + h\nu \rightarrow$ products
H29. $CF_2BrCF_2I + h\nu \rightarrow$ products

SO_x Photochemistry

I1. $SO_2 + h\nu \rightarrow SO + O$
$H_2S + h\nu \rightarrow HS + H$ (1)

I2. $CS_2 + h\nu \rightarrow CS + S$

I3. $OCS + h\nu \rightarrow CO + S$

I4. $SF_6 + h\nu \rightarrow$ products

Metal Photochemistry

J1. $NaOH\ h\nu \rightarrow Na + OH$

J2. $NaCl + h\nu \rightarrow Na + Cl$

---

(1) Hudson and Kieffer [351].
(2) Turco [787].
(3) Shaded entries indicate changes to the recommendation and/or the note since JPL 02-25.
(4) Shaded, bold indicate new entries, not previously evaluated

Table 4-1. Combined Uncertainties for Cross Sections and Quantum Yields

Species	Uncertainty	Notes
O_2 (Schumann-Runge bands)	1.2	
O_2 (Continua)	1.2	
O_3 (Cross Sections Only)	1.1	
$O_3 \rightarrow O(^1D)$, λ >310 nm	1.3	
$O_3 \rightarrow O(^1D)$, 290 < λ < 310 nm	1.2	
H_2O_2	1.3	
NO_2	1.2	
NO_3	1.5	
N_2O	1.2	
N_2O_5	2.0	
HNO_3	1.3	
HO_2NO_2	2.0	
CH_2O	1.4	
CH_3OOH	1.5	
$CH_3C(O)O_2NO_2$	1.3	λ < 300 nm
$CH_3C(O)O_2NO_2$	2.0	$\lambda \geq$ 300 nm
HCl	1.1	
HOCl	1.4	
ClOOCl	1.5	λ < 300 nm
ClOOCl	3.0	$\lambda \geq$ 300 nm
Cl_2O_3	1.5	λ < 300 nm
Cl_2O_3	3.0	$\lambda \geq$ 300 nm
$ClONO_2$	1.3	
CCl_4	1.1	
CCl_3F	1.1	
CCl_2F_2	1.1	
CH_3Cl	1.1	
CF_2O	2.0	
CF_3Br	1.3	
CF_2ClBr	2.0	
CF_2Br_2	2.0	
$C_2F_4Br_2$	2.0	
HOBr	2.0	λ < 350 nm
HOBr	10	$\lambda \geq$ 350 nm
$BrONO_2$	1.4	

A1. $O_2 + h\nu \rightarrow O + O$. The photodissociation of molecular oxygen in the stratosphere is due primarily to absorption of solar radiation in the 200–220 nm wavelength region, i.e., within the Herzberg continuum. The 185–200-nm region—the O_2 Schumann-Runge band spectral range—is also very important, since solar radiation penetrates efficiently into the stratosphere at those wavelengths.

Frederick and Mentall [251] Herman and Mentall [327] and Anderson and Hall [20, 21] estimated O_2 absorption cross sections from balloon measurements of solar irradiance in the stratosphere. These authors find the cross sections in the 200–210 nm range to be ~35% smaller than the smallest of the older laboratory results, which are those of Shardanand and Prasad Rao [727]. The more recent laboratory studies (Johnston et al. [389]; Cheung et al. [165, 166], Jenouvrier et al. [378]) confirm the lower values obtained from solar irradiance measurements. The recommended absorption cross section values between 205 and 240 nm are listed in Table 4-2; they are taken from Yoshino et al. [859] and are based on the latter set of laboratory measurements. Amoruso et al. [17] have also carried out cross section measurements in this wavelength range (the Herzberg continuum); their values are ~15% lower than those reported by Yoshino et al.

Table 4-2. Absorption Cross Sections of O_2 Between 205 and 240 nm

λ (nm)	$10^{24}\ \sigma$ (cm^2)	λ (nm)	$10^{24}\ \sigma$ (cm^2)
205	7.35	223	3.89
206	7.13	224	3.67
207	7.05	225	3.45
208	6.86	226	3.21
209	6.68	227	2.98
210	6.51	228	2.77
211	6.24	229	2.63
212	6.05	230	2.43
213	5.89	231	2.25
214	5.72	232	2.10
215	5.59	233	1.94
216	5.35	234	1.78
217	5.13	235	1.63
218	4.88	236	1.48
219	4.64	237	1.34
220	4.46	238	1.22
221	4.26	239	1.10
222	4.09	240	1.01

The studies of the penetration of solar radiation in the atmosphere in the Schumann-Runge wavelength region were based originally on laboratory measurements of cross sections that were affected by instrumental parameters due to insufficient spectral resolution. Yoshino et al. [870] reported high resolution O_2 cross section measurements at 300 K, between 179 and 202 nm, obtaining the first set of results, which is independent of the instrument width. Additional studies at other temperatures, wavelengths, and isotopic compositions have been carried out by Yoshino et al. [861, 864-866, 869], Lewis et al. [441, 442], Cheung et al. [164], and Chiu et al. [169]. More recently, Yoshino et al. [860] reported cross sections of the Schumann-Runge bands in the window region between the rotational lines for wavelengths between 180 and 195 nm; these measurements supersede their earlier ones. Minschwaner et al. [530] have fit temperature-dependent O_2 cross sections between 175 and 204 nm with polynomial expressions, providing accurate means of determining the Schumann-Runge band cross sections with a model that incorporates the most recent laboratory data. Coquart et al. [183] have reported Herzberg continuum absorption cross sections in the wavelength region 196–205 nm of the Schumann-Runge bands.

For parameterizations of the O_2 absorption in the Schumann-Runge bands used in atmospheric modeling calculations, see, e.g., the review in WMO Report No. 16 [851]. More recent work by Murtagh [567], Nicolet and Kennes, [585] and Minschwaner et al. [530] incorporates results of the later laboratory measurements into efficient schemes for computing broad-band transmission and photolysis rates. Transmission values obtained by Murtagh [567] agree well with the WMO [851] recommendations, although the high-resolution calculations of Minschwaner and Salawitch differ with the WMO values by as much as 10–20% at some wavelengths.

In view of the quality of the high-resolution laboratory measurements, the primary source of uncertainty in modeling O_2 photolysis in the Schumann-Runge bands (other than the issue of absolute solar irradiance) has shifted to the choice of broadband parameterization.

A2. $O_3 + h\nu \rightarrow O + O_2$. The O_3 absorption cross-sections in the 200-790 nm region can be separated into four systems: the Hartley band (200-300 nm), the Huggins bands (300-370 nm), the Chappuis band (370-790 nm), and the Wulf bands extending towards longer wavelengths. The Hartley band is the strongest band and peaks around 255 nm. Although its overall shape is very smooth, there is residual vibrational structure in the region 250-260 nm. The Huggins band consists of a series of individual peaks, and is marked with a drastic change of absorption cross-sections (over more than five orders of magnitude) and strong temperature dependence. The Chappuis band is composed of a vibrational band progression superimposed on a continuous absorption in the visible region and is about thousand times weaker than the Hartley band. The very weak near-infrared part of the Chappuis band is clearly structured and corresponds to a different electronic transition (called the "Wulf bands").

For the three main bands in the region 200-790 nm, there have been many different measurements of the absorption spectrum and cross-sections at various experimental (temperature and pressure) and instrumental conditions (resolution) during the last century as shown in the following survey. The available measurements can be organized into three groups: (A) measurements of absolute cross-sections at single wavelengths (e.g. at the Hg resonance line at 253.65 nm), (B) measurements of absolute cross-sections over broad spectral regions (typically covering a few hundred nm), and (C) measurements of relative O_3 absorption spectra over broad spectral regions that have been scaled to absolute spectra using results from other studies (Type A or B).

Table 4-4. Summary of O_3 Cross Section Measurements

Reference	Spectral Range, nm	Type	Resolution, nm	Temperature, K
Ny and Choong, 1933 [592]	213-353	B	0.05	298
Vassy and Vassy, 1948 [811]	450-601	A	not stated	291,231,193,168
Vigroux, 1953 [818]	230-793 245-345	B	0.05	291 181-393
Inn and Tanaka, 1953 [365]	200-350 400-750	B	~0.05 0.5	300
Tanaka et al., 1953 [772]	105-220	B	0.5	300
Hearn, 1961 [323]	253.7-577.0	A	0.01-0.09	295
DeMore and Raper, 1964 [211]	210-300	B	0.2	77, 273
Vigroux, 1967 [819]	304-341	B	0.05	291
Griggs, 1968 [304]	200-360 450-850	B	0.1 0.5	303
Vigroux, 1969 [820]	230-270	B	0.1	291
Simons et al., 1973 [736]	300-370	B	0.4	195,300,333
Astholz et al. 1982 [27]	210-320	B	3	300,500,720,900
McPeters and Bass, 1982 [511]	300-310	C	0.02	229,245,295
Daumont et al., 1983 [202]	310-350	B	0.012	223,294
Brion et al., 1983 [95]	310-350	B	0.012	223,294
Brion et al., 1984 [96]	310-350	B	0.012	223,294
Freeman et al., 1984 [252]	250-350	C*	0.002	195
Bass and Paur, 1985 [54]	230-350	C*	<0.025	200,298
Paur and Bass, 1985 [628]	245-340	C*	<0.025	203,218,228,243,273,298
Freeman et al., 1985 [253]	281-335	A	0.003	195,228,293
Molina and Molina, 1986 [542]	185-350	B	0.07	226,263,298
Mauersberger et. al., 1986 [500]	253.7	A	not stated	297.5
Mauersberger et. al., 1987 [501]	253.7	A	not stated	297.5
Barnes and Mauersberger, 1987 [40]	237.7	A,C	not stated	195,221,237,253,273, 297,318,335,351
Yoshino et al., 1988 [867]	238.2-344.4	A	0.13-0.003	195,228,295
Malicet et al., 1989 [469]	253.36	A	not stated	229,295
Cacciani et al., 1989 [130]	339-355	B	0.012	220,293
Amoruso et al., 1990 [15]	590-610	B	0.05	230,299
Daumont et al. 1992 [201]	195-345	B*	0.01	295
Anderson and Mauersberger, 1992 [23]	543.5-632.8	A	not stated	295
Anderson et al., 1993 [22]	750-975	A	not stated	295

Reference	Spectral Range, nm	Type	Resolution, nm	Temperature, K
Brion et al., 1993 [94];	195-345 300-345	B*	0.01	218,228,243,295 273
Yoshino et al., 1993 [862]	185-254	A,B	0.13-0.003	195,228,295
Burkholder and Talukdar, 1994 [117]	407-763	C*	0.2	220,240,260,280,298
Brion et al., 1998 [93]	345-830 515-650	B*	0.01	295 218
Burrows et al., 1999 [123]	231-794	B*	0.2 - 0.4	202,221,241,273,293
Voigt et al., 2001 [825]	230-850	C*	5 cm^{-1}	203,223,246,280,293
Bogumil et al., 2001[81]	230-2400	C*	0.17-1.44	203,293
Bogumil et al., 2003 [82]	230-1070	C*	0.2-0.4	203,223,243,273,293

Earlier reviews on the measured absorption cross-sections were presented by Inn and Tanaka, 1958 [366], Ackermann, 1971 [4], Hudson, 1974 [350], Nicolet, 1981 [584], Brion et al., 1985 [97], Steinfeld et al., 1987 [751] and the WMO Report No. 16 [851], which was the basis for the previous JPL-97-4 evaluation. Orphal, 2003 [612, 614] has recently critically reviewed the available laboratory measurements up to 2003, and the current JPL evaluation is partly based on his review. Relevant for his evaluation are the measurements of type B and C, particularly those studies whose data were digitally available and marked with an asterisk*. Unfortunately, the recommended data set for the JPL-97-4 evaluation of Molina and Molina, 1986 [542] was not considered in his review.

In the Hartley and Huggins bands (about 240-325 nm) there is generally very good agreement (better than 2-3%) between the data measured at room temperature (293-300 K) by Bass and Paur, 1985 [54] and Paur and Bass, 1985 [628], Molina and Molina, 1986 [542], the Reims-team (Daumont et al. 1992 [201], Brion et al., 1993 [94], Malicet et al., 1995 [470] and Brion et al. 1998 [93]), Yoshino et al., 1993 [862], and the Bremen-team (Burrows et al., 1999 [123], Voigt et al., 2001 [825] and Bogumil et al., 2003 [82]). The older data by Ny and Choong, 1933 [592], Inn and Tanaka, 1953 [365] and Vigroux 1953 [818] are about 8% larger than the data of Molina and Molina, 1986 [542]. The vibration structure between 240 and 270 nm was observed in most studies, except those of Inn and Tanaka, 1953 [365], DeMore and Raper, 1964 [211] and Astholz et al. 1982 [27], who used lower resolution instruments.

A comparison of the O_3 cross-sections at the Hg-line wavelength 253.7 nm was performed by Orphal [612, 614] involving 13 absolute measurements and provided a mean value of $(114.1 \pm 0.9) \times 10^{-19}$ cm^2 $molecule^{-1}$. It has to be noted that the data of Bass and Paur, 1985 [54] and Paur and Bass, 1985 [628] are normalized to the absolute value 114.7×10^{-19} cm^2 $molecule^{-1}$ at 253.7 nm and 295 K measured by Hearn, 1961 [323]. In the range 230-260 nm, the data of the Reims-team (Daumont-Brion-Malicet-Brion) are generally lower (up to 2.5%) than the data of Molina and Molina, 1986 [542], Bass and Paur, 1985 [54] and the Bremen-team (Burrows-Voigt-Bogumil). Furthermore, the data of Voigt et al., 2001 [825] show a strong baseline shift below 255 nm and in the range 310-320 nm; in addition, the spectra are very noisy in the Hartley band maximum. The data of Bogumil et al. 2001 [81] and 2003 [82] contain periodic artefacts of the order of 0.5–1.0% in the range 240-270 nm and a straylight feature around 305 nm in the order of 2%.

Below 225 nm the room temperature cross-sections of Molina and Molina, 1986 [542], DeMore and Raper, 1964 [211] and the Reims-team (Daumont-Brion-Malicet) agree within 1-2%, but are 2-5% larger than the measurements of Yoshino et al., 1993 [862]. Other reported values measured by Ny and Choong, 1933 [592], Inn and Tanaka, 1953 [365], Astholz et al. 1982 [27] and Griggs, 1968 [304] differ up to 15%.

In the Huggins bands (310-350 nm) the studies differ in spectral resolution, which is mostly relevant only to atmospheric remote sensing. At wavelengths larger than 310 nm the vibrational structure becomes pronounced. In the range 310-340 nm, the agreement between the different studies is rather good (about 2%) for the data of Bass and Paur, 1985 [54], the Reims-team (Daumont-Brion-Malicet-Brion) and Burrows et al. 1999 [123], although important differences (up to 13%) due to wavelength shifts and spectral resolution are noticed by Orphal, 2003 [612, 614]. The data of Bass and Paur, 1985 [54] and of Reims-team (Daumont-Brion-Malicet-Brion) show wavelength shift of more than 0.02 nm. The data of Voigt et al., 2001 [825] and Bogumil et al., 2003 [82] contain systematic baseline drifts. Above 312 nm, the data of Molina and Molina, 1986 [542], which are listed every 0.5 nm up to 350 nm, occasionally miss the maxima and minima of the peaks. The reported values by Cacciani et al., 1989 [130] are typically 5-8% lower than the values of Molina and Molina, 1986 [542] in the range 339-355 nm.

The O_3 absorption cross-sections in the 350-450 nm region between the Huggins and Chappuis bands are very small and the available measurements of absolute values scatter significantly. They have been measured by Brion et al., 1998 [93] and the Bremen team (Burrows-Voigt-Bogumil). At the minimum near 378 nm, the

reported absolute cross-sections at 298 K vary between 5×10^{-23} cm^2 molecule^{-1} of Voigt et al. [825] and 5×10^{-24} cm^2 molecule^{-1} of Brion et al., 1998 [93].

Absorption cross-section measurements of the Chappuis band of O_3 in the wavelength range 450-750 nm have been reported by Burkholder and Talukdar, 1994 [117], Brion et al., 1998 [93], the Bremen team (Burrows-Voigt-Bogumil) and at single wavelengths by Hearn, 1961 [323] and Anderson and Mauersberger, 1992 [23]. At the peak of the Chappuis band near 602 nm, the values agree within a few %, although the data of the Bremen-team (Burrows-Voigt-Bogumil) are consistently larger than those of Brion et al., 1998 [93] (by 2%) and Burkholder and Talukdar, 1994 [117] (by 4%) (the latter data are calibrated using the measurements of Anderson and Mauersberger, 1992 [23]). Note that there are pronounced deviations of data from Burkholder and Talukdar, 1994 [117] in the region 425-490 nm. The older values of Vassy and Vassy, 1948 [811], Vigroux, 1953 [818], Inn and Tanaka, 1953 [365], Griggs, 1968 [304] and Amoruso et al., 1990 [15] deviate up to 20%. Absorption cross-sections in the Wulf band region (>750 nm) have been reported by Anderson et al., 1993 [22] and Bogumil et al., 2003 [82].

The temperature dependence of the O_3 cross-sections has also been studied by several of the groups mentioned above, and tabulated in the survey. In his critical review, Orphal, 2003 [612, 614] calculated and compared the integrated cross-sections for 5 temperatures in the range 203 to 295 K in the different spectral regions of the O_3 spectrum. At all temperatures the agreement of the integrated cross-sections in the Hartley band is better than 2%, and less good agreement in the Chappuis band (4%). In particular, the integrated cross-sections of Burkholder and Talukdar, 1994 [117] lie systematically below the other measurements by about 3%, and the data of Burrows et al., 1999 [123] are always higher by 2%. In the Huggins bands and the blue tail of the Chappuis band the integrated cross-sections scatter by several percent (up to 5%), indicating systematic differences between the available data. The Hartley-band integrated cross-sections remain constant in the temperature range 203-293 K, within the experimental uncertainties. The integrated cross-sections in the Huggins bands decrease by more than 30% between 298 K and 203 K., and the differential cross sections of the bands increase significantly.

In the Hartley band most studies report a slight (0.9-1.6%) increase of the cross-section below 260 nm between room temperature and low temperatures 202-298 K, while Yoshino et al., 1993 [862] concluded that the temperature effect is negligible. Above 260 nm the cross-section decreases significantly at lower temperatures. This effect is due to the changing populations of the various vibrational and rotational quantum states of ozone, and has been analysed by Simons et al., 1973 [736]. The cross-section values are not linearly proportional to the temperature; instead the effect is larger at the maxima than it is at the minima of the spectral features.

The absorption cross-sections in the Huggins bands (310-350 nm) of O_3 decrease strongly with decreasing temperatures. Additionally, they depend on instrumental line shape and differences in wavelength calibration so that discrepancies up to 20% at the lowest temperatures are observed between the various studies. Comparison of the spectra obtained in the temperature range 220-229 K show good agreement (~3% at 325 nm, ~ 5% at 340 nm) with the data of Bass and Paur, 1985 [54], Molina and Molina, 1986 [542], the Brion team (Daumont-Brion-Malicet-Brion), and Burrows et al., 1999 [123]. The data of Voigt et al., 2001 [825] and Bogumil et al., 2003 [82] display sudden baseline jumps and are consistently lower than the other cited data sets. Voigt et al., 2001 [825] observed in the region 335-380 nm the presence of “hot bands”, which disappear with decreasing temperature, and “cold bands”, which become more pronounced at lower temperatures.

In the Chappuis band, the available cross-sections agree in showing a very small increase (1%) with decreasing temperature in the wavelength range 550-560 nm. However there is strong disagreement in the relative temperature dependence of the cross-sections in the wings (400-550 nm and 650-790 nm) of the Chappuis band. Burkholder and Talukdar, 1994 [117] report a decrease from 4% at 520 nm to 40% at 420 nm between 298 and 220 K., while Burrows et al. 1999 [123] observe a decrease at 420 nm to 70% at 221 K, and Bogumil et al., 2003 [82] a decrease of 20% at 223 K. These discrepancies could be due to baseline problems in the different measurements. It was also noted by the Bremen-team (Burrows-Voigt-Bogumil) that in the wings the differential cross-sections increase up to 10% between 298 and 203 K. In addition, the band structures between 400 and 500 nm shift toward shorter wavelengths with decreasing temperature.

Three different models have been proposed to reproduce the temperature-dependence of the O_3 cross-sections in the entire ultraviolet and visible regions within the experimental uncertainties. The first model was developed for the Hartley band by Adler-Golden [9] and uses an exponential function. The second model, developed by Bass and Paur 1985 [54], uses a quadratic polynomial to be applied in the Hartley and Huggins bands. The third model of Voigt et al., 2001 [825] uses a double exponential function. The accuracy of the models was checked by Orphal, 2003 [612, 614], who concluded that the experimental data are better reproduced using a quadratic polynomial.

The pressure dependence of the O_3 absorption cross-sections was investigated by Hearn, 1961 [323] in the Hartley band, and by Voigt et al., 2001 [825] in the entire spectral region 240-790 nm. Both groups did not

find experimental or theoretical support for pressure dependence, although Voigt et al., 2001 [825] proposed that temperature variations of the cross-sections around 400 nm might be due to the formation of a weakly bounded O_2-O_3 complex.

The recommended absorption cross sections are listed in Table 4-4, averaged over atmospheric intervals at 218 K and at room temperature (293-298 K). It has to be noted that cross sections are listed over 500 cm^{-1} intervals in the region 185-300 nm, over 1 nm intervals in the region 300 to 321 nm, over 2 nm intervals in the region 321.5 to 326.5 nm, and over 5 nm intervals in the region 330-825 nm. The 218 K values, measured by the Reims-team (Daumont-Brion-Malicet-Brion), are only listed for the range 196 to 340 nm. The room temperature data were selected for the range 185-233 nm from the data of Molina and Molina, 1986 [542], for the range 323-310 nm from Burrows et al. 1999 [123], and for the range 310-825 nm from the Reims team (Daumont-Brion-Malicet-Brion).

Table 4-5. Absorption Cross Sections of O_3 at 218 and 293-298 K

λ (nm)	10^{20} σ (cm^2) 218 K	10^{20} σ (cm^2) 293-298 K	λ (nm)	10^{20} σ (cm^2) 293-298 K
185.185–186.916		62.2	412.5–417.5	0.00295
186.916–188.679		57.6	417.5–422.5	0.00393
188.679–190.476		52.6	422.5–427.5	0.00656
190.476–192.308		47.7	427.5–432.5	0.00697
192.308–194.175		42.9	432.5–437.5	0.00882
194.175–196.078		38.5	437.5–442.5	0.0137
196.078–198.020	34.4	34.9	442.5–447.5	0.0165
198.020–200.000	32.0	32.4	447.5–452.5	0.0185
200.000–202.020	31.2	31.5	452.5–457.5	0.0218
202.020–204.082	32.4	32.6	457.5–462.5	0.0366
204.082–206.186	36.2	36.3	462.5–467.5	0.0367
206.186–208.333	43.2	43.3	467.5–472.5	0.0410
208.333–210.526	54.2	53.9	472.5–477.5	0.0481
210.526–212.766	69.6	69.3	477.5–482.5	0.0754
212.766–215.054	90.6	90.3	482.5–487.5	0.0813
215.054–217.391	119	118	487.5–492.5	0.0816
217.391–219.780	155	154	492.5–497.5	0.0908
219.780–222.222	201	199	497.5–502.5	0.121
222.222–224.719	256	255	502.5–507.5	0.160
224.719–227.273	323	322	507.5–512.5	0.158
227.273–229.885	403	401	512.5–517.5	0.166
229.885–232.558	492	490	517.5–522.5	0.183
232.558–235.294	589	590	522.5–527.5	0.219
235.294–238.095	692	693	527.5–532.5	0.267
238.095–240.964	799	802	532.5–537.5	0.287
240.964–243.902	905	908	537.5–542.5	0.295
243.902–246.914	995	1001	542.5–547.5	0.319
246.914–250.000	1074	1080	547.5–552.5	0.337
250.000–253.165	1116	1125	552.5–557.5	0.358
253.165–256.410	1136	1148	557.5–562.5	0.398
256.410–259.740	1105	1122	562.5–567.5	0.439
259.740–263.158	1047	1064	567.5–572.5	0.467
263.158–266.667	952	968	572.5–577.5	0.481
266.667–270.270	823	840	577.5–582.5	0.464
270.270–273.973	681	698	582.5–587.5	0.446
273.973–277.778	531	547	587.5–592.5	0.447
277.778–281.690	391	406	592.5–597.5	0.476
281.690–285.714	271	282	597.5–602.5	0.513
285.714–289.855	175	184	602.5–607.5	0.514
289.855–294.118	105	113	607.5–612.5	0.478
294.118–298.507	59.4	65.1	612.5–617.5	0.438
298.507-299.5	40.7	45.2	617.5–622.5	0.406
299.5-300.5	35.1	39.2	622.5–627.5	0.382
300.5-301.5	30.5	34.3	627.5–632.5	0.356
301.5-302.5	26.9	30.3	632.5–637.5	0.327
302.5-303.5	22.9	26.2	637.5–642.5	0.297
303.5-304.5	20.6	23.4	642.5–647.5	0.271
304.5-305.5	17.3	20.1	647.5–652.5	0.251
305.5-306.5	15.6	17.9	652.5–657.5	0.231
306.5-307.5	13.3	15.5	657.5–662.5	0.210
307.5-308.5	11.5	13.5	662.5–667.5	0.190
308.5-309.5	10.4	12.2	667.5–672.5	0.170
309.5-310.5	8.50	10.2	672.5–677.5	0.151
310.5-311.5	7.76	9.24	677.5–682.5	0.137

λ (nm)	10^{20} σ (cm^2) 218 K	293-298 K	λ (nm)	10^{20} σ (cm^2) 293-298 K
311.5-312.5	6.53	7.95	682.5–687.5	0.126
312.5-313.5	5.62	6.91	687.5–692.5	0.113
313.5-314.5	5.05	6.25	692.5–697.5	0.0989
314.5-315.5	4.08	5.19	697.5–702.5	0.0868
315.5-316.5	3.82	4.77	702.5-707.5	0.0784
316.5-317.5	3.11	4.02	707.5-712.5	0.0731
317.5-318.5	2.94	3.72	712.5-717.5	0.0696
318.5-319.5	2.11	2.89	717.5-722.5	0.0622
319.5-320.5	2.41	2.99	722.5-727.5	0.0543
320.5-321.5	1.43	2.10	727.5-732.5	0.0478
321.5-323.5	1.57	2.05	732.5-737.5	0.0442
323.5-325.5	1.02	1.41	737.5-742.5	0.0432
325.5-327.5	0.658	1.01	742.5-747.5	0.0447
327.5–332.5	0.483	0.697	747.5-752.5	0.0425
332.5–337.5	0.204	0.320	752.5-757.5	0.0338
337.5–342.5	0.0797	0.146	757.5-762.5	0.0286
342.5–347.5		0.0779	762.5-767.5	0.0262
347.5–352.5		0.0306	767.5-772.5	0.0260
352.5–357.5		0.0136	772.5-777.5	0.0294
357.5–362.5		0.00694	777.5-782.5	0.0318
362.5–367.5		0.00305	782.5-787.5	0.0262
367.5–372.5		0.00130	787.5-792.5	0.0208
372.5–377.5		0.000850	792.5-797.5	0.0173
377.5–382.5		0.000572	797.5-802.5	0.0157
382.5–387.5		0.000542	802.5-807.5	0.0156
387.5–392.5		0.000668	807.5-812.5	0.0186
392.5–397.5		0.000956	812.5-817.5	0.0221
397.5–402.5		0.00115	817.5-822.5	0.0206
402.5–407.5		0.00158	822.5-827.5	0.0145
407.5–412.5		0.00258		

Note:
T = 218 K, 196.078-342.5 nm, Reims team (1992-1995) (Daumont et al. 1992 [201], Brion et al., 1993 [94], Malicet et al., 1995 [470]),
T = 298 K, 185.185-232.558 nm, Molina and Molina, 1986 [542],
T = 293 K, 232.558-309.5 nm, Burrows et al. [123],
T = 295 K, 309.5-827.5 nm, Reims team (1992-1998) (Daumont et al. 1992 [201], Brion et al., 1993 [94], Malicet et al., 1995 [470], Brion et al. [93].

The recommendation for the $O(^1D)$ quantum yield from ozone photolysis as a function of wavelength and temperature is given by the expression,

$$\Phi(\lambda,T) = \left(\frac{q_1}{q_1+q_2}\right) \times A_1 \times \exp\left\{-\left(\frac{X_1-\lambda}{\omega_1}\right)^4\right\} + \left(\frac{q_2}{q_1+q_2}\right) \times A_2 \times \left(\frac{T}{300}\right)^2 \times \exp\left\{-\left(\frac{X_2-\lambda}{\omega_2}\right)^2\right\}$$
$$+ A_3 \times \left(\frac{T}{300}\right)^{1.5} \times \exp\left\{-\left(\frac{X_3-\lambda}{\omega_3}\right)^2\right\} + c$$

where $q_i = \exp\left(-\frac{\nu_i}{RT}\right)$ and X_{1-3}, A_{1-3}, ω_{1-3}, ν_{1-2} and c are best-fit parameters given in Table 4, λ is in nm, T is in K, and R = 0.695 (cm^{-1}/K). The parameter c is assumed to be temperature and wavelength independent.
This expression is valid only for the wavelength range 306–328 nm and temperature range 200–320 K.

Table 4-6. Parameters for the Calculation of $O(^1D)$ Quantum Yields

Parameter	i = 1	i = 2	i = 3
X_i (nm)	304.225	314.957	310.737
ω_i (nm)	5.576	6.601	2.187
A_i	0.8036	8.9061	0.1192
ν_i (cm^{-1})	0	825.518	–
c	0.0765	–	–

At room temperature (298 K) the uncertainties of the quantum yield values calculated with the above expression are estimated to be ±10 % (1σ) for $\Phi(\lambda, 298\ K) \geq 0.4$, while the uncertainties are estimated to be ±0.04 for $\Phi(\lambda, 298\ K) < 0.4$. At temperatures other than room temperature, the uncertainties are estimated to be ± 15 % for $\Phi(\lambda, T) \geq 0.4$ and ± 0.06 for $\Phi(\lambda, T) < 0.4$.

In the wavelength range 329–340 nm we recommend the value of $\Phi(O^1D) = 0.08 \pm 0.04$, independent of temperature. For $\lambda > 340$ nm, the quantum yield may be non-zero but no recommendation is made. For $\lambda < 306$ nm. the recommended quantum yield is 0.90, independent of temperature.

The recommendation for the temperature and wavelength dependences of the quantum yield for $O(^1D)$ production, $\Phi(O^1D)$, is taken from the review of Matsumi et al. [496]. Matsumi et al. derived the recommended values using the following procedure: The measured $O(^1D)$ quantum yields at 298 K between 306 and 328 nm from eight studies (Talukdar et al. [769], Takahashi et al. [762], Ball et al. [37], Armerding et al. [24], Bauer et al. [57], Brock and Watson [98], Trolier and Wiesenfeld [785] and Smith et al. [743], were normalized using $\Phi(O^1D) = 0.79$ at 308 nm. This value was derived from the studies listed in Table 1 of Matsumi et al. [496]. The resulting renormalized data were averaged. The wavelength dependence quantum yield data at various temperatures reported by Talukdar et al. [767, 769], Takahashi et al. [762], Hancock and Hofzumahaus [308] (this includes all the data from the Oxford group), Bauer et al. [57] and Smith et al. [743] were normalized to the value at 308 nm given above. These normalized data were used to obtain the best-fit parameters for eqn. 4-1 for the wavelength range 306–328 nm and temperature range 200–320 K. Because of the large number of studies upon which the 298 K evaluation is based, the averaged 298 K data were given a larger weight in the fitting procedure than the data at other temperatures.

The major differences between this recommendation and that of JPL 00-3 [703] are: (1) inclusion of more recent data from Smith et al., Hancock and Hofzumahaus, and Bauer et al., (2) selective deletion of data from the previous data from some of the groups, especially the use of data from Bauer et al. [57] which superseded the data of Silvente et al. [730] from the same group, (3) correcting for small differences in the absorption cross sections of ozone used by various groups, and (4) the normalization of all data to the selected value at 308 nm.

B1. $HO_2 + h\nu \rightarrow OH + H$. The absorption cross sections of the hydroperoxyl radical, HO_2, in the 190–260 nm region have been measured at room temperature by Paukert and Johnston [627], Hochanadel et al. [336], Cox and Burrows [187], McAdam et al. [505], Kurylo et al. [424], Moortgat et al. [559], Dagaut and Kurylo [200], Lightfoot and Jemi-Alade [450], who measured the cross sections up to 777 K, Crowley et al. [198], Maricq and Szente [482], Roehl et al. [677] and Sander et al. [704] at 227.5 nm. The absorption cross sections have been evaluated in earlier reviews by Lightfoot et al. [449] and Wallington et al. [832] who noted significant discrepancies in both the shapes of the spectra and the absolute magnitudes of the cross section values, particularly around 200 nm. The published ultraviolet absorption spectra have recently been reevaluated by Tyndall et al. [790]. Herein, the spectra were fitted to an analytical equation suggested by Maric et al. [479]:

$$\sigma = \frac{\sigma_{med}}{\left(1 - \frac{b}{\nu}\right)} \exp^{-a\left[\ln\left(\frac{\nu - b}{\nu_{med} - b}\right)\right]^2}$$

where $\sigma_{med} = 1.84 \times 10^{-18}$ cm^2 $molecule^{-1}$, a = 4.91, b = 30612 cm^{-1} and ν_{med}= 50260 cm^{-1}. Absolute cross sections were based on relative measurements of absorption cross sections of HO_2, CH_3O_2 and $C_2H_5O_2$ at 240 nm taken under identical conditions, combined with independent calibrations by Crowley et al. [198]. Table 4-7 lists the recommended cross sections, which are taken from the review by Tyndall et al. [790].

Lee [438] has detected $O(^1D)$ as a primary photodissociation product at 193 and at 248 nm, with a quantum yield that is about 15 times larger at the longer wavelength. The absolute quantum yield for $O(^1D)$ production has not been reported yet.

Photolysis of HO_2 in the stratosphere and troposphere is slow and can be neglected, but the UV absorption cross sections are important in laboratory studies of reaction kinetics.

Table 4-7. Absorption Cross Sections of HO_2

λ (nm)	$10^{20}\sigma$ (cm^2)
190	368
195	402
200	423
205	427
210	415
215	385
220	341
225	288
230	230
235	173
240	122
245	79.7
250	48.0
255	26.3
260	12.9

B2. $H_2O + h\nu \rightarrow H + OH$. Water vapor has a continuum absorption spectrum at wavelengths longer than 145 nm, with a maximum around 165 nm, the cross sections falling off rapidly toward longer wavelengths; the photodissociation threshold occurs at 246 nm. Below 69 nm the spectrum is also a continuum, and between 69 and 145 nm it consists of diffuse bands. In the atmosphere water vapor is photodissociated mainly by the solar Lyman alpha line (121.6 nm).

The absorption cross sections and the photochemistry of water vapor were reviewed by Hudson [349, 350], by Hudson and Kiefer [351], by Calvert and Pitts [136], and by Okabe [597].

The recommended absorption cross sections are taken from the review by Hudson and Kiefer [351] and are listed in Table 4-8 between 175 and 190 nm. At these wavelengths the quantum yield for production of H and OH is unity. At shorter wavelengths H_2 and O are also formed as primary products. Stief et al. [754] report a quantum yield of 0.11 for this process between 105 and 145 nm.

Table 4-8. Absorption Cross Sections of H_2O Vapor

λ(nm)	$10^{20}\sigma$ (cm^2)
175.5	262.8
177.5	185.4
180.0	78.1
182.5	23.0
185.0	5.5
186.0	3.1
187.5	1.6
189.3	0.7

B3. $H_2O_2 + h\nu \rightarrow OH + OH$. The recommended 298 K absorption cross section values, listed in Table 4-9, are the mean of the data of Lin et al. [455], Molina and Molina [539], Nicovich and Wine [586], and Vaghjiani and Ravishankara [799]. Molina and Molina [539] supersedes the earlier results of Molina et al. [546]. Nicovich and Wine measured the cross sections at $\lambda \pm 230$ relative to the values at 202.6, $\sigma = 4.32 \times 10^{-19}$ cm^2, and at 228.8 nm, $\sigma = 1.86 \times 10^{-19}$ cm^2. The values are within 2% of the recommended value.

Table 4-9. Absorption Cross Sections of H_2O_2 Vapor

λ (nm)	$10^{20}\sigma$ (cm^2)		λ (nm)	$10^{20}\sigma$ (cm^2)	
	298 K	355 K		298 K	355 K
190	67.2		270	3.3	3.5
195	56.4		275	2.6	2.8
200	47.5		280	2.0	2.2
205	40.8		285	1.5	1.6
210	35.7		290	1.2	1.3
215	30.7		295	0.90	1.0
220	25.8		300	0.68	0.79
225	21.7		305	0.51	0.58
230	18.2	18.4	310	0.39	0.46
235	15.0	15.2	315	0.29	0.36
240	12.4	12.6	320	0.22	0.27
245	10.2	10.8	325	0.16	0.21
250	8.3	8.5	330	0.13	0.17
255	6.7	6.9	335	0.10	0.13
260	5.3	5.5	340	0.07	0.10
265	4.2	4.4	345	0.05	0.06
			350	0.04	0.05

Nicovich and Wine have measured the temperature dependence of these cross sections. They expressed the measured cross sections as the sum of two components: σ_1, due to absorption from H_2O_2, which has the O–O stretch excited; and σ_0, due to absorption by ground state molecules. For atmospheric calculations the expression given in Table 4-10 may be used. The photodissociation quantum yield is believed to be unity. At and above 248 nm, the major photodissociation process is that leading to OH, i.e., the quantum yield for OH production is 2 (Vaghjiani and Ravishankara [800] and Vaghjiani et al. [801]). At 193 nm this quantum yield decreases to about 1.5 (Vaghjiani et al. [801]; Schiffman et al. [709]), and the quantum yield for O-atom production increases to about 0.16 (Vaghjiani et al. [801]).

Table 4-10. Mathematical Expression for Absorption Cross Sections of H_2O_2 as a Function of Temperature

$$10^{21}\,\sigma(\lambda,T) = \chi \sum_{n=0}^{7} A_n \lambda^n + (1-\chi) \sum_{n=0}^{4} B_n \lambda^n$$

Where T: temperature K; λ: nm; $\chi = (1 + \exp(-1265/T))^{-1}$

$A_0 = 6.4761 \times 10^4$	$B_0 = 6.8123 \times 10^3$
$A_1 = -9.2170972 \times 10^2$	$B_1 = -5.1351 \times 10^1$
$A_2 = 4.535649$	$B_2 = 1.1522 \times 10^{-1}$
$A_3 = -4.4589016 \times 10^{-3}$	$B_3 = -3.0493 \times 10^{-5}$
$A_4 = -4.035101 \times 10^{-5}$	$B_4 = -1.0924 \times 10^{-7}$
$A_5 = 1.6878206 \times 10^{-7}$	
$A_6 = -2.652014 \times 10^{-10}$	
$A_7 = 1.5534675 \times 10^{-13}$	

Range 260–350 nm; 200–400 K

C1. $NO_2 + h\nu \rightarrow NO + O(^3P)$. The NO_2 spectrum in the 200-800 nm region can be separated into two principal systems: the D-X band system below 250 nm, and the broad B-X and A-X band systems between 300 and 800 nm, with a maximum around 400 nm; due to interactions the forbidden C-X transition can also contribute to the visible spectrum. There is enormous spectral fine structure superimposed on the broad visible system. Due to the complexity of the electronic states of NO_2, it is impossible to predict its spectrum from molecular quantum theory within experimental accuracy. The absorption spectrum and cross sections of NO_2 have been measured at various resolutions during the last century as shown in the following survey.

Table 4-11. Summary of NO_2 Cross Section Measurements

Study	Range / nm	Type	Resolution / nm	Temperature / K
Holmes and Daniels, 1934 [337]	265-436	B	1	298
Dixon, 1940 [217]	400-700	A	1.5 and 4.0	295
Hall and Blacet, 1952 [307]	240-500	A	0.2-0.5	298
Nakayama et al., 1959 [571]	108-270	A	0.02	300
Jones and Bayes, 1973 [394]	297-579	B	0.2	300
Johnston and Graham, 1974 [387]	190-420	A	1.3	294
Bass et al., 1976 [53]	185-410	B	0.015-0.04	298,235
Harker et al., 1977 [311]	375-420	B	0.1	296
Hicks et al., 1979 [330]	425-450 at single λ	B	0.04	235,298
Schneider et al.,1987 [714]	200-700	A	0.04	298
Leroy et al., 1987 [440]	427-450	B	0.04	235,298
Koffend et al., 1987 [416]	391- 414/ intervals	B	0.005	251,300
Calvert et al., 1987 [135]	404.7	B	1.6	223,273,298,325,347, 370,406 496,566
Davidson et al., 1988 [204]	264-649	A	1.5 0.3-2.6 cm^{-1}	233,243,253,263,273,298 and higher up to 397
Corcoran et al., 1992 [184]	450-650/ intervals	A,B	0.075/0.003	295,573,673
Amoruso et al., 1993 [16]	440-460	B	0.134	220,298
Harwood and Jones, 1994 [314]	313-568	A	0.54	213,225,233,243,253, 263,273,298
Mérienne et al., 1995 [523]	300-500	A	0.01-0.015	293
Coquart et al., 1995 [182]	400-500	B	0.01	220,240,293
Vandaele et al., 1996 [806]	380-830	A	2.0 cm^{-1}	294
Frost et al. [254]	370-497	A	0.5 - 0.5 cm^{-1}	220
Jenouvrier et al., 1996 [377]	200-300	B	0.01	293
Mihalcea et al., 1996 [527]	395,670	B	0.001	296-774
Harder et al., 1997 [310]	350-585(294K) 350-560(low T)	A	0.15 cm^{-1}	217,230.2,238.6,293.8
Yoshino et al., 1997 [863]	360-470	B	0.14 cm^{-1}	298.5
Mérienne et al., 1997 [521]	200-400	A	0.05	220
Vandaele et al., 1998 [807]	238-1000	A	2.0 cm^{-1}	220,294
Burrows et al., 1998 [122]	231-794	C	0.2 - 0.4	221,241,273,293
Orphal et al., 1998 [615]	667-1111	B	0.012 cm^{-1}	298
Gierczak et al., 1999 [270]	413.4	B	1	259,298,323,348,385
Voigt et al., 2002 [826]	250-800	A	0.5-1.0 cm^{-1}	223,246,260,280,293
Vandaele et al., 2002 [804]	385-925	A	0.05-0.1 cm^{-1}	220,240,294
Bogumil et al., 2003 [82]	230-1070	C	0.2-0.4	203,223,243,273,293
Nizkorodov et al., 2004 [588]	415-525	B	0.06 cm^{-1}	215,230,250,273,298

The available studies can be organized into three groups: *type A*, measurements of *absolute* cross sections over broad spectral regions (typically covering a few hundred nm); *type B*, measurements of *absolute* cross sections at selected wavelengths or narrow spectral ranges; and *type C* measurements of *relative* NO_2 absorption spectra over broad spectral regions (typically a few hundred nm) that have been scaled to absolute spectra using results from other studies.

In the earlier years, the NO_2 ultraviolet-visible absorption cross section measurements were limited to lower spectral resolution. However since 1992 several sets of high-resolution measurements and their temperature and pressure dependence have been measured by several groups, mainly aimed at improving the accuracy of atmospheric measurements, in particular for the atmospheric remote sensing of NO_2. However laboratory measurements have been obtained at spectral resolutions that are limited by instrumental techniques.

The previous recommendations (JPL-97-04) [212] for the absorption cross sections of nitrogen dioxide were based on the work of Bass et al. [53], Schneider et al. [714] and by Davidson et al. [204]. Although at room temperature the agreement between these three sets of measurements is good (within 5% between 305 and 345 nm and within 10% at the longer wavelengths), serious non-uniform wavelength miscalibrations have

become apparent in the wavelength range 400-500 nm in the spectrum by Schneider et al. [714]. At the shorter wavelengths and at temperatures below 298 K the agreement is poor between the three sets of data. A possible cause for the discrepancies is the presence of N_2O_4, which is the weakly bound NO_2 dimer in equilibrium with the monomer, the ratio of the two species being pressure and temperature dependent. The corrections were needed to account for the presence of this species below 400 nm, especially in the near UV around 200 nm, where it absorbs strongly.

Kirmse et al. [409] analysed the spectra reported between 1976 and 1995 and concatenated selected (and corrected) cross sections to create a "new standard" spectrum in the range 300-708 nm at a resolution of 0.05 nm, and another spectrum extending to 908 nm at a lower resolution of 1 nm. This high resolution "new standard" spectrum consisted of the Mérienne et al. (1995) [523] cross sections from 300 to 500 nm, the Corcoran et al. [184] cross sections from 500 to 600 nm, and the Schneider et al. [714] cross sections from 600 to 710 nm. A critical review and evaluation of the cross section studies has been recently performed by Orphal (2002) [613] and Orphal (2003) [614], covering most studies published since 1995. In his evaluation Orphal [613, 614] considered baseline problems, wavelength calibration and integrated cross sections (after convolution of high-resolution cross sections of 0.1 nm or better). In addition, Vandaele et al. (2003) [805] derived temperature- and pressure-dependent parameters from high-resolution spectral data obtained since 1995. The current JPL (2006) evaluation is taken from the recommendations of Orphal (2003) [614] and Vandaele et al. (2003) [805].

At room temperature (295 ± 3 K) there is excellent agreement (better than 2-3%) between the absolute cross sections over the wavelength range covered by the measurements of Mérienne et al. (1995) [523], Coquart et al. [182], Vandaele et al. (1996) [806], Jenouvrier et al. [377], Yoshino et al. [863], Mérienne et al. (1997) [521], Vandaele et al. (1998) [807], Bogumil et al. [82] and Nizkorodov et al. [588]. Many of these studies differ in spectral resolution but this is much more relevant to atmospheric remote sensing. The cross sections of Harwood and Jones [314] are 6-8% below most of the other studies, while the data of Harder et al. [310] are slightly but systematically higher than the data of Vandaele et al. (1998) [807] (i.e. 2-5%) and show a systematic baseline drift of up to 10% at the lowest temperature.

The newest high-pressure cross-sections data of Vandaele et al. (2002) [804] and Vandaele et al. (2003) [805] are nearly 4% smaller than the Vandaele et al. (1996) [806] and Vandaele et al. (1998) [807] data. The cross sections of Burrows et al. [122] are about 6-8% lower than most recent high-resolution studies (Mérienne-95, Mérienne-97, Harder, Vandaele-96, Vandaele-98). The data of Voigt et al. [826] show several artificial peaks (probably Xenon lamp stray light) of a few percent and baseline shifts up to 10% (partly due to residual N_2O_4 absorption) at lower temperatures. The spectra of Bogumil et al. [82] were scaled to absolute values using the integrated cross section of Vandaele et al. (1998) [807].

The temperature effect on the NO_2 absorption cross sections has been studied by only a few research teams, as can be seen in the survey. The variation of the absorption consists mainly in an increase of the differential absorption cross sections with decreasing temperature. In his analysis of the temperature dependence of the cross sections in the 300-700 nm region, Orphal (2003) [614] observed a tilt in the baseline with decreasing temperature in the data of Davidson et al. [204], Burrows et al. [122], Bogumil et al. [82], but less pronounced in the data of Harwood and Jones [314], Harder et al. [310], and Vandaele et al. (2002) [804]. This is due to a change in the thermal population of the lower vibrational and rotational states, causing large discrepancies in the relative change and the absolute magnitude of the absorption cross sections. The comparison of the high-resolution absolute cross sections at temperatures below ambient reveals significant discrepancies in absolute magnitude of cross sections due to spectral resolution, baseline differences and possible wavelength calibration. For the temperatures 242 ± 2 and 220 ± 3 K, the overall agreement is within 15% in the region 350-500 nm, however outside this range the discrepancies are much larger. The integrated cross-sections for the range 400-500 nm were calculated by Orphal (2003) [614] to be $(4.50 \pm 0.10) \times 10^{-17}$ cm^2 $molecule^{-1}$ nm and are independent of temperature, as recently shown by Nizkorodov et al. [588] for the temperature range 215-298 K.

Orphal (2003) [614] and Vandaele et al. (2003) [805] compared the spectra after degrading the high-resolution spectra to a lower resolution. At 220 K the best agreement (within 1.6%) is obtained between the data of Coquart et al. [182], Mérienne et al. (1997) [521] and Vandaele et al. (1998) [807]. The data of Harder et al. [310] differ by 3.7% from the Vandaele et al. (1998) [807] data below 500 nm, but seem to contain more noise at larger wavelengths. The data of Voigt et al. [826] show larger disagreement, different at every temperature set. At 223 K their data are 22% lower than the Vandaele et al. (1998) [807] values.

The temperature dependence of the NO_2 cross sections in the entire ultraviolet and visible regions can be reproduced within the experimental uncertainties using analytical expressions at least at low and moderate spectral resolutions (i.e. 0.05 nm and less). Linear functions were proposed by Davidson et al. [204], Kirmse et al. [409] and Vandaele et al. (2002) [804], a quadratic polynomial by Burrows et al. [122] and a double exponential function by Voigt et al. [826]. For the high-resolution spectra Nizkorodov et al. [588] concluded that a linear temperature dependence is not valid, and a successful parameterisation needs further work.

The NO_2 cross sections are varying as a function of total pressure but these effects are only observed at high spectral resolution, i.e. better than 0.01 nm, as investigated by Harder et al. [310], Wennberg et al. [844], Vandaele et al. (1998) [807], Voigt et al. [826], Vandaele et al. (2002) [804], Nizkorodov et al. [588], using NO_2/N_2 (or air) mixtures at total pressures up to 1 atm. Nizkorodov et al. [588] showed that a simple Lorentzian broadening model, with linear dependence of the Lorentz width on pressure, provides an adequate description of the pressure broadening effects in NO_2.

The current recommendation is based on the data of Vandaele et al. (1998) [807]. Table 4- 12 displays cross sections for 294 and 220 K averaged over atmospheric intervals.

A number of studies of quantum yields of NO_2 photolysis for the atmospherically important 300–470 nm region have been reported: Jones and Bayes [394] for the wavelength range 295-445 nm and at selected wavelengths 492 nm, 546 nm and 579 nm; Gaedtke and Troe [259] in the range 313-416 nm; Harker et al. [311] for the range 375-420 nm at 1 nm intervals; Davenport [203] for the range 390-420 nm at 223 and 300 K; Gardner et al. [262] for the range 334-404 nm at 298 K, and at 404 nm at 273 and 370 K; and Roehl et al. [682] in the range 388-411nm at 248 and 298 K. In the range 360-398 nm the φ_1-values show a wide scatter, with differences as much as 60%, especially due to the data of Harker et al. [311]. Although Gardner et al. [262] obtained values of φ between 0.89 ± 0.05 and 0.97 ± 0.06 in the range 379-397 nm, they made a critical assessment of the quantum yield data and recommended that φ is near unity at wavelength up to and slightly beyond the dissociation limit of $\lambda_0 = 397.95$ nm (Jost et al., 1996; [395]) and then rapidly decreases to near zero at 424 nm. However Roehl et al. [682] determined $\varphi = (0.93 \pm 0.10)$ in the range 388-398 nm at 298 K, and $\varphi = (0.90 \pm 0.10)$ at 248 K. Troe [783] made a critical reanalysis of the quantum yield data of Gardner et al. [262] and Roehl et al. [682] below λ_0, and concluded that certain secondary reactions were not correctly accounted for, and recommended corrections for both data sets. The recommended quantum yield values listed in Table 4-13 are based on the data of Roehl et al. [682] corrected by Troe [783].

Table 4-12. Absorption Cross Sections of NO_2 at 220 and 294 K

λ (nm)	220 K x 10^{20}(cm^2)	294 K x 10^{20}(cm^2)	λ (nm)	220 K x 10^{20}(cm^2)	294 K x 10^{20}(cm^2)
240.964–243.902	4.14	5.77	442.5–447.5	47.9	48.8
243.902–246.914	0.961	2.79	447.5–452.5	49.3	49.8
246.914–250.000	0.859	1.62	452.5–457.5	40.6	41.6
250.000–253.165	0.191	0.998	457.5–462.5	43.5	43.6
253.165–256.410	0.496	1.05	462.5–467.5	41.5	41.4
256.410–259.740	0.872	1.28	467.5–472.5	32.7	33.7
259.740–263.158	1.26	1.58	472.5–477.5	38.8	38.7
263.158–266.667	1.77	2.05	477.5–482.5	33.4	33.7
266.667–270.270	2.36	2.64	482.5–487.5	24.0	25.4
270.270–273.973	3.03	3.24	487.5–492.5	30.9	30.8
273.973–277.778	3.94	4.07	492.5–497.5	29.4	29.4
277.778–281.690	5.16	5.21	497.5–502.5	16.7	18.2
281.690–285.714	6.29	6.23	502.5–507.5	24.4	24.3
285.714–289.855	7.72	7.59	507.5–512.5	22.8	23.1
289.855–294.118	9.64	9.51	512.5–517.5	14.8	16.0
294.118–298.507	11.6	11.5	517.5–522.5	17.7	16.1
298.507–303.030	13.2	13.2	522.5–527.5	17.5	17.9
303.030–307.692	16.0	16.1	527.5–532.5	14.9	15.3
307.692–312.5	18.5	18.8	532.5–537.5	9.71	10.6
312.5–317.5	20.8	21.6	537.5–542.5	10.3	10.8
317.5–322.5	24.2	25.3	542.5–547.5	12.6	12.7
322.5–327.5	27.2	28.7	547.5–552.5	10.4	11.0
327.5–332.5	29.4	31.7	552.5–557.5	7.40	7.97
332.5–337.5	33.0	35.8	557.5–562.5	5.56	6.05
337.5–342.5	37.0	40.2	562.5–567.5	8.62	8.70
342.5–347.5	38.6	41.8	567.5–572.5	8.25	8.48
347.5–352.5	43.5	46.2	572.5–577.5	4.12	4.71
352.5–357.5	47.7	49.7	577.5–582.5	4.11	4.47
357.5–362.5	49.2	50.9	582.5–587.5	4.60	4.69
362.5–367.5	53.7	54.9	587.5–592.5	5.14	5.39
367.5–372.5	55.2	56.1	592.5–597.5	3.82	4.08
372.5–377.5	58.4	59.0	597.5–602.5	3.71	3.95
377.5–382.5	58.5	59.3	602.5–607.5	1.56	1.85
382.5–387.5	59.2	60.1	607.5–612.5	2.38	2.54
387.5–392.5	62.4	63.0	612.5–617.5	3.47	3.53
392.5–397.5	58.5	59.7	617.5–622.5	2.39	2.57
397.5–402.5	64.0	64.4	622.5–627.5	1.77	1.96
402.5–407.5	57.0	58.2	627.5–632.5	1.00	1.21
407.5–412.5	61.8	62.4	632.5–637.5	1.23	1.33
412.5–417.5	58.3	59.1	637.5–642.5	1.48	1.53
417.5–422.5	59.3	59.9	642.5–647.5	1.86	1.92
422.5–427.5	56.0	57.0	647.5–652.5	1.24	1.35
427.5–432.5	53.7	54.4	652.5–657.5	0.755	0.873
432.5–437.5	55.5	55.9	657.5–662.5	0.508	0.566
437.5–442.5	47.5	48.8			

Note:
Integrated cross sections after Vandaele et al., 1998 [807].

Table 4-13. Quantum Yields for NO_2 Photolysis

λ, nm	Φ at 298 K	Φ at 248 K
300-398	1.00	1.00
399	0.95	0.94
400	0.88	0.86
401	0.75	0.69
402	0.62	0.56
403	0.53	0.44
404	0.44	0.34
405	0.37	0.28
406	0.30	0.22
407	0.26	0.18
408	0.22	0.14
409	0.18	0.12
410	0.15	0.10
411	0.13	0.08
412	0.11	0.07
413	0.09	0.06
414	0.08	0.04
415	0.06	0.03
416	0.05	0.02
417	0.04	0.02
418	0.03	0.02
419	0.02	0.01
420	0.02	0.01
422	0.01	0.01

Note:
after Troe et al. [783]

C2. $NO_3 + h\nu \rightarrow NO + O_2$ (1)
$NO_3 + h\nu \rightarrow NO_2 + O(^3P)$ (2)

The absorption spectrum of NO_3 shows about 20 diffuse bands between 400 and 700 nm. The most intense features, the 0-0 and 1-0 bands of the symmetric N-O stretching vibration in the excited state, are at 662 and 623 nm, with absorption cross sections of $\geq 2 \times 10^{-17}$ and $\geq 1.5 \times 10^{-17}$ cm^2 $molecule^{-1}$, respectively. The absorption cross section of the 0-0 band at 662 nm is of special interest, since it is used to monitor NO_3 both in the laboratory and in the atmosphere.

The absorption cross sections of NO_3 have been the subject of many laboratory studies in the last decades. Although agreement existed on the positions of the absorption features, estimates of the absolute cross sections varied by up to a factor of nearly two. The various studies and the cross sections measured at the 662-nm peak are listed in the following survey:

Table 4-14. Summary of NO_3 Cross Section Measurements

Reference	Year	NO_3 source Technique	Temperature (K)	Wavelength range (nm)	Resolution (nm)	σ(662 nm) (10^{-17} cm^2)
1) Schott and Davidson [716]	1958	N_2O_5 Shock pyrolysis	600, 650, 825, 1025	366-652	3.6	1.15 ± 0.4 [1]
2) Johnston and Graham [387]	1974	$N_2O_5 + O_3$ Equilibrium constant calculation	295	450-680	0.7	0.347 (±50%) 1.48 [2]
3) Graham and Johnston [296]	1978	$N_2O_5 + O_3$ Modulated photolysis	298	400-704	0.83	1.708
4) Mitchell et al. [534]	1980	$NO_2 + O_3$ Differential photomultiplier	294 ± 4	498-671	0.05	1.21 ± 0.20
5) Marinelli et al. [487]	1982	$NO_2 + O_3$ Tunable dye laser	296	654-671	0.05	1.90
6) Ravishankara and Wine [660]	1983	$F + HNO_3$ Discharge flow, dye laser	298	565-673	0.05	1.78 ± 0.23
7) Cox et al. [185]	1984	$Cl + ClONO_2$ Modulated photolysis, diode array spectrometer	296	662	0.4	1.63± 0.15
8) Burrows et al. [125]	1985	$F + HNO_3$, $Cl + HNO_3$ Modulated photolysis	298	615-670	1	1.85 ± 0.56
9) Ravishankara and Mauldin [658]	1986	$F + HNO_3$ Discharge flow, dye laser	298	652.5-672.5	0.05	1.90 ± 0.22
			240			2.31 ± 0.23
			220			2.71 ± 0.27
10) Sander [700]	1986	$Cl + ClONO_2$ Flash photolysis, diode array spectrometer $F + HNO_3$ Discharge flow	298	220-700	~0.4	2.28 ± 0.12 2.28 ± 0.34 [3]
			250			2.62 ± 0.13
			230			2.70 ±0.14
			298			1.83 ± 0.27
11) Canosa-Mas et al. [149]	1987	$F + HNO_3$ Discharge flow	296 ± 3	662	1.1	2.23 ± 0.35
12) Cantrell et al. [151]	1987	$NO_2 + O_3$ Fourier transform spectroscopy	348	662	0.22 (5 cm^{-1})	2.06 ± 0.27
			323			2.13 ± 0.22
			298			2.02 ± 0.20
			271			2.08 ± 0.18
			253			1.84 ± 0.43
			232			2.22 ± 0.33
			215			2.02 ± 0.24
			215-348			2.06 ± 0.32 (average)
13)Yokelson et al. [858]	1994	$Cl + ClONO_2$ Flash photolysis, diode array spectrometer	298	440-720	~0.1	2.23 ± 0.09
			258			2.49 ± 0.13
			230			2.76 ± 0.13
			200			2.99 ± 0.14
14) Wängberg et al. [836]	1997	$N_2O_5 \leftrightarrow NO_3 + NO_3$ Differential optical absorption spectroscopy	279.6-294.2	603-682	0.42	scaled to 2.10 [4]
15) Orphal et al. [616]	2003	$N_2O_5 + O_3$ Fourier transform spectroscopy	294	465-794	0.6 cm^{-1} (0.026 nm at 662 nm)	2.18

[1] Estimate for 300 K by Wayne et al. [840] from the data of Schott and Davidson [716].
[2] Improvement by Graham and Johnston [296] using their more actual kinetic data.
[3] The overall uncertainty (± 15%) includes the uncertainty of the absorbance measurement (± 5%) and the uncertainty of $\sigma(ClONO_2)$ (± 10%). The value for σ(662 nm) obtained by the flash photolysis method is preferred by Sander [700] over that obtained by the discharge flow method.
[4] Recommendation by Wayne et al. [840].

It is apparent from the above compilation that there are significant differences between the reported absorption cross sections for the strong 0-0 band near 662 nm. The previous JPL recommendation derived a value of $(2.00 \pm 0.25)x10^{-17}$ cm^2 $molecule^{-1}$, which is the average of the results of references Nr. 5, 6, and 8-12 in Table 4-14. The recommendation of Wayne et al. [840] averaged the data of the more recent studies, references Nr. 9-12, and resulted in the higher value of $(2.10 \pm 0.20)x10^{-17}$ cm^2 $molecule^{-1}$. Higher values for the absorption cross section at 662 nm (see Table 4-14) were obtained in two most recent studies of Yokelson et al. [858] and Orphal et al. [616]. We averaged the results of Sander [700] and Yokelson et al. [858] to derive a new recommendation at 662 nm of $(2.25 \pm 0.15)x10^{-17}$ cm^2 $molecule^{-1}$ (the results of Cantrell et al. [151] have not been included; see the next paragraph concerning the temperature dependence). To obtain the recommended absorption cross sections listed in Table 4-15, we normalized the data of Sander [700] to this peak value (which actually is a reduction by only 1.3%).

Measurements of the temperature dependence of the absorption spectrum indicated an increase of the absorption cross sections with decreasing temperature. At the 662-nm peak an increase by 42% between 298 and 220 K was observed by Ravishankara and Mauldin [658], by 17% between 298 and 230 K by Sander [700], and increases by 34% between 298 and 200 K and 24% between 298 and 230 K by Yokelson et al. [858]. The results of Cantrell et al. [151], who reported temperature-independent cross sections averagin around $2.06x10^{-17}$ cm^2 $molecule^{-1}$ at T = 210-348 K, are in disagreement with these findings. A linear interpolation of the cross sections measured at 662 nm between 200 and 298 K, $\sigma(662\ nm, T) = (4.56 - 0.00787\ T)x10^{-17}$ cm^2 $molecule^{-1}$, was derived by Yokelson et al. [858].

A similar empirical relation, $\sigma(662\ nm, T) = (4.59 - 0.00\ 837\ T)x10^{-17}$ cm^2 $molecule^{-1}$, based on the data of Sander [700], normalized to $\sigma(662\ nm) = 2.1 \times 10^{-17}$ cm^2 $molecule^{-1}$, was given in the IUPAC 2003 recommendation. Orphal et al. [616] explained the temperature effect as resulting from changing populations of the vibrational levels of NO_3 and derived a formula for the cross section ratio as function of temperature:

$$\sigma(T)/\sigma(298K) = \{1 - \exp(-1096.4/T) - 2\exp(-529.5/T)\} / \{1 - \exp(-1096.4/298.0) - 2\exp(-529.5/298.0)\}$$

where the values of 1096.4 K^{-1} and 529.5 K^{-1} are the vibrational energies of 762 cm^{-1} and 368 cm^{-1} divided by the Boltzmann constant. Considering the absorption cross section ratio $\sigma(T)/\sigma(298\ K)$ as a function of reciprocal temperature, there is excellent agreement between the curves calculated by the Orphal model and the empirical relation of Yokelson et al. [858].

The quantum yields φ_1 and φ_2 have been measured by Graham and Johnston [296], and at higher spectral resolution by Magnotta and Johnston [467], who report the product of the cross section times the quantum yield in the 400-to-630-nm range. The total quantum yield value, $\varphi_1 + \varphi_2$, computed from the results of this latter study and the cross sections of Graham and Johnston [296], is about 1.5 for $\lambda < 585$ nm, based on the nearly constant yield of the major product $O(^3P)$, and a quantum yield for the NO production φ_1 near zero. Because systematic errors seems to exist in these data, Wayne et al. [840] in their review normalize φ_2 quantum yields to unity at $\lambda < 585$ nm. The quantum yield for the NO production φ_1 rises from zero at 585 nm to a maximum of $\varphi_1 = 0.35$ at 595 nm, where $\varphi_2 = 0.65$. At longer wavelengths both quantum yields φ_1 and φ_2 decrease to become zero at $\lambda = 640$ nm. Orlando et al. [611] measured the $O(^3P)$ and NO quantum yields in the photolysis of NO_3 between 570 and 635 nm, confirm qualitatively the previous measurements by Johnston and coworkers, but provide more accurate data for both channels. The $O(^3P)$ quantum yield was found to be unity in the range 570 to 585 to decrease to 0.1 at 635 nm. They observed anomalously low $O(^3P)$ yields in the region of the strong absorption band near 623 nm. Quantum yield of NO were < 0.10 at 580 nm, and 0.20 ± 0.10 near 590 nm. The shapes of the φ_1 and φ_2 curves are similar to those recommended in the review of Wayne et al. [840].

In a molecular beam study, Davis et al. [208] investigated the photodissociation processes of NO_3 in the range 532-662 nm, and determined a very sharp threshold for the dissociation of internally cold NO_3 into NO_2 and $O(^3P)$ at a wavelength of 587 nm. At shorter wavelengths, e.g., 585 nm, the NO + O_2 yield has dropped to values smaller than 0.05. At excitation energies just below this threshold, i.e., $\lambda = 588$ nm, a large quantum yield (0.70 ± 0.10) for a concerted three-center rearrangement was observed, resulting in NO + $O_2(^3\Sigma_g^-, {}^1\Delta)$. The yield of this NO + O_2 process decreases at longer wavelengths to zero at 613 nm. At $\lambda > 588$ nm the O + NO_2 channel arises from vibrational excitation of the ground electronic state of NO_3. These results imply that for thermally equilibrated NO_3, the branching ratios for dissociation of both channels (1) and (2) will strongly depend on the temperature, especially near the threshold wavelength.

Johnston et al. [385] have reanalyzed the available laboratory data relevant to NO_3 photolysis, including quantum yield for NO and NO_2 formation, fluorescence, and threshold energies from the molecular beam experiments. Their model reproduces the wavelength-dependent quantum yield values for $\varphi(O + NO_2)$, $\varphi(NO + O_2)$ and Φ(fluorescence) for three temperatures: 190, 230 and 298 K. At 298 K the calculated $\varphi(O + NO_2)$ quantum yields agree reasonably well with those obtained by Orlando et al. [611], but

show some systematic offset in the range 605-620 nm. The calculated $\varphi(NO + O_2)$ product yield agree with those observed by Magnotta and Johnston [467] within experimental scatter.

The recommended quantum yields are taken from the work of Johnston et al. [385] and are listed in Table 4-16 for the range 685 to 640 nm at three temperatures 190, 230 and 298 K. For $\lambda < 585$ nm, $\varphi(O + NO_2) = 1$, and $\varphi(NO + O_2) = 0$; at $\lambda > 640$ nm, $\varphi(O + NO_2)$ and $\varphi(NO + O_2)$ are zero.

Photodissiociation rates have been calculated by Johnston et al. [385] for overhead sun in the stratosphere:

$$J_1(NO + O_2) = 0.0201\ s^{-1}$$

$$J_2(NO_2 + O) = 0.156\ s^{-1}$$

The spectroscopy of NO_3 has been reviewed by Wayne et al. [840].

Table 4-15. Absorption Cross Sections of NO_3 at 298 K

λ (nm)	10^{20} σ (cm^2)	λ (nm)	10^{20} σ (cm^2)	λ (nm)	10^{20} σ (cm^2)	λ (nm)	10^{20} σ (cm^2)	λ (nm)	10^{20} σ (cm^2)
403	2	461	41	519	165	577	362	635	154
404	0	462	42	520	180	578	354	636	181
405	3	463	43	521	196	579	347	637	222
406	2	464	51	522	206	580	358	638	217
407	1	465	54	523	189	581	380	639	169
408	3	466	58	524	176	582	351	640	132
409	0	467	61	525	169	583	314	641	108
410	1	468	60	526	175	584	302	642	99
411	2	469	62	527	193	585	310	643	104
412	5	470	63	528	225	586	355	644	102
413	5	471	66	529	257	587	446	645	92
414	2	472	69	530	239	588	540	646	80
415	6	473	66	531	224	589	656	647	75
416	7	474	66	532	216	590	638	648	66
417	8	475	73	533	209	591	583	649	58
418	5	476	84	534	218	592	548	650	53
419	9	477	83	535	247	593	490	651	59
420	9	478	78	536	275	594	449	652	65
421	9	479	78	537	276	595	460	653	76
422	10	480	75	538	251	596	495	654	88
423	12	481	76	539	219	597	467	655	105
424	10	482	76	540	225	598	393	656	142
425	8	483	77	541	219	599	333	657	184
426	15	484	83	542	201	600	296	658	260
427	15	485	88	543	180	601	307	659	436
428	13	486	98	544	183	602	355	660	798
429	12	487	99	545	210	603	408	661	1551
430	18	488	102	546	260	604	468	662	2250
431	14	489	103	547	312	605	467	663	1869
432	16	490	111	548	320	606	355	664	1210
433	19	491	106	549	290	607	258	665	794
434	20	492	107	550	265	608	198	666	532
435	17	493	109	551	261	609	184	667	326
436	16	494	109	552	264	610	189	668	203
437	20	495	113	553	271	611	204	669	134
438	23	496	129	554	298	612	239	670	102
439	22	497	130	555	334	613	282	671	85
440	21	498	128	556	349	614	273	672	81
441	20	499	125	557	352	615	242	673	69
442	23	500	121	558	376	616	224	674	55
443	19	501	118	559	399	617	226	675	51
444	21	502	118	560	355	618	256	676	52
445	22	503	119	561	320	619	274	677	63
446	26	504	135	562	311	620	350	678	80
447	31	505	137	563	300	621	562	679	84
448	26	506	143	564	291	622	1090	680	74
449	30	507	137	565	292	623	1578	681	57
450	31	508	136	566	305	624	1291	682	42
451	33	509	145	567	301	625	898	683	33
452	36	510	162	568	305	626	783	684	28
453	34	511	186	569	310	627	806	685	19
454	38	512	189	570	299	628	789	686	17
455	38	513	172	571	296	629	748	687	13
456	38	514	169	572	294	630	724	688	13
457	42	515	170	573	298	631	518	689	13

λ (nm)	10^{20} σ (cm^2)	λ (nm)	10^{20} σ (cm^2)	λ (nm)	10^{20} σ (cm^2)	λ (nm)	10^{20} σ (cm^2)	λ (nm)	10^{20} σ (cm^2)
458	39	516	167	574	306	632	350	690	11
459	45	517	160	575	330	633	233	691	8
460	42	518	154	576	350	634	176		

Note:
403-691 nm, data of Sander [700] normalized to 2.25×10^{-17} cm^2 $molecule^{-1}$ at 662 nm.

Table 4-16. Quantum Yields (multiplied by 1000) for the Product Channels $NO + O_2$ and $NO_2 + O(^3P)$ in the Photolysis of NO_3 at 298, 230 and 190 K

λ nm	φ(NO)			φ(NO_2)		
	298 K	230 K	190 K	298 K	230 K	190 K
585	0.0	0.0	0.0	983.0	996.0	999.0
586	15.2	26.4	37.9	967.0	970.0	961.0
587	39.1	66.7	94.4	943.0	930.0	905.0
588	97.1	161.0	221.0	885.0	836.0	779.0
589	128.0	209.0	283.0	854.0	788.0	716.0
590	190.0	300.0	397.0	793.0	696.0	602.0
591	220.0	343.0	448.0	763.0	653.0	551.0
592	249.0	383.0	495.0	734.0	614.0	505.0
593	303.0	455.0	575.0	680.0	542.0	424.0
594	328.0	487.0	610.0	654.0	510.0	390.0
595	359.0	517.0	630.0	608.0	453.0	332.0
596	357.0	501.0	598.0	587.0	429.0	307.0
597	318.0	430.0	493.0	567.0	406.0	285.0
598	323.0	421.0	468.0	531.0	367.0	249.0
599	314.0	396.0	429.0	509.0	345.0	229.0
600	291.0	346.0	355.0	472.0	307.0	196.0
601	296.0	338.0	335.0	438.0	275.0	170.0
602	291.0	322.0	310.0	415.0	254.0	153.0
603	283.0	294.0	267.0	371.0	215.0	123.0
604	280.0	282.0	249.0	351.0	198.0	111.0
605	264.0	253.0	213.0	323.0	176.0	94.4
606	271.0	251.0	205.0	296.0	155.0	80.0
607	268.0	243.0	194.0	280.0	143.0	71.9
608	250.0	217.0	167.0	259.0	128.0	62.1
609	248.0	208.0	155.0	238.0	113.0	53.0
610	236.0	193.0	140.0	226.0	105.0	48.1
611	205.0	159.0	111.0	210.0	94.7	42.2
612	200.0	150.0	101.0	193.0	84.0	36.2
613	190.0	138.0	90.6	181.0	77.3	32.6
614	166.0	114.0	71.2	166.0	68.4	28.0
615	166.0	110.0	66.1	147.0	58.3	22.9
616	160.0	102.0	59.7	137.0	52.7	20.2
617	141.0	85.5	47.5	124.0	46.5	17.3
618	143.0	83.5	44.8	108.0	38.6	13.8
619	139.0	78.4	40.9	99.3	34.6	12.1
620	131.0	71.5	36.0	89.7	30.3	10.2
621	127.0	66.0	32.0	76.9	24.8	8.03
622	122.0	61.9	29.2	70.4	22.1	6.99
623	117.0	57.6	26.5	64.3	19.7	6.07
624	106.0	49.6	21.9	55.2	16.2	4.8
625	98.5	44.5	19.0	48.7	13.8	3.94
626	92.3	40.6	16.8	44.2	12.2	3.39
627	84.8	36.0	14.5	39.3	10.5	2.83
628	73.9	29.9	11.5	33.9	8.67	2.26
629	69.9	27.4	10.2	29.4	7.23	1.81
630	64.9	24.7	9.01	26.4	6.29	1.53
631	57.8	21.3	7.52	23.6	5.45	1.29
632	50.8	17.8	6.02	19.5	4.29	0.969
633	46.6	15.9	5.23	17.7	3.8	0.838
634	42.6	14.2	4.54	16.1	3.36	0.724
635	37.3	12.0	3.73	14.6	2.97	0.624
636	32.3	9.86	2.93	11.9	2.3	0.462
637	29.4	8.7	2.52	10.7	2.02	0.396
638	26.6	7.66	2.16	9.57	1.77	0.338
639	23.5	6.53	1.78	8.56	1.54	0.288
640	20.3	5.38	1.41	7.15	1.24	0.224

[a] From Johnston et al. [385].

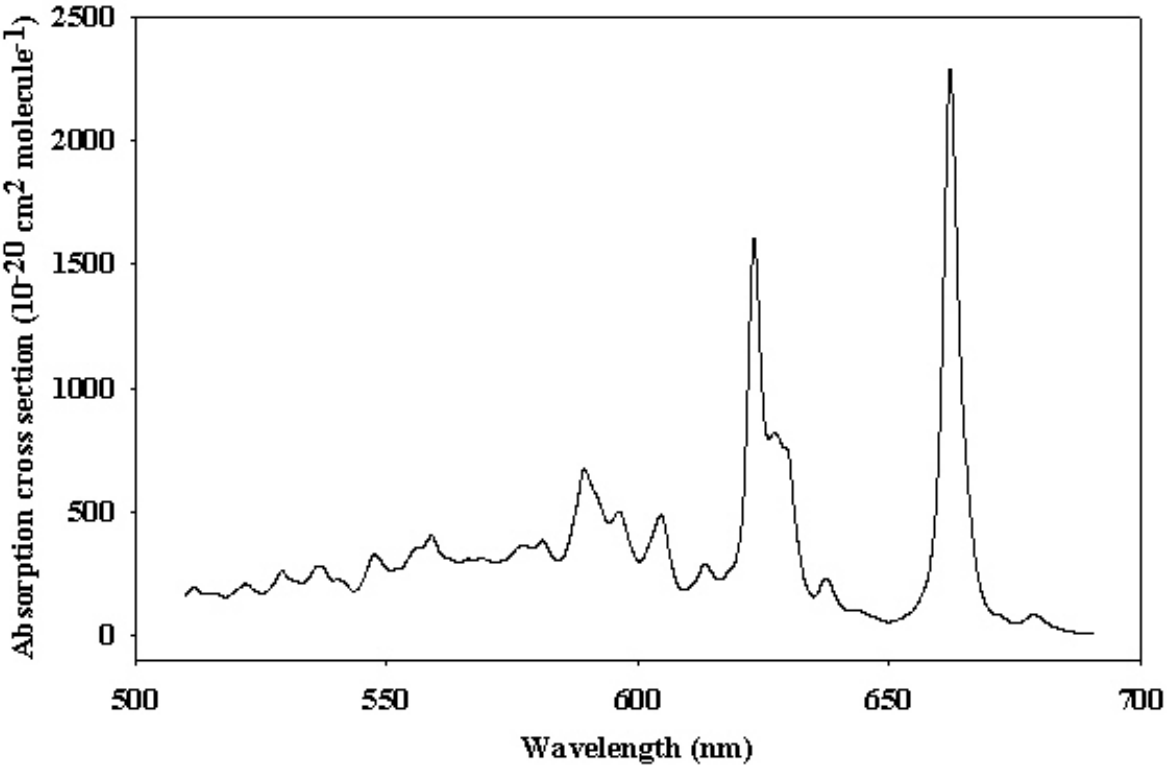

Figure 4-1. Absorption Spectrum of NO_3

C3. $N_2O + h\nu \rightarrow N_2 + O(^1D)$
$N_2O + h\nu \rightarrow N_2 + O(^3P)$
$N_2O + h\nu \rightarrow N(^4S) + NO(^2\Pi)$. Absorption cross sections of nitrous oxide NO_2 were measured in the VUV and UV spectral region between 108 and 315 nm and at temperatures between 194 and 302 K as shown in this survey:

Table 4-17. Summary of N_2O Cross Section Measurements

Reference	Year	Temperature (K)	Wavelength range (nm)	Spectral resolution (nm)
Romand and Mayence [685]	1949	291	139-231	not indicated
Zelikoff et al. [875]	1953	298	108-210	0.085
Zelikoff and Aschenbrand [874]	1954	298	184.9	not indicated
Thompson et al. [778]	1963	298	190-240	not indicated
Bates and Hays [55]	1967	298	190-315	not indicated
Johnston and Selwyn [390]	1975	298	210-300	not indicated
Selwyn et al. [722]	1977	194, 225, 243, 263, 302	173-240	0.7, 0.075
Hubrich and Stuhl [346]	1980	208, 298	160-235	0.3
Selwyn and Johnston [723]	1981	150-500	172-197	0.003, 0.05, 0.07
Yoshino et al. [868]	1984	295-299	169.6-222.6	0.0006
Mérienne et al. [522]	1990	220, 240, 296	200-240	0.02
Cantrell et al. [152]	1997	298, 353	184.9	<0.2
Creasy et al. [196]	2000	298	184.9	not indicated
von Hessberg et al. [828]	2004	233, 283	180-218	0.7, 1.1

The spectrum shows a broad absorption band between 160 and 260 nm with the maximum around 182 nm (σ_{max} = (1.24-1.47) × 10^{-19} cm^2 molecule^{-1}) and a stronger but smaller band between 137 and 160 nm with the maximum around 145 nm (σ_{max} = (5-6)) × 10^{-18} cm^2 molecule^{-1}). There is good agreement between the results of Selwyn et al. [722] and Hubrich and Stuhl [346] in the region of the broad absorption band. The agreement within this band is about 15%, around the 182 nm maximum better than 5%, with the data of Selwyn et al. [722] being somewhat larger than those of Hubrich and Stuhl [346]. The results of Mérienne et al. [522] for the region 220-240 nm are in excellent agreement (≤ 5%) with those of Selwyn et al. [722]. The

results of Cantrell et al. [152] and Creasy et al. [196] at 184.9 nm are in excellent agreement with the results of Selwyn et al. [722]. The high-resolution absorption curve reported by Yoshino et al. [868], showing vibrational structure around the maximum, lies very close to the absorption curve reported by Hubrich and Stuhl [346]. At wavelengths above 250 nm, there are large discrepancies between the results of Bates and Hayes [55] and those of Johnston and Selwyn [390]. Recommended cross sections are listed in Table 4-18. They are based on the room temperature results at 160, 165 and 170 nm of Hubrich and Stuhl [346] and the room temperature results between 173-240 nm of Selwyn et al. [722].

The temperature dependence of the absorption cross section in the atmospherically relevant wavelength region has been measured by Selwyn et al. [722], Hubrich and Stuhl [346], and Mérienne et al. [522] (see survey above). Their results are in excellent agreement. Absorption cross section decrease with decreasing temperature. Selwyn et al. [722] fitted their data with the expression shown in Table 4-19. Isotopomer specific cross sections for $^{14}N^{14}NO$, $^{15}N^{14}NO$, $^{14}N^{15}NO$, $^{15}N^{15}NO$ over the wavelength range 181-218 nm and at 233 and 283 K have been measured by von Hessberg et al. [828]; there is a slight decrease of the absorption cross sections of $^{14}N^{15}NO$ and $^{15}N^{5}NO$ as compared to those of $^{14}N^{14}NO$ and $^{15}N^{14}NO$, and again a decrease with decreasing temperature.

Quantum yield for photodissociation is unity, and products are almost exclusively N_2 and $O(^1D)$ (Zelikoff and Aschenbrand [874], Paraskevopoulos and Cvetanovic [621], Preston and Barr [645], Simonaitis et al. [735]). Yield of $N(^4S)$ and $NO(^2\Pi)$ is less than 1% (Greenblatt and Ravishankara [302]. The yield of $O(^3P)$ at 193 nm is reported to be 0.005±0.002 Nishida et al. [587].

Table 4-18. Absorption Cross Sections of N_2O at 298 K

λ (nm)	$10^{20}\sigma$ (cm^2)	λ (nm)	$10^{20}\sigma$ (cm^2)	λ (nm)	$10^{20}\sigma$ (cm^2)	λ (nm)	$10^{20}\sigma$ (cm^2)
160	4.30	188	12.5	206	1.65	224	0.0375
165	5.61	189	11.7	207	1.38	225	0.0303
170	8.30	190	11.1	208	1.16	226	0.0239
173	11.3	191	10.4	209	0.980	227	0.0190
174	11.9	192	9.75	210	0.755	228	0.0151
175	12.6	193	8.95	211	0.619	229	0.0120
176	13.4	194	8.11	212	0.518	230	0.00955
177	14.0	195	7.57	213	0.421	231	0.00760
178	13.9	196	6.82	214	0.342	232	0.00605
179	14.4	197	6.10	215	0.276	233	0.00478
180	14.6	198	5.35	216	0.223	234	0.00360
181	14.6	199	4.70	217	0.179	235	0.00301
182	14.7	200	4.09	218	0.142	236	0.00240
183	14.6	201	3.58	219	0.115	237	0.00191
184	14.4	202	3.09	220	0.0922	238	0.00152
185	14.3	203	2.67	221	0.0739	239	0.00123
186	13.6	204	2.30	222	0.0588	240	0.00101
187	13.1	205	1.95	223	0.0474		

Note:
160-170 nm, Hubrich and Stuhl [346],
173-240 nm, Selwyn et al. [722].

Table 4-19. Mathematical Expression for Absorption Cross Sections of N_2O as a Function of Temperature

$$\ln(\sigma(\lambda,T)) = \sum_{n=0}^{4} A_n \lambda^n + (T-300)\exp\left(\sum_{n=0}^{3} B_n \lambda^n\right)$$

Where T: temperature K; λ: nm;

$A_0 = 68.21023$ $B_0 = 123.4014$
$A_1 = -4.071805$ $B_1 = -2.116255$
$A_2 = 4.301146 \times 10^{-2}$ $B_2 = 1.111572 \times 10^{-2}$
$A_3 = -1.777846 \times 10^{-4}$ $B_3 = -1.881058 \times 10^{-5}$
$A_4 = 2.520672 \times 10^{-7}$

Ranges of applicability: 173 nm < λ < 240 nm; 194 K < T < 302 K

Several groups have investigated the isotopic fractionation of N_2O resulting from photolysis in the UV. Fractionation factors have been measured by several groups following photolysis at several wavelengths in the 193–213 nm range: Turatti et al. [786] employed high resolution FTIR spectroscopy; Röckmann et al. [675] used a modified isotope ratio mass spectrometric technique; and Rahn et al. [648] utilized conventional isotope ratio mass spectrometry. Zhang et al. [879] employed a low-resolution FTIR technique with N_2O photolysis at 213 nm, and Röckmann et al. [676] utilized a broadband photolysis source centered around 200 nm and simulating stratospheric actinic fluxes. The results are in reasonably good agreement, and indicate that the fractionation factors increase with photolysis wavelength from 193 to 213 nm. Furthermore, the fractionation factors show a clear dependence on the position of the ^{15}N atom, in agreement with the theoretical zero point energy model of Yung and Miller [872]; however, the Yung and Miller calculations underestimate the laboratory results by about a factor of two. A more detailed Hermite propagation model achieves better agreement with experimental enrichment factors (Johnson et al., [381]). Analysis of the isotopic composition of stratospheric air samples yields results that are in qualitative agreement with the laboratory results, confirming that photolysis is the predominant sink for N_2O [303, 676]. On the other hand, the fractionation factors measured in the atmospheric samples are smaller than those reported from the laboratory studies, indicating the influence of atmospheric diffusion and mixing [676].

C4. $N_2O_4 + h\nu \rightarrow 2\ NO_2$. The absorption cross sections of N_2O_4 have been derived from absorption measurements in NO_2-N_2O_4 mixtures. Data have been reported at 273 K and 265-405 nm by Holmes and Daniels [337]; at 300 K and 197 nm by Nakayama et al. [571]; at 298 K and 240-390 nm by Hall and Blacet [307] (as listed by Johnston and Graham [387]); at 273 K and 185-390 nm by Bass et al. [53]; at 298 K and 198-230 nm by Schneider et al. [714]; at 213, 225, 233, 243, and 253 K and 320-405 nm by Harwood et al. [314]; at 220 K and 200-390 nm by Mérienne et al. [521]; and at 220 K and 250-455 nm by Vandaele et al. [807]. The absorption spectrum of N_2O_4 exhibits an absorption band between 300 and 400 nm with the maximum at ~340 nm and a second, less pronounced maximum near ~265 nm followed by a sharp increase of the cross sections to another maximum in the region of ~190 nm. In the region 185-360 nm, there is good agreement between the various results as far as the shape of the absorption curve is concerned, with the exception that the spectrum reported by Bass et al. [53] is very noisy. In the region below 240 nm, there is good agreement between the absorption cross sections of Bass et al. [53] and Schneider et al. [714], whereas those reported by Mérienne et al. [521] are lower by ~30%. In the region between 250 and 300 nm, the results of Vandaele et al. [807] are systematically lower than the results of Mérienne et al. [521] by a factor ~0.85, whereas the results of Bass et al. [53] are higher by ~ 30%. In the region of the absorption band at 300-380 nm, there is good agreement between the results of Hall and Blacet [307], the low-temperature (213 and 224 K) data of Harwood et al. [314], and the results of Vandaele et al [807], the absorption cross sections for the maximum at 340 nm agreeing within 5%. The absorption curves reported by of Bass et al. [53] and Mérienne et al. [521] show higher values than the aforementioned ones, the differences for the absorption maximum being about 25% and 15%, respectively. As a recommendation we list in Table 4-20 the averages over 2-nm intervals of the high-resolution (0.01-0.03 nm) spectrum between 252 and 390 nm measured by Vandaele et al. [807].

Table 4-20. Absorption Cross Sections of N_2O_4 at 220 K

λ (nm)	10^{20} σ (cm^2)	λ (nm)	10^{20} σ (cm^2)	λ (nm)	10^{20} σ (cm^2)	λ (nm)	10^{20} σ (cm^2)
252	64.8	288	27.5	324	47.5	360	26.8
254	65.1	290	25.0	326	51.9	362	22.5
256	64.7	292	22.9	328	55.9	364	18.7
258	64.8	294	21.0	330	59.7	366	15.4
260	64.3	296	19.5	332	63.0	368	12.5
262	63.2	298	18.5	334	65.7	370	10.0
264	61.8	300	17.9	336	67.3	372	8.13
266	60.0	302	18.0	338	68.1	374	6.50
268	57.9	304	18.5	340	68.1	376	5.33
270	55.2	306	19.3	342	66.8	378	4.24
272	52.3	308	20.8	344	64.4	380	3.52
274	49.3	310	22.9	346	61.3	382	2.93
276	46.2	312	25.3	348	57.3	384	2.47
278	43.0	314	28.3	350	52.5	386	2.16
280	39.7	316	31.9	352	47.3	388	1.89
282	36.4	318	35.3	354	42.1	390	1.78

λ (nm)	10^{20} σ (cm^2)	λ (nm)	10^{20} σ (cm^2)	λ (nm)	10^{20} σ (cm^2)	λ (nm)	10^{20} σ (cm^2)
284	33.3	320	39.1	356	36.9		
286	30.3	322	43.2	358	31.7		

Note:
nm, Vandaele et al. [807].

C5. $N_2O_5 + h\nu \rightarrow NO_3 + NO_2$
$N_2O_5 + h\nu \rightarrow NO_3 + NO + O(^3P)$
$N_2O_5 + h\nu \rightarrow NO_3 + NO_2^*$. The absorption cross sections of dinitrogen pentoxide, N_2O_5 have been measured at 273 K and 265 and 280 nm by Holmes and Daniels [337] and at 280-380 nm by Jones and Wulf [393]; at room temperature and 210-290 nm by Johnston and Graham [387]; at 205-380 nm by Graham [295]; at 200-360 nm by Johnston et al. [384]; and at 208-398 nm by Harwood et al. [313]. The temperature dependence has been studied at 225 to 295 K and 290-380 nm by Yao et al. [856], at 273 and 295 K and 280-380 nm by Harwood et al. [316], and at 233-295 K and 240-420 nm by Harwood et al. [315]. Measurements in the far UV between 152 and 240 nm have been carried out at 195 K by Osborne et al. [617]. The absorption spectrum of N_2O_5 exhibits an absorption maximum at 160 nm and continuously decreasing absorption cross sections with increasing wavelength up to 420 nm.

The room temperature values of Yao et al. [856] and Harwood et al. [313, 315, 316] are in good agreement at wavelengths above 250 nm (within 10% in the region 250-280 nm and above 310 nm, and within 20% at ~290-310 nm). Below 250 nm, the cross sections reported by Yao et al. [856], which have been recommended in the 1997 evaluation, are systematically higher by up to a factor of ~2 at 208 nm than those reported by Harwood et al. [313]. A possible reason for this discrepancy could be contributions to the measured absorption from HNO_3 impurities as argued by Harwood et al. [313] who used N_2O_5 samples containing less than 1% HNO_3 impurities. This explanation was confirmed by the results of Osborne et al. [617], who also used thoroughly purified N_2O_5 samples and reported absorption cross sections (at 195 K indeed, but there is no temperature dependence at wavelengths smaller than 250 nm, see below) in excellent agreement with those of Harwood et al. [313] at 210-240 nm.

The recommended absorption cross sections listed in Table 4-21 are the mean of the data of Yao et al. [856] and Osborne [617] at 200-208 nm; the mean of the data of Yao et al. [856], Osborne et al. [617] (two data sets from different measurements), and Harwood et al. [313] at 210-240 nm; the data of Harwood et al. [313] at 242-398 nm, and the data of Harwood et al. [315] at 400-420 nm.

Temperature dependence of the absorption cross sections becomes significant at wavelengths above 280 nm. As observed in good agreement by Harwood et al. [313] and Yao et al. [856] the cross sections decrease with decreasing temperature, and the effect increases with increasing wavelength. The temperature coefficients A and B of a parameterization according to $\log_{10}(\sigma) = A + 1000B/T$ for T = 233-295 K, derived by Harwood et al. [315], are listed also in Table 4-21.

There are several studies on the primary photolysis products of N_2O_5: Swanson et al. [760] have measured the quantum yield for NO_3 production $\varphi_{248}(NO_3) = 0.89 \pm 0.15$ at 248 nm and $\varphi_{350}(NO_3) = 0.84 \pm 0.09$ at 350 nm, obtaining thus a value close to unity, which is consistent with the observations of Burrows et al. [124] for photolysis at 254 nm ($\varphi_{254}(NO_3) = 0.80$). Barker et al. [39] report a quantum yield for $O(^3P)$ production at 290 nm of less than 0.1, and 0.8 ± 0.2 for NO_3. For $O(^3P)$-atom production Margitan (private communication, 1985) measured a quantum yield value of 0.35 ± 0.10 at 266 nm, and Ravishankara et al. [662] report $\varphi(O^3P)$ values of 0.72 ± 0.09, 0.38 ± 0.08, 0.21 ± 0.03 and 0.15 ± 0.03 at 248, 266, 287, and 289 nm, respectively, with a quantum yield near unity for NO_3 production ($\varphi(NO_3) = 0.96 \pm 0.13$) at 248 nm. Quantum yields for NO_3 production were measured by Harwood et al. [313] at 248, 308 and 352.5 nm: $\varphi_{248}(NO_3) = 0.64 \pm 0.20$, $\varphi_{308}(NO_3) = 0.96 \pm 0.15$ and $\varphi_{352.5}(NO_3) = 1.03 \pm 0.15$.

Table 4-22 summarizes the above results. It appears, then, that NO_3 is produced with unity quantum yield at wavelengths above 300 nm, but that, based on the results by Harwood et al. [313], ($\varphi(NO_3)$ at $\lambda < 300$ nm is not well established. At e.g. 248 nm, the values vary between "near unity" and 0.64 ± 0.20. The $O(^3P)$-atom, and hence the NO yield, increases at shorter wavelengths, with a consequent decrease in the NO_2 yield.

The study of Oh et al. [595] indicates that, besides NO_3, the primary photolysis products are a wavelength-dependent mixture of NO_2, NO_2* and NO + O, where NO_2* represents one or more excited electronic states, most likely the $^2B_1$ state.

Table 4-21. Absorption cross sections N_2O_5 at 195-300 K and temperature coefficients

λ (nm)	10^{20} σ (cm^2)	A (cm^2)	B (cm^2 K^{-1})	λ (nm)	10^{20} σ (cm^2)	A (cm^2)	B (cm^2 K^{-1})	λ (nm)	10^{20} σ (cm^2)	A (cm^2)	B (cm^2 K^{-1})
200	910			270	16.2	-18.42	-0.104	340	0.368	-18.77	-0.492
202	842			272	14.9			342	0.328		
204	771			274	13.7			344	0.293		
206	682			276	12.4			346	0.262		
208	585			278	11.4			348	0.234		
210	445			280	10.5	-18.59	-0.112	350	0.210	-18.71	-0.583
212	381			282	9.59			352	0.188		
214	322			284	8.74			354	0.167		
216	267			286	7.94			356	0.149		
218	220			288	7.20			358	0.133		
220	181			290	6.52	-18.72	-0.135	360	0.120	-18.31	-0.770
222	151			292	5.88			362	0.107		
224	129			294	5.29			364	0.0958		
226	113			296	4.75			366	0.0852		
228	98.4			298	4.26			368	0.0763		
230	88.2			300	3.81	-18.84	-0.170	370	0.0685	-18.14	-0.885
232	80.5			302	3.40			372	0.0613		
234	74.0			304	3.03			374	0.0545		
236	69.2			306	2.70			376	0.0484		
238	64.6			308	2.40			378	0.0431		
240	59.8			310	2.13	-18.90	-0.226	380	0.0383	-18.01	-0.992
242	53.1			312	1.90			382	0.0341		
244	49.3			314	1.68			384	0.0305		
246	45.6			316	1.49			386	0.0273		
248	41.9			318	1.33			388	0.0242		
250	38.6			320	1.18	-18.93	-0.294	390	0.0215	-18.42	-0.949
252	35.5			322	1.05			392	0.0193		
254	32.6			324	0.930			394	0.0172		
256	29.9			326	0.826			396	0.0150		
258	27.5			328	0.735			398	0.0134		
260	25.2	-18.27	-0.091	330	0.654	-18.87	-0.388	400	0.014	-18.59	-0.966
262	23.1			332	0.582			410	0.009	-18.13	-1.160
264	21.1			334	0.518			420	0.005		
266	19.4			336	0.462						
268	17.8			338	0.412						

Note:
Absorption cross sections:
200-208 nm, mean of the data of Yao et al. [856] and Osborne et al. [617],
210-240 nm, mean of the data of Yao et al. [856], Osborne et al. [617] (two data sets), and Harwood et al. [313]
242-398 nm, data of Harwood et al. [313],
400-420 nm, data of Harwood et al. [315].
Temperature coefficients: 260-410 nm, Harwood et al. [315],
$\log_{10}(\sigma) = A + 1000B/T$ (T = 233-295 K). See text for a discussion of this parameterization.

Table 4-22. Quantum Yields from Photolysis of N_2O_5

λ (nm)	φ(NO_3)	φ(O^3P)	Reference
248	0.89 ± 0.15		Swanson et al. [760]
	0.96 ± 0.13	0.72 ± 0.09	Ravishankara et al. [662]
	0.64 ± 0.20		Harwood et al. [313]
254	0.80		Burrows et al. [124]
266		0.35 ±0.10	Margitan (private communication, 1985)
		0.38 ± 0.08	Ravishankara et al. [662]
287		0.21 ± 0.03	Ravishankara et al. [662]
289		0.15 ± 0.03	Ravishankara et al. [662]
290	0.8 ± 0.2	< 0.1	Barker et al. [39]
308	0.96 ± 0.15		Harwood et al. [313]
350	0.84 ± 0.09		Swanson et al. [760]
352.5	1.03 ± 0.15		Harwood et al. [313]

C6. $HONO + h\nu \rightarrow OH + NO$

$HONO + h\nu \rightarrow H + NO_2$. The absorption spectrum of HONO shows a structured absorption band between 300 and 400 nm, corresponding to vibrational progressions in the $A\,^1A'' \leftarrow X\,^1A'$ transition, with the highest peak near 354 nm. Below 270 nm there is a strong and broad absorption band with the maximum near 205 nm.

The absorption cross sections over the near-UV band have been measured at room temperature as shown in the following survey (the cross sections of the strongest vibrational band at 354 nm are given in the last column):

Table 4-23. Summary of HONO Cross Section Measurements

Reference	Year	Wavelength Range nm	Resolution nm	σ (354 nm) 10^{-19} cm^2
Johnston and Graham [387]	1974	300-399	0.87	1.23
Cox and Derwent [189]	1976	200-394	< 0.1	5.60
Perner [687]	1977	310-388	0.6	5.52
Stockwell and Calvert [755]	1978	310-396	< 1	4.96
Platt et al. [636]	1980	336-376	0.8	4.7
Vasudev [812]	1990	310-393	Not given	(4.97)*
Bongartz et al. [84]	1991	300-400	0.1 (λ<375 nm) 0.8 (λ<375 nm)	6.42**
Bongartz et al. [83]	1994	300-400	0.1 (λ<375 nm) 0.8 (λ>375 nm)	5.49**
Febo et al. [236]	1996	50-380	1	4.97**
Pagsberg et al. [618]	1997	348-376	0.06	5.02
Brust et al. [107]	2000	323-394	0.5	3.89
Stutz et al. [756]	2000	291-404	0.061±0.003	5.22
Wang and Zhang [835]	2000	352.2, 354.2, 357.0	< 0.1	4.89

* Normalized to the spectrum of Stockwell and Calvert [755].

** Bongartz et al. [83] corrected their 1991 results by a factor of 0.855.

There is good agreement between the various data sets as far as the peak positions are concerned. Discrepancies in the peak heights, generally, are a consequence of the different spectral resolutions used in the measurements. Stutz et al. [756] normalized the earlier cross section data to a resolution of 1 nm, which shows an agreement of better than 10% between their results and those of Bongartz et al. [83], Pagsberg et al. [618] and Vasudev [812]. The older measurements of Stockwell and Calvert [755] are in reasonable agreement with the more recent ones, whereas the data of Cox and Derwent [189] are higher by ~26% (presumably uncorrected NO_2 absorption) and those of Johnston and Graham [387] are smaller by 70% (presumably non equilibrium state of the $NO/NO_2/H_2O$ mixture during the measurements). The disagreement with the recent measurements of Brust et al. [107], whose results are smaller by ~25%, could not be explained.

Measurements in the region of the UV band have been carried out at 200-300 nm by Cox and Derwent [189] (resolution <0.1 nm) and at 184-274 nm by Kenner et al. [405] (resolution 0.38 nm). The reported spectra are in quantitative agreement over the wavelength range 220-270 nm. The sharp peak at 215 nm observed by Cox and Derwent [189], however, could not reproduced by Kenner et al. [405], who bring forward a number of arguments for the correctness of their results.

As recommended absorption cross sections, listed in Table 4-24, we choose for the region 184-274 nm the data of Kenner et al. [405] at 2-nm intervals (read from the plot given in their paper). The recommended absorption cross sections for the region 296-396 nm are based on the measurements of Stutz et al. [756]: for the regions 296-325 nm and 371-396 nm, we take the averages over 1-nm intervals of their high-resolution spectrum, and for the highly structured region 326-370 nm the averages over 0.5 nm intervals.

The quantum yield for OH radical production from the photolysis of HONO at 365 ± 5 nm was determined by Cox and Derwent [189] as (0.92 ± 0.16). The quantum yield for OH(A) production from the laser photolysis at 193 nm was measured as 1.8×10^{-5} by Kenner et al. [405]. Wollenhaupt et al. [852] determined an upper limit of 0.01 for the quantum yield of H-atom formation by the photolysis at 351 nm, using resonance fluorescence at 121.6 nm. The H + NO_2 ($X\ ^2A_1$, $A\ ^2B_2$, $B\ ^2B_1$, $C\ ^2A_2$) product channels in the photodissociation of HONO at 193.3 nm were recently examined by Amaral et al. [14], and branching ratios of the NO_2 electronic states estimated: $X\ ^2A_1 : A\ ^2B_2 : B\ ^2B_1 : C\ ^2A_2 \approx 0.13 : 0.21 : 0.66$.

Table 4-24. Absorption Cross Sections of HONO at 298 K

λ (nm)	10^{20} σ (cm^2)	λ (nm)	10^{20} σ (cm^2)	λ (nm)	10^{20} σ (cm^2)	λ (nm)	10^{20} σ (cm^2)
184	85.0	296	0.326	335.5	6.55	360.0	6.87
186	95.0	297	0.565	336.0	5.33	360.5	6.32
188	106	298	0.517	336.5	4.36	361.0	6.05
190	124	299	0.429	337.0	4.23	361.5	5.95
192	143	300	0.617	337.5	5.13	362.0	5.98
194	162	301	0.690	338.0	9.38	362.5	6.35
196	179	302	0.579	338.5	16.52	363.0	7.39
198	196	303	0.925	339.0	14.32	363.5	9.22
200	210	304	1.04	339.5	9.96	364.0	11.49
202	219	305	1.57	340.0	7.79	364.5	12.71
204	223	306	1.29	340.5	8.51	365.0	12.82
205	224	307	0.916	341.0	16.13	365.5	13.19
206	223	308	1.45	341.5	31.52	366.0	14.84
208	220	309	2.01	342.0	29.40	366.5	18.43
210	213	310	1.51	342.5	18.47	367.0	25.08
212	204	311	2.07	343.0	11.43	367.5	35.18
214	193	312	2.42	343.5	8.29	368.0	43.56
216	179	313	2.25	344.0	7.59	368.5	41.37
218	164	314	3.35	344.5	8.18	369.0	31.45
220	150	315	2.54	345.0	8.77	369.5	21.72
222	135	316	1.61	345.5	9.10	370	15.05
224	121	317	3.21	346.0	9.64	370	9.49
226	108	318	4.49	346.5	8.87	372	7.96
228	94.5	319	3.19	347.0	7.80	373	6.30
230	84.5	320	4.66	347.5	7.06	374	4.59
232	74.0	321	5.96	348.0	6.63	375	3.55
234	66.0	322	4.05	348.5	6.26	376	3.36
236	58.0	323	4.56	349.0	6.00	377	3.66
238	50.0	324	5.89	349.5	6.47	378	4.33
240	43.0	325	4.05	350.0	9.06	379	5.66
242	37.0	326	2.65	350.5	14.95	380	7.21
244	32.0	326.5	3.55	351.0	16.94	381	9.13
246	27.5	327.0	6.44	351.5	14.07	382	12.44
248	23.5	327.5	10.26	352.0	12.42	383	17.03
250	20.0	328.0	9.22	352.5	12.81	384	19.47
252	17.0	328.5	6.38	353.0	16.34	385	16.09
254	14.5	329.0	5.20	353.5	28.49	386	10.52
256	12.3	329.5	6.12	354.0	48.73	387	6.59
258	10.3	330.0	9.92	354.5	44.34	388	4.30
260	8.6	330.5	15.06	355.0	27.64	389	2.81
262	7.3	331.0	14.32	355.5	16.40	390	1.71
264	6.2	331.5	9.88	356.0	11.13	391	0.992
266	5.3	332.0	6.94	356.5	9.35	392	0.731
268	4.3	332.5	6.00	357.0	9.45	393	0.597
270	3.7	333.0	6.31	357.5	10.08	394	0.528
272	3.0	333.5	7.11	358.0	9.84	395	0.403
274	2.5	334.0	8.35	358.5	9.02	396	0.237
-	-	334.5	8.37	359.0	8.37		
-	-	335.0	7.71	359.5	7.67		

Note:
184-274 nm, Kenner et al. [405],
296-396 nm, Stutz et al. [756].

C7. $HNO_3 + h\nu \rightarrow OH + NO_2$ (1)
$HNO_3 + h\nu \rightarrow HONO + O(^3P)$ (2)
$HNO_3 + h\nu \rightarrow H + NO_3$ (3)
$HNO_3 + h\nu \rightarrow OH + NO_2^*(1^2B_2)$ (4)
$HNO_3 + h\nu \rightarrow HONO + O(^1D)$ (5)
$HNO_3 + h\nu \rightarrow HONO\ (a^3A) + O(^3P)$ (6)

The absorption spectrum of nitric acid shows a strong absorption band between 150 and 240 nm with the maximum near 183 nm and a second one, appearing as a shoulder above 240 nm on the long-wavelength wing of the strong band. The recommended absorption cross sections and their temperature dependence for the region 192-350 nm, listed in Table 4-25, are taken from the work of Burkholder et al. [119]. The temperature effect is very important for estimates of atmospheric photodissociation. The results of Burkholder et al. [119] agree well (within 10% above 200 nm) with those of Rattigan et al. [649, 650] measured at room temperature, whereas these latter authors report significantly smaller values at 239 K (smaller by 15-30% at 220-330 nm and smaller by ~50% at 330 nm). The recommended absorption cross sections at room temperature are in very good agreement (≤ 15% up to 310 nm) with the data of Molina and Molina [539]. These data are also in good agreement with the values reported by Biaume [68] and Johnston and Graham [386], except at the long wavelength ends. Okabe [598] has measured the cross sections in the 110–190 nm range and his results are 20–30% lower than those of Burkholder et al. [119], Biaume [68], and of Johnston and Graham [386] around 185–190 nm. Suto and Lee [758] have measured the cross sections between 105 and 210 nm, and their results are higher by 10-20% than those of Burkholder et al. [119], of Biaume [68], and of Johnston and Graham [386] around 185–190 nm, but show excellent agreement with the results of Molina and Molina [539] above 185 nm and with the results of Burkholder et al. [119] above 189 nm.

Johnston et al. [384] measured a quantum yield value of ~1 for the OH + NO_2 channel in the 200–315 nm range, using end product analysis. The quantum yield for O-atom production at 266 nm has been measured to be 0.03, and that for H-atom production ≤ 0.002, by Margitan and Watson [475], who looked directly for these products using atomic resonance fluorescence. Jolly et al. [391] measured a quantum yield for OH production of 0.89 ± 0.08 at 222 nm. Turnipseed et al. [789] have measured a quantum yield of (0.95 ± 0.09) for OH production at 248, (0.90 ± 0.11) at 222 nm, however, at 193 nm they reported φ(OH) be only 0.33 ± 0.06. They also measured the quantum yield for production of O-atoms [$O(^3P)$ + $O(^1D)$] to be about 0.031 ± 0.01, 0.20 ± 0.03 and 0.81 ±0.13 at 248, 222 and 193 nm. Both $O(^3P)$ and $O(^1D)$ were observed at 222 and 193 nm, but only $O(^3P)$ was detected at 248 nm. Moreover, 40% of the O atoms formed at both 193 and 222 nm were $O(^1D)$ atoms, giving a $O(^1D)$ yield of 0.28 ± 0.07 at 193 nm. Turnipseed et al. [789] measured upper limits for $H(^2S)$ quantum yields: ≤ 0.002 at 238 nm, ≤ 0.01 at 222 nm, and ≤ 0.012 at 193 nm. Schiffman et al. [709] reported a larger quantum yield for OH production of 0.47 ± 0.06 at 193 nm, and some lower yield 0.75 ± 0.10 at 248 nm. Thus, it appears from these studies that HONO is a major photolysis product at 193 nm.

Felder et al. [240] reported the yield for (OH + NO_2) to be φ(OH) = 0.6 ± 0.1 and for (O + HONO) to be φ(HONO) = 0.4 ± 0.1 in the photolysis of HNO_3 at 193 nm using molecular beam/photofragment translational spectroscopy. Also Myers et al. [570] used this technique to measure the primary processes in the photolysis at 193 nm from the different photofragment ions, and found evidence of the participation of all channels (1) to (6), expect process (4). They determined the branching ratio (OH + NO_2)/(O+HONO) = 0.50 ± 0.05. They obtained φ(OH) = 0.33 ± 0.04 in excellent agreement with the value obtained by Turnipseed et al. [789]. The $\varphi(O)_{total}$ = 0.67 ± 0.04 is lower than the 0.81 ± 0.13 value measured by Turnipseed et al. [789], but the latter authors included the contribution of the secondary dissociation of NO_2 produced in channel (1). The primary yield of $O(^1D)$ formation = $\varphi(O^1D)$ = 0.54 ±0.04 is much larger than the $\varphi O(^1D)$ yield of 0.28 ± 0.07 measured by Turnipseed et al. [789], and remains unexplained. In a similar experiment using LIF and REMPI –TOF, Li et al. [444] found evidence for channel (2) with a yield of about 0.06.

Recent studies by Donaldson et al. [219], Zhang et al. [878] and Brown et al. [102] have indicated that photodissociation of HNO_3 by excitation of the vibrational overtones $3\nu_{O-H}$ (~983 nm), $4\nu_{O-H}$ (~755 nm) and $5\nu_{O-H}$ (~618 nm) in the near IR and visible occurs in the atmosphere providing an additional OH source. The band strengths (integrated absorption cross sections in cm^2 $molecule^{-1}$ cm^{-1}) of 2.63×10^{-20} for $3\nu_{O-H}$ and 2.37×10^{-21} for $4\nu_{O-H}$ transitions have been measured by Donaldson et al. [219], while Zhang et al. [878] obtained band strengths of $(2.9 \pm 0.7) \times 10^{-20}$ for $3\nu_{O-H}$ and $(2.8 \pm 1.0) \times 10^{-21}$ for $4\nu_{O-H}$ transitions. Brown et al. [102] measured the band strengths for $4\nu_{O-H}$ as $(2.25 \pm 0.15) \times 10^{-21}$ at 296 K and $(2.25 \pm 0.15) \times 10^{-21}$ at 251 K, and for 5 ν_{O-H} as $(2.57 \pm 0.15) \times 10^{-22}$ at 296 K and $(2.41 \pm 0.35) \times 10^{-21}$ at 251 K. Although the contributions of enhanced production of OH of photolysis due to overtone absorption is small, the current values are larger than those previously estimated by Donaldson et al. [218].

Table 4-25. Absorption Cross Sections at 298 K and Temperature Coefficients of HNO_3 Vapor

λ (nm)	$10^{20}\sigma$ (cm^2)	10^3 B (K^{-1})	λ (nm)	$10^{20}\sigma$ (cm^2)	10^3 B (K^{-1})	λ (nm)	$10^{20}\sigma$ (cm^2)	10^3 B (K^{-1})
192	1225	0	246	2.06	1.61	300	0.263	3.10
194	1095	0	248	2.00	1.44	302	0.208	3.24
196	940	1.70	250	1.97	1.34	304	0.167	3.52
198	770	1.65	252	1.96	1.23	306	0.133	3.77
200	588	1.66	254	1.95	1.18	308	0.105	3.91
202	447	1.69	256	1.95	1.14	310	0.0814	4.23
204	328	1.74	258	1.93	1.12	312	0.0628	4.70
206	231	1.77	260	1.91	1.14	314	0.0468	5.15
208	156	1.85	262	1.87	1.14	316	0.0362	5.25
210	104	1.97	264	1.83	1.18	318	0.0271	5.74
212	67.5	2.08	266	1.77	1.22	320	0.0197	6.45
214	43.9	2.17	268	1.70	1.25	322	0.0154	6.70
216	29.2	2.17	270	1.62	1.45	324	0.0108	7.16
218	20.0	2.21	272	1.53	1.49	326	0.00820	7.55
220	14.9	2.15	274	1.44	1.56	328	0.00613	8.16
222	11.8	2.06	276	1.33	1.64	330	0.00431	9.75
224	9.61	1.96	278	1.23	1.69	332	0.00319	9.93
226	8.02	1.84	280	1.12	1.78	334	0.00243	9.60
228	6.82	1.78	282	1.01	1.87	336	0.00196	10.5
230	5.75	1.80	284	0.909	1.94	338	0.00142	10.8
232	4.87	1.86	286	0.807	2.04	340	0.00103	11.8
234	4.14	1.90	288	0.709	2.15	342	0.00086	11.8
236	3.36	1.97	290	0.615	2.27	344	0.00069	9.30
238	2.93	1.97	292	0.532	2.38	346	0.00050	12.1
240	2.58	1.97	294	0.453	2.52	348	0.00042	11.9
242	2.34	1.88	296	0.381	2.70	350	0.00042	9.30
244	2.16	1.75	298	0.316	2.92			

Note:
192-350 nm, absorption cross sections σ and temperature coefficients B
($\sigma(\lambda, T) = \sigma(\lambda, 298) \exp(B(\lambda)(T - 298))$; T in K) of Burkholder et al. [119].

C8. $HO_2NO_2 + h\nu \rightarrow HO_2 + NO_2$ (1)
$HO_2NO_2 + h\nu \rightarrow OH + NO_3$ (2)
$HO_2NO_2 + h\nu \rightarrow O(^3P) + HNO_3$ (3)
$HO_2NO_2 + h\nu \rightarrow H + NO_2 + O_2$ (4)
$HO_2NO_2 + h\nu \rightarrow OH + NO_2 + O$ (5)
$HO_2NO_2 + h\nu \rightarrow HO_2 + NO + O(^3P)$ (6)
$HO_2NO_2 + h\nu \rightarrow H + O(^3P) + NO_3$ (7)

There are six studies of the UV spectrum of HO_2NO_2 vapor: at 269 K and 190-330 nm by Cox and Patrick [191], at 284 K and 195-265 nm by Morel et al. [561]; at room temperature and 200-290 nm by Graham et al. [297]; at 298 K and 190-330 nm by Molina and Molina [539]; at 253, 273, and 298 K and 210-329 nm by Singer et al. [737]; and at 273, 296, 318, and 343 K and 220-350 nm by Knight et al. [414]. There is very good agreement (within 5%) between the results of Molina and Molina [539] and Singer et al. [737] at 210-290 nm, which provided the basis for the earlier recommendation; discrepancies (~15-60%) appear in the critical wavelength range for atmospheric photodissociation ($\lambda \geq 290$ nm). The agreement between the data of Graham et al. [297] and Morel et al. [561] with those of Molina and Molina [539] is only within 30% up to 255 and 280 nm, respectively, and the data of Cox and Patrick [191] diverge from those of Molina and Molina [539]. The recent study of Knight et al. [414] over the wavelength range 220-350 nm used the data of Molina and Molina [539] and Singer et al. [737] in the 250-270-nm region for calibration and yielded reliable data for the long-wavelength region. The recommended absorption cross sections, listed in Table 4-26, are the data of Molina and Molina [539] at 190-205 nm, the mean of the data of Molina and Molina [539] and Singer et al. [737] at 210-275 nm, and the data of Knight et al. [414] at 280-350 nm.

In contrast to the measurements of Singer et al. [737], who found no temperature dependence between 253 and 298 K, Knight et al. [414] observed a temperature dependence between 273 and 343 K, i.e., an increase of the absorption cross sections with increasing temperature. An empirical parameterization of the measured temperature dependence by a simple two component absorption model is (T in K):

$$\sigma(T, \lambda) = \sigma_0(\lambda)/Q + \sigma_1(\lambda)\ (1\text{-}1/Q),$$

where the partition function is given by $Q = 1 + \exp(-\Delta E/(0.69T))$ with $\Delta E = 988$ cm^{-1} (O-O stretching vibration).

MacLeod et al. [464] measured the quantum yield of OH radicals in the photolysis of HO_2NO_2 at 248 nm as $\varphi_{248}(OH) = 0.34 \pm 0.16$ (channels 2 and 5), relative to the OH yield in the photolysis of H_2O_2. Roehl et al. [679] determined the quantum yield of NO_2 in the photolysis at 248 nm (relative to the NO_2 yield in the photolysis of HNO_3) as $\varphi_{248}(NO_2) = 0.56 \pm 0.17$ (channels 1,4 and 5). Recently Jimenez et al. [380] measured the yield of OH and HO_2 (arising from channels 1 and 6) at 193 and 248 nm (relative to the photolysis of H_2O_2), and the yield of NO_3 (relative to the photolysis of $ClONO_2$) at 193, 248 and 308 nm over a pressure range 10 to 84 Torr. Jimenez et al. [380] obtained: $\varphi_{193}(OH) = 0.21 \pm 0.12$, $\varphi_{248}(OH) = 0.085 \pm 0.08$, $\varphi_{193}(HO_2) = 0.56 \pm 0.02$, $\varphi_{248}(HO_2) = 0.89 \pm 0.26$, $\varphi_{193}(NO_3) = 0.35 \pm 0.03$, $\varphi_{248}(NO_3) = 0.08 \pm 0.03$ and $\varphi_{308}(NO_3) = 0.05 \pm 0.02$. These latest results indicate that at 248 nm the yields of OH and NO_3 are nearly identical as 0.08, assuming that only channel (2) contributes to OH and NO_3. This lower yield is not in agreement with the earlier results of MacLeod et al. [464] and Roehl et al. [679] at 248 nm. The high HO_2 yield (0.89 ± 0.26) measured at 248 nm by Jimenez et al. [380] overlaps within the experimental uncertainties with the NO_2 yield (0.56 ± 0.17) of Roehl et al. [679], assuming that the HO_2 arises from channel (1). It cannot however not be excluded that the difference in NO_2 yields reflects the contribution of channel (6). The recommended quantum yields are summarized in Table 4-27. The values below 200 nm are taken from Jimenez et al. [380]. The values above 200 nm represent an average between the results of Jimenez et al., Roehl et al. and MacLeod et al..The uncertainties on the recommended quantum yields are ± 0.2.

Recent studies, e.g., Wennberg et al. [845], Salawitch et al. [698] and Evans et al. [231], have indicated that photodissociation of HO_2NO_2 by excitation of the vibrational overtones $3\nu_1$ and $4\nu_1$ in the near IR and visible (at ~991 and 763 nm, respectively) occurs in the atmosphere providing an additional HO_x source. The band strengths (= integrated absorption cross sections) (all in cm^2 molecule^{-1} cm^{-1}) $(3.8 \pm 1.1) \times 10^{-20}$ for $3\nu_1$ and $(3.0 \pm 1.8) \times 10^{-21}$ for $4\nu_1$ have been measured by Zhang et al. [877], and later $(3.3 \pm 0.7) \times 10^{-20}$ for $3\nu_1$ by Roehl et al. [680]. The latter group also measured absolute integrated band strengths and photodissociation quantum yields for 3 dissociative bands in the infrared region: $2\nu_1 + \nu_3$ (8242 cm^{-1}), $2\nu_1$ (6900 cm^{-1}) and $\nu_1 + 2\nu_3$(6252 cm^{-1}) as a function of temperature. The temperature-dependent cross sections and dissociation quantum yields are summarized in Table 4-27.

Table 4-26. Absorption Cross Sections of HO_2NO_2 at 296-298 K

λ (nm)	10^{20} σ (cm^2)	λ (nm)	10^{20} σ (cm^2)	λ (nm)	10^{20} σ (cm^2)	λ (nm)	10^{20} σ (cm^2)
190	1010	260	28.50	300	1.52	328	0.110
195	816	265	23.00	302	1.28	330	0.0926
200	563	270	18.05	304	1.05	332	0.0788
205	367	275	13.40	306	0.853	334	0.0650
210	239	280	9.29	308	0.702	336	0.0540
215	161	282	8.11	310	0.551	338	0.0456
220	117.5	284	6.93	312	0.465	340	0.0372
225	93.50	286	5.86	314	0.380	342	0.0320
230	79.20	288	4.91	316	0.313	344	0.0268
235	68.25	290	3.95	318	0.265	346	0.0228
240	58.10	292	3.37	320	0.216	348	0.0198
245	48.95	294	2.78	322	0.184	350	0.0168
250	41.25	296	2.30	324	0.152		
255	35.00	298	1.91	326	0.128		

Note:
190-205 nm, Molina and Molina [539],
10-275 nm, mean of the data of Molina and Molina [539] and Singer et al. [737],
280-350 nm, Knight et al. [414].

Table 4-27. Quantum Yields of HO_2NO_2

λ (nm)	Φ (OH)	Φ(NO_3)	Φ(HO_2)	Φ(NO_2)
<200	0.3	0.3	0.7	0.7
>200	0.2	0.2	0.8	0.8

Table 4-28. Photodissociation Band Strengths and Quantum Yields for Several Overtone and Combination Bands of HO_2NO_2

Band	Band center (cm^{-1})	$\int \sigma_{diss} \varphi_v \, d\nu$ Band strength cm^2 $molecule^{-1}$ cm^{-1}	Quantum yield
$4\nu_1$	13105	3.0×10^{-21} (b)	1
$3\nu_1$	10090	3.3×10^{-20}	1
$2\nu_1 + \nu_3$	8240	1.21×10^{-21}	0.76
$2\nu_1$	6900	$4.09 \times 10^{-18} \exp(-826.5/T)$ (195 K > T > 224 K	0.14
$\nu_1 + 2\nu_3$	6250	$1.87 \times 10^{-19} \exp(-1410.7/T)$ (195 K > T > 240 K)	0.02

Note:
a) Data from Roehl et al. [680]; b) from Zhang et al. [877].

PHOTOCHEM-D-Carbonyls

D1. $CH_2O + h\nu \rightarrow H + HCO$ ϕ_1
$CH_2O + h\nu \rightarrow H_2 + CO$ ϕ_2
$CH_2O + h\nu \rightarrow H + H + CO$ ϕ_3. The measurement of absorption spectra of formaldehyde at temperatures between 222 and 353 K have been the subject of many studies in the last four decades as shown in the following survey:

Table 4-29. Summary of CH_2O Cross Section Measurements

Reference	Year	Temperature (K)	Wavelength range (nm)	Resolution (nm)	Medium
McMillan [140]	1966	348	202-374	1	air
Bass et al. [52]	1980	223, 296	258-360	0.05	air
Moortgat et al.[555]	1980	285	215-370	0.5	air
Cantrell et al. [150]	1990	223, 233, 243, 253,263, 273, 283, 293, 296	300-358	1 cm^{-1} (~0.011)	vacuum
Rogers [683]	1990	296	235-365	0.04	vacuum
Meller and Moortgat [517]	2000	223, 298	224-373	~0.025	air
Bogumil et al. [82]	2003	293	247-400	0.25	air
Pope et al. [639]	2005	263, 294	313-320	0.1 cm^{-1} (~0.001)	air/vacuum
Pope et al. [640]	2005	294	308-320	0.1 cm^{-1}	air/vacuum

The UV absorption spectrum of formaldehyde displays a highly structured absorption band (of the $\tilde{A}^1A_2 - X^1A_1$ transition) between 240 and 380 nm. An overview of the measurements up to the year 2000, including description of the techniques and experimental details of CH_2O generation and absorption measurements as well as comparison of the various results, is given by Meller and Moortgat [517]. Low resolution spectra were obtained by Mc Millan [140], and Moortgat et al. [555], whereas medium-resolution measurements were reported by Bass et al. [52], Rogers [683], and Bogumil et al. [82]. The spectrum reported by Cantrell et al. [150] was measured with the highest resolution (0.011 nm) for the 300-358-nm region using Fourier transform spectroscopy. Meller and Moortgat [517] provided a high-resolution spectrum in the complete UV

absorption band (224-373 nm) using diode array spectroscopy. Recently, a very high resolution spectrum (close to the Doppler limit of 0.07 cm^{-1}) of CH_2O was measured by Pope et al. [639, 640] in the range 308-320 nm using cavity ring-down spectroscopy (CRDS).

In general, the agreement between the medium and higher resolution data is good, whereby the data of Bass et al. [52] and Rogers [683] are consistently lower than the Meller and Moortgat [517] data. The contours of the spectral features measured by Bogumil et al. [82] obtained with the SCIAMACHY pre-flight satellite instrument, agree with the data of Meller and Moortgat [517]. Also, after convolution with lower-resolution instrument functions, the very high-resolution CH_2O spectrum measured by Pope et al. [639, 640] is in excellent agreement with the spectra obtained by Cantrell et al. [150] and Meller and Moortgat [517]. The low resolution absorption cross sections reported by Chen and Zhu [160, 161] and Chen et al. [162] for the 280-330-nm region at 5- and 10-nm intervals and measured for the calibration of photolysis measurements of some other carbonyl compounds deviate substantially up to 50% from those reported by Meller and Moortgat [517].

The high-resolution absorption cross sections obtained by Meller and Moortgat [517] are recommended for the wavelength range 225-375 nm of the absorption band. They are ~5-10% larger than the previously recommended cross sections of Cantrell et al. [150]. Cross sections averaged over 1-nm intervals are listed in Table 4-30, and over intervals used in atmospheric modeling in Table 4-31.

The temperature dependence of the absorption cross sections has been studied by Bass et al. [52], Moortgat et al. [555], Cantrell et al. [150], Meller and Moortgat [517], and Pope et al. [639, 640] (see above). Temperature effects are the strongest at the maximum of the absorption bands, where the lower temperatures result in larger absorptions. This effect is reversed in the wings of the absorption bands, where higher temperatures result in a higher absorption. A temperature sensitivity coefficient, Γ, allowing the calculation of the UV absorption spectrum at temperatures between 223 and 323 K and in the wavelength range 250-356 nm was derived by Meller and Moortgat [517]. Γ is defined by the equation

$$\sigma(\lambda, T) = \sigma(\lambda, 298\ K) + \Gamma(T - 298\ K)$$

Values of Γ averaged over 1-nm intervals and intervals used in atmospheric modeling are listed in Table 4-30 and Table 4-31, respectively.

VUV absorption cross sections for the wavelength region 60-185 nm have been obtained by Gentieu and Mentall [265], Mentall et al. [520], and Glicker and Stief [285] using optical methods and by Cooper et al. [180] for the region 6-261 nm using (e, e) dipole spectroscopy.

In earlier studies quantum yields have been measured by McQuigg et al. [512], Calvert et al. [133] who established a general trend of increasing radical yield with decreasing wavelength in the range 290-360 nm. More precise wavelength dependent quantum yield studies using monochromatic light sources were performed by Lewis et al. [443], Marling [488], Horowitz and Calvert [338], Clark et al. [173], Moortgat et al. [558] and Tang et al. [774] using radical scavengers. Moortgat and Warneck [560] and Moortgat et al. [555, 557] measured the yields of CO and H_2 from the photolysis of CH_2O in air (thus giving respectively $\varphi_1 + \varphi_2$ and φ_2) as a function of wavelength and pressure at 300 and 220 K. They showed that the yield of CO was essential unity for $290 < \lambda < 330$ nm at all pressures with no systematic temperature effect. For $\lambda > 330$ nm, both temperature and pressure have a significant effect on ϕ_2 but a negligible effect on ϕ_1. Also the total CO yield decreased at $\lambda < 290$ nm to 0.76 at 240 nm. An evaluation of the quantum yields was performed by Calvert et al. [132] based on the results of previous studies, similar to the JPL-recommendation given by DeMore et al. [213], but including algorithms for estimating the pressure and temperature dependence of ϕ_2.

Smith et al. [744] measured relative quantum yields for the production of radical products H and HCO (φ_1) using NO-chemical amplification and subsequent detection of NO_2 with chemical ionization mass spectrometry. These authors measured the quantum yields in the range 269 to 339 nm with sufficient resolution (0.62 nm, fwhm) to observe structure in the wavelength dependence, which previously had not been reported, and which is believed to provide evidence for a complicated competition among the various dissociation pathways 1, 2 and 3. The ϕ_1 yields, normalized to 0.753 at 303.75 nm based on the JPL-1997 recommendation [213], agreed qualitatively with the previous determinations reported by Horowitz and Calvert [338] and Moortgat et al. [557]. However at $\lambda > 320$ nm the reported ϕ_1 yields (measured at 50 mbar) by Smith et al. [744] are somewhat larger than the values recommended by DeMore et al. [213], resulting in a larger (~ 8%) overall rate of radical production. Pope et al. [639, 640] simultaneously measured HCO radical and CH_2O absorption cross sections using CRDS, from which HCO-quantum yields were calculated. This work showed that HCO yields in the region 308-319 nm vary with the vibrational level of the $\tilde{A}^1A_2$ state of CH_2O and with the pressure of the bath gas.

The recommended quantum yields for photolysis of CH_2O are listed in Table 4-32, and are based on a fitting of the data for channel 1 (H + HCO) involving the data of Lewis et al. [443], Marling [488], Horowitz and Calvert [338], Clark et al. [173], Tang et al. [774], Moortgat et al. [557] and Smith et al. [744]. The parameters of the fitting expression

$\phi_1(\lambda) = a_0 + a_1 \lambda + a_2 \lambda^2 + a_3 \lambda^3 + a_4 \lambda^4$ (valid for the wavelength range $250 > \lambda > 338$ nm)

are $a_o = 717.057373$ $a_1 = -9.4955377$ $a_2 = 0.04665398$ $a_3 = -1.0065325 \times 10^{-4}$ $a_4 = 8.03898 \times 10^{-8}$

$\phi_2(\lambda)$ was optimized using the quantum data for CO (giving $\phi_{tot} = \phi_1 + \phi_2$) from Moortgat et al. [557] and the relation $\phi_2 = \phi_{tot} - \phi_1$.

The pressure and temperature dependence of ϕ_2 is based on the algorithm cited in Calvert et al. [132] and limited for values $\lambda > 330$ nm. The pressure dependence of ϕ_2 is represented in Stern-Volmer form

$$\phi_2(\lambda, p, T) = [(1/(1 - \phi_1(\lambda)) + \alpha(\lambda,T) \times P]^{-1}$$

where $\alpha(\lambda,T)$ is the quenching coefficient at pressure P, whose values at 300 K can be estimated directly from ϕ_1 and ϕ_2 (see Table 4-32 for quantum yields at atmospheric pressure P_{atm} and 300 K)**:**

$$\alpha(\lambda, 300) = 1/P_{atm} \; [\, 1/\phi_2(\lambda, P_{atm}, 300) \; - \; 1/(1 - \phi_1(\lambda))]$$

At temperatures T between 220 and 300 K the quenching coefficient $\alpha(\lambda, T)$ can be interpolated from

$$\alpha(\lambda, T) = \alpha(\lambda, 300) \{ 1 + 0.05 (\lambda - 329) [(T - 80)/80] \}$$

Table 4-30. Absorption Cross Sections of CH_2O at 298 K and Temperature Coefficients Averaged over 1-nm Intervals

λ (nm)	10^{20} σ (cm^2)	10^{24} Γ ($cm^2 \cdot K^{-1}$)	λ (nm)	10^{20} σ (cm^2)	$10^{24} \cdot$Γ ($cm^2 \cdot K^{-1}$)	λ (nm)	10^{20} σ (cm^2)	$10^{24} \cdot$Γ ($cm^2 \cdot K^{-1}$)
226	0.0179		276	2.59	-2.040	326	6.87	-5.640
227	0.0169		277	1.57	1.933	327	4.37	5.440
228	0.0177		278	1.03	1.427	328	1.22	5.067
229	0.0190		279	2.45	-2.547	329	3.12	-3.347
230	0.0205		280	2.34	-0.680	330	3.86	-2.173
231	0.0330		281	1.56	0.560	331	1.41	3.907
232	0.0335		282	0.972	0.809	332	0.346	1.792
233	0.0262		283	0.720	0.005	333	0.214	0.429
234	0.0325		284	4.27	-8.720	334	0.159	-0.228
235	0.0363		285	4.05	-1.800	335	0.0966	-0.005
236	0.0539		286	2.09	1.587	336	0.126	0.325
237	0.0771		287	1.15	0.760	337	0.383	0.329
238	0.0569		288	3.17	-4.707	338	1.92	1.600
239	0.0682		289	3.22	-1.213	339	5.50	-6.587
240	0.0782		290	1.17	1.707	340	3.15	5.520
241	0.0775		291	1.84	-1.160	341	0.978	5.863
242	0.123		292	0.796	1.155	342	0.504	1.216
243	0.159		293	3.11	-4.907	343	1.92	-2.987
244	0.109		294	7.15	-10.213	344	1.27	0.187
245	0.131		295	4.06	3.827	345	0.436	2.765
246	0.163		296	2.48	2.120	346	0.119	0.541
247	0.151		297	1.36	1.387	347	0.0441	-0.281
248	0.234		298	4.22	-4.933	348	0.0757	-0.664
249	0.318		299	3.17	1.480	349	0.0378	-0.560
250	0.257	0.203	300	0.963	4.267	350	0.0360	-0.728
251	0.204	0.177	301	1.63	-2.573	351	0.0894	-0.121
252	0.337	-0.072	302	0.852	-2.325	352	0.731	0.368
253	0.289	0.101	303	3.02	-3.600	353	2.28	-5.320
254	0.342	0.137	304	7.23	-4.827	354	1.65	0.600
255	0.450	0.272	305	4.74	4.173	355	0.696	2.456
256	0.629	0.169	306	4.29	0.320	356	0.148	-0.388
257	0.443	0.880	307	1.78	3.187	357	0.0344	
258	0.307	0.681	308	1.38	0.333	358	0.0186	
259	0.618	0.084	309	3.26	-3.867	359	0.0111	
260	0.604	0.447	310	1.74	2.360	360	0.0087	
261	0.660	0.093	311	0.461	0.075	361	0.0100	
262	0.602	0.635	312	1.19	-1.227	362	0.0211	
263	1.08	-0.813	313	0.902	-1.439	363	0.0141	
264	0.947	0.580	314	5.65	0.720	364	0.0094	
265	0.530	1.004	315	5.56	2.587	365	0.0088	
266	0.538	0.431	316	2.54	4.760	366	0.0085	
267	1.36	-0.880	317	5.79	-2.467	367	0.0091	
268	1.24	-0.120	318	3.15	3.307	368	0.0143	
269	0.990	1.116	319	0.975	2.532	369	0.0297	
270	0.960	0.748	320	1.19	0.240	370	0.0636	
271	1.94	-1.307	321	1.60	-2.187	371	0.0572	
272	1.43	1.000	322	0.721	0.149	372	0.0197	
273	0.810	1.228	323	0.327	0.389	373	0.0113	
274	0.657	0.871	324	0.861	-0.456	374	0.0091	
275	2.15	-2.733	325	1.54	2.213	375	0.0087	

Note: Absorption cross sections σ: 226-375 nm, Meller and Moortgat [517].
Temperature coefficients Γ: 250-356 nm, Meller and Moortgat [517],
$\sigma(\lambda, T) = \sigma(\lambda, 298\ K) + \Gamma(T - 298\ K)$ for the temperature range 223 -323 K.

Table 4-31. Absorption Cross Sections of CH_2O at 298 K and Temperature Coefficients Averaged over Intervals Used in Atmospheric Modeling

λ (nm)	λ range (nm)	10^{20} σ (cm^2) T = 298 K	10^{20} σ (cm^2) T = 223 K	10^{24} Γ (cm^2 K^{-1})
226.0	224.7 – 227.3	0.0166		
228.6	227.3 – 229.9	0.0181		
231.2	229.9 – 232.6	0.0303		
233.9	232.6 - 235.3	0.0313		
236.7	235.3 – 238.1	0.0625		
239.5	238.2 – 241.0	0.0704		
242.4	241.0 – 243.9	0.126		
245.4	243.9 – 246.9	0.139		
248.5	246.9 – 250.0	0.254		
251.6	250.0 – 253.2	0.270	0.2650	0.720
254.8	253.2 – 256.4	0.449	0.4350	1.77
258.1	256.4 – 259.7	0.478	0.4380	5.35
261.4	259.7 – 263.2	0.698	0.6870	1.45
264.9	263.2 – 266.7	0.736	0.6980	5.00
268.5	266.7 – 270.3	1.13	1.1100	2.80
272.1	270.3 – 274.0	1.30	1.2700	3.87
275.9	274.0 – 277.8	1.84	1.8900	-5.73
279.7	277.8 – 281.7	1.86	1.8900	-3.60
283.7	281.7 – 285.7	2.55	2.7200	-22.3
287.7	285.7 – 289.9	2.33	2.3800	-7.47
292.0	289.9 – 294.1	2.66	2.9300	-34.9
296.3	294.1 – 298.5	3.28	3.2300	5.73
300.8	298.5 – 303.0	1.60	1.5800	2.80
305.4	303.0 – 307.7	4.42	4.4300	-1.73
310.1	307.7 – 312.5	1.63	1.6700	-5.47
315	312.5 – 317.5	4.09	4.0300	8.40
320	317.5 – 322.5	1.53	1.4700	8.13
325	322.5 – 327.5	2.79	2.7600	3.87
330	327.5 – 332.5	1.99	1.9100	10.5
335	332.5 – 337.5	0.196	0.1830	1.71
340	337.5 – 342.5	2.390	2.2800	15.2
345	342.5 – 347.5	0.758	0.7550	0.480
350	347.5 – 352.5	0.194	0.2200	-3.40
355	352.5 – 357.5	0.961		
360	357.5 – 362.5	0.0139		
365	362.5 – 367.5	0.0010		
370	367.5 – 372.5	0.0369		

Note:
Absorption cross sections σ: 224.7-372.5 nm, Meller and Moortgat [517].
Temperature coefficients Γ: Meller and Moortgat [517]
$\sigma(\lambda, T) = \sigma(\lambda, 298\ K) + \Gamma(T - 298\ K)$ for the temperature range 223 -323 K

Table 4-32. Quantum Yields for Photolysis of CH_2O at 296-300 K

λ (nm)	Φ_1	Φ_2	λ (nm)	Φ_1	Φ_2	λ (nm)	Φ_1	Φ_2
250	0.317	0.483	288	0.669	0.291	326	0.463	0.537
251	0.311	0.489	289	0.680	0.284	327	0.435	0.565
252	0.307	0.493	290	0.690	0.278	328	0.406	0.594
253	0.304	0.496	291	0.700	0.272	329	0.375	0.625
254	0.303	0.497	292	0.710	0.266	330	0.343	0.657
255	0.303	0.497	293	0.718	0.262	331	0.310	0.690
256	0.305	0.495	294	0.726	0.259	332	0.276	0.714
257	0.307	0.493	295	0.734	0.256	333	0.240	0.740
258	0.311	0.489	296	0.740	0.255	334	0.203	0.737
259	0.316	0.484	297	0.746	0.254	335	0.165	0.735
260	0.322	0.478	298	0.751	0.249	336	0.126	0.724
261	0.329	0.471	299	0.755	0.245	337	0.085	0.695
262	0.337	0.468	300	0.758	0.242	338	0.043	0.687
263	0.346	0.464	301	0.761	0.239	339	0.0	0.665
264	0.355	0.460	302	0.762	0.238	340		0.650
265	0.366	0.454	303	0.762	0.238	341		0.620
266	0.377	0.448	304	0.762	0.238	342		0.590
267	0.388	0.442	305	0.760	0.240	343		0.560
268	0.400	0.435	306	0.758	0.242	344		0.530
269	0.413	0.427	307	0.754	0.246	345		0.500
270	0.425	0.420	308	0.749	0.251	346		0.480
271	0.439	0.411	309	0.744	0.256	347		0.450
272	0.452	0.403	310	0.737	0.263	348		0.430
273	0.466	0.394	311	0.729	0.271	349		0.400
274	0.480	0.385	312	0.720	0.280	350		0.380
275	0.494	0.376	313	0.709	0.291	351		0.350
276	0.508	0.367	314	0.698	0.302	352		0.320
277	0.623	0.357	315	0.685	0.315	353		0.280
278	0.537	0.358	316	0.671	0.329	354		0.250
279	0.551	0.349	317	0.656	0.344	355		0.220
280	0.565	0.342	318	0.639	0.361	356		0.180
281	0.579	0.334	319	0.622	0.378	357		0.160
282	0.593	0.327	320	0.603	0.397	358		0.130
283	0.607	0.320	321	0.583	0.417	359		0.009
284	0.620	0.313	322	0.561	0.439	360		0.004
285	0.633	0.307	323	0.539	0.461	361		0.0
286	0.645	0.302	324	0.515	0.485			
287	0.657	0.296	325	0.489	0.511			

Note:
The recommended quantum yields for photolysis of CH_2O are based on a fitting of the data for channel 1 (H + HCO) involving the data of Lewis et al. [443], Marling [488], Horowitz and Calvert [338], Clark et al. [173], Tang et al. [774], Moortgat et al. [557] and Smith et al. [744], and the data for channel 2 (H_2 + CO) from Moortgat et al. [557]; see also text.

D2. $CH_3CHO + h\nu \rightarrow CH_3 + HCO$ ϕ_1
$CH_3CHO + h\nu \rightarrow CH_4 + CO$ ϕ_2
$CH_3CHO + h\nu \rightarrow CH_3CO + H$ ϕ_3. The absorption spectrum of acetaldehyde has been measured at room temperature and 200-345 nm by McMillan [140]; at 221-345 nm by Meyrahn et al. [525]; at 197-362 nm by Schneider and Moortgat [687]; at 235-360 nm by Libuda et al. [445, 447]; at 202-365 nm by Martinez et al. [492]; and at 240-350 nm by Limão-Vieira et al. [453]. Absorption cross-sections at 5 nm wavelength intervals in the range 290-355 nm were reported by Weaver et al. [842]. The UV spectrum shows an absorption band between 200 and 350 nm with resolved vibrational structure (~12 maxima or shoulders) above 260 nm. The agreement between the various results is very good, mostly 5% and better, except for the results of Meyrahn et al. [525], which are appreciably lower (10%) in the structured features around the absorption maximum. Our recommendation is based on the data of Libuda et al. [445, 447] (1-nm averages of 0.6 nm-resolution data) and Martinez et al. [492] (4-nm averages of 0.5 nm-resolution data at 202-278 nm and 1-nm averages at 280-360 nm), for which the agreement is within 5% between 255 and 325 nm. The preferred values in Table 4-33 are the results of Martinez et al. [492] for the region 202-238 nm and the mean of the results of Martinez et al. [492] and Libuda et al. [445, 447] for the region 280-360 nm.

Measurements in the VUV were carried out at 150-180 nm by Lake and Harrison [429]; at 118-189 nm by Lucazeau and Sandorfy [462]; at 120-180 nm by Brint et al. [91]; and at 113-200 nm by Limão-Vieira et al. [453].

Quantum yield measurements have been reported by Calvert and Pitts [138], and Weaver et al. [842] at isolated wavelengths. Quantum yields of CO, CH_4 and CO_2 were determined in the photolysis of trace concentrations of CH_3CHO in air and N_2 in the spectral range 247-327 nm at 1 atmospheric pressure by Meyrahn et al. [525], which allowed the determination of ($\varphi_1 + \varphi_2$), φ_2, and φ_3, respectively. Product pressure-dependence was also investigated by Meyrahn [524] at 270, 303.4 and 313 nm. Horowitz et al. [340] and Horowitz and Calvert [339] measured the quantum yields of formation CO, CH_4 and H_2 at 290, 300, 313, 320 and 332 nm in the photolysis of CH_3CHO at various added pressures O_2, CO_2, from which φ_1 and φ_2 were derived. There seems to be evidence by Meyrahn et al. [524, 525] and Horowitz et al. [340] that some CO_2 is formed from secondary reactions of the CH_3CO radical, produced in channel (3). The quantum yield φ_3 was estimated as 0.025 at 300 nm, decreasing to zero at 320 nm. Both Meyrahn et al. [524, 525] and Horowitz et al. [339, 340] observed a pressure dependence of the products, from which Stern-Vollmer quenching coefficients were derived. These data were summarized by Calvert et al. [132] based on the results of previous studies.

Quantum yield recommendations are shown in Table 4-34 for atmospheric pressure, and are based on the evaluation by Atkinson and Lloyd [32] and on the measurements by Horowitz and Calvert [339], Meyrahn et al. [525] and Meyrahn [524]. A similar evaluation was performed by Calvert et al. [132].

Table 4-33. Absorption Cross Sections of CH_3CHO at 298-300 K

λ (nm)	10^{20} σ (cm^2)	λ (nm)	10^{20} σ (cm^2)	λ (nm)	10^{20} σ (cm^2)	λ (nm)	10^{20} σ (cm^2)
202	0.056	286	4.41	312	2.52	338	0.212
206	0.053	287	4.56	313	2.47	339	0.206
210	0.049	288	4.69	314	2.38	340	0.135
214	0.048	289	4.74	315	2.20	341	0.0664
218	0.052	290	4.86	316	2.07	342	0.0416
222	0.065	291	4.75	317	2.08	343	0.0305
226	0.096	292	4.66	318	1.98	344	0.0267
230	0.151	293	4.51	319	1.84	345	0.0210
234	0.241	294	4.31	320	1.70	346	0.0199
238	0.375	295	4.26	321	1.48	347	0.0149
242	0.639	296	4.24	322	1.38	348	0.0159
246	0.887	297	4.37	323	1.23	349	0.0664
250	1.18	298	4.41	324	1.06	350	0.00774
254	1.57	299	4.26	325	1.15	351	0.00695
258	2.03	300	4.15	326	1.09	352	0.00497
262	2.45	301	3.97	327	0.808	353	0.00552
266	3.06	302	3.87	328	0.715	354	0.00436
270	3.38	303	3.70	329	0.741	355	0.00500
274	4.03	304	3.46	330	0.699	356	0.00518
278	4.15	305	3.43	331	0.560	357	0.00345
280	4.48	306	3.41	332	0.496	358	0.00428
281	4.65	307	3.36	333	0.420	359	0.00207
282	4.66	308	3.31	334	0.333	360	0.00275
283	4.70	309	3.11	335	0.350		
284	4.58	310	2.92	336	0.227		
285	4.46	311	2.73	337	0.219		

Note:
202-238 nm, Martinez et al. [492],
240-360 nm, mean of Martinez et al. [492] and Libuda et al. [445, 447].

Table 4-34. Recommended Quantum Yields for the Photolysis of CH_3CHO at 1 bar Total Pressure

λ (nm)	Φ_1	Φ_2	λ (nm)	Φ_1
256	0.29	0.48	296	0.47
258	0.30	0.47	298	0.45
260	0.31	0.45	300	0.43
262	0.32	0.43	302	0.40
264	0.34	0.40	304	0.38
266	0.36	0.37	306	0.35
268	0.38	0.33	308	0.31
270	0.41	0.29	310	0.28
272	0.44	0.25	312	0.24
274	0.48	0.20	314	0.19
276	0.53	0.16	316	0.15
278	0.56	0.09	318	0.12
280	0.58	0.06	320	0.10
282	0.59	0.04	322	0.07
284	0.59	0.03	324	0.05
286	0.58	0.02	326	0.03
288	0.56	0.01	328	0.02
290	0.54	0.01	330	0.01
292	0.52	0.005	332	0
294	0.50	0		

D3. $C_2H_5CHO + h\nu \rightarrow C_2H_5 + CHO$ ϕ_1
$C_2H_5CHO + h\nu \rightarrow C_2H_6 + CO$ ϕ_2
$C_2H_5CHO + h\nu \rightarrow C_2H_4 + HCHO$ ϕ_3
$C_2H_5CHO + h\nu \rightarrow CH_3 + CH_2CHO$ ϕ_4. The absorption spectrum of propionaldehyde has been measured and room temperature at 118-190 nm by Lucazeau and Sandorfy [462], at 220-342 nm by McMillan [145], and at 262-365 nm by Martinez et al. [492]. The spectrum shows an absorption band between 200 and 360 nm with structured features (~9 maxima or shoulders) above 260 nm. Absorption cross sections have also been measured at isolated wavelengths by Blacet and Crane [76] in the range 187-313 nm, by Heicklen et al. [325] in the range 293-325 nm, and by Chen and Zhu [160] in the range 280-330 nm. The agreement between the results of the data Martinez et al. [492] and McMillan [140] is excellent, i.e., ≤ 5%, between 238 and 322 nm; at smaller wavelengths the differences increase to ~30%, at larger wavelengths up to nearly 50%. Three of the four data points reported by Heicklen et al. [325] fit well to the just mentioned absorption curves, the value reported for 293 nm however is lower by 20%. The cross sections measured at 5-nm intervals by Chen and Zhu [160] agree to within 10% with those reported by Martinez et al. [492], except the data at 285 and 330 nm which are 20% and 30% larger. The recommended absorption cross sections listed in Table 4-35 are those of Martinez et al. [492], which are the 4-nm averages of the 0.5 nm-resolution data at 202-278 nm and 1-nm averages at 280-360 nm.

Quantum yield measurements have been performed by Heicklen et al. [325] and recently by Chen and Zhu [160]. Heicklen et al. [325] investigated the laser photolysis at 298 K (at 294, 302, 312 and 325 nm) and the steady state photolysis at 263 and 298 K (at 254, 312 and 334 nm) of C_2H_5CHO in the presence of O_2. They measured the quantum yield of the HO_2 and $C_2H_5O_2$ radicals by UV absorption, yielding φ_1. From the determination of the products yields CO and C_2H_6, they derived $\varphi_1 = \varphi(CO) - \varphi(C_2H_6)$ and $\varphi_2 = \varphi(C_2H_6)$. A Stern-Volmer type pressure dependence of the quantum yields was observed at all wavelengths, giving lower quantum yields at higher pressures. At atmospheric pressure $\varphi_1 = 0.22$, 0.89, 0.85, 0.50, 0.26 and 0.15 were derived at 254, 294, 302, 313, 325 and 334 nm, respectively; at 254 nm Heicklen et al. [325] reported $\varphi_2 = 0.33$, but $\varphi_2 = 0$ at other larger wavelengths. The contribution of other primary processes (φ_3 and φ_4) was found to increase at $\lambda < 265$ nm from earlier studies cited in Calvert and Pitts [143].

Chen and Zhu [160] measured the yield of HCO radicals ($= \varphi_1$) in the wavelength range 280-330 nm using time-resolved cavity ring-down spectroscopy at 613.8 nm. The HCO yields were 0.85 ± 0.06 at 280 nm, 1.01 ± 0.07 at 285 nm, 0.95 ± 0.06 at 290 nm, 0.98 ± 0.06 at 295 nm, 0.92 ± 0.06 at 300 nm, 0.95 ± 0.08 at 305 nm, 0.98 ± 0.11 at 310 nm, 0.91 ± 0.05 at 315 nm, 1.08 ± 0.07 at 320 nm, 1.07 ± 0.14 at 325 nm, and 0.84 ± 0.08 at 330 nm. These values are quoted for zero-pressure, but the authors did not observe any pressure dependence upon addition of 400 Torr N_2.

Both quantum yield studies by Heicklen et al. [325] and Chen and Zhu [160] are only in agreement in the narrow wavelength range 290-305 nm. At $\lambda > 305$ nm, the data of Chen and Zhu do not show the decrease of φ_1 observed by Heicklen et al [325]. Because of the divergence of both data sets, no recommendation can be given.

Table 4-35. Absorption Cross Sections C_2H_5CHO at 298-300 K

λ (nm)	10^{20} σ (cm^2)	λ (nm)	10^{20} σ (cm^2)	λ (nm)	10^{20} σ (cm^2)	λ (nm)	10^{20} σ (cm^2)
202	0.049	285	5.86	310	3.60	335	0.325
206	0.049	286	5.82	311	3.53	336	0.280
210	0.057	287	5.72	312	3.50	337	0.230
214	0.069	288	5.59	313	3.32	338	0.185
218	0.080	289	5.52	314	3.06	339	0.166
222	0.091	290	5.56	315	2.77	340	0.155
226	0.115	291	5.68	316	2.43	341	0.119
230	0.163	292	5.81	317	2.18	342	0.076
234	0.257	293	5.88	318	2.00	343	0.045
238	0.407	294	5.80	319	1.86	344	0.031
242	0.622	295	5.57	320	1.83	345	0.025
246	0.909	296	5.37	321	1.78	346	0.019
250	1.29	297	5.16	322	1.66	347	0.016
254	1.75	298	5.02	323	1.58	348	0.014
258	2.25	299	5.02	324	1.49	349	0.013
262	2.88	300	5.04	325	1.30	350	0.010
266	3.43	301	5.09	326	1.13	351	0.008
270	4.12	302	5.07	327	0.996	352	0.007
274	4.59	303	4.94	328	0.828	353	0.005
278	5.17	304	4.69	329	0.685	354	0.004
280	5.16	305	4.32	330	0.575	355	0.002
281	5.21	306	4.04	331	0.494	356	0.001
282	5.35	307	3.81	332	0.466	357	0.001
283	5.57	308	3.65	333	0.430		
284	5.78	309	3.62	334	0.373		

Note:
202-357 nm, Martinez et al. [492].

D4. $CH_3O_2 + h\nu \rightarrow$ Products. The absorption cross sections of the methylperoxy radical, CH_3O_2, in the 195–310-nm region have been measured at room temperature by Parkes et al. [624], Hochanadel et al. [335], Parkes [623], Anastasi et al. [18], Kan et al. [402], Cox and Tyndall [193, 194] at 250 nm only; Adachi et al. [7], Sander and Watson [705] at 250 nm only; Pilling and Smith [635] at 254 nm only, Kurylo et al. [424], McAdam et al. [505], Jenkin et al. [374], Wallington et al. [831], Moortgat et al. [559], Dagaut and Kurylo [200], Simon et al. [731], Jenkin and Cox [373], Lightfoot and Jemi-Alade [450] who measured the cross sections up to 777 K., Maricq and Wallington [485], Wallington et al. [833], Roehl et al. [677], and Fahr et al. [233]. The absorption cross sections have been evaluated in earlier reviews by Lightfoot et al. [449] and Wallington et al. [832], who noted significant discrepancies in the both the shapes of the spectra and the absolute magnitude of the cross section values. The ultraviolet absorption spectra have recently been reevaluated by Tyndall et al. [790], who fitted the absorption spectra to a semilogarithmic Gaussian distribution function suggested by Lightfoot et al. [449] and Maric et al. [479] using:

$$\sigma = \sigma_{max} \exp^{-a\left[\ln\left(\frac{\lambda_{max}}{\lambda}\right)\right]^2}$$

Screening of the data suggested that most spectra published before 1987 did not constrain the shape of the spectrum very well as indicated by the large relative uncertainty of the width parameter a. The shape was determined by averaging the individual fitting parameters from McAdam et al. [505], Moortgat et al. [559], Simon et al. [731], Lightfoot and Jemi-Alade [450], Jenkin and Cox [373] and Maricq and Wallington [485], which were judged to be most reliable by Tyndall et al. [790]. Absolute cross sections were based on relative measurements of absorption cross sections of CH_3O_2 and $C_2H_5O_2$ at 240 nm taken under identical conditions (Wallington et al. [832], Maricq and Wallington [485], Fenter et al. [242] and Roehl et al. [677]), combined with independent calibrations by Dagaut and Kurylo [200], Simon et al. [731] and Lightfoot and Jemi-Alade

[450]. The fitting parameters are: $\sigma_{max} = 4.26 \times 10^{-18}$ cm^2 molecule^{-1}; a = 44.4; λ_{max} = 237.3 nm. Table 4-36 lists the recommended cross sections, which are taken from the review by Tyndall et al. [790].

Photolysis of CH_3O_2 in the stratosphere and troposphere is slow and can be neglected, but the UV absorption cross sections are important in laboratory studies of reaction kinetics.

Table 4-36. Absorption Cross Sections of CH_3O_2, $C_2H_5O_2$, and $CH_3C(O)O_2$

λ (nm)	10^{20} σ (cm^2)		
	CH_3O_2	$C_2H_5O_2$	$CH_3C(O)O_2$
195.0			389
200.0			564
205.0	165		665
210.0	219	195	656
215.0	276	257	564
220.0	330	319	451
225.0	376	374	366
230.0	408	418	326
235.0	424	444	319
240.0	424	452	326
245.0	407	440	330
250.0	378	412	322
255.0	339	372	300
260.0	294	324	268
265.0	248	273	229
270.0	203	222	187
275.0	162	176	147
280.0	126	136	111
285.0	96.1	102	81.2
290.0	71.5	74.6	57.3
295.0	52.0	53.3	
300.0		37.3	

D5. $C_2H_5O_2 + h\nu \rightarrow$ Products. The absorption cross sections of the ethylperoxy radical, $C_2H_5O_2$, in the 200–310-nm region have been measured at room temperature by Adachi et al. [6], Anastasi et al. [19], Cattell et al. [155], Wallington et al. [832], Bauer et al. [56], Maricq and Wallington [485], Fenter et al. [242], and Munk et al. [566]. The absorption cross sections have been evaluated in earlier reviews by Lightfoot et al. [449] and Wallington et al. [832], who noted significant discrepancies in the both the shapes of the spectra and the absolute magnitude of the cross section values. The ultraviolet absorption spectra have recently been reevaluated by Tyndall et al. [790], who fitted the absorption spectra to a semilogarithmic Gaussian distribution function suggested by Lightfoot et al. [449] and Maric et al. [479] using:

$$\sigma = \sigma_{max} \exp^{-a\left[\ln\left(\frac{\lambda_{max}}{\lambda}\right)\right]^2}$$

The shape was determined by averaging the individual fitting parameters from Wallington et al. [832], Bauer et al. [56], Maricq and Wallington [485] and Fenter et al. [242], which were judged to be most reliable by Tyndall et al. [790]. Absolute cross sections were based on relative measurements of absorption cross sections of CH_3O_2 and $C_2H_5O_2$ at 240 nm taken under identical conditions (Wallington et al. [832], Maricq and Wallington [485], Fenter et al. [242] and Roehl et al. [677]), combined with independent calibrations. The fitting parameters are $\sigma_{max} = 4.52 \times 10^{-18}$ cm^2 molecule^{-1}; a = 49.0; λ_{max} = 239.4 nm. Table 4-36 lists the recommended cross sections, which are taken from the review by Tyndall et al. [790].

Photolysis of $C_2H_5O_2$ in the stratosphere and troposphere is slow and can be neglected, but the UV absorption cross sections are important in laboratory studies of reaction kinetics.

D6. $CH_3C(O)O_2 + h\nu \rightarrow$ Products. The UV absorption spectrum of the acetylperoxy radical, $CH_3C(O)O_2$, exhibits two absorption maxima in the 185–285 nm region: a strong band near 207 nm, and a feature at 245 nm that is weaker by a factor of 2. The absorption cross sections have been measured at room temperature by Addison et al. [8], Basco and Parmer [50], Moortgat et al. [559], Maricq and Szente [484], and Roehl et al. [677]. The absorption cross sections have been evaluated in earlier reviews by Lightfoot et al. [449] and Wallington et al. [832], who noted significant discrepancies in the both the shapes of the spectra and the absolute magnitude of the cross section values. The ultraviolet absorption spectra have recently been

reevaluated by Tyndall et al. [790], who fitted the absorption spectra to the sum of two Gaussian-shaped absorption bands:

$$\sigma = \sigma_{max1} \exp^{-a_1\left[\ln\left(\frac{\lambda_{max1}}{\lambda}\right)\right]^2} + \sigma_{max2} \exp^{-a_2\left[\ln\left(\frac{\lambda_{max2}}{\lambda}\right)\right]^2}$$

The shape was determined by averaging the individual fitting parameters from Maricq and Szente [484] and Roehl et al. [677], which were judged to be the most reliable to date; the data by Maricq and Szente [484] were adjusted for their overcorrection for the contribution of CH_3O_2. Absolute cross sections were based on relative measurements of absorption cross sections of $C_2H_5O_2$ at 240 nm taken under identical conditions. The fitting parameters are
$\sigma_{max1} = 6.29 \times 10^{-18}$ cm^2 molecule^{-1}; $\lambda_{max1} = 206.0$ nm; $a_1 = 168.0$; $\sigma_{max2} = 3.26 \times 10^{-18}$ cm^2 molecule^{-1}; $\lambda_{max2} = 246.1$ nm; $a_2 = 64.2$. Table 4-36 lists the recommended cross sections, which are taken from the review by Tyndall et al. [790]

Photolysis of $CH_3C(O)O_2$ in the stratosphere and troposphere is slow and can be neglected, but the UV absorption cross sections are important in laboratory studies of reaction kinetics.

D7. $CH_3OOH + h\nu \rightarrow CH_3O + OH$. Vaghjiani and Ravishankara [799] measured the cross sections of CH_3OOH by monitoring the CH_3OOH concentration via trapping and titration. These results are recommended and are listed in Table 4-37. The earlier results of Molina and Arguello [547] are consistently 40% higher than the values shown in Table 4-37; this difference is believed to be due to difficulty in trapping CH_3OOH and measuring its concentration. CH_3OOH dissociates upon light absorption to give CH_3O with unit quantum yield (Vaghjiani and Ravishankara, [800]); these authors also observed some production of H and O atoms at shorter wavelengths (i.e., 193 nm). Thelen et al. [777] report unit quantum yield for OH production at 248 and 193 nm, in agreement with the results of Vaghjiani and Ravishankara [799].

Table 4-37. Absorption Cross Sections of CH_3OOH

λ (nm)	10^{20} σ (cm^2)	λ (nm)	10^{20} σ (cm^2)
210	31.2	290	0.691
215	20.9	295	0.551
220	15.4	300	0.413
225	12.2	305	0.313
230	9.62	310	0.239
235	7.61	315	0.182
240	6.05	320	0.137
245	4.88	325	0.105
250	3.98	330	0.079
255	3.23	335	0.061
260	2.56	340	0.047
265	2.11	345	0.035
270	1.70	350	0.027
275	1.39	355	0.021
280	1.09	360	0.016
285	0.863	365	0.012

D8. $HOCH_2OOH + h\nu \rightarrow HOCH_2O + OH$. The UV absorption spectrum of hydroxymethyl hydroperoxide, $HOCH_2OOH$, was measured at 298 K by Bauerle and Moortgat [59] in the range 205 to 360 nm. The cross sections are listed in Table 4-38. This photolysis is assumed to occur with unity quantum yield at wavelengths larger than 290 nm, in analogy with CH_3OOH.

Table 4-38. Absorption Cross Sections of $HOCH_2OOH$

λ (nm)	10^{20} σ (cm^2)	λ (nm)	10^{20} σ (cm^2)
205	26.9	285	0.75
210	22.6	290	0.63
215	18.7	295	0.51
220	15.5	300	0.40
225	12.5	305	0.29
230	10.1	310	0.22
235	7.89	315	0.18
240	5.98	320	0.13
245	4.68	325	0.10
250	3.78	330	0.073
255	2.88	335	0.059
260	2.31	340	0.045
265	1.81	345	0.036
270	1.48	350	0.028
275	1.21	355	0.022
280	0.93	360	0.017

D9. $CH_3C(O)O_2NO_2 + h\nu \rightarrow CH_3C(O)O_2 + NO_2$ φ_1

$CH_3C(O)O_2NO_2 + h\nu \rightarrow CH_3C(O)O + NO_3$ φ_2. The absorption cross sections of $CH_3C(O)O_2NO_2$ (peroxyacetyl nitrate, PAN) have been measured at room temperature and 220-450 nm by Stephens [752]; at 200-300 nm by Senum et al. [726]; at 210-250 nm by Basco and Parmar [51]; at 219-325 nm by Libuda and Zabel [446]; and at 250, 273, and 298 K and 196-350 nm by Talukdar et al. [766]. The five studies are in reasonable to good agreement over their range of overlap. The data of Talukdar et al. [766] and Libuda and Zabel [446] agree within 10% below 300 nm. The data of Stephens [752] are somewhat higher (up to 20%), those of Basco and Parmar [51] higher by up to about 45%, and those of Senum et al. [726] are smaller (within 20% and more beyond 280 nm) than the data of Talukdar et al. [766]. Libuda and Zabel [446] carried out simultaneous IR studies that showed that the measured cross sections need to be corrected for impurities that are transparent in the UV but contribute to the sample pressure in the absorption cell. These corrections are on the order of 20%. The recommended absorption cross section listed in Table 4-39 are those of Talukdar et al. [766] because of the good agreement with Libuda and Zabel [446] and the wider spectral coverage and temperature range of their study. The uncertainties in the reported cross sections are probably quite large (on the order of a factor of 2), decreasing to about 30% at shorter wavelengths.

A wavelength-dependent systematic decrease of the absorption cross sections with decreasing temperature was observed by Talukdar et al. [766]. The temperature dependence was parameterized to the expression

$$\ln \sigma(\lambda, T) = \ln \sigma(\lambda, 298K) + B(\lambda)(T-298)$$

to derive the temperature coefficients B(λ) which are also listed in Table 4-39.

Quantum yields for the production of NO_2 and NO_3 in the photolysis at 248 nm were reported by Mazely et al. [503, 504]: $\varphi(NO_2, 248\ nm) = 0.83 \pm 0.09$ and $\varphi(NO_3, 248\ nm) = 0.3 \pm 0.1$. The NO_3 quantum yield was obtained relative to the unity NO_3 quantum yield in the photolysis of N_2O_5 at 248 nm. However, this latter quantum yield was remeasured to be 0.8 ± 0.1 by Harwood et al. [313], so that the $\varphi(NO_3, 248\ nm)$ should be rescaled to 0.24. Quantum yields for the production of NO_3 in the photolysis of $CH_3C(O)O_2NO_2$ at 248 and 308 nm were recently measured by Harwood et al. [317]: $\varphi(NO_3, 248\ nm) = 0.19 \pm 0.04$ and $\varphi(NO_3, 308\ nm) = 0.41 \pm 0.10$. Assuming that only both product channels are produced and $\varphi_1 + \varphi_2 = 1$, it can be recommended that $\varphi_1 = 0.6$ and $\varphi_2 = 0.4$ at $\lambda > 300$ nm.

Table 4-39. Absorption Cross Sections of $CH_3C(O)O_2NO_2$ at 298 K, Temperature Coefficients B

λ (nm)	10^{20} σ (cm^2)	10^3 B (K^{-1})	λ (nm)	10^{20} σ (cm^2)	10^3 B (K^{-1})	λ (nm)	10^{20} σ (cm^2)	10^3 B (K^{-1})
196	429	2.02	248	14.6	3.64	300	0.189	8.44
198	398	1.73	250	12.9	3.76	302	0.152	8.61
200	361	1.36	252	11.4	3.87	304	0.125	8.76
202	325	1.07	254	10.0	3.98	306	0.0998	8.87
204	292	0.86	256	8.86	4.10	308	0.0816	9.01
206	261	0.75	258	7.80	4.23	310	0.0666	9.13
208	226	0.71	260	6.85	4.38	312	0.0538	9.30
210	196	0.75	262	6.01	4.53	314	0.0462	9.46
212	168	0.84	264	5.23	4.68	316	0.0363	9.57
214	143	0.97	266	4.54	4.82	318	0.0300	9.75
216	122	1.12	268	3.94	4.97	320	0.0252	10.0
218	104	1.29	270	3.37	5.14	322	0.0199	10.2
220	89.7	1.47	272	2.87	5.34	324	0.0166	10.4
222	77.7	1.64	274	2.45	5.55	326	0.0140	10.6
224	67.6	1.81	276	2.07	5.76	328	0.0117	10.7
226	59.3	1.98	278	1.74	5.98	330	0.0106	10.9
228	52.0	2.14	280	1.46	6.20	332	0.00857	11.2
230	45.8	2.30	282	1.21	6.43	334	0.00676	11.5
232	40.4	2.46	284	1.01	6.67	336	0.00615	11.7
234	35.5	2.63	286	0.810	6.90	338	0.00526	11.9
236	31.4	2.80	288	0.648	7.15	340	0.00502	12.2
238	27.9	2.96	290	0.537	7.39	342	0.00360	12.4
240	24.4	3.11	292	0.447	7.63	344	0.00241	12.5
242	21.5	3.25	294	0.369	7.86	346	0.00231	
244	18.8	3.39	296	0.297	8.08	348	0.00247	
246	16.6	3.52	298	0.245	8.27	350	0.00165	

Note:
Absorption cross sections σ: 196-350 nm, Talukdar et al. [766].
Temperature coefficients B: 250-298 K, Talukdar et al. [766] ($\ln \sigma(\lambda, T) = \ln \sigma(\lambda, 298\ K) + B(T-298)$).

D10. $C_2H_5C(O)O_2NO_2 + h\nu \rightarrow C_2H_5C(O)O_2 + NO_2$ φ_1
$C_2H_5C(O)O_2NO_2 + h\nu \rightarrow C_2H_5C(O)O + NO_3$ φ_2. The absorption cross sections of $C_2H_5C(O)O_2NO_2$ (peroxypropionyl nitrate, PPN) have been measured at room temperature and 200-300 nm by Senum et al. [726] and at 253, 273, and 296 K and 210-340 nm by Harwood et al. [317]. The absorption spectrum shows an exponential decrease of the cross sections with increasing wavelength. The absorption cross sections reported by Harwood et al. [317] are larger than those reported by Senum et al. [726] over the common wavelength range, larger by ~10% at 210 nm up to ~30% at 300 nm. A wavelength-dependent systematic decrease of the absorption cross sections with decreasing temperature was observed by Harwood et al. [317]. The temperature dependence was parameterized to the expression $\ln \sigma(\lambda, T) = \ln \sigma(\lambda, 296\ K) + B(\lambda)(T-296)$ to derive the temperature coefficients B(λ). We recommend the results of Harwood et al. [317], which are listed in Table 4-40.

Quantum yields for the production of NO_3 in the photolysis of $C_2H_5C(O)O_2NO_2$ at 248 and 308 nm were measured also by Harwood et al. [317]: $\varphi_2(248\ nm) = 0.22 \pm 0.04$ and $\varphi_2(308\ nm) = 0.39 \pm 0.04$.

Table 4-40. Absorption Cross Sections of $C_2H_5C(O)O_2NO_2$ at 296 K and Temperature Coefficients B

λ (nm)	10^{20} σ (cm^2)	10^3 B (K^{-1})	λ (nm)	10^{20} σ (cm^2)	10^3 B (K^{-1})	λ (nm)	10^{20} σ (cm^2)	10^3 B (K^{-1})
210	174	1.22	254	9.27	3.25	298	0.325	10.3
212	154	1.20	256	8.23	3.47	300	0.273	10.8
214	135	1.19	258	7.28	3.69	302	0.228	11.2
216	115	1.20	260	6.44	3.92	304	0.192	11.7
218	99.9	1.21	262	5.66	4.17	306	0.162	12.2
220	86.1	1.24	264	4.96	4.42	308	0.136	12.6
222	74.7	1.27	266	4.35	4.69	310	0.114	13.2
224	64.8	1.32	268	3.80	4.96	312	0.0962	13.6
226	56.9	1.37	270	3.31	5.25	314	0.0835	14.2
228	49.6	1.44	272	2.87	5.54	316	0.0689	14.7
230	43.6	1.52	274	2.48	5.85	318	0.0571	15.2
232	38.3	1.60	276	2.14	6.17	320	0.0491	15.8
234	33.6	1.70	278	1.84	6.49	322	0.0443	16.3
236	29.5	1.81	280	1.57	6.83	324	0.0354	16.9
238	25.8	1.93	282	1.33	7.18	326	0.0282	17.5
2400	22.6	2.06	284	1.12	7.54	328	0.0242	18.1
242	19.8	2.20	286	0.940	7.91	330	0.0206	18.7
244	17.4	2.35	288	0.790	8.29	332	0.0174	19.3
246	15.3	2.51	290	0.662	8.68	334	0.0146	19.9
248	13.5	2.68	292	0.551	9.08	336	0.0107	20.5
250	11.9	2.86	294	0.462	9.49	338	0.0090	21.2
252	10.5	3.05	296	0.389	9.91	340	0.0066	21.8

Note:
Absorption cross sections σ: 210-340 nm, Harwood et al. [317].
Temperature coefficients B: 253-296 K, Harwood et al. [317] ($\ln \sigma(\lambda, T) = \ln \sigma(\lambda, 298\ K) + B(T-298)$).

D11. CH_2=CHCHO + hν → CH_2=CH + CHO φ_1
CH_2=CHCHO + hν → C_2H_4 + CO φ_2
CH_2=CHCHO + hν → CH_2=CHCO + H φ_3. The absorption cross sections of acrolein (propenal) have been measured at room temperature and 227-380 nm by Gardner et al. [261] and at 192-431 nm by Magneron et al. [466]. The spectrum displays a broad absorption band between 250 and 400 nm, which is structured at wavelengths above 360 nm. The results of both teams agree to within 10% between 298 and 370 nm (with a few exceptions at 352, 360, 362 and 368 nm). Below 298 nm the differences increase up to ~40% with decreasing wavelength, above 368 nm the differences increase up to ~100% with increasing wavelength. Our preferred values listed in Table 4-41 are the 2-nm averages of the high-resolution data of Magneron et al. [466].

The photodecomposition was studied by Gardner et al. [261] at 313 and 334 nm in the pressure range 26-760 Torr air, who found that the photolysis is very inefficient at both wavelengths at high pressures but increases at low pressure. At 313 nm the quantum yield for photodissociation Φ_d of acrolein was $\Phi_d = 0.0065$ at 1 atm and 0.081 at 26 Torr. The pressure dependence was described by

$1/(\Phi_d - 0.004) = 0.086 + 1.613 \times 10^{-17}$ [M] (for $8 \times 10^{17} < M < 2.6 \times 10^{19}$ molecule cm^{-3}).

The dominant observed products were CO and C_2H_4. Magneron et al. [466] used broad-band photolysis (275-380 nm) of dilute mixtures of acrolein in air, but did not observe any products using long-path FTIR spectroscopy. An effective quantum yield for photolysis $\Phi_{eff} \leq 0.005$ nm was measured in the outdoor smog chamber.

Table 4-41. Absorption Cross Sections of CH_2=CHCHO at 298 K

λ (nm)	10^{20} σ (cm^2)	λ (nm)	10^{20} σ (cm^2)	λ (nm)	10^{20} σ (cm^2)	λ (nm)	10^{20} σ (cm^2)
282	0.84	310	3.59	338	5.46	366	3.74
284	0.97	312	3.92	340	5.31	368	3.82
286	1.08	314	4.15	342	5.10	370	2.17
288	1.23	316	4.21	344	5.12	372	1.58
290	1.46	318	4.47	346	5.30	374	1.14
292	1.62	320	4.65	348	5.17	376	1.14
294	1.80	322	5.08	350	5.94	378	1.24
296	1.97	324	5.17	352	5.79	380	1.10
298	2.18	326	5.34	354	4.18	382	0.84
300	2.47	328	5.20	356	3.63	384	0.79
302	2.70	330	5.31	358	3.28	386	1.18
304	2.85	332	5.44	360	3.92	388	0.49
306	3.09	334	5.80	362	3.72	390	0.25
308	3.29	336	6.24	364	2.86		

Note:
282-390 nm, Magneron et al. [466].

D12. CH_2=C(CH_3)CHO + hν → CH_2=CCH_3 + CHO Φ_1
CH_2=C(CH_3)CHO + hν → C_3H_6 + CO Φ_2
CH_2=C(CH_3)CHO + hν → H + CH_2=C(CH_3)CO Φ_3. The absorption cross sections of methacrolein (2-methylpropenal, MACR) have been measured at room temperature and 237-391 nm by Meller (see Röth et al. [687]) and Raber and Moortgat [646]; and at 214 and 250-395 nm by Gierczak et al. [271]. Both teams used diode array spectroscopy. A detailed vibrational-electronic analysis was reported by Birge et al. [71]. The spectrum exhibits a broad absorption band between 250 and 390 nm with vibrational structure above 310 nm. The results of both teams are in very good agreement in the region 261-351 nm where the agreement is between ~1 and 10%. Below 260 nm, the differences increase to nearly 100% at 250 nm, where the results of Gierczak et al. [271] are always larger than those of Meller [687] and Raber and Moortgat [646]. The peaks in the structured region above 328 nm reported by Meller [687] and Raber and Moortgat [646] are always higher due to the better resolution (0.07 nm) than those measured by Gierczak et al. [271] at a resolution of 0.5 nm. At the maximum, Raber and Moortgat [646] measured $\sigma = 7.64 \times 10^{-20}$ cm^2 $molecule^{-1}$ at 330.7 nm, while Gierczak et al. [271] measured $\sigma = 7.2 \times 10^{-20}$ cm^2 $molecule^{-1}$ at 331 nm. The latter group also reported $\sigma = (2.21 \pm 0.11) \times 10^{-17}$ cm^2 $molecule^{-1}$ at 213.86 nm (Zn lamp source). The 1-nm averages of both teams generally (with a few exceptions) are within 20% up to 376 nm. Above 380 nm, the results of Gierczak et al. [271] become larger with increasing wavelength up to nearly 80% than the results of Meller (see Röth et al. [687]) and Raber and Moortgat [646]. A wavelength shift of ~1 nm to longer wavelengths can be observed above 340 nm in the absorption curve of Gierczak et al. [271] as compared to that reported by Meller (see Röth et al. [687]) and Raber and Moortgat [646]. The recommended absorption cross sections listed in Table 4-42 are those of Gierczak et al. [271].

Overall quantum yields were measured by Raber and Moortgat [646] using broad band photolysis in the wavelength range 275-380 nm, and determination of the products by FTIR spectroscopy (CO, CO_2, HCHO, C_2H_4, C_3H_6, C_2H_2). An upper limit of 0.05 was reported at 760 Torr. Gierczak et al. [271] determined overall quantum yields at 308 nm $\Phi = 0.008 \pm 0.001$ and $\Phi = 0.005 \pm 0.001$ at 25 and 650 Torr total pressure, respectively, and at 351 nm $\Phi = 0.005 \pm 0.002$ and $\Phi = 0.003 \pm 0.001$ at 25 and 650 Torr, respectively. Endproducts were analyzed by GC and GC-MS. Both studies indicate a very low quantum yield for dissociation of methacrolein, and a value $\Phi < 0.01$ is recommended at $\lambda > 308$ nm.

Table 4-42. Absorption Cross Sections of $CH_2=C(CH_3)CHO$ at 298 K

λ (nm)	10^{20} σ (cm^2)	λ (nm)	10^{20} σ (cm^2)	λ (nm)	10^{20} σ (cm^2)	λ (nm)	10^{20} σ (cm^2)
250	0.207	287	1.67	324	6.58	361	4.28
251	0.194	288	1.79	325	6.74	362	3.61
252	0.187	289	1.90	326	6.73	363	2.86
253	0.180	290	2.03	327	6.68	364	2.68
254	0.179	291	2.16	328	6.83	365	2.33
255	0.177	292	2.28	329	7.07	366	1.92
256	0.180	293	2.39	330	7.15	367	1.62
257	0.180	294	2.52	331	7.16	368	1.40
258	0.186	295	2.68	332	7.03	369	1.31
259	0.193	296	2.85	333	6.69	370	1.42
260	0.201	297	2.99	334	6.41	371	1.67
261	0.211	298	3.13	335	6.08	372	1.53
262	0.224	299	3.26	336	5.97	373	1.43
263	0.241	300	3.44	337	6.25	374	1.08
264	0.263	301	3.61	338	6.38	375	0.977
265	0.283	302	3.76	339	6.37	376	1.00
266	0.305	303	3.91	340	6.24	377	1.07
267	0.333	304	4.04	341	6.02	378	1.35
268	0.363	305	4.19	342	5.98	379	2.18
269	0.398	306	4.40	343	6.58	380	1.30
270	0.436	307	4.58	344	6.79	381	0.984
271	0.479	308	4.71	345	6.53	382	0.555
272	0.520	309	4.81	346	6.11	383	0.456
273	0.567	310	4.92	347	5.63	384	0.364
274	0.616	311	5.13	348	5.22	385	0.331
275	0.673	312	5.35	349	4.55	386	0.246
276	0.732	313	5.50	350	4.16	387	0.205
277	0.793	314	5.61	351	3.85	388	0.181
278	0.863	315	5.70	352	3.89	389	0.161
279	0.936	316	5.87	353	4.35	390	0.147
280	1.01	317	6.04	354	4.31	391	0.156
281	1.09	318	6.19	355	4.14	392	0.159
282	1.18	319	6.28	356	3.62	393	0.153
283	1.26	320	6.27	357	3.53	394	0.149
284	1.35	321	6.18	358	3.46	395	0.123
285	1.45	322	6.21	359	3.81		
286	1.56	323	6.34	360	5.05		

Note:
250-395 nm, Gierczak et al. [271].

D13. $CH_3C(O)CH=CH_2 + h\nu \rightarrow CH_3\text{-}CH=CH_2 + CO$
$CH_3C(O)CH=CH_2 + h\nu \rightarrow CH=CH_2 + CH_3C(O)$
$CH_3C(O)CH=CH_2 + h\nu \rightarrow CH=CH_2C(O) + CH_3$. The absorption cross sections of methyl vinyl ketone (MVK) have been measured at room temperature and 240-398 nm by Schneider and Moortgat (see Röth et al. [687]); at 235-400 nm by Raber and Moortgat [646]; and at 216.86 nm and 250-395 nm by Gierzcak et al. [271]. A detailed vibrational-electronic analysis was reported by Birge et al. [71]. The spectrum displays some weak vibrational band structure, which is superimposed on the continuum envelope. The data of Schneider and Moortgat (see Röth et al. [687]) and Raber and Moortgat [646] are somewhat lower around the maximum at 334 nm (agreement within ~10% between 290 and 365 nm), and higher by up to 50% and lower by up to ~60% in the short- and long-wavelength tails, respectively, than the results of Gierczak et al. [271]. The latter group reported $\sigma = (6.6 \pm 0.04) \times 10^{-17}$ cm^2 $molecule^{-1}$ at 213.86 nm (Zn lamp source). They also determined the spectrum at reduced temperatures (range 250-298 K), and observed a small increase of < 2% at 250 K. We recommend the data of Gierzcak et al. [271] measured at 1-nm intervals as listed in Table 4-43.

Product quantum yields were measured by Raber and Moortgat [646], who monitored the products (major CO, C_3H_6 and HCHO; minor CO_2, HCOOH, CH_3OH, CH_3COOH) by FTIR using broadband photolysis in the range 275-380 nm. They quote $\Phi = 0.05$ at 760 Torr, increasing to $\Phi = 0.12$ at 54 Torr. Gierczak et al. [271] measured quantum yields at 308, 337 and 351 nm, by monitoring the disappearance of MVK at 25 and 650 Torr. At 308 nm they observed $\Phi = 0.16$ at 25 Torr and $\Phi = 0.04$ at 760 Torr; at 337 nm $\Phi = 0.04$ at 25 Torr and $\Phi = 0.01$ at 760 Torr; and at 351 nm $\Phi = 0.01$ independent of pressure. The data were fitted to the following empirical expression, taking into account the Stern-Volmer type pressure-dependence, which is our recommendation.

$$\Phi(\lambda,P) = \exp[-0.055\ (\lambda - 308)]\ /\ (5.5 + 9.2 \times 10^{-19}\ [M]),$$

where λ is in nm and [M] in molecule cm^{-3}.

Table 4-43. Absorption Cross Sections of $CH_3(O)CH=CH_2$ at 298 K

λ (nm)	10^{20} σ (cm^2)	λ (nm)	10^{20} σ (cm^2)	λ (nm)	10^{20} σ (cm^2)	λ (nm)	10^{20} σ (cm^2)
250	0.241	287	2.03	324	6.88	361	3.60
251	0.241	288	2.15	325	6.95	362	3.49
252	0.224	289	2.29	326	7.02	363	3.36
253	0.241	290	2.43	327	7.09	364	3.29
254	0.241	291	2.55	328	7.16	365	3.03
255	0.258	292	2.67	329	7.23	366	2.77
256	0.275	293	2.81	330	7.28	367	2.50
257	0.275	294	2.93	331	7.30	368	2.20
258	0.293	295	3.08	332	7.26	369	2.01
259	0.310	296	3.24	333	7.18	370	1.88
260	0.327	297	3.39	334	7.04	371	1.74
261	0.361	298	3.56	335	6.94	372	1.58
262	0.379	299	3.70	336	6.85	373	1.48
263	0.396	300	3.87	337	6.70	374	1.39
264	0.430	301	4.05	338	6.56	375	1.31
265	0.465	302	4.20	339	6.47	376	1.26
266	0.499	303	4.35	340	6.44	377	1.24
267	0.534	304	4.51	341	6.42	378	1.21
268	0.568	305	4.66	342	6.35	379	1.21
269	0.620	306	4.82	343	6.35	380	1.05
270	0.654	307	4.96	344	6.30	381	0.981
271	0.706	308	5.13	345	6.23	382	0.912
272	0.757	309	5.30	346	6.14	383	0.878
273	0.809	310	5.44	347	6.08	384	0.929
274	0.878	311	5.58	348	5.77	385	0.757
275	0.929	312	5.73	349	5.47	386	0.637
276	0.998	313	5.87	350	5.20	387	0.534
277	1.08	314	6.02	351	4.94	388	0.448
278	1.15	315	6.14	352	4.72	389	0.396
279	1.24	316	6.28	353	4.53	390	0.344
280	1.33	317	6.42	354	4.32	391	0.310
281	1.41	318	6.54	355	4.15	392	0.293
282	1.50	319	6.63	356	4.03	393	0.275
283	1.60	320	6.70	357	3.94	394	0.241
284	1.70	321	6.76	358	3.89	395	0.207
285	1.81	322	6.83	359	3.89		
286	1.91	323	6.85	360	3.68		

Note:
250-395 nm, Gierzcak et al. [271].

D14. $HOCH_2CHO + h\nu \rightarrow CH_2OH + HCO$ φ_1
$HOCH_2CHO + h\nu \rightarrow CH_3OH + CO$ φ_2
$HOCH_2CHO + h\nu \rightarrow OH + CH_2CHO$ φ_3
$HOCH_2CHO + h\nu \rightarrow HOCH_2CO + H$ φ_4. The absorption cross sections of $HOCH_2CHO$ (glycolaldehyde, hydroxyacetaldehyde) have been measured at room temperature and 205-335 nm by Bacher et al. [33]; and at 210-330 nm by Magneron et al. [465]. The spectrum consists of a strong absorption below 220 nm and a weaker absorption band centered near 280 nm with evidence of vibrational progressions. The measurements performed by Magneron et al. [465] were done at two different laboratories and are nearly identical, but reveal significant differences as compared to the spectrum measured by Bacher et al. [33], being about 20% at the maximum. The cross sections of Magneron et al. [465] are therefore recommended and are listed in Table 4-44.

The broad band photolysis (285 ± 25 nm) of glycolaldehyde in air performed by Bacher et al. [33] revealed an overall quantum yield $\Phi > 0.5$, relative to the quantum yield ($\Phi = 0.3$) of removal of acetone. Product studies by FTIR suggests that channel (1) is the major photolysis channel (65-80%), while channel (2) accounts to 15-20%, and channel (3) contributes up to 15%. The formation of channel (4) was suggested to produce $HOCH_2CO$ as a source for OH radicals, whose presence was indirectly invoked due the formation of glyoxal. Magneron et al. [465] also photolysed glycolaldehyde (broadband lamps 275-380 nm) and measured products by FTIR (CO, CO_2, HCHO and CH_3OH). They observed direct evidence for OH production via channel (3) using OH-scavenger and OH-tracer species, and performed additional photolysis experiments where glycolaldehyde was used an OH source to measure rate constants for OH with a series of dienes. The contribution of channel (2) was estimated to 10%, and that of channels (1) + (2) to 90%. No evidence was found for channel (4).

Based on the combined product studies we recommend quantum yields: $\varphi_1 = 0.70$, $\varphi_2 = 0.15$ and $\varphi_3 = 0.15$

Table 4-44. Absorption Cross Sections of $HOCH_2CHO$ at 298 K

λ (nm)	10^{20} σ (cm^2)	λ (nm)	10^{20} σ (cm^2)	λ (nm)	10^{20} σ (cm^2)	λ (nm)	10^{20} σ (cm^2)
212	8.24	242	1.48	272	6.62	302	3.26
214	4.85	244	1.77	274	6.90	304	2.69
216	2.97	246	2.10	276	6.91	306	2.29
218	1.68	248	2.41	278	6.88	308	1.89
220	0.904	250	2.76	280	6.85	310	1.57
222	0.569	252	3.19	282	6.93	312	1. 30
224	0.334	254	3.58	284	6.60	314	0.95
226	0.262	256	3.97	286	6.38	316	0.72
228	0.284	258	4.45	288	6.09	318	0.55
230	0.425	260	4.89	290	5.89	320	0.42
232	0.489	262	5.21	292	5.49	322	0.31
234	0.672	264	5.53	294	4.90	324	0.23
236	0.845	272	5.99	296	4.52	326	0.16
238	1.03	274	6.25	298	4.13	328	0.12
240	1.25	270	6.41	300	3.77	330	0.096

Note:
212-330 nm, Magneron et al. [465].

D15. $CH_3C(O)CH_3 + h\nu \rightarrow CH_3C(O) + CH_3$ ($\lambda_{threshold} > 338$ nm) φ_1
$CH_3C(O)CH_3 + h\nu \rightarrow 2\ CH_3 + CO$ ($\lambda_{threshold} > 299$ nm) φ_2. The absorption spectrum of acetone has been measured at room temperature and 159-203 nm by Lake and Harrison [429]; at 200-300 nm by McMillan [139, 510]; at 220-368 nm by Meyrahn et al. [524, 526]; at 196-366 nm by Schneider and Moortgat (see Röth et al. [687]); at 253.7 nm and 260-360 nm by Hynes et al. [355]; at 202-335 nm by Martinez et al. [492]; at 215–349 nm by Gierczak et al. [269]; at 220-346 nm by Wollenhaupt et al. [852]; and at 240-350 nm by Yujing and Mellouki [871]. Cross sections have been determined at isolated wavelengths: at 193 nm (also for $CD_3C(O)CD_3$) by Braun et al. [87] and Seki and Okabe [720]; at 216.51 nm by Krasnoperov and Mehta [421]; and at 184.9 nm (also for $CD_3C(O)CD_3$) by Gierczak et al. [272].

The spectrum below 200 nm is highly structured in the regions 160-170 nm and 180-195 nm. A broad absorption band was observed between 210 and 340 nm for which high-resolution measurements give evidence for the existence of two bands with maxima at about 273 and 278 nm. The results of the various research teams are in excellent agreement, i.e., ≤ 8% in the 240-320-nm region of the absorption band. The

measured absorption cross-sections for the maxima vary between 5.2×10^{-20} and 4.8×10^{-20} cm^2 molecule^{-1}. In the tails of the absorption band, the various data sets become more and more divergent with decreasing wavelength up to about 50% at 220 nm and with increasing wavelength up to more than 100% at 340 nm. The data measured by Meyrahn et al. [524, 526] are systematically higher than the other studies at wavelengths larger than 320 nm. Our recommendation for the region of the absorption band is based on the recent results of Martinez et al. [492], Gierczak et al. [269], Wollenhaupt et al. [852] and Yujing and Mellouki [871], which agree within 2.5% in the region of the absorption maximum and within 50% in the short- and long-wavelength tails.

The temperature dependence has been studied at 300-340 nm and 261-362 K by Hynes et al. [355]; at 215-349 nm and 235-298 K by Gierczak et al. [269]; and (also for $CD_3C(O)CD_3$) at 184.9 nm and 222-296 K by Gierczak et al. [272]. The absorption spectrum shows modest temperature dependence in the long-wavelength tail of the absorption band above 270 nm, with the cross sections decreasing with decreasing temperature. At shorter wavelengths the spectrum is essentially independent of temperature, the cross section changes by < 5% between 298 and 235 K. Gierczak et al. [269] parameterized the temperature dependent cross sections by a quadratic expression $\sigma(\lambda, T) = \sigma(\lambda, 298\ K)[1 + c_1(\lambda)T + c_2(\lambda)T^2]$, which later was superseded by Burkholder [109] by a cubic expression $\sigma(\lambda, T) = \sigma(\lambda, 298\ K)[1 + A(\lambda)T + B_2(\lambda)T^2 + C(\lambda)T^3]$. In Table 4-45 are listed the recommended absorption cross sections at 298 K taken from the work of Gierczak et al. [269] and the temperature coefficients A, B, and C of the cubic fit derived by Burkholder [109].

The absorption cross section of $CH_3C(O)CH_3$ at 184.9 nm decreases very slightly with decreasing temperature from 296 to 222 K leading to an average value of $(2.98 \pm 0.10) \times 10^{-18}$ cm^2 molecule^{-1}, whereas that of $CD_3C(O)CD_3$ increases noticeably from 3.91×10^{-18} cm^2 molecule^{-1} (average of six results) at 295 K to 4.61×10^{-18} cm^2 molecule^{-1} at 232 K, as reported by Gierczak et al. [272].

Gardner et al. [263] measured the acetone loss ($-\Phi_{AC}$) and formation of products CO_2, CO, CH_3OH and HCHO of the photolysis of dilute acetone-air mixtures at 4 wavelengths in the range 279-313 nm, 25-745 Torr and 271-301 K. At pressures larger than 300 Torr, they observed a near constant quantum yield $-\Phi_{AC} \approx \varphi_{CO2} = \varphi_1 = 0.077$ in the range 279-313 nm, to increase slightly at lower pressures. Meyrahn et al. [524, 526] measured the quantum yields of CO and CO_2 in the photolysis of dilute mixtures of acetone in air at nine wavelengths in the range 250-330 nm. At 1 atm, φ_{CO2} decreased from 1.59 at 250 nm to 0.11 at 310 nm, to increase again to 0.27 at 330 nm; the Φ_{CO} decreased from 0.45 at 250 nm to 0.02 at 310 nm and increased again to 0.09 at 330 nm. The quantum yield φ_{CO2} being larger than unity was explained by the participation of secondary reactions. The same authors also measured the quantum yield of peroxyacetyl nitrate φ_{PAN} (which is a direct measure of φ_1) of acetone /air/NO_2 mixtures to decrease from ~0.78 at 250-260 nm to 0.03 at 230-330 nm. Meyrahn et al. [524, 526] observed φ_{CO2} to increase at lower pressures (Stern-Volmer mechanism) at 330 nm. Emrich and Warneck [229, 230] also determined the φ_{PAN} of acetone /air/NO_2 mixtures at six wavelengths in the range 280-330 nm and the total pressure range 10 to 760 Torr. At 760 Torr, φ_{PAN} decreased from 1.00 at 280 nm to 0.06 at 320 nm, and increased again to 0.13 at 330 nm. These authors also observed Stern-Volmer type pressure dependence at all wavelengths. The results were explained in terms of the rate of photodissociation from the excited singlet $^1[AC]^*$ state of acetone and the competing intersystem crossing to the triplet $^3[AC]^*$, both relative to that of pressure quenching, as a function of energy above the dissociation threshold. It was proposed that

$$^1[AC]^* \rightarrow 2\ CH_3 + CO \text{ and } ^3[AC]^* \rightarrow CH_3C(O) + CH_3.$$

Gierczak et al. [269] determined $-\Phi_{AC}$ and φ_{CO2} in the laser photolysis of acetone at nine wavelengths in the range 248-337 nm as a function of pressure (25 to 760 Torr air) and temperature in the range 195-298 K. At $\lambda > 270$ nm Φ displayed a Stern-Volmer type pressure dependence, and the zero pressure quantum yield was found to increase at decreasing wavelength, to reach unity near 290 nm. The quantum yields were found to be temperature independent at 308 nm. Their results at 298 K were nearly identical to those of Emrich and Warneck [229]. Gierczak et al. [269] presented an algorithm for the quantum yield based on the parameterization of their own data. Warneck [838] evaluated the results of Gierczak et al. [269] and Emrich and Warneck [229] of the quantum yields for the dissociation of acetone Φ_{diss} to derive an expression for the dependence of Φ_{diss} on wavelength and pressure.

Aloisio and Francisco [13] measured the quantum yield of acetone photodissociation at 248 and 308 nm in the presence and absence of water vapor. At 248 nm the apparent quantum yield Φ_{eff} decreased from unity to 0.73 ± 0.07 in the presence of 9 Torr H_2O, and at 308 nm Φ_{eff} was reduced from 0.28 ± 0.07 to 0.06 ± 0.04.

Recently Blitz et al. [77, 78] measured the pressure and temperature (218-295 K) dependent quantum yields of acetone between 279 and 327.5 nm. These authors used a spectroscopic technique to detect the CH_3CO radical based on the detection of the OH radical formed by the reaction

$$CH_3CO + O_2 \rightarrow CH_3COO_2^* \rightarrow OH + \text{“other products”}.$$

They observed "classical" Stern-Volmer behavior at $\lambda < 302$ nm, but at $\lambda > 302$ nm an extended form of the Stern-Volmer expression was necessary for pressures below 15 Torr to fit their data, reflecting the dissociation and quenching from both $^1[AC]^*$ and $^3[AC]^*$ excited states (Arnold et al. [25]). These authors established the total quantum yield $\Phi_{TOTAL}(\lambda, p, T) = \varphi_{CH3CO}(\lambda, p, T) + \varphi_{CO}(\lambda, T) = \varphi_1 + \varphi_2$.

At the limit pressure p = 0 Blitz et al. [77, 78] determined at 248 nm and 295 K, $\Phi_{TOTAL} = 1$, $\varphi_{CH3CO} = 0.65$ and $\varphi_{CO} = 0.35$. At $\lambda < 310$ nm and 1 atm, there was very good agreement with the data of Gierczak et al. [269] and Emrich and Warneck [229]; however at $\lambda > 310$ nm, the measured quantum yields were significantly smaller, the time-resolved studies of Blitz et al. [77, 78] being more direct and sensitive than previous studies. The T-dependence of Φ_{TOTAL} is small below 295 nm, but quite striking at longer wavelengths: the ratio of the quantum yields at 295 and 218 K, Φ_{TOTAL} (295 K) / Φ_{TOTAL} (218 K) ≈ 4 and ≈ 20 at 310 nm and 322.5 nm, respectively.

The major difference in the study of Blitz et al, [77, 78] is that the OH radicals are detected before undergoing secondary reactions, so that the OH yields represent the CH_3CO radicals produced. The quantum yield determined by the other previous studies (Gierczak et al. [269] and Emrich and Warneck [229]) were based upon the removal of CH_3COCH_3, which is affected by the additional loss by reaction with the OH radicals which are produced in the decomposition of CH_3CO.

The quantum yield data of Blitz et al. [77, 78] are recommended in the current evaluation. The optimized parameterization of the quantum yields for the range 279-327.5 nm, temperature 218 to 295 K and pressure up to 1000 mbar, is given by the following expressions:

$$\Phi_{TOTAL}(\lambda, [M], T) = \varphi_{CH3CO}(\lambda, [M], T) + \varphi_{CO}(\lambda, T)$$

For λ = 279-327.5 nm

$$\varphi_{CO}(\lambda, T) = 1 / (1 + A_0)$$

where $A_0 = [a_0 / (1 - a_0)] \exp[b_0 \{\lambda - 248\}]$

$$a_0 = (0.350 \pm 0.003)\,(T/295)^{(-1.28 \pm 0.03)}$$

$$b_0 = (0.068 \pm 0.002)\,(T/295)^{(-2.65 \pm 0.20)}$$

For λ = 279-302 nm

$$\varphi_{CH3CO}(\lambda, [M], T) = \{1 - \varphi_{CO}(\lambda, T)\} / \{1 + A_1[M]\}$$

where $A_1 = a_1 \exp[-b_1 \{(10^7/\lambda) - 33113\}]$

$$a_1 = (1.600 \pm 0.032) \times 10^{-19}\,(T/295)^{(-2.38 \pm 0.08)}$$

$$b_1 = (0.55 \pm 0.02) \times 10^{-3}\,(T/295)^{(-3.19 \pm 0.13)}$$

For λ = 302-327.5 nm,

$$\varphi_{CH3CO}(\lambda, [M], T) = \{(1 + A_4[M] + A_3) / [(1 + A_2[M] + A_3)(1 + A_4[M])]\}\ \{1 - \varphi_{CO}(\lambda, T)\}$$

where $A_2 = a_2 \exp[-b_2 \{(10^7/\lambda) - 30488\}]$

$$a_2 = (1.62 \pm 0.06) \times 10^{-17}\,(T/295)^{(-10.03 \pm 0.20)}$$

$$b_2 = (1.79 \pm 0.02) \times 10^{-3}\,(T/295)^{(-1.364 \pm 0.036)}$$

$A_3 = a_3 \exp[-b_3 \{(10^7/\lambda) - c_3\}^2]$

$$a_3 = (26.29 \pm 0.88)\,(T/295)^{(-6.59 \pm 0.23)}$$

$$b_3 = (5.72 \pm 0.20) \times 10^{-7}\,(T/295)^{(-2.93 \pm 0.09)}$$

$$c_3 = (30006 \pm 41)\,(T/295)^{(-0.064 \pm 0.004)}$$

$A_4 = a_4 \exp[-b_4 \{(10^7/\lambda) - 30488\}]$

$$a_4 = (1.67 \pm 0.14) \times 10^{-15}\,(T/295)^{(-7.25 \pm 0.54)}$$

$$b_4 = (2.08 \pm 0.02) \times 10^{-3}\,(T/295)^{(-1.16 \pm 0.15)}$$

In all cases [M] is in molecule cm^{-3}, λ in nm and T in K.

These equations have been used to calculate the quantum yields in the region 279-327 nm at 218, 248, 273 and 295 K, as displayed in Table 4-46**.**

Table 4-45. Absorption Cross Sections of $CH_3C(O)CH_3$ at 298 K and Temperature Coefficients

λ (nm)	10^{20} σ (cm^2)	10^3 A (K^{-1})	10^5 B (K^{-2})	10^8 C (K^{-3})	λ (nm)	10^{20} σ (cm^2)	10^3 A (K^{-1})	10^5 B (K^{-2})	10^8 C (K^{-3})
215	0.167	-10.46	8.346	-16.43	283	4.71	1.137	-1.350	3.272
216	0.180	-9.192	7.357	-14.51	284	4.62	0.8530	-1.158	2.943
217	0.196	-6.233	5.039	-10.01	285	4.54	0.6518	-1.023	2.714
218	0.212	-3.190	2.651	-5.359	286	4.44	0.4907	-0.9154	2.531
219	0.228	-1.002	0.9314	-2.003	287	4.36	0.3190	-0.7992	2.332
220	0.246	0.4104	-0.1807	0.1679	288	4.28	0.1109	-0.6586	2.092
221	0.270	1.567	-1.090	1.936	289	4.15	-0.1230	-0.5036	1.833
222	0.294	2.962	-2.183	4.058	290	4.06	-0.3698	-0.3426	1.568
223	0.318	4.839	-3.651	6.909	291	3.95	-0.6430	-0.1615	1.265
224	0.346	6.940	-5.293	10.09	292	3.82	-0.9625	0.05796	0.8847
225	0.380	8.598	-6.588	12.60	293	3.71	-1.316	0.306	0.4472
226	0.419	9.380	-7.200	13.79	294	3.57	-1.650	0.535	0.0477
227	0.456	9.551	-7.336	14.06	295	3.42	-1.905	0.699	-0.2168
228	0.492	9.705	-7.462	14.31	296	3.26	-2.084	0.796	-0.3430
229	0.535	10.08	-7.761	14.89	297	3.11	-2.234	0.867	-0.4086
230	0.584	10.41	-8.023	15.41	298	2.98	-2.391	0.942	-0.4824
231	0.637	10.39	-8.002	15.36	299	2.82	-2.590	1.055	-0.6387
232	0.693	10.01	-7.707	14.79	300	2.67	-2.915	1.277	-1.020
233	0.750	9.534	-7.332	14.06	301	2.58	-3.421	1.649	-1.709
234	0.815	9.138	-7.022	13.46	302	2.45	-4.008	2.091	-2.543
235	0.885	8.851	-6.799	13.02	303	2.30	-4.508	2.465	-3.248
236	0.956	8.638	-6.634	12.70	304	2.18	-4.858	2.715	-3.699
237	1.03	8.471	-6.504	12.45	305	2.05	-5.120	2.880	-3.959
238	1.11	8.318	-6.385	12.22	306	1.89	-5.433	3.062	-4.219
239	1.21	8.125	-6.235	11.93	307	1.75	-6.010	3.429	-4.805
240	1.30	7.861	-6.031	11.53	308	1.61	-6.986	4.096	-5.954
241	1.40	7.554	-5.793	11.07	309	1.49	-8.135	4.899	-7.370
242	1.50	7.268	-5.571	10.64	310	1.36	-8.897	5.415	-8.255
243	1.60	7.035	-5.390	10.29	311	1.24	-8.923	5.378	-8.097
244	1.72	6.838	-5.237	9.994	312	1.14	-8.494	5.001	-7.305
245	1.83	6.649	-5.093	9.718	313	1.06	-8.228	4.754	-6.772
246	1.95	6.472	-4.960	9.464	314	0.944	-8.445	4.881	-6.959
247	2.07	6.326	-4.850	9.256	315	0.837	-8.966	5.240	-7.592
248	2.20	6.210	-4.763	9.091	316	0.760	-9.409	5.528	-8.076
249	2.33	6.099	-4.680	8.936	317	0.684	-9.584	5.588	-8.085
250	2.47	5.972	-4.587	8.763	318	0.598	-9.736	5.596	-7.946
251	2.60	5.832	-4.486	8.576	319	0.523	-10.39	5.958	-8.433
252	2.74	5.697	-4.389	8.399	320	0.455	-11.80	6.869	-9.933
253	2.87	5.581	-4.306	8.249	321	0.411	-13.48	7.962	-11.75
254	3.01	5.483	-4.235	8.120	322	0.348	-14.59	8.600	-12.67
255	3.15	5.385	-4.164	7.989	323	0.294	-14.98	8.670	-12.47
256	3.30	5.261	-4.075	7.825	324	0.248	-15.39	8.743	-12.27
257	3.44	5.101	-3.961	7.620	325	0.210	-16.28	9.187	-12.77
258	3.57	4.932	-3.843	7.410	326	0.174	-17.09	9.588	-13.21
259	3.69	4.802	-3.756	7.262	327	0.141	-17.21	9.471	-12.68
260	3.81	4.746	-3.723	7.215	328	0.113	-16.92	9.048	-11.58
261	3.94	4.744	-3.730	7.239	329	0.0913	-16.66	8.672	-10.62
262	4.07	4.734	-3.729	7.246	330	0.0740	-15.94	7.979	-9.099
263	4.20	4.651	-3.674	7.155	331	0.0586	-13.93	6.340	-5.829
264	4.32	4.482	-3.559	6.956	332	0.0465	-10.93	3.969	-1.214
265	4.41	4.271	-3.416	6.712	333	0.0375	-8.186	1.847	2.840
266	4.49	4.087	-3.296	6.513	334	0.0311	-6.530	0.6289	5.067
267	4.56	3.983	-3.234	6.420	335	0.0248	-5.692	0.1022	5.880

λ (nm)	10^{20} σ (cm^2)	10^3 A (K^{-1})	10^5 B (K^{-2})	10^8 C (K^{-3})	λ (nm)	10^{20} σ (cm^2)	10^3 A (K^{-1})	10^5 B (K^{-2})	10^8 C (K^{-3})
268	4.64	3.969	-3.235	6.440	336	0.0199	-4.656	-0.5382	6.860
269	4.72	4.009	-3.273	6.524	337	0.0162	-2.090	-2.355	10.09
270	4.79	4.025	-3.294	6.577	338	0.0135	3.113	-6.237	17.33
271	4.87	3.935	-3.240	6.494	339	0.0113	11.01	-12.26	28.77
272	4.91	3.704	-3.085	6.231	340	00912	20.02	-19.22	42.15
273	4.94	3.378	-2.861	5.845	341	00729	27.20	-24.83	53.03
274	4.94	3.061	-2.645	5.473	342	00583	29.63	-26.80	56.96
275	4.94	2.854	-2.508	5.243	343	00494	25.97	-24.04	51.78
276	4.93	2.790	-2.474	5.201	344	00365	16.35	-16.63	37.55
277	4.92	2.816	-2.505	5.276	345	0.00301	3.774	-6.858	18.72
278	4.94	2.820	-2.518	5.316	346	0.00235	-2.414	-1.987	9.304
279	4.92	2.692	-2.433	5.175	347	0.00158	7.880	-9.888	24.53
280	4.91	2.389	-2.222	4.803	348	0.00111	29.52	-26.61	56.78
281	4.86	1.963	-1.922	4.272	349	0.00107	41.03	-35.51	73.95
282	4.79	1.517	-1.612	3.726					

Note:
215-349 nm, Gierczak et al. [269], parameterization of the temperature dependence revised by J. Burkholder (2005) [109]: $\sigma(T, \lambda) = \sigma(298\ K, \lambda)\ (1 + A\ T + B\ T^2 + C\ T^3)$ for T = 235-298 K.

Table 4-46. Quantum Yields for the Photolysis of Acetone

λ (nm)	218 K	248 K	273 K	295 K
279	0.680	0.579	0.571	0.617
280	0.663	0.558	0.551	0.597
281	0.644	0.536	0.530	0.578
282	0.621	0.513	0.509	0.559
283	0.594	0.489	0.489	0.540
284	0.565	0.465	0.468	0.521
285	0.534	0.441	0.448	0.502
286	0.500	0.417	0.427	0.483
287	0.465	0.393	0.407	0.464
288	0.430	0.369	0.388	0.446
289	0.394	0.345	0.368	0.428
290	0.359	0.322	0.350	0.411
291	0.324	0.300	0.331	0.394
292	0.291	0.279	0.314	0.377
293	0.260	0.258	0.297	0.361
294	0.231	0.239	0.280	0.345
295	0.205	0.221	0.264	0.330
296	0.180	0.203	0.249	0.315
297	0.158	0.187	0.235	0.301
298	0.138	0.172	0.221	0.287
299	0.121	0.158	0.208	0.274
300	0.105	0.144	0.195	0.261
301	0.0915	0.132	0.183	0.249
302	0.0794	0.121	0.125	0.237
303	0.0735	0.101	0.105	0.213
304	0.0557	0.0810	0.0873	0.184
305	0.0421	0.0646	0.0728	0.159
306	0.0317	0.0514	0.0608	0.137
307	0.0239	0.0409	0.0508	0.119
308	0.0180	0.0325	0.0426	0.103
309	0.0135	0.0258	0.0358	0.0887
310	0.0101	0.0205	0.0301	0.0769
311	0.00762	0.0164	0.0255	0.0669
312	0.00574	0.0131	0.0216	0.0584
313	0.00433	0.0105	0.0184	0.0511
314	0.00328	0.00842	0.0158	0.0449
315	0.00249	0.00679	0.0136	0.0396
316	0.00190	0.00550	0.0117	0.0350
317	0.00145	0.00447	0.0101	0.0311
318	0.00111	0.00365	0.00882	0.0278
319	0.000858	0.00299	0.00771	0.0248
320	0.000664	0.00246	0.00676	0.0223
321	0.000515	0.00204	0.00595	0.0201
322	0.000400	0.00169	0.00526	0.0181
323	0.000312	0.00141	0.00466	0.0164
324	0.000244	0.00117	0.00414	0.0149
325	0.000191	0.000983	0.00369	0.0135
326	0.000149	0.000826	0.00329	0.0124
327	0.000117	0.000696	0.00295	0.0113

D16. $CH_3C(O)CH_2OH + h\nu \rightarrow CH_3C(O) + CH_2OH$
$CH_3C(O)CH_2OH + h\nu \rightarrow HOCH_2C(O) + CH_3$. The absorption cross sections of $CH_3C(O)CH_2OH$ (hydroxyacetone, acetol) have been measured at room temperature and 235-340 nm by Orlando et al. [610]. The spectrum shows an absorption band with the maximum at 266 nm. In Table 4-47 are listed the averages over 1-nm intervals of the spectrum recorded at medium resolution of ~0.6 nm.

Quantum yields for removal of hydroxyacetone were estimated by Orlando et al. [610] to be 0.65 ± 0.25 for the wavelength range 240-420 nm, and < 0.6 for wavelengths larger than 290 nm.

Table 4-47. Absorption Cross Sections of $CH_3C(O)CH_2OH$ at 298 K

λ (nm)	10^{20} σ (cm^2)	λ (nm)	10^{20} σ (cm^2)	λ (nm)	10^{20} σ (cm^2)	λ (nm)	10^{20} σ (cm^2)
236	2.13	262	6.61	288	3.34	314	0.177
237	2.29	263	6.68	289	3.11	315	0.157
238	2.43	264	6.72	290	2.87	316	0.142
239	2.59	265	6.74	291	2.66	317	0.133
240	2.78	266	6.74	292	2.45	318	0.117
241	2.94	267	6.74	293	2.26	319	0.104
242	3.14	268	6.71	294	2.06	320	0.095
243	3.34	269	6.67	295	1.87	321	0.087
244	3.55	270	6.61	296	1.69	322	0.078
245	3.74	271	6.53	297	1.52	323	0.072
246	3.95	272	6.42	298	1.36	324	0.067
247	4.14	273	6.30	299	1.22	325	0.063
248	4.34	274	6.18	300	1.08	326	0.065
249	4.56	275	6.05	301	0.961	327	0.057
250	4.76	276	5.90	302	0.843	328	0.051
251	4.98	277	5.73	303	0.743	329	0.051
252	5.18	278	5.54	304	0.652	330	0.046
253	5.36	279	5.33	305	0.569	331	0.041
254	5.54	280	5.12	306	0.493	332	0.037
255	5.72	281	4.91	307	0.431	333	0.036
256	5.89	282	4.69	308	0.379	334	0.037
257	6.06	283	4.48	309	0.331	335	0.035
258	6.19	284	4.27	310	0.287	336	0.031
259	6.30	285	4.05	311	0.249		
260	6.41	286	3.82	312	0.219		
261	6.50	287	3.58	313	0.192		

Note:
236-236 nm, Orlando et al. [610].

D17. $CHOCHO + h\nu \rightarrow HCO + HCO$ (1)
$CHOCHO + h\nu \rightarrow H_2 + 2\ CO$ (2)
$CHOCHO + h\nu \rightarrow HCHO + CO$ (3)
$CHOCHO + h\nu \rightarrow H + CO + HCO$ (4). The absorption spectrum of glyoxal has been measured at room temperature and 230-460 nm by Plum et al. [638]; at isolated wavelengths at 308 nm by Langford and Moore [432], at 193, 248, 308, and 351 nm by Zhu et al. [883], and between 290 and 420 nm at 10-nm intervals by Chen and Zhu [161]. Measurements at medium resolution were carried out with a diode-array spectrometer at 210-450 nm (resolution 0.6 nm) by Orlando and Tyndall [608], and at 210-480 nm (resolution 0.25 nm by Horowitz et al. [341], and measurements at high resolution using cavity ring-down spectroscopy in the narrow range 436-442 nm by Zhu and Johnston [882], and using a Fourier Transform spectrometer at 250-526 nm (resolution 1 cm^{-1} at 250-268 nm, 0.06 cm^{-1} at 368-526 nm) by Volkamer et al. [827]. The absorption spectrum exhibits two absorption bands in the region above 220 nm, a weak band with evidence of vibrational structure in the UV at 220-350 nm and a strong and highly structured band in the near UV and visible above 360 nm, with a maximum at 455 nm**.**

The data of Horowitz et al. [341] and Orlando and Tyndall [608] are in very good agreement, i.e., to better than 10% between 240 and 440 nm. The results of Chen and Zhu [161] agree to within 10% with those of Horowitz et al. [341] and Orlando and Tyndall [608] in the 290-310 nm region and at 330, 340, 400, and 420 nm, within 15% at 320, 370, and 390 nm, 20% at 360 and 410 nm, 35% at 380 nm, and 45% at 350 nm. The data of Plum et al. [638] agree to within 25% with these recent data except for the minimum near 350 nm and the region below 260 nm, where considerably lower absorption cross-section were observed by Plum et al. [638]. The absorption cross sections reported by Zhu et al. [883] at the excimer laser wavelengths 248, 308, and 351 nm also agree very well with the data of Horowitz et al. [341] and Orlando and Tyndall [608], and the strong absorption feature below 200 nm, indicated by the 193-nm measurement of Zhu et al. [883] ($\sigma = 4.8 \times 10^{-19}$ cm^2 $molecule^{-1}$), was also observed by Orlando and Tyndall [608].

The cross sections reported by Volkamer et al. [827] are in all spectral ranges roughly 10% larger than those reported by Horowitz et al. [341] and Orlando and Tyndall [608] (where comparison is possible), and this difference seems systematic. The UV spectrum reported by Volkamer et al. [827] is consistent with IR-spectral parameters, for which glyoxal photolysis is not a problem, and which were obtained by simultaneous recording of UV and IR spectra in identical glyoxal fillings of the absorption cell. As recommended room temperature absorption cross sections for glyoxal we choose the averages over 1-nm intervals (rounded to three significant figures) of the high-resolution spectrum of Volkamer et al. [827], which are listed in Table 4-48.

Calvert and Pitts [137] summarized the quantum yield data before 1966. Based on the work of Calvert and Layne [134] and Parmenter [625] it was established that channel (3) was the dominant photolysis channel (yield 0.84 to 0.6 in the range 254 to 435 nm) with little evidence for the radical channel (1). At 313 nm Plum et al. [638] measured a HCHO yield of 0.13 for wavelengths larger than 325 nm, but reported an "effective quantum yield" of $\phi_{eff} = 0.029$, based on measured outdoor relative photolysis rates compared to NO_2, $J_{CHOCHO}/J_{NO2} = 0.008 \pm 0.005$. Langford and Moore [432] determined HCO directly by resonance absorption and deduced total HCO yields of 0.8 ± 0.4 ($\Phi_1 \approx 0.4$) at 305 nm, and estimated quantum yields for the other two channels. Using cavity ring-down spectroscopy, Zhu et al. [883] found HCO yields of 1.5 ($\Phi_1 \approx 0.75$) at 351 nm, 069 ($\Phi_1 \approx 0.35$) at 308 nm, 0.52 ($\Phi_1 \approx 0.26$) at 248 nm and 0.42 ($\Phi_1 \approx 0.21$) at 193 nm. In a later study Chen and Zhu [161] determined zero pressure HCO yields $\phi_0(\lambda)$ at 10 nm intervals, to increase from 0.50 ± 0.01 at 290 nm to a maximum of 2.01 ± 0.08 at 390 nm and to drop to $0.74 \pm 0.08 \pm 400$ nm, 0.56 ± 0.04 at 410 nm and 0.48 ± 0.03 at 420 nm. HCO quantum yields were found independent of nitrogen buffer gas (10-400 Torr) in the 290-370 nm region, but decreased with increasing pressure in the 380-420 nm region. They deduced HCO quantum yields at 760 Torr N_2 to be 0.49 at 380 nm, 0.54 nm at 390 nm, 0.32 at 400 nm, 0.22 at 410 nm and 0.14 at 420 nm.

Tadić et al. [761] photolysed glyoxal with fluorescent broad-band lamps, overlapping selectively with one of the absorption bands of glyoxal, and determined the products CO, HCHO and HCOOH. Using 275-380 nm irradiation, the overall quantum yield was $\Phi_T = 0.97 \pm 0.05$ independent of pressure. The absolute quantum yields obtained with 390-470 nm radiation, covering the second absorption band of glyoxal, showed dependency on total pressure, ranging form $\Phi_T = 0.12$ at 100 Torr to $\Phi_T = 0.04$ at 700 Torr and which can be expressed as a Stern-Volmer equation $1/\Phi_T = 6.80 + [251.8 \times 10^{-4} \times P\ (\text{Torr})]$.

By combining the product yields with the literature data mentioned above, the quantum yields for channels (1), (2) and (3) were deduced, as summarized in Table 4-49. The product quantum yields indicate that dissociation into 2 HCO radicals is the most important pathway under atmospheric conditions. The mean photolysis rate was measured under solar radiation in the EUPHORE outdoor chamber to be $J_{obs} = 1.04 \pm 0.10 \times 10^{-4}\ s^{-1}$, corresponding to a mean effective quantum yield $\phi_{eff} = 0.035 \pm 0.007$ [554], [553]. Although glyoxal has a very low effective quantum yield, photolysis remains an important removal path in the atmosphere.

Table 4-48. Absorption Cross Sections of CHOCHO at 296 K

λ (nm)	10^{20} σ (cm^2)	λ (nm)	10^{20} σ (cm^2)	λ (nm)	10^{20} σ (cm^2)	λ (nm)	10^{20} σ (cm^2)	λ (nm)	10^{20} σ (cm^2)
250	1.73	306	3.22	362	0.706	418	7.87	474	0.108
251	1.52	307	3.20	363	0.639	419	9.13	475	0.159
252	1.48	308	3.15	364	0.680	420	5.60	476	0.155
253	1.55	309	3.12	365	0.665	421	7.19	477	0.181
254	1.60	310	3.10	366	0.743	422	6.99	478	0.255
255	1.67	311	3.22	367	0.860	423	13.0	479	0.142
256	1.62	312	3.34	368	1.01	424	8.24	480	0.074
257	1.81	313	3.39	369	1.06	425	10.4	481	0.070
258	1.82	314	3.23	370	1.14	426	16.4	482	0.065
259	1.85	315	2.80	371	1.18	427	16.1	483	0.053
260	1.83	316	2.65	372	1.14	428	21.4	484	0.071
261	1.96	317	2.46	373	1.21	429	6.50	485	0.050
262	2.03	318	2.21	374	1.35	430	7.03	486	0.041
263	2.14	319	1.93	375	1.33	431	6.52	487	0.056
264	2.18	320	1.85	376	1.38	432	6.08	488	0.070
265	2.26	321	1.89	377	1.47	433	5.66	489	0.042
266	2.33	322	1.77	378	1.61	434	6.81	490	0.045
267	2.37	323	1.72	379	1.53	435	7.66	491	0.041
268	2.36	324	1.68	380	1.93	436	13.2	492	0.039
269	2.48	325	1.60	381	2.46	437	9.19	493	0.040
270	2.51	326	1.61	382	2.02	438	13.8	494	0.041
271	2.61	327	1.70	383	2.07	439	12.1	495	0.042
272	2.72	328	1.94	384	1.94	440	25.9	496	0.045
273	2.81	329	1.86	385	1.89	441	13.1	497	0.033
274	2.92	330	1.69	386	1.83	442	9.01	498	0.035
275	3.00	331	1.13	387	2.29	443	11.1	499	0.032
276	3.06	332	1.05	388	3.00	444	13.5	500	0.033
277	3.09	333	0.966	389	3.21	445	15.1	501	0.038
278	3.08	334	0.919	390	3.48	446	7.82	502	0.031
279	3.09	335	0.737	391	3.92	447	3.73	503	0.042
280	3.13	336	0.630	392	3.80	448	4.14	504	0.034
281	3.22	337	0.589	393	2.85	449	5.53	505	0.035
282	3.32	338	0.647	394	3.15	450	8.68	506	0.046
283	3.45	339	0.585	395	3.86	451	13.8	507	0.042
284	3.57	340	0.553	396	3.68	452	15.9	508	0.037
285	3.67	341	0.563	397	3.36	453	30.4	509	0.030
286	3.80	342	0.510	398	4.32	454	26.9	510	0.023
287	3.79	343	0.499	399	4.35	455	52.0	511	0.023
288	3.81	344	0.649	400	3.87	456	15.7	512	0.030
289	3.80	345	0.624	401	4.46	457	2.66	513	0.023
290	3.73	346	0.733	402	5.84	458	2.20	514	0.030
291	3.64	347	0.631	403	7.16	459	0.902	515	0.053
292	3.65	348	0.604	404	6.24	460	1.20	516	0.035
293	3.68	349	0.415	405	4.49	461	0.883	517	0.051
294	3.73	350	0.391	406	4.48	462	0.588	518	0.102
295	3.81	351	0.395	407	4.07	463	0.322	519	0.065
296	3.82	352	0.423	408	3.44	464	0.339	520	0.100
297	3.92	353	0.415	409	4.01	465	0.330	521	0.169
298	4.07	354	0.403	410	5.66	466	0.416	522	0.037
299	4.12	355	0.422	411	7.22	467	0.522	523	0.011
300	4.04	356	0.443	412	7.41	468	0.149	524	0.007
301	3.91	357	0.431	413	10.8	469	0.091	525	0.004
302	3.78	358	0.471	414	10.1	470	0.076	526	0.000
303	3.57	359	0.503	415	10.2	471	0.086		
304	3.35	360	0.546	416	6.07	472	0.092		

λ (nm)	10^{20} σ (cm^2)	λ (nm)	10^{20} σ (cm^2)	λ (nm)	10^{20} σ (cm^2)	λ (nm)	10^{20} σ (cm^2)	λ (nm)	10^{20} σ (cm^2)
305	3.24	361	0.627	417	6.83	473	0.110		

Note:
250-526 nm, data of Volkamer et al. [827].

Table 4-49. Absolute Quantum Yields in the Photolysis of CHOCHO

λ (nm)	Φ_{tot}	Φ_1	Φ_2	Φ_3	λ (nm)	Φ_{tot}	Φ_1	Φ_2	Φ_3
225	1.0	0.241	0.560	0.199	**340**	0.978	0.648	0.051	0.279
230	1.0	0.246	0.535	0.219	**345**	0.856	0.616	0.036	0.204
235	1.0	0.251	0.504	0.245	**350**	0.691	0.520	0.021	0.150
240	1.0	0.256	0.475	0.269	**355**	0.540	0.424	0.008	0.108
245	1.0	0.261	0.448	0.291	**360**	0.404	0.332	0.0	0.072
250	1.0	0.266	0.420	0.314	**365**	0.293	0.253		0.040
255	1.0	0.271	0.395	0.334	**370**	0.213	0.191		0.022
260	1.0	0.278	0.370	0.352	**375**	0.156	0.142		0.014
265	1.0	0.286	0.345	0.369	**380**	0.115	0.104		0.011
270	1.0	0.293	0.320	0.387	**385**	0.085	0.077		0.008
275	1.0	0.301	0.295	0.404	**390**	0.064	0.057		0.007
280	1.0	0.310	0.270	0.420	**395**	0.048	0.043		0.005
285	1.0	0.320	0.250	0.430	**400**	0.037	0.033		0.004
290	1.0	0.330	0.230	0.440	**405**	0.029	0.026		0.003
295	1.0	0.343	0.206	0.451	**410**	0.022	0.020		0.002
300	1.0	0.357	0.186	0.457	**415**	0.017	0.016		0.001
305	1.0	0.374	0.166	0.460	**420**	0.013	0.013		0.0
310	1.0	0.396	0.146	0.458	**425**	0.010	0.010		
315	1.0	0.423	0.125	0.452	**430**	0.008	0.008		
320	1.0	0.457	0.110	0.433	**435**	0.006	0.006		
325	1.0	0.497	0.095	0.408	**440**	0.003	0.003		
330	1.0	0.541	0.080	0.379	**445**	0.001	0.001		
335	0.995	0.593	0.065	0.337					

D18. $CH_3C(O)C(O)H + h\nu \rightarrow CH_3CO + HCO$ (1)
$CH_3C(O)C(O)H + h\nu \rightarrow CH_4 + 2\ CO$ (2)
$CH_3C(O)C(O)H + h\nu \rightarrow CH_3CHO + CO$ (3). The absorption spectrum of methylglyoxal has been measured at room temperature and 230-470 nm by Plum et al. [638]; at 218-494 nm by Meller et al. [518]; and absorption cross-sections in 10 nm intervals at 290-440 nm by Chen et al. [159]. Measurements have been reported by Staffelbach et al. [749] at 248, 273, and 298 K and 205-474 nm, and by Kyle and Orchard [428] at 387 K and 436 nm. The absorption spectrum exhibits two absorption bands, a slightly structured band between 225 and 335 nm and a stronger band between 335 and 475 nm, which is highly structured in the region above 410 nm. A steep increase of the absorption cross sections was observed at shorter wavelengths going from 225 to 200 nm by Staffelbach et al. [749].

The room temperature values of Meller et al. [518] (measured at a spectral resolution of 0.07 nm) and Staffelbach et al. [749] (measured at a resolution of 0.125 nm) are in good agreement above 230 nm: in the weaker absorption band the data of Meller et al. [518] are higher by up to 10-15% than the data of Staffelbach et al. [749]. In the strong absorption band up to 400 nm, the data of Staffelbach et al. [749] are higher by up to ~10% than the data of Meller et al. [518], and at higher wavelengths the peak values reported by Meller et al. [518] are higher (due to the higher resolution used in their study) than those measured by Staffelbach et al. [749]. The data points of Chen et al. [159] determined at 10-nm intervals fit well to the absorption curves of Meller et al. [518] and Staffelbach et al. [749], except for the points at 380 and 400 nm were the differences are about 20%. The cross sections reported earlier by Plum et al. [638] are approximately only the half of the cross sections reported Meller et al. [518] and Staffelbach et al. [749]. The preferred absorption cross sections listed in Table 4-50 are the data points at 1-nm intervals selected from the data of Staffelbach et al. [749] at 200-218 nm and the averages over 1-nm intervals of the high-resolution data of Meller et al. [518] at 236-493 nm. For the region 219-235 nm, the mean of the values of Meller et al. [518] and Staffelbach et al. [749] have been chosen.

The temperature dependence of the absorption cross sections is not significant, only minor changes of the order of 10% were observed in the spectrum between 298 and 248 K by Staffelbach et al. [749]. The largest changes occur in the structured region between 410 and 450 nm, where the fine structure becomes more pronounced at lower temperatures.

Quantum yields have been measured by Staffelbach et al. [749] from the determination of products after photolysis of dilute mixtures of methylglyoxal in air using a Xe arc equipped with different band pass filters to isolate several regions of the spectrum. The observed products (CO, CO_2, HCHO, CH_3COOH, CH_3COOOH, CH_3OH and HCOOH,) let to the conclusion that only channel (1) is important in the photolysis range 240-480 nm. The quantum yields were derived by modeling the products, using a number of secondary radical reactions. At 760 Torr, the ϕ_1 yields were: 0.005 for the wavelength region 410-418 nm, 0.055 for 355-480 nm, 0.07 for 280-240 nm and 0.14 for 240-420 nm. Raber and Moortgat [646] irradiated methylglyoxal in air at different total pressures using two types of broad-band lamps and determined the products (CO, CO_2, HCHO, CH_3OOH, CH_3OH, HCOOH, CH_3CHO, CH_3COOH, CH_3COOOH and $CH_3COCOOH$). Quantum yield derived by modeling the products of the photolysis in the 275-380 nm region varied from 0.94 ± 0.04 at 54 Torr to 0.64 ± 0.03 at 760 Torr, and in the 390-470 nm region from 0.41 ± 0.04 to 0.23 ± 0.02.

Koch and Moortgat [415] determined the quantum yields of CO, HCHO and CH_3CHO formation at 298 K as a function of wavelength (260-440 nm) and pressure of synthetic air (30-900 Torr) using "broad" monochromatic light, with an optical resolution of 8.5 nm. For photolysis in the short wavelength band (260-320 nm), the overall quantum yield was found to be unity, independent of wavelength and pressure. The analysis of the data gave evidence that channel (1) is the predominant photolysis path. In the long-wavelength band (380-440 nm) ϕ_{CO} showed Stern-Volmer pressure dependence, but in addition, ϕ_{HCHO} increased with methylglyoxal pressure, which was attributed to the reaction of excited methylglyoxal with ground state methylglyoxal.

The quantum yield of channel (1) in the wavelength range 250-500 nm was expressed as:

$$1/\phi(\lambda) = 1/\phi_0(\lambda) + P(\text{Torr}) / k(\lambda)$$

where $\phi_0(\lambda) = 1$ for $\lambda < 380$ nm

$\phi_0(\lambda) = (8.15 \pm 0.7)\ 10^{-9}\ [\exp(7131 \pm 267) / \lambda]$ for $\lambda > 380$ nm

$k(\lambda) = (7.34 \pm 0.1)\ 10^{-9}\ [\exp(8793 \pm 300) / \lambda]$

Chen et al. [749] photolysed methylglyoxal in N_2 in the range 290-440 nm at 10 nm intervals using a tunable dye laser, and measured the yield of HCO radicals using cavity ring-down spectroscopy. The yield of HCO radicals was calibrated against HCO produced in the photolysis or HCHO or Cl_2/HCHO mixtures. The yield of HCO radicals were unity in the range 320-360 nm, but decreased slightly at shorter wavelengths to 0.82 ± 0.06 at 290 nm, and strongly at $\lambda \geq 370$ nm to 0.17 ± 0.02 at 440 nm. They observed a weak dependence of the HCO yield on the methylglyoxal partial pressure. The HCO yields were independent of 10-400 Torr N_2-pressure between 290 to 370 nm, but showed a Stern-Volmer pressure dependence at $\lambda \geq 380$ nm in the form

$$1/\phi(\lambda) = 1/\phi_0(\lambda) + k_Q(\lambda)\ P(\text{Torr}),$$

where $\phi_0(\lambda) = (3.63 \pm 0.32)\ 10^{-7}\ [\exp(5693 \pm 533) / \lambda]$

and $k_Q(\lambda) = (1.93 \pm 0.24) \times 10^4\ [\exp(-(5639 \pm 497) / \lambda]$

Both sets of zero pressure quantum yields $\phi_0(\lambda)$ are in good agreement at $\lambda \leq 420$ nm, but quantum yields at 760 Torr from Chen et al. [159] (extrapolated to higher pressures) and Koch and Moortgat [415] deviate by a factor 4 at $\lambda \geq 420$ nm. The data of Chen et al. [159] are recommended, since they were measured directly. Additional measurements are needed to establish the quantum yields in the long wavelength tail of the spectrum at atmospheric relevant pressures.

Table 4-50. Absorption Cross Sections of $CH_3COC(O)H$ at 295-298 K

λ (nm)	$10^{20}\ \sigma$ (cm^2)	λ (nm)	$10^{20}\ \sigma$ (cm^2)	λ (nm)	$10^{20}\ \sigma$ (cm^2)	λ (nm)	$10^{20}\ \sigma$ (cm^2)	λ (nm)	$10^{20}\ \sigma$ (cm^2)
200	33.8	259	3.25	318	1.82	377	2.10	436	11.1
201	30.6	260	3.29	319	1.68	378	2.18	437	10.0
202	27.0	261	3.33	320	1.50	379	2.30	438	10.6
203	23.0	262	3.36	321	1.34	380	2.42	439	11.0
204	18.6	263	3.42	322	1.22	381	2.54	440	9.94
205	15.3	264	3.49	323	1.14	382	2.70	441	10.4
206	12.1	265	3.59	324	1.01	383	2.88	442	10.2
207	10.0	266	3.73	325	0.924	384	3.03	443	10.2

λ (nm)	10^{20} σ (cm^2)	λ (nm)	10^{20} σ (cm^2)	λ (nm)	10^{20} σ (cm^2)	λ (nm)	10^{20} σ (cm^2)	λ (nm)	10^{20} σ (cm^2)
208	8.52	267	3.87	326	0.848	385	3.20	444	11.2
209	7.43	268	4.02	327	0.774	386	3.39	445	9.62
210	6.34	269	4.13	328	0.716	387	3.61	446	8.91
211	5.58	270	4.20	329	0.672	388	3.71	447	9.84
212	4.73	271	4.22	330	0.647	389	3.88	448	9.19
213	4.16	272	4.23	331	0.620	390	4.03	449	10.1
214	3.57	273	4.27	332	0.608	391	4.22	450	8.68
215	3.08	274	4.31	333	0.525	392	4.31	451	6.35
216	2.65	275	4.37	334	0.531	393	4.47	452	6.33
217	2.33	276	4.49	335	0.495	394	4.57	453	6.08
218	2.10	277	4.64	336	0.455	395	4.67	454	4.47
219	1.46	278	4.77	337	0.407	396	4.87	455	3.69
220	1.45	279	4.87	338	0.362	397	5.08	456	3.09
221	1.44	280	4.92	339	0.346	398	5.26	457	2.47
222	1.43	281	4.93	340	0.322	399	5.46	458	1.81
223	1.44	282	4.90	341	0.300	400	5.62	459	1.28
224	1.43	283	4.83	342	0.289	401	5.90	460	0.914
225	1.44	284	4.76	343	0.288	402	6.07	461	0.795
226	1.46	285	4.70	344	0.289	403	6.36	462	0.643
227	1.48	286	4.66	345	0.295	404	6.55	463	0.480
228	1.51	287	4.65	346	0.308	405	6.92	464	0.332
229	1.53	288	4.73	347	0.325	406	7.20	465	0.268
230	1.60	289	4.84	348	0.339	407	7.59	466	0.228
231	1.61	290	4.92	349	0.362	408	7.95	467	0.188
232	1.65	291	4.90	350	0.385	409	8.12	468	0.160
233	1.67	292	4.81	351	0.424	410	8.52	469	0.133
234	1.75	293	4.70	352	0.463	411	8.64	470	0.108
235	1.83	294	4.57	353	0.492	412	9.07	471	0.0998
236	1.86	295	4.37	354	0.523	413	9.38	472	0.0897
237	1.93	296	4.17	355	0.556	414	9.62	473	0.0776
238	1.96	297	4.00	356	0.597	415	9.69	474	0.0680
239	2.00	298	3.88	357	0.635	416	9.72	475	0.0627
240	2.07	299	3.76	358	0.676	417	10.0	476	0.0561
241	2.14	300	3.69	359	0.720	418	10.1	477	0.0515
242	2.19	301	3.70	360	0.765	419	10.1	478	0.0483
243	2.23	302	3.74	361	0.816	420	10.2	479	0.0462
244	2.27	303	3.74	362	0.872	421	10.3	480	0.0392
245	2.30	304	3.62	363	0.933	422	10.5	481	0.0366
246	2.33	305	3.38	364	1.00	423	10.5	482	0.0315
247	2.38	306	3.15	365	1.08	424	10.2	483	0.0278
248	2.46	307	2.92	366	1.15	425	10.3	484	0.0271
249	2.57	308	2.71	367	1.23	426	10.0	485	0.0243
250	2.64	309	2.52	368	1.31	427	9.84	486	0.0217
251	2.68	310	2.34	369	1.40	428	10.0	487	0.0186
252	2.71	311	2.18	370	1.47	429	9.94	488	0.0181
253	2.73	312	2.06	371	1.55	430	10.4	489	0.0170
254	2.76	313	1.97	372	1.64	431	10.5	490	0.0174
255	2.82	314	1.90	373	1.73	432	9.79	491	0.0162
256	2.93	315	1.86	374	1.81	433	10.6	492	0.0161
257	3.06	316	1.86	375	1.90	434	10.5	493	0.0138
258	3.17	317	1.87	376	2.02	435	10.8		

Note:
200-218 nm, Staffelbach et al. [749],
219-235 nm, mean of Meller et al. [518] and Staffelbach et al. [749],
219-493 nm, Meller et al. [518].

D19. $HC(O)OH + h\nu \rightarrow HCO + OH$ (1)
$HC(O)OH + h\nu \rightarrow H + COOH$ (2)
$HC(O)OH + h\nu \rightarrow HCOO + H$ (3)
$HC(O)OH + h\nu \rightarrow H_2 + CO_2$ (4)
$HC(O)OH + h\nu \rightarrow H_2O + CO$ (5)

$(HC(O)OH)_2 + h\nu \rightarrow HCO + OH + HCOOH$ (6)
$(HC(O)OH)_2 + h\nu \rightarrow CO + H_2O + HCOOH$ (7)
$(HC(O)OH)_2 + h\nu \rightarrow H_2 + CO_2 + HCOOH$ (8). The absorption cross sections of formic acid at its dimer have been measured at 300 K and three pressures (35.2, 16.4, and 2.45 Torr) in the region 200-249 nm by McMillan [141]; at 302 K and 29 pressures (0.5-22 Torr) in the region 195–250 nm by Singleton et al. [738]; in connection with quantum yield measurements at 222 nm and 298 K by Jolly et al. [392]; and at 296 and 356.2 K by Singleton et al. [740]. The absorption spectrum of the dimer shows a broad maximum near 205 nm and a monotonic decrease in intensity with increasing wavelength. The absorption maximum of the monomer seems to appear at larger wavelengths near 215 nm and is only one third as intense as that of the dimer. The decrease in cross sections with increasing wavelength is more rapid for the dimer than for the monomer, resulting in monomer values higher by up to a factor 10 at 250 nm. The three absorption curves reported by Mc Millan [141] have been derived assuming monomers only in spite of undefined amounts of monomer and dimer contributions. They lie between those reported by Singleton et al. [738] for the monomer and the dimer. The recommended absorption cross sections are listed in Table 4-51, taken from the data of Singleton et al [738] measured at a resolution of 1 nm.

Earlier studies reported yields of final products CO, CO_2, H_2, H_2O (Calvert and Pitts [147]) and favoured molecular elimination paths (4) and (5) in the range 220-260 nm, which were difficult to distinguish between primary photolytic products and subsequent secondary free-radical reactions, originating from both monomer and dimer. Jolly et al. [392] determined the quantum yield of OH formation via path (3) at 222 nm for the monomer to be $\phi_{3,M} = 1.05 \pm 0.14$ and essentially $\phi_{3,D}$ = zero for the dimer. In a follow-up study Singleton et al. [740] redetermined the OH-quantum yields at 222 nm at two temperatures: $\phi_{3,M}(OH) = 0.704 \pm 0.048$ at 298 K and 0.771 ± 0.030 at 356.2 K for the monomer, and $\phi_{3,D}(OH) = 0.153 \pm 0.028$ at 298 K for the dimer (the OH yield for the dimer at elevated temperatures was assumed to be zero). Photodissociation into the other radical channels (2) and (3) is minor, and has been discussed by He and Fang [322]. Photodissociation quantum yields for the dimer were determined by Singleton et al. [739] to be $\phi_{6,D} = 0.15$, $\phi_{7,D} = 0.81$ an $\phi_{8,D} = 0.04$.

Table 4-51. Absorption Cross Sections of HC(O)OH and $(HC(O)OH)_2$ at 302 K

λ (nm)	10^{20} σ (cm^2) monomer	dimer	λ (nm)	10^{20} σ (cm^2) monomer	dimer
195	9.18	27.4	223	11.9	17.0
196	9.96	29.1	224	11.3	15.5
197	9.57	30.8	225	10.9	14.1
198	10.0	32.2	226	9.87	12.7
199	10.7	33.3	227	10.4	11.3
200	10.7	34.6	228	9.24	10.1
201	11.5	35.4	229	9.15	8.87
202	11.9	36.2	230	8.12	7.78
203	12.5	36.7	231	7.18	6.77
204	12.5	37.3	232	7.07	5.87
205	13.8	37.4	233	6.44	5.01
206	13.6	37.4	234	6.68	4.26
207	13.7	37.2	235	5.24	3.58
208	13.6	36.9	236	5.40	2.95
209	14.1	36.2	237	4.10	2.46
210	14.4	35.5	238	4.32	2.03
211	14.2	34.6	239	3.58	1.63
212	13.6	33.6	240	3.79	1.31
213	14.3	32.4	241	2.79	1.02
214	14.9	31.0	242	2.83	0.795
215	15.0	29.4	243	1.98	0.659
216	13.7	28.1	244	2.10	0.490
217	13.6	26.7	245	1.73	0.337
218	13.4	25.1	246	1.79	0.267
219	13.5	23.4	247	1.18	0.190
220	12.9	21.8	248	1.23	0.134
221	11.6	20.2	249	0.855	0.093
222	12.4	18.6	250	0.861	0.072

Note:
199-250 nm, Singleton et al. [738].

D20. $CH_3C(O)OH + h\nu \rightarrow CH_4 + CO_2$ (1)
$CH_3C(O)OH + h\nu \rightarrow CH_3CO + OH$ (2)
$CH_3C(O)OH + h\nu \rightarrow CH_3 + COOH$ (3)
$CH_3C(O)OH + h\nu \rightarrow CH_3COO + H$ (4). The absorption cross sections of acetic acid at its dimer have been measured at 300 K and four pressures (12.9, 11.0, 8.3, and 3.6 Torr) in the region 200-241 nm by McMillan [146]; at 270 K and pressures of 0.15-1.5 Torr and at 298, 325, and 345 K and pressures of 0.12-3.6 Torr in the region 210-245 nm by Orlando and Tyndall [609]; and in connection with quantum yield measurements at 222 nm and 298 and 356.2 K by Singleton et al. [740]. The monomer spectrum reported by Orlando and Tyndall [609] displays a broad maximum near 207 nm and a monotonic decrease in intensity with increasing wavelength. The absorption maximum for the dimer appears at shorter wavelength below 205 nm and is twice as intense as that of the monomer. The decrease in cross sections with increasing wavelength is more rapid for the dimer than for the monomer, resulting in monomer values higher by up to a factor 6 than the dimer values at 240 nm. The four absorption curves reported by Calvert and Pitts [146] have been derived assuming monomers only in spite of undefined amounts of monomer and dimer contributions. The absorption curve for the highest pressure is close to the dimer curve reported by Orlando and Tyndall [609], and the other curves are shifted to lower absorption cross sections with decreasing temperature, but do not correspond with the monomer curve reported by Orlando and Tyndall [609]. The recommended absorption cross sections are listed in Table 4-52 at 2-nm intervals reported by Orlando and Tyndall [609] (measurements at 0.6-nm resolution).

Earlier studies reported yields of final products CO, CO_2, CH_4, and C_2H_6 (Calvert and Pitts [146]) and proposed molecular elimination path (1) and radical reactions (2) to (4) originating from the monomer. Hunnicutt et al. [354] photolysed acetic acid at 218 nm and determined channel (2) to be the dominant

photochemical path using photofragment laser fluorescence. Singleton et al. [740] determined the OH-quantum yield at 222 nm at two temperatures: $\phi_{2,M}(OH) = 0.546 \pm 0.097$ at 298 K, and 0.692 ± 0.024 at 356.2 K for the monomer, and $\phi_{2,D}(OH) = 0.038 \pm 0.026$ at 298 K for the dimer ($\phi_{2,D}(OH) = 0$ assumed for the dimer at elevated temperatures).

Table 4-52. Absorption Cross Sections of $CH_3C(O)OH$ and $(CH_3C(O)OH)_2$ at 298 K

λ (nm)	$10^{20}\sigma$ (cm^2) monomer	dimer	λ (nm)	$10^{20}\sigma$ (cm^2) monomer	dimer
210	15.1	23.4	228	6.00	3.60
212	14.7	20.9	230	5.09	2.45
214	13.5	18.4	232	4.20	1.71
216	12.5	15.8	234	3.44	1.11
218	11.7	13.2	236	2.71	0.65
220	10.5	10.9	238	2.11	0.45
222	9.33	8.54	240	1.64	0.27
224	8.19	6.68	242	1.19	
226	7.17	4.95	244	0.89	

Note:
210-244 nm, Orlando and Tyndall [609].

D21. $CH_3C(O)OOH + h\nu \rightarrow$ Products. The absorption cross sections of peracetic acid have been measured at 248 and 298 K and 205-340 nm by Orlando and Tyndall [609]. The absorption cross sections decrease in a monotonic, pseudo-exponential fashion with increasing wavelength. The spectrum recorded at 248 K shows an apparently faster fall-off with increasing wavelengths than that recorded at room temperature. In Table 4-53 are listed the data at 2-nm intervals reported by Orlando and Tyndall [609] (measurements at 0.6-nm resolution).

Table 4-53. Absorption Cross Sections $CH_3C(O)OOH$ at 298 K

λ (nm)	10^{20} σ (cm^2)	λ (nm)	10^{20} σ (cm^2)	λ (nm)	10^{20} σ (cm^2)	λ (nm)	10^{20} σ (cm^2)
210	38.1	244	4.31	278	0.574	312	0.045
212	33.1	246	3.82	280	0.506	314	0.044
214	29.5	248	3.41	282	0.444	316	0.040
216	25.4	250	3.05	284	0.386	318	0.035
218	21.7	252	2.71	286	0.334	320	0.025
220	18.9	254	2.42	288	0.297	322	0.020
222	16.0	256	2.16	290	0.256	324	0.020
224	13.9	258	1.93	292	0.226	326	0.017
226	12.0	260	1.71	294	0.193	328	0.014
228	10.5	262	1.53	296	0.170	330	0.009
230	9.10	264	1.35	298	0.141	332	0.011
232	8.01	266	1.21	300	0.123	334	0.011
234	7.03	268	1.06	302	0.107	336	0.009
236	6.31	270	0.945	304	0.094	338	0.009
238	5.61	272	0.835	306	0.078	340	0.006
240	5.03	274	0.742	308	0.069		
242	4.83	276	0.651	310	0.062		

Note:
Orlando and Tyndall [609].

D22. $C_2H_5C(O)OH + h\nu \rightarrow$ Products. Absorption cross sections for propionic acid and its dimer have been measured at 298 and 356.2 K and 222 nm by Singleton et al. [740]. At 298 K, $\sigma = 12.2 \times 10^{-20}$ cm^2 $molecule^{-1}$, and at 356.2 K, $\sigma = 10.6 \times 10^{-20}$ cm^2 $molecule^{-1}$ for the monomer. For the dimer at 298 K, $\sigma = 10.6 \times 10^{-20}$ cm^2 $molecule^{-1}$, and at 356.2 K , $\sigma = 25.6 \times 10^{-20}$ cm^2 $molecule^{-1}$ (obtained by an extrapolation procedure).

Quantum yields for the formation of OH radicals at 222 nm have been also measured by Singleton et al. [740]: For the monomer, $\Phi = 0.148 \pm 0.90$ and 0.341 ± 0.014 for the monomer at 297.6 and 375.0 K, respectively. For the dimer, $\Phi = 0.018 \pm 0.06$ at 297.6 K ($\Phi = 0$ assumed for the dimer at elevated temperatures).

D23. $CH_3C(O)C(O)OH + h\nu \rightarrow CH_3CHO + CO_2$ (1)
$CH_3C(O)C(O)OH + h\nu \rightarrow CH_3CO + COOH$ (2)
$CH_3C(O)C(O)OH + h\nu \rightarrow CH_3COOH + CO$ (3)
$CH_3C(O)C(O)OH + h\nu \rightarrow CH_3CO + CO + OH$ (4). The absorption cross sections of pyruvic acid have been measured at room temperature and at high resolution (diode array spectrometer) between 250 and 410 nm by Horowitz et al. [341] and between 290 and 380 nm by Mellouki and Mu [519]. The absorption spectrum of pyruvic acid, reported as a plot of relative absorbances vs. wavelength, was also measured at 358 K and 250-400 nm by Yamamoto and Back [855]. The value $\sigma = 3.82 \times 10^{-20}$ cm^2 $molecule^{-1}$ for the absorption maximum at 350 nm given by Yamamoto and Back [855] was used by Horowitz et al. [341] to normalize the relative spectrum. The general shapes of the three spectra are quite similar to each other. The spectrum obtained by Yamamoto and Back [855], however, is shifted to the red and the cross sections below 300 nm are considerably higher as compared with the spectrum reported by Horowitz et al. [341], differences which in part can be ascribed to the effect of temperature. The cross sections measured by Mellouki and Mu [519] are systematically higher than those obtained by Horowitz et al. [341]. This difference reaches a factor two for wavelengths below 295 nm and is ~20-30% between 305 and 370 nm. These discrepancies can be attributed to the difficulties in handling the pyruvic acid sample and measurement of the concentrations. The recommended absorption cross sections listed in Table 4-54 are 1-nm averages of the high-resolution data of Horowitz et al. [341] at 252-285 nm, the mean of the data of Horowitz et al. [341] and Mellouki and Mu [519] (both 1-nm averages) at 290-380 nm, and the data of Horowitz et al. [341] at 385-399 nm.

Vesley and Leermakers [816] reported quantum yields of CO_2 of 1.02 ± 0.06 and of CH_3CHO of 0.6 by the photolysis at 366 nm. Yamamoto and Back [855] measured quantum yields of CO_2 of 0.9 ± 0.1 and CH_3CHO of 0.45 at 366 nm and 340 K, but the CH_3CHO yields were more variable at 320 and 345 nm. Berges and Warneck [67] measured the quantum yields for the products CH_3CHO, CO_2 and CH_3COOH in the 350 nm decomposition to be 0.48 ± 0.01, 1.27 ± 0.18 and 0.14, respectively. In the presence of NO_2, the quantum yield of CH_3CHO was reduced to 0.30 ± 0.04 and PAN was formed with a quantum yield of 0.15 ± 0.02. Berges and Warneck [67] established the quantum yields for the photolysis channels: $\phi_1 = 0.48 \pm 0.01$

and $\phi_2 = 0.39 \pm 0.10$. Mellouki and Mu [519] used a laser flash photolysis system at 355 nm to photolyse pyruvic acid, and observed the formation of OH originating via channel (4) with a quantum yield of $\phi_4 = 0.05 \pm 0.03$. Effective quantum yields were obtained in an outdoor photoreactor to be $\phi_{eff} = 0.43 \pm 0.07$ as reported by Moortgat [553]. The analysis of the products CH_3CHO, CO, CH_3COOH by Winterhalter et al. [850] are consistent with the data of Berges and Warneck [67], and lead to a quantum yield of channel (3) $\phi_3 = 0.08 \pm 0.03$.

Table 4-54. Absorption Cross Sections of $CH_3C(O)C(O)OH$ at 298 K

λ (nm)	10^{20} σ (cm^2)	λ (nm)	10^{20} σ (cm^2)	λ (nm)	10^{20} σ (cm^2)	λ (nm)	10^{20} σ (cm^2)	λ (nm)	10^{20} σ (cm^2)
252	1.54	280	0.118	312	1.34	340	3.93	368	3.16
253	1.55	281	0.101	313	1.42	341	3.94	369	3.52
254	1.61	282	0.093	314	1.49	342	4.19	370	3.26
255	1.56	283	0.098	315	1.57	343	4.24	371	2.87
256	1.52	284	0.104	316	1.69	344	4.17	372	2.04
257	1.41	285	0.113	317	1.83	345	4.26	373	1.76
258	1.25	290	0.302	318	1.94	346	4.46	374	1.68
259	1.07	291	0.323	319	2.05	347	4.58	375	1.22
260	0.908	292	0.370	320	2.17	348	4.73	376	1.09
261	0.801	293	0.409	321	2.31	349	4.92	377	0.950
262	0.737	294	0.439	322	2.41	350	4.98	378	0.842
263	0.718	295	0.470	323	2.50	351	4.79	379	0.688
264	0.718	296	0.491	324	2.54	352	4.63	380	0.521
265	0.700	297	0.519	325	2.60	353	4.54	385	0.097
266	0.651	298	0.548	326	2.72	354	4.47	386	0.084
267	0.566	299	0.594	327	2.78	355	4.13	387	0.077
268	0.470	300	0.639	328	2.84	356	3.89	388	0.066
269	0.367	301	0.678	329	2.98	357	3.66	389	0.056
270	0.278	302	0.724	330	3.15	358	3.41	390	0.047
271	0.224	303	0.775	331	3.35	359	3.22	391	0.034
272	0.195	304	0.822	332	3.66	360	3.44	392	0.031
273	0.185	305	0.898	333	3.87	361	3.59	393	0.026
274	0.182	306	0.977	334	3.91	362	3.37	394	0.015
275	0.188	307	1.04	335	3.96	363	3.01	395	0.011
276	0.189	308	1.13	336	4.02	364	2.85	396	0.006
277	0.180	309	1.21	337	4.02	365	2.86	397	0.002
278	0.164	310	1.22	338	3.99	366	2.80	398	0.002
279	0.139	311	1.27	339	3.956	367	2.88	399	<0.001

Note:
252-285 nm, Horowitz et al. [341],
290-380 nm, mean of the data of Horowitz et al. [341] and Mellouki and Mu [519],
385-399 nm, Horowitz et al. [341].

D24. $HC(O)OCH_3 + h\nu \rightarrow$ Products. The absorption cross sections of methyl formate have been measured at room temperature and 201-260 nm by McMillan [142] and at 211-260 nm by Vésine and Mellouki [815]. The spectrum exhibits a structured absorption band with the maximum near 215 nm. There is very good agreement, i.e., ≤ 10%, between the results of both studies. As a recommendation we list in Table 4-55 the data of McMillan [142] at 202-210 nm (read from a plot) and the data of Vésine and Mellouki [815] at 211-260 nm, which are averages over 1- and 2-nm intervals in the ranges 211-230 and 230-260 nm, respectively, of the high-resolution (0.04 nm) spectrum.

Table 4-55. Absorption Cross Sections of $HC(O)OCH_3$ at 297-298 K

λ (nm)	10^{20} σ (cm^2)	λ (nm)	10^{20} σ (cm^2)	λ (nm)	10^{20} σ (cm^2)	λ (nm)	10^{20} σ (cm^2)
202	16.2	213	20.3	224	16.8	240	3.56
203	17.0	214	21.2	225	15.7	242	2.65
204	17.9	215	21.1	226	14.0	244	1.65
205	18.2	216	20.3	227	12.5	246	1.24
206	18.7	217	19.3	228	12.4	248	0.770
207	18.9	218	19.7	229	12.3	250	0.480
208	19.1	219	20.0	230	11.3	252	0.301
209	19.5	220	19.2	232	8.36	254	0.162
210	20.4	221	17.9	234	7.48	256	0.0717
211	20.4	222	16.7	236	6.11	258	0.0455
212	20.1	223	16.6	238	4.15	260	0.0281

Note:
202-210 nm, McMillan [142],
211-260 nm, Vésine and Mellouki [815].

D25. $HC(O)OC_2H_5 + h\nu \rightarrow$ Products. The absorption cross sections of ethyl formate have been measured at room temperature and 201-260 nm by McMillan [142] and at 211-260 nm by Vésine and Mellouki [815]. The spectrum exhibits a structured absorption band with the maximum near 215 nm. The agreement between the data of both studies is within ~15%, where the data of Vésine and Mellouki [815] are always lower than the data of McMillan [142] in the range 211-236 nm. An explanation for the discrepancy could not be found by Vésine and Mellouki [815]. As a recommendation we list in Table 4-56 the data of Vésine and Mellouki [815] at 211-260 nm, which are averages over 1- and 2-nm intervals in the ranges 211-230 and 230-260 nm, respectively, of the high-resolution (0.04 nm) spectrum.

Table 4-56. Absorption Cross Sections of $HC(O)OC_2H_5$ at 297 K

λ (nm)	10^{20} σ (cm^2)	λ (nm)	10^{20} σ (cm^2)	λ (nm)	10^{20} σ (cm^2)	λ (nm)	10^{20} σ (cm^2)
211	18.6	220	17.8	229	11.2	246	1.47
212	18.6	221	17.1	230	11.0	248	1.04
213	18.3	222	15.9	232	9.03	250	0.665
214	18.5	223	15.1	234	7.21	252	0.405
215	19.0	224	15.0	236	6.50	254	0.251
216	18.9	225	14.9	238	4.96	256	0.119
217	18.1	226	14.0	240	3.67	258	0.0611
218	17.5	227	12.6	242	3.00	260	0.0391
219	17.6	228	11.5	244	2.18		

Note:
211-260 nm, Vésine and Mellouki [815].

D26. $HCN + h\nu \rightarrow$ Products. Herzberg and Innes [329] have studied the spectroscopy of hydrogen cyanide, HCN, that starts absorbing weakly at $\lambda < 190$ nm.

The solar photodissociation rate for this molecule is rather small, even in the upper stratosphere; estimates of this rate would require additional studies of the absorption cross sections and quantum yields in the 200-nm region.

D27. $CH_3CN + h\nu \rightarrow$ Products. McElcheran et al. [506] have reported the spectrum of acetonitrile or methyl cyanide, CH_3CN; the first absorption band appears at $\lambda < 220$ nm. More recently, Suto and Lee [759] and Zetzsch [876] have measured the cross sections around 200 nm; solar photodissociation is unimportant compared to reaction with OH radicals.

PHOTOCHEM-E

E1. $FO_2 + h\nu \rightarrow F + O_2$. After two earlier studies with FO_2 in liquid argon at 87 K by Chegodaev and Tupikov [158] and Matchuk et al. [494], the absorption spectrum of the fluoroperoxy radical in the gas phase has been measured at room temperature and 206-250 nm by Pagsberg et al. [620]; at 186–276 nm by Maricq and Szente [481]; at 215-254 nm by Ellermann et al. [228]; and a single value for $\lambda = 215$ nm has been reported by Lyman and Holland [463]. The results of Maricq and Szente [481], Ellermann et al. [228], and Lyman and Holland [463] are in excellent agreement, whereas the cross sections reported by Pagsberg et al. [620] are

larger by a factor of 1.4-1.8 between 206 and 245 nm, and larger by a factor 3 at 250 nm. As a recommendation we list the absorption cross sections reported by Maricq and Szente [481] in Table 4-57.

Table 4-57. Absorption Cross Sections of FO_2 at 295 K

λ (nm)	10^{20} σ (cm^2)	λ (nm)	10^{20} σ (cm^2)	λ (nm)	10^{20} σ (cm^2)
185.9	950	214.2	1150	242.5	139
188.5	1050	216.8	1050	245.1	112
191.1	1130	219.4	933.	247.6	82
193.6	1180	221.9	796	250.2	60
196.2	1200	224.5	677	252.8	51
198.8	1260	227.1	558	255.3	43
201.4	1310	229.6	451	257.9	36
203.9	1330	232.2	368	260.5	32
206.5	1350	234.8	289	263.1	26
209.1	1300	237.4	233	265.6	20
211.6	1240	239.9	173		

Note: 185.9-265.6 nm, Maricq and Szente [481].

E2. $F_2O + h\nu \rightarrow F_2 + O$

$F_2O + h\nu \rightarrow F + FO$. The absorption spectrum of fluorine oxide has been measured at 273 K and 210-546 nm by Glissmann and Schuhmacher [286]. Their data are listed in Table 4-58.

Table 4-58. Absorption Cross Sections of F_2O at 273 K

λ (nm)	10^{20} σ (cm^2)	λ (nm)	10^{20} σ (cm^2)	λ (nm)	10^{20} σ (cm^2)	λ (nm)	10^{20} σ (cm^2)
210.2	4.88	239.9	0.65	296.7	0.12	404.0	0.020
211.4	3.39	244.7	0.50	302.7	0.12	421.0	0.023
213.7	3.06	248.2	0.37	313.1	0.11	428.0	0.021
216.5	2.73	253.7	0.27	334.0	0.087	435.8	0.018
218.1	2.60	257.6	0.21	350.0	0.072	445.0	0.017
221.0	2.21	265.5	0.15	365.0	0.064	458.0	0.015
223.6	1.95	270.0	0.13	378.0	0.055	471.5	0.012
225.3	1.76	275.9	0.12	380.0	0.044	491.6	0.0091
229.5	1.30	280.6	0.12	387.0	0.033	513.5	0.0052
234.5	1.14	289.3	0.12	395.0	0.023	546.0	0.0052
237.8	0.78	292.5	0.12	399.0	0.020		

Note:
210-546 nm, Glissmamm and Schuhmacher [286].

E3. $F_2O_2 + h\nu \rightarrow$ Products. The absorption cross sections of dioxygen difluoride in the gas phase have been measured at 273 K and 220-522.5 nm by Brodersen et al. [99], 193 K and 197-260 nm by Chegodaev and Tupikov [158], at 195 K and 350-600 nm by Matchuk et al. [494], and at 298 K and 215 nm by Lyman and Holland [463]. A measurement with liquid F_2O_2 in liquid freon at 77 K and 200-480 nm has been reported by Kirshenbaum and Streng [410]. The absorption spectrum shows the long-wavelength wing of an absorption band, whose maximum is somewhere below 200 nm, and a weak shoulder at ~250-300 nm. A hump around 405 nm observed by Brodersen et al. [99] did not appear in the spectra reported by Matchuk et al. [494] and Kirshenbaum and Streng [410]. There is good agreement at 220-250 nm (within 10-15%) between the data of Brodersen et al. [99] and Chegodaev and Tupikov [158]. The 250-360-nm region of the absorption curve reported by Brodersen et al. [99] connects well the absorptions curves reported by Chegodaev and Tupikov [158] and Matchuk et al. [494]. We therefore list as recommended values in Table 4-59 the results of Chegodaev and Tupikov [158] at 200-250 nm, those of Brodersen et al. [99] at 260-360 nm, and the data of Matchuk et al. [494] for the 370-600 nm region.

Table 4-59. Absorption Cross Sections of F_2O_2 at 193-195 and 273 K

λ (nm)	10^{20} σ (cm^2)	λ (nm)	10^{20} σ (cm^2)	λ (nm)	10^{20} σ (cm^2)
200	700	340	10.9	480	0.34
210	325	350	7.54	490	0.27
220	208	360	5.90	500	0.24
230	145	370	5.15	510	0.22
240	107	380	4.50	520	0.20
250	87.9	390	3.77	530	0.19
260	98.2	400	3.06	540	0.17
270	86.7	410	2.46	550	0.15
280	72.5	420	1.97	560	0.13
290	60.6	430	1.57	570	0.11
300	44.7	440	1.25	580	0.09
310	32.4	450	0.96	590	0.07
320	22.3	460	0.69	600	0.04
330	15.4	470	0.47		

Note:
200-250 nm (193 K), Chegodaev and Tupikov [158],
260-360 nm (273 K), Brodersen et al. [99],
370-600 nm (195 K), Matchuk et al. [494].

E4. $HF + h\nu \rightarrow H + F$. The ultraviolet absorption spectrum of HF has been measured at 289.5, 326, 373, and 438 K and 153-182 nm by Safary et al. [696] and Safary [695]; at room temperature and 107-145 nm by Nee et al. [575]; and, applying electron energy-loss spectroscopy, at 298 K and 8-155 nm by Carnovale et al. [153], and 30-200 nm by Hitchcock et al. [333]. There is no absorption at $\lambda > 180$ nm, so that photodissociation of HF should be unimportant in the stratosphere.

E5. $FNO + h\nu \rightarrow F + NO$. The absorption cross sections of nitrosyl fluoride have been measured at room temperature and 180-350 nm by Burley et al. [121], who report their results in graphical form as well as in tabular form at 1-nm intervals. The spectrum shows vibronic structure at wavelengths longer than 250 nm. The cross section values are listed in Table 4-60 at 2-nm intervals for the continuous part of the absorption curve and at 1-nm intervals for the structured part ($\lambda > 260$ nm). Two single values at 310.5 nm (strongest vibrational peak) and 195 K measured by Johnston and Bertin [383] and at 298 K measured by Pagsberg et al. [619] fit well to the absorption curve reported by Burley et al. [121]. The quantum yield for decomposition is expected to be unity (Brandon et al. [85], Reid et al. [670]).

Table 4-60. Absorption Cross Sections of FNO at 298 K

λ (nm)	10^{20} σ (cm^2)	λ (nm)	10^{20} σ (cm^2)	λ (nm)	10^{20} σ (cm^2)	λ (nm)	10^{20} σ (cm^2)
180	52.4	246	1.65	286	5.17	319	21.4
182	51.7	248	1.41	287	5.78	320	15.2
184	50.7	250	1.54	288	10.4	321	35.6
186	49.4	252	1.25	289	16.6	322	40.2
188	47.5	254	1.23	290	17.0	323	25.5
190	45.1	256	1.36	291	11.3	324	17.8
192	42.7	258	1.58	292	11.9	325	14.3
194	40.0	260	1.30	293	18.1	326	12.1
196	37.3	261	1.45	294	7.11	327	9.40
198	33.8	262	1.64	295	6.75	328	9.39
200	30.5	263	1.85	296	9.15	329	12.4
202	27.7	264	2.03	297	14.1	330	12.9
204	24.8	265	2.67	298	22.0	331	11.3
206	22.2	266	1.96	299	23.1	332	13.0
208	19.9	267	1.99	300	15.6	333	18.9
210	17.6	268	2.10	301	23.1	334	19.3
212	15.8	269	2.66	302	25.4	335	16.1
214	13.9	270	2.81	303	10.4	336	13.1
216	12.3	271	3.06	304	8.85	337	10.8
218	10.7	272	4.47	305	10.4	338	8.96
220	9.35	273	4.30	306	11.8	339	7.13
222	8.32	274	3.97	307	15.6	340	5.65
224	7.22	275	3.77	308	32.2	341	4.61
226	6.30	276	4.24	309	21.8	342	3.81
228	5.44	277	4.44	310	15.5	343	3.17
230	4.68	278	3.41	311	54.2	344	2.68
232	4.10	279	5.03	312	31.6	345	2.30
234	3.52	280	8.26	313	16.0	346	1.96
236	3.09	281	10.1	314	12.3	347	1.72
238	2.76	282	7.58	315	11.7	348	1.48
240	2.25	283	6.59	316	11.0	349	1.30
242	2.08	284	7.26	317	13.0	350	1.18
244	1.74	285	7.45	318	25.5		

Note:
180-350 nm, Burley et al. [121]

E6. $CF_4 + h\nu \rightarrow$ products. See note E7.

E7. $C_2F_6 + h\nu \rightarrow$ products. CF_4 and C_2F_6 do not absorb in the ultraviolet at wavelengths longer than 105 and 120 nm, respectively (Sauvageau et al. [707, 708]; Inn, [364]); therefore, they are not expected to photodissociate until they reach the mesosphere.

E8. $COF_2 + h\nu \rightarrow COF + F$. The absorption cross-sections of COF_2 (carbonyl difluoride, difluorophosgene) have been measured at room temperature and 185-226 nm by Chou et al. [170]; at 186-224 nm by Molina and Molina [540]; and at 199-232 nm by Nölle et al. [590]. This wavelength region covers the long-wavelength wing of an absorption band. The high-resolution spectrum reported by Nölle et al. [590] is highly structured. Comparison of values averaged over the 500-cm^{-1} intervals used for atmospheric modeling shows that the data of Nölle et al. [590] are somewhat higher than those of Molina and Molina [540] with differences between 1.5 and 22%. The data of Chou et al. [170] are in good agreement with the data of Molina and Molina [540] at 186-197 nm, but disagreement becomes steadily larger with increasing wavelength by up to more than 200%. We follow our earlier recommendation of 1997 and list in Table 4-61 the 500-cm^{-1} averages of Molina and Molina [540] for the range 186-199 nm and those of Nölle et al. [590] at larger wavelengths.

The COF + F quantum yields were determined at 193 nm using an excimer laser, and at 210 and 220 nm using a Hg medium pressure lamp by Nölle et al. [591]. The "apparent" quantum yields for pure COF_2, $\Phi' = 0.47 \pm 0.03$, 0.57 ± 0.05, and 0.11 ± 0.02 were obtained at 193, 210 and 220 nm, respectively. In the case of

the laser photolysis at 193 nm, where high concentrations of COF are formed, the self-reaction of the COF photodissociation product regenerates COF_2 via COF + COF → COF_2 + CO. Under the assumption that all COF radicals quantitatively react in this way, hence the quantum yield becomes $\Phi_{193} = 0.94 \pm 0.06$. The quantum yields at 210 and 220 nm obtained with the lamp are the "true" values. A quantum yield of 0.26 at 206 nm reported by Molina and Molina [540] is considered to be too low by Nölle et al. [591].

Table 4-61. Absorption Cross Sections of COF_2 at 298 K

λ (nm)	10^{20} σ (cm^2)	λ (nm)	10^{20} σ (cm^2)	λ (nm)	10^{20} σ (cm^2)
186.0	5.5	199.0	1.6	213.9	0.188
187.8	4.8	201.0	1.32	216.2	0.120
189.6	4.2	203.1	0.987	218.6	0.077
191.4	3.7	205.1	0.754	221.0	0.046
193.2	3.1	207.3	0.508	223.5	0.032
195.1	2.6	209.4	0.392	226.0	0.021
197.0	2.1	211.6	0.272	228.6	0.015

Note:
186-199 nm, Molina and Molina [540],
201-229 nm, Nölle et al. [590].

E9. COHF + hν → HF + CO
COHF + hν → H + FCO
COHF + hν → F + HCO. The absorption spectrum of COHF (formyl fluoride) has been measured at room temperature and 195-255 nm by Giddings and Innes [268]; at 194-267 nm by Meller (see Röth et al. [687]); and at 220-267 nm by Rattigan et al. [653]. The latter authors found the absorption cross-sections to be independent of temperature in the range 233-318 K. The high-resolution measurements show the long-wavelength wing of a highly structured absorption band. The absorption cross-sections measured using conventional methods by Giddings and Innes [268] are larger by nearly a factor two than the high-resolution (0.016 nm) data obtained by Meller (see Röth et al. [687]) using diode array spectrometry. The cross-sections measured by Rattigan et al. [653] at a resolution of 1.2 nm lie between the latter two data sets in the range 220-230 nm and nearer to the data of Giddings and Innes [268] at 230-245 nm. In Table 4-62 we recommend the averages over 1-nm intervals of the high-resolution data of Meller (see Röth et al. [687]).

Table 4-62. Absorption Cross Sections of COHF at 298 K

λ (nm)	10^{20} σ (cm^2)	λ (nm)	10^{20} σ (cm^2)	λ (nm)	10^{20} σ (cm^2)	λ (nm)	10^{20} σ (cm^2)
200	8.28	217	7.38	234	2.98	251	0.151
201	9.75	218	7.97	235	2.04	252	0.241
202	8.30	219	6.28	236	2.28	253	0.213
203	7.55	220	6.85	237	1.24	254	0.071
204	8.52	221	5.70	238	1.71	255	0.123
205	10.15	222	6.07	239	1.75	256	0.0674
206	8.28	223	6.58	240	1.55	257	0.0520
207	7.41	224	4.94	241	0.967	258	0.0382
208	8.44	225	5.33	242	1.19	259	0.0446
209	9.55	226	4.00	243	0.575	260	0.0427
210	7.76	227	4.65	244	0.765	261	0.0232
211	7.36	228	4.43	245	0.675	262	0.0153
212	7.92	229	4.61	246	0.719	263	0.0156
213	8.56	230	3.57	247	0.412	264	0.0170
214	9.22	231	2.55	248	0.484	265	0.0126
215	7.67	232	3.16	249	0.279	266	0.0118
216	6.51	233	3.09	250	0.210		

Note:
200-266 nm, Meller (see Röth et al. [687]).

E10. CF3OH + hν → Products. An upper limit of 10^{-21} cm^2 has been determined experimentally by Molina and Molina [544] for the absorption cross sections of CF_3OH in the 185–300-nm wavelength range. This upper

limit is in agreement with estimates based on similarities between CF_3OH and CH_3OH, as well as with quantum chemistry calculations, as reported by Schneider et al. [715].

E11. $CF_3OOCF_3 + h\nu \rightarrow 2\ CF_3O$. The absorption spectrum of hexafluorodimethyl peroxide has been measured at room temperature and 200-263 nm by Meller and Moortgat [515]. The spectrum shows a part of a broad absorption band originating near 265 nm and increasing cross sections with decreasing wavelengths. Absorption cross sections averaged over 1-nm intervals of the medium-resolution (0.2 nm) results of Meller and Moortgat [515] are listed in Table 4-63.

Table 4-63. Absorption Cross Sections CF_3OOCF_3 at 298 K.

λ (nm)	10^{20} σ (cm^2)	λ (nm)	10^{20} σ (cm^2)	λ (nm)	10^{20} σ (cm^2)	λ (nm)	10^{20} σ (cm^2)
200	3.61	216	1.25	232	0.501	248	0.204
201	3.37	217	1.18	233	0.462	249	0.195
202	3.13	218	1.10	234	0.433	250	0.183
203	2.92	219	1.04	235	0.408	251	0.174
204	2.73	220	0.983	236	0.380	252	0.166
205	2.53	221	0.926	237	0.361	253	0.157
206	2.35	222	0.869	238	0.339	254	0.147
207	2.20	223	0.822	239	0.323	255	0.138
208	2.06	224	0.778	240	0.303	256	0.132
209	1.94	225	0.737	241	0.288	257	0.125
210	1.80	226	0.693	242	0.274	258	0.119
211	1.69	227	0.654	243	0.263	259	0.112
212	1.61	228	0.614	244	0.246	260	0.107
213	1.51	229	0.584	245	0.240	261	0.101
214	1.42	230	0.555	246	0.227	262	0.096
215	1.33	231	0.525	247	0.214	263	0.091

Note:
200-263 nm, Meller and Moortgat [515].

E12. $CF_3O_3CF_3 + h\nu \rightarrow$ Products. The absorption spectrum of hexafluorodimethyl trioxide has been measured at room temperature and 200-312 nm by Meller and Moortgat [515]. The spectrum shows a part of a broad absorption band originating near 312 nm and increasing cross sections with decreasing wavelengths. Absorption cross sections averaged over 1-nm intervals of the medium-resolution (0.2 nm) results of Meller and Moortgat [515] are listed in Table 4-64.

Table 4-64. Absorption Cross Sections $CF_3O_3CF_3$ at 298 K.

λ (nm)	10^{20} σ (cm^2)	λ (nm)	10^{20} σ (cm^2)	λ (nm)	10^{20} σ (cm^2)	λ (nm)	10^{20} σ (cm^2)
200	46.9	229	20.3	258	4.26	287	0.565
201	45.5	230	19.5	259	3.99	288	0.526
202	44.2	231	18.8	260	3.73	289	0.491
203	42.8	232	18.0	261	3.51	290	0.458
204	41.4	233	17.2	262	3.28	291	0.427
205	40.2	234	16.5	263	3.07	292	0.400
206	39.0	235	15.7	264	2.86	293	0.373
207	37.9	236	15.0	265	2.67	294	0.347
208	37.0	237	14.3	266	2.50	295	0.325
209	36.1	238	13.7	267	2.33	296	0.302
210	35.2	239	13.0	268	2.17	297	0.281
211	34.4	240	12.3	269	2.03	298	0.262
212	33.6	241	11.7	270	1.89	299	0.244
213	32.8	242	11.1	271	1.76	300	0.228
214	32.1	243	10.5	272	1.64	301	0.213
215	31.3	244	10.0	273	1.53	302	0.197
216	30.5	245	9.46	274	1.43	303	0.185
217	29.8	246	8.95	275	1.33	304	0.174
218	29.0	247	8.45	276	1.24	305	0.164
219	28.2	248	7.95	277	1.15	306	0.154
220	27.4	249	7.48	278	1.07	307	0.143
221	26.7	250	7.04	279	0.999	308	0.133
222	25.9	251	6.64	280	0.929	309	0.122
223	25.1	252	6.25	281	0.860	310	0.112
224	24.3	253	5.87	282	0.800	311	0.106
225	23.5	254	5.52	283	0.748	312	0.096
226	22.7	255	5.18	284	0.699		
227	21.9	256	4.86	285	0.653		
228	21.1	257	4.56	286	0.608		

Note:
200-312 nm, Meller and Moortgat [515].

E13. $CF_3CHO + h\nu \rightarrow$ Products. The absorption cross sections of CF_3CHO (trifluoroacetaldehyde) have been measured at room temperature and at 118-182 and 250-357 nm by Lucazeau and Sandorfy [462]; at 229-364 nm by Meller et al. [514]; at 230-400 nm by Francisco and Williams [249]; and at 200-400 nm by Sellevåg et al. [721]. The absorption spectrum exhibits an absorption band in the near UV between 227 and ~360 nm, which is slightly structured at wavelength above 250 nm and has the maximum at 301 nm. The absorption cross sections reported by Francisco and Williams [249], Meller et al. [514], and Sellevåg et al. [721] are in good agreement, generally 10% and better, in the wavelength region between 245 and 354 nm, where the data of Sellevåg et al. [721] generally are the largest, those of Francisco and Williams [249] the smallest. Large discrepancies appear in the long and short wavelength wings of the absorption band, where the cross sections of Sellevåg et al. [721] are smaller than those of Francisco and Williams [249] and larger than those of Meller et al. [514]. The data of Lucazeau and Sandorfy [462], which are given as a plot only, are appreciably smaller than those reported by the other three teams, in the maximum even lower by ~30%. As a recommendation are listed in Table 4-65 the data of Sellevåg et al. [721] for the range 210-360 nm recorded at 1-nm intervals.

Effective quantum yields were obtained in an outdoor photoreactor to be $\Phi_{eff} < 0.02$ as reported by Sellevåg et al. [721].

Table 4-65. Absorption Cross Sections of CF_3CHO at 298 K

λ (nm)	10^{20} σ (cm^2)	λ (nm)	10^{20} σ (cm^2)	λ (nm)	10^{20} σ (cm^2)	λ (nm)	10^{20} σ (cm^2)
210	0.197	248	0.311	286	2.63	324	2.06
211	0.192	249	0.339	287	2.67	325	1.90
212	0.179	250	0.369	288	2.73	326	1.72
213	0.172	251	0.400	289	2.79	327	1.64
214	0.159	252	0.433	290	2.86	328	1.62
215	0.152	253	0.472	291	2.92	329	1.55
216	0.140	254	0.511	292	2.94	330	1.44
217	0.132	255	0.548	293	3.00	331	1.35
218	0.121	256	0.591	294	3.05	332	1.26
219	0.113	257	0.638	295	3.06	333	1.18
220	0.105	258	0.686	296	3.08	334	1.13
221	0.098	259	0.737	297	3.08	335	1.06
222	0.090	260	0.789	298	3.10	336	1.01
223	0.084	261	0.840	299	3.14	337	0.993
224	0.080	262	0.896	300	3.17	338	0.891
225	0.076	263	0.954	301	3.20	339	0.730
226	0.074	264	1.02	302	3.15	340	0.622
227	0.073	265	1.09	303	3.12	341	0.585
228	0.075	266	1.15	304	3.15	342	0.569
229	0.075	267	1.22	305	3.13	343	0.531
230	0.078	268	1.29	306	3.07	344	0.471
231	0.081	269	1.35	307	3.03	345	0.425
232	0.086	270	1.42	308	2.97	346	0.385
233	0.091	271	1.50	309	2.95	347	0.337
234	0.097	272	1.58	310	2.92	348	0.310
235	0.104	273	1.66	311	2.92	349	0.286
236	0.112	274	1.74	312	2.91	350	0.246
237	0.121	275	1.82	313	2.78	351	0.235
238	0.131	276	1.89	314	2.67	352	0.232
239	0.142	277	1.96	315	2.65	353	0.162
240	0.155	278	2.03	316	2.62	354	0.096
241	0.169	279	2.11	317	2.52	355	0.071
242	0.184	280	2.19	318	2.42	356	0.058
243	0.201	281	2.28	319	2.33	357	0.050
244	0.220	282	2.35	320	2.25	358	0.044
245	0.240	283	2.42	321	2.19	359	0.042
246	0.262	284	2.50	322	2.13	360	0.038
247	0.285	285	2.57	323	2.08		

Note:
210-360 nm, Sellevåg et al. [721].

E14. $CF_3C(O)F + h\nu \rightarrow$ Products. The absorption spectrum of $CF_3C(O)F$ (trifluoroacetyl fluoride) has been measured at room temperature and 200-281 nm by Meller [513] and 200-295 nm by Rattigan et al. [656]. These two studies are in agreement concerning the peak cross sections in this spectral region. However, the position of the absorption maximum observed by Rattigan et al. [656] is shifted by ~3 nm to longer wavelengths as compared to that observed by Meller [513]. The cross-sections agree within 0-13% up to 260 nm and then differ by 20-30% in the wing of the absorption band. As a recommendation we list in Table 4-66 the mean of the data (5-nm averages of high-resolution results) reported by Meller [513] and Rattigan et al. [656] at 200-275 nm and the value of Rattigan et al. [656] at 280 nm.

Table 4-66. Absorption Cross Sections of $CF_3C(O)F$ at 298 K

λ (nm)	10^{20} σ (cm^2)	λ (nm)	10^{20} σ (cm^2)	λ (nm)	10^{20} σ (cm^2)	λ (nm)	10^{20} σ (cm^2)
200	10.1	225	11.1	250	1.12	275	0.0036
205	12.2	230	8.67	255	0.492	280	0.0010
210	13.5	235	6.17	260	0.185		
215	13.8	240	3.93	265	0.0526		
220	12.9	245	2.21	270	0.0122		

Note:
200-275 nm, mean of Meller [513] and Rattigan et al. [656],
280 nm, Rattigan et al. [656]

E15. $CF_3C(O)Cl + h\nu \rightarrow$ Products. The absorption cross sections of $CF_3C(O)Cl$ (trifluoroacetyl chloride) have been measured at room temperature and 190-342 nm by Maricq and Szente [483]; at 233, 253 and 296 K and 220-330 nm by Rattigan et al. [656]; and at 223, 248, 273, and 298 K and 200-329 nm by Meller and Moortgat [516]. An absorption band was observed between 215 and 330 nm with the maximum around 254-255 nm and a strong increase of the absorption cross sections between 215 and 190 nm. The room temperature data of Rattigan et al. [656] and Meller and Moortgat [516] are in excellent agreement around the absorption maximum; the agreement is better than 5% between 240 and 315 nm. The data of Rattigan et al. [656] are smaller by nearly 70% than the data of Meller and Moortgat [516] around the absorption minimum at 215 nm, and become progressively smaller by up to 33% in the wing of the absorption band above 320 nm. Maricq and Szente [483] report an absorption maximum of 6.6×10^{-20} cm^2 $molecule^{-1}$ at ~255 nm compared to 6.8×10^{-20} cm^2 $molecule^{-1}$ and 6.7×10^{-20} cm^2 $molecule^{-1}$ observed by Rattigan et al. [656] and Meller and Moortgat [516], respectively. As a recommendation we list in Table 4-67 the mean of the data (5-nm averages of high-resolution results) reported by Rattigan et al. [656] and Meller and Moortgat [516] for the region 205-325 nm.

Both temperature studies show a decrease of the absorption cross sections with decreasing temperature from room temperature to 223 or 233 K in the wavelength regions below ~215 nm and above 255 nm. For the region between 215 and 255 nm, a very slight decrease of the absorption cross sections with decreasing temperature was observed by Rattigan et al. [656], whereas Meller and Moortgat [516] report nearly equal values for temperatures of 223–298 K and sometimes a slight increase of the cross sections between 248 and 223 K.

Table 4-67. Absorption Cross Sections of $CF_3C(O)Cl$ at 296-298 K

λ (nm)	10^{20} σ (cm^2)	λ (nm)	10^{20} σ (cm^2)	λ (nm)	10^{20} σ (cm^2)	λ (nm)	10^{20} σ (cm^2)
205	14.1	240	5.16	275	4.12	310	0.0756
215	1.38	250	6.57	285	2.12	320	0.00756
220	1.48	255	6.75	290	1.36	325	0.00233
225	2.10	260	6.55	295	0.794		
230	3.13	265	5.94	300	0.416		
235	4.17	270	5.08	305	0.194		

Note:
205-325 nm, mean of Rattigan et al. [656] and Meller and Moortgat [516].

E16. $CF_3C(O)O_2NO_2 + h\nu \rightarrow CF_3C(O)O_2 + NO_2$ φ_1
$CF_3C(O)O_2NO_2 + h\nu \rightarrow CF_3C(O)O + NO_3$ φ_2. The absorption cross sections of $CF_3C(O)O_2NO_2$ (trifluoroperoxyacetyl nitrate, FPAN) have been measured at room temperature and 227-305 nm by Libuda and Zabel [446]. Values averaged over 5-nm intervals of their medium-resolution (0.6 nm) data, which were reported with uncertainties of about 10% below 290 nm and of 15-45% at 295-305 nm, are listed in Table 4-68.

Table 4-68. Absorption Cross Sections of $CF_3(O)O_2NO_2$ at 298 K

λ (nm)	10^{20} σ (cm^2)	λ (nm)	10^{20} σ (cm^2)	λ (nm)	10^{20} σ (cm^2)
230	70.0	260	11.8	290	0.87
240	44.9	270	5.46	300	0.33
245	32.5	275	3.56	305	0.20
250	23.9	280	2.21		
255	17.0	285	1.40		

Note:
230-305 nm, Libuda and Zabel [446].

E17. $CF_3CH_2CHO + h\nu \rightarrow$ Products. The absorption spectrum of CF_3CH_2CHO (3,3,3-trifluoropropionaldehyde) has been measured at room temperature and 200-400 nm by Sellevåg et al. [721]. The spectrum exhibits a slightly structured absorption band between 220 and 343 nm (the data reported for the wavelength region above 343 nm show large noise effects). The recommendation is taken from these results. In Table 4-69 the results of Sellevåg et al. [721] are given for the wavelength region 200-343 nm.

Effective quantum yields were obtained in an outdoor photoreactor to be $\Phi_{eff} < 0.04$ as reported by Sellevåg et al. [721].

Table 4-69. Absorption Cross Sections of CF_3CH_2CHO at 298 K

λ (nm)	10^{20} σ (cm^2)	λ (nm)	10^{20} σ (cm^2)	λ (nm)	10^{20} σ (cm^2)	λ (nm)	10^{20} σ (cm^2)
200	0.939	236	0.309	272	2.43	308	3.04
201	0.825	237	0.324	273	2.58	309	3.07
202	0.732	238	0.344	274	2.72	310	3.13
203	0.668	239	0.362	275	2.83	311	3.15
204	0.611	240	0.377	276	2.89	312	3.04
205	0.542	241	0.395	277	2.92	313	2.83
206	0.483	242	0.422	278	2.94	314	2.56
207	0.432	243	0.443	279	2.98	315	2.30
208	0.397	244	0.474	280	3.07	316	2.11
209	0.367	245	0.513	281	3.22	317	1.97
210	0.334	246	0.552	282	3.37	318	1.93
211	0.311	247	0.593	283	3.49	319	1.93
212	0.309	248	0.629	284	3.55	320	1.92
213	0.298	249	0.671	285	3.54	321	1.95
214	0.285	250	0.728	286	3.53	322	1.97
215	0.273	251	0.788	287	3.51	323	1.93
216	0.267	252	0.842	288	3.51	324	1.79
217	0.266	253	0.904	289	3.59	325	1.59
218	0.263	254	0.963	290	3.69	326	1.32
219	0.263	255	1.01	291	3.80	327	1.09
220	0.270	256	1.08	292	3.85	328	0.938
221	0.266	257	1.15	293	3.81	329	0.818
222	0.265	258	1.25	294	3.76	330	0.757
223	0.266	259	1.34	295	3.72	331	0.740
224	0.256	260	1.40	296	3.65	332	0.742
225	0.270	261	1.48	297	3.62	333	0.718
226	0.268	262	1.53	298	3.61	334	0.717
227	0.270	263	1.61	299	3.67	335	0.706
228	0.269	264	1.71	300	3.75	336	0.673
229	0.273	265	1.84	301	3.76	337	0.607
230	0.272	266	1.96	302	3.67	338	0.506
231	0.281	267	2.06	303	3.53	339	0.390
232	0.288	268	2.13	304	3.37	340	0.277
233	0.298	269	2.17	305	3.21	341	0.206
234	0.300	270	2.22	306	3.11	342	0.138
235	0.307	271	2.30	307	3.06	343	0.103

Note:
200-343 nm, Sellevåg et al. [721].

E18. $CF_3C(O)OH + h\nu \rightarrow$ Products. The absorption cross sections of $CF_3C(O)OH$ (trifluoroacetic acid) have been measured at room temperature and 200-280 nm by Rattigan et al. [656]. The spectrum exhibits a single absorption band with a broad maximum near 215 nm, extending out to approximately 275 nm. In Table 4-70 are listed the averages over 5-nm intervals of the spectrum recorded at a resolution of 1.2 nm (diode-array spectrometer) by Rattigan et al. [656].

Table 4-70. Absorption Cross Sections of $CF_3C(O)OH$ at 296 K

λ (nm)	$10^{20}\,\sigma$ (cm^2)	λ (nm)	$10^{20}\,\sigma$ (cm^2)
200	5.20	245	1.69
205	6.48	250	0.870
210	7.23	255	0.390
215	7.59	260	0.155
220	7.76	265	0.050
225	7.21	270	0.013
230	6.03	275	0.006
235	4.46	280	0.000
240	2.89		

Note:
200-280 nm, Rattigan et al. [656].

E19. $CH_3C(O)F + h\nu \rightarrow$ Products. The absorption cross-sections of $CH_3C(O)F$ (acetyl fluoride) have been measured at room temperature and 200-310 nm by Rattigan et al. [656]. The spectrum exhibits a part of an absorption band with the maximum near 206 nm. In Table 4-71 are listed the averages over 5-nm intervals of the spectrum recorded at a resolution of 1.2 nm (diode-array spectrometer) by Rattigan et al. [656].

Table 4-71. Absorption Cross Sections of $CH_3C(O)F$ at 296 K

λ (nm)	$10^{20}\,\sigma$ (cm^2)	λ (nm)	$10^{20}\,\sigma$ (cm^2)	λ (nm)	$10^{20}\,\sigma$ (cm^2)	λ (nm)	$10^{20}\,\sigma$ (cm^2)
200	11.3	230	3.83	260	0.158	290	0.008
205	12.2	235	2.19	265	0.120	295	0.004
210	12.0	240	1.14	270	0.090	300	0.002
215	10.5	245	0.566	275	0.056	305	0.001
220	8.35	250	0.311	280	0.029	310	0.000
225	5.97	255	0.206	285	0.016		

Note:
200-310 nm, Rattigan et al. [656].

E20. $CH_2=CHCF_3 + h\nu \rightarrow$ Products. The absorption spectrum of $CH_2=CHCF_3$ (3,3,3-trifluoro-1-propene) has been measured at room temperature and 164-205 nm by Orkin et al. [601]. Their data recorded at 0.5-nm increments and selected at 1-nm intervals, are listed in Table 4-72.

Table 4-72. Absorption Cross Sections of $CH_2=CHCF_3$ at 295 K

λ (nm)	10^{20} σ (cm^2)	λ (nm)	10^{20} σ (cm^2)	λ (nm)	10^{20} σ (cm^2)
164	3569	178	168	192	0.681
165	3377	179	114	193	0.453
166	3146	180	77.7	194	0.298
167	2874	181	53.9	195	0.204
168	2538	182	36.5	196	0.131
169	2184	183	25.0	197	0.0872
170	1814	184	16.8	198	0.0581
171	1481	185	11.3	199	0.0404
172	1165	186	7.74	200	0.0278
173	899	187	5.22	201	0.0185
174	660	188	3.49	202	0.0129
175	475	189	2.32	203	0.00945
176	340	190	1.52	204	0.00669
177	240	191	1.02	205	0.00456

Note:
164-205 nm, Orkin et al. [601].

E21. $CH_2=CFCF_3 + h\nu \rightarrow$ Products. The absorption spectrum of $CH_2=CFCF_3$ (1,1,1,2-tetrafluoropropene) has been measured at room temperature and 164-186 nm by Orkin et al. [601]. Their data, recorded at 0.5-nm increments and selected at 1-nm intervals, are listed in Table 4-73.

Table 4-73. Absorption Cross Sections of $CH_2=CFCF_3$ at 295 K

λ (nm)	10^{20} σ (cm^2)	λ (nm)	10^{20} σ (cm^2)
164	3773	176	1130
165	3732	177	840
166	3730	178	600
167	3695	179	408
168	3594	180	273
169	3418	181	185
170	3176	182	124
171	2877	183	82.4
172	2535	184	55.5
173	2178	185	38.1
174	1802	186	26.2
175	1445		

Note:
164-186 nm, Orkin et al. [601].

E22. $CF_2=CF_2 + h\nu \rightarrow$ Products. The absorption spectrum of $CF_2=CF_2$ (tetrafluoroethylene) has been measured at room temperature and 185-209 nm by Sharpe et al. [728]; at 164–220 nm by Orkin et al. [601]; and at 115–320 nm by Eden et al. [227]. The spectrum shows a structured absorption band with five maxima and one shoulder between 170 and 220 nm (highest maximum near 189 nm). The results of Orkin et al. [601] and Eden et al. [227] agree within 10% at 164-182 nm, within 20% at 182-200 nm, and within 10% at 203-205 nm. Above 200 nm, a linear decrease of log σ is reported by Orkin et al. [601], whereas Eden et al. [227] reported a very noisy spectrum deviating from that of Orkin et al. [601]. The absorption curve reported by Sharpe et al. [728] shows a shift by 1-2 nm to shorter wavelengths. As recommended absorption cross sections are listed in Table 4-74, the mean of the data of Orkin et al. [601] and Eden et al. [227] for the region 164-205 nm, and the data of Orkin et al. [601] at 206-220 nm (selected at 1-nm intervals from the data reported at 0.5- and 0.1 nm-intervals, respectively).

Table 4-74. Absorption Cross Sections of $CF_2=CF_2$ at 295-298

λ (nm)	10^{20} σ (cm^2)	λ (nm)	10^{20} σ (cm^2)	λ (nm)	10^{20} σ (cm^2)	λ (nm)	10^{20} σ (cm^2)
164	335	179	341	194	423	209	0.429
165	324	180	362	195	387	210	0.257
166	300	181	432	196	263	211	0.162
167	272	182	521	197	169	212	0.0998
168	243	183	559	198	108	213	0.0633
169	227	184	485	199	64.0	214	0.0392
170	238	185	442	200	39.9	215	0.0249
171	268	186	491	201	23.8	216	0.0160
172	286	187	596	202	14.5	217	0.0105
173	281	188	682	203	8.74	218	0.00668
174	289	189	671	204	5.73	219	0.00443
175	327	190	507	205	3.23	220	0.00288
176	372	191	417	206	1.99		
177	390	192	399	207	1.17		
178	376	193	410	208	0.713		

Note:
164-205 nm, mean of the data of Orkin et al. [601] and Eden et al. [227],
206-220 nm, data of Orkin et al. [601].

E23. $CF_2=CFCF_3 + h\nu \rightarrow$ Products. The absorption spectrum of $CF_2=CFCF_3$ (hexafluoropropene) has been measured at room temperature and 185-209 nm by Sharpe et al. [728]; at 164–222 nm by Orkin et al. [601]; and at 115–330 nm by Eden et al. [226]. The spectrum shows an absorption band between 140 and 220 nm with two maxima at 155 and 158.5 nm ($\sigma \approx 3 \times 10^{-17}$ cm^2 $molecule^{-1}$) and two shoulders near 166 and 180 nm. In the region 164-200 nm, there is agreement within 15% between the result of Orkin et al. [601] and Eden et al. [226]; in the region 185-200 nm, the agreement between the results of the three teams is within 25%. Above 200 nm, a linear decrease of log σ is reported by Orkin et al. [601], whereas Eden et al. [226] reported a very noisy spectrum deviating from that of Orkin et al. [601]. As recommended absorption cross sections are listed in Table 4-75, the mean of the data of Orkin et al. [601] and Eden et al. [226] for the region 164-199 nm, and the data of Orkin et al. [601] at 200-222 nm (selected at 1-nm intervals from the data reported at 0.5- and 0.1 nm-intervals, respectively).

Table 4-75. Absorption Cross Sections of CF_2=$CFCF_3$ at 295-298 K

λ (nm)	10^{20} σ (cm^2)	λ (nm)	10^{20} σ (cm^2)	λ (nm)	10^{20} σ (cm^2)	λ (nm)	10^{20} σ (cm^2)
164	2290	179	929	194	97.8	209	0.585
165	2210	180	912	195	73.3	210	0.396
166	2130	181	880	196	54.7	211	0.269
167	2040	182	835	197	40.4	212	0.184
168	1920	183	779	198	29.7	213	0.125
169	1760	184	708	199	22.3	214	0.0838
170	1570	185	629	200	16.2	215	0.0564
171	1380	186	550	201	11.6	216	0.0381
172	1210	187	472	202	8.17	217	0.0261
173	1080	188	391	203	5.70	218	0.0177
174	995	189	321	204	3.95	219	0.0119
175	946	190	259	205	2.70	220	0.00795
176	930	191	207	206	1.85	221	0.00533
177	928	192	163	207	1.28	222	0.00354
178	931	193	127	208	0.866		

Note:
164-199 nm, mean of the data of Orkin et al. [601] and Eden et al. [226],
200-222 nm, data of Orkin et al. [601].

PHOTOCHEM-F-TOTAL CHLORINE

F1. $Cl_2 + h\nu \rightarrow Cl + Cl$. The recommended absorption cross sections are taken from the work of Maric et al. [477], who studied the absorption spectrum in the range 200-550 nm using a spectral resolution of 0.2 nm at 298 K. These authors also measured banded features in the range 476-496 nm at 0.04 nm resolution. The absorption cross sections can be calculated in the range 250-550 nm at various temperatures with the expression derived from their study and previous investigations, given at the bottom of Table 4-76. For convenience, some room temperature values are also listed in the table. Ganske et al. [260] have also measured the cross sections at room temperature, and the agreement with the recommended values is excellent. These two sets of data also agree well with the earlier recommendation, which was based on the work of Seery and Britton [719], which is in turn in good agreement with the results reported by Gibson and Bayliss [266], Fergusson et al. [243], and Burkholder and Bair [110]. At wavelengths larger than 250 nm, the absorption cross sections measured at room temperature by Hubinger and Nee [344] are in excellent agreement with the values of Maric et al. [477]. However, in the range 200-250 nm the cross sections deviate considerably between both groups. Room temperature cross sections have also been obtained by Roxlo and Mandl [692] for the range 170-214 nm. The low resolution absorption cross sections reported by Chen and Zhu [160, 161] and Chen et al. [162] for the 300-420-nm region at 5- and 10-nm intervals and measured for the calibration of quantum yield measurements of some carbonyl compounds deviate up to ~30% from those reported by Maric et al. [477].

The estimated atmospheric photodissociation rate is only weakly affected by the temperature dependency of the cross sections. Chininin [167] measured an upper limit of 5% for the branching ratio for excited atomic $Cl^*(^2P_{1/2})$ at 351 nm, in agreement with earlier studies by Bush et al. [128] and Park et al. [622], who determined an upper limit for Cl* formation of 0.01 in the photolysis of Cl_2 at 347.1 nm, and 308 and 340-355 nm, respectively.

Table 4-76. Absorption Cross Sections of Cl_2 at 298

λ (nm)	10^{20} σ (cm^2)	λ (nm)	10^{20} σ (cm^2)	λ (nm)	10^{20} σ (cm^2)
260	0.198	360	13.22	460	0.258
270	0.824	370	8.41	470	0.162
280	2.58	380	5.00	480	0.0957
290	6.22	390	2.94	490	0.0534
300	11.92	400	1.84	500	0.0283
310	18.50	410	1.28	510	0.0142
320	23.71	420	0.956	520	0.00681
330	25.55	430	0.732	530	0.00313
340	23.51	440	0.546	540	0.00137
350	18.77	450	0.387	550	0.00058

.

$$\sigma = 10^{-20}\alpha^{0.5}\left\{27.3\exp\left(-99.0\alpha\left(\ln\left(\frac{329.5}{\lambda}\right)\right)^2\right) + 0.932\exp\left(-91.5\alpha\left(\ln\left(\frac{406.5}{\lambda}\right)\right)^2\right)\right\}$$

where $\alpha = \tanh(402.7/T)$; λ in nm, $250 < \lambda < 550$ nm, and T in K; $300\ K > T > 195\ K$.

F2. $ClO + h\nu \rightarrow Cl + O$. The UV absorption spectrum of chlorine monoxide, ClO, shown in Figure 4-2, is partly composed of a continuum absorption band from 210 nm to the maximum near 265 nm, and a characterized banded structure of a strong $A\ ^2\Pi_{3/2} \leftarrow X\ ^2\Pi_{3/2}$ transition, superposing a weak $A\ ^2\Pi_{1/2} \leftarrow X\ ^2\Pi_{1/2}$ system, ranging from 265 nm to 315 nm. The cross sections have been reviewed by Watson [839]. The more recent measurements yield results in reasonable agreement with the earlier ones, (1) Mandelman and Nicholls [473] in the 250–310 nm region; (2) Wine et al. [849] around 283 nm; (3) Rigaud et al. [672] in the 272-324 nm range; (4) Jourdain et al. [397] in the 272-320 nm range; (5) Barton et al. [44] in the 274-306 nm range at 315 K, (6) Lang et al. [431] at 253.7 and 257.7 nm; (7) Sander and Friedl [702] at 275.2 nm, at 220, 298, and 400 K; (8) Trolier et al. [784] in the 270–310-nm region and 200-263 K temperature range; and (9) Simon et al. [732] between 240 and 310 nm. The peak cross section at the maximum of the continuum (near 265 nm) is 5.2×10^{-18} cm^2 $molecule^{-1}$, based on the average of studies 4, 7-9 and Johnston et al. [388]. At 257.7 nm an average value of $(4.86 \pm 0.04) \times 10^{-18}$ cm^2 $molecule^{-1}$ was calculated from the data of the studies 1,6-9. It should be noted that the cross sections on the structured part are extremely dependent on instrument resolution. Figure 4-2 shows a spectrum of ClO based on the data of Sander and Friedl [702]. The recommended absorption cross sections listed in Table 4-77 are the averages over 1-nm intervals of the continuous and banded spectrum measured at a resolution of 0.3 nm by Sander and Friedl [702]. In Table 4-78 are compared the absorption cross sections for the band heads of the v',v" = 1,0 to 21,0 bands measured at various spectral resolutions.

The cross sections of the continuum are independent of temperature (Trolier et al. [784]), while the structured part is extremely temperature dependent. The bands sharpen and grow with a decrease in temperature. Sander and Friedl [702] measured the temperature dependence at the peak of the 12-0 sub-band in the range 220-400K. Clyne and Coxon [175] determined the following relationship for the 11-0 sub-band relative to the 298 K value for the temperature range 294-240 K:

$$\sigma_{294} / \sigma_T = 1 + 0.0036\ (T-294K).$$

Recently, Maric and Burrows [476] performed a detailed analysis of the ClO spectrum and developed an analytical approach, which allows the calculation of the UV absorption spectrum for any temperature and spectral resolution.

The calculations of Coxon et al. [195] and Langhoff et al. [434] indicate that photodecomposition of ClO accounts for at most 2 to 3% of the total destruction rate of ClO in the stratosphere, which occurs predominantly by reaction with oxygen atoms and nitric oxide.

The photodissociation of thermal ClO radicals in the wavelength range $237<\lambda<270$ nm was studied by Schmidt et al. [711] using REMPI. Cl ($^2P_{3/2,1/2}$) and O(^1D) were formed with unity quantum yield. The cut-off excitation wavelength for O(^1D) was determined to be 263.4 nm.

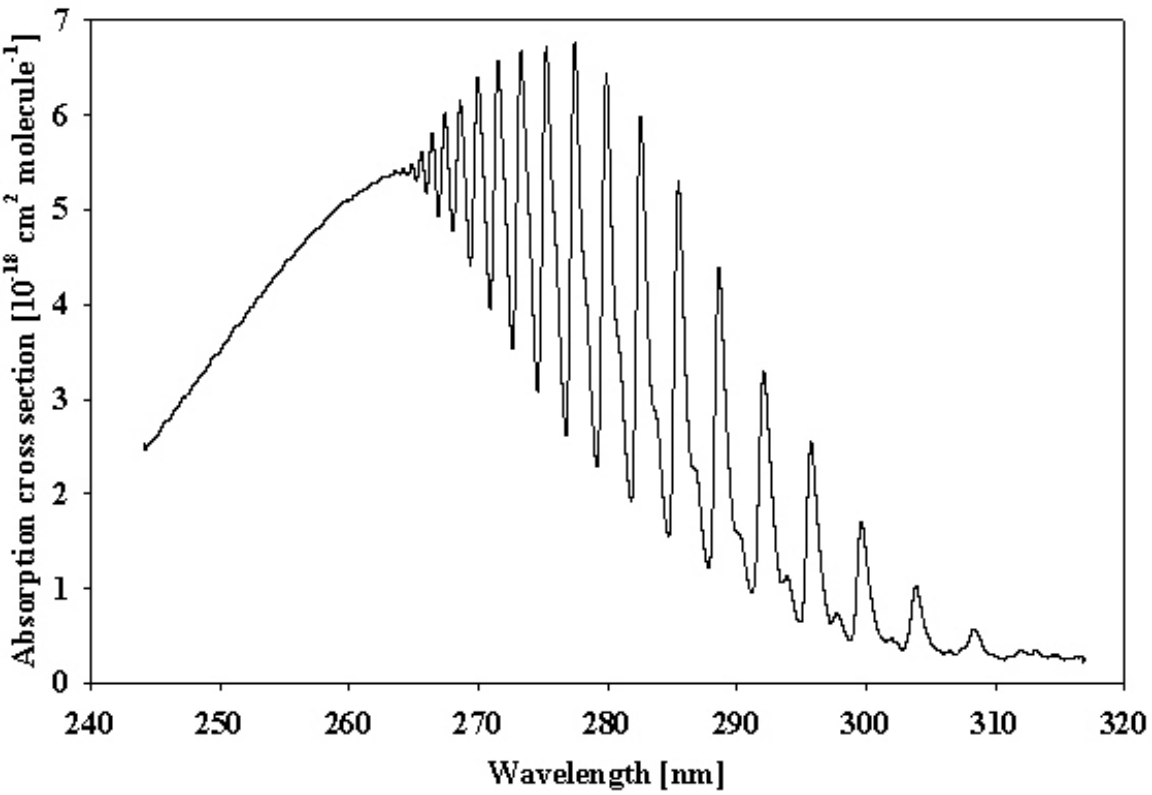

Figure 4-2. Absorption Spectrum of ClO

Table 4-77. Absorption Cross Sections of ClO at 298 K

λ (nm)	10^{20} σ (cm^2)	λ (nm)	10^{20} σ (cm^2)	λ (nm)	10^{20} σ (cm^2)	λ (nm)	10^{20} σ (cm^2)
245	260	263	536	281	329	299	74.8
246	279	264	540	282	311	300	133
247	297	265	541	283	445	301	56.6
248	315	266	549	284	245	302	45.2
249	333	267	546	285	292	303	44.9
250	352	268	529	286	362	304	87.8
251	371	269	529	287	200	305	45.5
252	388	270	575	288	197	306	33.2
253	407	271	489	289	337	307	33.1
254	425	272	532	290	165	308	47.7
255	442	273	515	291	111	309	41.9
256	457	274	470	292	270	310	28.7
257	473	275	507	293	161	311	27.3
258	486	276	456	294	102	312	33.1
259	500	277	418	295	94.5	313	32.5
260	511	278	501	296	206	314	28.9
261	520	279	283	297	83.1	315	27.8
262	529	280	538	298	65.1	316	26.8

Note:
Sander and Friedl [702]: Averages over 1-nm intervals of the continuous and banded spectrum measured at a resolution of 0.3 nm.

Table 4-78. Absorption Cross Sections of ClO at the band heads of the v′,v″ = 1,0 to 21,0 bands

Band v',v"	λ (nm)	10^{20} σ (cm^2)	λ (nm)	10^{20} σ (cm^2)	λ (nm)	10^{20} σ (cm^2)	λ (nm)	10^{20} σ (cm^2)	λ (nm)	10^{20} σ (cm^2)
	Trolier et al. resol. 0.6 nm		Sander, Friedl res. 0.3(0.18) nm		Simon et al. res. 0.3(0.03) nm		Mandelman resol. 0.22 nm		Jourdain et al. resol. 0.015 nm	
1,0			312.1	35					312.5	26
2,0	307.7	22	308.3	58	307.9	39	307.8	47	307.9	67
3,0	303.4	64	303.9	103	303.5	86	303.4	104	303.5	133
4,0	299.4	128	299.6	171	299.0	163	299.3	207	299.3	236
5,0	295.4	202	295.7	253	295.4	255	295.4	315	295.4	326
6,0	292.1	286	292.1	330	292.0	338 (400)	292.0	382	291.8	395
7,0	288.7	365	288.6	438	288.4	448 (502)	288.4	516	288.4	504
8,0	286.0	455	285.5	530	285.2	542	285.2	627	285.2	594
9,0	282.6	508	282.6	598	282.3	608	282.2	667	282.2	641
10,0	280.1	555	279.9	645	279.8	655	279.6	688	279.6	686
11,0	277.7	571	277.4	668	277.2	679	277.2	680	277.2	727
12,0	275.5	587	275.3	671 (836)	275.1	681	275.0	634	275.1	733
13,0	273.6	576	273.3	668					272.9	711
14,0	271.8	571	271.5	656						
15,0	269.9	556	270.0	640						
16,0	268.7	545	268.6	615						
17,0			267.4	603						
18,0			266.5	579						
19,0			265.6	562						
20,0			264.9	549						
21,0			264.2	543						

F3. $ClOO + h\nu \rightarrow ClO + O$. Johnston et al. [388] measured the absorption cross sections of the ClOO radical using a molecular modulation technique that required interpretation of a complex kinetic scheme. More recently, Mauldin et al. [502] reported cross section measurements in the range from 220 to 280 nm, and Baer et al. [34] from 240 to 300 nm. These two studies are in agreement, yielding cross section values that are more than twice as large as the older Johnston et al. [388] values. The recommended cross sections are listed in Table 4-79, and are taken from the work of Mauldin et al. [502].

Table 4-79. Absorption Cross Sections of ClOO

λ (nm)	10^{20} σ (cm^2)	λ (nm)	10^{20} σ (cm^2)
220	611	252	2630
222	670	254	2370
224	747	256	2120
226	951	258	1890
228	1100	260	1610
230	1400	262	1370
232	1650	264	1120
234	1960	266	905
236	2240	268	725
238	2520	270	596
240	2730	272	435
242	2910	274	344
244	2960	276	282
246	2980	278	210
248	2950	280	200

λ (nm)	10^{20} σ (cm^2)	λ (nm)	10^{20} σ (cm^2)
250	2800		

F4. $OClO + h\nu \rightarrow O(^3P) + ClO$
$OClO + h\nu \rightarrow Cl + O_2$ ($^3\Sigma_g^-$, $^1\Delta_g$)
$OClO + h\nu \rightarrow ClOO$ The spectrum of OClO (chlorine dioxide) is characterized by a series of well-developed progressions of bands extending from ~280 to 480 nm, corresponding to the A ($^2A_2$) (i,j,k) ← X ($^2B_1$) (0,0,0) vibronic transitions. The spectroscopy of this molecule has been studied extensively, and the quantum yield for photodissociation appears to be unity throughout the above wavelength range. See for example, the review by Watson [839]. Birks et al. [73] have estimated a half-life against atmospheric photodissociation of OClO of a few seconds. The measurement of absorption spectra at temperatures between 200 and 378 K has been the subject of many studies as shown in the following survey:

Table 4-80. Summary of Previous Measurements of OClO Cross Sections

Reference	Year	Temperature K	Wavelength Range nm	Resolution nm
Martin and Gareis [490]	1956	298	263-414	Not given
Knauth et al. [411]	1979	333	270-440	0.3-1
Wahner et al. [830]	1987	204, 296, 378	242-477	0.25
Hubinger and Nee [343]	1994	298	240-477	Not given
Frost et al. [255]	1996	200	390-454	0.0015-0.0021
Marston et al. [489]	1998	298	275-400	0.05
Kromminga et al. [423]	2003	213, 233, 253	312.5-440.5	0.01-0.02
Bogumil et al. [82]	2003	293	290-460	0.25

Absorption cross sections at 10-nm intervals for the region 270-440 nm and at 333 K have been reported by Knauth et al. [411], and for the 351.5-nm maximum at room temperature by Clyne and Coxon [175] and Basco and Dogra [46]. The absorption cross sections of Wahner et al. [830] obtained at a resolution of 0.25 nm and at 204, 296, and 378 K have been used by Hubinger and Nee [343], Frost et al. [255] and Marston et al. [489] for the calibration of their relative spectra. The values at the peaks of the main vibrational bands a(0) to a(26) (i.e., A ($^2A_2$) (i,0,0) ← X ($^2B_1$) (0,0,0), i = 0 to 26) reported by Wahner et al. [830] have been selected as recommended absorption cross sections of OClO in the four foregoing JPL reports. Most recently, Kromminga et al. [423] reported high- and medium-resolution absorption spectra at five temperatures between 213 and 293 K obtained by using Fourier-transform spectroscopy, which has the advantage of accurate wavelength calibration. There is a clear wavelength shift (~0.2-0.5 nm) between the spectra of Kromminga et al. [423] and Wahner et al. [830], which cannot be explained by the shift between measurements in air and in vacuum. The absorption cross sections for the band peaks a(3) to a(26) reported by Kromminga et al. [423] are smaller by 5-10% than those reported by Wahner et al. [830]. A decrease of the temperature causes a sharpening of the vibrational bands and an increase of the peak cross sections as observed between 293 and 213 K by Kromminga et al. [423] and between 378 and 200 K by Wahner at al. [830].

The recommended absorption cross sections of OClO are listed in Table 4-81, and represent the averages over 1-nm intervals of the spectrum measured at medium resolution (0.25 nm) by Wahner et al. [830]. In Table 4-82 are listed the a(16) to a(3) band peaks at 213, 233, 253, 273, and 293 K recorded in the medium-resolution (0.2-0.4 nm) spectra by Kromminga et al. [423]. The values for the a(17) to a(23) bands at 293 K are the results of Bogumil et al. [82], who have measured the OClO spectrum at medium resolution (0.24-0.44 nm) with the SCIAMACHY pre-flight satellite instrument and have scaled the absorption cross sections to those measured by Kromminga et al. [423]. In addition, the peak cross sections determined by Wahner et al. [830] are listed in Table 4-83. Figure 4-3 shows the spectrum of OClO at 204 K based on the data of Wahner et al. [830].

VUV absorption cross sections have been measured at 148-183 nm by Basco and Morse [49], at 50-207 nm by Flesch et al. [246], at 127-183 nm by Hubinger and Nee [343], and at 115-191 nm by Marston et al. [489].

The photochemistry of OClO is extremely complex, with several electronic excited states involved in the photodissociation dynamics. Several channels have been observed at wavelengths important in the stratosphere, including O + ClO, Cl + O_2 and isomerization to ClOO. Colussi [178] measured the quantum

yield for chlorine atom production to be less than 0.01, and for oxygen atom production to be unity (within experimental error), both at 308 nm. Vaida et al. [802] and Ruhl et al. [693] reported chlorine atom production at 362 nm; and Bishenden et al. [74, 75] measured the quantum yield for this process to be 0.15 ± 0.10 around that same wavelength. In contrast, Lawrence et al. [437] report a quantum yield for Cl-atom production in the 359–368-nm region of less than 5×10^{-4}. This conclusion is supported by photofragment studies of Davis and Lee [209] between 350 and 475 nm, who report Cl yields <0.2% in the wavelength range 350-370 nm, rising to a maximum of 3.9 ± 0.8% near 404 nm. In a later study Davis and Lee [207] report a substantial yield of $O_2(^1\Delta_g)$ and show that the branching ratio between O + ClO, and Cl + O_2 depends on the OClO($A\ ^2A_2$) excited state vibrational mode. Delmdahl et al. [210] measured the yield of nascent Cl atoms to be below 3.6% in the photolysis in the 365-450 nm range. At λ < 365 nm, there was a sharp increase of the Cl yield, which was attributed to the photolysis of vibrationally excited ClO (v≥4).

The recommendation is to use a quantum yield value of unity for the production of $O(^3P)$ atoms in the range 270-480 nm. An upper limit for the Cl yield can be set at 0.04 in the range 365-450 nm. While accurate absorption cross section values are valuable for atmospheric measurements of OClO levels, the identity of the photodissociation products is only of minor importance in the context of atmospheric processes.

Table 4-81. Absorption Cross Sections of OClO at 204 K (averages over 1-nm intervals)

λ (nm)	10^{20} σ (cm^2)	λ (nm)	10^{20} σ (cm^2)	λ (nm)	10^{20} σ (cm^2)	λ (nm)	10^{20} σ (cm^2)
247	35.6	304	96.1	361	477	418	107
248	34.4	305	276	362	173	419	75.1
249	33.7	306	328	363	179	420	81.4
250	34.6	307	190	364	207	421	323
251	34.3	308	116	365	361	422	151
252	34.6	309	85.4	366	403	423	50.0
253	34.1	310	168	367	625	424	23.8
254	34.9	311	511	368	919	425	23.3
255	34.3	312	338	369	903	426	14.5
256	34.8	313	174	370	268	427	43.8
257	34.8	314	107	371	107	428	99.5
258	35.1	315	94.2	372	180	429	46.9
259	35.0	316	239	373	170	430	44.3
260	35.8	317	686	374	364	431	23.3
261	36.5	318	360	375	376	432	47.0
262	37.5	319	176	376	554	433	173
263	38.2	320	114	377	718	434	69.6
264	38.0	321	125	378	881	435	24.6
265	38.8	322	279	379	278	436	11.2
266	39.9	323	873	380	92.4	437	7.68
267	40.4	324	443	381	135	438	9.09
268	42.3	325	192	382	148	439	5.13
269	44.6	326	121	383	266	440	12.5
270	44.3	327	147	384	298	441	47.8
271	45.7	328	221	385	440	442	23.2
272	49.9	329	838	386	345	443	14.7
273	49.1	330	782	387	762	444	7.59
274	48.1	331	285	388	591	445	3.96
275	54.8	332	155	389	173	446	46.8
276	58.3	333	147	390	71.4	447	55.2
277	52.5	334	208	391	123	448	18.4
278	54.3	335	355	392	109	449	7.17
279	67.4	336	1090	393	203	450	6.96
280	67.2	337	782	394	270	451	4.50
281	58.3	338	266	395	285	452	1.66
282	65.4	339	155	396	275	453	3.57
283	82.4	340	167	397	370	454	0.907
284	77.6	341	250	398	653	455	13.3
285	67.2	342	414	399	225	456	9.70
286	77.7	343	925	400	70.1	457	4.76

λ (nm)	10^{20} σ (cm^2)	λ (nm)	10^{20} σ (cm^2)	λ (nm)	10^{20} σ (cm^2)	λ (nm)	10^{20} σ (cm^2)
287	100	344	1090	401	45.6	458	4.25
288	93.7	345	388	402	96.9	459	3.98
289	79.4	346	176	403	56.3	460	1.84
290	90.5	347	161	404	196	461	17.1
291	127	348	258	405	194	462	17.9
292	116	349	320	406	185	463	11.8
293	90.9	350	581	407	160	464	10.0
294	94.1	351	1100	408	158	465	4.01
295	147	352	993	409	493	466	1.40
296	172	353	330	410	210	467	2.53
297	122	354	164	411	71.6	468	10.1
298	92.0	355	190	412	34.0	469	15.0
299	106	356	276	413	46.8	470	7.69
300	226	357	343	414	44.6	471	6.14
301	222	358	597	415	30.0	472	3.18
302	143	359	830	416	164		
303	94.3	360	1210	417	100		

Note:
246.5-472.5 nm, Wahner et al. [830].

Table 4-82. Absorption Cross Sections of OClO at the a(21) to a(3) Band Peaks at 213-293 K

band peak	λ (nm)	10^{20} σ (cm^2)	λ (nm)	10^{20} σ (cm2)	λ (nm)	10^{20} σ (cm^2)	λ (nm)	10^{20} σ (cm^2)	λ (nm)	10^{20} σ (cm^2)
	T = 213 K		T = 233 K		T = 253 K		T = 273 K		T = 293 K	
a(21)									292.05	79.32
a(20)									295.79	107.60
a(19)									300.96	171.03
a(18)									306.12	273.85
a(17)									311.58	391.16
a(16)									316.86	528.84
a(15)	322.96	846.62	322.96	812.45	323.02	786.75	323.02	756.88	323.02	707.16
a(14)	329.49	1054.25	329.49	1011.91	329.55	984.42	329.55	945.36	329.55	892.88
a(13)	336.41	1224.61	336.41	1181.30	336.41	1148.79	336.48	1098.73	336.48	1044.48
a(12)	343.77	1313.77	343.77	1269.99	343.77	1243.47	343.77	1189.35	343.77	1134.36
a(11)	351.53	1328.23	351.53	1289.25	351.53	1265.01	351.53	1212.13	351.53	1164.23
a(10)	359.73	1280.34	359.73	1243.39	359.73	1220.29	359.73	1171.14	359.73	1127.62
a(9)	368.39	1187.04	368.39	1153.33	368.39	1128.23	368.39	1083.63	368.47	1045.41
a(8)	377.56	1048.31	377.56	1019.56	377.56	992.21	377.56	951.69	377.65	916.95
a(7)	387.29	869.95	387.29	849.00	387.29	818.37	387.29	783.53	387.38	750.49
a(6)	397.90	696.60	397.99	683.65	397.90	661.61	397.99	643.31	397.99	619.46
a(5)	408.82	523.40	408.82	518.32	408.82	488.85	408.92	473.08	408.92	452.82
a(4)	420.56	350.83	420.45	350.30	420.45	319.18	420.45	317.13	420.45	301.27
a(3)	432.88	220.71	432.99	197.98	432.99	174.81	432.99	194.21	432.99	189.51

Note:
292-317 nm, Bogumil et al. [82],
323-433 nm, Kromminga et al. [423].

Table 4-83. Absorption Cross Sections of OClO at the Band Peaks (after Wahner et al. [830])

λ(nm)	10^{20} σ(cm^2)		
	204 K	296 K	378 K
475.53		13	
461.15	17	17	16
446.41	94	69	57
432.81	220	166	134
420.58	393	304	250
408.83	578	479	378
397.76	821	670	547
387.37	1046	844	698
377.44	1212	992	808
368.30	1365	1136	920
359.73	1454	1219	984
351.30	1531	1275	989
343.44	1507	1230	938
336.08	1441	1139	864
329.22	1243	974	746
322.78	1009	791	628
317.21	771	618	516
311.53	542	435	390
305.99	393	312	291
300.87	256	219	216
296.42	190	160	167
291.77	138	114	130
287.80	105	86	105
283.51	089	72	90
279.64	073	60	79
275.74	059	46	
272.93	053	33	

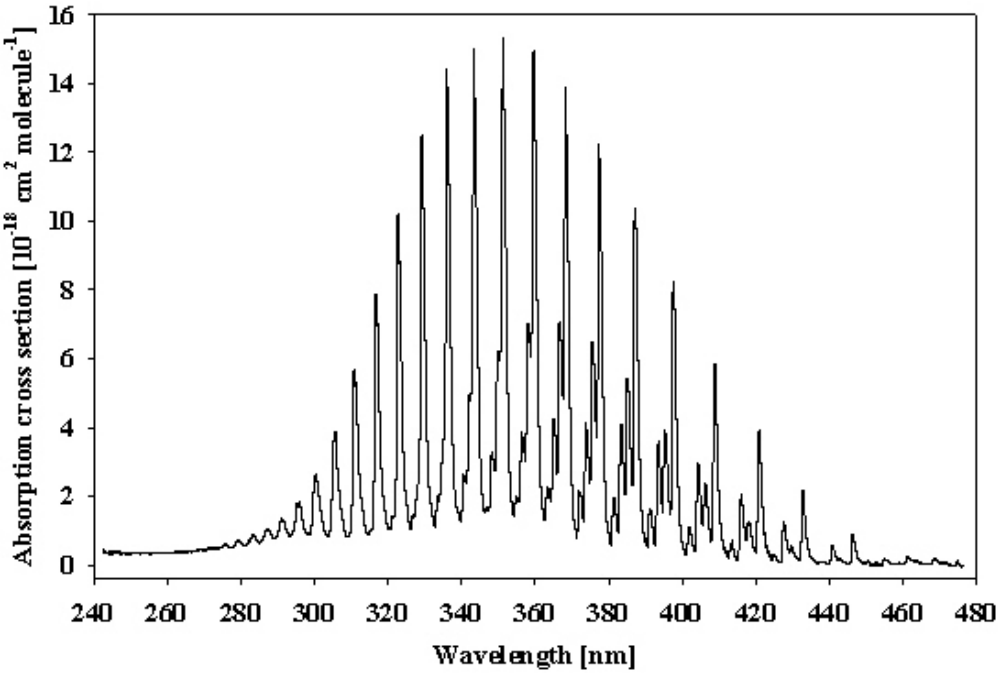

Figure 4-3. Absorption Spectrum of OClO at 204 K (after Wahner et al. [830])

F5. $ClO_3 + h\nu \rightarrow$ Products. The JPL-83 to JPL-90 recommendations for the absorption cross sections of the ClO_3 radical were based on the work of Goodeve and Richardson [288]. Lopez and Sicre [461], however, have shown that the spectrum reported by Goodeve and Richardson is most likely that of Cl_2O_6. Thermochemical estimates by Colussi et al. [179] further corroborate this assignment.

Grothe and Willner [305], [306] have reported the UV and IR spectra of ClO_3 trapped in a neon matrix following thermal decomposition of Cl_2O_4 or $FOClO_3$. By monitoring the amount of ClO formed as a photolysis product of ClO_3, they determined the absorption cross sections in the range 250-500 nm. The spectrum showing a highly structured absorption band around 320 nm ($\sigma \approx 3 \times 10^{-18}$ cm^2 molecule^{-1}) and a second band around 425 nm ($\sigma \approx 2.5 \times 10^{-18}$ cm^2 molecule^{-1}) is depicted in the review article of Wayne et al. [841]. A broad absorption spectrum between 280 and 450 nm peaking at ≈300 nm ($\sigma \approx 1.8 \times 10^{-17}$ cm^2 molecule^{-1}) was recorded for ClO_3 formed by radiolysis of aqueous solutions of chlorate ions.

For the absorption cross sections of ClO_3 in the gas phase no recommendation can be given at present.

F6. $Cl_2O + h\nu \rightarrow Cl + ClO$
$Cl_2O + h\nu \rightarrow Cl_2 + O(^3P)$
$Cl_2O + h\nu \rightarrow Cl_2 + O(^1D)$
$Cl_2O + h\nu \rightarrow O + 2Cl$. The absorption spectra of dichlorine monoxide have been measured at room temperature and 230-620 nm by Goodeve and Wallace [291], at 220-650 nm by Finkelnburg et al. [244], at 234-331 nm by Martin and Gareis [490], at 180-640 nm by Lin [454], at 200-450 nm by Molina and Molina [537], at 236-320 nm by Simon et al. [732], and at 190-399 nm by Smith et al. [742]. Johnsson et al. [382] measured the absorption spectrum at 210-350 nm of Cl_2O in Ar matrices and reported the absorption cross section at 260 nm for the gas phase. Measurements at 298 and 333 K and between 200 and 500 nm have been carried out by Knauth et al. [411]. The spectrum exhibits three absorption bands in the UV and visible regions: an asymmetrical band between ~220-380 nm with the maximum near 255 nm and a shoulder near 290 nm, and two weak bands at ~380-500 nm and ~500-650 nm with the maxima near 420 nm and 550 nm, respectively. The absorption cross sections measured by Lin et al. [454], Molina and Molina [537], Knauth et al. [411], and Smith et al. [742] are in very good agreement, i.e., within 10%, in the UV absorption band between 200 and ~350nm. The values reported by Molina and Molina [537] and Knauth et al. [411] are somewhat larger than those reported by Lin [454], which again are larger than those reported by Smith et al. [742]. The discrepancies between the various data sets become larger in the region of the absorption minimum, whereas above ~400 nm the agreement is again very good. The spectrum measured by Simon et al. [732] has been normalized to the data of Lin [454]. The earlier data reported by Goodeve and Wallace [291], Finkelnburg et al. [244], and Martin and Gareis [490] deviate substantially from the more recent results. VUV absorption cross sections have been reported by Nee [574] for the 150 –200 nm wavelength region, and by Motte-Tollet et al. [564] for the 128-190 nm region.

The recommended absorption cross sections for Cl_2O listed in Table 4-84 are based on the four spectra showing good agreement as outlined above: they are the mean of the data of Lin [454], Molina and Molina [537], Knauth et al. [411], and Smith et al. [742] at 200-350 nm; the mean of the data of Lin [454], Molina and Molina [537], and Knauth et al. [411], at 360-450 nm; the mean of the data of Lin [454] and Knauth et al. [411] at 460-500 nm; and the data of Lin [454] at 510-640 nm. Sander and Friedl [702] have measured the quantum yield for production of O-atoms to be 0.25 ± 0.05, using a broadband photolysis source extending from 180 nm to beyond 400 nm. The main photolysis products are Cl and ClO. Using a molecular beam technique, Nelson et al. [578] found Cl + ClO to be the only primary photodissociation channel at 308 nm, a major channel at 248 nm, and a minor channel at 193 nm. At 248 nm a fraction of the photoproduct ClO underwent spontaneous photodissociation. These authors find evidence that the dissociation in three atoms 2 Cl + O takes place at 193 nm, and that some O(^{1}D) atoms are generated as well. More recently, Nickolaisen et al. [582] reported that broadband photolysis at wavelengths beyond 300 nm results in pressure-dependent ClO quantum yields, which was explained by the rapid intercrossing between two metastable states. These states undergo competitive dissociation to ClO + Cl and collisional relaxation to the ground states. Furthermore, these authors detected a transient absorption spectrum, which they assigned to a long-lived metastable triplet state of Cl_2O. However Moore et al. [550] estimated the lifetime of this metastable excited state to be much shorter. Chichinin [167] and Tanaka et al. [773], also found evidence of ground state ($^2P_{3/2}$) and spin-orbit excited ($^2P_{1/2}$) atomic chlorine products.

The implication is that the photodecomposition quantum yield is less than unity at atmospherically relevant wavelengths, in spite of the continuous nature of the absorption spectrum. Additional experimental work is needed to corroborate this interpretation.

Table 4-84. Absorption Cross Sections of Cl_2O

λ (nm)	10^{20} σ (cm^2)	λ (nm)	10^{20} σ (cm^2)	λ (nm)	10^{20} σ (cm^2)
200	67.7	350	1.84	500	0.218
210	22.4	360	0.893	510	0.210
220	8.42	370	0.493	520	0.214
230	26.5	380	0.446	530	0.237
240	101	390	0.575	540	0.256
250	184	400	0.829	550	0.256
260	186	410	1.08	560	0.222
270	144	420	1.25	570	0.203
280	121	430	1.23	580	0.176
290	98.9	440	1.10	590	0.149
300	68.1	450	0.848	600	0.122
310	38.6	460	0.625	610	0.0956
320	18.7	470	0.446	620	0.0688
330	8.59	480	0.313	630	0.0344
340	3.90	490	0.247	640	0.0153

Note:
200-350 nm, mean of the data of Lin [454], Molina and Molina [537], Knauth et al. [411], and Smith et al. [742],
360-450 nm, mean of the data of Lin [454], Molina and Molina [537], and Knauth et al. [411],
460-500 nm, mean of the data of Lin [454] and Knauth et al. [411],
510-640 nm, data of Lin [454].

F7. $ClOOCl + h\nu \rightarrow Cl + ClOO$

$ClOOCl + h\nu \rightarrow ClO + ClO$. The absorption cross sections of ClOOCl have been measured at low temperatures: at 265 K and 220-360 nm by Cox and Hayman [190] (1), at 250 K and 211-426 nm by Burkholder et al. [115] (2), at 235 K and 210-290 nm by Permien et al. [630] (3), at 206 K and 190-400 nm by DeMore and Tschuikow-Roux [214] (4), at 230 K and 204-380 nm by Vogt and Schindler [823] (5), at 195 K and 200-400 nm by Huder and DeMore [348] (6), and at 183-245 K and 210 nm by Bloss et al. [79] (7). Recently, a theoretical photoabsorption spectrum of ClOOCl has been reported by Toniolo et al. [780]. The absorption spectrum shows decreasing cross sections between 190 and 220 nm, an absorption band above 220 nm with the maximum near 245 nm and $\sigma \approx (6.3\text{-}6.8) \times 10^{-18}$ cm^2 $molecule^{-1}$, and decreasing cross sections for wavelengths up to 450 nm. There is good agreement between the results of (1) to (6) in the region of the absorption band, agreement within 15% up to ~260 nm and about 30% up to ~290 nm. Larger discrepancies occur in the tail above 300 nm, where the spectrum is weak, which may be attributed to uncertainties in the spectral subtraction of impurities such as Cl_2O, Cl_2, and Cl_2O_2. A measurement at 210 nm over the temperature range 183-245 K by Bloss et al. [79] resulted in $\sigma = (2.94 \pm 0.86) \times 10^{-18}$ cm^2 $molecule^{-1}$, which is larger by ~25% than the values of (4) and (6). The absorption spectra reported and assigned to ClOOCl by Molina and Molina [543] and Basco and Hunt [48] differ significantly from the rest of the results.

The recommended absorption cross sections listed in Table 4-85 are unchanged from JPL02-25. They are based on the data of DeMore and Tschuikow-Roux at 190-200 nm, and the mean of the data of Cox and Hayman [190], DeMore and Tschuikow-Roux [214], Permien et al. [630], and Burkholder et al. [115] for the wavelength range 200-360 nm. Data at wavelengths greater than 360 nm were obtained from a linear extrapolation of the logarithm of the cross sections, using the expression, $\log (10^{20} \sigma(cm^2) = 7.589 - 0.01915 \lambda(nm)$. For $\lambda > 360$ nm the extrapolated data are considered to be more reliable than experimental measurements because of the very small dimer cross sections in this region.

The absorption studies also indicate that only one stable species is produced in the recombination reaction of ClO with itself, and that this species is dichlorine peroxide, ClOOCl, rather than ClOClO, or $ClClO_2$. Using submillimeter wave spectroscopy, Birk et al. [72] have further established the structure of the recombination product to be ClOOCl. These observations are in agreement with the results of quantum mechanical calculations (McGrath et al. [508, 509]; Jensen and Odershede [379]; Stanton et al. [750]).

Molina et al. [548] reported a quantum yield of approximately unity (1.03 ± 0.12) for the Cl + ClOO pathway from a flash photolysis study at 308 nm, in which the yield of Cl atoms was measured using time-resolved atomic resonance fluorescence. These results are in agreement with the steady-state photolysis study of Cox and Hayman [190]. In a molecular beam/flash-photolysis study Moore et al. [551] measured the relative Cl:ClO product yields from which the branching ratio for both photolysis channels ClOO + Cl and ClO +

ClO was derived: at 248 nm they obtained 0.88 ± 0.07 and 0.12 ± 0.07 respectively, and at 308 nm, 0.90 ± 0.1 and 0.10 ± 0.01. Kalekin and Morokuma [401] studied the photodissociation dynamics and predict the synchronous and sequential formation of $2Cl + O_2$ at 308 nm, and three possible fragmentation routes at 248 nm: $2Cl + O_2$, $Cl + O(^3P) + ClO$, and $2Cl + 2\ O(^3P)$. Similar theoretical calculations were performed by Toniolo et al. [779] for 264, 325 and 406 nm excitation energies, and predict $2Cl + O_2$ at all wavelengths with a small yield of 2ClO at the shortest wavelength. Recently Plenge et al. [637] measured the primary products from photolysis of ClO dimer at 250 and 308 nm, using photoionisation mass spectrometry. At both wavelengths exclusively formation of $2Cl + O_2$ is observed, corresponding to a primary Cl-quantum yield near unity; at 250 nm $\varphi_{Cl} \geq 0.98$ and at 308 nm $\varphi_{Cl} \geq 0.90$. At both photolysis wavelengths the pathway leading to ClO is not observed, corresponding to $\varphi_{ClO} \leq 0.02$ at 250 nm and $\varphi_{ClO} \leq 0.10$ at 308 nm.

A quantum yield of $\varphi_{Cl} = 1.0$ (± 0.1) is recommended throughout the range at wavelengths below 300 nm, while $\varphi_{Cl} = 0.9$ (± 0.1) is recommended at $\lambda > 300$ nm.

Table 4-85. Absorption Cross Sections of ClOOCl at 195-265 K

λ (nm)	$10^{20}\sigma(cm^2)$	λ (nm)	$10^{20}\sigma(cm^2)$	λ (nm)	$10^{20}\sigma(cm^2)$	λ (nm)	$10^{20}\sigma(cm^2)$
190	565.0	256	505.4	322	23.4	388	1.4
192	526.0	258	463.1	324	21.4	390	1.3
194	489.0	260	422.0	326	19.2	392	1.2
196	450.0	262	381.4	328	17.8	394	1.1
198	413.0	264	344.6	330	16.7	396	1.0
200	383.5	266	311.6	332	15.6	398	0.92
202	352.9	268	283.3	334	14.4	400	0.85
204	325.3	270	258.4	336	13.3	402	0.78
206	298.6	272	237.3	338	13.1	404	0.71
208	274.6	274	218.3	340	12.1	406	0.65
210	251.3	276	201.6	342	11.5	408	0.60
212	231.7	278	186.4	344	10.9	410	0.54
214	217.0	280	172.5	346	10.1	412	0.50
216	207.6	282	159.6	348	9.0	414	0.46
218	206.1	284	147.3	350	8.2	416	0.42
220	212.1	286	136.1	352	7.9	418	0.38
222	227.1	288	125.2	354	6.8	420	0.35
224	249.4	290	114.6	356	6.1	422	0.32
226	280.2	292	104.6	358	5.8	424	0.29
228	319.5	294	95.4	360	5.5	426	0.27
230	365.0	296	87.1	362	4.5	428	0.25
232	415.4	298	79.0	364	4.1	430	0.23
234	467.5	300	72.2	366	3.8	432	0.21
236	517.5	302	65.8	368	3.5	434	0.19
238	563.0	304	59.9	370	3.2	436	0.17
240	600.3	306	54.1	372	2.9	438	0.16
242	625.7	308	48.6	374	2.7	440	0.15
244	639.4	310	43.3	376	2.4	442	0.13
246	642.6	312	38.5	378	2.2	444	0.12
248	631.5	314	34.6	380	2.1	446	0.11
250	609.3	316	30.7	382	1.9	448	0.10
252	580.1	318	28.0	384	1.7	450	0.09
254	544.5	320	25.6	386	1.6		

Note:

190-200nm, DeMore and Tschuikow-Roux [214],
200-360 nm, mean of Cox and Hayman [190], Burkholder et al. [115], Permien et al. [630] and DeMore and Tschuikow-Roux [214],
362-450 nm, extrapolation $\log (10^{20}\ \sigma(cm^2) = 7.589 - 0.01915\ \lambda(nm)$

F8. $Cl_2O_3 + h\nu \rightarrow$ Products. The absorption cross sections of Cl_2O_3 have been measured at 293 K and 257.7 nm by Lipscomb et al. [457], at 233 K and 220-335 nm by Hayman and Cox [321], at 200-260 K and 220-320 nm by Burkholder et al. [113], at 223 K and 220-330 nm by Harwood et al. [318], and recently at room temperature and 201-320 nm by Green et al. [301]. Although the shape of the spectrum measured by the different group is in agreement, the cross sections are significantly different. Hayman and Cox [318] report the largest values, whereas the new data of Green et al. [301] are the lowest of all measurements. Particularly the spectrum of Green et al. [301] matches the shape of the spectrum measured by Burkholder et al. [113] more closely that it does those of Harwood et al. [318] or Hayman and Cox [318]. In addition, Burkholder et al. [113] and Green et al. [301] observed no long-wavelength tail in the region 300-450 nm, such as is observed by Harwood et al. [318] and Hayman and Cox [318]. At the maximum of the spectrum the values differ by 30%. Table 4-86 lists the recommended values. These are derived by averaging the spectra of Hayman and Cox [321], Burkholder et al. [113], Harwood et al. [318], and Green et al. [301]. Additional work is needed, particularly in the spectral region beyond 300 nm.

Table 4-86. Absorption Cross Sections of Cl_2O_3 at 220-260 K

λ (nm)	$10^{20}\,\sigma$ (cm^2)	λ (nm)	$10^{20}\,\sigma$ (cm^2)	λ (nm)	$10^{20}\,\sigma$ (cm^2)
220	1145	255	1443	290	763
225	1113	260	1596	295	566
230	1060	265	1661	300	417
235	1028	270	1614	305	294
240	1044	275	1464	310	212
245	1127	280	1239	315	159
250	1271	285	995	320	132

Note:
220-320 nm, mean of the data of Hayman and Cox [321], Burkholder et al. [113], Harwood et al. [318], and Green et al. [301].

F9. $Cl_2O_4 + h\nu \rightarrow$ Products. The absorption cross sections of Cl_2O_4 (dichlorine tetraoxide, chlorine perchlorate) have been measured at room temperature and 200-310 nm by Lopez and Sicre [460] and at 200-350 nm by Green et al. [300]. The absorption spectrum exhibits a weak band between 303 and 350 nm with the maximum at 327 nm, a stronger band between 212 and 303 nm with the maximum at 233 nm, and a further increase of the absorption cross sections below 212 nm. The absorption cross sections reported by Lopez and Sicre [460] and Green et al. [300], who applied a similar method of preparing Cl_2O_4, are in very good agreement in the region ~215-250 nm. Discrepancies are obvious below 215 nm, where the values of Lopez and Sicre [460] become larger by up to a factor ~1.7 at 200 nm than the values of Green et al. [300], and in the region of the weak absorption band, which has not been observed by Lopez and Sicre [460]. We follow the arguments of Green et al. [300] concerning their confidence in the accuracy of their measurements and recommend their results. Green et al. [300] report cross sections, which are the averages over 1-nm intervals of the data obtained at a resolution of 0.34 nm. We select the data for even wavelengths, which are listed in Table 4-87.

Table 4-87. Absorption Cross Sections of Cl_2O_4 at 298 K

λ (nm)	10^{20} σ (cm^2)	λ (nm)	10^{20} σ (cm2)	λ (nm)	10^{20} σ (cm^2)	λ (nm)	10^{20} σ (cm^2)
200	96.81	238	84.94	276	9.95	314	1.35
202	87.88	240	80.97	278	8.38	316	1.49
204	77.84	242	76.05	280	6.98	318	1.62
206	73.24	244	70.95	282	5.76	320	1.74
208	67.51	246	65.17	284	4.70	322	1.83
210	64.62	248	59.53	286	3.79	324	1.91
212	61.79	250	53.84	288	3.03	326	1.96
214	61.74	252	48.55	290	2.40	328	1.98
216	63.46	254	43.30	292	1.89	330	1.96
218	66.58	256	38.52	294	1.50	332	1.92
220	70.82	258	34.33	296	1.21	334	1.85
222	74.95	260	30.28	298	1.01	336	1.75
224	79.70	262	26.63	300	0.88	338	1.63
226	83.84	264	23.55	302	0.83	340	1.50
228	87.21	266	20.58	304	0.83	342	1.36
230	89.19	268	17.97	306	0.88	344	1.23
232	90.06	270	15.81	308	0.97	346	1.11
234	89.67	272	13.62	310	1.08	348	1.02
236	87.86	274	11.77	312	1.21	350	0.98

Note:
200-350 nm, Green et al. [300].

F10. $Cl_2O_6 + h\nu \rightarrow$ Products. The absorption cross sections for Cl_2O_6 (chlorine hexoxide, chloryl perchlorate) have been measured at room temperature and 200-386 nm by Lopez and Sicre [461], at 268 nm by Jansen et al. [369], and at 200-450 nm by Green et al. [300]. A spectrum measured by Goodeve and Richardson [288] and originally attributed to ClO_3, was shown by Lopez and Sicre [461] to be most likely that of Cl_2O_6. The cross sections measured by Lopez and Sicre [461] are several times larger than those reported by Goodeve and Richardson [288], but the shape of the spectrum is similar. There is excellent agreement between the data of Lopez and Sicre [461] and Green et al. [300] at wavelengths between 210 and 310 nm; the data of Green et al. [300] are smaller by ~10% than those of Lopez and Sicre [461] at 200 nm, and become increasingly larger at wavelengths above 320 nm by up to a factor ~ 3 at 380 nm. The absorption curve reported by Green et al. [300] shows a logarithmic decrease at wavelengths 300-390 nm. We recommend the most recent data of Green et al. [300] who report cross sections, which are the averages over 1-nm intervals of the data obtained at a resolution of 0.34 nm. We select the data for even wavelengths, which are listed in Table 4-88.

Table 4-88. Absorption Cross Sections of Cl_2O_6 at 298 K

λ (nm)	10^{20} σ (cm^2)	λ (nm)	10^{20} σ (cm^2)	λ (nm)	10^{20} σ (cm^2)	λ (nm)	10^{20} σ (cm^2)
200	1104	248	1085	296	1173	344	195
202	1135	250	1111	298	1115	346	180
204	1161	252	1142	300	1056	348	167
206	1208	254	1177	302	997	350	153
208	1233	256	1217	304	939	352	141
210	1254	258	1256	306	880	354	130
212	1261	260	1297	308	822	356	121
214	1266	262	1337	310	767	358	111
216	1260	264	1375	312	714	360	103
218	1245	266	1410	314	664	362	96
220	1230	268	1440	316	615	364	89
222	1207	270	1466	318	569	366	81
224	1182	272	1485	320	526	368	75
226	1156	274	1496	322	485	370	71
228	1132	276	1500	324	447	372	66
230	1108	278	1497	326	412	374	61
232	1086	280	1488	328	380	376	57
234	1066	282	1469	330	350	378	52
236	1052	284	1444	332	322	380	49
238	1042	286	1411	334	296	382	46
240	1039	288	1373	336	271	384	43
242	1041	290	1329	338	251	386	40
244	1049	292	1281	340	231	388	37
246	1065	294	1229	342	212	390	36

Note:
200-390 nm, Green et al. [300].

F11. $Cl_2O_7 + h\nu \rightarrow$ Products. The absorption cross sections of chlorine heptoxide have been measured at room temperature and 222-302 nm by Goodeve and Windsor [292] and at 180-310 nm by Lin [454]. There is agreement between the two data sets only near 290 nm. The cross sections reported by Goodeve and Windsor [292] become larger at shorter wavelengths than those reported by Lin [454], larger by up to a factor of more than 4 at 225 nm, and smaller at longer wavelengths by up to a factor ~3 at 300 nm. In Table 4-89 are listed the absorption cross sections of Cl_2O_7 measured by Lin [454].

Table 4-89. Absorption Cross Sections of Cl_2O_7 at 298 K

λ (nm)	10^{20} σ (cm^2)	λ (nm)	10^{20} σ (cm^2)	λ (nm)	10^{20} σ (cm^2)
180	1188	225	79.7	270	3.77
185	908.5	230	61.0	275	2.57
190	674.7	235	45.6	280	1.70
195	475.3	240	34.6	285	1.20
200	322	245	24.7	290	0.705
205	231	250	17.5	295	0.521
210	169	255	12.0	300	0.368
215	132	260	7.74	305	0.203
220	102	265	5.37	310	0.104

Note:
180-310 nm. Lin [454].

F12. $ClClO_2 + h\nu \rightarrow$ Products. The absorption cross sections of chloryl chloride have been measured in the gas phase at room temperature and 220-390 nm with a spectral resolution of 0.4 - 1 nm (and in noble gas matrices at low temperatures) by Müller and Willner [565], and reinvestigated using the same spectrometer between 180 and 390 nm by Jacobs et al. [367]. The spectrum exhibits two absorption maxima at 226 nm ($\sigma = 1.38 \times 10^{-17}$ cm^2 $molecule^{-1}$) and 296 nm ($\sigma = 1.51 \times 10^{-17}$ cm^2 $molecule^{-1}$), two minima at 192 and 261 nm, and a decrease of the cross sections above 300 nm. Absorption cross sections at 5-nm intervals as listed by Müller and Willner [565] are given in Table 4-90. Photolysis experiments of matrix isolated $ClClO_2$ suggest it to

absorb in the visible region, nevertheless cross section between 500 and 800 nm is estimated to be below 10^{-20} cm^2 $molecule^{-1}$.

Table 4-90. Absorption Cross Sections of $ClClO_2$ at 298 K

λ (nm)	10^{20} σ (cm^2)	λ (nm)	10^{20} σ (cm^2)	λ (nm)	10^{20} σ (cm^2)	λ (nm)	10^{20} σ (cm^2)
220	920	265	550	310	1120	355	50
225	1160	270	660	315	870	360	40
230	1270	275	830	320	630	365	40
235	1210	280	1050	325	430	370	30
240	1060	285	1260	330	280	375	30
245	880	290	1430	335	190	380	20
250	720	295	1500	340	120	385	20
255	590	300	1470	345	80	390	20
260	530	305	1330	350	60		

Note: Müller and Willner [565]

F13. $HCl + h\nu \rightarrow H + Cl$ ($^2P_{3/2}$ and $^2P_{1/2}$).

$DCl + h\nu \rightarrow D + Cl$. The absorption cross sections of HCl have been measured at room temperature and 139-207 nm by Romand and Vodar [686] and Romand [684], at 140-200 nm by Myer and Samson [568], at 140-220 nm by Inn [363], at 170-215 nm by Roxlo and Mandl [692], at 132-185 nm by Nee et al. [577], and at 120-230 nm (also for DCl) by Bahou et al. [36] and Cheng et al. [163]. Single absorption cross sections have been measured for 121.6 nm by Vatsa and Volpp [814], for 193 nm by Mo et al. [535], and for 135 nm by Hanf et al. [309]. Absorption cross sections obtained by dipole (e,e) spectroscopy have been reported for the region 8-40 eV (155-31 nm) by Daviel et al. [206]. The spectrum exhibits a broad absorption band between 135 and 230 nm, corresponding to the $A\ ^1\Pi \leftarrow X\ ^1\Sigma^+$ transition, with the maximum at ~154 nm for HCl and ~156 nm for DCl. There is good agreement within the experimental uncertainties among the recent data of Bahou et al. [36] / Cheng et al. [163] with those of Nee et al. [577], and Inn [363]. The values of Bahou et al. [36] / Cheng et al. [163] generally are larger than those of Nee et al. [577], larger by less than 10% at 132-170 nm and larger by less than 25% above 170 nm. Also the values of Bahou et al. [36] / Cheng et al. [163] generally are slightly smaller, by less than 10%, than those of Inn [363] except for the region above 210 nm. The absorption curve of Inn [363], who measured the cross sections at 2.5- nm intervals, seem to have shoulders near 147.5 nm and 160 nm around the distinct maximum at ~155 nm. This is in contrast to the results of Bahou et al. [36] / Cheng et al. [163] obtained at a resolution of 0.1 nm and those of Nee et al. [577] obtained at a resolution of 0.05 nm: their absorption curves show a smooth and continuous behavior around absorption maximum. As recommended absorption cross sections for HCl and DCl we choose the most recent results of Bahou et al. [36] / Cheng et al. [163]. In Table 4-91 are listed averages over 2.5- and 5-nm intervals of their data measured at 0.1-nm resolution as reported by Bahou et al. [36].

Photodissociation of HCl was studied by Matsumi et al. [497-499, 782] and the branching fraction Cl ($^2P_{1/2}$) / (Cl ($^2P_{1/2}$) + Cl ($^2P_{3/2}$)) determined to be 0.33 ± 0.05 at 193 nm and 0.45-0.47 (± 0.04) at 157 nm; Lambert et al. [430] measured branching fractions between 0.47 and 0.33 for eight wavelengths between 193 and 235 nm for HCl; Zhang et al. [880] obtained 0.41 ± 0.01 at 193.3 nm; Regan et al. [668] obtained values between 0.42 and 0.48 for 5 wavelengths in the range 201-210 nm, and Regan et al. [667] values between 0.41 to 0.53 for selected rovibrational states at 235 nm. The latter 4 studies and the results from Liyanage et al. [458] are in good agreement with calculations of Alexander et al. [11].

Table 4-91. Absorption Cross Sections of HCl and DCl at 298 K

λ (nm)	10^{20} σ (cm^2)		λ (nm)	10^{20} σ (cm^2)	
	HCl	DCl		HCl	DCl
135.0	123	45.5	**175.0**	106	87.1
137.5	152	75.9	**177.5**	79.6	58.9
140.0	205	120	**180.0**	58.9	38.5
142.5	238	184	**182.5**	42.3	23.9
145.0	279	248	**185.0**	29.4	14.5
147.5	311	308	**187.5**	20.3	8.80
150.0	334	364	**190.0**	13.8	4.93
152.5	342	393	**195.0**	5.96	1.67
155.0	343	415	**200.0**	2.39	0.485
157.5	327	407	**205.0**	0.903	0.136
160.0	306	367	**210.0**	0.310	0.040
162.5	273	321	**215.0**	0.101	0.011
165.0	240	267	**220.0**	0.030	0.0027
167.5	199	211	**225.0**	0.010	
170.0	163	166	**230.0**	0.0034	
172.5	136	119			

Note:
135-230 nm, Bahou et al. [36]

F14. $HOCl + h\nu \rightarrow OH + Cl$

$HOCl + h\nu \rightarrow HCl + O(^3P)$. The absorption spectrum of HOCl exhibits an intensive singlet-singlet absorption in the near-UV region with a strong maximum near 240 nm (mostly the $2\ ^1A' \leftarrow 1\ ^1A'$ transition), and a weak shoulder near 300 nm (arising from the $1\ ^1A'' \leftarrow 1\ ^1A'$ transition). The absorption cross sections of HOCl vapor have been measured by several groups. Molina and Molina [537] and Knauth et al. [411] produced this species using equilibrium mixtures with Cl_2O and H_2O; their results provided the basis for the earlier recommendation. More recently, Mishalanie et al. [533] and Permien et al. [630] used a dynamic source to generate the HOCl vapor. The cross section values reported by Molina and Molina [537], Mishalanie et al. [533], and Permien et al. [630] are in reasonable agreement between 250 and 330 nm. In this wavelength range, the values reported by Knauth et al. [411] are significantly smaller, e.g., a factor of 4 at 280 nm. Beyond 340 nm, the cross sections of Mishalanie et al. are much smaller than those obtained by the other three groups. At 365 nm, the discrepancy is about an order of magnitude.

Burkholder [108] has remeasured the absorption spectrum of HOCl over the wavelength range 200 to 380 nm, following photolysis of equilibrium mixtures of Cl_2O-H_2O-HOCl. The obtained spectrum displays two absorption maxima at 242 and 304 nm, and is in excellent agreement with the work of Knauth et al. [411], but in poor agreement with the measurements of Mishalanie et al. [533] and Permien et al. [630]. The discrepancies can be attributed mostly to difficulties in correcting the measured absorptions for the presence of Cl_2 and Cl_2O. In the study by Burkholder [108], several control experiments were carried out in order to check the internal consistency of the data. Moreover, Barnes et al. [42] examined the near-UV spectrum of HOCl by monitoring the OH fragments resulting from photodissociation, and revealed a third weak band centered at 387 nm extending down to 480 nm, arising from a weak singlet-triplet transition (Minaev [529]). The recommended cross sections up to 420 nm, calculated from an analytical expression provided by Barnes et al. [42] and based on the values of Burkholder [108] and Barnes et al. [42], are listed in Table 4-92. The work by Jungkamp et al. [400] yields cross section values in excellent agreement with this recommendation for wavelengths < 350 nm.

Molina et al. [549] observed production of OH radicals in the laser photolysis of HOCl around 310 nm, and Butler and Phillips [129] found no evidence for O-atom production at 308 nm, placing an upper limit of ~0.02 for the primary quantum yield for the HCl + O channel. Vogt and Schindler [824] used broadband photolysis in the 290–390 nm wavelength range, determining a quantum yield for OH production of >0.95. Schindler et al. [710] measured the quantum yield for atomic Cl as 1.00 ± 0.05 at 308 nm. These authors also determined the probability P to generate $Cl^*(^2P_{1/2})$ relative to Cl ($^2P_{3/2}$), P = 0.035 ± 0.02 at 308 nm, and P = 0.35 ± 0.02 at 235 nm, in agreement with P = 0.30 ± 0.07 at 236 nm reported by Bell et al. [65]. Fujiwara and Ishiwata [256] determined the relative yield of $OH(^2\Pi_{3/2})$ / $OH(^2\Pi_{1/2})$ to be 2.0 at 266 nm and 1.5 at 355 nm.

Table 4-92. Absorption Cross Sections of HOCl

λ (nm)	10^{20} σ (cm^2)	λ (nm)	10^{20} σ (cm^2)	λ (nm)	10^{20} σ (cm^2)
200	7.18	274	5.26	348	1.55
202	6.39	276	4.94	350	1.43
204	5.81	278	4.74	352	1.33
206	5.46	280	4.64	354	1.24
208	5.37	282	4.62	356	1.17
210	5.54	284	4.68	358	1.11
212	5.98	286	4.79	360	1.06
214	6.68	288	4.95	362	1.02
216	7.63	290	5.13	364	0.985
218	8.81	292	5.33	366	0.951
220	10.2	294	5.52	368	0.919
222	11.6	296	5.71	370	0.888
224	13.2	298	5.86	372	0.855
226	14.7	300	5.99	374	0.822
228	16.2	302	6.08	376	0.786
230	17.5	304	6.12	378	0.748
232	18.7	306	6.12	380	0.708
234	19.6	308	6.07	382	0.667
236	20.2	310	5.97	384	0.624
238	20.5	312	5.84	386	0.580
240	20.6	314	5.66	388	0.535
242	20.3	316	5.45	390	0.491
244	19.8	318	5.21	392	0.447
246	19.0	320	4.95	394	0.405
248	18.1	322	4.67	396	0.364
250	17.0	324	4.38	398	0.325
252	15.8	326	4.09	400	0.288
254	14.6	328	3.79	402	0.254
256	13.3	330	3.50	404	0.222
258	12.1	332	3.21	406	0.194
260	10.9	334	2.94	406	0.168
262	9.73	336	2.68	410	0.144
264	8.68	338	2.44	412	0.124
266	7.75	340	2.22	414	0.105
268	6.94	342	2.02	416	0.089
270	6.25	344	1.84	418	0.075
272	5.69	346	1.69	420	0.063

F15. $ClNO + h\nu \rightarrow Cl + NO$. Nitrosyl chloride has a continuous absorption extending beyond 650 nm. There is good agreement between the work of Martin and Gareis [490] for the 240-to-420-nm wavelength region, of Ballash and Armstrong [38] for the 185 to 540 nm region, of Illies and Takacs [360] for the 190-to-400-nm region, and of Tyndall et al. [792] for the 190-to-350-nm region except around 230 nm, where the values of Ballash and Armstrong are larger by almost a factor of two. Roehl et al. [681] measured the absorption cross sections between 350 and 650 nm at several temperatures between 223 and 343 K. Their room temperature results agree to within 15% with those of Martin and Gareis [490], Ballash and Amstrong [38], and Tyndall et al. [792]. Table 4-93 lists the recommended cross sections: these are taken from the work of Tyndall et al. [792] between 190 and 350 nm (unchanged from the previous recommendation), and from Roehl et al. [681] beyond 350 nm.

The quantum yield for the primary photolytic process has been reviewed by Calvert and Pitts [136]. It is unity over the entire visible and near-ultraviolet bands. Chichinin [167] found evidence of ground state ($^2P_{3/2}$) and excited ($^2P_{1/2}$) atomic chlorine products and measured a relative quantum yield $Cl(^2P_{1/2})/ (Cl(^2P_{1/2}) + Cl(^2P_{3/2}))$ to be 0.88 ± 0.12 at 248 nm and 0.90 ± 0.10 at 351 nm; Felder and Morley [239] obtained 0.80 at 248 nm; Skorokhodov et al. [741] obtained 0.48 ± 0.03 at 212 nm, 0.30 at 235 nm., and 0.52 ± 0.03 at 248 nm.

Table 4-93. Absorption Cross Sections of ClNO

λ (nm)	10^{20} σ (cm^2)	λ (nm)	10^{20} σ (cm^2)	λ (nm)	10^{20} σ (cm^2)	λ (nm)	10^{20} σ (cm^2)
190	4320	246	45.2	302	10.3	370	11.0
192	5340	248	37.7	304	10.5	375	9.95
194	6150	250	31.7	306	10.8	380	8.86
196	6480	252	27.4	308	11.1	385	7.82
198	6310	254	23.7	310	11.5	390	6.86
200	5860	256	21.3	312	11.9	395	5.97
202	5250	258	19.0	314	12.2	400	5.13
204	4540	260	17.5	316	12.5	405	4.40
206	3840	262	16.5	318	13.0	410	3.83
208	3210	264	15.3	320	13.4	415	3.38
210	2630	266	14.4	322	13.6	420	2.89
212	2180	268	13.6	324	14.0	425	2.45
214	1760	270	12.9	326	14.3	430	2.21
216	1400	272	12.3	328	14.6	435	2.20
218	1110	274	11.8	330	14.7	440	2.20
220	896	276	11.3	332	14.9	445	2.07
222	707	278	10.7	334	15.1	450	1.87
224	552	280	10.6	336	15.3	455	1.79
226	436	282	10.2	338	15.3	460	1.95
228	339	284	9.99	340	15.2	465	2.25
230	266	286	9.84	342	15.3	470	2.50
232	212	288	9.71	344	15.1	475	2.61
234	164	290	9.64	346	15.1	480	2.53
236	120	292	9.63	348	14.9	485	2.33
238	101	294	9.69	350	14.2	490	2.07
240	82.5	296	9.71	355	13.6	495	1.78
242	67.2	298	9.89	360	12.9	500	1.50
244	55.2	300	10.0	365	12.0		

F16 $ClNO_2 + h\nu \rightarrow Cl + NO_2$

$ClNO_2 + h\nu \rightarrow ClNO + O$. The absorption cross sections of nitryl chloride, $ClNO_2$, have been measured between 230 and 330 nm by Martin and Gareis [490], between 185 and 400 nm by Illies and Takacs [360], between 270 and 370 nm by Nelson and Johnston [580], by Ganske et al. [260] between 200 and 370 nm, and between 190 and 450 nm by Furlan et al. [258]. The absorption spectrum starts at ~400 nm and shows three broad bands, a weak band at ~300 nm and two stronger bands at ~215 nm and below 185 nm. In the range 220-280 nm weak, but distinct vibrational structure has been observed by Furlan et al. [258]. A major source of discrepancies in the data results from the presence of impurities. Table 4-94 lists the recommended values, which are the mean values of the data of Illies and Takacs [360] (as listed in the paper) and of Furlan et al. [258] (5-nm averages of their high-resolution data).

Nelson and Johnston [580] report a value of 0.93 ± 0.15 for the quantum yield for production of chlorine atoms; they also report a negligible quantum yield for the production of oxygen atoms (< 0.02). Carter et al. [154] reported at 235 nm the formation of NO_2 in the electronic ground state (yield 0.15 ± 0.05) and in the excited state (yield 0.85 ± 0.05).

Table 4-94. Absorption Cross Sections of $ClNO_2$ at 298 K

λ (nm)	10^{20} σ (cm^2)	λ (nm)	10^{20} σ (cm^2)
195	1060	280	20.7
200	445	290	16.3
205	310	300	14.1
210	321	310	12.1
215	339	320	9.40
220	325	330	6.79
225	279	340	4.62
230	221	350	3.05
235	169	360	1.86
240	132	370	1.12
250	90.9	380	0.772
260	58.7	390	0.475
270	33.7	400	0.327

F17. $ClONO + h\nu \rightarrow$ Products. Measurements in the near-ultraviolet of the cross sections of chlorine nitrite (ClONO) have been made by Molina and Molina [536]. Their results are listed in Table 4-95. The characteristics of the spectrum and the instability of ClONO strongly suggest that the quantum yield for decomposition is unity. The Cl–O bond strength is only about 20 kcal $mole^{-1}$, so that chlorine atoms are likely photolysis products.

Table 4-95. Absorption Cross Sections of ClONO at 231 K

λ (nm)	10^{20} σ (cm^2)	λ (nm)	10^{20} σ (cm^2)
235	215.0	320	80.3
240	176.0	325	75.4
245	137.0	330	58.7
250	106.0	335	57.7
255	65.0	340	43.7
260	64.6	345	35.7
265	69.3	350	26.9
270	90.3	355	22.9
275	110.0	360	16.1
280	132.0	365	11.3
285	144.0	370	9.0
290	144.0	375	6.9
295	142.0	380	4.1
300	129.0	385	3.3
305	114.0	390	2.2
310	105.0	395	1.5
315	98.1	400	0.6

F18. $ClONO_2 + h\nu \rightarrow Cl + NO_3$
$ClONO_2 + h\nu \rightarrow ClO + NO_2$
$ClONO_2 + h\nu \rightarrow O(^3P) + ClONO$. The recommended cross sections are taken from the work of Burkholder et al. [118]; the values are listed in Table 4-96, together with the parameters needed to compute their temperature dependency. These values are in very good agreement with those reported by Molina and Molina [538], which provided the basis for the previous recommendation, and which supersedes the earlier work of Rowland et al. [689].

Several groups have investigated the identity of the primary photolytic fragments. Smith et al. [745] report O + ClONO as the most likely products, using endproduct analysis and steady-state photolysis. The results of Chang et al. [157], who employed the very low-pressure photolysis (VLPPh) technique, indicate that the products are $Cl + NO_3$, with a quantum yield of 1.0 ± 0.2. Adler-Golden and Wiesenfeld [10], using a flash photolysis atomic absorption technique, find O-atoms to be the predominant photolysis product and report a quantum yield for Cl-atom production of less than 4%. Marinelli and Johnston [486] report a quantum yield

for NO_3 production at 249 nm between 0.45 and 0.85, with a most likely value of 0.55; they monitored NO_3 by tunable dye-laser absorption at 662 nm. Margitan [474] used atomic resonance fluorescence detection of O- and Cl-atoms and found the quantum yield at 266 nm and at 355 nm to be 0.9 ± 0.1 for Cl-atom production and ~0.1 for O-atom production, with no discernible difference at the two wavelengths. These results were confirmed by Knauth and Schindler [412], who used end-product analysis to infer the quantum yields from photolysis studies at 265 and 313 nm. Burrows et al. [126] report also Cl and NO_3 as the photolysis products at 254 nm, with a quantum yield of unity within experimental error, and a O atom quantum yield of 0.24. In contrast, Nikolaisen et al. [583] using broadband photolysis found that at $\lambda > 200$ nm the relative branching ratios are 0.61 ± 0.20 for the channel ClO + NO_2 and 0.39 ± 0.20 for the channel Cl + NO_3; in the $\lambda > 300$ nm region the quantum yields are found to be 0.44 ± 0.08 for production of ClO and NO_2 and 0.56 ± 0.08 for production of Cl and NO_3. Minton et al. [532], Nelson et al. [579], and Moore et al. [552] made the first direct measurements of ClO and obtained comparable yields for the Cl + NO_3 and the ClO + NO_2 channels, using a molecular beam technique: at 193, they obtained respectively 0.64 ± 0.08 and 0.36 ± 0.08, at 248 nm 0.54 ± 0.08 and 0.46 ± 0.08, and at 308 nm 0.67 ± 0.06 and 0.33 ± 0.06. These authors found no evidence for channel O + ClONO, and placed an upper limit for this channel of 0.04. Tyndall et al. [791] observed quantum yields of 0.80 ± 0.08 and 0.28 ± 0.12 for Cl and ClO at 308 nm using resonance fluorescence detection methods, and reported a very small $O(^3P)$ yield ≤ 0.05. Ravishankara [657], Goldfarb et al. [287] and Yokelson et al. [857] have studied the photodissociation of $ClONO_2$ at 193, 222, 248 and 308 nm, using both atomic resonance fluorescence and time-resolved absorption methods. They found that Cl and ClO are the two major dissociation products at 222, 248 and 308 nm, whereas at 193 nm, the quantum yield of O atoms became larger than the yield of ClO. At 193, 222, 248 and 308 nm, the yield of Cl was 0.53 ± 0.10, 0.46 ± 0.10, 0.41 ± 0.13 and 0.64 ± 0.20, respectively; the O-atom yield 0.73 ± 0.08, 0.17 ± 0.08, <0.10 and <0.05; and the ClO yield 0.29 ± 0.20, 0.64 ± 0.20, 0.39 ± 0.19 and 0.37 ± 0.19. The yield of NO_3 was also determined by Yokelson et al. [857] as 0.93 ± 0.24 at 352.5 nm, 0.67 ± 0.09 at 308 nm, 0.60 ± 0.09 at 248 nm, and 0.18 ± 0.04 at 193 nm. In addition, they measured the Cl atom yield as 0.73 ± 0.14 at 308 nm, 0.60 ± 0.12 at 248 nm and 0.45 ± 0.08 at 193 nm, and the O atom yield as <0.4 at 248 nm and < 0.9 at 193 nm. Recently, Zou et al. [886] determined absolute quantum yields for the Cl and ClO channels at 235 nm to be 0.42 ± 0.1 and 0.58 ± 0.1, respectively, using molecular beam techniques and TOFMS/REMPI. The recommended quantum yield values for production of Cl + NO_3 (ϕ_1) and ClO + NO_2 (ϕ_2) are given at the bottom of Table 4-96 and are based on the work of Nelson et al. [579], Moore et al. [552], Nickolaisen et al. [583], and Ravishankara [657]. For wavelengths shorter than 308 nm the value of ϕ_1 is 0.6, and for ϕ_2 it is 0.4. For longer wavelengths ϕ_1 increases linearly to 0.9 at 350 nm, with the corresponding decrease in ϕ_2 to 0.1. There is no evidence for production of O + ClONO in the more recent work; the production of O-atoms reported in some of the earlier studies might have resulted from decomposition of excited NO_3. Zou et al. [886] determined the quantum yield of spontaneous decomposition of NO_3 into NO_2 + O to be 0.20, and into NO + O_2 to be 0.006.

Recent work by Nickolaisen et al. [583] indicates that the photodissociation quantum yield is less than unity at wavelengths longer than about 330 nm, because of the formation of a long-lived intermediate that might be quenched under atmospheric conditions (a situation analogous to that of Cl_2O). Additional work is needed to address these issues, which have potentially important atmospheric consequences.

Table 4-96. Absorption Cross Sections and Temperature Coefficients of $ClONO_2$

$\sigma(\lambda, T) = \sigma(\lambda, 296)\,(1 + A1\,(T - 296) + A2\,(T - 296)2)$; T in K

λ (nm)	$10^{20}\sigma(\lambda, 296)$ (cm^2)	A1*) (K^{-1})	A2*) (K^{-1})	λ (nm)	$10^{20}\sigma(\lambda, 296)$ (cm^2)	A1*) (K^{-1})	A2*) (K^{-1})
196	310	9.90 (–5)	–8.38 (–6)	316	1.07	5.07 (–3)	1.56 (–5)
198	294	6.72 (–5)	–8.03 (–6)	318	0.947	5.24 (–3)	1.69 (–5)
200	282	–5.34 (–6)	–7.64 (–6)	320	0.831	5.40 (–3)	1.84 (–5)
202	277	–1.19 (–4)	–7.45 (–6)	322	0.731	5.55 (–3)	2.00 (–5)
204	280	–2.60 (–4)	–7.50 (–6)	324	0.647	5.68 (–3)	2.18 (–5)
206	288	–4.12 (–4)	–7.73 (–6)	326	0.578	5.80 (–3)	2.36 (–5)
208	300	–5.62 (–4)	–8.05 (–6)	328	0.518	5.88 (–3)	2.54 (–5)
210	314	–6.96 (–4)	–8.41 (–6)	330	0.466	5.92 (–3)	2.70 (–5)
212	329	–8.04 (–4)	–8.75 (–6)	332	0.420	5.92 (–3)	2.84 (–5)
214	339	–8.74 (–4)	–9.04 (–6)	334	0.382	5.88 (–3)	2.96 (–5)
216	345	–9.03 (–4)	–9.24 (–6)	336	0.351	5.80 (–3)	3.05 (–5)
218	341	–8.86 (–4)	–9.35 (–6)	338	0.326	5.68 (–3)	3.10 (–5)
220	332	–8.28 (–4)	–9.38 (–6)	340	0.302	5.51 (–3)	3.11 (–5)
222	314	–7.31 (–4)	–9.34 (–6)	342	0.282	5.32 (–3)	3.08 (–5)

λ (nm)	$10^{20}\sigma(\lambda, 296)$ (cm^2)	A1*) (K^{-1})	A2*) (K^{-1})	λ (nm)	$10^{20}\sigma(\lambda, 296)$ (cm^2)	A1*) (K^{-1})	A2*) (K^{-1})
224	291	–6.04 (–4)	–9.24 (–6)	344	0.264	5.07 (–3)	2.96 (–5)
226	264	–4.53 (–4)	–9.06 (–6)	346	0.252	4.76 (–3)	2.74 (–5)
228	235	–2.88 (–4)	–8.77 (–6)	348	0.243	4.39 (–3)	2.42 (–5)
230	208	–1.13 (–4)	–8.33 (–6)	350	0.229	4.02 (–3)	2.07 (–5)
232	182	6.18 (–5)	–7.74 (–6)	352	0.218	3.68 (–3)	1.76 (–5)
234	158	2.27 (–4)	–7.10 (–6)	354	0.212	3.40 (–3)	1.50 (–5)
236	138	3.72 (–4)	–6.52 (–6)	356	0.205	3.15 (–3)	1.27 (–5)
238	120	4.91 (–4)	–6.14 (–6)	358	0.203	2.92 (–3)	1.06 (–5)
240	105	5.86 (–4)	–5.98 (–6)	360	0.200	2.70 (–3)	8.59 (–6)
242	91.9	6.64 (–4)	–6.04 (–6)	362	0.190	2.47 (–3)	6.38 (–6)
244	81.2	7.33 (–4)	–6.27 (–6)	364	0.184	2.22 (–3)	3.66 (–6)
246	71.6	8.03 (–4)	–6.51 (–6)	366	0.175	1.93 (–3)	2.42 (–7)
248	62.4	8.85 (–4)	–6.59 (–6)	368	0.166	1.62 (–3)	–3.62 (–6)
250	56.0	9.84 (–4)	–6.40 (–6)	370	0.159	1.33 (–3)	–7.40 (–6)
252	50.2	1.10 (–3)	–5.93 (–6)	372	0.151	1.07 (–3)	–1.07 (–5)
254	45.3	1.22 (–3)	–5.33 (–6)	374	0.144	8.60 (–4)	–1.33 (–5)
256	41.0	1.33 (–3)	–4.73 (–6)	376	0.138	6.73 (–4)	–1.54 (–5)
258	37.2	1.44 (–3)	–4.22 (–6)	378	0.129	5.01 (–4)	–1.74 (–5)
260	33.8	1.53 (–3)	–3.79 (–6)	380	0.121	3.53 (–4)	–1.91 (–5)
262	30.6	1.62 (–3)	–3.37 (–6)	382	0.115	2.54 (–4)	–2.05 (–5)
264	27.8	1.70 (–3)	–2.94 (–6)	384	0.108	2.25 (–4)	–2.11 (–5)
266	25.2	1.78 (–3)	–2.48 (–6)	386	0.103	2.62 (–4)	–2.11 (–5)
268	22.7	1.86 (–3)	–2.00 (–6)	388	0.0970	3.33 (–4)	–2.08 (–5)
270	20.5	1.94 (–3)	–1.50 (–6)	390	0.0909	4.10 (–4)	–2.05 (–5)
272	18.5	2.02 (–3)	–1.01 (–6)	392	0.0849	5.04 (–4)	–2.02 (–5)
274	16.6	2.11 (–3)	–4.84 (–7)	394	0.0780	6.62 (–4)	–1.94 (–5)
276	14.9	2.20 (–3)**	9.02 (–8)	396	0.0740	8.95 (–4)	–1.79 (–5)
278	13.3	2.29 (–3)	6.72 (–7)	398	0.0710	1.14 (–3)	–1.61 (–5)
280	11.9	2.38 (–3)	1.21 (–6)	400	0.0638	1.38 (–3)	–1.42 (–5)
282	10.5	2.47 (–3)	1.72 (–6)	402	0.0599	1.63 (–3)	–1.20 (–5)
284	9.35	2.56 (–3)	2.21 (–6)	404	0.0568	1.96 (–3)	–8.97 (–6)
286	8.26	2.66 (–3)	2.68 (–6)	406	0.0513	2.36 (–3)	–5.15 (–6)
288	7.24	2.75 (–3)	3.09 (–6)	408	0.0481	2.84 (–3)	–6.64 (–7)
290	6.41	2.84 (–3)	3.41 (–6)	410	0.0444	3.38 (–3)	4.47 (–6)
292	5.50	2.95 (–3)	3.74 (–6)	412	0.0413	3.96 (–3)	1.00 (–5)
294	4.67	3.08 (–3)	4.27 (–6)	414	0.0373	4.56 (–3)	1.60 (–5)
296	4.09	3.25 (–3)	5.13 (–6)	416	0.0356	5.22 (–3)	2.28 (–5)
298	3.57	3.45 (–3)	6.23 (–6)	418	0.0317	5.96 (–3)	3.07 (–5)
300	3.13	3.64 (–3)	7.36 (–6)	420	0.0316	6.70 (–3)	3.87 (–5)
302	2.74	3.83 (–3)	8.38 (–6)	422	0.0275	7.30 (–3)	4.58 (–5)
304	2.39	4.01 (–3)	9.30 (–6)	424	0.0242	7.82 (–3)	5.22 (–5)
306	2.09	4.18 (–3)	1.02 (–5)	426	0.0222	8.41 (–3)	5.95 (–5)
308	1.83	4.36 (–3)	1.11 (–5)	428	0.0207	9.11 (–3)	6.79 (–5)
310	1.60	4.53 (–3)	1.20 (–5)	430	0.0189	9.72 (–3)	7.52 (–5)
312	1.40	4.71 (–3)	1.30 (–5)	432	0.0188	9.96 (–3)	7.81 (–5)
314	1.22	4.89 (–3)	1.42 (–5)				

Notes:

*) (-n) means $x10^{-n}$.

**) Value corrected for an obvious misprint.

Quantum yields:

$$ClONO_2 + h\nu \rightarrow Cl + NO_3$$

$\phi_1 = 0.6$ ($\lambda < 308$ nm)

$\phi_1 = 7.143 \times 10^{-3}\ \lambda\ (nm) - 1.60$ (308 nm < λ < 364 nm)

$\phi_1 = 1.0$ ($\lambda > 364$ nm)

$$ClONO_2 + h\nu \rightarrow ClO + NO_2$$

$$\phi_2 = 1 - \phi_1$$

F19. $CCl_4 + h\nu \rightarrow$ Products. The absorption cross sections of CCl_4 have been measured at room temperature and 110–200 nm by Russell et al. [694] and Causley and Russell [156]; at 204–250 nm by Gordus and Bernstein [293]; at 186–226 nm by Rowland and Molina [688]; at 170–230 nm by Roxlo and Mandl [692]; and at 160–275 nm by Hubrich and Stuhl [346]; at 105-210 nm by Ibuki et al. [357]; and at 135 and 195 nm by Hanf et al. [309]; at 297–477 K and 250 nm by Currie et al. [199], at 279 and 296 K and 190–252 nm by Vanlaethem-Meurée et al. [808]; at 225–295 K and 174–250 nm by Simon et al. [734]; and at 220–300 K and 186–240 nm by Prahlad and Kumar [644]. The room temperature data agree within 10% between 190 and 235 nm and within 20% and 40% at 240 and 250 nm (except the value at 250 nm reported by Currie et al [199], which is lower than the half of the other values). The absorption curve based on the data (reported at 0.5-nm intervals) of Prahlad and Kumar [644] shows wiggles over the whole range 186–240 nm obviously due to experimental uncertainties. In the range 180–186 nm, the values reported by Hubrich and Stuhl [346] are higher by up to 25% than those reported by Simon et al. [734], and the value at 186 nm reported by Prahlad and Kumar [644] is lower by 18% than the value of Simon et al. [734]. In the maximum near 176 nm, the absorption cross section is 1.01×10^{-17} cm^2, as reported by Hubrich and Stuhl [346] and Simon et al. [734], whereas the plotted spectrum reported by Roxlo and Mandl [692] shows a lower value of $\sim 7 \times 10^{-18}$ cm^2. For a wavelength of 313 nm, an absorption cross section of $\leq 3.7 \times 10^{-26}$ cm^2 was derived by Rebbert and Ausloos [663] from the C_2H_5Cl yield in the photolysis of CCl_4-C_2H_6 mixtures. The preferred absorption cross sections at room temperature, listed in Table 4-97, are the mean of the values reported by Hubrich and Stuhl [346] and Simon et al. [734] at 174–192 nm, the values of Simon et al. [734] at 194–250 nm, and the data of Hubrich and Stuhl [346] at 255–275 nm. Absorption cross sections obtained by using synchrotron radiation as a tunable photoexcitation source have been reported for the region 4.9-200 nm by Ho [334] and for the region 50-200 nm by Seccombe et al. [718]. Cross sections for the region 6.4-225 nm were obtained by dipole (e,e) spectroscopy by Burton et al. [127].

The temperature dependence of the absorption cross sections becomes significant at wavelengths above 205 nm, where the cross sections decrease with decreasing temperature between 300 and 210 K as observed in good agreement by Simon et al. [734] and Prahlad and Kumar [644]. Simon et al. [734] parameterized the cross sections and the temperature dependence by the polynomial expansion

$$\log_{10} \sigma(\lambda, T) = \sum A_n \lambda^n + (T - 273) \times \sum B_n \lambda^n$$

and reported smoothed values for T = 210, 230, 250, 270, and 295 K, every 2 nm, and at wavelengths corresponding to the wavenumber intervals generally used in stratospheric photodissociation calculations. The parameters An and Bn for the ranges T = 210–300 K and λ = 194–250 nm are as follows:

$A_0 = -37.104$	$B_0 = 1.0739$
$A_1 = -5.8218 \times 10^{-1}$	$B_1 = -1.6275 \times 10^{-2}$
$A_2 = 9.9974 \times 10^{-3}$	$B_2 = 8.8141 \times 10^{-5}$
$A_3 = -4.6765 \times 10^{-5}$	$B_3 = -1.9811 \times 10^{-7}$
$A_4 = 6.8501 \times 10^{-8}$	$B_4 = 1.5022 \times 10^{-10}$

Quantum yields ≥ 0.9 and ~0.75 for the photodissociative processes $CCl_4 + h\nu \rightarrow CCl_3 + Cl$ at 213.9 nm and $CCl_4 + h\nu \rightarrow CCl_2 + 2Cl$ at 163.3 nm, respectively, were derived from the gas-phase photolysis of CCl_4 in the presence of HCl, HBr, and C_2H_6 by Rebbert and Ausloos [663]. A quantum yield for $Cl^*(^2P_{1/2})$ atom formation in the broad band photolysis of CCl_4, $\Phi(Cl^*) = 0.78 \pm 0.27$, was reported by Clark and Husain [174]. Photolysis of CCl_4 after pulsed laser excitation at 193 and 135 nm resulted in the quantum yields $\Phi(Cl) = 1.1 \pm 0.05$ and $\Phi(Cl^*) = 0.4 \pm 0.02$ (thus $\Phi(Cl + Cl^*) = 1.5 \pm 0.1$) at 193 nm and $\Phi(Cl) = 1.5 \pm 0.07$ and $\Phi(Cl^*) = 0.4 \pm 0.02$ (thus $\Phi(Cl + Cl^*) = 1.9 \pm 0.1$) at 135 nm as reported by Hanf et al. [309].

Table 4-97. Absorption Cross Sections of CCl_4 at 295–298 K

λ (nm)	10^{20} σ (cm^2)	λ (nm)	10^{20} σ (cm^2)	λ (nm)	10^{20} σ (cm^2)
174	956	204	61.0	234	2.20
176	1010	206	57.0	236	1.60
178	982.5	208	52.5	238	1.16
180	806	210	46.9	240	0.830
182	647	212	41.0	242	0.590
184	478.5	214	34.5	244	0.413
186	338.5	216	27.8	246	0.290
188	227	218	22.1	248	0.210
190	145.5	220	17.5	250	0.148
192	99.6	222	13.6	255	0.0661
194	76.7	224	10.2	260	0.0253
196	69.5	226	7.60	265	0.0126
198	68.0	228	5.65	270	0.00610
200	66.0	230	4.28	275	0.00239
202	63.8	232	3.04		

Notes:

174–192 nm: mean of Hubrich and Stuhl [346] and Simon et al. [734]
194–250 nm: Simon et al. [734]
255–275 nm: Hubrich and Stuhl [346].

F20. $CH_3OCl + h\nu \rightarrow CH_3O + Cl$

$CH_3OCl + h\nu \rightarrow CH_2O + HCl$. The absorption cross sections of CH_3OCl have been determined by Crowley et al. [197] in the wavelength range 400-460 nm and by Jungkamp et al. [400] in the range 230-400 nm. The preferred cross sections, listed in Table 4-98, are the mean of the values reported by these two groups. The agreement between the two sets of measurements is excellent at wavelengths longer than 250 nm; at the maximum near 230 nm the results of Jungkamp et al. [400] are about 15% smaller.

Schindler et al. [710] measured the quantum yield $\varphi = 0.95 \pm 0.05$ for the product channel $Cl + CH_3O$ at 308 nm. They also determined an upper limit of < 0.01 for HCl at 248 nm and the ratio $Cl^*(^2P_{1/2})/ Cl(^2P_{1/2})$ following photolysis at 235 and 238 nm to be 1.45 ± 0.05. Krisch et al. [422] used photofragment translational spectroscopy to confirm photodissociation of CH_3OCl at 248 nm resulted in cleavage of only the O-Cl bond and the formation of Cl and CH_3O.

Table 4-98. Absorption Cross Sections of CH_3OCl

λ (nm)	10^{20} σ (cm^2)	λ (nm)	10^{20} σ (cm^2)	λ (nm)	10^{20} σ (cm^2)
230	14.9	290	1.32	350	0.662
232	15.4	292	1.34	352	0.611
234	15.7	294	1.35	354	0.574
236	15.9	296	1.37	356	0.529
238	15.8	298	1.40	358	0.482
240	15.5	300	1.43	360	0.445
242	14.9	302	1.45	362	0.411
244	14.2	304	1.47	364	0.389
246	13.2	306	1.48	366	0.356
248	12.2	308	1.49	368	0.331
250	11.1	310	1.49	370	0.298
252	9.96	312	1.48	372	0.273
254	8.86	314	1.47	374	0.246
256	7.77	316	1.46	376	0.225
258	6.80	318	1.43	378	0.209
260	5.87	320	1.41	380	0.202
262	5.05	322	1.37	382	0.186
264	4.31	324	1.33	384	0.17
266	3.69	326	1.30	386	0.16
268	3.16	328	1.24	388	0.15
270	2.71	330	1.20	390	0.13

λ (nm)	10^{20} σ (cm^2)	λ (nm)	10^{20} σ (cm^2)	λ (nm)	10^{20} σ (cm^2)
272	2.35	332	1.14	392	0.14
274	2.06	334	1.09	394	0.13
276	1.83	336	1.04		
278	1.64	338	0.980		
280	1.53	340	0.918		
282	1.42	342	0.875		
284	1.37	344	0.822		
286	1.33	346	0.760		
288	1.32	348	0.709		

F21. $CHCl_3 + h\nu \rightarrow$ Products. The absorption cross sections of $CHCl_3$ have been measured at room temperature and in the far UV region at 113–182 nm by Lucazeau and Sandorfy [462]; at the Lyman-α line at 121.6 nm by Brownsword et al. [104]; and at 110–200 nm by Russell et al. [694]; at room temperature and 222.7 nm by Gordus and Bernstein [293]; at 160–255 nm by Hubrich and Stuhl [346]; at 279 and 296 K and 190–230 nm by Vanlaethem-Meurée et al. [808]; and at 225–295 K and 174–240 nm by Simon et al. [734]. The room temperature data of Vanlaethem- Meurée et al. [808] and Simon et al. [734] are identical at 190–210 nm and increasingly deviate up to ~15% at 212–240 nm. The data of Hubrich and Stuhl [346] and Simon et al. [734] agree to within 10% between 180 and 234 nm. The discrepancy increases to ~25% in the long-wavelength tail with the values of Hubrich and Stuhl [346] being larger than those of Simon et al. [734]. In the region of the absorption maximum at ~176 nm, there is the largest spread: a cross section of $\sim 5 \times 10^{-18}$ cm^2 was measured by Simon et al. [734] compared with 3.7×10^{-18} cm^2 reported by Hubrich and Stuhl [346] and $< 2 \times 10^{-18}$ cm^2 given in a plot by Lucazeau and Sandorfy [462]. We therefore recommend absorption cross sections only for the region above 180 nm. The values, listed in Table 4-99, are the mean of the values reported by Hubrich and Stuhl [346] and Simon et al. [734] for the range 180–240 nm. For the range 242–256 nm, these have been extrapolated ($\log \sigma = -1.2277 - 0.0844\ \lambda$) (in italics).

The temperature dependence of the absorption cross sections becomes significant at wavelengths above 194 nm, where the cross sections decrease with decreasing temperature between 295 and 210 K. Simon et al. [734] parameterized the cross sections and the temperature dependence by the polynomial expansion,

$$\log_{10} \sigma(\lambda, T) = \sum A_n \lambda^n + (T - 273) \times \sum B_n \lambda^n$$

and reported smoothed values for T = 210, 230, 250, 270, and 295 K, every 2 nm, and at wavelengths corresponding to the wavenumber intervals generally used in stratospheric photodissociation calculations. The parameters A_n and B_n for the ranges T = 210–300 K and λ = 190–240 nm are as follows:

$A_0 = 269.80$ $\quad B_0 = 3.7973$
$A_1 = -6.0908$ $\quad B_1 = -7.0913 \times 10^{-2}$
$A_2 = 4.7830 \times 10^{-2}$ $\quad B_2 = 4.9397 \times 10^{-4}$
$A_3 = -1.6427 \times 10^{-4}$ $\quad B_3 = -1.5226 \times 10^{-6}$
$A_4 = 2.0682 \times 10^{-7}$ $\quad B_4 = 1.7555 \times 10^{-9}$

Quantum yields for H atom formation have been measured in the far UV by Brownsword et al. [104], [103]: $\Phi(H) = 0.23 \pm 0.03$ and 0.13 at 121.6 and 157.6 nm, respectively, whereas H atoms could not be detected in the photolysis at 193.3 nm.

Table 4-99. Absorption Cross Sections of $CHCl_3$ at 295–298 K

λ (nm)	10^{20} σ (cm^2)	λ (nm)	10^{20} σ (cm^2)	λ (nm)	10^{20} σ (cm^2)
180	372	206	20.7	232	0.158
182	317	208	15.1	234	0.107
184	248	210	10.7	236	0.0730
186	186	212	7.48	238	0.0503
188	144	214	5.24	240	0.0347
190	113	216	3.60	*242*	*0.0223*
192	89.9	218	2.48	*244*	*0.0151*
194	76.1	220	1.69	*246*	*0.01023*
196	64.2	222	1.13	*248*	*0.00694*
198	53.0	224	0.750	*250*	*0.00470*
200	42.6	226	0.503	*252*	*0.00319*
202	34.4	228	0.342	*254*	*0.00216*
204	27.2	230	0.234	*256*	*0.00147*

Note:

180–240 nm: mean of Hubrich and Stuhl [346] and Simon et al. [734]
242–256 nm: extrapolation of mean of Hubrich and Stuhl [346] and Simon et al. [734] data.

F22. $CH_2Cl_2 + h\nu \rightarrow$ Products. The absorption cross sections of CH_2Cl_2 have been measured at room temperature and 110–200 nm by Russell et al. [694]; at the Lyman-α line at 121.6 nm by Brownsword et al. [104]; at 213 nm by Gordus and Bernstein [293], at 160–255 nm by Hubrich and Stuhl [346]; at 279 and 296 K and 176–216 nm by Vanlaethem-Meurée et al. [808]; and at 225–295 K and 176–220 nm by Simon et al. [734]. The room temperature data of Vanlaethem-Meurée et al. [808] and Simon et al. [734] are nearly identical. The cross sections of Hubrich and Stuhl [346] are up to 12% larger than those of Simon et al. [734] in the 176–206 nm wavelength range, increasing to 50% in the 185–220 nm range. The preferred absorption cross sections, listed in Table 4-100, are the mean of the values reported by Hubrich and Stuhl [346] and Simon et al. [734] at 176–220 nm. For wavelengths above 220 nm, the average of their data at 200–210 nm has been extrapolated ($\log \sigma = -2.1337 - 0.08439\ \lambda$) (in italics) at wavelengths up to 256 nm. The measured values of Hubrich and Stuhl [346] are smaller by up to 7% below 230 nm and become larger by up to 50% between 235 and 255 nm than the extrapolated values.

The temperature dependence of the absorption cross sections becomes significant at wavelengths above 190 nm, where the cross sections decrease with decreasing temperature between 295 and 210 K. Simon et al. [734] parameterized the cross sections and the temperature dependence by the polynomial expansion

$$\log_{10} \sigma(\lambda, T) = \sum A_n \lambda^n + (T - 273) \times \sum B_n \lambda^n$$

and reported smoothed values for T = 210, 230, 250, 270, and 295 K, every 2 nm, and at wavelengths corresponding to the wavenumber intervals generally used in stratospheric photodissociation calculations. The parameters A_n and B_n for the ranges T = 210–300 K and
λ = 176–220 nm are as follows:

$A_0 = -1431.8$	$B_0 = -3.1171$
$A_1 = 27.395$	$B_1 = 6.7874 \times 10^{-2}$
$A_2 = -1.9807 \times 10^{-1}$	$B_2 = -5.5000 \times 10^{-4}$
$A_3 = 6.3468 \times 10^{-4}$	$B_3 = 1.9649 \times 10^{-6}$
$A_4 = -7.6298 \times 10^{-7}$	$B_4 = -2.6101 \times 10^{-9}$

Quantum yields for H atom formation have been measured in the far UV by Brownsword et al. [104], [103]: Φ(H) = 0.28 ± 0.03, 0.23, and 0.002 ± 0.001 at 121.6, 157.6, and 193.3 nm, respectively.

Table 4-100. Absorption Cross Sections of CH_2Cl_2 at 295–298 K

λ (nm)	10^{20} σ (cm^2)	λ (nm)	10^{20} σ (cm^2)	λ (nm)	10^{20} σ (cm^2)
176	186	204	4.41	*232*	*0.0194*
178	182	206	3.07	*234*	*0.0132*
180	173	208	2.13	*236*	*0.00892*
182	156	210	1.45	*238*	*0.00605*
184	135	212	0.978	*240*	*0.00410*
186	110	214	0.651	*242*	*0.00278*
188	84.2	216	0.435	*244*	*0.00188*
190	61.0	218	0.291	*246*	*0.00128*
192	43.9	220	0.190	*248*	*0.000866*
194	30.5	*222*	*0.135*	*250*	*0.000587*
196	20.6	*224*	*0.0918*	*252*	*0.000398*
198	14.1	*226*	*0.0623*	*254*	*0.000270*
200	9.48	*228*	*0.0422*	*256*	*0.000183*
202	6.40	*230*	*0.0286*		

Note:

176–220 nm: mean of Hubrich and Stuhl [346] and Simon et al. [734]
222–256 nm: extrapolation of mean of Hubrich and Stuhl [346] and Simon et al. [734] data.

F23. $CH_3Cl + h\nu \rightarrow$ Products. The absorption cross sections of CH_3Cl have been measured at room temperature and 110–200 nm by Russell et al. [694]; at the Lyman-α line at 121.6 nm by Brownsword et al. [104]; at 171.2 nm by Felps et al. [241]; and at 174–220 nm by Robbins [673]; at 208 and 298 K and 158–235 nm by Hubrich et al. [347]; at 255, 279, and 296 K and 186–216 nm by Vanlaethem-Meurée et al. [808]; and at 225–295 K and 174–216 nm by Simon et al. [734]. The room temperature data generally agree within 10% in the

wavelength range 174–216 nm, those of Vanlaethem-Meurée et al. [808] and Simon et al. [734] are nearly identical. The value at 171 nm of Felps et al. [103] is smaller by ~15% than that of Hubrich et al. [347]. The preferred absorption cross sections, listed in Table 4-101, are the mean of the values reported by Robbins [673], Hubrich et al. [347], and Simon et al. [734] at 174–184 nm, the mean of the values reported by Robbins [673], Hubrich et al. [347], Vanlaethem-Meurée et al. [808], and Simon et al. [734] at 186–216 nm, and the mean of the values reported by Robbins [673] and Hubrich et al. [347] at 218–220 nm. The values for the wavelength range 222–236 nm have been taken from an interpolation (at 2-nm intervals) of the 200–235-nm data of Hubrich et al. [347] ($\log \sigma = -0.24164 - 0.09743\ \lambda$).

The temperature dependence of the absorption cross sections becomes significant at wavelengths above 194 nm, where the cross sections decrease with decreasing temperature between 295 and 210 K. There is very good agreement between the low-temperature values at 250–255 K of Vanlaethem-Meurée et al. [808] and Simon et al. [734]. The latter authors parameterized the cross sections and the temperature dependence by the polynomial expansion $\log_{10} \sigma(\lambda, T) = \Sigma A_n \lambda^n + (T - 273) \times \Sigma B_n \lambda^n$ and reported smoothed values for T = 210, 230, 250, 270, and 295 K, every 2 nm, and at wavelengths corresponding to the wavenumber intervals generally used in stratospheric photodissociation calculations. The parameters A_n and B_n for the ranges T = 210–300 K and λ = 174–216 nm are as follows:

$A_0 = -299.80$ $\quad B_0 = -7.1727$

$A_1 = 5.1047$ $\quad B_1 = 1.4837 \times 10^{-1}$

$A_2 = -3.3630 \times 10^{-2}$ $\quad B_2 = -1.1463 \times 10^{-3}$

$A_3 = 9.5805 \times 10^{-5}$ $\quad B_3 = 3.9188 \times 10^{-6}$

$A_4 = -1.0135 \times 10^{-7}$ $\quad B_4 = -4.9994 \times 10^{-9}$

Note: There was a typographical error in the value for A_3 in JPL02-25 that has been corrected in this evaluation.

Quantum yields for H atom formation have been measured in the far UV by Brownsword et al. [104], [103]: $\Phi(H) = 0.53 \pm 0.05$, 0.29, 0.012 ± 0.006 at 121.6, 157.6, and 193.3 nm, respectively.

Table 4-101. Absorption Cross Sections of CH_3Cl at 295–298 K

λ (nm)	$10^{20}\ \sigma$ (cm^2)	λ (nm)	$10^{20}\ \sigma$ (cm^2)	λ (nm)	$10^{20}\ \sigma$ (cm^2)
174	110	196	3.96	218	0.0345
176	93.9	198	2.68	220	0.0220
178	78.2	200	1.77	*222*	*0.0135*
180	63.6	202	1.13	*224*	*0.00859*
182	46.5	204	0.731	*226*	*0.00549*
184	35.0	206	0.482	*228*	*0.00350*
186	25.8	208	0.313	*230*	*0.00224*
188	18.4	210	0.200	*232*	*0.00143*
190	12.8	212	0.127	*234*	*0.000911*
192	8.84	214	0.0860	*236*	*0.000582*
194	5.83	216	0.0534		

Note:
174–184 nm: mean of Robbins [673], Hubrich et al. [347], and Simon et al. [734]
186–216 nm: mean of Robbins [673], Hubrich et al. [347], Vanlaethem-Meurée et al. [808] and Simon et al. [734]
218–220 nm: mean of Robbins [673] and Hubrich et al. [347]
222–236 nm: extrapolation of Hubrich et al. [347] data.

F24. $CH_3CCl_3 + h\nu \rightarrow$ Products. The absorption cross sections of CH_3CCl_3 have been measured at room temperature and 147 nm by Salomon et al. [699], and at 160–255 nm by Hubrich and Stuhl [346], who corrected (< 10.7%) the absorption cross sections in the range 170–190 nm for the concentration and absorption cross sections of a 1,4-dioxane stabilizer present during the experiments. Measurements at 220–295 K and 182–240 nm were carried out by Vanlaethem-Meurée et al. [810] and at 223–333 K and 160 240 nm by Nayak et al. [573]. The latter authors also measured the absorption cross sections in the liquid phase at 235–260 nm and used a wavelength-shift procedure to convert the liquid-phase data into gas-phase data. The agreement of the room temperature data is within 20% at 165–205 nm (at 160 nm, the value reported by Nayak et al. [573] is larger by 50% than that reported by Hubrich and Stuhl [346]). Between 210 and 240 nm, the data of Vanlaethem-Meurée et al. [810] and Nayak et al. [573] are within 15%, whereas those of Hubrich and Stuhl [346] are larger by 100–150%. The preferred absorption cross sections, listed in Table 4-102, are the mean of the values reported by Hubrich and Stuhl [346] and Nayak et al. [573] at 170–180 nm, the mean of the values reported by Vanlaethem-Meurée et al. [810], Hubrich and Stuhl [346], and

Nayak et al. [573] at 185–205 nm, and the mean of the values reported by Vanlaethem-Meurée et al. [810] and Nayak et al. [573] at 210–240 nm. For wavelengths above 240 nm, the average of their data at 220–240 nm has been extrapolated ($\log \sigma = -1.59792 - 0.08066\ \lambda$) at wavelengths up to 255 nm. The measured values of Hubrich and Stuhl [346] are larger by up to ~140% at 250 nm and smaller by ~80% at 255 nm than the recommended values.

The temperature dependence of the absorption cross sections becomes significant at wavelengths above 210 nm, where the cross sections decrease with decreasing temperature, as observed in good agreement at 333–223 K by Nayak et al. [573] and at 295–210 K by Vanlaethem-Meurée et al. [810]. The latter authors parameterized the cross sections and the temperature dependence by the polynomial expansion $\log_{10} \sigma(\lambda, T) = \sum A_n \lambda^n + (T - 273) \times \sum B_n \lambda^n$ and reported smoothed values for T = 210, 230, 250, 270, and 295 K, every 2 nm, and at wavelengths corresponding to the wavenumber intervals generally used in stratospheric photodissociation calculations. The parameters A_n and B_n for the ranges T = 210–300 K and λ = 182–240 nm reported by Gillotay and Simon [281] are as follows:

$A_0 = 341.085191$ $\quad B_0 = -1.660090$
$A_1 = -7.273362$ $\quad B_1 = 3.079969 \times 10^{-2}$
$A_2 = 5.498387 \times 10^{-2}$ $\quad B_2 = -2.106719 \times 10^{-4}$
$A_3 = -1.827552 \times 10^{-4}$ $\quad B_3 = 6.264984 \times 10^{-7}$
$A_4 = 2.238640 \times 10^{-7}$ $\quad B_4 = -6.781342 \times 10^{-10}$

Table 4-102. Absorption Cross Sections of CH_3CCl_3 at 295–298 K

λ (nm)	10^{20} σ (cm^2)	λ (nm)	10^{20} σ (cm^2)	λ (nm)	10^{20} σ (cm^2)
170	406	200	92.1	230	0.717
175	424	205	52.0	235	0.276
180	404	210	25.5	240	0.111
185	301	215	10.9	*245*	*0.0437*
190	212	220	4.47	*250*	*0.0173*
195	147	225	1.82	*255*	*0.00682*

Note:
170–180 nm: mean of Hubrich and Stuhl [346] and Nayak et al. [573]
185–205 nm: mean of Vanlaethem-Meurée et al. [810], Hubrich and Stuhl [346] and Nayak et al. [573]
210–240 nm: mean of Vanlaethem-Meurée et al. [810] and Nayak et al. [573]
245–255 nm: extrapolation of mean of Vanlaethem-Meurée et al. [810] and Nayak et al. [573] data.

F25. $CH_3CH_2Cl + h\nu \rightarrow$ Products. The absorption cross sections of CH_3CH_2Cl have been measured at room temperature and 147 nm by Ichimura et al. [358] and at 160–240 nm by Hubrich and Stuhl [346]. The data of Hubrich and Stuhl [346] are listed in Table 4-103.

Table 4-103. Absorption Cross Sections of CH_3CH_2Cl at 298 K

λ (nm)	10^{20} σ (cm^2)	λ (nm)	10^{20} σ (cm^2)	λ (nm)	10^{20} σ (cm^2)
160	189.0	190	6.85	220	0.0127
165	110.0	195	2.56	225	0.00463
170	70.5	200	1.17	230	0.00117
175	44.4	205	0.375	235	0.000395
180	30.4	210	0.147	240	0.000156
185	13.6	215	0.0433		

Note:
160–240 nm, Hubrich and Stuhl [346].

F26. $CH_3CHClCH_3 + h\nu \rightarrow$ Products. In a compilation of ultraviolet absorption cross sections of halocarbons by Gillotay and Simon [278] results are reported (erroneously) for $CH_3CH_2ClCH_3$, which presumably should be $CH_3CHClCH_3$. The data are listed in Table 4-104.

Table 4-104. Absorption Cross Sections of $CH_3CHClCH_3$ at 295 K

λ (nm)	10^{20} σ (cm^2)	λ (nm)	10^{20} σ (cm^2)	λ (nm)	10^{20} σ (cm^2)
170	31.7	192	4.67	214	0.0965
172	27.0	194	3.49	216	0.0652
174	24.3	196	2.58	218	0.0444
176	22.1	198	1.88	220	0.0308
178	20.3	200	1.34	222	0.0212

λ (nm)	10^{20} σ (cm^2)	λ (nm)	10^{20} σ (cm^2)	λ (nm)	10^{20} σ (cm^2)
180	18.0	202	0.954	224	0.0144
182	15.0	204	0.671	226	0.0107
184	12.2	206	0.463	228	0.00752
186	9.99	208	0.311	230	0.00580
188	7.93	210	0.214		
190	6.06	212	0.144		

Note:

170–230 nm, Gillotay and Simon [278].

F27. $CH_2ClCH_2Cl + h\nu \rightarrow$ Products.

F28. $CH_2ClCH_2CH_2Cl + h\nu \rightarrow$ Products.

F29. $CH_2Cl(CH_2)_2CH_2Cl + h\nu \rightarrow$ Products. Absorption cross sections for these three dichloroalkanes at room temperature and 118–200 nm have been reported by Russell et al. [694].

F30. $COCl_2 + h\nu \rightarrow CO + Cl_2$
$COCl_2 + h\nu \rightarrow COCl + Cl$
$COCl_2 + h\nu \rightarrow CO + 2\ Cl$
$COCl_2 + h\nu \rightarrow CCl_2 + O$. The absorption cross-sections of $COCl_2$ (carbonyl dichloride, phosgene) have been measured at room temperature and 185-226 nm by Chou et al. [170], at 240-280 nm by Okabe [596], at 200-315 nm by Meller et al. [514], at 172-220 nm by Jäger et al. [368], at some singular points between 147 and 254 nm by Okabe [599, 600], and Glicker and Okabe [284]; and at 210-295 K and 166-308 nm by Gillotay et al. [282]. The spectrum shows a weak absorption band between 215 and 310 nm with the maximum at ~235 nm and a strong absorption band below 200 nm with the maximum at ~174 nm. The room temperature values reported by the various teams are in very good agreement, generally within 10%; exceptions are the region of the absorption minimum and the region around 200 nm where the values of Jäger at al. [368] are lower than those of Gillotay et al. [282] by up to 20%. Around the absorption minimum the values of Chou et al. [170] and Meller et al. [514] are between those of Gillotay et al. [282] and Jäger et al. [368].

The preferred absorption cross-sections listed in Table 4-105 as averages over the 500-cm^{-1} intervals used for atmospheric modeling are the values of Gillotay et al. [282] at 168.10-173.15 nm, the mean of the values of Gillotay et al. [282] and Jäger et al. [368] at 174.65-182.65 nm, the mean of the values of Chou et al. [170], Gillotay et al. [282], and Jäger et al. [368] at 184.35-199.00 nm, the mean of the values of Chou et al. [170], Gillotay et al. [282], Meller et al. [514], and Jäger et al. [368] at 201.01-218.59 nm, the mean of the values of Chou et al. [170], Gillotay et al. [282], and Meller et al. [514] at 221.00-226.00 nm, and the mean of the values of Gillotay et al. [282] and Meller et al. [514] at 228.58-305.36 nm.

The temperature dependence becomes significant only in the regions below 175 nm and above 250 nm as reported by Gillotay et al. [282]. The strong absorption band is shifted slightly to shorter wavelengths with deceasing temperature and becomes higher by nearly 20% between 295 and 210 K; in the region above 250 nm the absorption cross-sections become smaller with decreasing temperature, the differences increase up to about 80% at 305 nm.

Phosgene is a useful actinometer in the region 200-280 nm. The photodissociation processes $COCl_2 + h\nu \rightarrow COCl + Cl$ with subsequent decay of $COCl \rightarrow CO + Cl$, produces CO with unity quantum yield (see Okabe, [596], Wijnen, [847], Heicklen [324], Calvert and Pitts [136]).

Table 4-105. Absorption Cross Sections of $COCl_2$ at 294-298 K

λ (nm)	10^{20} σ (cm^2)	λ (nm)	10^{20} σ (cm^2)	λ (nm)	10^{20} σ (cm^2)	λ (nm)	10^{20} σ (cm^2)
168.10	301	193.25	68.8	223.47	12.6	264.92	2.68
170.95	433	195.15	52.1	226.00	13.0	268.50	1.85
173.15	493	197.05	40.6	228.58	13.2	272.12	1.17
174.65	509	199.00	31.7	231.23	13.4	275.88	0.689
176.20	475	201.01	25.7	233.93	13.5	279.74	0.370
177.80	427	203.05	20.7	236.69	13.0	283.70	0.182
179.40	369	205.14	17.2	239.53	12.4	287.78	0.0771
181.00	313	207.26	14.7	242.43	11.5	291.99	0.0298
182.65	261	209.43	13.0	245.41	10.4	296.32	0.0104
184.35	210	211.65	11.9	248.45	9.07	300.77	0.00323
186.05	178	213.89	11.4	251.59	7.75	305.36	0.000964
187.80	137	216.20	11.3	254.79	6.32		
189.60	112	218.59	11.5	258.08	5.02		
191.40	88.9	221.00	12.2	261.45	3.77		

Note:
168.10-173.15 nm, Gillotay et al. [282],
174.65-182.65 nm, mean of Gillotay et al. [282] and Jäger et al. [368],
184.35-199.00 nm, mean of Chou et al. [170], Gillotay et al. [282], and Jäger et al. [368],
201.01-218.59 nm, mean of Chou et al [170], Gillotay et al. [282], Meller et al. [514], and Jäger et al. [368],
221.00-226.00 nm, mean of Chou et al. [170], Gillotay et al. [282], and Meller et al. [514],
228.58-305.36 nm, mean of Gillotay et al. [282] and Meller et al. [514].

F31. $COHCl + h\nu \rightarrow$ Products. The absorption spectrum of COHCl (formyl chloride) was measured at room temperature and 239-307 nm by Libuda et al. [448]. The absorption spectrum exhibits a highly structured absorption band with the maximum near 260 nm. In Table 4-106 are listed the averages over 1-nm intervals of the medium-resolution (0.7 nm) data of Libuda et al. [448].

Table 4-106. Absorption Cross Sections of COHCl at 298 K

λ (nm)	10^{20} σ (cm^2)	λ (nm)	10^{20} σ (cm^2)	λ (nm)	10^{20} σ (cm^2)	λ (nm)	10^{20} σ (cm^2)
240	2.76	257	3.92	274	3.53	291	0.624
241	3.36	258	5.03	275	2.30	292	0.605
242	3.41	259	4.45	276	3.28	293	0.342
243	3.32	260	5.46	277	2.38	294	0.431
244	3.03	261	5.09	278	2.09	295	0.303
245	3.53	262	4.66	279	1.89	296	0.275
246	4.01	263	4.54	280	2.22	297	0.184
247	4.64	264	4.03	281	1.06	298	0.165
248	4.44	265	3.83	282	1.98	299	0.178
249	4.27	266	4.72	283	1.36	300	0.0562
250	3.92	267	3.76	284	1.15	301	0.0912
251	4.38	268	4.83	285	1.51	302	0.0805
252	4.57	269	3.79	286	1.00	303	0.0319
253	4.98	270	3.34	287	0.784	304	0.0587
254	5.20	271	3.72	288	0.748	305	0.0275
255	4.59	272	2.68	289	0.880	306	0.0157
256	5.07	273	2.74	290	0.371	307	0.0131

Note:

240-307 nm, Libuda [448].

F32. $COFCl + h\nu \rightarrow COF + Cl$
$COFCl + h\nu \rightarrow COCl + F$
$COFCl + h\nu \rightarrow CO + F + Cl$. The absorption cross-sections of COFCl (carbonyl chlorofluoride, fluorochlorophosgene) have been measured at room temperature and 186-226 nm by Chou et al. [170] and Hermann et al. [328] and at 223, 248, 273, and 298 K and 200-262 nm by by Nölle et al. [589] [591]. The spectrum exhibits monotonically decreasing absorptions cross-sections with increasing wavelengths with a shoulder around 200 nm. The room temperature data of both teams are in excellent agreement in the common wavelength range with differences ≤6%. The preferred absorption cross-sections listed in Table 4-107, the averages over the 500-cm^{-1} intervals used for atmospheric modeling, are the data of Chou et al. [170] and Hermann et al. [328] at 186-199 nm, the mean of the data of Chou et al. [170], Hermann et al. [328] and Nölle et al. [589] [591] at 201 and 203.1 nm, and the data of Nölle et al. [589] [591] at wavelengths above 205 nm.

The study of the temperature dependence by Nölle et al. [589] [591] shows the following effects: a decrease of the absorption cross-section with decreasing temperature from 298 to 223 K was observed above 210 nm, where the difference between the 298- and 223-K values increases with increasing wavelength to about 40% at 260 nm. The reverse effect was observed below 210 nm, where the difference between the 298 and 223 K values increases with decreasing wavelength to about 18% at 201 nm.

The photolysis quantum yields of COFCl were determined at 193 nm using an excimer laser by Hermann et al. [328], at 210, 222.5 and 230 nm using an excimer pumped dye laser system, at 248 nm using an excimer laser, and at 210 nm using a Hg medium pressure lamp by Nölle et al. [591]. The relative distribution of the products CO and COF_2 was shown by Hermann et al. [328] to depend on the total pressure (range 10-to 900 mbar). The apparent quantum yields were taken as the quantum yields for the decomposition into COF + Cl and CO + F + Cl since the parent molecule cannot be reformed (as in the case of COF_2) and COCl is known to be unstable. The quantum yields are as follows:

λ in nm	193	210	222.5	230	248	254
Φ	0.98 ± 0.09	0.85 ± 0.25 (laser)	0.77 ± 0.33	0.71 ± 0.30	0.52 ± 0.14	0.90 ± 0.05 (Hg lamp)

Table 4-107. Absorption Cross Sections of COFCl at 296-298 K

λ (nm)	10^{20} σ (cm^2)	λ (nm)	10^{20} σ (cm^2)	λ (nm)	10^{20} σ (cm^2)	λ (nm)	10^{20} σ (cm^2)
186.0	15.6	201.0	12.2	218.6	5.79	239.5	0.459
187.8	14.0	203.1	11.9	221.0	4.77	242.4	0.292
189.6	13.4	205.1	11.5	223.5	3.81	245.4	0.178
191.4	12.9	207.3	10.8	226.0	2.93	248.5	0.103
193.2	12.7	209.4	9.91	228.6	2.19	251.6	0.0635
195.1	12.5	211.6	8.96	231.2	1.57	254.8	0.0409
197.0	12.4	213.9	7.90	233.9	1.09	258.1	0.0279
199.0	12.3	216.2	6.84	236.7	0.724	261.4	0.0214

Note:
186.0-199.0 nm, Chou et al. [170] and Hermann et al. [328],
201.0 and 203.1 nm, mean of Chou et al. [170], Hermann et al. [328] and Nölle et al. [591],
205.1-261 4 nm, Nölle et al. [591].

F33. $CFCl_3$ (CFC-11) + hν → Products. The absorption cross sections of $CFCl_3$ have been measured at room temperature and 225 nm by Gordus and Bernstein [293], at 186–226 nm by Rowland and Molina [688], at 174–226 nm by Robbins and Stolarski [674], at 186–209 nm by Greene and Wayne [299]; at 213–296 K and 185–226 nm by Chou et al. [172]; at 208 and 298 K and 158–260 nm by Hubrich et al. [347] and Hubrich and Stuhl [346]; at 255, 279, and 296 K and 190–220 nm by Vanlaethem-Meurée et al. [809]; at 225–295 K and 174–230 nm by Simon et al. [734]; and at 220, 240, and 296 K and 200–238 nm by Mérienne et al. [522]. The room temperature data are in good agreement, generally within 10–15%. Absorption cross sections at 148–225 nm have also been derived from electron energy-loss measurements by Huebner et al. [353], which are up to 30% higher than the values obtained by optical measurements. The preferred absorption cross sections, listed in Table 4-108, are the values of Simon et al. [734] at 174–198 nm, the mean of the values reported by Simon et al. [734] and Mérienne et al. [522] at 200–230 nm, and the data of Hubrich and Stuhl [346] at 235–260 nm. Measurements in the far UV at 60–145 nm have been reported by Gilbert et al. [273], and at 120–200 nm by Doucet et al. [222].

The temperature dependence becomes significant at wavelengths above 185 nm, where the cross sections decrease with decreasing temperature between 296 and 210 K (Hubrich et al. [347] observed such a behavior only above 200 nm). Simon et al. [734] parameterized the temperature dependence of the cross sections by the polynomial expansion $\log_{10} \sigma(\lambda, T) = \Sigma A_n \lambda^n + (T - 273) \times \Sigma B_n \lambda^n$and reported smoothed values for T = 210, 230, 250, 270, and 295 K, every 2 nm, and at wavelengths corresponding to the wavenumber intervals generally used in stratospheric photo- dissociation calculations. Parameters A_n and B_n for the ranges T = 210–300 K and λ = 174–230 nm are as follows:

$A_0 = -84.611$ $B_0 = -5.7912$
$A_1 = 7.9551 \times 10^{-1}$ $B_1 = 1.1689 \times 10^{-1}$
$A_2 = -2.0550 \times 10^{-3}$ $B_2 = -8.8069 \times 10^{-4}$
$A_3 = -4.4812 \times 10^{-6}$ $B_3 = 2.9335 \times 10^{-6}$
$A_4 = 1.5838 \times 10^{-8}$ $B_4 = -3.6421 \times 10^{-9}$

A similar polynomial expansion, $\ln \sigma(\lambda, T) = \Sigma a_n (\lambda - 200)^n + (T - 296) \times \Sigma b_n(\lambda - 200)^n$, for the ranges T = 220–296 K and λ = 200–238 nm was used by Mérienne et al. [522] with the following parameters a_n and b_n:

$a_0 = -41.925548$ $b_0 = 3.58977 \times 10^{-4}$
$a_1 = -1.142857 \times 10^{-1}$ $b_1 = 3.02973 \times 10^{-4}$
$a_2 = -3.12034 \times 10^{-3}$ $b_2 = -1.13 \times 10^{-8}$
$a_3 = 3.6699 \times 10^{-5}$

A quantum yield for $Cl^*(^2P_{1/2})$ atom formation in the broad band photolysis of $CFCl_3$, Φ (Cl*) = 0.79 ± 0.27, was reported by Clark and Husain [174].

Table 4-108. Absorption Cross Sections of $CFCl_3$ at 295–298 K

λ (nm)	10^{20} σ (cm^2)	λ (nm)	10^{20} σ (cm^2)	λ (nm)	10^{20} σ (cm^2)
174	313.0	198	78.0	222	1.72
176	324.0	200	63.2	224	1.17
178	323.5	202	49.1	226	0.790
180	314.0	204	37.3	228	0.532
182	296.0	206	28.1	230	0.354
184	272.0	208	20.4	235	0.132
186	243.0	210	15.1	240	0.0470
188	213.0	212	10.7	245	0.0174
190	179.0	214	7.54	250	0.0066
192	154.0	216	5.25	255	0.0029
194	124.3	218	3.65	260	0.0015
196	99.1	220	2.51		

Note:

174–198 nm: Simon et al. [734]
200–230 nm: mean of Simon et al. [734] and Mérienne et al. [522]
235–260 nm: Hubrich and Stuhl [346].

F34. CF_2Cl_2 (CFC-12) + hν → Products. The absorption cross sections of CF_2Cl_2 have been measured at room temperature and 210 nm by Gordus and Bernstein [293], at 186–216 nm by Rowland and Molina [688], at 174–216 nm by Robbins and Stolarski [674], at 186–206 nm by Greene and Wayne [299]; at 234–442 K and 213.9 nm by Rebbert and Ausloos [664]; at 212, 252, and 296 K and 184–221 nm by Chou et al. [172]; at 208 and 298 K and 159–240 nm by Hubrich et al. [347]; at 255, 279, and 296 K and 190–216 nm by Vanlaethem-Meurée et al. [809]; at 225–295 K and 174–230 nm by Simon et al. [734]; and at 220, 240, and 296 K and 200–231 nm by Mérienne et al. [522]. The room temperature data are in good agreement, generally within 10–15%, except the data of Green and Wayne [299] above 195 nm and the data of Rowland and Molina [688] around 210 nm. Absorption cross sections at 148–218 nm have also been derived from electron energy-loss measurements by Huebner et al. [353], which agree within 10% with the data obtained by optical measurements around the absorption maximum and become higher than the optical data by up to 100% above 196 nm. The preferred absorption cross sections, listed in Table 4-109, are values of Hubrich et al. [347] at 170–172 nm, the mean of the values reported by Hubrich et al. [347] and Simon et al. [734] at 174–178 nm, the values of Simon et al. [734] at 180–198 nm, mean of the values reported by Simon et al. [734] and Mérienne et al. [522] at 200–226 nm, and the data of Mérienne et al. [522] at 228–230 nm. For the range 232–240 nm, absorption curve above 210 nm of Mérienne et al. [522] has been extrapolated ($\log \sigma = 2.1448 - 0.1061\ \lambda$). The measured values of Hubrich et al. [347] are lower by up to ~40% at 240 nm than the extrapolated values.

High-resolution absorption cross section measurements have been carried out by Seccombe et al. [717] between 50 and 150 nm, and by Limao-Vieira et al. [451] between 113 and 225 nm using a synchrotron radiation light source. The results of Limao-Vieira et al. [451] for the absorption band at 170–204 nm are in very good agreement with the recommendation in Table 4-109 (at wavelengths above 204 nm, noise effects become significant). The new cross section measurements for the far UV region from both recent studies significantly improve upon the earlier data of Gilbert et al. [273] for the wavelength range 60–135 nm and of Doucet et al. [222] for the wavelength range 120–200 nm.

The temperature dependence becomes significant at wavelengths above 186 nm, where the cross sections decrease with decreasing temperature between 296 and 210 K.A polynomial expansion, $\ln \sigma(\lambda, T) = \sum a_n (\lambda - 200)^n + (T - 296) \times \sum b_n(\lambda - 200)^n$, for the ranges T = 220–296 K and λ = 200–231 nm was used by Mérienne et al. [522] with the following parameters a_n and b_n:

$a_0 = -43.8954569$ $\quad b_0 = 4.8438 \times 10^{-3}$
$a_1 = -2.403597 \times 10^{-1}$ $\quad b_1 = 4.96145 \times 10^{-4}$
$a_2 = -4.2619 \times 10^{-4}$ $\quad b_2 = -5.6953 \times 10^{-6}$
$a_3 = 9.8743 \times 10^{-6}$

Simon et al. [734] parameterized the temperature dependence of the cross sections by the polynomial expansion $\log_{10} \sigma(\lambda, T) = \sum A_n \lambda^n + (T - 273) \times \sum B_n \lambda^n$. **Note: The parameters reported by Simon et al. contain typographical error(s) that were reproduced in JPL02-25. The correct parameters are not known, and therefore the fitting parameters of Simon et al. are not given in this evaluation.**

A quantum yield for $Cl^*(^2P_{1/2})$ atom formation in the broad band photolysis of CF_2Cl_2, $\Phi(Cl^*) = 0.75 \pm 0.26$, was reported by Clark and Husain [174].

Table 4-109. Absorption Cross Sections of CF_2Cl_2 at 295–298 K

λ (nm)	10^{20} σ (cm^2)	λ (nm)	10^{20} σ (cm^2)	λ (nm)	10^{20} σ (cm^2)
170	124.0	194	31.5	218	0.103
172	151.0	196	21.1	220	0.0624
174	168.0	198	13.9	222	0.0381
176	185.5	200	8.71	224	0.0233
178	189.5	202	5.42	226	0.0140
180	179.0	204	3.37	228	0.0090
182	160.0	206	2.06	230	0.0057
184	134.0	208	1.26	*232*	*0.0034*
186	107.0	210	0.762	*234*	*0.0021*
188	82.8	212	0.458	*236*	*0.0013*
190	63.2	214	0.274	*238*	*0.0008*
192	45.50	216	0.163	*240*	*0.0005*

Note:
170–172 nm, Hubrich et al. [347],
174–178 nm, the mean of Hubrich et al. [347] and Simon et al. [734],
180–198 nm, Simon et al. [734],
200–230 nm, mean of Simon et al. [734] and Mérienne et al. [522],
232–240 nm, extrapolation of Mérienne et al. [522] data.

F35. CF_3Cl (CFC-13) + hν → Products. The absorption cross sections of CF_3Cl have been measured at room temperature and 184–203 nm by Chou et al. [171]; at 255, 279, and 296 K and 172–200 nm by Vanlaethem-Meurée et al. [809]; at 208 and 298 K and 160–220 nm by Hubrich and Stuhl [346]; and at 225–295 K and 172–200 nm by Simon et al. [734]. The values of Vanlaethem-Meurée et al. [809] and Simon et al. [734] are identical, the room temperature values of Hubrich and Stuhl [346] deviate from the latter by up to about ±25%, and the data of Chou et al. [171] are always larger by about 15–30% in the region 185–200 nm. The recommended absorption cross sections for CF_3Cl, presented in Table 4-110, are taken from Simon et al. [734] for the range 172–200 nm. The values at 202–220 nm are obtained by extrapolation of the absorption curve above 200 nm ($\log \sigma = -5.048 - 0.0834\ \lambda$) of Simon et al. [734].

Measurements in the far UV at 65–130 nm have been reported by Gilbert et al. [273] and at 120–160 nm by Doucet et al. [222]. Measurements at the Lyman-α line at 121.6 nm have been carried out by Ravishankara et al. [659].

Temperature effects, if any, could not be detected by Vanlaethem-Meurée et al. [809] and Simon et al. [734], whereas Hubrich and Stuhl [346] report a decrease of the absorption cross sections between 298 and 208 K by 4% at160 nm to 74% at 205 nm. Simon et al. [734] parameterized the cross sections and the temperature dependence of the absorption cross sections by the polynomial expansion

$$\log_{10} \sigma(\lambda, T) = \sum A_n \lambda^n + (T - 273) \times \sum B_n \lambda^n \text{ (with all } B_n = 0),$$

and reported smoothed values for T = 295 K, every 2 nm, and at wavelengths corresponding to the wavenumber intervals generally used in stratospheric photodissociation calculations. The parameters A_n for the ranges T = 210–300 K and λ = 172–200 nm are:

$$A_0 = -1.55.88,\ A_1 = 2.0993,\ A_2 = -1.0486 \times 10^{-2},\ A_3 = 1.6718 \times 10^{-5}.$$

A quantum yield for $Cl^*(^2P_{1/2})$ atom formation in the broad band photolysis of CF_3Cl, $\Phi(Cl^*) = 0.86 \pm 0.29$, was reported by Clark and Husain [174].

Table 4-110. Absorption Cross Sections of CF_3Cl at 295 K

λ (nm)	10^{20} σ (cm^2)	λ (nm)	10^{20} σ (cm^2)	λ (nm)	10^{20} σ (cm^2)
172	1.100	190	0.128	*206*	*0.00595*
174	0.970	192	0.0900	*208*	*0.00406*
176	0.825	194	0.0610	*210*	*0.00276*
178	0.681	196	0.0410	*212*	*0.00188*
180	0.542	198	0.0280	*214*	*0.00128*
182	0.425	200	0.0190	*216*	*0.000872*
184	0.326	200	0.0189	*218*	*0.000594*
186	0.244	202	*0.0128*	*220*	*0.000405*
188	0.175	204	*0.00874*		

Note:

172–200 nm, Simon et al. [734],
202–220 nm, extrapolation of Simon et al. [734] data.

F36. $CF_2ClCFCl_2$ (CFC-113) + hν → Products. The absorption cross sections of $CF_2ClCFCl_2$ have been measured at 298 K and 184–224 nm by Chou et al. [171]; at 208 and 298 K and 160–250 nm by Hubrich and Stuhl [346]; and at 225–295 K and 184–230 nm by Simon et al. [733]. The room temperature values agree within about 10% except in the region around 190 nm where the values of Hubrich and Stuhl [346] are smaller by up to 20% than the other values. The preferred absorption cross sections, listed in Table 4-111, are the values of Hubrich and Stuhl [346] at 175–180 nm, a value at 184 nm interpolated between those of Hubrich and Stuhl [346] at 180 nm and Simon et al. [733] at 186 nm, and the values of Simon et al. [733] at 186–230 nm. For the range 232–250 nm, the absorption curve of Simon et al. [733] above 230 nm has been extrapolated ($\log \sigma = -0.9860 - 0.0894\ \lambda$). The measured values of Hubrich and Stuhl [346] are larger than the extrapolated values by ~20–80% at 232–250 nm.

Measurements in the far UV at 110–200 nm have been carried out by Doucet et al. [223].

The temperature dependence becomes significant at wavelengths above 194 nm and below 170 nm, where the cross sections decrease with decreasing temperature. This was observed by Simon et al. [733] at 295–225 K and by Hubrich and Stuhl [346] at 298 and 208 K. Simon et al. [733] parameterized the temperature dependence of the cross sections by the polynomial expansion $\log_{10} \sigma(\lambda, T) = \sum A_n \lambda^n + (T - 273) \times \sum B_n \lambda^n$ and reported smoothed values for T = 210, 230, 250, 270, and 295 K, every 2 nm, and at wavelengths corresponding to the wavenumber intervals generally used in stratospheric photodissociation calculations. The parameters A_n and B_n for the ranges T = 210–300 K and λ = 182–230 nm are as follows:

$A_0 = -1087.9$ $\quad B_0 = 12.493$
$A_1 = 20.004$ $\quad B_1 = -2.3937 \times 10^{-1}$
$A_2 = -1.3920 \times 10^{-1}$ $\quad B_2 = 1.7142 \times 10^{-3}$
$A_3 = 4.2828 \times 10^{-4}$ $\quad B_3 = -5.4393 \times 10^{-6}$
$A_4 = -4.9384 \times 10^{-7}$ $\quad B_4 = 6.4548 \times 10^{-9}$.

Note: There was a typographical error in JPL02-25 for parameter B4 which has been corrected in this evaluation.

Table 4-111. Absorption Cross Sections of $CF_2ClCFCl_2$ at 295–298 K

λ (nm)	10^{20} σ (cm^2)	λ (nm)	10^{20} σ (cm^2)	λ (nm)	10^{20} σ (cm^2)
175	192	204	5.80	228	0.0410
180	155	206	4.00	230	0.0270
184	*123*	208	2.65	232	0.0188
186	104	210	1.80	234	0.0124
188	83.5	212	1.15	236	0.00824
190	64.5	214	0.760	238	0.00546
192	48.8	216	0.505	240	0.00361
194	36.0	218	0.318	242	0.00239
196	26.0	220	0.220	244	0.00159
198	18.3	222	0.145	246	0.00105
200	12.5	224	0.0950	248	0.000696
202	8.60	226	0.0630	250	0.000461

Note:
175–180 nm: Hubrich and Stuhl [346]
184 nm: interpolation: Hubrich and Stuhl and Simon et al.
186–230 nm: Simon et al. [733]
232–250 nm: extrapolation of Simon et al. [733] data.

F37. CF_2ClCF_2Cl (CFC-114) + hν → Products. The absorption cross sections of CF_2ClCF_2Cl have been measured at room temperature and 184–219 nm by Chou et al. [171]; at 208 and 298 K and 160–235 nm by Hubrich and Stuhl [346]; and at 225–295 K and 182–220 nm by Simon et al. [733]. The room temperature values of Simon et al. [733] and Chou et al. [171] agree within 5% except for a hump around 195 nm in the absorption curve reported by Chou et al. [171]. The values of Hubrich and Stuhl [346] are always larger than those of Simon et al. [733], around 190 nm by up to ~40% and between 200 and 220 nm up to ~50% with increasing

wavelength. The recommended absorption cross sections, listed in Table 4-112, are the values of Simon et al. [733] at 172–220 nm. For the range 222–235 nm, the absorption curve above 200 nm of Simon et al. [733] has been extrapolated ($\log \sigma = -1.8233 - 0.00913\ \lambda$). The measured values of Hubrich et al. [346] are larger by ~40% in that range than the extrapolated values.

Measurements at the Lyman-α line at 121.6 nm have been carried out by Ravishankara et al. [659]; and at 110–190 nm by Doucet et al. [223].

The temperature dependence has been observed at wavelengths above 190 nm, where Simon et al. [733] report decreasing cross sections with decreasing temperature 295–210 K. Hubrich and Stuhl [346] report for the range 160–210 nm and between 298 and 208 K a small decrease of the cross sections (generally <10%, except two data points). Simon et al. [733] parameterized the temperature dependence of the cross sections by the polynomial expansion $\log_{10} \sigma(\lambda, T) = \sum A_n \lambda^n + (T - 273) \times \sum B_n \lambda^n$ and reported smoothed values for T = 210, 230, 250, 270, and 295 K, every 2 nm, and at wavelengths corresponding to the wavenumber intervals generally used in stratospheric photodissociation calculations. The parameters A_n and B_n for the ranges T = 210–300 K, λ = 172–220 nm are as follows:

$A_0 = -160.50$ $\quad B_0 = -1.5296$
$A_1 = 2.4807$ $\quad B_1 = 3.5248 \times 10^{-2}$
$A_2 = -1.5202 \times 10^{-2}$ $\quad B_2 = -2.9951 \times 10^{-4}$
$A_3 = 3.8412 \times 10^{-5}$ $\quad B_3 = 1.1129 \times 10^{-6}$
$A_4 = -3.4373 \times 10^{-8}$ $\quad B_4 = -1.5259 \times 10^{-9}$

Table 4-112. Absorption Cross Sections of CF_2ClCF_2Cl at 295 K

λ (nm)	10^{20} σ (cm^2)	λ (nm)	10^{20} σ (cm^2)	λ (nm)	10^{20} σ (cm^2)
172	69.0	194	2.56	216	0.0290
174	55.0	196	1.75	218	0.0190
176	43.0	198	1.20	220	0.0122
178	34.0	200	0.800	*222*	*0.00809*
180	26.2	202	0.540	*224*	*0.00531*
182	19.8	204	0.370	*226*	*0.00349*
184	15.0	206	0.245	*228*	*0.00229*
186	11.0	208	0.160	*230*	*0.00151*
188	7.80	210	0.104	*232*	*0.00099*
190	5.35	212	0.0680	*234*	*0.00065*
192	3.70	214	0.0440	*235*	*0.00053*

Note:
172–220 nm: Simon et al. [733]
222–235 nm: extrapolation of Simon et al. [733] data.

F38. CF_3CF_2Cl (CFC-115) + hν → Products. The absorption cross sections of CF_3CF_2Cl have been measured at room temperature and 184–207 nm by Chou et al. [171]; at 208 and 298 K and 160–230 nm by Hubrich and Stuhl [346]; and at 225–295 K and 172–204 nm by Simon et al. [733]. The room temperature data of Simon et al. [733] and Hubrich and Stuhl [346] agree within ~20%, where Hubrich and Stuhl [346] report the larger values over the range 172–204 nm. The data of Chou et al. [171] are larger by up to more than 50% than those of Simon et al. [733]. The preferred absorption cross sections, listed in Table 4-113, are the mean of the values reported by Hubrich and Stuhl [346] and Simon et al. [733] at 172–204 nm. The mean of the values measured by Hubrich and Stuhl [346] and those obtained by extrapolating the absorption curve of Simon et al. [733] ($\log \sigma = -6.2191 - 0.0756\ \lambda$) were taken for the range 205–230 nm (the extrapolated values become larger by up to nearly 50% with increasing wavelength than the measured values of Hubrich and Stuhl [346]).

Measurements at the Lyman-α line at 121.6 nm have been carried out by Ravishankara et al. [659]; and at 120–175 nm by Doucet et al. [223].

Temperature effects, if any, could not be detected for this highly fluorinated species. Simon et al. [733] parameterized the absorption cross sections by the polynomial expansion

$\log_{10} \sigma(\lambda, T) = \sum A_n \lambda^n + (T - 273) \times \sum B_n \lambda^n$ (with all $B_n = 0$),

and reported smoothed values for T = 295 K, every 2 nm, and at wavelengths corresponding to the wavenumber intervals generally used in stratospheric photodissociation calculations. The parameters A_n for the ranges T = 210–300 K and λ = 172–204 nm are

$$A_0 = 5.8281,\ A_1 = -2.990 \times 10^{-1},\ A_2 = 1.3525 \times 10^{-3},\ A_3 = -2.6851 \times 10^{-6}.$$

Note: There were typographical errors in JPL02-25 for parameters A_1 and A_2 which have been corrected in the present evaluation.

Table 4-113. Absorption Cross Sections of CF_3CF_2Cl at 295–298 K

λ (nm)	10^{20} σ (cm^2)	λ (nm)	10^{20} σ (cm^2)	λ (nm)	10^{20} σ (cm^2)
172	5.50	188	0.403	204	0.0218
174	4.13	190	0.287	*205*	*0.0187*
176	3.08	192	0.203	*210*	*0.00700*
178	2.25	194	0.143	*215*	*0.00273*
180	1.58	196	0.0985	*220*	*0.00107*
182	1.13	198	0.0685	*225*	*0.00046*
184	0.790	200	0.0474	*230*	*0.00018*
186	0.563	202	0.0325		

Note:
172–204 nm: mean of Hubrich and Stuhl [346] and Simon et al. [733]
205–230 nm: mean of Hubrich and Stuhl [346] and extrapolated Simon et al. [733] data.

F39. $CHFCl_2$ (HCFC-21) + hν → Products. The absorption cross sections of $CHFCl_2$ have been measured at room temperature and 208 nm by Gordus and Bernstein [293]; at 174–222 nm by Robbins and Stolarski [674]; at 184–205 nm by and Green and Wayne [299]; and at 213.9 nm by Rebbert et al. [666]; at 208 and 298 K and 158–235 nm by Hubrich et al. [347]; and at 225–295 K and 174–222 nm by Simon et al. [734]. The results of these groups (except those of Green and Wayne [299] which deviate strongly) are in good agreement, generally within 15%, although the data of Hubrich et al. [347] show humps around 205 and 220 nm, where the agreement is only ~40%. The preferred absorption cross sections, listed in Table 4-114, are the values of Simon et al. [734] at 174–222 nm. For the range 224–236 nm, the absorption curve above 200 nm of Simon et al. [734] has been extrapolated ($\log \sigma = 0.9806 - 0.1014\ \lambda$). The measured values of Hubrich et al. [347] deviate from the extrapolated values by up to ~–20% and +50%.

Measurements in the far UV at 60–120 nm have been reported by Gilbert et al. [273], measurements at 120–200 nm by Doucet et al. [222], and a measurement at 147 nm by Rebbert et al. [666].

The temperature dependence becomes significant at wavelengths above 190 nm, where the cross sections decrease with decreasing temperature between 296 and 210 K. Simon et al. [734] parameterized the temperature dependence of the cross sections by the polynomial expansion

$$\log_{10} \sigma(\lambda, T) = \sum A_n \lambda^n + (T - 273) \times \sum B_n \lambda^n$$

and reported smoothed values for T = 210, 230, 250, 270, and 295 K, every 2 nm, and at wavelengths corresponding to the wavenumber intervals generally used in stratospheric photodissociation calculations. The parameters A_n and B_n for the ranges T = 210–300 K and λ = 174–222 nm are as follows:

$A_0 = -514.56$ $B_0 = -3.0577$
$A_1 = 8.7940$ $B_1 = 6.6539 \times 10^{-2}$
$A_2 = -5.6840 \times 10^{-2}$ $B_2 = -5.3964 \times 10^{-4}$
$A_3 = 1.5894 \times 10^{-4}$ $B_3 = 1.9322 \times 10^{-6}$
$A_4 = 1.6345 \times 10^{-7}$

Table 4-114. Absorption Cross Sections of $CHFCl_2$ at 295–298 K

λ (nm)	10^{20} σ (cm^2)	λ (nm)	10^{20} σ (cm^2)	λ (nm)	10^{20} σ (cm^2)
174	166.0	198	8.10	222	0.0319
176	164.5	200	5.24	*224*	*0.0195*
178	155.0	202	3.35	*225*	*0.0154*
180	138.0	204	2.12	*226*	*0.0122*
182	116.0	206	1.34	*228*	*0.00766*
184	92.4	208	0.836	*230*	*0.00480*
186	71.5	210	0.522	*232*	*0.00301*
188	53.2	212	0.325	*234*	*0.00189*
190	38.4	214	0.203	*235*	*0.00150*
192	26.9	216	0.127	*236*	*0.00119*
194	18.4	218	0.0797		
196	12.3	220	0.0503		

Note:
174–222 nm: Simon et al. [734]
224–236 nm: extrapolation of Simon et al. [734] data.

F40. CHF_2Cl (HCFC-22) + hν → Products. The absorption cross sections of CHF_2Cl have been measured at room temperature and 174–202 nm by Robbins and Stolarski [674] and at 181–194 nm by Green and Wayne [299]; at 208 K and 298 K and 158–220 nm by Hubrich et al. [347], and at 225–295 K and 174–204 nm by Simon et al. [734]. The results of Robbins and Stolarski [674], Hubrich et al. [347], and Simon et al. [734] are in good agreement generally within 15–20%, however those of Green and Wayne [299] deviate strongly. The preferred absorption cross sections, listed in Table 4-115, are the values of Hubrich et al. [347] at 170–172 nm and the values of Simon et al. [734] at 174–204 nm. For the range 206–220 nm, the absorption curve above 190 nm of Simon et al. [734] has been extrapolated ($\log \sigma = -4.1001 - 0.0870\ \lambda$). The measured values of Hubrich et al. [347] deviate from the extrapolated values by up to 20%.

Measurements in the far UV at 60–160 nm have been reported by Gilbert et al. [273], and measurements at 120–200 nm by Doucet et al. [222].

A weak temperature dependence has been observed above 190 nm, where the cross sections decrease with decreasing temperature between 296 and 210 K. Simon et al. [734] parameterized the cross sections and the temperature dependence by the polynomial expansion

$$\log_{10} \sigma(\lambda, T) = \sum A_n \lambda^n + (T - 273) \times \sum B_n \lambda^n$$

and reported smoothed values for T = 210, 230, 250, 270, and 295 K, every 2 nm, and at wavelengths corresponding to the wavenumber intervals generally used in stratospheric photodissociation calculations. The parameters A_n and B_n for the ranges T = 210–300 K and λ = 174–204 nm are as follows:

$A_0 = -106.029$ $\quad B_0 = -1.3399 \times 10^{-1}$
$A_1 = 1.5038$ $\quad B_1 = 2.7405 \times 10^{-3}$
$A_2 = -8.2476 \times 10^{-3}$ $\quad B_2 = -1.8028 \times 10^{-5}$
$A_3 = 1.4206 \times 10^{-5}$ $\quad B_3 = 3.8504 \times 10^{-8}$

Table 4-115. Absorption Cross Sections of CHF_2Cl at 295–298 K

λ (nm)	10^{20} σ (cm^2)	λ (nm)	10^{20} σ (cm^2)	λ (nm)	10^{20} σ (cm^2)
170	12.9	188	0.372	*206*	*0.00842*
172	9.79	190	0.245	*208*	*0.00636*
174	5.72	192	0.156	*210*	*0.00426*
176	4.04	194	0.103	*212*	*0.00285*
178	2.76	196	0.072	*214*	*0.00191*
180	1.91	198	0.048	*216*	*0.00128*
182	1.28	200	0.032	*218*	*0.00086*
184	0.842	202	0.0220	*220*	*0.00057*
186	0.576	204	0.0142		

Note:
170–172 nm: Hubrich et al. [347]
174–204 nm: Simon et al. [734]
206–220 nm: extrapolation of Simon et al. [734] data.

F41. CH_2FCl (HCFC-31) + hν → Products. The absorption cross sections of CH_2FCl have been measured at 208 and 298 K and 160–230 nm by Hubrich and Stuhl [346]. The room temperature data at 160–230 nm are listed in Table 4-116.

Measurements in the far UV at 60–120 nm have been reported by Gilbert et al. [273], and measurements at 120–200 nm by Doucet et al. [222].

Table 4-116. Absorption Cross Sections of CH_2FCl at 298 K

λ (nm)	10^{20} σ (cm^2)	λ (nm)	10^{20} σ (cm^2)	λ (nm)	10^{20} σ (cm^2)
160	47.9	185	4.20	210	0.0188
165	55.9	190	1.95	215	0.00560
170	43.0	195	0.544	220	0.00215
175	23.3	200	0.209	225	0.00049
180	12.5	205	0.069	230	0.00026

Note:
160–230 nm: Hubrich and Stuhl [346].

F42. CF_3CHCl_2 (HCFC-123) + hν → Products. The absorption cross sections of CF_3CHCl_2 have been measured at room temperature and 185–204 nm by Green and Wayne [299]; at 225–295 K and 170–250 nm by Gillotay and Simon [279]; at 203–295 K and 190–230 nm by Orlando et al. [607]; and at 223–333 K and 160–230 nm by Nayak et al. [572]. The agreement between the results of the latter three groups is within 25% in the region below 220 nm. The results of Green and Wayne [299] are very different below 200 nm. The preferred absorption cross sections at 295 K, listed in Table 4-117, are the mean of the values reported by Gillotay and Simon [279] and Nayak et al. [572] at 170–188 nm and the mean of the values reported by Gillotay and Simon [279], Orlando et al. [607], and Nayak et al. [572] at 190–230 nm. For the range 232–250 nm, the absorption curve above 210 nm of Orlando et al. [607] has been extrapolated ($\log \sigma = -3.1097 - 0.0794\ \lambda$).

The studies of the temperature dependence show a decrease of the absorption cross sections with decreasing temperature at wavelengths above 178–180 nm and below 170 nm. Between 170–180 nm, the reverse behavior was observed by Gillotay and Simon [279] and Nayak et al. [572]. An irregular temperature dependence was reported by Orlando et al. [607] for the range 210–230 nm, where the absorption curves show wiggles.

Various parameterized fits, i.e., polynomial expansions of the logarithm of the absorption cross section, have been proposed for the temperature dependence. Gillotay and Simon [279] parameterized the cross sections and the temperature dependence by the polynomial expansion $\log_{10} \sigma(\lambda, T) = \sum A_n \lambda^n + (T - 273) \times \sum B_n \lambda^n$ and reported smoothed values for T = 210, 230, 250, 270, and 295 K, every 2 nm, and at wavelengths corresponding to the wavenumber intervals generally used in stratospheric photodissociation calculations. The parameters A_n and B_n for the ranges T = 210–300 K and λ = 182–250 nm are as follows:

$A_0 = -513.996354$ $B_0 = 1.757133$
$A_1 = 9.089141$ $B_1 = -3.499205 \times 10^{-2}$
$A_2 = -6.136794 \times 10^{-2}$ $B_2 = 2.593563 \times 10^{-4}$
$A_3 = 1.814826 \times 10^{-4}$ $B_3 = -8.489357 \times 10^{-7}$
$A_4 = -1.999514 \times 10^{-7}$ $B_4 = 1.037756 \times 10^{-9}$.

Nayak et al. [572] report sixth-order polynomial coefficients for the functions $\log_{10}(\sigma_T) = \sum C_n (\lambda - 170)^n$ at T = 223, 233, 253, 273, 295, 313, and 333 K and for the range 160–230 nm. The parameters C_n are as follows:

	223 K	273 K	295 K	333 K
C_0	–17.6732	–17.6773	–17.6792	–17.6722
C_1	1.70233×10^{-2}	1.3636×10^{-2}	1.19392×10^{-2}	9.07941×10^{-3}
C_2	-7.39366×10^{-4}	-4.98553×10^{-4}	-3.71661×10^{-4}	-1.29566×10^{-4}
C_3	-1.83761×10^{-4}	-1.70566×10^{-4}	-1.61218×10^{-4}	-1.56667×10^{-4}
C_4	7.80778×10^{-6}	6.73373×10^{-6}	6.03101×10^{-6}	5.56409×10^{-6}
C_5	-1.29836×10^{-7}	-1.02726×10^{-7}	-8.76762×10^{-8}	-7.77379×10^{-8}
C_6	8.05415×10^{-10}	5.66688×10^{-10}	4.61745×10^{-10}	3.93859×10^{-10}

A double expansion in terms of twelve parameters, $\ln \sigma(\lambda, T) = \sum (\sum a_{ij} (T-245.4)^{j-1}) (\lambda - 206.214)^{i-1}$, i = 1–4,
j = 1–3, T = 203–295 K, λ = 190–230 nm, was used by Orlando et al. [607]:

$a_{11} = -4.500 \times 10^{1}$	$a_{12} = 3.529 \times 10^{-3}$	$a_{13} = -4.181 \times 10^{-8}$
$a_{21} = -1.985 \times 10^{-1}$	$a_{22} = 6.826 \times 10^{-5}$	$a_{23} = 1.555 \times 10^{-6}$
$a_{31} = -2.802 \times 10^{-4}$	$a_{32} = -1.018 \times 10^{-5}$	$a_{33} = 4.037 \times 10^{-8}$
$a_{41} = 6.312 \times 10^{-5}$	$a_{42} = -3.055 \times 10^{-7}$	$a_{43} = -2.473 \times 10^{-9}$

Note: There was a typographical error in JPL02-25 for parameter a_{11} which has been corrected in this evaluation.

Table 4-117. Absorption Cross Sections of CF_3CHCl_2 at 295 K

λ (nm)	10^{20} σ (cm^2)	λ (nm)	10^{20} σ (cm^2)	λ (nm)	10^{20} σ (cm^2)
170	192	198	17.1	226	0.0880
172	207	200	11.9	228	0.0599
174	214	202	8.24	230	0.0451
176	213	204	5.70	*232*	*0.0295*
178	202	206	3.89	*234*	*0.0205*
180	184	208	2.67	*236*	*0.0142*
182	161	210	1.82	*238*	*0.0098*
184	135	212	1.23	*240*	*0.0068*
186	109	214	0.838	*242*	*0.0047*
188	85.5	216	0.573	*244*	*0.0033*
190	62.2	218	0.384	*246*	*0.0023*
192	46.4	220	0.266	*248*	*0.0016*
194	33.9	222	0.180	*250*	*0.0011*
196	24.2	224	0.124		

Note: 170–188 nm: mean of the values of Gillotay and Simon [279] and Nayak et al. [572]
190–230 nm: mean of the values of Gillotay and Simon [279], Orlando et al. [607], and Nayak et al. [572]
232–250 nm: extrapolation of Orlando et al. [607] data.

F43. CF_3CHFCl (HCFC-124) + hν → Products. The absorption cross sections of CF_3CHFCl have been measured at 203–295 K and 190–230 nm by Orlando et al. [607]; and at 210–295 K and 170–230 nm by Gillotay and Simon [280]. The agreement is better than 10% between 190 and 220 nm, whereas above 220 nm the values of Orlando et al. [607] become increasingly larger by up to 133% than those of Gillotay and Simon [280]. The preferred room temperature values, listed in Table 4-118, are the values of Gillotay and Simon [280] at 170–188 nm and 222–230 nm and the mean of the values reported by Gillotay and Simon [280] and Orlando et al. [607] at 190–220 nm.

The temperature dependence of the cross sections has been measured by both groups and a decrease of the absorption cross sections with decreasing temperature was observed at 170–230 nm by Gillotay and Simon [280] and at 190–215 nm by Orlando et al. [607]. An irregular temperature behavior was reported by Orlando et al. [607] for the range 215–230 nm, where the absorption curves show wiggles. Parameterized fits, i.e., polynomial expansions of the logarithm of the absorption cross section, have been derived. Gillotay and Simon [280] parameterized the cross sections and the temperature dependence by the polynomial expansion

$$\log_{10} \sigma(\lambda, T) = \sum A_n \lambda^n + (T - 273) \times \sum B_n \lambda^n$$

and reported smoothed values for T = 210, 230, 250, 270, and 295 K, every 2 nm, and at wavelengths corresponding to the wavenumber intervals generally used in stratospheric photodissociation calculations. The parameters A_n and B_n for the ranges T = 210–300 K and λ = 170–230 nm are as follows:

$A_0 = -101.230250$ $\quad B_0 = -5.795712 \times 10^{-2}$
$A_1 = 1.333519$ $\quad B_1 = 1.053901 \times 10^{-3}$
$A_2 = -6.888672 \times 10^{-3}$ $\quad B_2 = -6.530379 \times 10^{-6}$
$A_3 = 1.114172 \times 10^{-5}$ $\quad B_3 = 1.382056 \times 10^{-8}$

A double expansion in terms of twelve parameters, $\ln \sigma(\lambda, T) = \sum (\sum a_{ij} (T-251.7)^{j-1}) (\lambda - 206.214)^{i-1}$, i = 1–4, j = 1–3, T = 203–295 K, λ = 190–230 nm, was used by Orlando et al. [607]:

$a_{11} = -4.967 \times 10^{1}$ $\quad a_{12} = 6.562 \times 10^{-3}$ $\quad a_{13} = 1.735 \times 10^{-5}$
$a_{21} = -2.025 \times 10^{-1}$ $\quad a_{22} = 2.788 \times 10^{-4}$ $\quad a_{23} = -3.974 \times 10^{-6}$
$a_{31} = 6.839 \times 10^{-4}$ $\quad a_{32} = 5.523 \times 10^{-6}$ $\quad a_{33} = -3.092 \times 10^{-7}$
$a_{41} = 1.275 \times 10^{-4}$ $\quad a_{42} = -2.959 \times 10^{-7}$ $\quad a_{43} = -1.182 \times 10^{-8}$

Note: There was a typographical error in JPL02-25 for parameter a_{11} which has been corrected in this evaluation.

Table 4-118. Absorption Cross Sections of CF_3CHFCl at 295 K

λ (nm)	10^{20} σ (cm^2)	λ (nm)	10^{20} σ (cm^2)	λ (nm)	10^{20} σ (cm^2)
170	13.6	192	0.548	214	0.00859
172	11.1	194	0.387	216	0.00610
174	8.85	196	0.267	218	0.00431
176	6.93	198	0.185	220	0.00312
178	5.33	200	0.128	222	0.00214
180	4.03	202	0.0868	224	0.00153
182	3.00	204	0.0594	226	0.00111
184	2.20	206	0.0401	228	0.00082
186	1.60	208	0.0269	230	0.00061
188	1.14	210	0.0186		
190	0.772	212	0.0126		

Note:
170–188 nm, Gillotay and Simon [280],
190–220 nm, mean of the values of Gillotay and Simon [280] and Orlando et al. [607],
222–230 nm, Gillotay and Simon [280].

F44. CF_3CH_2Cl (HCFC-133) + hν → Products. The absorption cross sections of CF_3CH_2Cl have been measured at room temperature and 147 nm ($\sigma = 1.35 \times 10^{-17}$ cm^2) by Ichimura et al. [359], and 186–203 nm by Green and Wayne [299], and at 208 and 298 K and 160–245 nm by Hubrich and Stuhl [346]. There is no good agreement between the results at wavelengths above 180 nm. Table 4-119 gives the recommended room temperature data of Hubrich and Stuhl [346].

Table 4-119. Absorption Cross Sections of CF_3CH_2Cl at 298 K

λ (nm)	10^{20} σ (cm^2)	λ (nm)	10^{20} σ (cm^2)	λ (nm)	10^{20} σ (cm^2)
160	59.4	190	6.20	220	0.0887
165	64.6	195	2.95	225	0.0226
170	56.4	200	1.14	230	0.0147
175	37.3	205	0.598	235	0.00404
180	22.8	210	0.328	240	0.00181
185	11.6	215	0.169	245	0.00054

Note:
160–245 nm, Hubrich and Stuhl [346].

F45. CH_3CFCl_2 (HCFC-141b) + hν → Products. The absorption cross sections of CH_3CFCl_2 have been measured at 210–295 K and 170–240 nm by Gillotay and Simon [279]; at 203–295 K and 190–230 nm by Orlando et al. [607] (data of Orlando et al. reported by Gillotay and Simon [281]); at 203–295 K and 190–230 nm by Talukdar et al. [764]; and at room temperature and 190–240 nm by Fahr et al. [232], who investigated the spectrum both for the gas and liquid phases and used a wavelength-shift procedure to convert the liquid-phase data into gas-phase data. The agreement between the values reported by Gillotay and Simon [279] and Fahr et al. [232] for the 190–240-nm region is very good (1–10% up to 236 nm); the results of Orlando et al. [607] are also in good agreement with these, but only in the region 190–210 nm. The agreement of the results of Talukdar et al. [764] is not as good, their absorption cross sections become smaller below 210 nm by up to ~20% and become larger above 210 nm by up to about 70% than the above mentioned data. The preferred absorption cross sections, listed in Table 4-120, are the values of Gillotay and Simon [279] at 170–188 nm and the mean of the values reported by Gillotay and Simon [279] and Fahr et al. [232] at 190–240 nm.

A decrease of the absorption cross sections with decreasing temperature at wavelengths above 188 nm and below 172 nm and the reverse behavior between 172 and 188 nm was observed by Gillotay and Simon [279]. They parameterized the cross sections and the temperature dependence of the absorption cross sections using the polynomial expansion $\log_{10}$

$\sigma(\lambda, T) = \sum A_n \lambda^n + (T - 273) \times \sum B_n \lambda^n$. They derived the parameters

$A_0 = -682.913042$ $B_0 = 4.074747$
$A_1 = 12.122290$ $B_1 = -8.053899 \times 10^{-2}$
$A_2 = -8.187699 \times 10^{-2}$ $B_2 = 5.946552 \times 10^{-4}$
$A_3 = 2.437244 \times 10^{-4}$ $B_3 = -1.945048 \times 10^{-6}$
$A_4 = -2.719103 \times 10^{-7}$ $B_4 = 2.380143 \times 10^{-9}$

for the ranges 210–300 K and 172–240 nm and list smoothed values for T = 210, 230, 250, 270, and 295 K at 2-nm intervals and at wavelengths corresponding to the wavenumber intervals generally used in stratospheric photodissociation calculations. **Note: There were typographical errors in JPL02-25 for parameters B_0 and B_1 which have been corrected in this evaluation.**

A similar temperature behavior was observed by Orlando et al. [607] only between 190 and 210 nm, and by Talukdar et al. [764] only above 197 nm.

Table 4-120. Absorption Cross Sections of CH_3CFCl_2 at 295–298 K

λ (nm)	10^{20} σ (cm^2)	λ (nm)	10^{20} σ (cm^2)	λ (nm)	10^{20} σ (cm^2)
170	143.1	194	47.2	218	0.382
172	145.1	196	34.1	220	0.248
174	154.2	198	24.0	222	0.161
176	162.9	200	16.6	224	0.105
178	172.6	202	11.3	226	0.0680
180	172.3	204	7.56	228	0.0444
182	162.9	206	5.02	230	0.0290
184	146.4	208	3.30	232	0.0189
186	125.7	210	2.16	234	0.0123
188	103.6	212	1.40	236	0.00801
190	83.0	214	0.909	238	0.00518
192	63.6	216	0.589	240	0.00334

Note:
170–188 nm, Gillotay and Simon [279],
190–240 nm, mean of Gillotay and Simon [279] and Fahr et al. [232].

F46. CH_3CF_2Cl (HCFC-142b) + hν → Products. The absorption cross sections of CH_3CF_2Cl have been measured at room temperature and 120–180 nm by Doucet et al. [223]; at 184–210 nm by Green and Wayne [299]; at 298 and 208 K and 160–230 nm by Hubrich and Stuhl [346]; at 210–295 K and 170–230 nm by Gillotay and Simon [279]; at 203–295 K and 190–230 nm by Orlando et al. [607]; and at 223–333 K and 160–210 nm by Nayak et al. [572]. At wavelengths below 200 nm, the values of Hubrich and Stuhl [346] and Nayak et al. [572] are within 15%, those of Gillotay and Simon [279] and Orlando et al. [607] are lower than the latter by up to 30%. At wavelengths between 200 and 215 nm, the values of Gillotay and Simon [279], Orlando et al. [607], and Nayak et al [572] agree within 15%. Above 215 nm, the absorption curve reported by Orlando et [607] shows wiggles with deviations by up to 100% from the data of Gillotay and Simon [279]. Also the values reported for the range 205–230 nm by Hubrich and Stuhl [346] become increasingly large by up to 600% than those of Gillotay and Simon [279]. The results of Green and Wayne [299] are very different from all other data. The preferred room temperature absorption cross sections, listed in Table 4-121, are the mean of the values reported by Hubrich and Stuhl [346], Gillotay and Simon [279], and Nayak et al. [572] at 175–185 nm, the mean of the values reported by Gillotay and Simon [279], Orlando et al. [607], and Nayak et al. [572] at 190–210 nm, and the values reported by Gillotay and Simon [279] at 212–230 nm.

A decrease of the absorption cross sections with decreasing temperature was observed by Gillotay and Simon [279] and Nayak et al. [572] over the wavelength range 160–230 nm and by Orlando et al. [607] between 190 and 200 nm. An irregular temperature behavior was reported by Orlando et al. [607] for the range 215–230 nm, where the absorption curves for the various temperatures show several crossings. Various parameterized fits for the temperature dependence of the absorption cross sections have been offered. Gillotay and Simon [279] used the polynomial expansion

$$\log_{10} \sigma(\lambda, T) = \sum A_n \lambda^n + (T - 273) \times \sum B_n \lambda^n$$

and reported smoothed values for
T = 210, 230, 250, 270, and 295 K, every 2 nm, and at wavelengths corresponding to the wavenumber intervals generally used in stratospheric photodissociation calculations. Their parameters A_n and B_n for the ranges
T = 210–300 K and λ = 172–230 nm are as follows:

$A_0 = -328.092008$ $\quad B_0 = 4.289533 \times 10^{-1}$
$A_1 = 6.342799$ $\quad B_1 = -9.042817 \times 10^{-3}$
$A_2 = -4.810362 \times 10^{-2}$ $\quad B_2 = 7.018009 \times 10^{-5}$
$A_3 = 1.611991 \times 10^{-4}$ $\quad B_3 = -2.389065 \times 10^{-7}$
$A_4 = -2.042613 \times 10^{-7}$ $\quad B_4 = 3.039799 \times 10^{-10}$

Nayak et al. [572] report fourth-order polynomial coefficients $C_n(T)$ for the functions $\log_{10}(\sigma_T) = \sum C_n (\lambda - 160)^n$ at T = 223, 233, 253, 273, 295, 313, and 333 K and for the range 160–210 nm. The parameters C_n are as follows

	223 K	273 K	295 K	333 K
C_0	–18.2361	–18.2441	–18.2406	–18.1777
C_1	-1.26669×10^{-2}	-7.37889×10^{-3}	-6.48269×10^{-3}	-2.39647×10^{-2}
C_2	-2.32945×10^{-3}	-2.66537×10^{-3}	-2.80923×10^{-3}	-7.23910×10^{-4}
C_3	2.81933×10^{-5}	4.19193×10^{-5}	5.01979×10^{-5}	-1.08049×10^{-5}
C_4	-1.37963×10^{-7}	-2.88472×10^{-7}	-3.96860×10^{-7}	1.37618×10^{-7}

A double expansion in terms of twelve parameters,

$\ln \sigma(\lambda, T) = \sum (\sum a_{ij} (T-245.4)^{j-1}) (\lambda - 206.214)^{i-1}$, i = 1–4, j = 1–3, T = 203–295 K, λ = 190–230 nm,

was used by Orlando et al. [607]:

$a_{11} = -4.973 \times 10^{1}$ $a_{12} = 9.077 \times 10^{-3}$ $a_{13} = -4.651 \times 10^{-5}$

$a_{21} = -2.175 \times 10^{-1}$ $a_{22} = 4.712 \times 10^{-4}$ $a_{23} = -1.005 \times 10^{-5}$

$a_{31} = 4.133 \times 10^{-4}$ $a_{32} = -6.432 \times 10^{-5}$ $a_{33} = 1.141 \times 10^{-6}$

$a_{41} = 7.145 \times 10^{-5}$ $a_{42} = -5.396 \times 10^{-6}$ $a_{43} = 1.187 \times 10^{-7}$

Note: There was a typographical error in JPL02-25 for parameter a_{11} which has been corrected in this evaluation.

Quantum yields for Cl ($^2P_{3/2}$) and Cl*($^2P_{1/2}$) atom formation in the photolysis of CH_3CF_2Cl at 193.3 nm have been measured by Brownsword et al. [106] and quantum yields for H atom formation in the photolysis at 121.6 and 193.3 nm by Brownsword et al. [105]: Φ(Cl + Cl*) = 0.90 ± 0.17 with Φ(Cl) = 0.65 ± 0.12 and Φ(Cl*) = 0.25 ± 0.05 at 193.3 nm, and Φ(H) = 0.53 ± 0.12 and 0.06 ± 0.02 at 121.6 and 193.3 nm, respectively.

Table 4-121. Absorption Cross Sections of CH_3CF_2Cl at 295–298 K

λ (nm)	10^{20} σ (cm^2)	λ (nm)	10^{20} σ (cm^2)	λ (nm)	10^{20} σ (cm^2)
170	27.1	200	0.145	218	0.00243
175	14.0	202	0.0949	220	0.00145
180	6.38	204	0.0622	222	0.000845
185	2.73	206	0.0399	224	0.000484
190	1.02	208	0.0256	226	0.000271
192	0.706	210	0.0161	228	0.000148
194	0.482	212	0.0105	230	0.0000783
196	0.324	214	0.00652		
198	0.218	216	0.00401		

Note:
170–185 nm: mean of Gillotay and Simon [279], Hubrich and Stuhl [346], and Nayak et al. [572]
190–210 nm: mean of Gillotay and Simon [279], Orlando et al. [607], and Nayak et al. [572]
212–230 nm: Gillotay and Simon [279].

F47. $CH_2ClCHO + h\nu \rightarrow$ Products. The absorption spectrum of CH_2ClCHO (chloroacetaldehyde) has been measured at room temperature and 118-182 nm by Lucazeau and Sandorfy [462] and at 235–360 nm by Libuda [445] who report a slightly structured absorption band with the maximum around 290 nm. In Table 4-122 are listed the average absorption cross-sections over 1-nm intervals of the medium-resolution data (0.6 nm) of Libuda [445] for the range 240-357 nm.

Table 4-122. Absorption Cross Sections of CH_2ClCHO at 298 K

λ (nm)	10^{20} σ (cm^2)	λ (nm)	10^{20} σ (cm^2)	λ (nm)	10^{20} σ (cm^2)	λ (nm)	10^{20} σ (cm^2)
240	0.952	270	2.46	300	5.57	330	1.64
241	0.887	271	2.65	301	5.10	331	1.52
242	0.885	272	2.85	302	4.92	332	1.68
243	0.881	273	2.98	303	5.01	333	1.42
244	0.845	274	3.04	304	5.30	334	1.36
245	0.814	275	3.13	305	5.27	335	1.06
246	0.815	276	3.29	306	5.48	336	0.747
247	0.841	277	3.38	307	5.34	337	0.622
248	0.857	278	3.57	308	5.44	338	0.502
249	0.864	279	3.82	309	5.37	339	0.411
250	0.875	280	3.99	310	5.03	340	0.340
251	0.884	281	4.23	311	4.61	341	0.281
252	0.926	282	4.09	312	3.92	342	0.247
253	0.959	283	4.15	313	3.71	343	0.213
254	0.977	284	4.31	314	3.73	344	0.190
255	1.01	285	4.55	315	3.96	345	0.159
256	1.08	286	4.64	316	3.85	346	0.136
257	1.18	287	4.80	317	4.16	347	0.0977
258	1.23	288	4.99	318	3.84	348	0.0791
259	1.28	289	5.03	319	3.78	349	0.0623
260	1.33	290	5.20	320	3.84	350	0.0545
261	1.42	291	4.95	321	3.43	351	0.0558
262	1.53	292	4.94	322	3.26	352	0.0603
263	1.68	293	5.14	323	2.49	353	0.0633
264	1.84	294	5.48	324	2.11	354	0.0565
265	1.91	295	5.47	325	1.92	355	0.0377
266	1.98	296	5.64	326	1.87	356	0.0239
267	2.08	297	5.56	327	1.87	357	0.0123
268	2.23	298	5.75	328	1.70		
269	2.33	299	5.63	329	1.92		

Note:
240-357 nm, Libuda et al. [445].

F48. $CHCl_2CHO + h\nu \rightarrow$ Products. The absorption spectrum of $CHCl_2CHO$ (dichloroacetaldehyde) has been measured at room temperature and 118-182 nm by Lucazeau and Sandorfy [462] and at 253–360 nm by Libuda [445] who report an absorption band slightly structured around the maximum at about 300 nm. In Table 4-123 are listed the averages over 1-nm intervals of the medium-resolution data (0.6 nm) of Libuda [445] for the range 256-354 nm.

Table 4-123. Absorption Cross Sections of $CHCl_2CHO$ at 298 K

λ (nm)	10^{20} σ (cm^2)	λ (nm)	10^{20} σ (cm^2)	λ (nm)	10^{20} σ (cm^2)	λ (nm)	10^{20} σ (cm^2)
256	0.0462	281	3.66	306	5.76	331	1.47
257	0.0787	282	3.85	307	5.70	332	1.34
258	0.167	283	4.02	308	5.49	333	1.22
259	0.221	284	4.23	309	5.36	334	1.21
260	0.247	285	4.43	310	5.25	335	1.05
261	0.313	286	4.63	311	4.99	336	0.859
262	0.445	287	4.88	312	4.58	337	0.720
263	0.596	288	4.96	313	4.40	338	0.594
264	0.705	289	5.17	314	4.26	339	0.495
265	0.785	290	5.32	315	4.11	340	0.418
266	0.914	291	5.38	316	3.98	341	0.362
267	1.09	292	5.51	317	3.85	342	0.315
268	1.30	293	5.68	318	3.73	343	0.259
269	1.49	294	5.85	319	3.51	344	0.209
270	1.67	295	5.88	320	3.30	345	0.182
271	1.77	296	6.06	321	3.18	346	0.155
272	1.91	297	5.97	322	3.00	347	0.134
273	2.08	298	6.04	323	2.73	348	0.117
274	2.28	299	6.02	324	2.48	349	0.102
275	2.57	300	6.14	325	2.27	350	0.0844
276	2.74	301	5.94	326	2.14	351	0.0707
277	3.01	302	5.97	327	1.99	352	0.0697
278	3.14	303	5.93	328	1.80	353	0.0638
279	3.26	304	5.90	329	1.67		
280	3.48	305	5.77	330	1.58		

Note:
256-354 nm, Libuda et al. [445].

F49. $CF_2ClCHO + h\nu \rightarrow$ Products. The absorption spectrum of CF_2ClCHO (difluorochloroacetaldehyde) has been measured at room temperature and 235-355 nm by Libuda [445] and at 245-298 K and 235-370 nm by Rattigan et al. [655]. The spectrum displays an absorption band in that wavelength region with a maximum at 300 nm. The room temperature data are in very good agreement, within 3-10%, between 270 and 335 nm, where the data of Rattigan et al. [655] are always larger than those of Libuda [445]. Above 340 nm, the data of Rattigan et al. [655] become larger by up to 25% than the data of Libuda [445], and going from 265 to 235 nm, the data of Rattigan et al. [655] become increasingly larger by 15-~300% than the data of Libuda [445]. The preferred absorption cross-sections listed at 5-nm intervals in Table 4-124 are the mean values of the data of Libuda [445] (selected from 1-nm averages of medium-resolution (0.6 nm) data) and Rattigan et al. [655] (given as 5-nm averages of medium-resolution (0.6 nm) data) at 235-350 nm, and the data of Rattigan et al. [655] at 355-370 nm.

The temperature studies at several temperatures between 245 and 298 K show an increase of the absorption cross sections over the absorption band up to 340 nm and a decrease in the long-wavelength wing with decreasing temperature. A simple empirical relation for the temperature dependence between 245 and 298 K, $\ln \sigma(\lambda, T) = \ln \sigma(\lambda, 298K) + B(\lambda)\cdot(T-298)$, and temperature coefficients $B(\lambda)$ for λ = 235-370 nm at 5-nm intervals are given by Rattigan et al. [655]. These temperature coefficients B are also listed in Table 4-124.

Table 4-124. Absorption Cross Sections of CF_2ClCHO at 298 K and Temperature Coefficients

λ (nm)	10^{20} σ (cm^2)	10^4 B (K^{-1})	λ (nm)	10^{20} σ (cm^2)	10^4 B (K^{-1})	λ (nm)	10^{20} σ (cm^2)	10^4 B (K^{-1})
235	0.120	-29.0	285	11.8	-10.2	335	4.64	-2.83
240	0.295	-17.9	290	13.7	-10.6	340	2.66	-2.84
245	0.584	-13.5	295	15.2	-9.54	345	1.46	14.0
250	1.07	-11.8	300	16.0	-10.4	350	0.670	37.3
255	1.78	-10.7	305	15.6	-7.09	355	0.148	68.1
260	2.78	-10.5	310	15.2	-9.73	360	0.036	75.8
265	4.09	-10.4	315	13.0	-8.32	365	0.012	52.9
270	5.75	-10.5	320	11.4	-7.71	370	0.003	63.1
275	7.67	-9.96	325	9.07	-5.02			
280	9.79	-10.6	330	6.38	-3.03			

Note:
Absorption cross-sections σ: 235-350 nm, mean of Libuda [445] and Rattigan et al. [655], 355-370 nm, Rattigan et al. [655].
Temperature coefficients B: 245-298 K, Rattigan et al. [655] ($\ln \sigma(\lambda, T) = \ln \sigma(\lambda, 298\ K) + B(T-298)$).

F50. $CFCl_2CHO + h\nu \rightarrow$ Products. The absorption spectrum of $CFCl_2CHO$ (fluorodichloroacetaldehyde) has been measured at room temperature and 235-355 nm by Libuda [445] and at 253-298 K and 235-370 nm by Rattigan et al. [655]. There is an absorption band in that wavelength region with a maximum near 296 nm. The data of Libuda [445] are larger by 10-30% than the data of Rattigan et al. [655] over the whole absorption band (except for a few points in the wings). The preferred absorption cross-sections listed at 5-nm intervals in Table 4-125 are the mean values of the data of Libuda [445] (selected from 1-nm averages of medium-resolution (0.6 nm) data) and Rattigan et al. [655] (given as 5-nm averages of medium-resolution (0.6 nm) data) at 235-355 nm, and the data of Rattigan et al. [655] at 355-370 nm.

The temperature studies at several temperatures between 253 and 298 K show an increase of the absorption cross sections around the absorption maximum at 260-305 nm and a decrease in the long- and short-wavelength wings with decreasing temperature. A simple empirical relation for the temperature dependence between 253 and 298 K, $\ln \sigma(\lambda, T) = \ln \sigma(\lambda, 298K) + B(\lambda)\cdot(T-298)$, and temperature coefficients $B(\lambda)$ for λ = 235-370 nm at 5-nm intervals are given by Rattigan et al. [655]. These temperature coefficients B are also listed in Table 4-125.

Table 4-125. Absorption Cross Sections of $CFCl_2CHO$ at 298 K and Temperature Coefficients

λ (nm)	10^{20} σ (cm^2)	10^4 B (K-1)	λ (nm)	10^{20} σ (cm^2)	10^4 B (K-1)	λ (nm)	10^{20} σ (cm^2)	10^4 B (K-1)
235	0.305	136.0	285	14.1	-7.82	335	2.50	24.60
240	0.599	87.0	290	15.3	-6.89	340	1.20	36.50
245	1.22	30.6	295	16.1	-6.41	345	0.616	58.10
250	1.91	6.41	300	15.7	-4.50	350	0.245	84.90
255	2.89	1.24	305	14.9	-2.93	355	0.067	92.80
260	4.21	-6.12	310	13.0	1.73	360	0.017	93.20
265	5.89	-7.55	315	10.9	2.70	365	0.007	103.2
270	7.84	-8.11	320	8.66	6.97	370	0.002	138.3
275	9.95	-8.28	325	5.97	12.2			
280	12.1	-8.04	330	4.11	15.6			

Note:
Absorption cross-sections σ: 235-355 nm, mean of Libuda [445] and Rattigan et al. [655], 360-370 nm, Rattigan et al. [655].
Temperature coefficients B: 253-298 K, Rattigan et al. [655] ($\ln \sigma(\lambda, T) = \ln \sigma(\lambda, 298\ K) + B(T-298)$).

F51. $CCl_3CHO + h\nu \rightarrow CCl_3 + CHO$
$CCl_3CHO + h\nu \rightarrow CCl_3CO + H$
$CCl_3CHO + h\nu \rightarrow Cl + CCl_2CHO$

$CCl_3CHO + h\nu \rightarrow CCl_3H + CO$. The absorption spectrum of CCl_3CHO (trichloroacetaldehyde, chloral) has been measured at room temperature and at 118-182 and 250-357 nm by Lucazeau and Sandorfy [462]; at 235-350 nm by Libuda [445]; at 243-298 K and 200-360 nm by Rattigan et al. [656], [655]; at 210-295 K and 166-348 nm by Gillotay et al. [282]; and at 200-360 nm by Talukdar et al. [770]. An absorption band was observed between 240 and 360 nm with the maximum near 290 nm and a stronger absorption feature at shorter wavelengths. Except for the data of Lucazeau and Sandorfy [462], the results for the region of the absorption band are in good agreement within the experimental uncertainties: Gillotay et al. [282] report the highest values, Libuda [445] the lowest, the agreement around the maximum is within 20%. For the data of Rattigan et al. [655] and Talukdar et al. [770] the agreement is even better than 10% around the absorption maximum. The data of the latter two teams are nearly identical above 300 nm, whereas those of Gillotay et al [282] become appreciably higher, the difference becoming greater than a factor of 2 with increasing wavelength up to 335 nm. There is no explanation for these differences. As recommended absorption cross-sections, listed in Table 4-126, we chose the results of Talukdar et al. [770] who report data at 2-nm increments measured at a resolution of 1 nm by using a diode array spectrometer.

The studies of the temperature dependence at 233-296 K by Rattigan et al. [656], [655]; at 210-295 K Gillotay et al. [282]; and at 240-360 K by Talukdar et al. [770] in agreement show that the absorption cross sections clearly decrease with decreasing temperature below ~260 nm and above ~290 nm. The temperature dependence of the absorption cross-sections was parameterized by the empirical relation,

$$\ln \sigma(\lambda, T) = \ln \sigma(\lambda, 298K) + B(\lambda)\cdot(T-298).$$

Rattigan et al. [655] derived temperature coefficients $B(\lambda)$ for T = 233-296 K and λ = 200-355 nm, Talukdar et al. [770] for T = 240-360 K and 200-344 nm. The temperature coefficients B of Talukdar et al. [770] are also listed in Table 4-126.

Quantum yields for the production of H, $O(^3P)$, and Cl atoms in the photolysis of CCl_3CHO at 193, 248, and 308 nm have been measured by Talukdar et al. [770]. The yields of H and O atoms were found to be small or below the detection limit, $\Phi(O(^3P)) < 0.02$ and < 0.01 at 248 and 308 nm, $\Phi(H) = 0.04 \pm 0.005$, < 0.01, and < 0.002 at 193, 248, and 308 nm. Despite of the major expected channel to be the production of $CCl_3 + CHO$, Cl atoms were found to be the primary photolysis products at 308 nm with $\Phi(Cl) = 1.3 \pm 0.3$.

Table 4-126. Absorption Cross Sections of CCl_3CHO at 298 K and Temperature Coefficients

λ (nm)	$10^{20}\,\sigma$ (cm^2)	10^4 B (K-1)	λ (nm)	$10^{20}\,\sigma$ (cm^2)	10^4 B (K-1)	λ (nm)	$10^{20}\,\sigma$ (cm^2)	10^4 B (K-1)
200	187	22.0	250	2.18	3.73	300	9.25	3.07
202	153	23.9	252	2.54	1.50	302	8.77	3.60
204	122	27.2	254	2.92	0.324	304	8.17	4.37
206	95.7	30.6	256	3.36	-0.569	306	7.50	5.25
208	73.8	34.1	258	3.84	-0.877	308	6.86	6.10
210	56.3	37.5	260	4.35	-1.23	310	6.18	6.91
212	42.6	40.9	262	4.90	-1.65	312	5.58	7.90
214	31.8	44.0	264	5.48	-1.62	314	4.98	9.30
216	23.8	47.2	266	6.07	-1.50	316	4.33	11.2
218	17.1	50.2	268	6.68	-1.41	318	3.68	13.2
220	13.1	52.9	270	7.28	-1.22	320	3.09	15.1
222	9.75	55.6	272	7.88	-1.07	322	2.51	16.7
224	7.24	57.6	274	8.46	-0.931	324	2.09	18.5
226	5.39	59.0	276	8.99	-0.584	326	1.76	21.1
228	4.06	60.4	278	9.49	-0.412	328	1.43	25.0
230	3.07	60.5	280	9.94	-0.481	330	1.12	30.3
232	2.39	59.5	282	10.3	-0.235	332	0.849	36.6
234	1.90	55.9	284	10.6	0.242	334	0.590	43.3
236	1.62	49.2	286	10.8	0.475	336	0.373	49.8
238	1.43	41.6	288	10.9	0.750	338	0.261	55.6
240	1.39	33.0	290	10.9	1.09	340	0.188	60.2
242	1.41	24.0	292	10.8	1.51	342	0.136	65.0
244	1.53	16.4	294	10.6	1.96	344	0.100	69.0
246	1.66	10.4	296	10.3	2.38			
248	1.91	6.50	298	9.92	2.71			

Note:

Absorption cross-sections σ: 200-344 nm, Talukdar et al. [770].
Temperature coefficients B: 240-360 K, Talukdar et al. [770] ($\ln \sigma(\lambda, T) = \ln \sigma(\lambda, 298\ K) + B(T-298)$).

F52. $CH_3C(O)Cl + h\nu \rightarrow$ Products. The absorption spectrum of $CH_3C(O)Cl$ (acetyl chloride) has been measured at room temperature and 233-300 nm by Libuda [445] and 190-341 nm by Maricq [480]. Both authors in agreement report an absorption band with a maximum of (1.15-1.17) × 10^{-19} cm^2 $molecule^{-1}$ in the 242-245-nm region. The band observed by Libuda [445], however, is narrower than that observed by Maricq [480] due to an obvious asymmetry on the short-wavelength wing and the maximum is shifted somewhat to larger wavelength. The data reported by Maricq [480] therefore become increasingly larger by up to ~50% between 242 and 233 nm than the data reported by Libuda [445]. Above 292 nm there are large differences between the data reported by both authors: the absorption curve reported by Libuda [445] shows a regular and continuous decrease with increasing wavelengths up to 302 nm, whereas the data of Maricq [480] show large variations obviously due to noise effects. As recommended absorption cross-sections we chose the 1-nm averages of the medium-resolution (0.5 nm) data of Maricq [480] for the region 191-292 nm and the 1-nm averages of the medium-resolution (0.6 nm) data of Libuda [445] for the region 293-302 nm as listed in Table 4-127.

Table 4-127. Absorption Cross Sections of $CH_3C(O)Cl$ at 295-298 K

λ (nm)	10^{20} σ (cm^2)	λ (nm)	10^{20} σ (cm^2)	λ (nm)	10^{20} σ (cm^2)	λ (nm)	10^{20} σ (cm^2)
191	34.7	219	5.95	247	11.0	275	1.98
192	26.3	220	6.28	248	10.9	276	1.90
193	23.6	221	6.57	249	10.6	277	1.67
194	20.5	222	6.93	250	10.4	278	1.42
195	17.1	223	7.15	251	10.1	279	1.24
196	14.1	224	7.53	252	9.76	280	1.12
197	11.4	225	7.99	253	9.51	281	0.959
198	9.08	226	8.23	254	9.17	282	0.781
199	7.53	227	8.59	255	8.77	283	0.653
200	6.37	228	8.98	256	8.36	284	0.479
201	5.17	229	9.27	257	8.03	285	0.391
202	4.34	230	9.61	258	7.67	286	0.389
203	3.83	231	9.93	259	7.27	287	0.327
204	3.54	232	10.1	260	6.86	288	0.307
205	3.45	233	10.3	261	6.55	289	0.267
206	3.28	234	10.5	262	6.20	290	0.213
207	3.12	235	10.7	263	5.79	291	0.200
208	3.16	236	10.9	264	5.40	292	0.173
209	3.35	237	11.2	265	5.11	293	0.129
210	3.48	238	11.3	266	4.76	294	0.103
211	3.72	239	11.3	267	4.39	295	0.0846
212	3.89	240	11.4	268	4.03	296	0.0716
213	4.06	241	11.5	269	3.70	297	0.0599
214	4.40	242	11.5	270	3.36	298	0.0500
215	4.68	243	11.4	271	3.06	299	0.0404
216	4.88	244	11.3	272	2.77	300	0.0336
217	5.14	245	11.2	273	2.49	301	0.0298
218	5.54	246	11.1	274	2.19	302	0.0265

Note:
191-292 nm, Maricq [480],
293-302 nm, Libuda [445].

F53. $CH_2ClC(O)Cl + h\nu \rightarrow$ Products. The absorption spectrum of $CH_2ClC(O)Cl$ (chloroacetyl chloride) has been measured at room temperature and 234-342 nm by Libuda [445]. The spectrum exhibits an absorption band with the maximum around 248 nm. Above 315 nm the data points show a somewhat irregular behavior. We therefore recommend the 1-nm averages of Libuda's [445] medium-resolution (0.6 nm) data for the region 235-316 nm, which are listed in Table 4-128.

Table 4-128. Absorption Cross Sections of $CH_2ClC(O)Cl$ at 298 K

λ (nm)	10^{20} σ (cm^2)	λ (nm)	10^{20} σ (cm^2)	λ (nm)	10^{20} σ (cm^2)	λ (nm)	10^{20} σ (cm^2)
235	9.50	256	11.2	277	4.00	298	0.409
236	10.0	257	11.0	278	3.71	299	0.353
237	10.4	258	10.7	279	3.41	300	0.300
238	11.0	259	10.4	280	3.15	301	0.248
239	11.5	260	10.0	281	2.89	302	0.199
240	11.8	261	9.67	282	2.65	303	0.170
241	12.0	262	9.32	283	2.43	304	0.157
242	12.3	263	8.94	284	2.21	305	0.131
243	12.5	264	8.55	285	2.03	306	0.113
244	12.7	265	8.16	286	1.85	307	0.0909
245	12.7	266	7.80	287	1.67	308	0.0809
246	12.7	267	7.41	288	1.50	309	0.0657
247	12.7	268	7.06	289	1.33	310	0.0547
248	12.8	269	6.72	290	1.17	311	0.0522
249	12.7	270	6.30	291	1.04	312	0.0419
250	12.5	271	5.90	292	0.918	313	0.0380
251	12.4	272	5.53	293	0.814	314	0.0311
252	12.3	273	5.23	294	0.717	315	0.0286
253	12.1	274	4.93	295	0.628	316	0.0214
254	11.8	275	4.61	296	0.546		
255	11.5	276	4.33	297	0.473		

Note:
235-316 nm, Libuda [445].

F54. $CHCl_2C(O)Cl + h\nu \rightarrow$ Products. The absorption spectrum of $CHCl_2C(O)Cl$ (dichloroacetyl chloride) has been measured at room temperature and 235-338 nm by Libuda [445] and 200-300 nm by Villenave et al. [821]. An absorption band with the maximum around 258 nm was observed in that wavelength region. The reported data are in very good agreement between 242 and 300 nm, where the data of Villenave et al. [821] are smaller by 1-10% than the data of Libuda [445]. At shorter wavelengths the absorption cross-sections reported by Libuda [445] become smaller by up to ~25% at 235 nm than those reported by Villenave et al. [821]. The latter authors observed a minimum near 232 nm and increasing cross-sections between 230 and 220 nm. At longer wavelengths the absorption curve reported by Libuda [445] shows a regular behavior up to 316 nm. In Table 4-129 are listed as a recommendation the absorption cross sections measured at 10-nm increments for 200-300 nm by Villenave et al. [821].

Table 4-129. Absorption Cross Sections of $CHCl_2C(O)Cl$ at 298 K

λ (nm)	10^{20} σ (cm^2)
220	21.7
230	13.2
240	15.7
250	20.0
256	20.9
260	20.8
270	17.1
280	10.5
290	4.7
300	1.4

Note:
220 -300 nm, Villenave et al. [821].

F55. $CCl_3C(O)Cl + h\nu \rightarrow$ Products. The absorption spectrum of $CCl_3C(O)Cl$ (trichloroacetyl chloride) has been measured at room temperature and 235-342 nm by Libuda [445] and 220-290 nm by Villenave et al. [821]; and at 210-295 K and 166-338 nm by Gillotay et al. [282]. An absorption band between 230 and 340 nm with a maximum of ~2.3×10^{-19} cm^2 $molecule^{-1}$ around 256 nm and a strong increase of the absorption cross-sections below 230 nm was observed in good agreement by Gillotay et al. [282] and Villenave et al. [821]. Gillotay et al. [282] report a second maximum of ~7.2×10^{-18} cm^2 $molecule^{-1}$ around 175 nm. The absorption curve reported by Libuda [445] is very shallow in the region 240-270 nm, it crosses the other two curves at ~245 nm and is higher by 30-40% at 235 nm and lower by 10-14% in the region of the maximum. In the wing of the absorption band above 290 nm the data reported by Libuda [445] become smaller by up to about 70% than the data reported by Gillotay et al. [282]. Since the data of Villenave et al. [821] and Gillotay et al. [282] are in good agreement, but Villenave et al. [821] measured absorption cross-sections at 10-nm increments only, we list in Table 4-130 the room temperature data of Gillotay et al. [282], which are averages over the 500-cm^{-1} and 5-nm intervals of the high-resolution spectrum (0.015 nm) generally used in stratospheric photodissociation calculations.

The temperature studies at 210-295 K by Gillotay et al. [282] show an increase of the absorption cross-sections with increasing temperature all over the observed wavelength region.

Table 4-130. Absorption Cross Sections of $CCl_3C(O)Cl$ at 295 K

λ (nm)	10^{20} σ (cm^2)	λ (nm)	10^{20} σ (cm^2)	λ (nm)	10^{20} σ (cm^2)
166.7 – 169.5	671	204.1 - 206.2	231	256.4 - 259.7	22.6
169.5 - 172.4	699	206.2 - 208.3	194	259.7 - 263.2	22.3
172.4 - 173.9	712	208.3 - 210.5	160	263.2 - 266.7	21.1
173.9 - 175.4	716	210.5 - 212.8	129	266.7 - 270.3	19.1
175.4 - 177.0	717	212.8 - 215.0	102	270.3 - 274.0	16.6
177.0 - 178.6	714	215.0 - 217.4	78.9	274.0 - 277.8	13.7
178.6 - 180.2	706	217.4 - 219.8	59.5	277.8 - 281.7	10.7
180.2 - 181.8	694	219.8 - 222.2	44.0	281.7 - 285.7	8.14
181.8 - 183.5	677	222.2 - 224.7	31.8	285.7 - 289.9	5.86
183.5 - 185.2	655	224.7 - 227.3	25.8	289.9 - 294.1	4.03
185.2 - 186.9	630	227.3 - 229.9	21.9	294.1 - 298.5	2.67
186.9 - 188.7	599	229.9 - 232.6	19.5	298.5 - 303.0	1.68
188.7 - 190.5	567	232.6 - 235.3	18.3	303.0 - 307.7	0.921
190.5 - 192.3	528	235.3 - 238.1	17.9	307.7 - 312.5	0.605
192.3 - 194.2	487	238.1 - 241.0	18.1	312.5 - 317.5	0.339
194.2 - 196.1	445	241.0 - 243.9	18.7	317.5 - 322.5	0.188
196.1 - 198.0	402	243.9 - 246.9	19.7	322.5 - 327.5	0.104
198.0 - 200.0	358	246.9 - 250.0	20.9	327.5 - 332.5	0.0578
200.0 - 202.0	314	250.0 - 253.2	21.8	332.5 - 337.5	0.0326
202.0 - 204.1	272	253.2 - 256.4	22.3		

Note:
166.7-337.5 nm, Gillotay et al. [282].

F56. $CF_3CF_2CHCl_2$ (HCFC-225ca) + hν → Products.

F57. CF_2ClCF_2CHFCl (HCFC-225cb) + hν → Products. The absorption spectra of these compounds in the gaseous and liquid phases at 298 K have been measured by Braun et al. [86]. Table 4-131 lists the absorption cross sections for the gas phase taken from this work. The originally listed (0.5-nm intervals) absorption coefficients ε in $(atm, 298\ K)^{-1}$ cm^{-1} ($\sigma = 4.06 \times 10^{-20}\ \varepsilon$) for both phases have been fitted with third-order polynomial expansions $\log_{10} \varepsilon = \sum a_n(\lambda - 160)^n$ with

$a_0 = 1.425$, $a_1 = 4.542 \times 10^{-2}$, $a_2 = -2.036 \times 10^{-3}$, $a_3 = 1.042 \times 10^{-5}$ for HCFC-225ca at 170–270 nm,

$a_0 = 1.677$, $a_1 = -2.175 \times 10^{-2}$, $a_2 = -1.484 \times 10^{-3}$, $a_3 = 1.147 \times 10^{-5}$ for HCFC-225cb at 165–250 nm.

Table 4-131. Absorption Cross Sections of $CF_3CF_2CHCl_2$ and CF_2ClCF_2CFCl at 298 K

λ (nm)	10^{20} σ (cm^2) $CF_3CF_2CHCl_2$ (HCFC-225ca)	CF_2ClCF_2CFCl (HCFC-225cb)	λ (nm)	10^{20} σ (cm^2) $CF_3CF_2CHCl_2$ (HCFC-225ca)	CF_2ClCF_2CFCl (HCFC-225cb)
160	268.7	187.9	202	11.58	0.479
162	236.8	173.3	204	8.185	0.369
164	207.6	154.8	206	5.802	0.291
166	189.0	135.1	208	4.084	0.254
168	181.4	113.2	210	2.903	0.250
170	182.7	91.35	212	2.042	
172	182.8	70.68	214	1.429	
174	189.0	54.73	216	1.05	
176	190.9	40.68	218	0.727	
178	187.9	30.04	220	0.463	
180	177.5	21.11	222	0.308	
182	161.1	14.90	224	0.209	
184	140.3	10.47	226	0.145	
186	118.3	7.308	228	0.0987	
188	96.51	5.075	230	0.0653	
190	74.30	3.492	232	0.0434	
192	57.08	2.412	234	0.0299	
194	42.83	1.661	236	0.0193	
196	31.75	1.165	238	0.0134	
198	23.22	0.873	239	0.0119	
200	16.24	0.633			

Note:
HCFC-225ca, 160–239 nm, Braun et al. [86],
HCFC-225cb, 160–210 nm, Braun et al. [86].

F58. $CH_3C(O)CH_2Cl + h\nu \rightarrow$ Products. The absorption cross sections of chloroacetone have been measured at 243-296 K and 210-370 nm by Burkholder et al. [111] at a resolution of 0.6 nm using a diode array spectrometer. The spectrum shows two absorption bands, a strong band with the maximum at ~223-224 nm and $\sigma = 3.35 \times 10^{-19}$ cm^2 $molecule^{-1}$ at room temperature and a weaker and broader one with the maximum at ~290-293 nm and $\sigma = 1.02 \times 10^{-19}$ cm^2 $molecule^{-1}$. The averages over 1-nm intervals of the medium-resolution absorption spectrum are listed in Table 4-132. A systematic decrease of the absorption cross-sections with decreasing temperature from 296 to 243 K was observed in the weaker absorption band above ~260 nm. Also a decrease of the absorption cross-sections is observed in the short-wavelength absorption band from the measurement made at 296, 273 to 243 K. However, the values obtained at 253 K are larger than those at 273 K below ~240 nm, and even larger than those at 296 K below ~230 nm.

Photodissociation quantum yields were measured by Burkholder et al. [111] as 0.5 ± 0.08 at 308 nm and 351 nm. At both wavelengths, the yields of CO and CO_2 were 0.50 and ~0.25, respectively, whereas the yield of HCOOH was measured as 0.25 and of HCl as 0.5.

Table 4-132. Absorption Cross Sections of $CH_3C(O)CH_2Cl$ at 296 K

λ (nm)	10^{20} σ (cm^2)	λ (nm)	10^{20} σ (cm^2)	λ (nm)	10^{20} σ (cm^2)	λ (nm)	10^{20} σ (cm^2)
210	22.0	248	3.36	286	9.89	324	2.58
211	23.0	249	3.11	287	9.98	325	2.37
212	24.3	250	2.96	288	10.00	326	2.16
213	25.5	251	2.90	289	10.10	327	1.95
214	26.4	252	2.92	290	10.20	328	1.73
215	27.5	253	3.00	291	10.20	329	1.52
216	28.9	254	3.10	292	10.20	330	1.33
217	30.1	255	3.24	293	10.20	331	1.14
218	30.9	256	3.39	294	10.10	332	0.979
219	31.7	257	3.56	295	10.00	333	0.832
220	32.4	258	3.75	296	9.89	334	0.707
221	32.8	259	3.97	297	9.77	335	0.598
222	33.2	260	4.19	298	9.66	336	0.506
223	33.5	261	4.40	299	9.54	337	0.427
224	33.5	262	4.63	300	9.41	338	0.361
225	33.0	263	4.86	301	9.25	339	0.302
226	32.3	264	5.12	302	9.04	340	0.2520
227	31.8	265	5.38	303	8.80	341	0.212
228	31.3	266	5.65	304	8.53	342	0.176
229	30.3	267	5.89	305	8.24	343	0.145
230	28.9	268	6.14	306	7.94	344	0.120
231	27.3	269	6.39	307	7.63	345	0.103
232	25.7	270	6.65	308	7.34	346	0.0887
233	24.0	271	6.93	309	7.06	347	0.0757
234	22.2	272	7.20	310	6.77	348	0.0642
235	20.3	273	7.47	311	6.50	349	0.0547
236	18.4	274	7.71	312	6.22	350	0.0458
237	16.5	275	7.94	313	5.93	351	0.0411
238	14.6	276	8.16	314	5.61	352	0.0328
239	12.7	277	8.37	315	5.28	353	0.0319
240	11.0	278	8.59	316	4.92	354	0.0220
241	9.50	279	8.82	317	4.57	355	0.0193
242	8.15	280	9.03	318	4.22	356	0.0138
243	6.93	281	9.23	319	3.89	357	0.0134
244	5.85	282	9.41	320	3.58	358	0.00917
245	4.95	283	9.56	321	3.30	359	0.0155
246	4.26	284	9.69	322	3.04	360	0.0128
247	3.74	285	9.80	323	2.80		

Note:
210-360 nm, Burkholder et al. [111].

PHOTOCHEM-G-TOTAL BROMINE

G1. $Br_2 + h\nu \rightarrow 2\ Br$. The absorption spectrum of bromine has repeatedly been measured during the last century as shown in the following survey:

Table 4-133. Summary of Cross Section Measurements of Br_2

Reference	Year	Temperature, K	Wavelength Range, nm
Ribaud [671]	1919	289, 593, 893	356-608
Gray and Style [298]	1930	294	240-579
Acton et al. [5]	1936	293, 400, 531, 657, 767, 906	327.4-571.7
Seery and Britton [719]	1964	298	320-590
McMillan [144]	1966	298	200-599
Passchier et al. [626]	1967	298, 348, 423, 298, 573, 648, 713	200-750
Wen and Noyes [843]	1972	303	220-290
Hemenway et al. [326]	1979	296	556-616.3
Roxlo and Mandl [692]	1980	298	170-230
Röth et al. [687]	1991	294	315.2-512.4 504.0-552.6
Hubinger and Nee [345]	1995	295	190-600

The spectrum of Br_2 exhibits an absorption band between 190 and 300 nm with the maximum near 223 nm and another band between 300 and 600 nm, which is composed of three overlapping bands with the maxima at ~412, 480, and 549 nm. The results of the various research teams are in very good agreement in the region of the UV-visible absorption band. Discrepancies are observed above 550 nm, where the data of McMillan [144] and Hemenway et al. [326] are respectively up to 60% and 100% lower than the values measured by the other groups. Large discrepancies arise in the region of the absorption minimum between 230 and 340 nm due to a pressure-dependent component of the Br_2 vapor, possibly a Br_2-Br_2 collision dimer. A detailed discussion of the available absorption data of Br_2 and an evaluation is given by Maric et al. [478]. These authors fitted the most reliable data, i.e., those of Passchier et al. [626] and Wen and Noyes [843], to a four-band semi-logarithmic distribution function and derived a mathematical expression which allows the calculation of a smooth absorption curve for Br_2 in the wavelength region 200-650 nm:

$$\sigma(298\ K) = 1.06 \times 10^{-20}\ cm^2 \times \exp\{-52.3x[\ln(223.3\ nm/\lambda)]^2\}$$
$$+ 6.19 \times 10^{-19}\ cm^2 \times \exp\{-108.5[\ln(411.9\ nm/\lambda)]^2\}$$
$$+ 3.39 \times x10^{-19}\ cm^2 \times \exp\{-106.8[\ln(480.2\ nm/\lambda)]^2\}$$
$$+ 3.78 \times 10^{-20}\ cm^2 \times \exp\{-112.0[\ln(549.3\ nm/\lambda)]^2\}$$

The recommended absorption cross sections calculated from that expression are listed in Table 4-134. The results of Maric et al. [478] have been generally confirmed in a later study by Hubinger and Nee [345], who reported absorption cross sections for the wavelength range 190-600 nm; only the cross sections with values below 10^{-21} cm^2 $molecule^{-1}$, i.e., between 260 and 340 nm, are different from the recommended data of Maric et al. [478] and can only be considered as upper limits.

Studies of the temperature dependence at 293-906 K by Acton et al. [5] and at 298-713 K by Passchier et al. [626] show a decrease of the cross sections around the absorption maximum between ~380 and ~500 nm and an increase in the short- and long-wavelength tails with increasing temperature.

Photodissociation of Br_2 leads to the formation of Br atoms in the ground $Br(^2P_{3/2})$ and excited $Br^*(^2P_{1/2})$ state. A few studies have been performed to establish the relative quantum yields of (Br+Br) and (Br+Br*) at various wavelengths. Peterson and Smith [631] measured the yield of Br* atoms to increase from 0.4 to 0.89 in the range 444-510 nm, and to further decrease to ~ 0.4 at 530 nm. Lindeman and Wiesenfeld [456] observed the relative quantum yield (Br+Br*) to increase from 0.07 at 434 nm to 0.64 at 482 nm and then to decrease to 0.57 at 511 nm. Haugen et al. [320] determined the relative quantum yield (Br+Br*) to increase from 0.44 at 445 nm to 0.87 at 500 nm, followed by a decrease to 0.40 at 530 nm. Cooper et al. [181] measured the relative (Br+Br*) yield to be zero in the range 360 to 430 nm and to increase at longer wavelengths to 0.79 at 580 nm; at 260 nm they observed (Br+Br*) to be dominant. Jee at al. [370, 371] measured the relative yield of the photodissociation channel into (Br+Br*) at 234 nm to be unity and at 265 nm to be 0.96. Zaraga et al. [873] calculated the zero-pressure predissociation quantum yield from high-resolution spectroscopic studies of a banded region ($B\ ^3\Pi(0_u^+)$ state) overlapping a continuum at 588 nm to be near unity.

Table 4-134. Absorption Cross Sections of Br_2 at 298 K

λ (nm)	10^{20} σ (cm^2)	λ (nm)	10^{20} σ (cm^2)	λ (nm)	10^{20} σ (cm^2)	λ (nm)	10^{20} σ (cm^2)
200	0.562	315	0.0274	430	60.1	545	10.1
205	0.723	320	0.0626	435	57.1	550	8.68
210	0.870	325	0.141	440	54.0	555	7.47
215	0.983	330	0.300	445	51.2	560	6.43
220	1.05	335	0.602	450	48.8	565	5.54
225	1.06	340	1.14	455	46.8	570	4.77
230	1.01	345	2.05	460	45.2	575	4.09
235	0.925	350	3.49	465	44.0	580	3.50
240	0.808	355	5.63	470	42.8	585	2.98
245	0.676	360	8.66	475	41.6	590	2.52
250	0.544	365	12.7	480	40.3	595	2.11
255	0.422	370	17.8	485	38.6	600	1.76
260	0.316	375	23.9	490	36.6	605	1.45
265	0.229	380	30.7	495	34.3	610	1.19
270	0.161	385	37.9	500	31.8	615	0.958
275	0.110	390	45.1	505	29.0	620	0.767
280	0.0728	395	51.8	510	26.2	625	0.607
285	0.0472	400	57.4	515	23.4	630	0.475
290	0.0299	405	61.6	520	20.6	635	0.368
295	0.0187	410	64.2	525	18.0	640	0.282
300	0.0122	415	65.1	530	15.7	645	0.214
305	0.0100	420	64.5	535	13.6	650	0.161
310	0.0135	425	62.8	540	11.7		

Note: Cross sections calculated from the expression given by Maric et al. [478].

G2. $HBr + h\nu \rightarrow H + Br$. The absorption cross sections of HBr have been repeatedly measured at room temperature and in the UV region as shown in the following survey:

Table 4-135. Summary of Cross Section Measurements of HBr

Reference	Year	Temperature, K	Wavelength Range, nm
Goodeve and Taylor [289]	1935	298	182-286
Romand [684]	1949	298	139-228
Huebert and Martin [352]	1968	297	170-230
Bridges and White [90]	1973	298	214
Okabe [596]	1977	296	240-270
Ravishankara et al. [661]	1979	298	184.9
Roxlo and Mandl [692]	1980	298	170-230
Okabe [600]	1983	296	184.9
Brion et al. [92]	1985	298	30-177
Nee et al. [576]	1986	298	105-238
Vaghjiani [798]	1993	296	193
Barone et al. [43]	1994	298	184.9,193.0

The spectrum exhibits a broad absorption band at wavelengths above 155 nm with the maximum near 178 nm and a large number of strong and sharp bands at shorter wavelengths down to 105 nm. The absorption cross sections near the maximum of the absorption band reported by Nee et al. [576] and Huebert and Martin [352] are in good agreement, whereas those reported by Romand [684] and Roxlo and Mandl [692] are lower: the absorption cross sections reported for the maximum are 2.4×10^{-18}, 2.7×10^{-18}, 2×10^{-18}, and 1.4×10^{-18} cm^2 $molecule^{-1}$, respectively. The results of Vaghjiani [798] and Barone et al. [43] for 193 nm fit well to the absorption curves reported by Nee et al. [576] and Huebert and Martin [352]. The cross section at 184.9 nm measured by Ravishankara et al. [661] and Barone et al. [43] lies between those reported by Nee et al. [576] and Huebert and Martin [352], that measured by Okabe [596] between those of Goodeve and Taylor [289] and Romand [684]. The recommended values, listed in Table 4-136, are derived as follows: the spectra of Goodeve and Taylor [289], Romand [684], Huebert and Martin [352], and Nee et al. [576] have been

normalized to the value $\sigma = 2.21 \times 10^{-18}$ cm^2 molecule^{-1} at 184.9 nm, which is the mean of the values reported by Okabe [596], Ravishankara et al. [661], and Barone et al. [43]; the normalized spectra have then been averaged, for 152-168 nm those of Romand [684] and Nee et al. [576], for 170-180 nm those of Romand [684], Huebert and Martin [352], and Nee et al. [576], and for 182-230 nm those of Goodeve and Taylor[289], Romand [684], Huebert and Martin [352], and Nee et al. [576].

The branching fraction for the formation of excited Br*($^2P_{3/2}$) atoms was determined by Regan et al. [669] in the wavelength range 201-253 nm to vary between 015 and 0.23. Baumfalk et al. [63] obtained a value for the branching fraction for Br* of 0.20 ± 0.03 at 243 nm, and a value of 0.18 ± 0.03 at 193 nm.

Table 4-136. Absorption Cross Sections of HBr at 296-298 K

λ (nm)	10^{20} σ (cm^2)	λ (nm)	10^{20} σ (cm^2)	λ (nm)	10^{20} σ (cm^2)	λ (nm)	10^{20} σ (cm^2)
152	139	172	233	192	181	212	54.8
154	124	174	240	194	168	214	45.7
156	138	176	244	196	154	216	38.8
158	148	178	244	198	140	218	33.0
160	161	180	242	200	125	220	28.0
162	176	182	233	202	111	222	22.9
164	189	184	225	204	98.1	224	18.2
166	201	186	217	206	85.5	226	14.4
168	211	188	206	208	74.7	228	11.7
170	225	190	194	210	64.4	230	9.32

Note:
Normalization of the data of Goodeve and Taylor [289], Romand [684], Huebert and Martin [352], and Nee et al. [576] to $\sigma = 2.21 \times 10^{-18}$ cm^2 molecule^{-1} at 184.9 nm and averaging:
152-168 nm, mean of Romand [684] and Nee et al. [576];
170-180 nm, mean of Romand [684], Huebert and Martin [352] and Nee et al. [576],
182-230 nm, mean of Goodeve and Taylor [289], Romand [684], Huebert and Martin [352] and Nee et al. [576].

G3. $BrO + h\nu \rightarrow Br + O$. The BrO radical has a banded spectrum in the 290–380 nm range, which is attributed to the A $^2\Pi_{3/2} \leftarrow$ X $^2\Pi_{3/2}$ transition. The absorption spectrum has been measured in the region of this absorption band, and cross sections have been also determined for single absorption peaks, the strongest, the (7, 0) peak at 338.5 nm and the (11, 0) and (12, 0) peaks at 320.8 nm and 317.3 nm.

Table 4-137. Summary of Cross Section Measurements of BrO

Reference	Year	Temperature, K	Wavelength Range, nm	Resolution, nm
Clyne and Cruse [176]	1970	293	338.3	0.15
Basco and Dogra [45]	1971	298	320.8, 338.3	not given
Cox et al. [192]	1982	298	296-370	0.22
Wahner et al. [829]	1988	228, 243, 298	312-380	0.4
Sander and Friedl [702]	1989	220, 298	338.5	0.06-1.25
Orlando et al. [606]	1991	298	338.5	0.4
Laszlo et al [435]	1997	295	338.5	0.6
Gilles et al. [274]	1997	204, 222, 237, 252, 273, 298, 329, 369	338.5	0.5
Wheeler et al. [846]	1998	298	338, 317	4 cm^{-1}
Wilmouth et al. [848]	1999	298	317-388	1.0 cm^{-1}
Wilmouth et al. [848]	1999	228, 298	286-386	10 cm^{-1}
Fleischmann et al. [245]	2003	203, 223, 243, 273, 298	300-385	4 cm^{-1}

The measured cross sections are both temperature- and resolution-dependent, i.e., the peaks of the vibrational bands become higher and sharper with decreasing temperature and lower resolution. As an example, the spectrum measured by Wahner et al. [829] is shown in Figure 4-4. Wilmouth et al. [848] used their 10-cm^{-1} absorption spectra for an analysis of the results of Cox et al. [192], Wahner et al. [829], Orlando et al. [606], Laszlo et al.

[435], and Gilles et al. [274] at a common resolution of 0.40 nm (details of this procedure are described in the paper of Wilmouth et al. [848]).

The absorption cross sections for the peaks of the vibrational bands of the A ← X transition at 298 ± 2 and 228 ± 2 K obtained by this analysis are listed in Table 4-138. Averages over 0.5-nm intervals of the spectrum of Wilmouth et al. [848] are listed in Table 4-139.

Absorption cross sections for the rotational peaks of the (7,0) and (12,0) bands were measured at high-resolution (1.0 cm^{-1}) by Wilmouth et al. [848]: $\sigma = 2.17 \times 10^{-17}$ cm^2 $molecule^{-1}$ for the apex of the (7,0) band and $\sigma = 1.38 \times 10^{-17}$ cm^2 $molecule^{-1}$ for the apex of the (12,0) band.

The temperature dependence of the (7,0) absorption maximum (338 nm) is reported by Gilles et al. [274] for the range 204-388 K for a resolution of 0.5 nm by the following expression:

$$\sigma(T)_{338} = 3.29 - (5.58 \times 10^{-3}) \times T, \text{ in units of } 10^{-17} \text{ cm}^2 \text{ molecule}^{-1}.$$

Table 4-138. Absorption Cross Sections at the Vibrational Band Peaks in the A ← X Spectrum of BrO (0.4 nm resolution)

v', v''	λ, nm	10^{20} σ, cm^2 $molecule^{-1}$	
		298 ± 2 K	228 ± 2 K
26, 0	286.46	107	88.3
25, 0	287.38	132	133
24, 0	288.45	145	175
23, 0	289.83	188	208
22, 0	291.40	188	267
21, 0	292.99	242	284
20, 0	294.88	295	348
19, 0	296.97	356	441
18, 0	299.30	447	541
17, 0	301.81	523	636
16, 0	304.54	601	728
15, 0	307.46	679	819
14, 0	310.54	772	932
13, 0	313.81	904	1090
12, 0	317.29	1190	1480
11, 0	321.20	1360	1670
10, 0	325.37	1260	1510
9, 0	329.56	1210	1430
8, 0	333.89	1250	1510
7, 0	338.69	1580	1970
6, 0	344.04	923	1060
5, 0	349.09	715	828
4, 0	355.02	723	864
3, 0	360.64	267	287
4, 1	364.32	126	95.4
2, 0	367.94	128	129
1, 0	374.69	74.5	77.3
2, 1	381.27	27.5	27.4
0, 0	286.46	22.5	
1, 1	287.38	9.86	

Note:
Wilmouth et al. [848]: The own data and data of Cox et al. [192], Wahner et al. [829], Orlando et al. [606], Laszlo et al. [435], Gilles et al. [274] were normalized to a common resolution of 0.40 nm and then averaged.

Table 4-139. Absorption Cross Sections of BrO at 298 K

λ (nm)	10^{20} σ (cm^2)	λ (nm)	10^{20} σ (cm^2)	λ (nm)	10^{20} σ (cm^2)	λ (nm)	10^{20} σ (cm^2)
286.5	104.8	311.5	453.1	336.5	258.7	361.5	226.6
287.0	106.5	312.0	294.8	337.0	222.1	362.0	182.9
287.5	128.8	312.5	203.7	337.5	202.0	362.5	145.2
288.0	95.04	313.0	197.3	338.0	201.8	363.0	119.9
288.5	147.7	313.5	723.9	338.5	1287.0	363.5	103.7
289.0	109.8	314.0	901.3	339.0	1296.0	364.0	113.3
289.5	126.4	314.5	650.8	339.5	734.4	364.5	122.2
290.0	183.8	315.0	443.2	340.0	444.8	365.0	99.15
290.5	133.1	315.5	310.9	340.5	303.1	365.5	87.15
291.0	133.5	316.0	231.7	341.0	243.1	366.0	86.23
291.5	188.6	316.5	173.7	341.5	217.5	366.5	91.26
292.0	157.2	317.0	721.1	342.0	235.0	367.0	105.0
292.5	128.3	317.5	1136.0	342.5	291.6	367.5	123.4
293.0	248.2	318.0	730.7	343.0	423.8	368.0	130.5
293.5	192.5	318.5	482.3	343.5	711.9	368.5	119.5
294.0	140.4	319.0	344.6	344.0	967.8	369.0	100.9
294.5	161.5	319.5	275.1	344.5	814.4	369.5	86.11
295.0	294.4	320.0	251.4	345.0	542.1	370.0	74.79
295.5	216.1	320.5	293.7	345.5	345.0	370.5	64.46
296.0	163.9	321.0	1138.0	346.0	225.9	371.0	53.91
296.5	152.9	321.5	1155.0	346.5	160.3	371.5	46.47
297.0	361.1	322.0	676.9	347.0	146.4	372.0	39.44
297.5	276.5	322.5	419.6	347.5	162.2	372.5	35.13
298.0	193.5	323.0	300.6	348.0	257.8	373.0	34.13
298.5	156.4	323.5	261.7	348.5	529.5	373.5	35.68
299.0	284.0	324.0	288.2	349.0	747.7	374.0	48.08
299.5	421.1	324.5	433.6	349.5	667.4	374.5	74.97
300.0	275.3	325.0	982.6	350.0	499.2	375.0	70.53
300.5	193.5	325.5	1283.0	350.5	363.4	375.5	51.46
301.0	180.1	326.0	837.6	351.0	272.4	376.0	35.44
301.5	350.9	326.5	494.8	351.5	215.3	376.5	30.47
302.0	502.3	327.0	312.0	352.0	181.9	377.0	27.46
302.5	318.4	327.5	231.1	352.5	165.9	377.5	25.66
303.0	217.4	328.0	223.5	353.0	162.8	378.0	25.61
303.5	195.9	328.5	343.1	353.5	163.2	378.5	21.82
304.0	274.0	329.0	789.1	354.0	179.5	379.0	18.60
304.5	609.6	329.5	1261.0	354.5	309.3	379.5	14.96
305.0	466.2	330.0	1058.0	355.0	789.4	380.0	12.28
305.5	298.4	330.5	706.2	355.5	498.6	380.5	13.03
306.0	221.1	331.0	453.4	356.0	276.2	381.0	19.55
306.5	209.7	331.5	295.9	356.5	166.2	381.5	20.93
307.0	407.2	332.0	203.1	357.0	119.9	382.0	16.76
307.5	703.1	332.5	164.7	357.5	111.1	382.5	9.049
308.0	518.3	333.0	259.8	358.0	115.3	383.0	3.059
308.5	343.6	333.5	952.8	358.5	123.6	383.5	4.924
309.0	227.6	334.0	1294.0	359.0	143.6	384.0	3.892
309.5	193.6	334.5	963.3	359.5	182.7	384.5	6.695
310.0	395.5	335.0	652.3	360.0	236.4	385.0	10.93
310.5	798.9	335.5	457.5	360.5	272.3		
311.0	659.2	336.0	338.8	361.0	264.4		

Note:
Wilmouth et al. [848]: Averages over 0.5-nm intervals of the high-resolution spectrum.

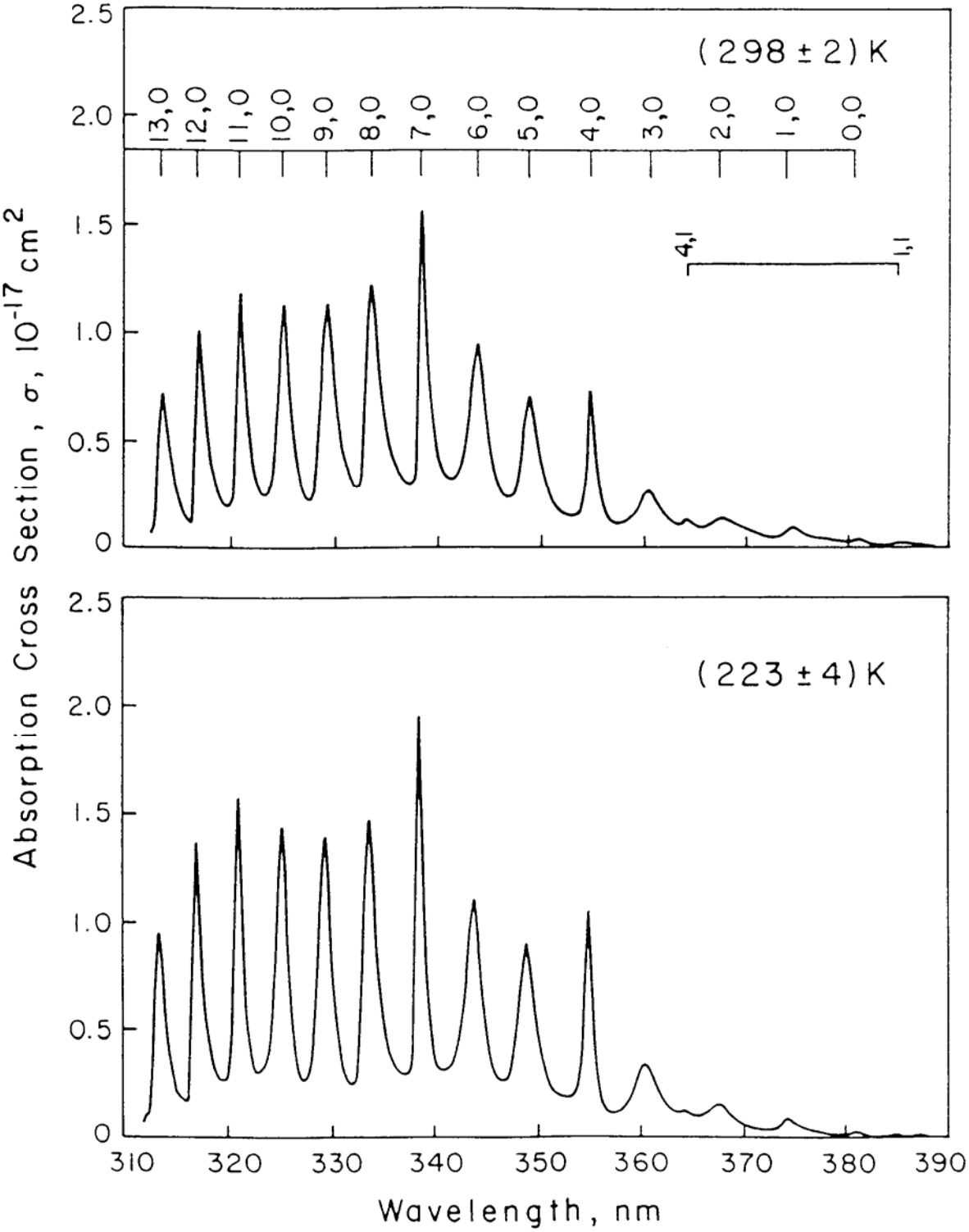

Figure 4-4. Absorption Spectrum of BrO (after Wahner et al. [829])

G4. $OBrO + h\nu \rightarrow BrO + O(^3P)$

$OBrO + h\nu \rightarrow Br + O_2$..The visible absorption spectrum of bromine dioxide has been measured in the 400-600-nm region at 273, 298, and 338 K by Rattigan et al. [651], at 298 K by Rowley et al. [690], at ~250 K by Miller et al. [528], and at 298 K by Knight et al. [413]. The spectrum shows a highly structured absorption band consisting of a progression of doublets with a maximum intensity near 500 nm and a progression of less intense bands between the doublets. The spectrum was identified as arising from the $C\ ^2A_2 \leftarrow X\ ^2B_1$ electronic transition by Miller et al. [528] who combined *ab initio* calculations of the lowest doublet electronic states of OBrO with Franck-Condon simulations. Whereas Rattigan et al. [651], Rowley et al. [690], and Miller et al. [528] observed only qualitative spectra, Knight et al. [413] were the first who measured the absorption cross sections. In Table 4-140 are listed the peak positions and corresponding absorption cross sections for the vibrational progressions (n,0,0)←(0,0,0) and (n,1,0)←(0,0,0). In Table 4-141 are listed the averages over 1-nm intervals of the spectrum measured at a resolution of 0.66 nm.

No quantum yields are available, but theoretical calculations by Vetter et al. [817] indicate that photodissociation occurs via $BrO + O(^3P)$ because of a large transition dipole moment for the $C\ ^2A_2 \leftarrow X\ ^2B_1$ transition. Photodissociation into $Br + O_2$ occurs via the 1^2B_2 state, which is less probably reached from the ground state, and therefore of minor importance.

Table 4-140. Peak Absorption Cross Sections of OBrO at 298 K

n	(n,0,0)←(0,0,0) λ (nm)	10^{20} σ (cm^2)	(n,1,0)←(0,0,0) λ (nm)	10^{20} σ (cm^2)
0	630.4		622.0	
1	606.1		598.4	
2	583.8		576.8	
3	563.4	1080	556.8	1350
4	544.4	1450	538.5	1740
5	527.1	1640	521.6	1910
6	510.7	1770	505.5	1960
7	495.5	1720	490.7	1760
8	481.2	1670	476.9	1510
9	468.2	1440	464.1	1260
10	455.8	1210	452.2	960
11	444.4	1020	440.8	720
12	433.7	790	430.4	490
13	423.5	570	420.6	310
14	414.1	400	411.0	220
15	405.1	260	402.3	130

Note:
Peak absorption cross sections, Knight et al. [413].

Table 4-141. Absorption Cross Sections of OBrO at 298 K

λ (nm)	10^{20} σ (cm^2)	λ (nm)	10^{20} σ (cm^2)	λ (nm)	10^{20} σ (cm^2)	λ (nm)	10^{20} σ (cm^2)
401	66.7	443	363	485	301	527	1530
402	112	444	834	486	463	528	1100
403	116	445	777	487	368	529	584
404	153	446	452	488	298	530	326
405	243	447	292	489	425	531	218
406	180	448	254	490	868	532	347
407	131	449	214	491	1580	533	547
408	113	450	180	492	993	534	361
409	105	451	323	493	641	535	344
410	128	452	854	494	583	536	539
411	201	453	672	495	1160	537	434
412	171	454	394	496	1430	538	1200
413	239	455	633	497	826	539	1500
414	380	456	1110	498	458	540	888
415	260	457	729	499	291	541	546
416	180	458	426	500	405	542	442
417	156	459	292	501	512	543	312
418	133	460	314	502	336	544	991
419	147	461	262	503	419	545	1230
420	269	462	213	504	483	546	716
421	274	463	399	505	1230	547	395
422	229	464	1100	506	1650	548	252
423	479	465	868	507	962	549	161
424	481	466	506	508	651	550	302
425	287	467	562	509	556	551	476
426	207	468	1230	510	1030	552	300
427	175	469	1020	511	1570	553	255
428	149	470	568	512	953	554	461
429	194	471	341	513	506	555	349
430	422	472	298	514	307	556	532
431	382	473	362	515	282	557	1250
432	274	474	239	516	532	558	870
433	577	475	286	517	433	559	472
434	661	476	563	518	303	560	350
435	392	477	1390	519	529	561	267
436	251	478	990	520	504	562	204
437	208	479	567	521	1390	563	791
438	179	480	577	522	1610	564	885
439	166	481	1260	523	921	565	504
440	363	482	1310	524	622	566	275
441	651	483	745	525	516	567	170
442	425	484	403	526	654	568	107

Note:
401-568 nm, Knight et al. [413] (columns 1, 3, 5, 7: center of interval).

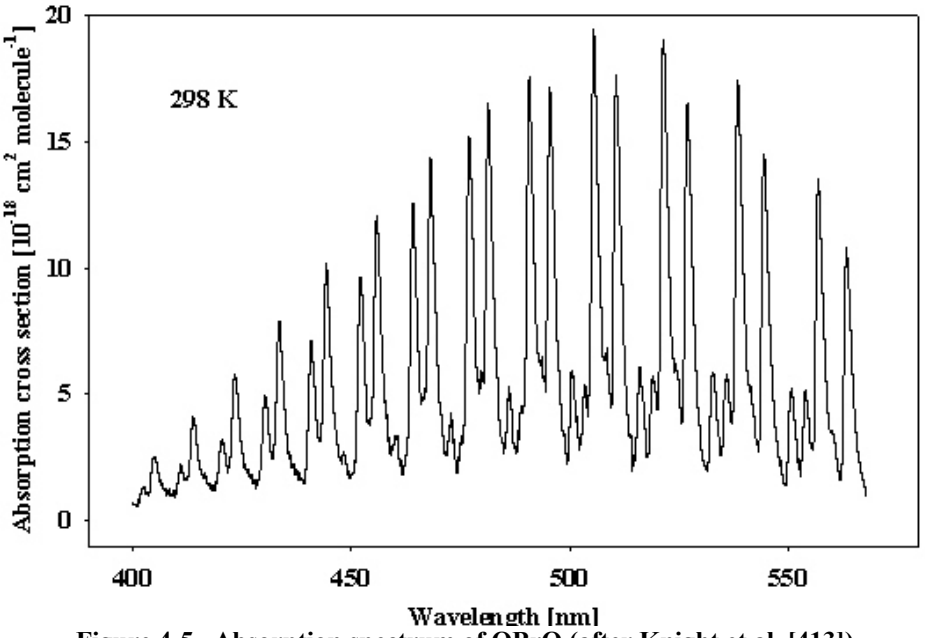

Figure 4-5. Absorption spectrum of OBrO (after Knight et al. [413])

G5. $Br_2O + h\nu \rightarrow$ Products. The absorption spectrum of dibromine monoxide has been measured at room temperature and 196-432 nm by Orlando and Burkholder [605], at 240-515 nm by Rattigan et al. [652], and at 208-444 nm by Deters et al. [215]. The spectrum exhibits a strong narrow absorption band below 220 nm with a maximum at 200 nm ($\sigma = 2 \times 10^{-17}$ cm^2 molecule^{-1}), a weaker and broader absorption band extending from 250 nm to about 450-470 nm with a maximum at 313 nm ($\sigma \approx (2.0\text{-}2.3) \times 10^{-18}$ cm^2 molecule^{-1}) and a shoulder near 350 nm ($\sigma = (1.74\text{-}1.95) \times 10^{-18}$ cm^2 molecule^{-1}), and two weak bands at 460-580 nm and 580-750 nm with maxima at ~520 nm ($\sigma \sim 4 \times 10^{-20}$ cm^2 molecule^{-1}) and ~665 nm ($\sigma \sim 6.2 \times 10^{-20}$ cm^2 molecule^{-1}). There is very good agreement between the various data sets in the wavelength region below 380 nm, where the data of Orlando and Burkholder [605] and Deters et al. [215] are nearly identical, and those of Rattigan et al. [652] are smaller by ~10% below 250 nm and above 290 nm and smaller by up to ~25% in the region of the absorption minimum near 270 nm. Large discrepancies between the three data sets are at wavelengths above 380 nm: The absorption cross sections reported by Orlando and Burkholder [605] and Deters et al. [215] rapidly decrease to values $\leq 1 \times 10^{-20}$ cm^2 molecule^{-1}, whereas the values reported by Rattigan et al. [652] show an exponential decrease at 400-470 nm followed by a new absorption band. The cutoff at 440 nm of the absorption curve reported by Orlando and Burkholder [605] is a result of the assumption that the absorbance of Br_2O is zero at 440 nm and beyond. The correction procedure used by Rattigan et al. [652] taking vibrational structure of the Br_2 spectrum into account resulted in appreciable absorption for Br_2O at wavelengths above 440 nm. The recommended cross sections listed in Table 4-142 are the data of Orlando and Burkholder [605] at 196 and 200 nm, the mean of the data of Orlando and Burkholder [605] and Deters et al. [215] at 210-230 nm, and the mean of the data of Orlando and Burkholder [605], Deters et al. [215], and Rattigan et al. [652] at 240-400 nm. No recommendation is given at wavelengths above 400 nm.

Table 4-142. Absorption Cross Sections of Br_2O at 298 K

λ (nm)	$10^{20}\,\sigma$ (cm^2)	λ (nm)	$10^{20}\,\sigma$ (cm^2)
196	1740	300	167
200	2000	310	220
210	1050	320	212
220	288	330	192
230	140	340	188
240	85.8	350	186
250	45.4	360	162
260	24.6	370	132
270	18.8	380	99.0
280	33.5	390	74.8
290	85.5	400	54.0

Note: 196, 200 nm, Orlando and Burkholder [605],
210-230 nm, mean of Orlando and Burkholder [605] and Deters et al. [215],
240-400 nm, mean of Orlando and Burkholder [605], Deters et al. [215] and Rattigan et al. [652].

G6. $HOBr + h\nu \rightarrow OH + Br$

$HOBr + h\nu \rightarrow HBr + O(^3P)$. The absorption spectrum of HOBr has been measured by Orlando and Burkholder [605], Deters et al. [215], Benter et al. [66], Rattigan et al. [652], and Ingham et al. [361]. The spectra cluster has been measured in two groups. Orlando and Burkholder [605], Deters et al. [215], and Benter et al. [66] observe between 240 and 400 nm two absorption bands with maxima near 284 and 351 nm; the spectra agree reasonably well in their shape, but show a sharp decrease in cross section above 400 nm. In contrast, the cross sections reported by Rattigan et al. [652] and Ingham et al. [361] are roughly 50% larger between 300 and 400 nm.

In addition, the spectrum obtained by Rattigan et al. [652] shows a pronounced tail extending to 520 nm, whereas Ingham et al. [361] observe unambiguously a third weaker absorption band ranging to 550 nm with a maximum at 457 nm. These last two studies confirm the observations of Barnes et al. [41], who showed that laser photolysis of HOBr between 440–600 nm gives rise to OH fragments. The presence of a weak band beyond 400 nm is attributable to the presence of a forbidden transition from the ground electronic to a triplet state predicted by the *ab initio* calculations of Francisco et al. [248] and Minaev [529]. The differences in the spectral shapes are probably attributable to impurities such as Br_2O and Br_2, and/or the use of different Br_2O cross sections. However, the presence of impurities alone cannot explain the large difference in cross sections at the peak of the absorption bands.

The recommended absorption cross sections are listed in Table 4-143 over the range from 250 to 550 nm; below 250 nm the data are uncertain and no recommendation is given. The cross section values in the table are based on the latest study by Ingham et al. [361]. These authors generated HOBr in situ by laser photolytic production of OH in the presence of Br_2, and determined the HOBr spectrum using a gated diode camera shortly after the pulse, circumventing the problem associated with the presence of the strong absorbing impurity Br_2O, which was encountered in previous studies. The calibration of the absorption cross sections was made relative to the established cross sections of Br_2.

The data presented in Table 4-143 are computed with the following expression taken from Ingham et al. [361], which is based on a combination of three Gaussian fits, one for each absorption band:

$$\sigma(\lambda) = 24.77\exp\left\{-109.80\left[\ln\left(\frac{284.01}{\lambda}\right)\right]^2\right\} + 12.22\exp\left\{-93.63\left[\ln\left(\frac{350.57}{\lambda}\right)\right]^2\right\} + 2.283\exp\left\{-242.40\left[\ln\left(\frac{457.38}{\lambda}\right)\right]^2\right\}$$

$\sigma(\lambda)$: 10^{-20} cm^2 molecule^{-1}; $250 < \lambda < 550$ nm.

Benter et al. [66] measured quantum yields for HOBr photolysis at 261 and 363 nm (near the peaks of the second absorption bands). The observed quantum yield for Br formation at 363 nm was greater than 0.95, and a unity quantum yield into the product channel OH + Br is recommended. The other channel O + HBr was not observed. The laser photofragment study of Barnes et al. [41] claimed that OH was the major photolysis product at wavelengths beyond 400 nm. Lock et al. [459] found that at 490 and 510 nm OH and Br fragments are in their respective vibrational and spin-orbit ground states. The assumption of unit quantum yield of OH formation should be confirmed experimentally.

Table 4-143. Absorption Cross Sections of HOBr

λ (nm)	10^{20} σ (cm^2)	λ (nm)	10^{20} σ (cm^2)	λ (nm)	10^{20} σ (cm^2)
250	4.15	355	12.1	460	2.28
255	6.19	360	11.5	465	2.14
260	10.5	365	10.5	470	1.91
265	14.6	370	9.32	475	1.62
270	18.7	375	7.99	480	1.30
275	22.1	380	6.65	485	0.993
280	24.3	385	5.38	490	0.723
285	25.0	390	4.22	495	0.502
290	24.0	395	3.23	500	0.333
295	21.9	400	2.43	505	0.212
300	19.1	405	1.80	510	0.129
305	16.2	410	1.36	515	0.076
310	13.6	415	1.08	520	0.042
315	11.8	420	0.967	525	0.023
320	10.8	425	0.998	530	0.012
325	10.5	430	1.15	535	0.0059

λ (nm)	10^{20} σ (cm^2)	λ (nm)	10^{20} σ (cm^2)	λ (nm)	10^{20} σ (cm^2)
330	10.8	435	1.40	540	0.0029
335	11.3	440	1.68	545	0.0013
340	11.9	445	1.96	550	0.0006
345	12.3	450	2.18		
350	12.4	455	2.29		

Note:

250-550 nm, Ingham et al. [361]

G7. $BrNO + h\nu \rightarrow Br + NO$. The absorption spectrum of nitrosyl bromide has been measured at room temperature and 275-550 nm by Eden et al. [225], at 200-800 nm by Houel and Van den Bergh [342] and at 189-300 nm by Uthman et al. [797], and single cross sections have been reported for 266 nm by Hippler et al. [332] and for 270 nm by Maloney and Palmer [471]. The spectrum exhibits three absorption bands between 200 and 800 nm: a strong absorption band between 190 and 290 nm with the maximum at ~213 nm, a weaker band between 290 and 600 nm with the maximum at 338 nm and a shoulder near 420 nm, and a still weaker band between 600 and 800 nm with the maximum at 708 nm. The results of the various research teams are (after correction of an error in the paper of Maloney and Palmer [471]) in very good agreement. In Table 4-144 are listed the results of Uthman et al. [797] for the UV absorption band at 189-300 nm and the cross sections at the maxima and the shoulder in the near UV and visible regions reported by Houel and Van den Bergh [342] (these authors as well as Eden et al. [225] only give plots of their measured spectra).

Table 4-144. Absorption cross sections of BrNO at 298 K

λ(nm)	10^{20} σ (cm^2)	λ(nm)	10^{20} σ (cm^2)
189	18.3	224	4740
193	39.0	230	2990
194	46.2	235	1920
197	166	240	1090
200	566	250	360
201	861	260	117
203	1690	270	40.1
205.5	2950	280	19.5
207	4340	290	16.8
210	6470	300	18.0
211	6910		
213	7270	338	31.0
216	7060	416	20.1
220	6070	708	2.94

Note:
189-300 nm, Uthman et al. [797],
338, 416, 708 nm, Houel and Van den Bergh [342].

G8. BrONO + hν → Products. The absorption spectrum of *cis*-BrONO (bromine nitrite) has been measured in the range 228 to 296 K and 200-365 nm by Burkholder and Orlando [114]. The spectrum exhibits a strong absorption band between 200 and 270 nm with the maximum at 228 nm and a broader and weaker band between 270 and 364 nm with the maximum at 316 nm. The relative shape of the BrONO spectrum was independent of the temperature within the uncertainties of the measurements. The results of Burkholder and Orlando [114] are listed in Table 4-145.

Table 4-145. Absorption Cross Sections of BrONO at 253 K

λ (nm)	10^{20} σ (cm^2)	λ (nm)	10^{20} σ (cm^2)	λ (nm)	10^{20} σ (cm^2)	λ (nm)	10^{20} σ (cm^2)
200	0	242	1070	284	247	326	400
202	116	244	874	286	262	328	394
204	221	246	720	288	277	330	387
206	358	248	602	290	293	332	382
208	496	250	514	292	310	334	375
210	687	252	446	294	331	336	364
212	822	254	391	296	350	338	350
214	107	256	345	298	366	340	332
216	128	258	306	300	377	342	308
218	161	260	273	302	386	344	284
220	194	262	244	304	393	346	263
222	224	264	221	306	400	348	248
224	252	266	205	308	407	350	233
226	263	268	196	310	413	352	214
228	271	270	192	312	415	354	195
230	262	272	191	314	413	356	176
232	239	274	194	316	409	358	157
234	217	276	200	318	406	360	138
236	186	278	211	320	406	362	123
238	155	280	223	322	406	364	117
240	124	282	235	324	405		

Note:
200-364 nm, Burkholder and Orlando [114].

G9. $BrONO_2 + h\nu \rightarrow Br + NO_3$

$BrONO_2 + h\nu \rightarrow BrO + NO_2$

$BrONO_2 + h\nu \rightarrow BrO + NO + O(^3P)$. The bromine nitrate cross sections have been measured at room temperature and 186-390 nm by Spencer and Rowland [748], at 220, 250, and 298 K and 200-500 nm by Burkholder et al. [116], and at 230 and 298 K and 210-500 nm by Deters et al. [216]. The results of Burkholder et al. [116] and Deters et al. [216] are nearly identical over the range of spectral overlap. The results of Spencer and Rowland [748] agree generally within 10% with those of Burkholder et al. [116] and Deters et al. [216] except for the region between 315 and 350 nm where the Spencer data are higher by 10-20%.

The temperature dependence of the absorption cross sections generally is small. Burkholder et al. [116] observed decreasing cross sections with decreasing temperature between 200 and 215 nm and between 230 and 500 nm and a slight increase between 215 and 230 nm.; the ratio $\sigma(220\ K)/\sigma(298\ K)$ has values of ~0.8 to 1.03 between 200-235 nm, a minimum of 0.90 at 260 nm, nearly constant values of ~0.95 between 290 and 370 nm, a minimum of ~0.87 at 430 nm, two maxima of ~ 0.98 around 440-450 nm, and rapidly decreases to ~0.5 at 500 nm. The measurements of Deters et al. [216] show a similar behavior of the $\sigma(230\ K)/\sigma(298\ K)$ vs. λ curve with the difference that all values lie below 1, i.e., the decrease of the cross sections with decreasing temperature is observed over the entire wavelength range 210 and 500 nm. As a recommendation we list in Table 4-146 the data of Burkholder et al. [116] for 296 K and the temperature coefficients A1 and A2 obtained from the parameterization of the temperature dependence by the relation

$$\sigma(\lambda,T) = \sigma(\lambda, 296\ K)\ [1 + A1\ (T - 296) + A2\ (T - 296)^2].$$

The quantum yields for NO_3 production were measured by Harwood et al. [313]: $\varphi(NO_3) = 0.28 \pm 0.09$ at 248 nm, 1.01 ± 0.35 at 305 nm and 0.92 ± 0.43 at 352.5 nm. The quantum yields for BrO and Br were also estimated at 248 nm to be $\varphi(BrO) \approx 0.5$ and $\varphi(Br) \approx 0.5$. Recently Soller et al. [746] investigated the production of Br, $O(^3P)$ and BrO from the photolysis of $BrONO_2$ in the wavelength range 248-355 nm. The quantum yield for the Br atom are 0.35 ± 0.08, 0.65 ± 0.14, $>0.62 \pm 0.11$, and 0.77 ± 0.19 at 248, 266, 308 and 355 nm, respectively. The values for the $O(^3P)$ atom quantum yields are 0.66 ± 0.15, 0.18 ± 0.04, $<0.13 \pm 0.03$, and <0.02 at 248, 266, 308 and 355 nm, respectively. The measured quantum yields for BrO are 0.37 ± 0.12 at 266 nm and 0.23 ± 0.08 at 355 nm. The measured quantum yields are summarized below.

Wavelength nm	NO_3	Br	BrO	$O(^3P)$
248	0.28 ± 0.09[a]	≈ 0.5[a] 0.35 ± 0.08[b]	≈ 0.5[a]	0.66 ± 0.15[b]
266		0.65 ± 0.14[b]	0.37 ± 0.12[b]	0.18 ± 0.04[b]
305	1.01 ± 0.35[a]			
308		$>0.62 \pm 0.11$[b]		$<0.13 \pm 0.03$[b]
352.5	0.92 ± 0.43[a]			
355		0.77 ± 0.19[b]	0.23 ± 0.08[b]	<0.02[b]

[a]Harwood et al. [313]
[b]Soller et al. [746]

A recommendation is only given for wavelengths above 300 nm, where total quantum yield Φ_{BrONO2} is unity, $\Phi_{Br+NO_3} = 0.85$ and $\Phi_{BrO+NO_2} = 0.15$. There is no recommendation for wavelengths below 300 nm.

Table 4-146. Absorption Cross Sections of $BrONO_2$ at 296 K and Temperature Coefficients

λ (nm)	10^{20} σ (cm^2)	10^3 A1 (K^{-1})	10^6 A2 (K^{-2})	λ (nm)	10^{20} σ (cm^2)	10^3 A1 (K^{-1})	10^6 A2 (K^{-2})	λ (nm)	10^{20} σ (cm^2)	10^3 A1 (K^{-1})	10^6 A2 (K^{-2})
200	680	0.852	-26.0	302	17.5	0.781	0.784	404	2.04	1.91	3.64
202	616	0.608	-26.1	304	16.6	0.870	1.88	406	1.95	1.86	2.63
204	552	0.308	-26.2	306	15.8	0.872	1.62	408	1.88	1.78	1.52
206	488	0.138	-23.7	308	15.0	0.772	-0.229	410	1.81	1.70	0.316
208	425	0.158	-17.5	310	14.2	0.660	-2.28	412	1.75	1.59	-0.981
210	361	0.184	-9.09	312	13.5	0.652	-1.95	414	1.69	1.49	-2.37
212	334	0.401	-2.61	314	12.8	0.643	-1.58	416	1.63	1.40	-2.60
214	307	0.657	5.03	316	12.1	0.652	-1.42	418	1.56	1.35	-1.54
216	286	0.882	11.2	318	11.6	0.684	-1.48	420	1.50	1.29	-0.381
218	272	1.05	15.3	320	11.0	0.719	-1.56	422	1.45	1.00	-2.34
220	258	1.24	19.7	322	10.5	0.719	-1.06	424	1.40	0.694	-4.43
222	247	1.19	19.7	324	10.1	0.720	-0.508	426	1.36	0.599	-4.31
224	236	1.12	19.6	326	9.64	0.743	0.087	428	1.33	0.734	-1.78
226	226	1.14	20.3	328	9.29	0.791	0.722	430	1.30	0.877	0.880
228	215	1.26	21.8	330	8.94	0.843	1.41	432	1.26	0.747	0.484
230	205	1.40	23.4	332	8.65	0.825	1.33	434	1.22	0.609	0.0625
232	193	1.40	23.1	334	8.36	0.806	1.25	436	1.18	0.519	0.0968
234	180	1.41	22.8	336	8.10	0.800	1.30	438	1.15	0.484	0.632
236	167	1.47	22.8	338	7.87	0.809	1.49	440	1.11	0.447	1.20
238	153	1.59	23.4	340	7.64	0.818	1.70	442	1.08	0.384	-0.388
240	139	1.73	24.0	342	7.45	0.898	2.52	444	1.05	0.318	-2.06
242	126	1.65	20.9	344	7.26	0.982	3.38	446	1.02	0.335	-1.82
244	113	1.56	17.2	346	7.07	0.991	3.48	448	0.974	0.446	0.568
246	101	1.62	15.5	348	6.86	0.918	2.75	450	0.930	0.567	3.18
248	90.0	1.88	16.8	350	6.66	0.842	1.98	452	0.892	0.739	4.40
250	79.5	2.22	18.5	352	6.48	0.942	2.83	454	0.853	0.926	5.74
252	71.7	2.24	17.4	354	6.30	1.05	3.74	456	0.816	1.09	6.94
254	64.0	2.27	16.0	356	6.11	1.08	4.10	458	0.779	1.23	8.00
256	57.5	2.30	14.9	358	5.90	1.03	3.87	460	0.743	1.39	9.16
258	52.3	2.32	14.6	360	5.69	0.969	3.62	462	0.707	1.32	5.99
260	47.1	2.36	14.1	362	5.48	1.02	4.08	464	0.670	1.24	2.46
262	43.8	2.38	14.4	364	5.27	1.08	4.57	466	0.635	1.39	1.87
264	40.5	2.40	14.7	366	5.07	1.13	5.16	468	0.600	1.83	4.74
266	37.9	2.38	14.6	368	4.86	1.18	5.87	470	0.566	2.32	7.95
268	35.8	2.31	14.0	370	4.66	1.24	6.63	472	0.524	2.72	10.9
270	33.8	2.22	13.4	372	4.46	1.29	6.93	474	0.482	3.18	14.4
272	32.5	2.19	13.6	374	4.26	1.35	7.25	476	0.447	3.75	17.9
274	31.2	2.16	13.8	376	4.07	1.44	7.74	478	0.418	4.45	21.4
276	30.0	2.10	13.7	378	3.88	1.54	8.41	480	0.390	5.24	25.4
278	28.9	2.01	13.2	380	3.69	1.66	9.15	482	0.344	5.92	36.6
280	27.9	1.91	12.7	382	3.51	1.60	8.15	484	0.298	6.80	51.2
282	27.0	1.85	12.5	384	3.32	1.54	7.04	486	0.269	7.91	61.2
284	26.1	1.78	12.3	386	3.16	1.62	7.02	488	0.256	9.11	63.1
286	25.1	1.66	11.2	388	3.02	1.85	8.28	490	0.243	10.4	65.2
288	24.2	1.46	9.01	390	2.88	2.11	9.67	492	0.231	11.7	70.6
290	23.2	1.24	6.66	392	2.74	2.16	9.74	494	0.220	13.2	76.5
292	22.2	1.01	4.11	394	2.60	2.22	9.83	496	0.198	14.5	85.0
294	21.2	0.758	1.31	396	2.47	2.21	9.05	498	0.167	16.0	98.6
296	20.2	0.636	-0.188	398	2.36	2.10	7.28	500	0.135	18.2	119
298	19.3	0.666	-0.197	400	2.25	1.98	5.34				
300	18.4	0.699	-0.207	402	2.15	1.95	4.53				

Note:

Absorption cross sections σ and temperature coefficients A1 and A2, 200-500 nm, Burkholder et al. [116] ($\sigma(\lambda,T) = \sigma(\lambda, 296\ K)\ [1 + A1\ (T - 296) + A2\ (T - 296)^2]$).

G10. $BrCl + h\nu \rightarrow Br + Cl$. The absorption spectrum of bromine chloride has been measured at room temperature and 240-313 nm and 546 nm by Gray and Style [298], at 486-548 nm by Jost [396], at 220-510 nm by Seery and Britton [719], at 200-600 nm by Maric et al. [478], at 190-560 nm by Hubinger and Nee [345], and at 200-600 nm by Tellinghuisen [776]. The spectrum exhibits a small absorption band between 190 and 290 nm with the maximum at 230 nm ($\sigma \approx (6.0\text{-}7.2) \times 10^{-20}$ cm^2 molecule^{-1}) and a strong absorption band between 290 and 600 nm with the maximum at 375 nm ($\sigma \approx (3.9\text{-}4.1) \times 10^{-19}$ cm^2 molecule^{-1} and a shoulder near 470 nm. There is good agreement between the results of the six studies except for the values at 289 and 297 nm reported by Gray and Style [298] which are smaller by factors 2.5-6 and 2.5-4, respectively, than the rest of the results. The agreement is within 20% in the small absorption band around 230 nm between the results of Seery and Britton [719], Maric et al. [478], and Hubinger and Nee [345], where Seery and Britton [719] report the highest, Hubinger and Nee [345] the lowest values. Very good agreement within ~5-15% is in the strong absorption band around 375 nm, where Seery and Britton [719] and Tellinghuisen [776] report the highest, Hubinger and Nee [345] the lowest values. The discrepancies are larger, up to 50%, in the region of the absorption minimum around 290 nm, where Seery and Britton [719] and Hubinger and Nee [345] report the highest cross sections, Tellinghuisen [776] the lowest. Excellent agreement is to be observed in the long-wavelength tail above 450 nm between the data of Maric et al. [478] and Tellinghuisen [776], whereas those of Hubinger and Nee [345] are larger by 50% and more and those of Jost [396] are lower by ~20-40%. Maric et al. [478] fitted their data measured at a resolution of 0.2 nm to a three-band semi-logarithmic Gaussian distribution function and derived a mathematical expression which allows the calculation of a smooth absorption curve for BrCl in the wavelength region 200-600 nm:

$$\begin{aligned}\sigma(298\text{ K}) = {} & 6.52\text{x}10^{-20}\text{ cm}^2 \times \exp\{-54.1\,[\ln(227.6\text{ nm}/\lambda)]^2\} \\ & + 3.86\text{x}10^{-19}\text{ cm}^2 \times \exp\{-97.6\,[\ln(372.5\text{ nm}/\lambda)]^2\} \\ & + 9.99\text{x}10^{-20}\text{ cm}^2 \times \exp\{-66.9\,[\ln(442.4\text{ nm}/\lambda)]^2\}\end{aligned}$$

The recommended absorption cross sections calculated at 5-nm intervals from that expression are listed in Table 4.147.

The temperature dependence of the BrCl absorption cross sections has not been measured. A semiempirical expression based on the theory of Sulzer and Wieland [757], which describes the temperature and wavelength dependence of the absorption spectrum, was derived by Maric et al. [478]:

$$\begin{aligned}\sigma(T, \lambda) = {} & 7.34\text{x}10^{-20}\text{ cm}^2 \times \tanh^{0.5} \times \exp\{-68.6 \times \tanh \times [\ln(227.6\text{ nm}/\lambda)]^2\} \\ & + 4.35\text{x}10^{-19}\text{ cm}^2 \times \tanh^{0.5} \times \exp\{-123.6 \times \tanh \times [\ln(372.5\text{ nm}/\lambda)]^2\} \\ & + 1.12\text{x}10^{-19}\text{ cm}^2 \times \tanh^{0.5} \times \exp\{-84.8 \times \tanh \times [\ln(442.4\text{ nm}/l)]^2\}\end{aligned}$$

where λ is the wavelength in vacuum (200-600 nm), tanh = tanh ($hc\omega_e/2KT$) = tanh(318.8/T) (with ω_e = 443.1cm^{-1}), and T the temperature (195-300 K).

No quantum yield data are available, but is expected that BrCl photodissociates with unity quantum yield.

Table 4-147. Absorption Cross Sections of BrCl at 298 K

λ (nm)	10^{20} σ (cm^2)	λ (nm)	10^{20} σ (cm^2)	λ (nm)	10^{20} σ (cm^2)	λ (nm)	10^{20} σ (cm^2)
200	2.64	305	0.845	410	22.51	515	2.13
205	3.61	310	1.47	415	19.95	520	1.74
210	4.59	315	2.51	420	17.80	525	1.41
215	5.47	320	4.08	425	16.04	530	1.13
220	6.13	325	6.30	430	14.63	535	0.892
225	6.47	330	9.25	435	13.49	540	0.700
230	6.48	335	12.92	440	12.55	545	0.544
235	6.17	340	17.21	445	11.73	550	0.419
240	5.60	345	21.90	450	10.98	555	0.320
245	4.86	350	26.68	455	10.25	560	0.243
250	4.05	355	31.18	460	9.52	565	0.182
255	3.24	360	35.03	465	8.78	570	0.136
260	2.50	365	37.91	470	8.02	575	0.101
265	1.86	370	39.61	475	7.24	580	0.0739
270	1.35	375	40.04	480	6.47	585	0.0539
275	0.945	380	39.26	485	5.72	590	0.0390
280	0.653	385	37.45	490	4.99	595	0.0281
285	0.458	390	34.87	495	4.31	600	0.0200
290	0.357	395	31.82	500	3.68		
295	0.360	400	28.59	505	3.10		
300	0.504	405	25.43	510	2.59		

Note:
200-600 nm, Maric et al. [478]

G11. $BrOCl + h\nu \rightarrow$ Products. Absorption spectrum of bromine-chlorine monoxide has been measured at room temperature and 230-390 nm by Burkholder et al. [112]. Results are in Table 4-148.

Table 4-148. Absorption Cross Sections of BrOCl at 298 K

λ (nm)	10^{20} σ (cm^2)	λ (nm)	10^{20} σ (cm^2)	λ (nm)	10^{20} σ (cm^2)	λ (nm)	10^{20} σ (cm^2)
230	16.8	272	200	314	55.8	338	46.7
232	15.4	274	199	316	56.6	358	22.5
234	15.2	276	191	318	57.2	360	20.2
236	15.5	278	179	320	57.4	362	18.1
238	16.6	280	165	322	57.3	364	16.1
240	18.6	282	149	324	56.9	366	14.2
242	21.7	284	132	326	56.1	368	12.3
244	26.1	286	115	328	55.1	370	10.6
246	31.6	288	100	330	53.8	372	8.66
248	39.1	290	87.2	332	52.3	374	7.34
250	48.1	292	76.3	334	50.6	376	6.12
252	59.9	294	67.9	336	48.7	378	5.01
254	73.8	296	61.6	340	44.5	380	4.00
256	89.4	298	57.0	342	42.3	382	3.10
258	107	300	54.0	344	39.9	384	2.30
260	126	302	52.4	346	37.3	386	1.62
262	145	304	52.1	348	34.7	388	1.03
264	163	306	52.3	350	32.4	390	0.55
266	179	308	53.0	352	29.8		
268	192	310	53.9	354	27.2		
270	198	312	54.7	356	24.8		

Note:
230-390 nm, Burkholder et al. [112].

G12. $CH_3Br + h\nu \rightarrow$ Products**.** The absorption cross sections of CH_3Br have been measured at room temperature and 205–270 nm by Davidson [205]; at 204–260 nm by Gordus and Bernstein [293]; at 174–270 nm by Robbins [673]; at 200–260 nm by Uthman et al. [797]; at 190–290 nm by Molina et al. [545]; at 201.6 nm by Felps et al. [241]; at 180–264 nm by Man et al. [472]; and at 210–295 K and 180–280 nm by Gillotay and Simon [276]. Above 180 nm and below 270 nm, the room temperature values of Gordus and Bernstein [293], Robbins [673], Uthman et al. [797], Molina et al. [545], Gillotay and Simon [276], and the values of Davidson [205] above 210 nm are in very good agreement, i.e., generally within 10% and around the absorption maximum at 200–202 nm within 2%. The value at 202 nm of Felps et al. [241] is lower by ~10% than the rest of the data. The data of Man et al. [472], given as a plot in their paper, are lower by 20–30% over the whole absorption band than the above-mentioned agreeing data sets. The preferred absorption cross sections, listed in Table 4-149, are the values of Robbins [673] at 174–178 nm; the mean of the values reported by Gillotay and Simon [276] and Robbins [673] at 180–188 nm; the mean of the values reported by Gillotay and Simon [276], Uthman et al. [797], and Robbins [673] at 190–198 nm; the mean of the values reported by Gillotay and Simon [276], Molina et al. [545], Uthman et al. [797], and Robbins [673] at 200–260 nm; the mean of the values reported by Gillotay and Simon [276], Molina et al. [545], and Robbins [673] at 262–268 nm; the mean of the values reported by Gillotay and Simon [276] and Molina et al. [545] at 270–280 nm; and the data of Molina et al. [545] at 285–290 nm.

A slight temperature dependence was observed above 220 nm, where the absorption cross sections decrease with decreasing temperature 295–210 K. Gillotay and Simon [276] parameterized the cross sections and the temperature dependence by the polynomial expansion $\log_{10} \sigma(\lambda, T) = \sum A_n \lambda^n + (T - 273) \times \sum B_n \lambda^n$ and reported smoothed values for T = 210, 230, 250, 270, and 295 K, every 2 nm, and at wavelengths corresponding to the wavenumber intervals generally used in stratospheric photodissociation calculations. The parameters A_n and B_n for the ranges T = 210–300 K and λ = 200–280 nm are as follows:

$A_0 = 46.520$ $\quad B_0 = 9.3408 \times 10^{-1}$

$A_1 = -1.4580$ $\quad B_1 = -1.6887 \times 10^{-2}$

$A_2 = 1.1469 \times 10^{-2}$ $\quad B_2 = 1.1487 \times 10^{-4}$

$A_3 = -3.7627 \times 10^{-5}$ $\quad B_3 = -3.4881 \times 10^{-7}$

$A_4 = 4.3264 \times 10^{-8}$ $\quad B_4 = 3.9945 \times 10^{-10}$

Quantum yields for Br and H atom formation in the photodissociation of CH_3Br were measured at 298 K by Talukdar et al. [771]. The quantum yields for Br atom formation were found to be close to unity, $\Phi(Br) = 1.05 \pm 0.11$, 1.10 ± 0.20, and 1.01 ± 0.16 at 193, 222, and 248 nm, respectively; the quantum yield for H atom formation in the photolysis at 193 nm was measured to be $\Phi(H) = 0.002 \pm 0.001$, whereas H atoms could not be detected in the photolysis at 222 and 248 nm. Broad band flash photolysis of CH_3Br produced $Br^*(^2P_{1/2})$ atoms with a quantum yield $\Phi(Br^*) = 0.15 \pm 0.12$ as reported by Ebenstein et al. [224].

Table 4-149. Absorption Cross Sections of CH_3Br at 295–296 K

λ (nm)	$10^{20}\sigma$ (cm^2)	λ (nm)	$10^{20}\sigma$ (cm^2)	λ (nm)	$10^{20}\sigma$ (cm^2)
174	533	212	59.9	250	0.921
176	1010	214	54.2	252	0.683
178	1280	216	47.9	254	0.484
180	44.6	218	42.3	256	0.340
182	19.8	220	36.6	258	0.240
184	21.0	222	31.1	260	0.162
186	27.8	224	26.6	262	0.115
188	35.2	226	22.2	264	0.0795
190	44.2	228	18.1	266	0.0551
192	53.8	230	14.7	268	0.0356
194	62.6	232	11.9	270	0.0246
196	69.7	234	9.41	272	0.0172
198	76.1	236	7.38	274	0.0114
200	79.0	238	5.73	276	0.00808
202	79.2	240	4.32	278	0.00553
204	78.0	242	3.27	280	0.00382
206	75.2	244	2.37	285	0.00110
208	70.4	246	1.81	290	0.00030
210	65.5	248	1.31		

Note:

174–178 nm, Robbins [673],
180–188 nm, mean of Gillotay and Simon [276] and Robbins [673],
190–198 nm, mean of Gillotay ad Simon [276], Uthman et al. [797], and Robbins [673],
200–260 nm, mean of Gillotay and Simon [276], Molina et al. [545], Uthman et al. [797] and Robbins [673],
262–268 nm, mean of Gillotay and Simon [276], Molina et al. [545], and Robbins [673],
270–280 nm, mean of Gillotay and Simon [276] and Molina et al. [545],
285–290 nm, Molina et al. [545].

G13. $CH_2Br_2 + h\nu \rightarrow CH_2Br + Br$. The absorption cross sections of CH_2Br_2 have been measured at room temperature and 200–300 nm by Molina et al. [545]; at 210–295 K and 174–290 nm by Gillotay et al. [281], [278]; and at 250–348 K and 215–300 nm by Mössinger et al. [563]. The results are in good agreement, at 200–255 nm within 10% and up to 275 nm within 30%. The preferred room temperature values, listed in Table 4-150, are the values of Gillotay et al. [281], [278] at 174–198 nm; the mean of the values reported by Molina et al. [545] and Gillotay et al. [281], [278] for the wavelength range 200–215 nm; the mean of the values reported by the three groups for the wavelength range 220–290 nm; and values of Mössinger et al. [563] at 295–300 nm.

Both studies of the temperature dependence show a decrease of the absorption cross sections with decreasing temperature at wavelength above ~235–239 nm, and the reverse behavior around the absorption maximum down to 207 nm. At lower wavelengths, Gillotay et al. [278, 281] report between 210 and 295 K a slight increase of σ at 175–189 nm and a slight decrease around the weaker absorption maximum at 198–201 nm. The latter group parameterized the cross sections and the temperature dependence by the polynomial expansion
$\log_{10} \sigma(\lambda, T) = \sum A_n \lambda^n + (T - 273) \times \sum B_n \lambda^n$ and report smoothed values for T = 210, 230, 250, 270, and 295 K, every 2 nm, and at wavelengths corresponding to the wavenumber intervals generally used in stratospheric photodissociation calculations. The parameters A_n and B_n for the ranges 210–290 nm and 210–300 K are as follows:

$A_0 = -70.211776$	$B_0 = 2.899280$
$A_1 = 1.940326 \times 10^{-1}$	$B_1 = -4.327724 \times 10^{-2}$
$A_2 = 2.726152 \times 10^{-3}$	$B_2 = 2.391599 \times 10^{-4}$
$A_3 = -1.695472 \times 10^{-5}$	$B_3 = -5.807506 \times 10^{-7}$
$A_4 = 2.500066 \times 10^{-8}$	$B_4 = 5.244883 \times 10^{-10}$

Mössinger et al. [563] list the temperature coefficients $B(\lambda)$ at 5-nm intervals for the ranges 215–300 nm and 250–348 K for the empirical relation $\ln \sigma(\lambda, T) = \ln \sigma(\lambda, 298K) + B(\lambda)x(T–298)$. Formulae used by Gillotay et al. [278, 281] and Mössinger et al. [563] produce cross sections that agree at 250 K within 5% in the range 215–265 nm and within 10% in the range 270–285 nm.

There are no quantum yield measurements, but it is expected that photolysis will rupture the C-Br bond with unity quantum yield.

Table 4-150. Absorption Cross Sections of CH_2Br_2 at 295–298 K

λ (nm)	10^{20} σ (cm^2)	λ (nm)	10^{20} σ (cm^2)	10^3 B (K^{-1})	λ (nm)	10^{20} σ (cm^2)	10^3 B (K^{-1})
174	1170.9	198	226.0		255	14.10	3.91
176	662.4	200	225.6		260	6.607	5.16
178	377.2	205	215.3		265	3.037	6.33
180	241.0	210	234.5		270	1.347	7.75
182	178.4	215	263.2	–2.02	275	0.590	8.74
184	154.4	220	272.0	–1.79	280	0.255	11.6
186	153.5	225	247.4	–1.50	285	0.114	13.8
188	166.1	230	195.8	–0.96	290	0.0499	15.3
190	187.0	235	138.9	–0.04	295	0.0210	16.5
192	209.3	240	88.60	0.71	300	0.0090	21.9
194	222.5	245	51.90	1.80			
196	228.3	250	28.03	2.70			

Note:
Absorption cross sections σ: 174–198 nm, Gillotay et al. [281], [278],
200–210 nm, mean of Molina et al. [545] and Gillotay et al. [281], [278],
215–290 nm, mean of Molina et al [545], Gillotay et al. [281], [278], and Mössinger et al. [563],
295–300 nm, Mössinger et al. [563].

Temperature coefficients B: 215–300 nm, Mössinger et al. [563].

G14. $CHBr_3 + h\nu \rightarrow CHBr_2 + Br$

$CHBr_3 + h\nu \rightarrow CHBr + Br_2$. The absorption cross sections of $CHBr_3$ have been measured at 240–295 K and 170–310 nm by Gillotay et al. [275] and at 256–296 K and 286–362 nm by Moortgat et al. [556]; the agreement in the overlap region is excellent. The recommended cross sections at room temperature, listed in Table 4-151, are the values of Gillotay et al. [275] for the range 170–284 nm; the mean of the values reported by Gillotay et al. [275] and Moortgat et al. [556] for the range 286–310 nm; and the values of Moortgat et al. [556] at 286–362 nm.

The studies of the temperature dependence show an increase of the absorption cross sections with decreasing temperature around the three absorption maxima at 178–189 nm, 194–208 nm, and 208–234 nm, and a decrease of the absorption cross sections below 179 nm, at 189–194 nm and above 235 nm. Gillotay et al. [275] parameterized the cross sections and the temperature dependence by the polynomial expansion

$$\log_{10}(\sigma(\lambda, T)) = \sum A_n \lambda^n + (T - 273) \times \sum B_n \lambda^n$$

and report smoothed values for T = 210, 230, 250, 270, and 295 K, every 2 nm, and at wavelengths corresponding to the wavenumber intervals generally used in stratospheric photodissociation calculations. The parameters A_n and B_n for the ranges 240–310 nm and 210–300 K are given by Gillotay and Simon [278]:

$A_0 = -110.2782$ $\quad B_0 = -1.5312 \times 10^{-1}$
$A_1 = 1.0281$ $\quad B_1 = 1.6109 \times 10^{-3}$
$A_2 = -3.6626 \times 10^{-3}$ $\quad B_2 = -5.8075 \times 10^{-6}$
$A_3 = 4.1226 \times 10^{-6}$ $\quad B_3 = 7.2893 \times 10^{-9}$

For wavelengths longer than 290 nm, the atmospherically important range, Moortgat et al. [556] give the expression

$$\sigma(\lambda,T) = \exp\{(0.06183 - 0.000241\,\lambda)(273 - T) - (2.376 + 0.14757\,\lambda)\}\ (\lambda = 290\text{–}340\text{ nm}, T = 210\text{–}300\text{ K})$$

These two formulae produce continuous absorption curves for the range 240–340 nm also at low temperatures

At wavelengths longer than 290 nm, the cross sections are relatively small; the presence of impurities as well as optical artifacts arising, e.g., from adsorption of $CHBr_3$ on the cell windows, complicate the measurements. Hence, additional investigations of the spectrum would be useful.

The quantum yield for the formation of Br atoms were determined by Bayes et al. [64] between 266 and 324 nm. For 303 to 306 nm, the Br-atom quantum yield is unity within experimental error. At longer wavelengths, the quantum yields decreases to 0.76 at 324 nm, but the authors claim that the lower than unity values is the result of systematic and random errors and/or incorrect absorption cross sections. Support for unity quantum yield at λ > 300 nm comes from theoretical calculations by Peterson and Francisco [632], and is recommended for modeling in the troposphere. At 266 nm, the Br-atom quantum yield is 0.76 ± 0.03,

indicating that another photodissociation channel becomes important. Xu et al. [854] measured atomic Br and molecular Br_2 by TOF mass spectrometry from bromoform photolysis at 234 and 267 nm and report evidence for the formation of CHBr + Br_2. At 234 nm the $\varphi(Br) = 0.74$ and $\varphi(Br_2) = 0.26$, while at 267 nm $\varphi(Br) = 0.84$ and $\varphi(Br_2) = 0.16$.

It is recommended that the Br-atom quantum yield is unity at wavelengths above 300 nm.

Table 4-151. Absorption Cross Sections of $CHBr_3$ at 295–296 K

λ (nm)	$10^{20}\sigma$ (cm^2)	λ (nm)	$10^{20}\sigma$ (cm^2)	λ (nm)	$10^{20}\sigma$ (cm^2)
170	1603.8	236	323.9	302	0.534
172	1173.2	238	294.7	304	0.397
174	969.6	240	272.8	306	0.297
176	872.0	242	253.3	308	0.222
178	857.6	244	233.7	310	0.165
180	831.3	246	214.4	312	0.127
182	770.3	248	193.9	314	0.0952
184	683.3	250	174.1	316	0.0712
186	570.4	252	157.7	318	0.0529
188	470.8	254	136.1	320	0.0390
190	399.1	256	116.4	322	0.0289
192	360.2	258	98.6	324	0.0215
194	351.3	260	82.8	326	0.0162
196	366.1	262	68.9	328	0.0121
198	393.6	264	56.9	330	0.00916
200	416.4	266	46.7	332	0.00690
202	433.6	268	38.0	334	0.00525
204	440.6	270	30.8	336	0.00396
206	445.0	272	24.8	338	0.00307
208	451.4	274	19.8	340	0.00240
210	468.5	276	15.8	342	0.00176
212	493.4	278	12.5	344	0.00135
214	524.2	280	9.88	346	0.00102
216	553.5	282	7.77	348	0.00080
218	573.9	284	6.10	350	0.00064
220	582.6	286	4.79	352	0.00054
222	578.0	288	3.74	354	0.00046
224	557.8	290	2.89	356	0.00032
226	527.2	292	2.20	358	0.00024
228	486.8	294	1.69	360	0.00017
230	441.2	296	1.28	362	0.00013
232	397.4	298	0.956		
234	361.8	300	0.719		

Note:
170–284 nm, Gillotay et al. [275],
286–310 nm, mean of Gillotay et al. [275] and Moortgat et al. [556],
312–362 nm, Moortgat et al. [556].

G15. $CH_2BrCH_2Br + h\nu \rightarrow$ Products. Absorption cross sections of CH_2BrCH_2Br have been measured at room temperature and 190–270 nm by Uthman et al. [797]. Their data are listed in Table 4-152.

Table 4-152. Absorption Cross Sections of CH_2BrCH_2Br at 295 K

λ (nm)	10^{20} σ (cm^2)	λ (nm)	10^{20} σ (cm^2)	λ (nm)	10^{20} σ (cm^2)
190	230	218	170	246	9.3
192	250	220	150	248	7.1
194	270	222	130	250	5.9
196	290	224	110	252	4.4
198	300	226	89	254	4.0
200	310	228	75	256	2.8
202	310	230	62	258	2.1
204	300	232	50	260	1.9
206	290	234	41	262	1.7
208	280	236	32	264	1.4
210	260	238	26	266	1.1
212	230	240	20	268	0.9
214	210	242	16	270	0.7
216	190	244	11		

Note:
190–270 nm, Uthman et al. [797].

G16. $C_2H_5Br + h\nu \rightarrow$ Products. The absorption cross sections of C_2H_5Br have been measured at 295 K and 200–260 nm by Zhang et al. [881]. This wavelength range shows part of an absorption band with a maximum of ~ 6×10^{-19} cm^2 at ~200 nm. Estimated values at 5-nm intervals, read from a logarithmic plot, are presented in Table 4-153.

Table 4-153. Absorption Cross Sections of C_2H_5Br at 295 K

λ (nm)	10^{20} σ (cm^2)	λ (nm)	10^{20} σ (cm^2)	λ (nm)	10^{20} σ (cm^2)
200	61	225	24	250	1.1
205	60	230	15	255	0.5
210	54	235	8.3	260	0.2
215	45	240	4.3		
220	34	245	2.3		

Note:
200–260 nm, Zhang et al. [881], estimated values read from logarithmic plot.

G17. $COBr_2 + h\nu \rightarrow$ Products. The absorption cross-sections of $COBr_2$ (carbonyl dibromide, dibromophosgene) have been measured at room temperature and 235-353 nm by Libuda et al. [447] and Libuda [445]. The spectrum exhibits monotonically decreasing absorption cross-sections with increasing wavelength, the maximum obviously lies below 235 nm. As a recommendation are listed in Table 4-154 the averages over 1-nm intervals of the medium-resolution data (0.6 nm) for the range 240-331 nm where the absorption curve shows a regular behavior.

Table 4-154. Absorption Cross Sections of $COBr_2$ at 298 K

λ (nm)	10^{20} σ (cm^2)	λ (nm)	10^{20} σ (cm^2)	λ (nm)	10^{20} σ (cm^2)	λ (nm)	10^{20} σ (cm^2)
240	58.3	263	20.9	286	4.50	309	0.301
241	56.5	264	19.9	287	4.13	310	0.260
242	55.3	265	18.8	288	3.73	311	0.230
243	54.1	266	17.9	289	3.38	312	0.204
244	52.3	267	17.0	290	3.09	313	0.178
245	50.6	268	16.1	291	2.81	314	0.159
246	48.8	269	15.2	292	2.58	315	0.143
247	47.1	270	14.4	293	2.32	316	0.127
248	45.2	271	13.6	294	2.07	317	0.114
249	43.2	272	12.8	295	1.82	318	0.0995
250	41.3	273	12.0	296	1.62	319	0.0892
251	39.5	274	11.4	297	1.42	320	0.0789
252	37.7	275	10.7	298	1.26	321	0.0694
253	35.7	276	9.98	299	1.11	322	0.0633
254	33.7	277	9.24	300	0.971	323	0.0578
255	32.0	278	8.56	301	0.858	324	0.0528
256	30.4	279	7.99	302	0.750	325	0.0499
257	28.9	280	7.44	303	0.661	326	0.0449
258	27.4	281	6.91	304	0.578	327	0.0397
259	26.0	282	6.35	305	0.501	328	0.0336
260	24.5	283	5.81	306	0.437	329	0.0296
261	23.3	284	5.34	307	0.386	330	0.0264
262	22.1	285	4.92	308	0.331	331	0.0229

Note:
240-331 nm, Libuda et al. [447], Libuda [445].

G18. $COHBr + h\nu \rightarrow$ Products. The absorption spectrum of COHBr (formyl bromide) has been measured at room temperature and 240-340 nm by Libuda et al. [447] and Libuda [445]. The absorption spectrum exhibits a highly structured absorption band with the maximum near 268 nm. In Table 4-155 are listed the averages over 1-nm intervals of the medium-resolution (0.6 nm) data for the range 240-324 nm where the absorption curve shows a regular behavior.

Table 4-155. Absorption Cross Sections of COHBr at 298 K

λ (nm)	10^{20} σ (cm^2)	λ (nm)	10^{20} σ (cm^2)	λ (nm)	10^{20} σ (cm^2)	λ (nm)	10^{20} σ (cm^2)
240	18.7	262	32.4	284	21.7	306	2.77
241	20.1	263	29.9	285	20.1	307	2.43
242	19.4	264	31.1	286	19.1	308	2.12
243	19.8	265	29.9	287	17.5	309	1.90
244	19.1	266	32.5	288	17.3	310	1.65
245	20.0	267	31.6	289	14.9	311	1.51
246	22.6	268	33.8	290	15.5	312	1.34
247	22.6	269	30.9	291	12.7	313	1.13
248	23.6	270	31.9	292	13.3	314	1.01
249	22.5	271	30.9	293	11.1	315	0.801
250	22.3	272	29.6	294	10.8	316	0.687
251	24.0	273	31.4	295	9.79	317	0.613
252	25.0	274	29.3	296	9.08	318	0.611
253	27.1	275	31.5	297	8.03	319	0.576
254	26.9	276	28.5	298	7.35	320	0.522
255	27.5	277	29.1	299	5.97	321	0.476
256	27.5	278	26.8	300	5.86	322	0.424
257	26.9	279	25.6	301	5.25	323	0.363
258	28.8	280	25.1	302	4.47	324	0.308
259	28.9	281	23.2	303	4.38		
260	31.9	282	23.8	304	3.53		
261	30.1	283	22.0	305	3.18		

Note:
240-324 nm, Libuda [447].

G19. CH_2ClBr (Halon-1011) + hν → Products**.** The absorption cross sections of CH_2ClBr have been measured at room temperature and 210–260 nm by Cadman and Simons [131], and at 187–290 nm by Orkin et al. [603]. The data of Cadman and Simons [131], which are given only on a plot in their paper, are smaller by ≤20% than the data of Orkin et al. [603]. The recommended absorption cross sections, listed in Table 4-156, are the data of Orkin et al. [603].

Quantum yields for Br ($^2P_{3/2}$) and Br*($^2P_{1/2}$) atom formation in the photolysis of CH_2ClBr at 193–242 nm and 248–268 nm have been measured by Zou et al. [884] and McGivern et al. [507], respectively. Reported values are as follows:

	193 nm	234 nm	248.5 nm	261.5 nm	266.7 nm:
Φ(Br ($^2P_{3/2}$))	0.82 ± 0.10	0.80 ± 0.10	0.86 ± 0.10	0.84 ± 0.10	0.91 ± 0.10
Φ(Br*($^2P_{1/2}$))	0.18 ± 0.10	0.20 ± 0.10	0.14 ± 0.10	0.16 ± 0.10	0.09 ± 0.10

Table 4-156. Absorption Cross Sections of CH_2ClBr at 295 K

λ (nm)	10^{20} σ (cm^2)	λ (nm)	10^{20} σ (cm^2)	λ (nm)	10^{20} σ (cm^2)
187	151.1	222	57.4	258	1.45
188	126.4	224	50.5	260	1.09
190	104.6	226	44.1	262	0.807
192	100.5	228	38.2	264	0.596
194	104.7	230	32.8	266	0.440
196	111.8	232	28.0	268	0.322
198	119.4	234	23.6	270	0.235
200	124.7	236	19.7	272	0.170
202	127.1	238	16.3	274	0.123
204	126.3	240	13.4	276	0.089
206	122.5	242	10.8	278	0.064
208	116.3	244	8.73	280	0.046
210	108.4	246	6.94	282	0.033
212	99.6	248	5.46	284	0.024
214	90.5	250	4.24	286	0.0178
216	81.5	252	3.29	288	0.0129
218	72.9	254	2.52	290	0.0098
220	64.8	256	1.92		

Note:
187–290 nm, Orkin et al. [603].

G20. $CHClBr_2$ (Halon-1012) + hν $\rightarrow$ CH_2Cl + Br ($^2P_{3/2}$)
$CHClBr_2$ (Halon-1012) + hν $\rightarrow$ CH_2Cl + Br*($^2P_{1/2}$)
$CHClBr_2$ (Halon-1012) + hν $\rightarrow$ CH_2Br + Cl ($^2P_{3/2}$)
$CHClBr_2$ (Halon-1012) + hν $\rightarrow$ CH_2Br + Cl*($^2P_{1/2}$). The absorption cross sections of $CHClBr_2$ have been measured at room temperature and 106–200 nm by Ibuki et al. [356]; at 240, 261, and 296 K and 200–310 nm by Bilde et al. [69]; and at 295 K and 193.3 nm by Taketani et al. [763]. Two absorption bands are apparent above 200 nm, one maximizing near 206 nm and the other near 240 nm. Near the band maxima, the cross sections at 240 K are approximately higher by 10% than those at room temperature. A positive temperature dependence of the cross sections is evident in the long-wavelength tail of the spectrum, the room temperature cross section being about 15% higher at 270 nm than that obtained at 240 K. The recommended absorption cross sections, listed in Table 4-157, are the room temperature data of Bilde et al. [69] (originally listed at 1-nm intervals); values at 2-nm intervals are given for wavelengths above 212 nm, and values at 1-nm intervals are given or the region of the first absorption maximum (200–212 nm), where the absorption curve shows a somewhat irregular behavior. Taketani et al. [763] reported a value of 304×10^{20} cm^2 $molecule^{-1}$ at 193.3 nm.

Quantum yields for dissociation have been measured by Tzeng et al. [793] at 193 and 248 nm; by McGivern et al. [507] from 248 to 268 nm; by Zou et al, [884] between 193 and 242 nm; by Lee et al. [439] at 234 nm; and by Taketani et al. [763] at 193.3 nm. In the range 248-262 nm, $CHClBr_2$ undergoes C-Br bond rupture exclusively, whereas in the range 193-242 nm it predominantly dissociates via C-Br bond rupture, with a minor contribution from C-Cl bond rupture. The relative quantum yield for ground state Br($^2P_{3/2}$) varies from 0.80 to 0.90 in the range 193 to 267 nm, whereas the quantum yield for spin excited Br*($^2P_{1/2}$) ranges from 0.20 to 0.10.

Table 4-157. Absorption Cross Sections of $CHClBr_2$ at 296 K

λ (nm)	10^{20} σ (cm^2)	λ (nm)	10^{20} σ (cm^2)	λ (nm)	10^{20} σ (cm^2)
200	274.6	230	141.4	272	9.415
201	282.8	232	136.4	274	7.552
202	293.9	234	131.4	276	5.950
203	306.7	236	126.8	278	4.687
204	314.2	238	122.2	280	3.691
205	320.6	240	116.0	282	2.884
206	324.9	242	109.2	284	2.261
207	323.7	244	101.2	286	1.734
208	322.9	246	92.70	288	1.331
209	324.6	248	83.52	290	1.016
210	317.8	250	74.04	292	0.7907
211	306.2	252	64.83	294	0.6116
212	297.4	254	55.95	296	0.4583
214	279.4	256	47.67	298	0.3489
216	261.7	258	39.92	300	0.2692
218	234.9	260	33.35	302	0.2076
220	215.1	262	27.50	304	0.1588
222	199.1	264	22.50	306	0.1208
224	184.5	266	18.28	308	0.0945
226	165.3	268	14.78	310	0.0742
228	151.7	270	11.82		

Note:
200–310 nm, Bilde et al. [69]

G21. $CHCl_2Br$ (Halon-1021) + hν → Products. The absorption cross sections of $CHCl_2Br$ have been measured at room temperature and 106–200 nm by Ibuki [356]; at room temperature and 201–270 nm by Cadman and Simons [131]; and at 253, 273 and 298 K and 200–320 nm by Bilde et al. [69]. The data of Cadman and Simons [131], which are given only in a plot in their paper, agree between 200 and 260 nm within ≤15% with the room temperature data of Bilde et al. [69], the absorption maximum, however, is shifted to lower wavelengths. The recommended absorption cross sections, listed in Table 4-158, are those reported by Bilde et al. [69].

A decrease of the absorption cross sections with decreasing temperature was observed between 298 and 253 K over the whole spectrum. The cross section in the absorption maximum, which has been observed at 220 nm by Bilde et al. [69], is approximately 6% lower at 253 K than at room temperature. An increasingly positive temperature dependence was observed at longer wavelengths, the room temperature cross section at 320 nm becoming about four times larger than those at 253 K.

Table 4-158. Absorption Cross Sections of $CHCl_2Br$ at 298 K

λ (nm)	10^{20} σ (cm^2)	λ (nm)	10^{20} σ (cm^2)	λ (nm)	10^{20} σ (cm^2)
200	115.0	230	58.1	276	1.63
202	93.8	232	54.6	278	1.32
204	81.1	234	50.0	280	1.07
206	73.6	236	45.8	282	0.865
208	69.0	238	41.6	284	0.694
209	69.8	240	37.3	286	0.573
210	68.8	242	33.0	288	0.454
211	67.4	244	29.3	290	0.384
212	68.4	246	25.8	292	0.317
213	70.0	248	22.2	294	0.265
214	70.1	250	19.2	296	0.217
215	70.2	252	16.5	298	0.176
216	71.1	254	13.6	300	0.146
217	71.0	256	11.5	302	0.118
218	70.7	258	9.75	304	0.0962
219	71.3	260	8.19	306	0.0761
220	71.6	262	6.82	308	0.0617
221	70.6	264	5.61	310	0.0496
222	69.3	266	4.68	312	0.0395
223	68.7	268	3.74	314	0.0317
224	68.2	270	3.01	316	0.0259
226	65.2	272	2.48	318	0.0210
228	62.2	274	2.02	320	0.0171

Note:
200–320 nm, Bilde et al. [69].

G22. CCl_3Br (Halon-1031) + hν → CCl_3 + Br. The absorption cross sections of CCl_3Br have been measured at room temperature and 207–305 nm by Cadman and Simons [131], at 365 nm by Sidebottom et al. [729], at 170–230 nm by Roxlo and Mandl [692], at 105-198 nm by Ibuki et al. [357], and at 50-200 nm by Seccombe et al. [718]. The absorption spectrum shows a strong absorption band between 170 and 220 nm with the maximum near 185 nm and $\sigma \approx (1.1\text{-}1.4) \times 10^{-17}$ cm^2 $molecule^{-1}$ followed by a weak shoulder at 220-305 nm. The absorption cross sections for the wavelength region 235-305 nm listed in Table4-159 have been read at 5-nm intervals from a plot in the paper of Cadman and Simons [131], the value for 365 nm has been reported by Sidebottom et al. [729].

Product quantum yield were studied at 365 nm by Sidebottom et al. [729], showing evidence that Br + CCl_3 are the primary products, being pressure and temperature dependent. Quantum yields for $Br^*(^2P_{1/2})$ atom formation in the photolysis at 234 and 265 nm, $\Phi(Br^*) = 0.31 \pm 0.01$ and 0.68 ± 0.02, respectively, were reported by Jung et al. [399].

Table 4-159. Absorption Cross Sections of CCl_3Br at 298 K

λ (nm)	10^{20} σ (cm^2)	λ (nm)	10^{20} σ (cm^2)
235	50	275	11
240	50	280	7.2
245	49	285	5.0
250	48	290	3.3
255	46	295	2.2
260	42	300	1.4
265	34	305	1.0
270	19	365	0.0077

Note:
235–305 nm, Cadman and Simons [131],
365 nm, Sidebottom et al. [729].

G23. CHF_2Br (Halon-1201) + hν → Products The absorption cross sections of CHF_2Br have been measured at room temperature and 207–255 nm by Davidson [205]; at 190–280 nm by Talukdar et al. [765]; and at 190–280 nm by Orkin and Kasimovskaya [602]. Gillotay et al. [281] carried out measurements at 210–295 K and

in the wavelength range 166–267 nm and report only smoothed values for T = 210, 230, 250, 270, and 295 K and at wavelengths corresponding to the wavenumber intervals generally used in stratospheric photodissociation calculations. The results of Davidson [205], Orkin and Kasimovskaya [602], and Gillotay et al. [281] are in excellent agreement at wavelengths below 240 nm; the values of Gillotay et al. [281] become increasingly smaller by up to about 40% at 260 nm, and those of Davidson [205] become smaller by up to about 30% at 250 nm than the values of Orkin and Kasimovskaya [602]. The results of Talukdar et al. [765], who report a plot on a logarithmic scale for measured values at 190–280 nm and extrapolated values up to 360 nm, appear to be in agreement with the results of Orkin and Kasimovskaya [602]. The preferred values, listed in Table 4-160, are the values of Gillotay et al. [281] at the centers of the 500-cm^{-1} intervals between 168 and 188 nm, and the values of Orkin and Kasimovskaya [602] at 190–280 nm.

With decreasing temperature 295–210 K, an increase of the absorption cross sections around the absorption maximum at 168–215 nm and a decrease at wavelengths above 215 nm was observed by Gillotay et al. [281] (the interpolation formula has not been reported for this molecule).

Table 4-160. Absorption Cross Sections of CHF_2Br at 298 K

λ (nm)	10^{20} σ (cm^2)	λ (nm)	10^{20} σ (cm^2)	λ (nm)	10^{20} σ (cm^2)
168.10	3.97	206	23.2	246	0.299
170.95	8.21	208	21.2	248	0.220
173.15	12.5	210	19.0	250	0.161
174.65	15.6	212	16.8	252	0.117
176.20	18.8	214	14.6	254	0.0849
177.80	21.9	216	12.6	256	0.0615
179.40	24.5	218	10.6	258	0.0444
181.00	26.6	220	8.85	260	0.0319
182.65	28.3	222	7.25	262	0.0230
184.35	29.6	224	5.88	264	0.0166
186.05	30.6	226	4.71	266	0.0121
187.80	31.4	228	3.73	268	0.0087
190	32.5	230	2.91	270	0.0063
192	32.4	232	2.24	272	0.0046
194	31.8	234	1.71	274	0.0034
196	31.0	236	1.30	276	0.0024
198	29.9	238	0.982	278	0.0018
200	28.6	240	0.735	280	0.0012
202	27.0	242	0.547		
204	25.2	244	0.405		

Note:
168–188 nm, Gillotay et al. [281],
190–280 nm, Orkin and Kasimovskaya [602].

G24. CF_2Br_2 (Halon-1202) + hν → Products. The absorption cross sections of CF_2Br_2 have been measured at room temperature and 215–290 nm by Davidson [205]; at 200–310 nm by Walton [834]; at 190–340 nm by Molina et al. [545]; at 190–320 nm by Orkin and Kasimovskaya [602]; at 210–295 K and 170–304 nm by Gillotay and Simon [277]; and at 210–296 K and 190–320 nm by Burkholder et al. [120]. The room temperature data, except those of Walton [834], are in good agreement, i.e., better than 10%, over their common wavelength range from 190 to 300 nm. In the absorption maximum around 226 nm, the older data of Davidson [205] and Molina et al. [545] are the highest and lowest, respectively, and the more recent data agree within 5% (the absorption maximum reported by Walton [834] is larger by ~50%). At wavelengths above 300 nm, the values of Orkin and Kasimovskaya [602] and Burkholder et al. [120] agree within 15%, whereas those of Molina et al. [545] become increasingly larger by up to ~200% at 320 nm (and larger by up to ~660% than the extrapolated values at 340 nm, see below). The preferred absorption cross sections, listed in Table 4-161, are the values of Gillotay and Simon [277] at 170–188 nm; the mean of the values reported by Gillotay and Simon [277], Orkin and Kasimovskaya [602], and Burkholder et al. [120] for the wavelength range 190–304 nm; and the mean of the values reported by the latter two groups for the range 306–320 nm. For wavelengths 322–340 nm, the mean of the values of Orkin and Kasimovskaya [602], and Burkholder et al. [120] for the range 306–320 nm have been extrapolated ($\log \sigma = 1.85109 - 0.07755\ \lambda$).

Measurements in the far UV were reported by Doucet et al. [221] for the wavelength range 60–220 nm and by Seccombe et al. [717] for the wavelength range 55–175 nm.

Both studies of the temperature dependence show an increase of the absorption cross sections in the two absorption bands around 190 and 226 nm with decreasing temperature 296–210 K and the reverse effect at wavelengths above 240 nm and below 177 nm. Gillotay and Simon [277] observed a regular temperature

behavior, i.e., an increase of the maximum absorption cross section at ~225 nm by ~0.09×10^{-18} cm^2 $molecule^{-1}$ per 20-K temperature decrease. Burkholder et al. [120] observed a less pronounced temperature behavior below 250 K (the maximum absorption cross sections agree within 1%), so that their maximum cross section at 210 K is 5% lower than that observed by Gillotay and Simon [277] (in contrast to the cross sections at room temperature which are nearly identical). Different parameterizations for the temperature dependence of the absorption cross section was proposed. Gillotay and Simon [277] give the polynomial expansion

$$\log_{10} \sigma(\lambda, T) = \sum A_n \lambda^n + (T - 273) \times \sum B_n \lambda^n$$

and report smoothed values for T = 210, 230, 250, 270, and 295 K, every 2 nm, and at wavelengths corresponding to the wavenumber intervals generally used in stratospheric photodissociation calculations. The parameters A_n and B_n for the ranges 222–304 nm and 210–300 K are as follows:

$A_0 = -206.2$	$B_0 = 1.0460 \times 10^{-1}$
$A_1 = 2.3726$	$B_1 = -1.4124 \times 10^{-3}$
$A_2 = -1.0527 \times 10^{-2}$	$B_2 = 6.9015 \times 10^{-6}$
$A_3 = 1.9239 \times 10^{-5}$	$B_3 = -1.5164 \times 10^{-8}$
$A_4 = -1.2242 \times 10^{-8}$	$B_4 = 1.3990 \times 10^{-11}$

Burkholder et al. [120] give the expansion

$$\ln \sigma(\lambda, T) = (\sum A_i (\lambda - 268.7998)^i) (1 + (296–T) \sum B_i (\lambda - 268.7998)^i)$$

and report the following parameters A_i and B_i for the ranges 235–260 nm and 210–296 K:

$A_0 = -44.42756$	$B_0 = 1.481886 \times 10^{-4}$
$A_1 = -1.464955 \times 10^{-1}$	$B_1 = 6.77182 \times 10^{-6}$
$A_2 = -5.692188 \times 10^{-4}$	$B_2 = 1.154347 \times 10^{-7}$
$A_3 = 1.155366 \times 10^{-5}$	$B_3 = -2.77145 \times 10^{-11}$
$A_4 = -1.399502 \times 10^{-7}$	$B_4 = -6.619515 \times 10^{-11}$

Burkholder et al. [120] also report a parameterization for cross sections extrapolated to 400 nm:

$$\ln \sigma(\lambda, T) = (\sum A_i (\lambda - 301.0104)^i) (1 + (296–T) \sum B_i (\lambda - 301.0104)^i)$$

and report the following parameters A_i and B_i for the ranges 260-400 nm and 210-296 K:

$A_0 = -49.50456$	$B_0 = 3.616315 \times 10^{-4}$
$A_1 = -1.633525 \times 10^{-1}$	$B_1 = 5.534952 \times 10^{-6}$
$A_2 = 5.170758 \times 10^{-6}$	$B_2 = -1.997903 \times 10^{-8}$
$A_3 = 4.332654 \times 10^{-6}$	$B_3 = -9.234512 \times 10^{-11}$
$A_4 = -3.899051 \times 10^{-8}$	$B_4 = 1.776346 \times 10^{-12}$

According to J. Burkholder (priv. comm.), there are several errors in the original Burkholder et al. publication [120]. In this paper, the parameterization equation is written in terms of $\log_{10}(\sigma(\lambda,T))$ but the correct expression should be given in terms of $\ln(\sigma(\lambda,T))$. In addition, the parameterization equation for extrapolated cross section data is incorrect. These errors were repeated in JPL02-25 but have been corrected in this evaluation.

The quantum yield for formation of CF_2O and Br_2 in the photolysis of CF_2Br_2 at 206, 248, and 302 nm, in the presence of O_2 has been measured to be unity by Molina and Molina [541], independent of pressure, in contrast to an earlier report by Walton [834] that the quantum yield at 265 nm decreases from unity when the system pressure is raised to 50 Torr of CO_2. Primary quantum yields for Br atom formation, $\Phi(Br) = 1.96 \pm 0.27$, 1.63 ± 0.19, and 1.01 ± 0.15, in the photodissociation of CF_2Br_2 at 193, 222, and 248 nm, respectively, were measured at 298 K by Talukdar et al. [771]. A quantum yield for CF_2 formation, $\Phi(CF_2) = 1.15 \pm 0.30$, in the 193-nm photolysis was reported by Talukdar et al. [768].

The transient CF_2Br was detected by molecular beam [420] and spectroscopic studies [294, 813] during photolysis at 248 nm, and confirm that the C-Br bond is broken.

Table 4-161. Absorption Cross Sections of CF_2Br_2 at 295–296 K

λ (nm)	10^{20} σ (cm^2)	λ (nm)	10^{20} σ (cm^2)	λ (nm)	10^{20} σ (cm^2)
170	124.5	228	253.4	286	0.336
172	78.1	230	244.7	288	0.245
174	55.3	232	230.2	290	0.178
176	49.5	234	211.9	292	0.128
178	60.3	236	191.6	294	0.0926
180	75.0	238	169.3	296	0.0672
182	86.6	240	147.3	298	0.0487
184	100.9	242	125.8	300	0.0352
186	111.8	244	106.0	302	0.0253
188	118.0	246	87.8	304	0.0183
190	115.9	248	72.0	306	0.0130
192	110.3	250	58.3	308	0.00919
194	101.6	252	46.5	310	0.00650
196	91.4	254	36.8	312	0.00456
198	82.1	256	28.9	314	0.00319
200	74.9	258	22.4	316	0.00222
202	71.7	260	17.3	318	0.00157
204	73.4	262	13.1	320	0.00105
206	80.7	264	9.90	*322*	*0.000759*
208	93.0	266	7.47	*324*	*0.000531*
210	110.0	268	5.59	*326*	*0.000371*
212	131.0	270	4.17	*328*	*0.000260*
214	154.9	272	3.08	*330*	*0.000182*
216	180.4	274	2.27	*332*	*0.000127*
218	204.7	276	1.66	*334*	*0.000089*
220	226.0	278	1.21	*336*	*0.000062*
222	244.2	280	0.888	*338*	*0.000044*
224	253.3	282	0.647	*340*	*0.000030*
226	256.8	284	0.470		

Note:
170 188 nm: Gillotay and Simon [277]
190–304 nm: mean of Gillotay and Simon [277], Orkin and Kasimovskaya [602], and Burkholder et al. [120]
306–320 nm: mean of Orkin and Kasimovskaya [602] and Burkholder et al. [120]
322–340 nm: extrapolation of mean of Orkin and Kasimovskaya [602], and Burkholder et al. [120] data.

G25. CF_2ClBr (Halon-1211) + hν → Products. The absorption cross sections of CF_2ClBr have been measured at room temperature and 191–307 nm by Giolando et al. [283]; at 190–330 nm by Molina et al. [545]; at 190–304 nm by Orkin and Kasimovskaya [602]; at 210–295 K and 170–302 nm by Gillotay and Simon [277]; and at 210–296 K and 190–320 nm by Burkholder et al. [120]. The agreement between the room temperature data of Orkin and Kasimovskaya [602], Gillotay and Simon [277], and Burkholder et al. [120] is very good in the region of the absorption band, i.e., within 10% over the range 190–240 nm and within 3% in the maximum at 205–206 nm, with one exception: Gillotay and Simon [277] observed a structure near the absorption maximum, different from the other observations, which resulted in values higher by about 10% at 200–202 nm. Molina et al. [545] reported values for the range 190–240 nm which are lower by 10–20% than the above mentioned data. The few data points (at 10-nm intervals) of Giolando et al. [283] fit well to the absorption curves reported by Orkin and Kasimovskaya [602], Gillotay and Simon [277], and Burkholder et al. [120]. The deviations between the various data sets increase at longer wavelengths to ≤30% at 300 nm and up to 55% at 320 nm. The preferred absorption cross sections at 295–298 K, listed in Table 4-162, are the values of Gillotay and Simon [277] at 170–188 nm; the mean of the values reported by Molina et al. [545], Gillotay and Simon [277], Burkholder et al. [120] and Orkin and Kasimovskaya [602] at 190–302 nm; the mean of the values reported by Molina et al. [545], Burkholder et al. [120], and Orkin and Kasimovskaya [602] at 304 nm; and the mean of the values reported by Molina et al. [545] and Burkholder et al. [120] at 306–320 nm.

Measurements in the far UV at 60–220 nm were reported by Doucet et al. [221].

Both studies of the temperature dependence show an increase of the absorption cross sections in the absorption band around 204–206 nm with decreasing temperature 296–210 K and the reverse effect at wavelengths above 233 nm and below 180 nm. Gillotay and Simon [277] observed a regular temperature behavior, i.e., an increase of the maximum absorption cross section by ~0.05×10^{-18} cm^2 $molecule^{-1}$ per 20 K temperature decrease. Burkholder et al. [120] observed a less pronounced temperature behavior (the maximum absorption cross sections agree within 2.5%), so that their maximum cross section at 210 K is lower by 15% than that observed by Gillotay and Simon [277] (in contrast to the cross sections at room temperature which are within 4%). Different parameterizations for the temperature dependence of the absorption cross section have been proposed. Gillotay and Simon [277] give the polynomial expansion

$$\log_{10} \sigma(\lambda, T) = \sum A_n \lambda^n + (T - 273) \times \sum B_n \lambda^n$$

and report smoothed values for T = 210, 230, 250, 270, and 295 K, every 2 nm, and at wavelengths corresponding to the wavenumber intervals generally used in stratospheric photodissociation calculations. The parameters A_n and B_n for the ranges 200–302 nm and 210–300 K are as follows:

$A_0 = -134.80$	$B_0 = 3.3070 \times 10^{-1}$
$A_1 = 1.7084$	$B_1 = -5.0957 \times 10^{-3}$
$A_2 = -9.1540 \times 10^{-3}$	$B_2 = 2.9361 \times 10^{-5}$
$A_3 = 2.1644 \times 10^{-5}$	$B_3 = -7.6198 \times 10^{-8}$
$A_4 = -1.9863 \times 10^{-8}$	$B_4 = 7.6825 \times 10^{-11}$

Burkholder et al. [120] give the expansion

$$\ln \sigma(\lambda, T) = (\sum A_i (\lambda - 259.8989)^i) (1 + (296 - T) \sum B_i (\lambda - 259.8989)^i)$$

and report the following parameters A_i and B_i for the ranges 220–260 nm and 210–296 K:

$A_0 = -45.4087$	$B_0 = 1.528905 \times 10^{-4}$
$A_1 = -1.304811 \times 10^{-1}$	$B_1 = 6.024833 \times 10^{-6}$
$A_2 = -6.995443 \times 10^{-4}$	$B_2 = 1.030995 \times 10^{-7}$
$A_3 = 6.159709 \times 10^{-6}$	$B_3 = -6.387931 \times 10^{-11}$
$A_4 = -9.384074 \times 10^{-9}$	$B_4 = -3.718503 \times 10^{-11}$

Burkholder et al. [120] also report a parameterization for cross sections extrapolated to 400 nm:

$$\ln \sigma(\lambda, T) = (\sum A_i (\lambda - 292.2083)^i) (1 + (296-T) \sum B_i (\lambda - 292.2083)^i)$$

and report the following parameters A_i and B_i for the ranges 260-400 nm and 210-296 K:

$A_0 = -50.15428$	$B_0 = 3.778659 \times 10^{-4}$
$A_1 = -1.547025 \times 10^{-1}$	$B_1 = 6.338322 \times 10^{-6}$
$A_2 = -9.551083 \times 10^{-5}$	$B_2 = -1.294407 \times 10^{-8}$
$A_3 = 4.076334 \times 10^{-6}$	$B_3 = -2.430137 \times 10^{-10}$
$A_4 = -2.747685 \times 10^{-8}$	$B_4 = 2.234599 \times 10^{-12}$

According to J. Burkholder (priv. comm.), there are several errors in the original Burkholder et al. publication [120]. In this paper, the parameterization equation is written in terms of $\log_{10}(\sigma(\lambda,T))$ but the correct expression should be given in terms of $\ln(\sigma(\lambda,T))$. In addition, the parameterization equation for extrapolated cross section data is incorrect. These errors were repeated in JPL02-25 but have been corrected in this evaluation.

Quantum yields for Cl and Br atom formation in the photodissociation of CF_2ClBr at 193, 222, and 248 nm, $\Phi(Cl) = 1.03 \pm 0.14$, 0.27 ± 0.04, and 0.18 ± 003, $\Phi(Br) = 1.04 \pm 0.13$, 0.86 ± 0.11, and 0.75 ± 0.13, respectively, and a quantum yield for CF_2 formation in the 193-nm photolysis, $\Phi(CF_2) = 0.91 \pm 0.30$, were measured at 298 K by Talukdar et al. [768].

Table 4-162. Absorption Cross Sections of CF_2ClBr at 295–298 K

λ (nm)	10^{20} σ (cm^2)	λ (nm)	10^{20} σ (cm^2)	λ (nm)	10^{20} σ (cm^2)
170	323.0	222	68.3	274	0.250
172	234.2	224	60.4	276	0.184
174	176.0	226	52.7	278	0.135
176	120.9	228	45.7	280	0.0991
178	84.7	230	39.2	282	0.0724
180	58.1	232	33.8	284	0.0527
182	41.9	234	28.8	286	0.0385
184	35.0	236	24.4	288	0.0282
186	34.1	238	20.4	290	0.0205
188	38.9	240	16.9	292	0.0148
190	46.1	242	13.9	294	0.0106
192	57.0	244	11.4	296	0.00764
194	69.1	246	9.28	298	0.00544
196	81.4	248	7.50	300	0.00391
198	93.5	250	5.99	302	0.00279
200	106.0	252	4.76	304	0.00207
202	113.3	254	3.76	306	0.00161
204	117.4	256	2.94	308	0.00113
206	118.7	258	2.29	310	0.000803
208	117.7	260	1.76	312	0.000569
210	114.2	262	1.36	314	0.000403
212	108.5	264	1.03	316	0.000288
214	101.5	266	0.784	318	0.000213
216	93.6	268	0.593	320	0.000159
218	85.3	270	0.447		
220	76.8	272	0.336		

Note:
170–188 nm: Gillotay and Simon [277]
190–302 nm: mean of Molina et al. [545], Gillotay and Simon [277], Burkholder et al. [120], and Orkin and Kasimovskaya [602]
304 nm: mean of Molina et al. [545], Burkholder et al. [120], and Orkin and Kasimovskaya [602]
306–320 nm: mean of Molina et al. [545] and Burkholder et al. [120].

G26. CF_3Br (Halon-1301) + hν → CF_3 + Br. The absorption cross sections of CF_3Br have been measured at room temperature and 207–255 nm by Davidson [205]; at 170–230 nm by Roxlo and Mandl [692]; at 180–400 nm by Pence et al. [629]; at 190–300 nm by Molina et al. [545]; at 190–270 nm by Orkin and Kasimovskaya [602]; at 210–295 K and 168–280 nm by Gillotay and Simon [277]; and at 210–296 K and 190–285 nm by Burkholder et al. [120]. The agreement between the room temperature data is very good, i.e., 10% and better, in the region of the absorption band between 190 and 230 nm with the exception of the data of Davidson [205] below 210 nm and the whole data set of Roxlo and Mandl [692]. Pence et al. [629] report a plot of the absorbance (in arbitrary units) and give for 193 nm an absorption cross section smaller by one order of magnitude than the rest of the data for 193 nm. At wavelengths above 250 nm, Burkholder et al. [120] and Orkin and Kasimovskaya [602] measured higher values (up to ~ 35% at 270 nm) than those reported by Molina et al. [545] and Gillotay and Simon [277]. The preferred absorption cross sections at 295–298 K, listed in Table 4-163, are the values of Gillotay and Simon [277] at 168–188 nm, the mean of the values reported by Molina et al. [545], Gillotay and Simon [277], Burkholder et al. [120], and Orkin and Kasimovskaya [602] at 190–270 nm, the mean of the values reported by Molina et al. [545], Gillotay and Simon [277], and Burkholder et al. [120] at 272–280 nm, and the values of Molina et al. [545] at 295–300 nm.

Measurements in the far UV at 60–220 nm were reported by Doucet et al. [221].

Both studies of the temperature dependence show an increase of the absorption cross sections in the absorption band between 174 and 216 nm with decreasing temperature 296–210 K and the reverse effect at wavelengths above 218 nm and below 174 nm. Gillotay and Simon [277] observed a regular temperature behavior, i.e., an increase of the maximum absorption cross section by ~0.06×10^{-19} cm^2 $molecule^{-1}$ per 20 K temperature decrease. Burkholder et al. [120] observed a less pronounced temperature behavior (the maximum absorption cross sections agree within 2%), so that their maximum cross section at 210 K is lower by ~25% than that observed by Gillotay and Simon [277] (in contrast to the cross sections at room

temperature which are within 6%). Different parameterizations for the temperature dependence of the absorption cross section have been proposed. Gillotay and Simon [277] give the polynomial expansion

$$\log_{10} \sigma(\lambda, T) = \sum A_n \lambda^n + (T - 273) \times \sum B_n \lambda^n$$

and report smoothed values for T = 210, 230, 250, 270, and 295 K, every 2 nm, and at wavelengths corresponding to the wavenumber intervals generally used in stratospheric photodissociation calculations. The parameters A_n and B_n for the ranges 178–280 nm and 210–300 K are as follows:

$A_0 = 62.563$	$B_0 = -9.1755 \times 10^{-1}$
$A_1 = -2.0068$	$B_1 = 1.8575 \times 10^{-2}$
$A_2 = 1.6592 \times 10^{-2}$	$B_2 = -1.3857 \times 10^{-4}$
$A_3 = -5.6465 \times 10^{-5}$	$B_3 = 4.5066 \times 10^{-7}$
$A_4 = 6.7459 \times 10^{-8}$	$B_4 = -5.3803 \times 10^{-10}$

Burkholder et al. [120] give the expansion

$$\ln \sigma(\lambda, T) = (\sum A_i (\lambda - 242.2466)^i) (1 + (296 - T) \sum B_i (\lambda - 242.266)^i)$$

and report the following parameters A_i and B_i for the ranges 214–285 nm and 210–296 K:

$A_0 = -46.70542$	$B_0 = 1.694026 \times 10^{-4}$
$A_1 = -1.55047 \times 10^{-1}$	$B_1 = 8.723247 \times 10^{-6}$
$A_2 = -1.020187 \times 10^{-3}$	$B_2 = 5.953165 \times 10^{-9}$
$A_3 = 2.246169 \times 10^{-5}$	$B_3 = -3.872168 \times 10^{-9}$
$A_4 = -1.300982 \times 10^{-7}$	$B_4 = -1.803325 \times 10^{-11}$

According to J. Burkholder (priv. comm.) there is a typographical error in the original Burkholder et al. publication [120]. In this paper, the parameterization equation is written in terms of $\log_{10} \sigma(\lambda, T)$ but the correct expression should be given in terms of $\ln \sigma(\lambda, T)$. This error was repeated in JPL02-25 but has been corrected in this evaluation.

Quantum yields for Br ($Br(^2P_{3/2}$ + $Br^*(^2P_{1/2})$) atom formation in the photodissociation of CF_3Br at 193 and 222 nm, $\Phi(Br+Br^*) = 1.12 \pm 0.16$ and 0.92 ± 0.15, respectively, were measured at 298 K by Talukdar et al. [771]. A quantum yield for $Br^*(^2P_{1/2})$ atom formation at 193 nm, $\Phi(Br^*) = 0.56 \pm 0.05$, was reported by Pence et al. [629].

Table 4-163. Absorption Cross Sections of CF_3Br at 295–298 K

λ (nm)	10^{20} σ (cm^2)	λ (nm)	10^{20} σ (cm^2)	λ (nm)	10^{20} σ (cm^2)
168	0.517	210	12.1	252	0.107
170	0.696	212	11.4	254	0.0743
172	0.928	214	10.6	256	0.0516
174	1.22	216	9.71	258	0.0357
176	1.60	218	8.65	260	0.0248
178	2.05	220	7.56	262	0.0171
180	2.61	222	6.50	264	0.0118
182	3.26	224	5.47	266	0.00827
184	4.02	226	4.52	268	0.00580
186	4.88	228	3.69	270	0.00399
188	5.82	230	2.91	272	0.00271
190	6.56	232	2.32	274	0.00188
192	7.58	234	1.80	276	0.00129
194	8.63	236	1.39	278	0.00092
196	9.61	238	1.04	280	0.00064
198	10.5	240	0.766	285	0.00022
200	11.3	242	0.563	290	0.00008
202	11.9	244	0.414	295	0.00003
204	12.4	246	0.296	300	0.00001
206	12.5	248	0.212		
208	12.4	250	0.149		

Note:
170–188 nm: Gillotay and Simon [277]
190–270 nm: mean of Molina et al. [545], Gillotay and Simon [277], Burkholder et al. [120] and Orkin and Kasimovskaya [602]
272–280 nm: mean of Molina et al. [545] and Burkholder et al. [120]
285–300 nm: Molina et al. [545].

G27. CH_2=CHBr + hν → Products. The absorption spectrum of bromoethene (vinylbromide) has been measured at room temperature and 164 -254 nm by Orkin et al. [604]. The spectrum shows a very strong absorption band with the maximum at 192 nm, characteristic of the CH_2=CBr- group, and the absorption band of the CH_2=CH- group around 170 nm. Orkin et al. [604] recorded the spectrum at 0.5-nm increments. In Table 4-164 are listed their data selected at 2-nm intervals for the wavelength region 184-254 nm.

Table 4-164. Absorption Cross Sections of CH_2=CHBr at 295 K

λ (nm)	10^{20} σ (cm^2)	λ (nm)	10^{20} σ (cm^2)	λ (nm)	10^{20} σ (cm^2)
184	1970	208	306	232	18.2
186	2320	210	266	234	12.6
188	2710	212	232	236	8.47
190	3000	214	198	238	5.70
192	3160	216	166	240	3.69
194	2950	218	136	242	2.43
196	2470	220	109	244	1.58
198	1800	222	85.9	246	1.03
200	996	224	65.3	248	0.683
202	605	226	49.1	250	0.454
204	440	228	35.7	252	0.315
206	359	230	25.5	254	0.225

Note:
184-254 nm, Orkin et al. [604].

G28. $CHBr=CF_2$ + hν → Products. The absorption spectrum of 1-bromo-2,2-difluoroethene has been measured at room temperature and 164-266 nm by Orkin et al. [604]. The spectrum shows strong absorption bands between 164 and 190 nm, a weaker and less pronounced band between 190 and 210 nm (maximum 194 nm), and a still weaker band above 210 nm with the maximum near 220 nm. Orkin et al. [604] recorded the spectrum at 0.5-nm increments. In Table 4-165 are listed their data selected at 2-nm intervals for the wavelength region 184-266 nm.

Table 4-165. Absorption Cross Sections of $CHBr=CF_2$ at 295 K

λ (nm)	10^{20} σ (cm^2)	λ (nm)	10^{20} σ (cm^2)	λ (nm)	10^{20} σ (cm^2)	λ (nm)	10^{20} σ (cm^2)
184	2160	206	87.6	228	74.0	250	8.81
186	1020	208	70.1	230	68.2	252	6.51
188	670	210	63.4	232	61.3	254	4.75
190	635	212	63.5	234	53.7	256	3.49
192	671	214	66.7	236	45.9	258	2.54
194	703	216	71.1	238	38.8	260	1.86
196	610	218	75.8	240	31.7	262	1.37
198	471	220	79.3	242	25.5	264	1.04
200	306	222	80.7	244	20.1	266	0.796
202	193	224	80.6	246	15.4		
204	124	226	78.4	248	11.7		

Note:
184-266 nm, Orkin et al. [604].

G29. $CFBr=CF_2 + h\nu \rightarrow$ Products. The absorption spectrum of trifluorobromoethene has been measured at room temperature and 164-274 nm by Orkin et al. [604]. The spectrum shows strong absorption bands between 164 and 188 nm, a weaker and less pronounced band between 188 and 213 nm (maximum 194.5 nm), and a still weaker band above 213 nm with the maximum near 229 nm. Orkin et al. [604] recorded the spectrum at 0.5-nm increments. In Table 4-166 are listed their data selected at 2-nm intervals for the wavelength region 184-274 nm.

Table 4-166. Absorption Cross Sections of $CFBr=CF_2$ at 295 K

λ (nm)	10^{20} σ (cm^2)	λ (nm)	10^{20} σ (cm^2)	λ (nm)	10^{20} σ (cm^2)	λ (nm)	10^{20} σ (cm^2)
184	456	208	56.1	232	58.1	256	6.87
186	367	210	39.5	234	54.7	258	5.15
188	350	212	34.1	236	50.4	260	3.77
190	373	214	34.5	238	45.1	262	2.78
192	415	216	37.7	240	39.5	264	2.04
194	439	218	42.2	242	33.9	266	1.49
196	434	220	47.2	244	28.5	268	1.09
198	412	222	52.1	246	23.5	270	0.812
200	354	224	56.2	248	19.2	272	0.613
202	263	226	59.0	250	15.2	274	0.469
204	167	228	60.4	252	11.8		
206	95.1	230	60.0	254	9.03		

Note:
184-274 nm, Orkin et al. [604].

G30. $CH_2=CBrCF_3 + h\nu \rightarrow$ Products. The absorption spectrum of 2-bromo-3,3,3-trifluoro-1-propene has been measured at room temperature and 164-254 nm by Orkin et al. [604]. The spectrum shows a very strong absorption band above 174 nm with the maximum at 194 nm, characteristic of the $CH_2=CBr-$ group. Orkin et al. [604] recorded the spectrum at 0.5–nm increments. In Table 4-167 are listed their data selected at 2-nm intervals for the wavelength region 184-252 nm.

Table 4-167. Absorption Cross Sections of CH_2=$CBrCF_3$ at 295 K

λ (nm)	10^{20} σ (cm^2)	λ (nm)	10^{20} σ (cm^2)	λ (nm)	10^{20} σ (cm^2)	λ (nm)	10^{20} σ (cm^2)
184	1370	202	1520	220	126	238	6.97
186	1700	204	1080	222	97.3	240	4.77
188	2040	206	774	224	73.1	242	3.26
190	2350	208	581	226	54.9	244	2.22
192	2590	210	440	228	40.1	246	1.50
194	2700	212	338	230	28.8	248	1.02
196	2620	214	263	232	20.5	250	0.705
198	2370	216	208	234	14.4	252	0.496
200	1980	218	162	236	10.2		

Note:
184-252 nm, Orkin et al. [604].

G31. CF_3CH_2Br (Halon-2301) + hν → Products. The absorption cross sections of CF_3CH_2Br have been measured at 295 K and 190–294 nm by Orkin and Kasimovskaya [602]. Their results are listed in Table 4-168.

Table 4-168. Absorption Cross Sections of CF_3CH_2Br at 295 K

λ (nm)	10^{20} σ (cm^2)	λ (nm)	10^{20} σ (cm^2)	λ (nm)	10^{20} σ (cm^2)
190	45.4	226	16.6	262	0.190
192	49.5	228	14.1	264	0.137
194	52.5	230	11.9	266	0.0983
196	54.4	232	9.85	268	0.0705
198	55.1	234	8.10	270	0.0504
200	54.7	236	6.58	272	0.0361
202	53.3	238	5.28	274	0.0258
204	51.2	240	4.20	276	0.0184
206	48.6	242	3.31	278	0.0132
208	45.7	244	2.58	280	0.0096
210	42.5	246	2.01	282	0.0069
212	39.1	248	1.53	284	0.0048
214	35.7	250	1.16	286	0.0034
216	32.2	252	0.876	288	0.0025
218	28.8	254	0.653	290	0.0018
220	25.5	256	0.484	292	0.0013
222	22.3	258	0.357	294	0.0011
224	19.4	260	0.261		

Note:
190–294 nm, Orkin and Kasimovskaya [602].

G32. $CF_3CHClBr$ (Halon-2311) + hν →. CF_3CHCl + Br

$CF_3CHClBr$ (Halon-2311) + hν →. CF_3CHBr + Cl. The absorption cross sections of $CF_3CHClBr$ have been measured at room temperature and 190–310 nm by Orkin and Kasimovskaya [602]; at 210–295 K and 170–290 nm by Gillotay et al. [281]; at 223–298 K and 200–310 nm by Bilde et al. [69]; and at 295 K and 193.3 nm by Taketani et al. [763]. The room temperature values are in good agreement within 5–15% at wavelengths below 280 nm, where Gillotay et al. [281], [278] report the lowest, Orkin and Kasimovskaya [602] the highest values. At wavelengths above 280 nm, the data of Bilde et al. [69] become increasingly higher (up to 100% at 310 nm) than those of Orkin and Kasimovskaya [602]. The preferred absorption cross sections, listed in Table 4-169, are the values of Gillotay et al. [281] at 170–188 nm; the mean of the values reported by Gillotay et al. [281] and Orkin and Kasimovskaya [602] at 190–198 nm; the mean of the values reported by the three groups at 200–290 nm; and the mean of the values reported by Orkin and Kasimovskaya [602] and Bilde et al. [69] at 292–310 nm. Taketani et al. [763] reported a value of 107×10^{-20} cm^2 $molecule^{-1}$ at 193.3 nm.

The study of the temperature dependence by Gillotay et al. [281] shows an increase of the absorption cross sections in the absorption band between 192 and 238 nm with decreasing temperature 295–210 K and the reverse effect at wavelengths above 238 nm and below 192 nm; the increase in the absorption maximum at ~202 nm is ~0.024×10^{-18} cm^2 $molecule^{-1}$ per 20 K temperature decrease, i.e., an increase by ~10% between 295 and 210 K. Bilde et al. [69] observed a less pronounced temperature behavior in the absorption band (the

maximum absorption cross sections agree within 3%) and a decrease of the absorption cross sections with decreasing temperature at wavelengths above 214 nm.

Gillotay and Simon [281] parameterized the cross sections and the temperature dependence of the absorption cross section by the polynomial expansion

$$\log_{10} \sigma(\lambda, T) = \sum A_n \lambda^n + (T - 273) \times \sum B_n \lambda^n$$

and report smoothed values for T = 210, 230, 250, 270, and 295 K, every 2 nm, and at wavelengths corresponding to the wavenumber intervals generally used in stratospheric photodissociation calculations. The parameters A_n and B_n for the ranges 190–290 nm and 210–300 K are as follows:

$A_0 = -127.157358$	$B_0 = -7.959828 \times 10^{-2}$
$A_1 = 1.635435$	$B_1 = 1.978026 \times 10^{-3}$
$A_2 = -9.002683 \times 10^{-3}$	$B_2 = -1.627866 \times 10^{-5}$
$A_3 = 2.190678 \times 10^{-5}$	$B_3 = 5.480744 \times 10^{-8}$
$A_4 = -2.062651 \times 10^{-8}$	$B_4 = -6.480935 \times 10^{-11}$

Note: There was a typographical error in JPL02-25 for parameter A_4. The error has been corrected in the present evaluation.

Taketani et al. [763] reported the total yield of Cl atoms as 0.28 ± 0.02 in the photodissociation of $CF_3CHClBr$ at 193.3 nm, implying that the rupture of the C-Br bond should be dominant photodissociation channel.

Table 4-169. Absorption Cross Sections of $CF_3CHClBr$ at 295–298 K

λ (nm)	10^{20} σ (cm^2)	λ (nm)	10^{20} σ (cm^2)	λ (nm)	10^{20} σ (cm^2)
170	702.6	218	78.7	266	0.980
172	614.6	220	71.0	268	0.765
174	496.8	222	63.3	270	0.575
176	379.8	224	56.3	272	0.444
178	281.1	226	49.5	274	0.339
180	206.1	228	43.3	276	0.258
182	153.3	230	37.3	278	0.196
184	118.4	232	32.2	280	0.149
186	97.1	234	27.6	282	0.111
188	86.6	236	23.6	284	0.0818
190	93.4	238	20.0	286	0.0606
192	99.8	240	16.8	288	0.0448
194	107.1	242	14.0	290	0.0331
196	114.3	244	11.7	292	0.0263
198	119.7	246	9.51	294	0.0198
200	121.5	248	7.79	296	0.0147
202	123.0	250	6.38	298	0.0109
204	122.3	252	5.15	300	0.00808
206	119.7	254	4.13	302	0.00583
208	115.1	256	3.31	304	0.00450
210	109.0	258	2.63	306	0.00313
212	102.0	260	2.06	308	0.00235
214	94.6	262	1.61	310	0.00180
216	86.7	264	1.26		

Note:
170–188 nm, Gillotay et al. [281], [278],
190–198 nm, mean of Gillotay et al. [278, 281] and Orkin and Kasimovskaya [602],
200–290 nm, mean of Gillotay et al. [278, 281], Orkin and Kasimovskaya [602], and Bilde et al. [69],
292–310 nm, mean of Orkin and Kasimovskaya [602] and Bilde et al. [69].

G33. CF_3CHFBr (Halon-2401) + hν → Products. The absorption cross sections of CF_3CHFBr have been measured at 295 K and 190–280 nm by Orkin and Kasimovskaya [602]. Their results are listed in Table 4-170.

Table 4-170. Absorption Cross Sections of CF_3CHFBr at 295 K

λ (nm)	10^{20} σ (cm^2)	λ (nm)	10^{20} σ (cm^2)	λ (nm)	10^{20} σ (cm^2)
190	24.9	222	11.0	254	0.226
192	26.1	224	9.38	256	0.166
194	27.0	226	7.91	258	0.121
196	27.5	228	6.58	260	0.0873
198	27.7	230	5.42	262	0.0628
200	27.4	232	4.42	264	0.0450
202	26.9	234	3.53	266	0.0325
204	26.0	236	2.79	268	0.0235
206	24.8	238	2.19	270	0.0171
208	23.4	240	1.69	272	0.0124
210	21.9	242	1.30	274	0.0093
212	20.2	244	0.991	276	0.0069
214	18.3	246	0.736	278	0.0053
216	16.5	248	0.556	280	0.0040
218	14.6	250	0.416		
220	12.8	252	0.308		

Note:
190–280 nm, Orkin and Kasimovskaya [602].

G34. CF_2BrCF_2Br (Halon-2402) + hν → Products. The absorption cross sections of CF_2BrCF_2Br have been measured at room temperature and 195–320 nm by Molina et al. [545] and at 190–300 nm by Orkin and Kasimovskaya [602]; at 210–295 K and 170–280 nm by Gillotay et al. [281], and at 210–296 K and 190–320 nm by Burkholder et al. [120]. The room temperature data are in very good agreement, in the absorption band at 180–240 nm generally within 10%, in the absorption maximum at ~200 nm within 5%, and in the long-wavelength tail up to 310 nm within 15%. The preferred absorption cross sections at 295–298 K, listed in Table 4-171, are the values of Gillotay et al. [281] at 170–186 nm; the mean of the values reported by Molina et al. [545], Gillotay et al. [281], Burkholder et al. [120], and Orkin and Kasimovskaya [602] at 196–280 nm; the mean of the values reported by Molina et al. [545], Burkholder et al. [120], and Orkin and Kasimovskaya [602] at 282–300 nm; and the mean of the values reported by Molina et al. [545] and Burkholder et al. [120] at 302–320 nm. In the region around 190 nm, there is some uncertainty, because there is no continuous transition between the absorption curve of Gillotay et al. [281] and that obtained by averaging the data of Gillotay et al. [281], Burkholder et al. [120], and Orkin and Kasimovskaya [602]. We therefore smoothed the absorption curve between 186 and 196 nm and give estimated values for 188, 190, 192, and 194 nm.

The results of the two temperature studies are rather controversial. A regular, but weak decrease of the absorption cross sections at 194–280 nm with decreasing temperature 295 to 210 K and the reverse effect below 194 nm was observed by Gillotay et al. [281]; the decrease in the absorption maximum at ~200 nm is $\sim 0.010 \times 10^{-18}$ cm^2 $molecule^{-1}$ per 20-K temperature decrease, i.e., a decrease by ~4% between 295 and 210 K. Burkholder et al. [120] observed a strong increase over the whole absorption band (increase of the absorption maximum by 20%) with decreasing temperature 296–210 K, and the reverse effect above 230 nm. So, low-temperature data of these two groups are not comparable. Different parameterizations of the temperature dependence of the absorption cross section have been proposed. Gillotay and Simon [281] give the polynomial expansion

$$\log_{10} \sigma(\lambda, T) = \sum A_n \lambda^n + (T - 273) \times \sum B_n \lambda^n$$

and report smoothed values for T = 210, 230, 250, 270, and 295 K, every 2 nm, and at wavelengths corresponding to the wavenumber intervals generally used in stratospheric photodissociation calculations. The parameters A_n and B_n for the ranges 190–290 nm and 210–300 K are as follows:

$A_0 = 34.026000$ $\quad B_0 = 4.010664 \times 10^{-1}$
$A_1 = -1.152616$ $\quad B_1 = -8.358968 \times 10^{-3}$
$A_2 = 8.959798 \times 10^{-3}$ $\quad B_2 = 6.415741 \times 10^{-5}$
$A_3 = -2.9089 \times 10^{-5}$ $\quad B_3 = -2.157554 \times 10^{-7}$
$A_4 = 3.307212 \times 10^{-8}$ $\quad B_4 = 2.691871 \times 10^{-10}$

Burkholder et al. [120] give the expansion

$$\ln \sigma(\lambda, T) = (\sum A_i (\lambda - 242.4015)^i) (1 + (296–T) \sum B_i (\lambda - 242.4015)^i)$$

and report the following parameters A_i and B_i for the ranges 190–320 nm and 210–296 K:

$A_0 = -43.69218$ $B_0 = 3.301341 \times 10^{-5}$
$A_1 = -1.124704 \times 10^{-1}$ $B_1 = 4.695917 \times 10^{-6}$
$A_2 = -1.213301 \times 10^{-3}$ $B_2 = 6.128629 \times 10^{-8}$
$A_3 = 5.275007 \times 10^{-6}$ $B_3 = -5.443107 \times 10^{-10}$
$A_4 = 6.936195 \times 10^{-8}$ $B_4 = -1.035596 \times 10^{-11}$

According to J. Burkholder (priv. comm.) there is a typographical error in the original Burkholder et al. publication [120]. In this paper, the parameterization equation is written in terms of $\log_{10} \sigma(\lambda, T)$ but the correct expression should be given in terms of $\ln \sigma(\lambda, T)$. This error was repeated in JPL02-25 but has been corrected in this evaluation.

Quantum yields for Br atom formation in the photodissociation of CF_2BrCF_2Br at 193, 233, and 266 nm, $\Phi(Br) = 1.9 \pm 0.1$, 1.9 ± 0.1, and 1.4 ± 0.1, respectively, were measured at room temperature by Zou et al. [885]. These values indicate bond breaking of both C–Br bonds in nearly all the CF_2BrCF_2Br molecules at 193 and 233 nm and in an appreciable fraction of the parent molecules still at 266 nm.

Table 4-171. Absorption Cross Sections of CF_2BrCF_2Br at 296 K

λ (nm)	10^{20} σ (cm^2)	λ (nm)	10^{20} σ (cm^2)	λ (nm)	10^{20} σ (cm^2)
170	50.9	222	59.6	274	0.112
172	56.4	224	52.6	276	0.0813
174	62.3	226	45.9	278	0.0592
176	68.5	228	39.7	280	0.0428
178	75.1	230	33.9	282	0.0300
180	81.8	232	28.8	284	0.0216
182	88.6	234	24.1	286	0.0152
184	95.3	236	19.9	288	0.0109
186	101.8	238	16.4	290	0.00784
188	*107.0*	240	13.2	292	0.00569
190	*112.0*	242	10.6	294	0.00410
192	*116.5*	244	8.45	296	0.00301
194	*120.0*	246	6.68	298	0.00219
196	122.3	248	5.25	300	0.00161
198	123.7	250	4.03	302	0.00124
200	124.3	252	3.12	304	0.00094
202	123.6	254	2.37	306	0.00071
204	120.3	256	1.78	308	0.00054
206	115.9	258	1.34	310	0.00042
208	110.4	260	0.973	312	0.00033
210	104.2	262	0.718	314	0.00026
212	97.4	264	0.529	316	0.00020
214	90.1	266	0.390	318	0.00016
216	82.4	268	0.287	320	0.00014
218	74.8	270	0.211		
220	67.0	272	0.154		

Note: 170–186 nm: Gillotay et al. [281]
188–194 nm: values estimated by smoothing the absorption curve
196–280 nm: mean of Molina et al. [545], Gillotay et al. [281], Burkholder et al. [120], and Orkin and Kasimovskaya [602]
282–300 nm: mean of Molina et al. [545], Burkholder et al. [120], and Orkin and Kasimovskaya [602]
302–320 nm: mean of Molina et al. [545] and Burkholder et al. [120].

G35. CF_3CF_2Br (Halon-2501) + hν → Products. Table 4-172 lists the absorption cross sections of CF_3CF_2Br measured at room temperature and reported at 5-nm intervals by Molina et al. [545]. The results of Zhang et al. [881], who report a plot on a logarithmic scale for measured values at 200–250 nm, are about 30% larger over that wavelength range than the results of Molina et al. [545]. Pence et al. [629] measured the absorption cross sections at 180–400 nm, report a plot of the absorbance (in arbitrary units) and give for 193 nm an absorption cross section smaller by ~ 40% than that reported by Molina et al. [545].

Broad band flash photolysis of CF_3CF_2Br produced $Br^*(^2P_{1/2})$ atoms with a quantum yield $\Phi(Br^*) = 0.48 \pm 0.02$ as reported by Ebenstein et al. [224]. A quantum yield for $Br^*(^2P_{1/2})$ atom formation at 193 nm, $\Phi(Br^*)$

= 0.16 ± 0.08, was reported by Pence et al. [629].

Table 4-172. Absorption Cross Sections of CF_3CF_2Br at 298 K

λ (nm)	10^{20} σ (cm^2)	λ (nm)	10^{20} σ (cm^2)	λ (nm)	10^{20} σ (cm^2)
190	18.1	230	3.83	270	0.0112
195	18.4	235	2.22	275	0.00505
200	18.1	240	1.20	280	0.00218
205	16.9	245	0.620	285	0.00100
210	14.8	250	0.305	290	0.00045
215	12.0	255	0.135	295	0.00020
220	8.94	260	0.0590	300	0.00009
225	6.13	265	0.0260		

Note:
190–300 nm, Molina et al. [545].

G36. $CH_3CH_2CH_2Br + h\nu \rightarrow$ Products.

G37. $CH_3CHBrCH_3 + h\nu \rightarrow$ Products. The absorption spectra of 1-bromopropane (n-propyl bromide) and 2-bromopropane (isopropyl bromide) have been measured at room temperature and 164-270 nm by Kozlov et al. [419]. The spectra show an absorption band above 180 nm with maxima at~201 nm for 1-bromopropane and ~209 nm for 2-bromopropane, respectively, and structured features below 180 nm characteristic of the C-Br band absorptions in bromoalkanes. In Table 4-173 are listed the absorption cross sections reported by Kozlov et al. [419] at 2-nm intervals over the stratospheric transparency window near 200 nm

Table 4-173. Absorption Cross Sections of $CH_3CH_2CH_2Br$ and $CH_3CHBrCH_3$ at 295 K

λ (nm)	10^{20} σ (cm^2)		λ (nm)	10^{20} σ (cm^2)	
	$CH_3CH_2CH_2Br$	$CH_3CHBrCH_3$		$CH_3CH_2CH_2Br$	$CH_3CHBrCH_3$
180	108.5	220.2	206	68.8	43.5
182	29.9	36.5	208	65.2	44.2
184	29.5	18.2	210	61.0	44.2
186	35.6	17.6	212	56.5	43.6
188	42.7	19.4	214	51.5	42.2
190	49.8	22.1	216	46.6	40.1
192	56.5	24.8	218	41.4	37.4
194	62.5	28.0	220	35.8	34.1
196	67.0	31.3	222	30.8	30.7
198	70.2	34.3	224	26.0	27.1
200	71.8	37.3	226	21.8	23.6
202	72.6	39.9	228	17.8	20.2
204	71.2	42.0	230	14.4	16.8

Note: 180-230 nm, Kozlov et al. [419].

G38. $CH_3C(O)CH_2Br + h\nu \rightarrow$ Products. The absorption cross sections of bromoacetone have been measured at 238-296 K and 210-370 nm by Burkholder et al. [111] at a resolution of .6 nm using a diode array spectrometer. The spectrum shows an absorption band above 255 nm with the maximum at ~299 nm of $\sigma = 1.15 \times 10^{-19}$ cm^2 $molecule^{-1}$ at room temperature and a rapid increase of the absorption cross sections below 255 nm to a second stronger band at or below 210 nm with $\sigma \leq 6 \times 10^{-19}$ cm^2 $molecule^{-1}$ at room temperature. The averages over 1-nm intervals of the medium-resolution absorption spectrum are listed in Table 4-174. A slight, but not systematic, decrease of the absorption cross-sections with decreasing temperature was observed only around the absorption minimum and in the long-wavelength wings of both absorption bands.

Photodissociation quantum yields were measured by Burkholder et al. [111] as 1.6 ± 0.25 at 308 nm and 1.0 ± 0.15 at 351 nm. At both wavelengths, the yields of CO and CO_2 were unity and ~0.5, respectively, whereas the yield of HCOOH was measured as 0.15 and that of HBr as ~0.15.

Table 4-174. Absorption Cross Sections of $CH_3C(O)CH_2Br$ at 296 K

λ (nm)	10^{20} σ (cm^2)	λ (nm)	10^{20} σ (cm^2)	λ (nm)	10^{20} σ (cm^2)	λ (nm)	10^{20} σ (cm^2)
210	59.2	248	6.40	286	9.78	324	5.55
211	58.0	249	6.07	287	9.98	325	5.20
212	57.5	250	5.77	288	10.2	326	4.87
213	56.2	251	5.49	289	10.4	327	4.55
214	53.2	252	5.25	290	10.6	328	4.24
215	50.7	253	5.14	291	10.8	329	3.94
216	48.4	254	4.98	292	11.0	330	3.64
217	46.2	255	4.88	293	11.1	331	3.35
218	43.9	256	4.76	294	11.2	332	3.06
219	41.8	257	4.68	295	11.3	333	2.77
220	39.7	258	4.62	296	11.4	334	2.51
221	37.5	259	4.66	297	11.4	335	2.26
222	35.6	260	4.70	298	11.5	336	2.02
223	33.9	261	4.76	299	11.5	337	1.80
224	32.0	262	4.72	300	11.5	338	1.60
225	30.1	263	4.79	301	11.4	339	1.41
226	28.5	264	4.91	302	11.4	340	1.24
227	26.8	265	5.01	303	11.3	341	1.09
228	25.2	266	5.12	304	11.2	342	0.955
229	23.7	267	5.39	305	11.1	343	0.831
230	22.1	268	5.44	306	11.1	344	0.724
231	20.7	269	5.57	307	10.9	345	0.627
232	19.4	270	5.77	308	10.7	346	0.545
233	18.1	271	6.03	309	10.4	347	0.473
234	16.9	272	6.25	310	10.2	348	0.408
235	15.7	273	6.48	311	9.89	349	0.351
236	14.7	274	6.68	312	9.62	350	0.303
237	13.6	275	6.90	313	9.36	351	0.259
238	12.6	276	7.16	314	9.10	352	0.223
239	11.7	277	7.45	315	8.82	353	0.190
240	10.9	278	7.74	316	8.52	354	0.164
241	10.2	279	8.00	317	8.19	355	0.140
242	9.47	280	8.25	318	7.83	356	0.120
243	8.80	281	8.50	319	7.45	357	0.108
244	8.18	282	8.75	320	7.06	358	0.0952
245	7.68	283	9.04	321	6.66	359	0.0838
246	7.22	284	9.29	322	6.28	360	0.0784
247	6.79	285	9.58	323	5.89		

Note:
210-360 nm, Burkholder et al. [111].

PHOTOCHEM-H- IODINE

H1. $I_2 + h\nu \rightarrow 2\ I$. The absorption cross sections of iodine have been measured at room temperature and 440-650 nm by Rabinowitch and Wood [647]; at 105-220 nm by Myer and Samson [569]; at 420-800 nm by Tellinghuisen [775]; at 170-230 nm by Roxlo and Mandl [692]; and at 182-750 nm by Saiz-Lopez et al. [697]. Measurements at single wavelengths (436 and 500 nm) were reported by Bauer et al. [58]. The rest of the measurements (from the years 1923 to 1966) have been carried out at elevated temperatures: at 321-673 K and 400-600 nm by Vogt and Koenigsberger [822]; at 353 K and 450-580 nm and at 613 K and 230-600 nm by Kortüm and Friedheim [418]; at 423 to 1323 K and 360-740 nm by Sulzer and Wieland [757]; at 393 K and 600-800 nm by Mathieson and Rees [495]; and at 348 K and 400-650 nm by McMillan [144, 510].

The UV absorption spectrum of iodine shows strong absorption below 200 nm with maxima near 187-188 nm and 183 nm ($\sigma \approx (2\text{-}4) \times 10^{-17}$ cm^2 molecule^{-1}) and a rapid decrease of the cross sections down to $\sigma \approx 1 \times 10^{-20}$ cm^2 molecule^{-1} between 360 and 400 nm. The visible absorption spectrum shows a broad band between 400 and 650 nm, which is continuous below 500 nm, but shows pronounced rovibrational structure between 500 and 630 nm, which is due to the transition from the $X^1\Sigma$ ground state into the bound $B^3\Pi$ upper state. There is also a weaker underlying continuum in the structured region, due to the transition to the $^1\Pi$ repulsive state. The maximum is near 533 nm. At longer wavelengths above 650 nm, there is evidence for another weak absorption band.

The most recent room temperature results of Saiz-Lopez et al. [697] were obtained with a Fourier transform spectrometer at a resolution of 4 cm^{-1} (0.1 nm at 500 nm). The room temperature cross sections of Tellinghuisen [775], who recorded the spectrum with a continuum source of moderate resolution (~2.5 nm), are lower than those of Saiz-Lopez et al. [697] in the continuous region, i.e. lower within 30% at 420-450 nm and within 10% at 450-500 nm. Considering averages over 5-nm intervals of the high-resolution spectrum of Saiz-Lopez et al. [697] for the banded region, there is again good agreement (within 15%) with the results of Tellinghuisen [775]. Discrepancies between these two spectra appear above 600 nm: the results of Saiz-Lopez et al. [697] are larger by up to 35% than those of Tellinghuisen [775] at 600-670 nm; above 670 nm a more rapid decrease of the cross sections is observed by Saiz-Lopez et al. [697] compared to that observed by Tellinghuisen [775], where the cross sections of Saiz-Lopez et al [697] become lower by factors ~2 and ~20 at 710 and 740 nm, respectively. The cross sections obtained by Bauer et al. [58] $(1.41 \pm 0.05) \times 10^{-18}$ at 436 nm and $(2.25 \pm 0.09) \times 10^{-18}$ cm^2 molecule^{-1} at 500 nm are in close agreement with the integrated averages of Saiz-Lopez et al. [697]. The absorption curve reported by Rabinowitch and Wood [647] is different from those described above: it is shifted to lower wavelengths with the maximum at 500 nm and a hump near 550 nm.

It has to be noted that in the structured region the measurements of the cross sections have been found to be very dependent on the experimental conditions such as absolute I_2 concentrations and the bath gas pressure. The measurements of Saiz-Lopez et al. [697] were performed at high bath gas pressure and high resolution, so to better define the shape of the spectrum. As recommended absorption cross sections for iodine in the UV and visible regions, listed in Table 4-175, we take the averages over 5-nm intervals calculated from the reported values (at 1-nm intervals for the regions 182-500 nm and 640-750nm, and at 0.1-nm intervals at 500-640 nm) by Saiz-Lopez et al. [697]. In Table 4-176 are given the absorption cross sections for the maxima and minima in the banded region reported by Saiz-Lopez et al. [697].

The photodissociation quantum yields for the production of I atoms were obtained by Brewer and Tellinghuisen [88] by measuring the $I(^2P_{3/2})$ yield using the atomic fluorescence technique under condition of steady-state irradiation of I_2 at 12 wavelengths in the region 500-630 nm. The reported yields were determined relative to the purely dissociative continuum at 292 nm, where a unity quantum yield is assumed.

Table 4-175. Absorption Cross Sections of I_2 at 295 K

λ (nm)	10^{20} σ (cm^2)	λ (nm)	10^{20} σ (cm^2)	λ (nm)	10^{20} σ (cm^2)	λ (nm)	10^{20} σ (cm^2)
185	1853	315	15.1	445	25.8	575	96.6
190	2012	320	12.2	450	33.3	580	92.7
195	1226	325	10.5	455	44.0	585	74.1
200	732	330	7.79	460	57.1	590	65.8
205	519	335	6.18	465	72.2	595	59.4
210	418	340	4.71	470	89.7	600	47.4
215	352	345	4.08	475	109	605	43.3
220	302	350	2.58	480	131	610	40.8
225	290	355	1.94	485	155	615	34.4
230	225	360	1.24	490	179	620	30.5
235	197	365	1.02	495	204	625	28.2
240	169	370	0.659	500	228	630	28.0
245	147	375	0.823	505	254	635	22.6
250	128	380	1.14	510	277	640	23.6
255	110	385	1.01	515	297	645	22.8
260	97.1	390	0.925	520	309	650	21.6
265	84.2	395	1.11	525	319	655	20.7
270	72.9	400	2.93	530	326	660	19.0
275	63.1	405	3.89	535	320	665	17.3
280	54.4	410	4.43	540	306	670	17.7
285	45.9	415	5.44	545	281	675	15.9
290	38.9	420	5.96	550	265	680	14.9
295	32.4	425	8.32	555	237	685	13.9
300	27.4	430	13.5	560	191	690	12.8
305	23.1	435	15.7	565	155	695	10.9
310	18.1	440	20.3	570	130	700	10.3

Note:
185-700 nm, Saiz-Lopez et al. [697].

Table 4-176. Cross Sections at the Maxima and Minima of I_2 at 295 K

λ (nm) Maximum	10^{20} σ (cm^2)	λ (nm) minimum	10^{20} σ (cm^2)	λ (nm) maximum	10^{20} σ (cm^2)	λ (nm) minimum	10^{20} σ (cm^2)
500.6	232.5	500.7	231.5	543.6	406.7	545.1	225.3
500.8	233.9	501.0	231.0	545.4	240.5	545.6	219.9
501.1	235.9	501.2	233.7	545.8	371.9	547.4	231.3
501.4	236.6	501.6	234.8	547.6	246.7	548.1	208.0
501.8	239.6	501.9	236.3	548.4	372.2	549.7	226.5
502.1	240.5	502.4	238.8	550.0	251.7	550.6	197.1
502.6	246.5	502.8	240.6	550.8	347.6	552.1	220.6
503.0	247.8	503.3	240.6	552.4	256.8	553.2	187.0
503.5	252.3	503.8	241.0	553.5	321.4	554.6	211.2
504.0	254.4	504.4	243.7	554.8	257.7	555.8	176.3
504.5	255.6	504.9	245.1	556.2	299.4	557.1	200.3
505.2	263.2	505.6	252.0	557.5	254.2	558.6	161.2
505.8	268.7	506.2	252.7	559.0	263.9	559.8	186.1
506.5	271.6	507.0	252.3	560.1	250.0	561.5	126.8
507.2	275.4	507.7	253.7	561.9	203.1	562.7	153.9
507.9	281.7	508.5	254.6	562.9	216.0	564.5	103.7
508.7	284.4	509.3	255.0	564.9	175.0	565.4	143.7
509.6	291.1	510.3	262.8	565.8	208.0	567.5	96.9
510.5	301.6	511.2	264.1	568.1	142.9	568.4	115.4
511.5	308.1	512.2	266.0	568.7	203.5	569.5	131.4
512.5	309.9	513.3	263.0	569.9	139.8	570.7	70.3
513.6	323.1	514.4	266.1	571.0	127.5	571.4	113.9
514.7	325.9	515.6	266.4	571.7	147.2	573.9	76.1
515.9	334.3	516.8	265.0	574.9	131.8	577.3	68.8
517.1	345.9	518.1	269.2	578.1	122.6	580.7	62.7
518.3	353.6	519.4	266.0	581.4	109.7	584.3	51.8
519.8	356.6	520.9	267.1	585.1	105.4	587.8	48.6
521.1	371.0	522.3	267.3	588.7	95.9	591.7	42.4
522.7	379.3	523.9	259.8	592.1	85.7	595.4	42.8
524.2	384.5	525.4	261.4	596.0	80.5	599.1	34.3
525.8	393.7	527.2	252.8	599.6	76.0	603.0	31.6
527.4	398.8	528.9	258.7	603.5	64.3	606.8	28.8
529.2	407.8	530.8	252.2	607.6	53.8	610.8	30.3
531.0	415.9	532.7	242.1	611.8	49.1	614.6	26.4
533.0	423.8	534.7	242.8	615.5	42.5	618.8	26.7
534.9	416.4	536.7	232.6	620.0	37.4	622.2	22.3
537.0	414.8	538.8	224.4	623.6	35.8	627.0	23.1
539.1	409.3	541.0	216.5	628.2	31.8	629.8	24.0
541.4	406.1	543.0	218.5				

Note:
500.6-629.8 nm, Saiz-Lopez et al [697].

H2. $IO + h\nu \rightarrow I + O(^3P)$

$IO + h\nu \rightarrow I + O(^1D)$. The absorption cross sections of iodine monoxide have been measured in the region of the A $^2\Pi_{3/2} \leftarrow$ X $^2\Pi_{3/2}$ electronic transition between 338 and 488 nm. The A –X band shows a smooth shoulder between 340 and 380 nm and some broad peaks superimposed on the continuum which maximizes around 400 nm. Pronounced vibrational structure is seen above 400 nm, the (7,0) to (0,0) and (3,1) to (1,1) bands could be assigned in the absorption spectra recorded at medium resolution. Of special interest (e.g., for the study of the reaction kinetics of IO) is the absorption cross section of the strongest vibrational peak (4,0) at 427.2 nm. The various studies (photolysis of N_2O/I_2, N_2O/CF_3I, and O_3/I_2 mixtures) and the corresponding (4,0) peak cross sections at room temperature are compiled in the following summary:

Table 4-177. Summary of Cross Section Measurements of IO

Reference	Year	Temperature, K	Wavelength Range, nm	Resolution, nm	σ(427.2 nm), 10^{-17} cm^2
Cox and Coker [188]	1983	303	415-470	0.27	3.1 (+2.0/-1.5)
Jenkin and Cox [372]	1985	303	426.9	0.27	2.2 ± 0.5
Sander [701]	1986	250, 273, 298, 317, 341, 373	427.2	0.17	3.1 ± 0.3
Stickel et al. [753]	1988	300	420-455 444.8-446.4	0.3 0.025	3.1 ± 0.6
Laszlo et al. [436]	1995	295	340-447	0.3	2.8 ± 0.5
Harwood et al [312]	1997	203, 220, 250, 338-488		0.14	3.6 ± 0.5*
		253, 275, 298, 323, 353, 373		0.44	3.0 ± 0.4
Atkinson et al. [28]	1999	295	444.48-447.83, 454.98-457.88	0.0013	
			445.04, 455.17	0.7	
Bloss et al. [15]	2001	220, 250, 273, 295, 325	342-455	1.13	1.9 ± 0.17

* Average value between 203 and 373 K (see text below)

At ambient temperature the general shape of the vibrational spectrum is similar for the spectra reported by Laszlo et al. [436], Harwood et al. [312] and Bloss et al. [80], however the difference in the size of the structural features depends on the resolution employed in the various studies. The absorption cross sections measured by Harwood et al. [312] at a resolution of 0.44 nm and scaled to 0.83 of the value obtained for the (4,0) maximum at high (0.14 nm) resolution generally (with exceptions for the region 350-415 nm, see below) are higher than those measured at a resolution of 0.3 nm by Lazlo et al [436] and of 1.13 nm by Bloss et al. [80]. The latter data are the lowest throughout the spectral region 340-465 nm; they are smaller than the values reported by Harwood et al. [312] by factors mostly of 1.5 in the continuous part of the spectrum and at the vibrational maxima, and smaller by factors up to 5 at the minima. Bloss et al. [80] attributed this difference to an underlying absorption due to the absorbing species I_2O_2, considered to be a product of the IO self-reaction.

The absorption curve reported by Laszlo et al. [436] is higher by a factor of ~1.2-1.5 at 350-370 nm and in the maxima of the 395-405-nm region than those reported by Harwood et al. [312], and is very similar to that curve in the region of the (6,0) to (4,0) maxima. The absorption cross section measured by Atkinson et al. [28] at an ultra-high resolution of 0.0013 nm for the (2,0) maximum is higher by a factor of nearly 5 than that measured by Harwood et al. [312], whereas the cross sections reported by Atkinson et al. [28] and Harwood et al. [312] for the (1,0) maximum are nearly the same.

The recommended cross sections were obtained by the following procedure: (1) the spectra of Harwood et al. [312] and Laszlo et al. [436] were degraded to the resolution of the spectrum of Bloss et al. [80] (1.13 nm), (2) the degraded spectra of Harwood et al. [312] were normalized to the (4,0) peak value of Bloss et al. [80], (3) the mean of the degraded and normalized spectra of Harwood et al. [312] and Laszlo et al. [436] and that of Bloss et al. [80] were calculated and averaged over 1 nm intervals. These values are listed in Table 4-178. The recent studies from Dillon et al. and Gómez Martin et al. are noted but were not considered in the present evaluation.

The temperature dependence of the absorption cross section of the (4,0) peak has been studied at 250-373 K by Sander [701]; at 203-373 K by Harwood et al. [312]; and at 220-325 K by Bloss et al. [80]. Sander [701]

observed a significant increase of σ(427 nm) from (2.1 ± 0.1) × 10^{-17} cm^2 $molecule^{-1}$ at 373 K to (5.3 ± 0.5) × 10^{-17} cm $molecule^{-1}$ at 250 K upon flash photolysis of O_2/I_2 mixtures. Bloss et al. [80] observed a less pronounced increase of the absorption cross sections by approximately 40% (σ(T)/σ(295 K) ≈ 0.85 to 1.23) between 325 and 220 K (laser flash photolysis of O_2/I_2 mixtures). Harwood et al. [312], applying laser flash photolysis of N_2O/CF_3I, O_3/I_2, and N_2O/I_2 mixtures, measured absorption cross sections between (3.1 ± 0.4) × 10^{-17} and (3.9 ± 0.1) × 10^{-17} cm^2 $molecule^{-1}$ independent of the temperature (203–373 K) and derived an average value of (3.6 ± 0.5) × 10^{-17} cm^2 $molecule^{-1}$ from the data obtained with the N_2O/CF_3I system.

The quantum yield for $O(^3P)$ formation following photolysis of IO at 355 nm was measured relative to NO_2 photolysis at the same wavelength and was determined as 0.91 ($^{+019}_{-0.26}$) by Ingham et al. [362]. The lifetime of the A $^2\Pi_{3/2}$ was observed to be < 20 ns by Turnipseed et al. [788], indicating that electronic collisional quenching cannot compete with the dissociation into $O(^3P)$ + I, thus confirming the results of Ingham et al. [362].

Table 4-178. Absorption Cross Sections of IO at 298 K

λ (nm)	10^{20} σ (cm^2)	λ (nm)	10^{20} σ (cm^2)	λ (nm)	10^{20} σ (cm^2)	λ (nm)	10^{20} σ (cm^2)
339	81.2	373	381	407	606	441	219
340	118	374	413	408	578	442	168
341	100	375	422	409	643	443	183
342	107	376	402	410	813	444	195
343	89	377	413	411	1010	445	957
344	96.2	378	435	412	976	446	805
345	86.2	379	463	413	786	447	392
346	126	380	504	414	589	448	214
347	112	381	548	415	568	449	269
348	108	382	472	416	414	450	156
349	142	383	435	417	460	451	96.9
350	160	384	523	418	734	452	102
351	154	385	560	419	1380	453	87.3
352	165	386	591	420	1200	454	100
353	163	387	603	421	681	455	457
354	181	388	580	422	365	456	441
355	185	389	598	423	253	457	213
356	194	390	622	424	204	458	132
357	207	391	620	425	205	459	183
358	223	392	617	426	302	460	123
359	230	393	642	427	2050	461	82.3
360	242	394	684	428	1370	462	51.9
361	247	395	694	429	543	463	53.6
362	242	396	709	430	309	464	38.2
363	241	397	701	431	208	465	43.4
364	268	398	654	432	173	466	118
365	273	399	671	433	166	467	134
366	291	400	671	434	177	468	67.2
367	313	401	700	435	653	469	24.2
368	326	402	765	436	1880	470	125
369	343	403	859	437	807	471	76.4
370	346	404	864	438	381		
371	339	405	787	439	249		
372	360	406	667	440	256		

Note:
339-471 nm: see text

H3. $OIO + h\nu \rightarrow IO(^2\Pi) + O(^3P)$

$OIO + h\nu \rightarrow I(^2P_J) + O_2$. A qualitative absorption spectrum (optical densities vs. wavelengths) at 298 K and 476-667 nm was first reported by Himmelmann et al. [331], who observed a highly structured absorption band belonging to the A ($^2A_2$) (i,j,k) ← X ($^2B_1$) (0,0,0) vibronic transitions with vibrational progressions of the symmetric I-O stretch (i = 0-9) and the O-I-O bend (j = 0, 1, 2) in the upper electronic state. A first assessment indicated that the absorption cross section at 549.1 nm (in air, resolution of 0.3 nm) is larger than 2.5×10^{-17} cm^2 molecule^{-1} (see however Table 4-179). Absorption cross sections have been measured at room temperature and 514-573 nm at medium resolution of 1.13 nm by Cox et al. [186] and Bloss et al. [80], and at 558-578 nm at high resolution better than 0.006 nm (cavity ring-down spectroscopy) by Ashworth et al. [26]. The vibrational peaks at 562 and 568 nm recorded at high resolution are higher by a factor ~1.7 than those reported at medium resolution. As a recommendation (with a factor of 3 uncertainty) are listed in Table 4-179 the averages over 1-nm intervals of the data reported (at intervals of 0.22 and 0.23 nm) by Bloss et al. [80].

Photodissociation of OIO was studied at a laser wavelength of 532 nm by Ingham et al. [362]. O(^{3}P) atoms were not detected, which enabled the authors to place an upper limit to the quantum yield of $\Phi(O(^3P)) < 0.012$ (this assessment however is based on too high an absorption cross section of $(2.4 \pm 1.0) \times 10^{-17}$ cm^2 molecule^{-1} for OIO at 532 nm). Since photolysis to IO +O can be excluded, Ashworth et al. [26] implied that OIO must largely predissociate to I + O_2 via the upper $^2B_2$ state. Ingham et al. [362] detected I(^2P_J) atoms at very high laser fluence, presumably in a sequential two-photon process. An upper limit for the quantum yield, $\Phi(I(^2P_J)) < 0.15$, was determined.

Table 4-179. Absorption Cross Sections of OIO at 295 K

λ (nm)	10^{20} σ (cm^2)	λ (nm)	10^{20} σ (cm^2)	λ (nm)	10^{20} σ (cm^2)	λ (nm)	10^{20} σ (cm^2)
516	833	531	989	546	582	561	476
517	696	532	1012	547	513	562	769
518	565	533	779	548	665	563	709
519	599	534	636	549	1030	564	524
520	719	535	519	550	842	565	442
521	626	536	643	551	575	566	384
522	573	537	709	552	429	567	613
523	517	538	640	553	377	568	937
524	496	539	548	554	609	569	699
525	534	540	470	555	661	570	475
526	754	541	451	556	604	571	322
527	840	542	494	557	474	572	224
528	697	543	715	558	393		
529	626	544	817	559	373		
530	651	545	676	560	350		

Note:
516-572 nm, Bloss et al. [80].

H4. $HI + h\nu \rightarrow H + I(^2P_{3/2})$

$HI + h\nu \rightarrow H + I^*(^2P_{1/2})$. The absorption spectrum of hydrogen iodide has been measured at room temperature and 200-368 nm by Goodeve and Taylor [290]; at 149-159, 164-175, and 178-244 nm by Romand [684]; at 200-300 nm by Huebert and Martin [352]; at 192-313 nm by Ogilvie [593]; at 170-230 nm by Roxlo and Mandl [692]; at 198–341 nm by Campuzano-Jost and Crowley [148]; and at 195 K and 180-195 K by Huebert and Martin [352]. Single cross sections at room temperature and 254 nm and 147 nm were reported by Bridges and White [90] and Rebbert et al. [665], respectively. The spectrum shows, according to the most recent measurements by Campuzano-Jost and Crowley [148] and those of Huebert and Martin [352], Ogilvie [593], and Roxlo and Mandl [692], an absorption band between 185 and 375 nm with the maximum near 222 nm and a strong absorption peak at 176 nm. There is good agreement between the results of Campuzano-Jost and Crowley [148], Ogilvie [593], and Huebert and Martin [352]: the data reported by Huebert and Martin [352] and Campuzano-Jost and Crowley [148] are nearly identical around the absorption maximum up to ~275 nm; the data reported by Ogilvie [593] are slightly larger over the absorption band than those of the two former authors, where the agreement is better than 10% up to 290 nm and even better than 5% around the maximum from ~215 to 235 nm and in the wing between 255 and 285 nm. At wavelengths above ~280 nm, the three absorption curves are somewhat divergent: the cross sections reported by Huebert and Martin [352] become increasingly larger by up to 27%, those of Ogilvie [593] are smaller (within ~15%) than the cross sections reported by Campuzano-Jost and Crowley [148]. As a recommendation are listed in Table 4-180 the averages over 1-nm intervals of the high-resolution (0.08 nm) data of Campuzano-Jost and Crowley [148].

Martin and Willard [491] measured the quantum yield for H and I atoms in the photolysis at 184.9 and 253.7 nm to be near unity. The relative quantum yield for the formation of $I^*(^2P_{1/2}) = 0.47 \pm 0.03$ at 248 nm was determined by Brewer et al. [89]. Using a broadband flash photolysis, Donohue and Wiesenfeld [220] obtained a yield $I^*(^2P_{1/2}) = 0.10 \pm 0.05$. Recently a detailed study was performed by Langford et al. [433], measuring the branching ratio $I^*(^2P_{1/2}) / I(^2P_{3/2})$ at 24 different wavelengths in the range 200 to 303 nm, which they observed to increase from 0.2 near 208 nm to a maximum value of 1.7 near 252 nm, and to decrease again to 0.1 at 303 nm. In their paper, these authors review several similar studies performed previously and should be consulted for more detailed information.

Table 4-180. Absorption Cross Sections of HI at 298 K

λ (nm)	10^{20} σ (cm^2)	λ (nm)	10^{20} σ (cm^2)	λ (nm)	10^{20} σ (cm^2)	λ (nm)	10^{20} σ (cm^2)
199	59.7	235	71.9	271	16.1	307	1.29
200	61.1	236	70.6	272	15.1	308	1.19
201	62.4	237	69.2	273	14.2	309	1.10
202	63.7	238	67.6	274	13.3	310	1.01
203	65.0	239	66.2	275	12.5	311	0.929
204	66.4	240	64.6	276	11.7	312	0.852
205	67.7	241	62.9	277	10.9	313	0.781
206	69.0	242	61.3	278	10.2	314	0.715
207	70.3	243	59.6	279	9.57	315	0.653
208	71.5	244	57.9	280	8.94	316	0.596
209	72.7	245	56.1	281	8.36	317	0.544
210	73.8	246	54.2	282	7.81	318	0.495
211	74.8	247	52.5	283	7.30	319	0.450
212	75.9	248	50.7	284	6.82	320	0.409
213	76.9	249	48.8	285	6.37	321	0.371
214	77.7	250	47.0	286	5.94	322	0.336
215	78.4	251	45.2	287	5.55	323	0.303
216	79.1	252	43.5	288	5.18	324	0.274
217	79.7	253	41.7	289	4.83	325	0.247
218	80.2	254	39.9	290	4.51	326	0.223
219	80.5	255	38.2	291	4.21	327	0.200
220	80.8	256	36.5	292	3.92	328	0.180
221	80.9	257	34.8	293	3.66	329	0.162
222	81.0	258	33.2	294	3.41	330	0.145
223	80.9	259	31.6	295	3.18	331	0.130
224	80.7	260	30.0	296	2.96	332	0.116
225	80.4	261	28.5	297	2.76	333	0.104
226	80.0	262	27.1	298	2.57	334	0.0928
227	79.5	263	25.7	299	2.40	335	0.0828
228	78.9	264	24.3	300	2.23	336	0.0740
229	78.2	265	23.0	301	2.07	337	0.0660
230	77.4	266	21.7	302	1.92	338	0.0591
231	76.5	267	20.5	303	1.77	339	0.0528
232	75.5	268	19.4	304	1.64	340	0.0470
233	74.4	269	18.3	305	1.52		
234	73.2	270	17.2	306	1.40		

Note:
199-340 nm, Campuzano-Jost and Crowley [148].

H5. $HOI + h\nu \rightarrow OH + I$. The absorption spectrum of hypoiodous acid has been measured at room temperature and 280-500 nm by Bauer et al. [58], and at 280-450 nm by Rowley et al. [691]. Two absorption bands of comparable intensity were observed, one between 280 and ~375 nm with the maximum near 340 nm, and another on between ~375 and 500 nm with the maximum near 404-410 nm. The spectra of Bauer et al. [58] and Rowley et al. [691] are in reasonable agreement. Differences comparing the results of Rowley et al. [691] with those of Bauer et al. [58] are: the absorption maxima are shifted by 2-3 nm to smaller wavelengths; the low-wavelength maximum is slightly higher (~3%), whereas the long-wavelength maximum is smaller by ~15%. As a recommendation are listed in Table 4-181 the mean of the values reported by Rowley et al. [691] and Bauer et al. [58].

Table 4-181. Absorption Cross Sections HOI at 295-298 K

λ (nm)	10^{20} σ (cm^2)	λ (nm)	10^{20} σ (cm^2)	λ (nm)	10^{20} σ (cm^2)	λ (nm)	10^{20} σ (cm^2)
280	0.077	332	36.1	384	20.8	436	11.9
282	0.121	334	37.6	386	22.1	438	10.6
284	0.186	336	38.5	388	23.4	440	9.30
286	0.281	338	39.1	390	24.8	442	8.10
288	0.417	340	39.2	392	26.1	444	7.03
290	0.608	342	38.9	394	27.3	446	6.05
292	0.867	344	38.2	396	28.4	448	5.17
294	1.22	346	37.1	398	29.4	450	4.40
296	1.68	348	35.6	400	30.1	452	3.72
298	2.27	350	33.9	402	30.6	454	3.13
300	3.02	352	32.0	404	30.9	456	2.61
302	3.95	354	30.1	406	30.9	458	2.17
304	5.09	356	28.0	408	30.7	460	1.79
306	6.44	358	26.0	410	30.2	462	1.47
308	8.03	360	24.1	412	29.5	464	1.20
310	9.85	362	22.4	414	28.5	466	0.973
312	11.9	364	20.8	416	27.4	468	0.785
314	14.2	366	19.5	418	26.1	470	0.632
316	16.6	368	18.5	420	24.7	472	0.505
318	19.2	370	17.8	422	23.1	474	0.402
320	21.9	372	17.4	424	21.5	476	0.318
322	24.6	374	17.3	426	19.9	478	0.250
324	27.3	376	17.5	428	18.2	480	0.196
326	29.9	378	18.0	430	16.6		
328	32.2	380	18.8	432	15.0		
330	34.3	382	19.7	434	13.4		

Note:
280-480 nm, mean of the data of Bauer et al. [58] and Rowley et al. [691].

H6. $ICl + h\nu \rightarrow I(^3P_{3/2}) + Cl(^3P_{3/2})$ (1)
$ICl + h\nu \rightarrow I(^3P_{3/2}) + Cl^*(^3P_{1/2})$ (2)
$ICl + h\nu \rightarrow I^*(^3P_{1/2}) + Cl(^3P_{3/2})$ (3)
$ICl + h\nu \rightarrow I^*(^3P_{1/2}) + Cl^*(^3P_{1/2})$ (4). The absorption spectrum of iodine chloride has been measured at room temperature and 380-570 nm by Gibson and Ramsperger [267], at 220-600 nm by Seery and Britton [719], and at 210-690 nm by Jenkin et al. [375]. Measurements at 293, 387, 489, and 685 K and 216.5-310.0 nm have been carried out by Binder [70]. The spectrum shows two absorption bands of nearly equal height, one between 220 and 350 nm with the maximum at ~240-244 nm, and one between 350 and 600 nm with the maximum near 470 nm. The latter band is asymmetric because of the overlap of two or three bands corresponding to the transitions $B\ ^3\Pi_{0+} \leftarrow X\ ^1\Sigma_{0+}$, $^1\Pi \leftarrow X\ ^1\Sigma_{0+}$, and $A\ ^3\Pi_i \leftarrow X\ ^1\Sigma_{0+}$ as shown by Seery and Britton [719] and Mashnin et al. [493]. The experimental data of Seery and Britton [719] and Jenkin et al. [375] are in excellent agreement in the region of the visible absorption band, but appreciably higher (by ~35% in the maximum) than the earlier data of Gibson and Ramsperger [267]. The UV maximum observed by Jenkin et al. [375] is higher by ~14% than those observed by Gibson and Ramsperger [267] and Seery and Britton [719]. The higher absorption cross sections observed by Seery and Britton [719] between the two absorption bands between 290 and 360 nm are certainly due to Cl_2 impurities as argued by Jenkin et al. [375] who used purified samples and subtracted possible Cl_2 contributions in their spectral analysis.

Jenkin et al. [375] give a plot of the absorption spectrum and two numerical values for the absorption maxima: 5.00×10^{-19} cm^2 molecule^{-1} at 244 nm and 4.20×10^{-19} cm^2 molecule^{-1} at 467 nm; further numerical data are no more available. We therefore list in Table 4-182 these values together with the absorption cross sections read at 10-nm intervals from Fig.5 of the paper of Jenkin et al. [375]. For the region between the absorption bands at 310-350 nm, values $<1\times10^{-20}$ cm^2 molecule^{-1} can only be read from the plot (linear scaling of the σ axis) of Jenkin et al. [375].

The temperature study of Binder [70] shows a decrease of the absorption cross sections in the UV band with increasing temperature: in the maximum at 240 nm from 4.40×10^{-19} cm^2 molecule^{-1} at 293 K to 3.53×10^{-19} cm^2 molecule^{-1} at 685 K.

The relative quantum yields Cl*/(Cl* + Cl) in the photodissociation of ICl have been measured by several groups. The work of Mashnin et al. [493] shows that at longer wavelengths (437-532 nm) the Cl*($^3P_{1/2}$) are produced from the channel (2, I +Cl*), with a relative quantum yield varying between 0.41 ± 0.02 and 0.79 ± 0.02. Ni and Flynn [581] measured Cl*/(Cl* + Cl) at 237 nm as 0.17 ± 0.04, while Chichinin [167] obtained 0.67 ± 0.05 at 248 nm, and Chichinin et al. [168] 0.55 ± 0.05 at 530 nm. Tonokura et al. [781] measured in the wavelength range 235-248 nm, the contribution of channels (1, I + Cl), (2, I + Cl*) and (3, I* + Cl) to be 0.2, 0.4 and 0.4, respectively. The branching ratio I*/I = 0.71 ± 0.27 was also determined by Tonokura et al. [781], and by Jung et al. [398] at 304 nm as I*/I = 0.43.

Table 4-182. Absorption Cross Sections of ICl at 298 K

λ (nm)	10^{20} σ (cm^2)	λ (nm)	10^{20} σ (cm^2)	λ (nm)	10^{20} σ (cm^2)
210	7.4	340	<1	480	41.8
220	21.3	350	<1	490	40.0
230	40.0	360	2.3	500	35.4
240	49.0	370	4.6	510	29.0
244	50.0	380	8.74	520	21.1
250	47.8	390	13.8	530	15.6
260	36.8	400	19.0	540	11.0
270	24.4	410	25.0	550	7.3
280	12.9	420	28.5	560	5.5
290	6.4	430	32.0	570	4.2
300	3.2	440	35.4	580	3.4
310	<1	450	38.8	590	2.9
320	<1	460	41.7	600	2.1
330	<1	470	42.0		

Note:
210-600 nm, Jenkin et al. [375].

H7. $IBr + h\nu \rightarrow I(^3P_{3/2}) + Br(^3P_{3/2})$ (1)
$IBr + h\nu \rightarrow I(^3P_{3/2}) + Br^*(^3P_{1/2})$ (2)
$IBr + h\nu \rightarrow I^*(^3P_{1/2}) + Br(^3P_{3/2})$ (3)
$IBr + h\nu \rightarrow I^*(^3P_{1/2}) + Br^*(^3P_{1/2})$ (4). The absorption spectrum of iodine bromide has been measured at room temperature and 220-600 nm by Seery and Britton [719]. The spectrum shows two absorption bands, a weak one between 220 and 350 nm with the maximum at ~270 nm, and a stronger one between 350 and 600 nm with the maximum at ~500 nm. The absorption cross sections reported by Seery and Britton [719] are listed in Table 4-183.

Absolute quantum yields for Br* formation upon IBr photodissociation were measured by Haugen et al. [319] in the range 450-530 nm. The quantum yields show a steady increase from 0.28 at 450 nm to reach a maximum of 0.73 near 500 nm. Relative Br*/(Br + Br*) quantum yields measured by Peterson and Smith [631] varying from ~0.3 at 444 nm to a maximum of unity near 520 nm, declining to ~0.1 at 670 nm, and of Wrede et al. [853] in the range 440-544 nm display a similar trend. Kim et al. [406] measured at 267 nm the relative quantum yields for the photolysis channels (1, I + Br), (2, I + Br*) and (3, I* + Br) to be respectively 0.23, 0.35 and 0.42.

Table 4-183. Absorption Cross Sections of IBr at 298 K

λ (nm)	10^{20} σ (cm^2)	λ (nm)	10^{20} σ (cm^2)	λ (nm)	10^{20} σ (cm^2)
220	3.59	350	1.45	480	111
230	5.70	360	1.52	490	120
240	10.2	370	2.37	500	122
250	16.7	380	4.17	510	116
260	21.4	390	6.96	520	103
270	23.1	400	12.0	530	85.8
280	21.1	410	20.5	540	67.5
290	16.8	420	31.7	550	52.3
300	12.4	430	44.8	560	36.6
310	7.95	440	58.7	570	27.2
320	5.39	450	71.9	580	19.9
330	3.36	460	85.2	590	14.6
340	2.14	470	98.5	600	11.3

Note:
220-600 nm, Seery and Britton [719].

H8. $INO + h\nu \rightarrow I + NO$. The absorption cross sections of INO (nitrosyl iodide) have been measured at room temperature and 390-470 nm by Porter et al. [643], around 265 and 410 nm by van den Bergh and Troe [803], at 220-460 nm by Basco and Hunt [47], and at 223-300 nm and around 410 nm by Forte et al. [247]. The spectrum shows two absorption bands, a strong and asymmetric one in the UV between 220 and 300 nm with the maximum at 238 nm, and a second one, weaker by two orders of magnitude, between 355 and 470 nm with the maximum near 410 nm. The results for the UV band are in good agreement except for the region around 250 nm, where the absorption curve reported by Basco and Hunt [47] shows a hump and an absorption cross section larger by a factor of ~1.5 than that reported by Forte et al. [247]. The absorption curve in the near UV and visible reported by Porter et al. [643] is shifted to longer wavelengths by ~20 nm and the absorption cross sections are smaller by 50-30% at 400-430 nm compared to the results of Basco and Hunt [47].

As recommended absorption cross sections for the UV band we take the mean of the data of Basco and Hunt [47] and Forte et al. [247] at 223- 290 nm, and the data of Basco and Hunt [47] at 300 and 310 nm. For the absorption band in the near UV and visible we adopt the IUPAC (1982-2000) [61], [31], [30], [29] recommendations (which should be the mean of the data of Van den Berg and Troe [803], Basco and Hunt [47], and Forte et al. [247]), however after correcting the old errors for the values at 400 and 410 nm. The recommended cross sections are listed in Table 4-184.

Table 4-184. Absorption Cross Sections of INO at 298 K

λ (nm)	10^{20} σ (cm^2)	λ (nm)	10^{20} σ (cm^2)
223	225	360	45
230	1690	370	59
235	5640	380	65
238	6850	390	78
245	6000	400	92*
251	4880	410	110*
260	2270	420	100
270	1040	430	94
280	500	440	80
290	187	450	60
300	92	460	40
310	41		

Note:
223-290 nm, mean of Basco and Hunt [47] and Forte et al. [247],

300, 310 nm, Basco and Hunt [47],
360-460 nm, IUPAC-1982-2000 recommendations (* corrected) [61], [31], [30], [29].

H9. $IONO + h\nu \rightarrow I + NO_2$. The absorption cross sections of iodine nitrite have been measured at room temperature and 210-390 nm by Bröske [100]. The spectrum shows three broad bands with maxima of 4.20×10^{-18}, 9.6×10^{-19}, and 3.9×10^{-19} cm^2 $molecule^{-1}$ at 240, 282, and 342 nm, respectively. These values are only upper limits of the absorption cross sections assuming stoichiometric conversion of NO_2 to IONO in the photolysis of I_2 - NO_2 mixtures. The values listed in Table 4-185, which have to be considered as provisional, are taken from the IUPAC evaluation by Atkinson et al. [29].

Table 4-185. Absorption Cross Sections of IONO at 298 K

λ (nm)	10^{20} σ (cm^2)	λ (nm)	10^{20} σ (cm^2)	λ (nm)	10^{20} σ (cm^2)	λ (nm)	10^{20} σ (cm^2)
210	236	260	162	310	24.7	360	27.1
215	187	265	99.6	315	25.1	365	20.7
220	196	270	87.1	320	27.5	370	14.9
225	279	275	89.8	325	32.5	375	7.40
230	347	280	99.6	330	31.2	380	2.40
235	399	285	92.2	335	34.9	385	0.00
240	422	290	81.0	340	37.3	390	0.00
245	400	295	62.0	345	37.3		
250	330	300	37.3	350	29.8		
255	234	305	30.8	355	29.5		

Note:
210-390 m, Bröske [100], from IUPAC evaluation: Atkinson et al. [29].

H10. $IONO_2 + h\nu \rightarrow IO + NO_2$
$IONO_2 + h\nu \rightarrow I + NO$. The absorption cross sections of iodine nitrate produced in the gas phase by laser flash photolysis of $NO_2/CF_3I/N_2$ mixtures have been measured at room temperature in the spectral region 245-335 nm at a resolution of 1.67 nm and at 385-415 nm with a resolution of 0.55 nm by Mössinger et al. [562]. The cross sections for 335-385 nm, where absorption could not be recorded, were obtained by interpolation. The spectrum consists of a broad continuous absorption band. The cross sections averaged over 5-nm intervals are listed in Table 4-186.

Table 4-186. Absorption Cross Sections of $IONO_2$ at 298 K

λ (nm)	10^{20} σ (cm^2)	λ (nm)	10^{20} σ (cm^2)	λ (nm)	10^{20} σ (cm^2)	λ (nm)	10^{20} σ (cm^2)
245	1210	290	631	335	374	380	184
250	1170	295	577	340	360	385	153
255	1060	300	525	345	348	390	130
260	946	305	495	350	334	395	103
265	880	310	462	355	316	400	78.0
270	797	315	441	360	294	405	60.5
275	772	320	404	365	270	410	49.6
280	741	325	396	370	242	415	41.6
285	691	330	380	375	213		

Note:
245-415 nm, Mössinger et al. [562].

H11. $CH_3I + h\nu \rightarrow CH_3 + I(^2P_{3/2})$.
$CH_3I + h\nu \rightarrow CH_3 + I^*(^2P_{1/2})$. The absorption cross sections of CH_3I have been measured at room temperature and 147 nm by Rebbert et al. [665], at 200–360 nm by Porret and Goodeve [641], at 200–310 nm by Baughcum and Leone [60], at 180–400 nm by Pence et al. [629]; at 257.7 nm by Felps et al. [241], at 205–335 nm by Jenkin et al. [376], at 205–360 nm by Man et al. [472], and at 192–225 nm by Kwok and Phillips [427], who also measured the CH_3I spectrum in cyclohexane solution. Measurements were also carried out at 223–333 K and 160–330 nm by Fahr et al. [235]; at 243–333 K and 235–365 nm by Rattigan et al. [654]; and at 210–298 K and 200–350 nm by Roehl et al. [678]. Fahr et al. [235] also measured the absorption cross

sections at 330–400 nm for the liquid phase and used a wavelength-shift procedure to convert them into gas-phase values. The room temperature data for the absorption band at 210–305 nm are in reasonable to good agreement, whereby Rattigan et al. [654] report the lowest values and Fahr et al. [235] the highest values over the whole absorption band. The agreement generally is better than 15% except for the region around the absorption maximum where the spread is ~30%: Rattigan et al. [654] and Fahr et al. [235] report values of 1.07×10^{-18} cm^2 and 1.4×10^{-18} cm^2, respectively, for the maximum at ~260 nm, and the rest of the data ranges between 1.15×10^{-18} cm^2 and 1.22×10^{-18} cm^2. At wavelengths 305–330 nm, the agreement is still within 20%. At wavelengths below 210 nm, the few data points reported by Jenkin et al. [376] and Roehl et al. [678] and the absorption curve reported by Kwok and Phillips [426] obviously fit into the strong and highly structured band system observed by Fahr et al. [235] between 160 and 205 nm. The preferred room temperature absorption cross sections for the wavelength range above 210 nm, listed in Table 4-187, are the mean of the values reported by Jenkin et al. [376], Fahr et al. [235], and Roehl et al. [678] at 210–230 nm; the mean of the values reported by Jenkin et al. [376], Fahr et al. [235], Rattigan et al. [654], and Roehl et al. [678] at 235–330 nm; the mean of the values reported by Fahr et al. [235], Rattigan et al. [654], and Roehl et al. [678] at 335–350 nm; and the values of Rattigan et al. [654] at 355–365 nm. The data of Man et al. [472] are given only as a plot in their paper and have therefore not been included in the evaluation.

The three temperature studies are in qualitative agreement. An increase of the absorption cross sections in the absorption band at 210–270 nm with decreasing temperature 333–210 K has been observed. Very small temperature effects are reported by Rattigan et al. [654] for the temperature range 243–333 K, and by Fahr et al. [235] and Roehl et al. [678] for the range between room temperature and ~240–250 K and at 313–333 K. At wavelengths above 270 nm and below 210 nm, the absorption cross sections decrease with decreasing temperature. The low temperature absorption spectra observed by the three groups differ in the same manner as their room temperature spectra, i.e., Fahr et al. [235] report the highest and Rattigan et al. [654] the lowest values for the absorption band.

A simple analytical expression for the temperature dependence,

$$\sigma(\lambda, T) = \sigma(298\ K)\ (1 + a_1(T–298) + a_2(T–298)^2)$$

and the fitting parameters $a_1(\lambda)$ and $a_2(\lambda)$ for λ = 200–350 nm and T = 210– 298 K give Roehl et al. [678]. Another simple parameterization, $\ln \sigma(\lambda, T) = \ln \sigma(\lambda, 298\ K) + B(T–298)$, and parameters $B(\lambda)$ for λ = 235–355 nm and T = 243–333 K report Rattigan et al. [654]. The parameters a_1, a_2, and B are listed also in Table 4-187.

Quantum yields for I*($^2P_{1/2}$) atom formation in the photolysis of CH_3I at several wavelengths between 222 and 333.5 nm have been reported: $\Phi(I^*) = 0.63 \pm 0.02$, 0.79 ± 0.02, 0.69 ± 0.02, and 0.43 ± 0.02 at 222, 266, 280, and ~305 nm by Uma and Das [794], [795], [796]; $\Phi(I^*) = 0.72 \pm 0.08$ at 248 nm by Gedanken [796], $\Phi(I^*) = 0.81 \pm 0.03$ and ~ 0.05 at 248 and 308 nm by Pence et al. [629], $\Phi(I^*) = 0.30$ at 304 nm by Kang et al. [403]; and $\Phi(I^*) = 0.47$, 0.77, and 0.92 at 325.8, 329.4, and 333.5 nm by Ogorzalek Loo et al. [594]. The latter authors report also quantum yields for CD_3I:

$\Phi(I^*)$:	0.66	0.59	0.83	0.91	0.90	0.57	0.80	0.92	>0.95	0.61	0.84
λ, nm:	312.6	314.4	317.0	319.8	322.9	324.5	327.8	330.5	333.8	336.2	339.3 3

Brewer et al. [89] report $\Phi(I^*) = 0.75 \pm 0.02$ at 248 nm for CD_3I.

Quantum yields for I($^2P_{3/2}$) atom formation, $\Phi(I)$, can be derived from $\Phi(I) = 1 – \Phi(I^*)$.

Table 4-187. Absorption Cross Sections of CH_3I at 296–298 K and Temperature Coefficients

λ (nm)	10^{20} σ (cm^2)	10^3 $a_1(K^{-1})$	10^5 $a_2(K^{-2})$	10^3 $B(K^{-1})$	λ (nm)	10^{20} σ (cm^2)	10^3 $a_1(K^{-1})$	10^5 $a_2(K^{-2})$	10^3 $B(K^{-1})$
210	3.62	3.07	2.42		290	8.04	6.14	• 2.57	4.98
215	5.08	2.61	2.28		295	4.00	7.27	2.91	6.38
220	6.90	1.06	1.22		300	2.06	7.82	3.53	6.97
225	9.11	1.74	1.96		305	1.10	7.82	3.85	6.84
230	12.6	1.47	1.67		310	0.621	7.37	3.71	6.78
235	20.5	1.91	2.04	0.67	315	0.359	6.98	3.47	6.75
240	38.1	1.74	2.06	0.61	320	0.221	7.39	3.54	6.53
245	65.6	1.52	2.15	0.34	325	0.126	7.23	2.82	6.79
250	96.3	1.20	2.11	0.08	330	0.0684	8.93	3.74	7.82
255	117.7	0.890	1.95	–0.10	335	0.0388	10.88	4.88	9.34
260	119.7	0.882	1.93	–0.12	340	0.0212	11.30	4.46	10.95
265	102.9	1.21	2.00	0.10	345	0.0114	15.68	8.44	13.58
270	75.9	1.77	2.11	0.54	350	0.00609	15.94	8.22	16.83
275	49.6	2.52	2.12	1.33	355	0.00320			18.91
280	29.2	3.62	2.24	2.43	360	0.00190			17.28
285	15.6	4.84	2.38	3.74	365	0.00090			23.63

Note:
Absorption cross sections σ: 210–230 nm: mean of Jenkin et al. [376], Fahr et al. [235], and Roehl et al. [678],
235–330 nm: mean of Jenkin et al. [376], Fahr et al. [235], Rattigan et al. [654], and Roehl et al. [678],
335–350 nm: mean of Fahr et al. [235], Rattigan et al. [654], and Roehl et al. [678],
355–365 nm: Rattigan et al. [654].
Temperature coefficients a_1 and a_2: 210–298 K, Roehl et al. [678]:
$\sigma(\lambda, T) = \sigma(298\ K)\ [1 + a_1(T–298) + a_2(T–298)^2]$,
Temperature coefficients B: 243–333 K, Rattigan et al. [654]:
$\ln \sigma(\lambda, T) = \ln \sigma(\lambda, 298\ K) + B(T–298)$.

H12. $CH_2I_2 + h\nu \rightarrow CH_2I + I(^2P_{3/2})$.
$CH_2I_2 + h\nu \rightarrow CH_2I + I^*(^2P_{1/2})$. The absorption cross sections of CH_2I_2 have been measured at room temperature and 180–400 nm by Pence et al. [629], at 220–360 nm by Schmitt and Comes [712], at 200–360 nm by Baughcum and Leone [60], at 265–341 nm by Koffend and Leone [417]; and at 220–400 nm by Kwok and Phillips [425], who measured the spectrum also in methanol and cyclohexane. Measurements at 273 and 298 K and 205–380 nm have also been carried out by Roehl et al. [678]; and at 273, 298, and 348 K and 215–385 nm by Mössinger et al. [563]. There are absorption maxima at or below 215 nm, and around 250 and 290 nm. The room temperature data of the various teams (except those of Kwok and Phillips [425], which are presented only as a plot) are in very good agreement, i.e., generally within 5–10% between 230 and 380 nm, were the older data of Schmitt and Comes [712] and Koffend and Leone [417] for the prominent absorption band around 290 nm are higher than those of Roehl et al. [678] and Mössinger et al. [563]. The values of Kwok and Phillips [425] for the prominent absorption band around 290 nm are lower by 15–20% than the rest of the data. The preferred room temperature absorption cross sections, listed in Table 4-188, are the values of Roehl et al. [678] at 205–215 nm, the mean of the values reported by Roehl et al. [678] and Mössinger et al. [563] at 220–380 nm, which are very close, and the value of Mössinger et al. [563] at 385 nm.

Both temperature studies show, that decreasing the temperature from 298 or 348 K to 273 K causes a slight increase of the absorption cross sections between 275 and 300 nm (~2% in the maximum at 290 nm between 298 and 273 K) and a slight decrease outside this wavelength region. A simple empirical relation for the temperature dependence between 273 and 348 K, $\ln \sigma(\lambda, T) = \ln \sigma(\lambda, 298K) + B(\lambda)\cdot(T–298)$, and temperature coefficients $B(\lambda)$ for λ = 205–375 nm at 5-nm intervals are given by Mössinger et al. [563]. The temperature coefficients B are also listed in Table 4-188 (an erroneous B value at 305 nm has been corrected by Dr. Mössinger via a personal communication).

Quantum yields for $I^*(^2P_{1/2})$ atom formation in the photolysis of CH_2I_2 at 193, 248, and 308 nm, $\Phi(I^*)$ = ~0.05, 0.46 ± 0.04, and 0.25 ± 0.02, respectively, were reported by Pence et al. [629]. Quantum yields for $I(^2P_{3/2})$ atom formation, $\Phi(I)$, can be derived from $\Phi(I) = 1 – \Phi(I^*)$.

Table 4-188. Absorption Cross Sections of CH_2I_2 at 298 K

λ (nm)	10^{20} σ (cm^2)	10^3 B (K^{-1})	λ (nm)	10^{20} σ (cm^2)	10^3 B (K^{-1})
205	407.0		300	357.0	–0.37
210	404.0		305	338.5	–0.16
215	366.0	0.15	310	313.5	0.07
220	260.0	0.14	315	280.0	0.15
225	197.5	0.19	320	244.0	0.27
230	133.0	0.51	325	203.0	0.27
235	109.0	0.56	330	161.5	0.51
240	122.5	0.15	335	120.5	0.55
245	150.0	0.18	340	83.3	1.36
250	157.0	0.67	345	53.7	1.99
255	139.5	1.58	350	32.6	3.19
260	120.5	2.04	355	19.2	4.09
265	130.0	1.30	360	10.9	5.39
270	178.5	0.00	365	6.05	6.77
275	255.0	–0.71	370	3.45	8.25
280	328.5	–1.24	375	1.93	11.3
285	371.5	–1.21	380	1.17	
290	380.5	–0.94	385	0.769	
295	371.5	–0.58			

Note:
Absorption cross sections σ: 205–215 nm, Roehl et al. [678],
220–380 nm, mean of Roehl et al. [678] and Mössinger et al. [563],
385 nm, Mössinger et al. [563].
Temperature coefficients B: 273–348 K, Mössinger et al. [563]:
$\ln \sigma(\lambda, T) = \ln \sigma(\lambda, 298\ K) + B(T–298)$.

H13. $C_2H_5I + h\nu \rightarrow C_2H_5 + I(^2P_{3/2})$.
$C_2H_5I + h\nu \rightarrow C_2H_5 + I^*(^2P_{1/2})$. The absorption cross sections of C_2H_5I have been measured at room temperature and 147 nm ($\sigma = 1.48 \times 10^{-17}$ cm^2) by Rebbert et al. [665], at 205–360 nm by Porret and Goodeve [642]; at 223–298 K and 205–365 nm by Roehl et al. [678], at 243–333 K and 235–355 nm by Rattigan et al. [654], and at 323 K and 220–320 nm by Zhang et al. [881]. The room temperature data are in good agreement, the values of Roehl et al.[678] are higher by 5–15% at 235–325 nm and become increasingly higher up to 125% at 355 nm than the values of Rattigan et al. [654]. The latter authors found their data to agree within 10–15% with the plotted values of Porret and Goodeve [642]. The preferred absorption cross sections, listed in Table 4-189, are the mean of the values reported by Roehl et al. [678] and Rattigan et al. [654] in the common wavelength range 235–355 nm, and the data of Roehl et al. [678] at 215–230 nm.

The temperature studies of Roehl et al. [678] and Rattigan et al. [654] show, that decreasing the temperature in the range 333–223 K causes an increase of the absorption cross section in the absorption band at ~230–270 nm and a decrease at longer wavelengths. The differences between the low-temperature data of the two groups are comparable with those between the room temperature data. The data for 323 K, reported by Zhang et al. [881] as a plot on a logarithmic scale, are larger by 10–40% around the absorption maximum and up to more than 200% in the long-wavelength tail than the data for 313 and 333 K reported by Rattigan et al. [654]. A simple analytical expression for the temperature dependence,

$$\sigma(\lambda, T) = \sigma(298\ K)\ [1 + a_1(T–298) + a_2(T–298)^2],$$

and the fitting parameters $a_1(\lambda)$ and $a_2(\lambda)$ for λ = 205–365 nm and T = 223–298 K give Roehl et al. [678]. Another simple parameterization, $\ln \sigma(\lambda, T) = \ln \sigma(\lambda, 298\ K) + B(T–298)$, and parameters $B(\lambda)$ for λ = 235–355 nm and T = 243–333 K is reported by Rattigan et al. [654]. The parameters a_1, a_2, and B are listed also in Table 4-189.

Quantum yields for $I^*(^2P_{1/2})$ atom formation in the photolysis of C_2H_5I at a few wavelengths between 222 and 305 nm have been reported: Φ(I*) = 0.57 ± 0.02, 0.72 (or 0.73) ± 0.02, 060 ± 0.02, and 0.39 ± 0.02 at 222, 266, 280, and ~305 nm by Uma and Das [794], [795], [796]; Φ(I*) = 0.78 ± 0.07 at 248 nm by Gedanken [264]; Φ(I*) = 0.68 ± 0.02 at 248 nm by Brewer et al. [89], Φ(I*) = 0.22 at 304 nm by Kang et al. [403]. Quantum yields for $I(^2P_{3/2})$ atom formation, Φ(I), can be derived from Φ(I) = 1 – Φ(I*).

At 147 nm, the overall process $C_2H_5I + h\nu \rightarrow C_2H_4 + H + I$ was observed with a quantum yield of 0.75 by Rebbert et al. [665].

Table 4-189. Absorption Cross Sections of C_2H_5I at 298 K and Temperature Coefficients

λ (nm)	10^{20} σ (cm^2)	10^3 $a_1(K^{-1})$	10^5 $a_2(K^{-2})$	10^3 $B(K^{-1})$	λ (nm)	10^{20} σ (cm^2)	10^3 $a_1(K^{-1})$	10^5 $a_2(K^{-2})$	10^3 $B(K^{-1})$
205	11.9	6.38	3.15		285	19.1	3.85	0.926	3.61
210	4.22	4.07	6.28		290	10.3	5.47	1.65	4.83
215	4.56	4.93	6.75		295	5.38	7.00	2.52	6.33
220	6.18	4.06	5.70		300	2.78	8.56	4.11	7.48
225	9.09	2.81	3.81		305	1.44	9.31	4.89	8.08
230	14.3	2.62	3.83		310	0.777	10.56	6.87	7.55
235	23.2	1.28	2.17	–0.27	315	0.416	10.83	6.81	7.92
240	41.7	0.876	1.96	–0.40	320	0.227	11.98	9.76	8.27
245	69.3	0.233	1.62	–0.62	325	0.127	12.98	11.3	8.81
250	99.3	–0.111	1.58	–0.79	330	0.0743	14.56	17.5	9.30
255	119.7	–1.03	0.606	–0.82	335	0.0403	18.81	24.6	10.20
260	121.8	–1.48	–0.0332	–0.75	340	0.0246	13.90	9.08	11.16
265	105.9	–1.09	1.2×10^{-6}	–0.44	345	0.0133	18.86	22.1	12.41
270	80.6	–0.538	–0.257	0.36	350	0.00840	20.19	20.1	11.28
275	54.4	0.770	0.0299	1.23	355	0.00488	–7.04	–40.5	12.20
280	33.5	2.01	0.110	2.36					

Note:
Absorption cross sections σ: 205–230 nm, Roehl et al. [678],
235–355 nm, mean of Roehl et al. [678] and Rattigan et al. [654].
Temperature coefficients a_1 and a_2: 223–298 K, Roehl et al. [678]:
$\sigma(\lambda, T) = \sigma(298\ K)\ [1 + a_1(T–298) + a_2(T–298)^2]$,
Temperature coefficients B: 243–333 K, Rattigan et al. [654]:
$\ln \sigma(\lambda, T) = \ln \sigma(\lambda, 298\ K) + B(T–298)$.

H14. $CH_3CHI_2 + h\nu \rightarrow$ Products. The absorption cross sections of CH_3CHI_2 have been measured at 298 K and 220–360 nm by Schmitt and Comes [712]. Their data are listed in Table 4-190.

Table 4-190. Absorption Cross Sections of CH_3CHI_2 at 298 K

λ (nm)	10^{20} σ (cm^2)	λ (nm)	10^{20} σ (cm^2)	λ (nm)	10^{20} σ (cm^2)
220	304	270	183	320	222
225	240	275	243	325	201
230	181	280	304	330	175
235	144	285	352	335	138
240	138	290	374	340	107
245	151	295	366	345	75.7
250	157	300	339	350	49.3
255	143	305	305	355	31.7
260	133	310	273	360	19.1
265	145	315	247		

Note:
220–360 nm, Schmitt and Comes [712].

H15. $CH_3CH_2CH_2I + h\nu \rightarrow$ Products.

H16. $CH_3CHICH_3 + h\nu \rightarrow$ Products. The absorption cross sections of 1-C_3H_7I have been measured at 223–298 K and 205–335 nm, those of 2-C_3H_7I at 223–298 K and 205–380 nm by Roehl et al. [678]. The absorption cross sections of 2-C_3H_7I in the gas phase and in cyclohexane solution have also been measured at room temperature and 235–305 nm by Phillips et al. [634]. The gas-phase data reported by Phillips et al. [634] and given as a plot in their paper are larger by 30–70% over the whole absorption band than the data of Roehl et al. [678]. Room temperature values at 147 nm for 1-C_3H_7I and 2-C_3H_7I have been reported by Rebbert et al. [665]. The recommended room temperature values for 1-C_3H_7I and 2-C_3H_7I, listed in Table 4-191, are taken from the paper of Roehl et al. [678].

Decreasing the temperature in the range 298–223 K causes an increase of the absorption cross sections around the absorption maximum, at 245–265 nm for 1-C_3H_7I and at 240–270 nm for 2-C_3H_7I, and a decrease

in the long-wavelength tail. Decrease of the absorption cross sections with decreasing temperature generally has been observed in the short-wavelength tail of the absorption band except for slight increases between 273 and 248 K in the case of 1-C_3H_7I and between 248 and 223 K in the case of 2-C_3H_7I. At wavelengths below the minimum (~210 nm), the absorption cross sections decrease with decreasing temperature between 298 and 223 K. The temperature dependence has been parameterized by the analytical expression

$$\sigma(\lambda, T) = \sigma(298\ K)\ [1 + a_1(T–298) + a_2(T–298)^2]$$

and the fitting parameters $a_1(\lambda)$ and $a_2(\lambda)$ for T = 223–298 K and λ = 205–335 nm (1-C_3H_7I) and λ = 205–380 nm (2-C_3H_7I) are reported by Roehl et al. [678]. These are listed also in Table 4-190.

Quantum yields for I*($^2P_{1/2}$) atom formation in the photolysis of C_3H_7I at a few wavelengths have been reported: Φ(I*) = 0.54 ± 0.02, 0.66 ± 002, 0.56 ± 0.02, and 0.35 ± 0.02 at 222, 266, 280, and ~305 nm by Uma and Das [794], [796]; Φ(I*) = 0.60 ± 0.02 at 248 nm by Brewer et al. [89], Φ(I*) = 0.20 at 304 nm by Kang et al. [403] for 1-C_3H_7I; Φ(I*) = 0.40 ± 0.02, 0.44 ± 0.03, and 0.19 ± 0.02 at 222, 266, and ~305 nm by Uma and Das [795], and Φ(I*) = 0.26 ± 0.02 at 248 nm by Brewer et al. [89] for 2-C_3H_7I. Quantum yields for I($^2P_{3/2}$) atom formation, Φ(I), can be derived from Φ(I) = 1 – Φ(I*).

At 147 nm, Rebbert et al. [665] observed the main overall processes

1-$C_3H_7I + h\nu \rightarrow C_3H_6 + H + I$ and

1-$C_3H_7I + h\nu \rightarrow CH_3 + C_2H_4 + I$

with quantum yields 0.38 and 0.47 and the processes

2-$C_3H_7I + h\nu \rightarrow C_3H_6 + H + I$ and

2-$C_3H_7I + h\nu \rightarrow CH_3 + C_2H_4 + I$

with quantum yields 0.80 and 0.07.

Table 4-191. Absorption Cross Sections of C_3H_7I at 298 K and Temperature Coefficients

λ (nm)	1-C_3H_7I			2-C_3H_7I		
	10^{20} σ (cm^2)	10^3 a_1 (K^{-1})	10^5 a_2 (K^{-2})	10^{20} σ (cm^2)	10^3 a_1 (K^{-1})	10^5 a_2 (K^{-2})
205	15.6	7.60	4.37	44.9	15.14	8.46
210	5.05	0.283	1.57	4.53	7.84	7.23
215	5.14	–1.49	–2.46	3.57	4.96	5.08
220	6.84	–1.59	–2.97	4.20	1.55	1.27
225	10.4	–0.891	–2.14	6.45	2.21	1.99
230	17.7	–0.375	–1.26	11.0	1.60	1.80
235	32.8	–0.311	–1.04	20.4	0.480	0.681
240	58.1	–0.611	–0.804	38.2	–0.333	0.121
245	91.9	–0.949	–0.609	66.7	–0.680	0.0947
250	124	–1.22	–0.611	102	–0.795	0.289
255	141	–1.55	–0.776	133	–0.966	0.570
260	136	–1.44	–0.867	148	–1.14	0.512
265	113	–1.02	–1.04	143	–0.589	0.824
270	82.2	–0.306	–1.16	120	–0.439,	0.281
275	53.4	0.524	–1.50	90.2	0.792	0.873
280	32.0	1.68	–1.66	61.4	1.65	0.466
285	18.1	3.08	–1.44	38.6	2.88	0.534
290	9.96	5.56	0.812	22.6	4.13	0.559
295	5.42	6.76	2.05	12.8	5.71	1.04
300	2.96	7.16	2.90,	6.94	7.20	1.93
305	1.63	6.90	3.20	3.73	8.19	2.33
310	0.945	7.10	4.01	2.04	8.75	2.81
315	0.532	5.59	2.78	1.09	8.49	2.25
320	0.301	3.68	0.0140	0.627	10.79	4.36
325	0.177	4.23	0.0238	0.348	9.54	2.76
330	0.110	11.40	12.3	0.202	10.99	5.94
335	0.0627	15.76	25.8	0.115	12.37	7.58
340				0.0688	13.69	12.2
345				0.0402	16.32	17.1
350				0.0253	18.50	24.7
355				0.0150	19.41	24.3
360				0.0105	18.61	13.9
365				0.00666	29.85	50.9
370				0.00479	37.24	76.8
375				0.00535	36.71	80.7
380				0.00530	22.00	40.0

Note:
Absorption cross sections σ: 205–380 nm, Roehl et al. [678],
Temperature coefficients a_1 and a_2: 223–298 K, Roehl et al. [678]:
$\sigma(\lambda, T) = \sigma(298\ K)\ [1 + a_1(T–298) + a_2(T–298)^2]$.

H17. $C_4H_9I + h\nu \rightarrow C_4H_9 + I(^2P_{3/2})$.
$C_4H_9I + h\nu \rightarrow C_4H_9 + I^*(^2P_{1/2})$.

H18. $(CH_3)_2CHCH_2I + h\nu \rightarrow (CH_3)_2CCH_2 + I(^2P_{3/2})$.
$(CH_3)_2CHCH_2I + h\nu \rightarrow (CH_3)_2CCH_2 + I^*(^2P_{1/2})$.

H19. $(CH_3)_3CI + h\nu \rightarrow (CH_3)_3C + I(^2P_{3/2})$.
$(CH_3)_3CI + h\nu \rightarrow (CH_3)_3C + I^*(^2P_{1/2})$. Absorption cross sections for *n*- and *iso*-C_4H_9I are not available. Absorption cross sections of *tert*-C_4H_9I have been measured at 323 K by Phillips et al. [634]. An absorptions band between 230 and 310 nm exhibits a maximum of ~2.1×10^{-18} cm^2 at ~268 nm. Estimated values at 5-nm intervals, read from a logarithmic plot, are presented in Table 4-192.

Quantum yields for $I^*(^2P_{1/2})$ atom formation in the photolysis of *n*-C_4H_9I at several wavelengths between 222 and 305 nm have been reported: $\Phi(I^*) = 0.51 \pm 0.02$, 0.64 ± 0.03, 0.50 ± 0.03, and 0.30 ± 0.02 at 222, 266, 280, and ~305 nm by Uma and Das [794], [796]; $\Phi(I^*) = 0.53 \pm 0.03$ at 248 nm by Brewer et al. [89], $\Phi(I^*) = 0.14$ at 304 nm by Kang et al. [403].

Quantum yields for $I^*(^2P_{1/2})$ atom formation in the photolysis of *iso*-C_4H_9I, $\Phi(I^*) = 0.71 \pm 0.01$, 0.56 ± 0.03, and 0.35 ± 0.02 at 266, 280, and ~305 nm, have been reported by Uma and Das [796], $\Phi(I^*) = 0.20 \pm 0.02$ at 248 nm by Brewer et al. [89].

Quantum yields for I atom formation in the photolysis of *tert*-C_4H_9I, $\Phi(I(^2P_{3/2})+I^*(^2P_{1/2})) = 0.93$ and 0.92 at 277 and 304 nm, have been reported by Kim et al. [408]. Quantum yields for $I^*(^2P_{1/2})$ atom formation, $\Phi(I^*(^2P_{1/2})) = 0.33 \pm 0.03$, 0.20 ± 0.03, and 0.12 ± 0.03, in the photolysis at 222, 266, and ~305 nm, have been reported by Uma and Das [795], $I^*(^2P_{1/2}) = 0.41 \pm 0.10$ and 0.03 ± 0.02 at 248 nm by Gedanken [264] and Brewer et al. [89], respectively.

Table 4-192. Absorption Cross Sections of $(CH_3)_3CI$ at 298 K

λ (nm)	10^{20} σ (cm^2)	λ (nm)	10^{20} σ (cm^2)	λ (nm)	10^{20} σ (cm^2)
235	28.5	265	209	295	54.0
240	42.5	270	211	300	34.0
245	64.8	275	186	305	21.5
250	98.0	280	150	310	14.0
255	140	285	116		
260	180	290	83.0		

Note:
235–310 nm, Phillips et al. [634], read from logarithmic plot.

H20. $C_5H_{11}I + h\nu \rightarrow C_5H_{11} + I(^2P_{3/2})$.
$C_5H_{11}I + h\nu \rightarrow C_5H_{11} + I^*(^2P_{1/2})$. Absorption cross sections for *n*-$C_5H_{11}I$ are not available. A quantum yield for $I^*(^2P_{1/2})$ atom formation in the photolysis of *n*-$C_5H_{11}I$ at 222 nm, $\Phi(I^*) = 0.50 \pm 0.03$, has been measured by Uma and Das [794].

H21. $CF_3I + h\nu \rightarrow CF_3 + I(^2P_{3/2})$
$CF_3I + h\nu \rightarrow CF_3 + I^*(^2P_{1/2})$. The absorption cross sections of CF_3I have been measured at room temperature and 170–230 nm by Roxlo and Mandl [692]; at room temperature and in shock waves at 625 and 1050 K and 220–360 nm by Brouwer and Troe [101]; at 200–298 K and 216–370 nm by Solomon et al. [747]; at 218–333 K and 160–350 nm by Fahr et al. [234]; at 243–333 K and 235–390 nm by Rattigan et al. [654], and at 205-325 nm (and in the VUV at 113-181 nm) by Limão-Vieira et al. [452]. Measurements in the long-wavelength tail of the absorption band up to 455 nm and at temperatures up to ~4000 K were also carried out with hot molecules excited by IR laser pulses by Bagratashvili et al. [35] and Abel et al. [2, 3].

There is good agreement between the room temperature values above 200 nm, i.e., better than 20% around the absorption maximum at 265–270 nm and better than 15% below 255 nm and at 280–350 nm. Fahr et al. [234] report the highest absorption maximum of 7×10^{-19} cm^2, compared to 6.7×10^{-19}, 6.4×10^{-19}, 6.2×10^{-19}, and 5.9×10^{-19} cm^2 reported by Limão-Vieira et al. [452], Solomon et al. [747], Brouwer and Troe [101], and Rattigan et al. [654], respectively. The long-wavelength data of Solomon et al. [747] become increasingly higher by up to ~70% than those of Rattigan et al. [654]. The new data of Limão-Vieira et al. [452] confirm the JPL-97 recommendation between 230 and 310 nm better than the JPL-2002 recommendation, i.e., the absorption curve lies between those of Solomon et al. [747] and Fahr et al. [234], and the cross sections are higher than those of the JPL-2002 recommendation. In the wings (below 230 nm and above 310 nm) there are deviations from the rest of the result, i.e., the absorption curve shows an irregular behavior. We keep at the JPL-2002 recommendation, i.e., the preferred absorption cross sections, listed in Table 4-193 are the data of Fahr et al. [234] at 180–215 nm; the mean of the values reported by Brouwer and Troe [101], Solomon et al. [747], and Fahr et al. [234] at 220–230 nm; the mean of the values reported by Brouwer and Troe [101], Solomon et al. [747], Fahr et al. [234], and Rattigan et al. [654], at 235–310 nm; the mean of the values reported by Solomon et al. [747], Fahr et al. [234], and Rattigan et al. [654] at 315–350 nm; and the values of Rattigan et al. [654] at 355–385 nm.

Fahr et al. [234] and Limão-Vieira et al. [452] observed in the short-wavelength region a band centered at about 171 nm with cross sections up to 3.6×10^{-17} and 7.4×10^{-17} cm^2, which shows vibrational structure, and a structured band with a maximum approaching values of $\sim1 \times 10^{-16}$ cm^2 at or below 160 nm. The plotted spectrum at 170–230 nm reported by Roxlo and Mandl [692] is not in agreement with the results of Fahr et al. [234] and Limão-Vieira et al. [452]. Four strong and structured bands are observed at still shorter wavelengths between 158 and 115 nm in the high-resolution spectrum reported by Limão-Vieira et al. [452].

The temperature studies of Solomon et al. [747], Fahr et al. [234], and Rattigan et al. [654] agree in the observation, that the absorption cross sections increase in the region of the maximum (~240–280 nm) with decreasing temperature from 333 K or room temperature down to temperatures of 240–250 K; the ratios σ(298 K)/σ(~240 K) and σ(333 K)/σ(~240 K) around the maximum are ~0.9, the ratios σ(333 K)/σ(298 K) are ~1. Solomon et al. [747] observed a further increase of the cross sections down to 200 K, whereas Fahr at al. [234] observed a slight decrease between 253 and 218 K. A decrease of the absorption cross sections above 280 nm and between 333 and 200 K was observed by the three groups; the ratios σ(298 K)/σ(~240 K) increase from ~1.0 to ~1.9 at 280–340 nm, the ratios σ(333 K)/σ(298 K) are around 1.3. Thus, the temperature dependences reported by the three groups are compatible at least in the range 240–333 K.

Solomon et al. [747] and Rattigan et al. [654] fitted their spectra to the expression

$$\ln \sigma(\lambda, T) = \ln \sigma(\lambda, 298\ K) + B(T–298)$$

and report the temperature coefficients $B(\lambda)$ for T = 200–298 K and λ = 216–344 nm (at 2-nm intervals) and for T = 243–333 K and λ = 235–390 nm (at 5-nm intervals), respectively. The temperature coefficients B reported by Solomon et al. [747] are nearly constantly larger by $\sim0.8 \times 10^{-3}$ than those of Rattigan et al. [654] at 235–300 nm and become smaller by up to 1.75×10^{-3} between 315 and 345 nm. The B values reported by Rattigan et al. [654] for the ranges 235–385 nm and 243–333 K are listed also in Table 4-193.

Fahr et al. [234] gave fits for the long-wavelength tail using the expressions
$\sigma(\lambda) = \sigma_0(\lambda) \exp(–L/\lambda)$ for $\lambda > 320$ nm and $\sigma(T) = \sigma_0(T) \exp(–\theta/T)$ and reported values for the parameters $\sigma_0(\lambda)$ and L at T = 218, 235, 253, 273, 295, and 333 K and for $\sigma_0(T)$ and θ at 300, 310, 320, 330, 340, and 350 nm.

In the short-wavelength region at 160–180 nm, a decrease of the absorption cross sections with decreasing temperature 333–218 K has been observed by Fahr et al. [234].

Since CF_3I serves as model system for studying the dynamics of $I^*(^2P_{1/2})$ atom production by UV photolysis, there is a great number of studies which measure $I^*(^2P_{1/2})/I(^2P_{3/2})$ branching ratios and $I^*(^2P_{1/2})$ quantum yields from CF_3I photolysis in the wavelength region of the absorption band. The following quantum yields were reported for the range between 248 and 308 nm:

$\Phi(I^*) = 0.89 \pm 0.01$, 0.87 ± 0.04, and 0.88 at 248 nm by Brewer et al. [89], Gedanken et al. [264], and Felder [237], respectively;

$\Phi(I^*) = 0.89 \pm 0.05$, 0.79 ± 0.03 and 0.63 ± 0.02 at 266, 280, and ~305 nm by Kavita and Das [404];

$\Phi(I^*) = 0.87$ at 277 nm by Kim et al. [407]; $\Phi(I^*) = 0.69$ at 304 nm by Kang et al. [403];

$\Phi(I^*) = 0.21$ at 308 nm by Felder [238], and

$\Phi(I^*)$	0.99 ± 0.01	0.91 ± 0.01	0.89 ± 0.01	0.84 ± 0.01	0.81 ± 0.01	0.69 ± 0.01
λ (nm)	275	279	283	290	293	295
$\Phi(I^*)$	0.68 ± 0.01	0.63 ± 0.02	0.61 ± 0.02	0.47 ± 0.01	0.41 ± 0.0	0.37 ± 0.01
λ (nm)	296	297	298	300	302	303

by Furlan et al. [257].

Quantum yields for $I(^2P_{3/2})$ atom formation, $\Phi(I)$, can be derived from $\Phi(I) = 1 - \Phi(I^*)$.

Table 4-193. Absorption Cross Sections of CF_3I at 295-300 K

λ (nm)	$10^{20}\,\sigma$ (cm^2)	10^3 B (K^{-1})	λ (nm)	$10^{20}\,\sigma$ (cm^2)	10^3 B (K^{-1})
180	3.11		285	33.4	0.55
185	0.75		290	22.7	1.65
190	0.28		295	14.3	2.98
195	0.16		300	8.6	4.22
200	0.15		305	5.06	5.61
205	0.19		310	2.82	6.84
210	0.34		315	1.62	7.68
215	0.68		320	0.905	8.27
220	1.52		325	0.485	8.74
225	2.88		330	0.262	9.25
230	5.03		335	0.142	9.92
235	8.21	0.16	340	0.0750	10.27
240	13.6	-0.16	345	0.0407	11.71
245	21.8	-0.52	350	0.0210	12.85
250	32.4	-0.86	355	0.0115	13.26
255	45.2	-1.17	360	0.0064	14.65
260	56.9	-1.37	365	0.0036	14.63
265	63.4	-1.43	370	0.002	15.49
270	63.1	-1.30	375	0.0011	17.14
275	56.1	-0.94	380	0.0007	17.66
280	45.1	-0.62	385	0.0004	19.71

Note: Absorption cross sections σ:
180–215 nm: Fahr et al. [234],
220–230 nm: mean of Brouwer and Troe [101], Solomon et al. [747], and Fahr et al.[234],
235–310 nm: mean of Brouwer and Troe [101], Solomon et al. [747], Fahr et al. [234], and Rattigan et al. [654],
315–350 nm: mean of Solomon et al. [747], Fahr et al. [234], and Rattigan et al. [654],
355–385 nm: Rattigan et al. [654].
Temperature coefficients B:
243–333 K, Rattigan et al. [654]: $\ln \sigma(\lambda, T) = \ln \sigma(\lambda, 298\ K) + B(T–298)$.

H22. $CF_2I_2 + h\nu \rightarrow CF_2I + I(^2P_{3/2})$
$CF_2I_2 + h\nu \rightarrow CF_2I + I^*(^2P_{1/2})$
$CF_2I_2 + h\nu \rightarrow CF_2 + I(^2P_{3/2}) + I(^2P_{3/2})$
$CF_2I_2 + h\nu \rightarrow CF_2 + I(^2P_{3/2}) + I^*(^2P_{1/2})$. The photodissociation of CF_2I_2 has been studied at room temperature and wavelengths 248, 308, 337, and 351 nm by Wannenmacher et al. [837] and Baum et al. [62]. These authors report also plots of the absorption spectrum at room temperature and between 190 and 420 nm, which suggest the presence of at least two overlapping transitions corresponding to the different dissociation processes. Numerical absorption data belonging to Wannenmacher et al. [837] and Baum et al. [62] were obtained via personal communication by Pfister and Huber [633]. The absorption cross sections listed in Table 4-194 are normalized to a

maximum value $\sigma = 2.929 \times 10^{-18}$ cm^2·molecule^{-1} at 300 nm, which was derived from five different spectra and has an uncertainty of ±16%.

Table 4-194. Absorption Cross Sections of CF_2I_2 at 294 K

λ (nm)	10^{20} σ (cm^2)	λ (nm)	10^{20} σ (cm^2)	λ (nm)	10^{20} σ (cm^2)
190	3163	270	203.1	350	66.24
195	4616	275	215.7	355	57.76
200	4070	280	224.3	360	49.81
205	2285	285	236.4	365	41.51
210	837.0	290	259.5	370	33.92
215	238.1	295	281.9	375	26.85
220	75.78	300	292.9	380	18.90
225	36.39	305	288.5	385	13.60
230	29.50	310	266.7	390	9.892
235	35.51	315	235.6	395	6.713
240	47.34	320	198.6	400	4.240
245	66.07	325	163.9	405	3.356
250	89.21	330	135.5	410	1.943
255	118.0	335	111.6	415	1.413
260	150.1	340	91.33	420	0.7066
265	180.5	345	78.25		

Note:
190–420 nm, Wannenmacher et al. [837], Baum et al. [62], and Pfister and Huber [633].

H23. $C_2F_5I + h\nu \rightarrow C_2F_5 + I(^2P_{3/2})$.

$C_2F_5I + h\nu \rightarrow C_2F_5 + I^*(^2P_{1/2})$. The absorption cross sections of C_2F_5I were measured at 295 K and 268 nm ($\sigma = 6.39 \times 10^{-19}$ cm^2) by Pence et al. [629] and at 323 K and 220–320 nm by Zhang et al. [881]. The absorption band extending over the 220–320-nm range has a maximum of ~ 6.7×10^{-19} cm^2 at ~269 nm. Estimated values at 5-nm intervals, read from a logarithmic plot, are in Table 4-195.

Quantum yields for $I^*(^2P_{1/2})$ atom formation in the photolysis of C_2F_5I at 266, 288, and ~305 nm, $\Phi(I^*) = 0.97 \pm 0.03$, 0.75 ± 0.03, and 0.83 ± 0.05, respectively, have been reported by Kavita and Das [404]. Quantum yields for $I(^2P_{3/2})$ atom formation, $\Phi(I)$, can be derived from $\Phi(I) = 1 - \Phi(I^*)$.

Table 4-195. Absorption Cross Sections of C_2F_5I at 323 K

λ (nm)	10^{20} σ (cm^2)	λ (nm)	10^{20} σ (cm^2)	λ (nm)	10^{20} σ (cm^2)
220	1.95	255	49.8	290	35.3
225	3.27	260	60.0	295	25.0
230	5.60	265	65.5	300	16.3
235	9.40	270	66.8	305	10.4
240	16.0	275	63.2	310	6.4
245	25.3	280	56.1	315	3.9
250	37.5	285	46.5	320	2.3

Note:
235–310 nm, Zhang et al. [881], read from logarithmic plot.

H24. $C_3F_7I + h\nu \rightarrow C_3F_7 + I(^2P_{3/2})$.

$C_3F_7I + h\nu \rightarrow C_3F_7 + I^*(^2P_{1/2})$. The absorption cross sections of 1-C_3F_7I have been measured at room temperature and 265–341 nm by Koffend and Leone [417] and at 180–400 nm by Pence et al. [629]. The latter authors report a plot of the absorbance (in arbitrary units), which shows an absorption band between ~220 and 340 nm with the maximum at ~268 nm, and absorption cross sections only for 248, 268, and 308 nm. The data for 268 and 308 nm are in good agreement with the corresponding data reported by Koffend and Leone [417]. The recommended absorption cross sections of 1-C_3F_7I, listed in Table 4-196, are the value for 248 nm reported by Pence et al. [629]; the mean of the values of Pence et al. [629] and Koffend and Leone [417] at 268 nm; and, for the range 270–340 nm, values obtained by interpolation and extrapolation at 5-nm intervals of the data reported at odd wavelength by Koffend and Leone [417].

Quantum yields for $I^*(^2P_{1/2})$ atom formation in the photolysis of C_3F_7I at 266, 288, and ~305 nm,

$\Phi(I^*) = 0.83 \pm 0.02$, 0.89 ± 0.03, and 0.90 ± 0.05 for 1-C_3F_7I and

$\Phi(I^*) = 0.83 \pm 0.01$, 0.80 ± 0.03, and 0.89 ± 0.02 for 2-C_3F_7I,

have been reported by Kavita and Das [404].

Quantum yields for $I(^2P_{3/2})$ atom formation, $\Phi(I)$, can be derived from $\Phi(I) = 1 - \Phi(I^*)$.

Table 4-196. Absorption Cross Sections of 1-C_3F_7I at 295–298 K

λ (nm)	10^{20} σ (cm^2)	λ (nm)	10^{20} σ (cm^2)	λ (nm)	10^{20} σ (cm^2)
248	31.0	290	43.7	320	3.3
268	77.3	295	31.8	325	2.0
270	77.0	300	21.3	330	1.2
275	74.0	305	14.2	335	0.70
280	66.5	310	9.2	340	0.42
285	56.2	315	5.5		

Note:
248 nm, Pence et al. [629],
268 nm, mean of Pence et al. [629] and Koffend and Leone [417]
270–340 nm, 5-nm inter- and extrapolation of Koffend and Leone [417] data.

H25. $C_4F_9I + h\nu \rightarrow C_4F_9 + I(^2P_{3/2})$.
$C_4F_9I + h\nu \; C_4F_9 + I^*(^2P_{1/2})$.

H26. $C_6F_{13}I + h\nu \rightarrow C_6F_{13} + I(^2P_{3/2})$.
$C_6F_{13}I + h\nu \rightarrow C_6F_{13} + I^*(^2P_{1/2})$. Absorption cross sections are not available for these perfluoroalkyl iodides.

Quantum yields for $I^*(^2P_{1/2})$ atom formation in the photolysis of both iodides at 266, 288, and ~305 nm. $\Phi(I^*) = 0.75 \pm 0.03$, 0.80 ± 0.03, and 0.87 ± 0.02 for *n*-C_4F_9I and $\Phi(I^*) = 0.82 \pm 0.02$, 0.74 ± 0.03, and 0.82 ± 0.01 for *n*-$C_6F_{13}I$, have been reported by Kavita and Das [404]. Quantum yields for $I(^2P_{3/2})$ atom formation, $\Phi(I)$, can be derived from $\Phi(I) = 1 - \Phi(I^*)$.

H27. $CH_2ICl + h\nu \rightarrow CH_2Cl + I$
$CH_2ICl + h\nu \rightarrow CH_2I + Cl$. The absorption cross sections of CH_2ICl have been measured at room temperature and 205–330 nm by Schmitt and Comes [713]; at 192–225 nm and 215–400 nm by Kwok and Phillips [427], [426], who also measured the CH_2ICl spectrum in cyclohexane solution. Measurements have also been carried out at 223–298 K and 205–355 nm by Roehl et al. [678] and at 243–333 K and 235–390 nm by Rattigan et al. [654]. The room temperature data of Roehl et al. [678] and Rattigan et al. [654] are in good agreement, where the values of Rattigan et al. [654] are lower by ≤10% between 240 and 345 nm. The older data of Schmitt and Comes [713] and the data of Kwok and Phillips [426] are higher with absorption maxima near 270 nm of 1.94×10^{-18} and 1.5×10^{-18} cm^2, respectively, compared to 1.35×10^{-18} and 1.21×10^{-18} cm^2 reported by the other two groups. The data of Kwok and Phillips [427] at 205 and 210 nm are lower by more than 80% than the data of Roehl et al. [678]. The preferred absorption cross sections, listed in Table 4-197, are the data of Roehl et al. [678] at 205–230 nm; the mean of the values reported by Roehl et al. [678] and Rattigan et al. [654] at 235–355 nm; and the data of Rattigan et al. [654] at 360–390 nm. The data of Schmitt and Comes [713] and Kwok and Phillips [427], [426] are given only as a plots in their papers and have therefore not been included in the evaluation.

Both temperature studies show an increase of the absorption cross sections around the absorption maximum (~250–285 nm) with decreasing temperature between 333 and 223 K and the reverse effect above 285 nm. The absorption maxima at ~250 K reported by the two groups agree within 15%. A simple analytical expression for the temperature dependence,

$$\sigma(\lambda, T) = \sigma(298\ K)\,[1 + a_1(T–298) + a_2(T–298)^2]$$

and the fitting parameters $a_1(\lambda)$ and $a_2(\lambda)$ for λ = 205–355 nm and T = 223– 298 K give Roehl et al. [678]. Another simple parameterization, $\ln \sigma(\lambda, T) = \ln \sigma(\lambda, 298\ K) + B(T–298)$, and parameters $B(\lambda)$ for

λ = 235–390 nm and T = 243–333 K report Rattigan et al. [654]. The temperature coefficients a_1, a_2, and B are given also in Table 4-197.

The relative quantum yield of $I^*(^2P_{1/2})/(I(^2P_{3/2}) + I^*(^2P_{1/2}))$ has been determined by Senapati et al. [725] at 5 different wavelengths: 0.47 ± 0.02 at 222 nm, 0.51 ± 0.01 at 236 nm, 0.51 ± 0.02 at 266 nm, 0.55 ± 0.03 at 280 nm, and 0.38 ± 0.01 at 304 nm. Relative quantum yields of $Cl^*(^2P_{1/2})/(Cl(^2P_{3/2}) + Cl^*(^2P_{1/2}))$ were recently measured by Senapati and Das [724] at 4 different wavelengths: 0.44 at 222 nm, 0.44 at 266 nm, 0.30 at 280 nm, and 0.22 at 304 nm.

Table 4-197. Absorption Cross Sections of CH_2ICl at 298 K and Temperature Coefficients

λ (nm)	10^{20} σ (cm^2)	10^3 $a_1(K^{-1})$	10^5 $a_2(K^{-2})$	10^3 $B(K^{-1})$	λ (nm)	10^{20} σ (cm^2)	10^3 $a_1(K^{-1})$	10^5 $a_2(K^{-2})$	10^3 $B(K^{-1})$
205	132	–1.59	–3.83		300	25.9	2.38	–0.0473	2.56
210	42.1	8.47	3.76		305	16.7	3.13	0.394	3.08
215	11.1	6.12	4.30		310	10.9	3.13	0.303	3.50
220	7.50	0.232	0.129		315	7.16	2.74	–0.317	3.56
225	9.76	–0.0938	0.660		320	4.79	2.44	–0.533	3.46
230	14.9	–0.268	-1.4×10^{-6}		325	3.23	2.87	0.140	3.44
235	21.2	–0.512	–0.388	0.24	330	2.14	8.52	–4.21	3.72
240	32.1	–0.793	–0.664	0.12	335	1.40	2.02	–2.25	4.09
245	45.9	–0.929	–0.758	–0.02	340	0.906	5.20	4.54	4.87
250	63.3	–1.22	–1.13	–0.11	345	0.569	7.05	6.88	5.69
255	84.5	–1.25	–0.998	–0.28	350	0.350	9.12	11.7	6.88
260	106	–1.56	–1.14	–0.44	355	0.225	12.27	18.9	8.16
265	122	–1.05	–0.294	–0.55	360	0.133			9.01
270	128	–1.33	–0.593	–0.59	365	0.081			11.06
275	121	–1.07	–0.298	–0.47	370	0.048			11.47
280	104	–0.618	–0.309	–0.18	375	0.027			12.77
285	81.1	–0.326	–0.554	0.32	380	0.017			15.14
290	58.5	0.300	–0.711	0.99	385	0.008			19.12
295	39.9	1.55	–0.245	1.73	390	0.006			20.48

Note:
Absorption cross sections σ: 205–230 nm, Roehl et al. [678],
235–355 nm, mean of Roehl et al. [678] and Rattigan et al. [654],
360–390 nm, Rattigan et al. [654].
Temperature coefficients a_1 and a_2: 223–298 K, Roehl et al. [678]
$(\sigma(\lambda, T) = \sigma(298\ K)\ [1 + a_1(T–298) + a_2(T–298)2])$.
Temperature coefficients B: 243–333 K, Rattigan et al. [654]:
$\ln \sigma(\lambda, T) = \ln \sigma(\lambda, 298\ K) + B(T–298)$.

H28. $CH_2BrI + h\nu \rightarrow CH_2I + Br$.

$CH_2BrI + h\nu \rightarrow CH_2Br + I$. The absorption cross sections of CH_2BrI have been measured at room temperature and 180–360 nm by Man et al. [472]; and at 273, 298, and 348 K and 215–390 nm by Mössinger et al. [563]. The spectrum exhibits two absorption bands with maxima near 210 and 267 nm, which can be assigned to electronic transitions to repulsive states antibonding in C–Br and C–I, respectively. The results of the two studies are not in quantitative agreement: Mössinger et al. [563] report room temperature absorption cross sections of 5.7×10^{-18} and 2.3×10^{-18} cm^2 at 215 and 270 nm, whereas a plot in the paper of Man et al. [472] gives the larger values of $\sim 1 \times 10^{-17}$ and 3.5×10^{-18} cm^2, respectively. We recommend the data of Mössinger et al. [563], which are listed in Table 4-198.

The absorption cross sections increase with decreasing temperature around the band maxima and decrease in their long-wavelength tails at 220–240 nm and above 290 nm. The temperature dependence was parameterized by Mössinger et al. [563] by the empirical relation $\ln \sigma(\lambda, T) = \ln \sigma(\lambda, 298\ K) + B(T–298)$. The temperature coefficients B(λ) are listed also in Table 4-198 (an erroneous B value at 280 nm has been corrected by Dr. Mössinger via a personal communication).

Table 4-198. Absorption Cross Sections of CH_2BrI at 298 K and Temperature Coefficients

λ (nm)	10^{20} σ (cm^2)	10^3 B (K^{-1})	λ (nm)	10^{20} σ (cm^2)	10^3 B (K^{-1})	λ (nm)	10^{20} σ (cm^2)	10^3 B (K^{-1})
215	567	–2.16	275	214	–1.22	335	5.52	3.89
220	423	–0.12	280	184	–0.94	340	3.50	4.79
225	269	1.34	285	150	–0.53	345	2.24	5.74
230	155	2.06	290	110	0.10	350	1.41	6.73
235	97.9	2.05	295	82.5	0.63	355	0.817	9.47
240	80.9	1.01	300	60.6	1.03	360	0.498	11.5
245	93.7	0.00	305	42.9	1.13	365	0.303	11.6
250	125	–0.58	310	31.4	1.41	370	0.165	14.3
255	170	–1.16	315	23.1	1.52	375	0.098	17.4
260	207	–1.29	320	16.8	1.71	380	0.070	
265	228	–1.45	325	11.5	2.36	385	0.039	
270	229	–1.73	330	8.02	2.99	390	0.025	

Note:
Absorption cross sections σ: 205–380 nm, Mössinger et al. [563].
Temperature coefficients B: 273–348 K, Mössinger et al. [563]:
$\ln \sigma(\lambda, T) = \ln \sigma(\lambda, 298\ K) + B(T–298)$.

H29. $CF_2BrCF_2I + h\nu \rightarrow CF_2BrCF_2 + I$.
$CF_2BrCF_2I + h\nu \rightarrow CF_2ICF_2 + Br$. The absorption spectrum of CF_2BrCF_2I has been measured at room temperature and 190– 350 nm by Pence et al. [629]. The spectrum, reported as a plot (with arbitrary absorbance units), exhibits an absorption band with the maximum near 268 nm corresponding to the C–I bond and part of an absorption band with the maximum at or below 193 nm corresponding to the C–Br bond. A cross section $\sigma = 2.36 \times 10^{-18}$ cm^2 and a quantum yield for Br*($^2P_{1/2}$) atom formation, $\Phi(Br^*) = 0.07 \pm 0.05$, at 193 nm have been reported.

4.4 References

1. *The Stratosphere 1981: Theory and Measurements*; National Aeronautics and Space Administration, 1982.
2. Abel, B., B. Herzog, H. Hippler and J. Troe, 1989, J. Chem. Phys., 91, 890-899, 900-905.
3. Abel, B., H. Hippler and J. Troe, 1992, J. Chem. Phys., 96, 8863-8871.
4. Ackermann, M. In *Mesospheric Models and Related Experiments*; G. Fiocco, Ed., 1971; pp 149-159.
5. Acton, A. P., R. G. Aickin and N. S. Bayliss, 1936, J. Chem. Phys., 4, 474-479.
6. Adachi, H., N. Basco and D. G. L. James, 1979, Int. J. Chem. Kinet., 11, 1211-1229.
7. Adachi, H., N. Basco and D. G. L. James, 1980, Int. J. Chem. Kinet., 12, 949-977.
8. Addison, M. C., J. P. Burrows, R. A. Cox and R. Patrick, 1980, Chem. Phys. Lett., 73, 283-287.
9. Adler-Golden, S. M., 1983, J. Quant. Spectrosc. Radiat. Transfer, 30, 175-185.
10. Adler-Golden, S. M. and J. R. Wiesenfeld, 1981, Chem. Phys. Lett., 82, 281-284.
11. Alexander, M. H., B. Pouilly and T. Duhoo, 1993, J. Chem. Phys., 99, 1752-1764.
12. Allen, M. and J. E. Frederick, 1982, J. Atmos. Sci., 39, 2066-2075.
13. Aloisio, S. and J. S. Francisco, 2000, Chem. Phys. Lett., 329, 179-184.
14. Amaral, G., K. Xu and J. Zhang, 2001, J. Phys. Chem., A, 105, 1465-1475.
15. Amoruso, A., M. Cacciani, A. di Sarra and G. Fiocco, 1990, J. Geophys. Res., 95, 20565.
16. Amoruso, A., L. Crescentini, G. Fiocco and M. Volpe, 1993, J. Geophys. Res., 98, 16857-16863.
17. Amoruso, A., L. Crescentini, M. Silvia Cola and G. Fiocco, 1996, J. Quant. Spectrosc. Radiat. Transfer, 56, 145- 152.
18. Anastasi, C., I. W. M. Smith and D. A. Parkes, 1978, J. Chem. Soc. Faraday Trans. 1, 74, 1693-1701.
19. Anastasi, C., D. J. Waddington and A. Woolley, 1983, J. Chem. Soc. Faraday Trans., 79, 505-516.
20. Anderson, G. P. and L. A. Hall, 1983, J. Geophys. Res., 88, 6801-6806.
21. Anderson, G. P. and L. A. Hall, 1986, J. Geophys. Res., 91, 14509-14514.
22. Anderson, M., P. Hupalo and K. Mauersberger, 1993, Geophys. Res. Lett., 20, 1579-1582.
23. Anderson, S. M. and K. Mauersberger, 1992, Geophys. Res. Lett., 19, 933-936.
24. Armerding, W., F. J. Comes and B. Schulke, 1995, J. Phys. Chem., 99, 3137-3143.
25. Arnold, S. R., M. P. Chipperfield, M. A. Blitz, D. E. Heard and M. J. Pilling, 2004, Geophys. Res. Lett., L07110, doi:10.1029/2003GL019099.
26. Ashworth, S. H., B. J. Allan and J. M. C. Plane, 2002, Geophys. Res. Lett., 29, 65-1 - 65-4.
27. Astholz, D. C., A. E. Croce and J. Troe, 1982, J. Phys. Chem., 86, 696-699.
28. Atkinson, D. B., J. W. Hudjens and A. J. Orr-Ewing, 1999, J. Phys. Chem. A, 103, 6173-6180.
29. Atkinson, R., D. L. Baulch, R. A. Cox, R. F. Hampson, Jr., J. A. Kerr, M. J. Rossi and J. Troe, 2000, J. Phys. Chem. Ref. Data, 29, 167-266.
30. Atkinson, R., D. L. Baulch, R. A. Cox, R. F. Hampson, J. A. Kerr, M. J. Rossi and J. Troe, 1997, J. Phys. Chem. Ref. Data, 26, 521-1011.
31. Atkinson, R., D. L. Baulch, R. A. Cox, R. F. Hampson, J. A. Kerr and J. Troe, 1992, J. Phys. Chem. Ref. Data, 21, 1125-1568.
32. Atkinson, R. and A. C. Lloyd, 1984, J. Phys. Chem. Ref. Data, 13, 315-444.
33. Bacher, C., G. S. Tyndall and J. J. Orlando, 2001, J. Atmos. Chem., 39, 171-189.
34. Baer, S., H. Hippler, R. Rahn, M. Siefke, N. Seitzinger and J. Troe, 1991, J. Chem. Phys., 95, 6463-6470.
35. Bagratashvili, V. N., S. I. Ionov, G. V. Mishakov and V. A. Semchishen, 1985, Chem. Phys. Lett., 115, 144-148.
36. Bahou, M., C.-Y. Chung, Y.-P. Lee, B. M. Cheng, Y. L. Yung and L. C. Lee, 2001, Astrophys. J., 559, L179-L182.
37. Ball, S. M., G. Hancock, S. E. Martin and J. C. Pinot de Moira, 1997, Chem. Phys. Lett., 264, 531-538.
38. Ballash, N. M. and D. A. Armstrong, 1974, Spectrochim Acta, 30A, 941-944.
39. Barker, J. R., L. Brouwer, R. Patrick, M. J. Rossi, P. L. Trevor and D. M. Golden, 1985, Int. J. Chem. Kinet., 17, 991-1006.
40. Barnes, J. and K. Mauersberger, 1987, J. Geophys. Res., 92, 14861-14864.
41. Barnes, R. J., M. Lock, J. Coleman and A. Sinha, 1996, J. Phys. Chem., 100, 453-457.
42. Barnes, R. J., A. Sinha and H. A. Michelsen, 1998, J. Phys. Chem. A, 102, 8855-8859.
43. Barone, S. B., A. A. Turnipseed, T. Gierczak and A. R. Ravishankara, 1994, J. Phys. Chem., 98, 11969-11977.
44. Barton, S. A., J. A. Coxon and U. K. Roychowdhury, 1984, Can. J. Phys., 62, 473-486.
45. Basco, N. and S. K. Dogra, 1971, Proc. Roy. Soc. A., 323, 417-429.
46. Basco, N. and S. K. Dogra, 1971, Proc. Roy. Soc. A., 323, 29-68.
47. Basco, N. and J. E. Hunt, 1978, Int. J. Chem Kinet., 10, 733-743.
48. Basco, N. and J. E. Hunt, 1979, Int. J. Chem. Kinet., 11, 649-664.
49. Basco, N. and R. D. Morse, 1974, Proc. Roy. Soc. London, A 336, 495-505.
50. Basco, N. and S. S. Parmar, 1985, Int. J. Chem. Kinet., 17, 891-900.
51. Basco, N. and S. S. Parmar, 1987, Int. J. Chem. Kinet., 19, 115-128.

52. Bass, A. M., L. C. Glasgow, C. Miller, J. P. Jesson and S. L. Filken, 1980, Planet. Space Sci. , 28, 675-679.
53. Bass, A. M., A. E. Ledford and A. H. Laufer, 1976, J. Res. Natl. Bur. Stand., 80A, 143-166.
54. Bass, A. M. and R. J. Paur. In *Atmospheric Ozone*; C. S. Zerefos and A. Ghazi, Eds., 1985; pp 606-610.
55. Bates, D. R. and P. B. Hays, 1967, Planet. Space Sci., 15, 189-197.
56. Bauer, D., J. N. Crowley and G. K. Moortgat, 1992, J. Photochem. and Photobiol., A65, 3530-3538.
57. Bauer, D., L. D'Ottone and A. J. Hynes, 2000, Phys. Chem. Chem. Phys., 2, 1421-1424.
58. Bauer, D., T. Ingham, S. A. Carl, G. K. Moortgat and J. N. Crowley, 1998, J. Phys. Chem., 102, 2857-2864.
59. Bauerle, S. and G. K. Moortgat, 1999, Chem. Phys. Lett., 309, 43-48.
60. Baughum, S. L. and S. R. Leone, 1980, J. Chem. Phys., 72, 6531-6545.
61. Baulch, D. L., R. A. Cox, P. J. Crutzen, R. F. Hampson, Jr., J. A. Kerr, J. Troe and R. T. Watson, 1982, J. Phys. Chem. Ref. Data, 11, 327-496.
62. Baum, G. P., P. Felder and R. J. Huber, 1993, J. Chem. Phys., 98, 1999-2010.
63. Baumfalk, R., U. Buck, C. Frischkorn, N. H. Nahler and L. Hüwel, 1999, J. Chem. Phys., 111, 2595-2605.
64. Bayes, K. D., D. W. Toohey, R. R. Friedl and S. P. Sander, 2003, J. Geophys. Res., 108, 4095, doi:10.29/2002JD002877.
65. Bell, A. J., S. A. Boggis, J. M. Dyke, J. R. Frey, R. Richter, N. Shaw and M. Tabrizchi, 1994, J. Chem. Soc. Faraday Trans., 90, 17-21.
66. Benter, T., C. Feldmann, U. Kirchner, M. Schmidt, S. Schmidt and R. N. Schindler, 1995, Ber. Bunsenges. Phys. Chem., 99, 1144-1147.
67. Berges, M. G. M. and P. Warneck, 1992, Ber. Bunsenges. Phys. Chem., 96, 413-416.
68. Biaume, F., 1973, J. Photochem., 2, 139-149.
69. Bilde, M., T. J. Wallington, G. Ferronato, J. J. Orlando, G. S. Tyndall, E. Estupinan and S. Haberkorn, 1998, J. Phys.Chem. A, 102, 1976-1986.
70. Binder, J. L., 1938, Phys. Rev., 54, 114-117.
71. Birge, R. R., W. C. Pringle and P. A. Leermakers, 1971, J. Am. Chem. Soc., 93, 6715-6726.
72. Birk, M., R. R. Friedl, E. A. Cohen, H. M. Pickett and S. P. Sander, 1989, J. Chem. Phys., 91, 6588-6597.
73. Birks, J. W., B. Shoemaker, T. J. Leck, R. A. Borders and L. J. Hart, 1977, J. Chem. Phys., 66, 4591-4599.
74. Bishenden, E., J. Haddock and D. J. Donaldson, 1991, J. Phys. Chem., 95, 2113-2115.
75. Bishenden, E., J. Haddock and D. J. Donaldson, 1992, J. Phys. Chem., 96, 6513.
76. Blacet, F. E. and R. A. Crane, 1954, J. Am. Chem. Soc., 76, 5337-5340.
77. Blitz, M. A., D. E. Heard, M. J. Pilling, S. R. Arnold and M. P. Chipperfield, 2004, Geophys. Res. Lett., 31, L09104, doi:10.1029/2004GL020182 (correction).
78. Blitz, M. A., D. E. Heard, M. J. Pilling, S. R. Arnold and M. P. Chipperfield, 2004, Geophys. Res. Lett., 31, L06111, doi:1029/2003GL018793.
79. Bloss, W. J., S. L. Nickolaisen, R. J. Salawitch, R. R. Friedl and S. P. Sander, 2001, J. Phys. Chem. A, 105, 11226-11239.
80. Bloss, W. J., D. M. Rowley, R. A. Cox and R. L. Jones, 2001, J. Phys. Chem. A, 105, 7840-7854.
81. Bogumil, K., J. Orphal, J. P. Burrows and J.-M. Flaud, 2001, Chem. Phys. Lett., 349, 241-248.
82. Bogumil, K., J. Orphal, T. Homann, S. Voigt, P. Spietz, O. C. Fleischmann, A. Vogel, M. Hartmann, H. Krominga, H. Bovensmann, J. Frerick and J. P. Burrows, 2003, J. Photochem. Photobiol. A.: Chem., 157, 167-184.
83. Bongartz, A., J. Kames, U. Schurath, C. George, P. Mirabel and J. L. Ponche, 1994, J. Atmos. Chem., 18, 149-169.
84. Bongartz, A., J. Kames, F. Welter and U. Schurath, 1991, J. Phys. Chem., 95, 1076-1082.
85. Brandon, J. T., S. A. Reid, D. C. Robie and H. Reisler, 1992, J. Chem. Phys., 97, 5246.
86. Braun, M., A. Fahr, R. Klein, M. J. Kurylo and R. E. Huie, 1991, J. Geophys. Res., 96, 13009-13015.
87. Braun, W., R. Klein, A. Fahr, H. Okabe and A. Mele, 1990, Chem. Phys. Lett., 166, 397-403.
88. Brewer, L. and J. Tellinghuisen, 1972, J. Chem. Phys., 56, 3929-3938.
89. Brewer, P., P. Das, G. Ondrey and R. Bersohn, 1983, J. Chem. Phys., 79, 720-723.
90. Bridges, L. and J. M. White, 1973, J. Phys. Chem., 77, 295-298.
91. Brint, P., L. O'Toole, C. A. Mayhew and W. Dussa, 1990, J. Chem. Soc. Faraday Trans., 86, 3349-3354.
92. Brion, C. E., Y. Iida, F. Carnovale and J. P. Thomson, 1985, Chem. Phys., 98, 327-339.
93. Brion, J., A. Chakir, J. Charbonnier, D. Daumont, C. Parisse and J. Malicet, 1998, J. Atmos. Chem., 30, 291-299.
94. Brion, J., A. Chakir, D. Daumont, J. Malicet and C. Parisse, 1993, Chem. Phys. Lett., 213, 610-612.
95. Brion, J., D. Daumont and J. Malicet, 1983, C. R. Acad. Sc. Paris, 297, 401-404.
96. Brion, J., D. Daumont and J. Malicet, 1984, J. Physique. Lett., 45, L57-L60.
97. Brion, J., D. Daumont, J. Malicet and P. Marché, 1985, J. Physique. Lett., 46, L105-L110.
98. Brock, J. C. and R. T. Watson, 1980, Chem. Phys., 46, 477-484.
99. Brodersen, P. H., P. Frisch and H.-J. Schumacher, 1937, Z. Phys. Chem. B, 37, 25-29.
100. Broske, R. Ph.D. Thesis, University of Wuppertal, Germany, 1999.

101. Brouwer, L. and J. Troe, 1981, Chem. Phys. Lett., 82, 1-4.
102. Brown, S. S., R. W. Wilson and A. R. Ravishankara, 2000, J. Phys. Chem., A, 104, 4963-4976.
103. Brownsword, R. A., M. Hillenkamp, T. Laurent, R. K. Vatsa, H.-R. Volpp and J. Wolfrum, 1997, J. Phys. Chem. A, 101, 5222-5227.
104. Brownsword, R. A., M. Hillenkamp, T. Laurent, R. K. Vatsa, H.-R. Volpp and J. Wolfrum, 1997, J. Chem. Phys., 106, 1359-1366.
105. Brownsword, R. A., M. Hillenkamp, T. Laurent, J. Wolfrum, H.-R. Volpp, R. K. Vatsa and H.-S. Yoo, 1997, J. Chem. Phys., 107, 779-785.
106. Brownsword, R. A., P. Schmiechen, H.-R. Volpp, H. P. Upadhyaya, Y. J. Jung and K.-H. Jung, 1999, J. Chem. Phys., 110, 11823-11829.
107. Brust, A. S., K. H. Becker, J. Kleffmann and P. Wiesen, 2000, Atmos. Environ., 34, 13-19.
108. Burkholder, J. B., 1993, J. Geophys. Res., 98, 2963-2974.
109. Burkholder, J. B., personal communication to the NASA JPL Panel.
110. Burkholder, J. B. and E. J. Bair, 1983, J. Phys. Chem., 87, 1859-1863.
111. Burkholder, J. B., M. K. Gilles, T. Gierczak and A. R. Ravishankara, 2002, Geophys. Res. Lett., 29, 1822, doi:10.1029/2002GL014712.
112. Burkholder, J. B., G. P. Knight and J. J. Orlando, 2000, J. Photochem. Photobiol. A: Chem., 134, 133-137.
113. Burkholder, J. B., R. L. Mauldin, R. J. Yokelson, S. Solomon and A. R. Ravishankara, 1993, J. Phys. Chem., 97, 7597-7605.
114. Burkholder, J. B. and J. J. Orlando, 2000, Chem. Phys. Lett., 317, 603-608.
115. Burkholder, J. B., J. J. Orlando and C. J. Howard, 1990, J. Phys. Chem., 94, 687-695.
116. Burkholder, J. B., A. R. Ravishankara and S. Solomon, 1995, J. Geophys. Res., 100, 16793-16800.
117. Burkholder, J. B. and R. K. Talukdar, 1994, Geophys. Res. Lett., 21, 581-584.
118. Burkholder, J. B., R. K. Talukdar and A. R. Ravishankara, 1994, Geophys. Res. Lett., 21, 585-588.
119. Burkholder, J. B., R. K. Talukdar, A. R. Ravishankara and S. Solomon, 1993, J. Geophys. Res., 98, 22937-22948.
120. Burkholder, J. B., R. R. Wilson, T. Gierczak, R. Talukdar, S. A. McKeen, J. J. Orlando, G. L. Vaghjiani and A. R. Ravishankara, 1991, J. Geophys. Res., 96, 5025-5043.
121. Burley, J. D., C. E. Miller and H. S. Johnston, 1993, J. Molec. Spec, 158, 377-391.
122. Burrows, J. P., A. Dehn, B. Deters, S. Himmelmann, A. Richter, S. Voigt and J. Orphal, 1998, J. Quant. Spectrosc. Radiat. Transfer, 60, 1025-1031.
123. Burrows, J. P., A. Richter, A. Dehn, B. Deters, S. Himmelmann, S. Voigt and J. Orphal, 1999, J. Quant. Spectrosc. Radiat. Transfer, 61, 509-517.
124. Burrows, J. P., G. S. Tyndall and G. K. Moortgat. 16th Informal Conf. on Photochemistry, 1984, Boston.
125. Burrows, J. P., G. S. Tyndall and G. K. Moortgat, 1985, J. Phys. Chem., 89, 4848-4856.
126. Burrows, J. P., G. S. Tyndall and G. K. Moortgat, 1988, J. Phys. Chem., 92, 4340-4348.
127. Burton, G. R., W. F. Chan, G. Cooper and C. E. Brion, 1994, Chem. Phys., 181, 147-172.
128. Bush, G. E., R. T. Mahoney, R. I. Morse and K. R. Wilson, 1969, J. Chem. Phys., 51, 449-450.
129. Butler, P. J. D. and L. F. Phillips, 1983, J. Phys. Chem., 87, 183-184.
130. Cacciani, M., A. D. di Sarra, G. Fiocco and A. Amoruso, 1989, J. Geophys. Res., 94, 8485-8490.
131. Cadman, P. and J. P. Simons, 1966, Trans. Faraday Soc., 62, 631-641.
132. Calvert, J. G., R. Atkinson, J. A. Kerr, S. Madronich, G. K. Moortgat, T. J. Wallington and Y. G. *The mechanisms of atmospheric oxidation of the alkenes*; Oxford University Press: New York - Oxford, 2000.
133. Calvert, J. G., J. A. Kerr, K. L. Demerjian and R. D. McQuigg, 1972, Science, 175, 751-752.
134. Calvert, J. G. and G. S. Layne, 1953, J. Am. Chem. Soc., 75, 856-859.
135. Calvert, J. G., S. Madronich, E. P. Gardner, J. A. Davidson, C. A. Cantrell and R. E. Shetter, 1987, J. Phys. Chem., 91, 6339-6341.
136. Calvert, J. G. and J. N. Pitts. In *Photochemistry*; John Wiley & Sons, Inc.: New York, 1966; pp 230-231.
137. Calvert, J. G. and J. N. Pitts *Photochemistry*; John Wiley & Sons, Inc.: New York, 1966.
138. Calvert, J. G. and J. N. Pitts Jr. In *Photochemistry*; John Wiley & Sons, Inc.: New York, 1966; pp 371.
139. Calvert, J. G. and J. N. Pitts Jr. In *Photochemistry*; John Wiley & Sons, Inc.: New York, 1966; pp 377.
140. Calvert, J. G. and J. N. Pitts Jr. In *Photochemistry*; John Wiley & Sons, Inc.: New York, 1966; pp 368.
141. Calvert, J. G. and J. N. Pitts Jr. In *Photochemistry*; John Wiley & Sons, Inc.: New York, 1966; pp 428.
142. Calvert, J. G. and J. N. Pitts Jr. In *Photochemistry*; John Wiley & Sons, Inc.: New York, 1966; pp 429.
143. Calvert, J. G. and J. N. Pitts Jr. In *Photochemistry*; John Wiley & Sons, Inc.: New York, 1966; pp 372.
144. Calvert, J. G. and J. N. Pitts Jr. In *Photochemistry*; John Wiley & Sons, Inc.: New York, 1966; pp 184.
145. Calvert, J. G. and J. N. Pitts Jr. In *Photochemistry*; John Wiley & Sons, Inc.: New York, 1966; pp 369.
146. Calvert, J. G. and J. N. Pitts Jr. In *Photochemistry*; John Wiley & Sons, Inc.: New York, 1966; pp 431.
147. Calvert, J. G. and J. N. Pitts Jr. In *Photochemistry*; John Wiley & Sons, Inc.: New York, 1966; pp 430.
148. Campuzano-Jost, P. and J. N. Crowley, 1999, J. Phys. Chem. A, 103, 2712-2719.
149. Canosa-Mas, C. E., M. Fowles, P. J. Houghton and R. P. Wayne, 1987, J. Chem. Soc. Faraday Trans. 2, 83, 1465-1474.

150. Cantrell, C. A., J. A. Davidson, A. H. McDaniel, R. E. Shetter and J. G. Calvert, 1990, J. Phys. Chem., 94, 3902-3908.
151. Cantrell, C. A., J. A. Davidson, R. E. Shetter, B. A. Anderson and J. G. Calvert, 1987, J. Phys. Chem., 91, 5858-5863.
152. Cantrell, C. A., A. Zimmer and G. S. Tyndall, 1997, Geophys. Res. Lett., 24, 2195-2198, 2687 (Erratum).
153. Carnovale, F., R. Tseng and C. E. Brion, 1981, J. Phys. B: Atom. Mol. Phys., 14, 4771-4785.
154. Carter, R. T., A. Hallou and R. J. Huber, 1999, Chem. Phys. Lett., 310, 166-172.
155. Cattell, F. C., J. Cavanagh, R. A. Cox and M. E. Jenkin, 1986, J. Chem. Soc. Faraday Trans. 2, 82, 1999-2018.
156. Causley, G. C. and B. R. Russell, 1977, J. Electron Spectrosc. Relat. Phenom., 11, 383-397.
157. Chang, J. S., J. R. Barker, J. E. Davenport and D. M. Golden, 1979, Chem. Phys. Lett., 60, 385-390.
158. Chegodaev, P. P. and B. I. Tubikov, 1973, Dokl. Akad. Nauk. SSSR, 210, 647-649.
159. Chen, Y., W. Wang and L. Zhu, 2000, J. Phys. Chem. A, 104, 11126-11131.
160. Chen, Y. and L. Zhu, 2001, J. Phys. Chem. A,, 105, 9689-9696.
161. Chen, Y. and L. Zhu, 2003, J. Chem. Phys. A,, 107, 4643-4651.
162. Chen, Y., L. Zhu and J. S. Francisco, 2002, J. Chem. Phys. A, 106, 7755-7763.
163. Cheng, B. M., C.-Y. Chung, M. Bahou, Y.-P. Lee and L. C. Lee, 2002, J. Chem. Phys., 117, 4293-4298.
164. Cheung, A. S. C., K. Yoshino, J. R. Esmond, S. S. L. Chiu, D. E. Freeman and W. H. Parkinson, 1990, J. Chem. Phys., 92, 842-849.
165. Cheung, A. S. C., K. Yoshino, W. H. Parkinson and D. E. Freeman, 1984, Geophys. Res. Lett., 11, 580-582.
166. Cheung, A. S. C., K. Yoshino, W. H. Parkinson, S. L. Guberman and D. E. Freeman, 1986, Planet. Space Sci., 34, 1007-1021.
167. Chichinin, A. I., 1993, Chem. Phys. Lett., 209, 459-463.
168. Chichinin, A. I., S. A. Chasovnikov and L. N. Krasnoperov, 1987, Chem.Phys.Lett., 138, 371-376.
169. Chiu, S. S. L., A. S. C. Cheung, K. Yoshino, J. R. Esmond, D. E. Freeman and W. H. Parkinson, 1990, J. Chem. Phys., 93, 5539-5543.
170. Chou, C. C., G. Crescentini, H. Vera-Ruiz, W. S. Smith and F. S. Rowland. "Stratospheric Photochemistry of CF_2O, CClFO, and CCl_2O"; 173rd American Chemical Society Meeting, 1977, New Orleans, LA.
171. Chou, C. C., R. J. Milstein, W. S. Smith, H. Vera-Ruiz, M. J. Molina and F. S. Rowland, 1978, J. Phys. Chem., 82, 1-7.
172. Chou, C. C., W. S. Smith, H. V. Ruiz, K. Moe, G. Crescentini, M. J. Molina and F. S. Rowland, 1977, J. Phys. Chem., 81, 286-290.
173. Clark, J. H., C. B. Moore and N. S. Nogar, 1978, J. Chem. Phys., 68, 1264-1271.
174. Clark, R. H. and D. Husain, 1984, J. Photochem., 24, 103-115.
175. Clyne, M. A. A. and J. A. Coxon, 1968, Proc. Roy. Soc. A, 303, 207-231.
176. Clyne, M. A. A. and H. W. Cruse, 1970, Trans. Faraday Soc., 66, 2214-2226.
177. CODATA, 1982, J. Phys. Chem. Ref. Data, 11, 327-496.
178. Colussi, A. J., 1990, J. Phys. Chem., 94, 8922-8926.
179. Colussi, A. J., S. P. Sander and R. R. Friedl, 1992, J. Phys.Chem., 96, 4442-4445.
180. Cooper, G., J. E. Anderson and C. E. Brion, 1996, Chem. Phys., 209, 61-77.
181. Cooper, M. J., E. Wrede, A. J. Orr-Ewing and M. N. R. Ashfold, 1998, J. Chem. Soc. Faraday Trans., 94, 2901-2907.
182. Coquart, B., A. Jenouvier and M. F. Merienne, 1995, J. Atm. Chem, 21, 251-261.
183. Coquart, B., M. F. Merienne and A. Jenouvrier, 1990, Planet. Space Sci., 38, 287.
184. Corcoran, T. C., E. J. Beiting and M. O. Mitchell, 1992, J. Molecular Spectroscopy, 154, 119-128.
185. Cox, R. A., R. A. Barton, E. Ljungstrum and D. W. Stocker, 1984, Chem. Phys. Lett., 108, 228-232.
186. Cox, R. A., W. J. Bloss, R. L. Jones and D. M. Rowley, 1999, Geophys. Res. Lett., 26, 1857-1860.
187. Cox, R. A. and J. P. Burrows, 1979, J. Phys. Chem., 83, 2560-2568.
188. Cox, R. A. and G. B. Coker, 1983, J. Phys. Chem., 87, 4478-4484.
189. Cox, R. A. and R. G. Derwent, 1976, J. Photochem., 52, 23-34.
190. Cox, R. A. and G. D. Hayman, 1988, Nature, 332, 796-800.
191. Cox, R. A. and R. Patrick, 1979, Int. J. Chem. Kinet., 11, 635-648.
192. Cox, R. A., D. W. Sheppard and M. P. Stevens, 1982, J. Photochem., 19, 189-207.
193. Cox, R. A. and G. Tyndall, 1979, Chem. Phys. Lett., 65, 357-360.
194. Cox, R. A. and G. S. Tyndall, 1980, J. Chem. Soc. Faraday Trans. 2, 76, 153-163.
195. Coxon, J. A., W. E. Jones and D. A. Ramsey. 12th International Symposium on Free Radicals, 1976, Laguna Beach, California.
196. Creasey, D. J., D. E. Heard and J. D. Lee, 2000, Geophys. Res. Lett., 27, 1651-1654.
197. Crowley, J. N., R. Helleis, R. Muller, G. K. Moortgat, P. J. Crutzen and J. J. Orlando, 1994, J. Geophys. Res., 99, 20683-20688.

198. Crowley, J. N., F. G. Simon, J. P. Burrows, G. K. Moortgat, M. E. Jenkin and R. A. Cox, 1991, J. Photochem. and Photobiol. A: Chem., 60, 1-10.
199. Currie, J., J. H. Sidebottom and J. Tedder, 1974, Int. J. Chem. Kinet., 6, 481-492.
200. Dagaut, P. and M. J. Kurylo, 1990, J. Photochem. and Photobiol. A:Chem., 51, 133-140.
201. Daumont, D., J. Brion, J. Charbonnier and J. Malicet, 1992, J. Atmos. Chem., 15, 145-155.
202. Daumont, D., J. Brion and J. Malicet, 1983, Planet. Space Sci., 31, 1229-1234.
203. Davenport, J. E. "Determination of NO_2 Photolysis Parameters for Stratospheric Modeling," FAA-EQ-78-14, Federal Aviation Administration, Washington, DC. 1978.
204. Davidson, J. A., C. A. Cantrell, A. H. McDaniel, R. E. Shetter, S. Madronich and J. G. Calvert, 1988, J. Geophys. Res., 93, 7105-7112.
205. Davidson, N., 1951, J. Am. Chem. Soc., 73, 467-468.
206. Daviel, S., Y. Iida, F. Carnovale and C. E. Brion, 1984, Chem. Phys., 83, 319-406.
207. Davis, F. H. and Y. T. Lee, 1996, J. Chem. Phys., 105, 8142-8163.
208. Davis, H. F., B. Kim, H. S. Johnston and Y.-T. Lee, 1993, J. Phys. Chem., 97, 2172-2180.
209. Davis, H. F. and Y. T. Lee, 1992, J. Phys. Chem., 96, 5681-5684.
210. Delmdahl, R. F., S. Ulrich and K.-H. Gericke, 1998, J. Phys. Chem. A,, 102, 7680-7685.
211. DeMore, W. B. and O. Raper, 1964, J. Phys. Chem., 68, 412-414.
212. DeMore, W. B., S. P. Sander, D. M. Golden, R. F. Hampson, M. J. Kurylo, C. J. Howard, A. R. Ravishankara, C. E. Kolb and M. J. Molina, 1997, JPL Publication 97-4, Evaluation 12.
213. DeMore, W. B., S. P. Sander, D. M. Golden, R. F. Hampson, M. J. Kurylo, C. J. Howard, A. R. Ravishankara, C. E. Kolb and M. J. Molina "Chemical Kinetics and Photochemical Data for Use in Stratospheric Modeling, Evaluation Number 12," JPL Publication 97-4, Jet Propulsion Laboratory, California Institute of Technology, Pasadena, CA, 1997.
214. DeMore, W. B. and E. Tschuikow-Roux, 1990, J. Phys. Chem., 94, 5856-5860.
215. Deters, B., J. P. Burrows, S. Himmelmann and C. Blindauer, 1996, Ann. Geophysicae, 14, 468-475.
216. Deters, B., J. P. Burrows and J. Orphal, 1998, J. Geophys. Res., 103, 3563-3570.
217. Dixon, J. K., 1940, J. Chem. Phys., 8, 157-160.
218. Donaldson, D. J., G. J. Frost, K. H. Rosenlof, A. F. Tuck and V. Vaida, 1997, Geophys. Res. Lett., 24, 2651-2654.
219. Donaldson, J., J. J. Orlando, S. Amann, G. S. Tyndall, R. J. Proos, B. R. Henry and V. Vaida, 1998, J. Phys. Chem., 102, 5171-5174.
220. Donohue, T. and J. R. Wiesenfeld, 1975, J. Chem. Phys., 63, 3130-3135.
221. Doucet, J., J. R. Gilbert, P. Sauvageau and C. Sandorfy, 1975, J. Chem. Phys., 62, 366-369.
222. Doucet, J., P. Sauvageau and C. Sandorfy, 1973, J. Chem. Phys., 58, 3708-3716.
223. Doucet, J., P. Sauvageau and C. Sandorfy, 1975, J. Chem. Phys., 62, 355-359.
224. Ebenstein, W. L., J. R. Wiesenfeld and G. L. Wolk, 1978, Chem. Phys. Lett., 53, 185-189.
225. Eden, C., H. Feilchenfeld and S. Manor, 1969, Anal. Chem, 41, 1150-1151.
226. Eden, S., P. Limão-Vieira, S. V. Hoffmann and N. J. Mason, 2003, Chem. Phys. Lett., 379, 170-176.
227. Eden, S., P. Limão-Vieira, P. A. Kendall, N. J. Mason, J. Delwich, M.-J. Hubin-Franskin, T. Tanaka, M. Kitajima, H. Tanaka, H. Cho and S. V. Hoffmann, 2004, Chem. Phys., 297, 257-269.
228. Ellerman, T., J. Sehested, O. J. Nielson, P. Pagsberg and T. J. Wallington, 1994, Chem. Phys. Lett., 218, 287-294.
229. Emrich, M. and P. Warneck, 2000, J. Phys. Chem. A, 104, 9436-9442.
230. Emrich, M. and P. Warneck, 2005, J. Phys. Chem. A, 109, 1752.
231. Evans, J. T., M. P. Chipperfield, H. Oelhaf, M. Stowasser and G. Wetzel, 2003, Geophys. Res. Lett., 29, 10.1029/2002GL016470, 27-21 - 27-24.
232. Fahr, A., W. Braun and M. J. Kurylo, 1993, J. Geophys. Res., 98, 20467-20472.
233. Fahr, A., A. H. Laufer, M. Kraus and R. Osman, 1997, J. Phys. Chem A, 101, 4879-4886.
234. Fahr, A., A. K. Nayak and R. E. Huie, 1995, Chem. Phys., 199, 275-284.
235. Fahr, A., A. K. Nayak and M. J. Kurylo, 1995, Chem. Phys., 197, 195-203.
236. Febo, A., C. Perrino and I. Allegrini, 1996, Atmos. Environ., 30, 3599-3609.
237. Felder, P., 1991, Chem. Phys., 155, 435-445.
238. Felder, P., 1992, Chem. Phys. Lett., 197, 425-432.
239. Felder, P. and G. P. Morley, 1994, Chem. Phys., 185, 145-151.
240. Felder, P., X. Yang and J. R. Huber, 1993, Chem. Phys. Lett., 215, 221-227.
241. Felps, W. S., K. Rupnik and S. P. McGlynn, 1991, J. Phys. Chem., 95, 639-656.
242. Fenter, F. F., V. Catoire, R. Lesclaux and P. D. Lightfoot, 1993, J. Phys. Chem., 97, 3530-3538.
243. Fergusson, W. C., L. Slotin and W. G. Style, 1936, Trans. Far. Soc., 32, 956-962.
244. Finkelnburg, W., H.-J. Schumacher and G. Stieger, 1931, Z. Phys. Chem., B15, 127-156.
245. Fleischmann, O. C., J. P. Burrows and J. Orphal, 2003, Photochem. Photobiol, A: Chem., 157, 127-136.
246. Flesch, R., E. Rühl, K. Hottmann and H. Baumgärtel, 1993, J. Phys. Chem., 97, 837-844.
247. Forte, E., H. Hippler and H. van den Bergh, 1981, Int. J. Chem. Kinet., 13, 1227-1233.

248. Francisco, J. S., M. R. Hand and I. H. Williams, 1996, J. Phys. Chem., 100, 9250-9253.
249. Francisco, J. S. and I. H. Williams, 1992, Mol. Phys., 76, 1433-1441.
250. Frederick, J. E. and R. D. Hudson, 1979, J. Atmos. Sci., 36, 737-745.
251. Frederick, J. E. and J. E. Mentall, 1982, Geophys. Res. Lett., 9, 461-464.
252. Freeman, D. E., K. Yoshino, J. R. Esmond and W. H. Parkinson, 1984, Planet. Space Sci., 32, 239-248.
253. Freeman, D. E., K. Yoshino, J. R. Esmond and W. H. Parkinson. In *Atmospheric Ozone*; C. S. Zerefos and A. Ghazi, Eds., 1985; pp 622-624.
254. Frost, G. J., L. M. Goss and V. Vaida, 1996, J. Geophys. Res, 101, 3869-3877.
255. Frost, G. J., L. M. Goss and V. Vaida, 1996, J. Geophys. Res., 101, 3879-3884.
256. Fujiwara, H. and T. Ishiwata, 1998, J. Phys. Chem., 102, 3856-3859.
257. Furlan, A., T. Gejo and R. J. Huber, 1996, J. Phys. Chem., 100, 7956-7961.
258. Furlan, A., M. A. Haeberli and R. J. Huber, 2000, J. Phys. Chem. A, 104, 10392-10397.
259. Gaedtke, H. and J. Troe, 1975, Ber. Bunsenges. Phys. Chem., 79, 184-191.
260. Ganske, J. A., H. N. Berko and B. J. Finlayson-Pitts, 1992, J. Geophys. Res., 97, 7651-7656.
261. Gardner, E. P., P. D. Sperry and J. G. Calvert, 1987, J. Phys. Chem., 91, 1922-1930.
262. Gardner, E. P., P. D. Sperry and J. G. Calvert, 1987, J. Geophys. Res., 92, 6642-6652.
263. Gardner, E. P., R. D. Wijayaratne and J. G. Calvert, 1984, J. Phys. Chem., 88, 5069-5076.
264. Gedanken, A., 1987, Chem. Phys. Lett., 137, 462-466.
265. Gentieu, E. P. and J. E. Mentall, 1970, Science, 169, 681-683.
266. Gibson, G. E. and N. S. Bayliss, 1933, Phys. Rev., 44, 188-192.
267. Gibson, G. E. and H. C. Ramsperger, 1927, Phys. Rev., 30, 598-600.
268. Giddings, L. E., Jr. and K. K. Innes, 1961, J. Mol. Spectrosc., 6, 528-549.
269. Gierczak, T., J. B. Burkholder, S. Bauerle and A. R. Ravishankara, 1998, Chem. Phys., 231, 229-244.
270. Gierczak, T., J. B. Burkholder and A. R. Ravishankara, 1999, J. Phys. Chem. A, 103, 877-883.
271. Gierczak, T., J. B. Burkholder, R. K. Talukdar, A. Mellouki, S. B. Barone and A. R. Ravishankara, 1997, J. Photochem. Photobiol. A: Chem., 110, 1-10.
272. Gierczak, T., M. K. Gilles, S. Bauerle and A. R. Ravishankara, 2003, J. Phys. Chem. A, 107, 5014-5020.
273. Gilbert, R., P. Sauvageau and C. Sandorfy, 1974, J. Chem. Phys., 60, 4820-4824.
274. Gilles, M. K., A. A. Turnipseed, J. B. Burkholder and A. R. Ravishankara, 1997, J. Phys. Chem. A, 101, 5526-5534.
275. Gillotay, D., A. Jenouvrier, B. Coquart, M. F. Mérienne and P. C. Simon, 1989, Planet. Space Sci., 37, 1127-1140.
276. Gillotay, D. and P. C. Simon, 1988, Annales Geophysicae, 6, 211-215.
277. Gillotay, D. and P. C. Simon, 1989, J. Atmos. Chem., 8, 41-62.
278. Gillotay, D. and P. C. Simon, 1990, Aeronomica Acta A, A356, 1-173.
279. Gillotay, D. and P. C. Simon, 1991, J. Atmos. Chem., 12, 269-285.
280. Gillotay, D. and P. C. Simon, 1991, J. Atmos. Chem., 13, 289-299.
281. Gillotay, D., P. C. Simon and L. Dierickx, 1988, Aeronomica Acta, A335, 1-25.
282. Gillotay, D., P. C. Simon and L. Dierickx, 1993, Aeronomica Acta, A368, 1-15.
283. Giolando, D. M., G. B. Fazekas, W. D. Taylor and G. A. Takacs, 1980, J. Photochem., 14, 335-339.
284. Glicker, S. and H. Okabe, 1987, J. Phys. Chem., 91, 437-440.
285. Glicker, S. and L. J. Stief, 1971, J. Chem. Phys., 54, 2852-2857.
286. Glissmann, A. and H.-J. Schumacher, 1934, Z. Phys. Chem. B, 24, 328-334.
287. Goldfarb, L., A.-M. Schmoltner, M. K. Gilles, J. Burkholder and A. R. Ravishankara, 1997, J. Phys. Chem. A., 101, 6658-6666.
288. Goodeve, C. F. and F. D. Richardson, 1937, Trans. Faraday. Soc., 33, 453-457.
289. Goodeve, C. F. and A. W. C. Taylor, 1935, Proc. Roy. Soc. London, A 152, 221-230.
290. Goodeve, C. F. and A. W. C. Taylor, 1936, Proc. Roy. Soc. London, A 154, 181-187.
291. Goodeve, C. F. and J. I. Wallace, 1930, Trans. Faraday Soc., 26, 254-260.
292. Goodeve, C. F. and B. A. M. Windsor, 1936, Trans. Faraday Soc., 32, 1518-1519.
293. Gordus, A. A. and R. B. Bernstein, 1954, J. Chem. Phys., 22, 790-795.
294. Gosnell, R. R., A. J. Taylor and J. L. Lyman, 1991, J. Chem. Phys., 94, 5949-5953.
295. Graham, R. A. Photochemistry of NO_3 and the Kinetics of the N_2O_5-O_3 System, Ph. D. Thesis, University of California, Berkeley, CA, 1975.
296. Graham, R. A. and H. S. Johnston, 1978, J. Phys. Chem., 82, 254-268.
297. Graham, R. A., A. M. Winer and J. N. Pitts, Jr., 1978, Geophys. Res. Lett., 5, 909-911.
298. Gray, L. T. M. and D. W. G. Style, 1930, Proc. Roy. Soc. London, A 126, 603-612.
299. Green, R. G. and R. P. Wayne, 1976/77, J. Photochem., 6, 375-377.
300. Green, T. J., M. Islam, C. Canosa-Mas, G. Marston and R. P. Wayne, 2004, J. Photochem. Photobiol. A: Chem., 162, 353-370.
301. Green, T. J., M. Islam, P. Guest, K. Hickson, C. E. Canosa-Mas, and R. P. Wayne, 2003, Phys. Chem. Chem. Phys.,, 5, 5409-5418.

302. Greenblatt, G. D. and A. R. Ravishankara, 1990, J. Geophys. Res., 95, 3539-3547.
303. Griffith, D. W. T., G. C. Toon, B. Sen, J.-F. Blavier and R. A. Toth, 2000, Geophys. Res. Lett., 27, 2485-2488.
304. Griggs, M., 1968, J. Phys. Chem., 49, 857-859.
305. Grothe, H. and H. Willner, 1994, Angew. Chem., 106, 1581-1584.
306. Grothe, H. and H. Willner, personal communication to Wayne et al. (1995).
307. Hall, J., T. C. and F. E. Blacet, 1952, J. Chem. Phys., 20, 1745-1749.
308. Hancock, G. and A. Hofzumahaus "Experimental Study of the Altitude Dependence of the Tropospheric Ozone Photolysis Frequency, J(O(1D)) Between 0 and 12 km Height (ATOP)," ENV4-CT95-0158, EU R and D Programme Environment and Climate 1997.
309. Hanf, A., A. Laüter and H.-R. Volpp, 2003, Chem. Phys. Lett., 368, 445-451.
310. Harder, J. W., J. W. Brault, P. V. Johnston and G. H. Mount, 1997, J. Geophys. Res., D102, 3681-3879.
311. Harker, A. B., W. Ho and J. J. Ratto, 1977, Chem. Phys. Lett., 50, 394-397.
312. Harwood, M. H., J. B. Burkholder, M. Hunter, R. W. Fox and A. R. Ravishankara, 1997, J. Phys. Chem. A, 101, 853-863.
313. Harwood, M. H., J. B. Burkholder and A. R. Ravishankara, 1998, J. Phys. Chem. A, 102, 1309-1317.
314. Harwood, M. H. and R. L. Jones, 1994, J. Geophys. Res., 99, 22955-22964.
315. Harwood, M. H., R. L. Jones, R. A. Cox, E. Lutman and O. V. Rattigan, 1993, J. Photochem. Photobiol. A: Chem., 73, 167-175.
316. Harwood, M. H., O. V. Rattigan, R. L. Jones and R. A. Cox, 1992, Proc. SPIE Int. Soc. Opt. Eng., 1715, 113-124.
317. Harwood, M. H., J. M. Roberts, G. J. Frost, A. R. Ravishankara and J. B. Burkholder, 2003, J. Phys. Chem. A, 107, 1148-1154.
318. Harwood, M. H., D. M. Rowley, R. A. Freshwater, R. A. Cox and R. L. Jones, 1995, J. Chem. Soc. Faraday Trans, 91, 3027-3032.
319. Haugen, H. K., E. Weitz and S. R. Leone, 1964, J. Chem. Phys., 83, 3402-3412.
320. Haugen, H. K., E. Weitz and S. R. Leone, 1985, J. Chem. Phys., 83, 3402-3412.
321. Hayman, G. D. and R. A. Cox, 1989, Chem. Phys. Lett., 155, 1-7.
322. He, H.-Y. and W.-H. Fang, 2003, J. Am. Chem. Soc., 125, 16139-16147.
323. Hearn, A. G., 1961, Proc. Phys. Soc. London, 78, 932-940.
324. Heicklen, J., 1965, J. Am. Chem. Soc., 87, 445-453.
325. Heicklen, J., J. Desai, A. Bahta, C. Harper and R. Simonaitis, 1986, J. Photochem., 34, 117-135.
326. Hemenway, C. P., T. G. Lindeman and J. R. Wiesenfeld, 1979, J. Chem. Phys., 70, 3560-3561.
327. Herman, J. R. and J. E. Mentall, 1982, J. Geophys. Res., 87, 8967-8975.
328. Hermann, M., A. Nölle and H. Heydtmann, 1994, Chem. Phys. Lett., 226, 559-562.
329. Herzberg, G. and K. K. Innes, 1957, Can. J. Phys., 35, 842-879.
330. Hicks, E., B. Leroy, P. Rigaud, J.-L. Joudain and G. Le Bras, 1979, J. Chem. Phys., 76, 693-698.
331. Himmelmann, S., J. Orphal, H. Bovensmann, A. Richter, A. Ladstätter-Weissenmayer and J. P. Burrows, 1996, Chem. Phys. Lett., 251, 330-334.
332. Hippler, H., S. Luu, H. Teitelbaum and J. Troe, 1978, Int. J. Chem. Kinet., 10, 155-169.
333. Hitchcock, A. P., G. R. J. Williams, C. E. Brion and P. W. Langhoff, 1984, Chem. Phys., 88, 65-80.
334. Ho, G. H., 1998, Chem. Phys., 226, 101-111.
335. Hochanadel, C. J., J. A. Ghormley, J. W. Boyle and P. J. Ogren, 1977, J. Phys. Chem., 81, 3-7.
336. Hochanadel, C. J., J. A. Ghormley and P. J. Ogren, 1972, J. Chem. Phys., 56, 4426-4432.
337. Holmes, H. H. and F. Daniels, 1934, J. Am. Chem. Soc., 56, 630-637.
338. Horowitz, A. and J. G. Calvert, 1978, Int. J. Chem. Kinet., 10, 805-819.
339. Horowitz, A. and J. G. Calvert, 1982, J. Phys. Chem., 86, 3105-3114.
340. Horowitz, A., C. J. Kershner and J. G. Calvert, 1982, J. Phys. Chem., 86, 3094-3104.
341. Horowitz, A., R. Meller and G. K. Moortgat, 2001, J. Photochem. Photobiol. A: Chem., 146, 19-27.
342. Houel, N. and H. Van den Bergh, 1977, Int. J. Chem. Kinet., 9, 867-874.
343. Hubinger, S. and J. B. Nee, 1994, Chem. Phys., 181, 247-257.
344. Hubinger, S. and J. B. Nee, 1995, J. Photochem. Photobiol. , 86, 1-7.
345. Hubinger, S. and J. B. Nee, 1995, J. Photochem. and Photobiol. A: Chem., 86, 1-7.
346. Hubrich, C. and F. Stuhl, 1980, J. Photochem., 12, 93-107.
347. Hubrich, C., C. Zetzsch and F. Stuhl, 1977, Ber. Bunsenges. Phys. Chem., 81, 437-442.
348. Huder, K. J. and W. B. DeMore, 1995, J. Phys. Chem., 99, 3905-3908.
349. Hudson, R. D., 1971, Reviews of Geophysics and Space Physics, 9, 305-399.
350. Hudson, R. D., 1974, Canad. J. Chem., 52, 1465-1478.
351. Hudson, R. D. and L. J. Kieffer. Absorption Cross Sections of Stratospheric Molecules. In *The Natural Stratosphere of 1974*; CIAP, 1975; Vol. Monograph 1; pp (5-156)-(5-194).
352. Huebert, B. J. and R. M. Martin, 1968, J. Phys. Chem., 72, 3046-3048.

353. Huebner, R. H., J. Bushnell, D. L., R. J. Celotta, S. R. Mielczarek and C. E. Kuyatt, 1975, Nature, 257, 376-378.
354. Hunnicutt, S. S., L. D. Waits and J. A. Guest, 1989, J. Phys. Chem., 93, 5188-5195.
355. Hynes, A. J., E. A. Kenyon, A. J. Pounds and P. H. Wine, 1992, Spectrochim. Acta, 48A, 1235-1242.
356. Ibuki, T., 1992, J. Chem. Phys., 96, 8793-8798.
357. Ibuki, T., N. Takahashi, A. Hiraya and K. Shobatake, 1986, J. Chem. Phys., 85, 5717-5722.
358. Ichimura, T., A. W. Kirk, G. Kramer and E. Tschuikow-Roux, 1976/1977, J. Photochem., 6, 77-90.
359. Ichimura, T., A. W. Kirk and E. Tschuikow-Roux, 1977, J. Phys. Chem., 81, 1153-1156.
360. Illies, A. J. and G. A. Takacs, 1976, J. Photochem., 6, 35-42.
361. Ingham, T., D. Bauer, J. Landgraf and J. N. Crowley, 1998, J. Phys. Chem. A, 102, 3293-3298.
362. Ingham, T., M. Cameron and J. N. Crowley, 2000, J. Phys. Chem. A, 104, 8001-8010.
363. Inn, E. C. Y., 1975, J. Atmos. Sci., 32, 2375-2377.
364. Inn, E. C. Y., 1980, J. Geophys. Res., 85, 7493-7494.
365. Inn, E. C. Y. and Y. Tanaka, 1953, J. Opt. Soc. Am., 43, 870-873.
366. Inn, E. C. Y. and Y. Tanaka, 1958, Adv. Chem. Ser., 21, 263-268.
367. Jacobs, J., M. Kronberg, H. S. P. Müller and H. Willner, 1994, J. Am. Chem. Soc., 116, 1106-1114.
368. Jäger, M., H. Heydtmann and C. Zetzsch, 1996, Chem. Phys. Lett., 263, 817-821.
369. Jansen, M., G. Schatte, K. M. Tobias and H. Willner, 1988, Inorg. Chem., 27, 1703-1706.
370. Jee, Y.-J., Y.-S. Jung and K.-H. Jung, 2001, J. Chem. Phys., 115, 9739-9746.
371. Jee, Y.-J., M. S. Park, Y. S. Kim, Y.-S. Jung and K.-H. Jung, 1998, Chem. Phys. Lett., 287, 701-708.
372. Jenkin, M. E. and R. A. Cox, 1985, J. Phys. Chem., 89, 192-199.
373. Jenkin, M. E. and R. A. Cox, 1991, J. Phys. Chem., 95, 3229-3237.
374. Jenkin, M. E., R. A. Cox, G. Hayman and L. J. Whyte, 1988, J. Chem. Soc. Faraday Trans. 2, 84, 913-930.
375. Jenkin, M. E., R. A. Cox, A. Mellouki, G. Le Bras and G. Poulet, 1990, J. Phys. Chem., 94, 2927-2934.
376. Jenkin, M. E., T. P. Murrells, S. J. Shalliker and G. D. Hayman, 1993, J. Chem. Soc. Faraday Trans., 89, 433-446.
377. Jenouvrier, A., B. Coquart and M.-F. Mérienne, 1996, J. Atmos. Chem., 25, 21-32.
378. Jenouvrier, A., B. Coquart and M. F. Merienne, 1986, J. Quant. Spectros. Radiat. Transfer 36, 349-354.
379. Jensen, F. and J. Oddershede, 1990, J. Phys. Chem., 94, 2235-2237.
380. Jimenez, E., T. Gierczak, H. Stark, J. B. Burkholder and A. R. Ravishankara, 2005, Phys. Chem. Chem. Phys., 7, 342-348.
381. Johnson, M. S., G. D. Billing, A. Gruodis and M. H. M. Janssen, 2001, J. Phys. Chem. A, 105, 8672-8680.
382. Johnsson, K., A. Engdahl and B. Nelander, 1995, J. Phys. Chem., 99, 3965-3968.
383. Johnston, H. S. and H. J. Bertin, Jr., 1959, J. Mol. Spectrosc., 3, 683-696.
384. Johnston, H. S., S. Chang and G. Whitten, 1974, J. Phys. Chem., 78, 1-7.
385. Johnston, H. S., H. F. Davis and Y. T. Lee, 1996, J. Phys. Chem., 100, 4713-4723.
386. Johnston, H. S. and R. Graham, 1973, J. Phys. Chem., 77, 62-63.
387. Johnston, H. S. and R. Graham, 1974, Canad. J. Chem., 52, 1415-1423.
388. Johnston, H. S., E. D. Morris, Jr. and J. Van den Bogaerde, 1969, J. Am. Chem. Soc., 91, 7712-7727.
389. Johnston, H. S., M. Paige and F. Yao, 1984, J. Geophys. Res., 89, 661.
390. Johnston, H. S. and G. S. Selwyn, 1975, Geophys. Res. Lett., 2, 549-551.
391. Jolly, G. S., D. L. Singleton, D. J. McKenney and G. Paraskevopoulos, 1986, J. Chem. Phys., 84, 6662-6667.
392. Jolly, G. S., D. L. Singleton and G. Paraskevopoulos, 1987, J. Phys. Chem., 91, 3463-3465.
393. Jones, E. L. and O. R. Wulf, 1937, J. Chem. Phys., 5, 873-877.
394. Jones, I. T. N. and K. Bayes, 1973, J. Chem. Phys., 59, 4836-4844.
395. Jost, R., J. Nygard, A. Pasinski and A. Delon, 1996, J. Chem. Phys., 105, 1287-1290.
396. Jost, W., 1931, Z. Phys. Chem. A, 153, 143-152.
397. Jourdain, J. L., G. Le Bras, G. Poulet, J. Combourieu, P. Rigaud and B. LeRoy, 1978, Chem. Phys. Lett., 57, 109-112.
398. Jung, K.-W., T. S. Ahmadi and M. A. El-Sayed, 1997, J. Phys. Chem. A, 101, 6562-6567.
399. Jung, Y.-J., M. S. Park, Y. S. Kim, K.-H. Jung and H.-R. Volpp, 1999, J. Chem. Phys., 111, 4005-4012.
400. Jungkamp, T. P. W., U. Kirchner, M. Schmidt and R. N. Schindler, 1995, J. Photochem. Photobiol. A: Chemistry, 99, 1-6.
401. Kalekin, A. L. and K. Morokuma, 2000, J. Chem. Phys., 113, 5750-5762.
402. Kan, C. S., R. D. McQuigg, M. R. Whitbeck and J. G. Calvert, 1979, Int. J. Chem. Kinet., 11, 921-933.
403. Kang, W. K., K. W. Jung, D.-C. Kim and K.-H. Jung, 1996, J. Chem. Phys., 104, 5815-5820.
404. Kavita, K. and P. K. Das, 2000, J. Chem. Phys., 112, 8426-8431.
405. Kenner, R. D., F. Rohrer and F. Stuhl, 1986, J. Phys. Chem., 90, 2635-2639.
406. Kim, Y. S., Y. J. Jung and K.-H. Jung, 1997, J. Chem. Phys., 107, 3805-3812.
407. Kim, Y. S., W. K. Kang and K.-H. Jung, 1996, J. Chem. Phys., 105, 551-557.
408. Kim, Y. S., W. K. Kang, D.-C. Kim and K.-H. Jung, 1997, J. Phys. Chem. A, 101, 7576-7581.

409. Kirmse, B., A. Delon and R. Jost, 1997, J. Geophys. Res., D103, 16089-16098.
410. Kirshenbaum, A. D. and A. G. Streng, 1961, J. Chem. Phys., 35, 1440-1442.
411. Knauth, H. D., H. Alberti and H. Clausen, 1979, J. Phys. Chem., 83, 1604-1612.
412. Knauth, H. D. and R. N. Schindler, 1983, Z. Naturforsch., 38a, 893-895.
413. Knight, G. P., A. R. Ravishankara and J. B. Burkholder, 2000, J. Phys. Chem. A, 104, 11121-11125.
414. Knight, G. P., A. R. Ravishankara and J. B. Burkholder, 2002, Phys. Chem. Chem. Phys., 4, 1432-1437.
415. Koch, S. and G. K. Moortgat, 1998, J. Phys. Chem. A, 102, 9142-9153.
416. Koffend, J. B., J. S. Holloway, M. A. Kwok and R. F. Heidner III, 1987, J. Quant. Spectrosc. Radiat. Transfer, 37, 449-453.
417. Koffend, J. B. and S. R. Leone, 1981, Chem. Phys. Lett., 81, 136-141.
418. Kortüm, G. and G. Friedheim, 1947, Z. Naturforsch., 2a, 20-27.
419. Kozlov, S. N., V. L. Orkin, R. E. Huie and M. J. Kurylo, 2003, J. Phys. Chem. A, 107, 1333-1338.
420. Krajnovich, D., Z. Zhang, L. Butler and Y. T. Lee, 1984, J. Chem. Phys., 88, 4561-4566.
421. Krasnoperov, L. N. and K. Mehta, 1999, J. Phys. Chem. A, 103, 8008-8020.
422. Krisch, M. J., L. R. McCunn, K. Takematsu, L. J. Butler, F. R. Blase and J. Shu, 2004, J. Phys. Chem., A, 108, 1650-1656.
423. Kromminga, J., J. Orphal, P. Spietz, S. Voigt and J. P. Burrows, 2003, J. Photochem. Photobiol. A: Chem., 157, 149-160.
424. Kurylo, M. J., T. J. Wallington and P. A. Ouellette, 1987, J. Photochem., 39, 201-215.
425. Kwok, W. M. and D. L. Phillips, 1996, J. Chem. Phys., 104, 2529-2540.
426. Kwok, W. M. and D. L. Phillips, 1997, Mol. Phys., 90, 315-326.
427. Kwok, W. M. and D. L. Phillips, 1997, Chem. Phys. Lett., 270, 506-516.
428. Kyle, E. and S. W. Orchard, 1977, J. Photochem., 7, 305-317.
429. Lake, J. S. and A. J. Harrison, 1959, J. Chem. Phys., 30, 361-362.
430. Lambert, H. M., P. J. Dagdigian and M. H. Alexander, 1998, J. Chem. Phys., 108, 4460-4466.
431. Lang, V. I., S. P. Sander and R. R. Friedl, 1988, J. Mol. Spectrosc., 132, 89-103.
432. Langford, A. O. and C. B. Moore, 1984, J. Chem. Phys., 80, 4211-4221.
433. Langford, S. R., P. M. Regan, A. J. Orr-Ewing and N. M. R. Ashfold, 1998, Chem. Phys., 231, 245-260.
434. Langhoff, S. R., L. Jaffe and J. O. Arnold, 1977, J. Quant. Spectrosc. Radiat. Transfer, 18, 227-235.
435. Laszlo, B., R. E. Huie, M. J. Kurylo and A. W. Miziolek, 1997, J. Geophys. Res., 102, 1523-1532.
436. Laszlo, B., M. J. Kurylo and R. E. Huie, 1995, J. Phys. Chem., 99, 11701-11707.
437. Lawrence, W. G., K. C. Clemitshaw and V. A. Apkarian, 1990, J. Geophys. Res., 95, 18591-18595.
438. Lee, L. C., 1982, J. Chem. Phys., 76, 4909-4915.
439. Lee, S.-H., Y.-J. Jung and K.-H. Jung, 2000, Chem. Phys., 260, 143-150.
440. Leroy, B., P. Rigaud and E. Hicks, 1987, Ann. Geophys. A., 5, 247-250.
441. Lewis, B. R., L. Berzins and J. H. Carver, 1986, J. Quant. Spectrosc. Radiat. Transfer, 36, 209-232.
442. Lewis, B. R., L. Berzins, J. H. Carver and S. T. Gibson, 1986, J. Quant. Spectrosc. Radiat. Transfer, 36, 187-207.
443. Lewis, R. S., K. Y. Tang and E. K. C. Lee, 1976, J. Chem. Phys., 65, 2910-2911.
444. Li, Q., R. T. Carter and J. R. Huber, 2001, Chem. Phys. Lett., 334, 39-46.
445. Libuda, H. G. Spektroskopische und kinetische Untersuchungen an halogenierten Carbonylverbindungen von atmosphärischem Interesse, PhD-Thesis, University of Wuppertal, Germany, 1992.
446. Libuda, H. G. and F. Zabel, 1995, Ber. Bunsenges. Phys. Chem., 99, 1205-1213.
447. Libuda, H. G., F. Zabel and K. H. Becker. "UV spectra of some organic chlorine and bromine compounds of atmospheric interest"; Kinetics and Mechanisms for the Reactions of Halogenated Organic Compounds in the Troposphere. STEP-HALOCSIDE/AFEAS WORKSHOP, 1991, Dublin, Ireland.
448. Libuda, H. G., F. Zabel, E. H. Fink and K. H. Becker, 1990, J. Phys. Chem., 94, 5860-5865.
449. Lightfoot, P. D., R. A. Cox, J. N. Crowley, M. Destriau, G. D. Hayman, M. E. Jenkin, G. K. Moortgat and F. Zabel, 1992, Atmos. Environ., 26A, 1805-1961.
450. Lightfoot, P. D. and A. A. Jemi-Alade, 1991, J. Photochem. and Photobiol. A: Chem., 59, 1-10.
451. Limao-Vieira, P., S. Eden, P. A. Kendall, N. J. Mason and S. V. Hoffmann, 2002, Chem. Phys. Lett., 364, 535-541.
452. Limão-Vieira, P., S. Eden and N. J. Mason, 2003, Radiation Phys. Chem., 68, 187-192.
453. Limão-Vieira, P., S. Eden, N. J. Mason and S. V. Hoffmann, 2003, Chem. Phys. Lett., 376, 737-747.
454. Lin, C. L., 1976, J. Chem. Eng. Data, 21, 411-413.
455. Lin, C. L., N. K. Rohatgi and W. B. DeMore, 1978, Geophys. Res. Lett., 5, 113-115.
456. Lindeman, T. G. and J. R. Wiesenfeld, 1979, J. Chem. Phys., 70, 2882-2888.
457. Lipscomb, F. J., R. G. W. Norrish and B. A. Thrush, 1956, Proc. Roy. Soc. London, A 233, 455-464.
458. Liyanage, R., Y.-A. Yang, S. Hashimoto, R. J. Gordon and R. W. Field, 1995, J. Chem. Phys., 103, 6811-6814.
459. Lock, M., R. J. Barmes and A. Sinha, 1996, J. Phys. Chem., 100, 7972-7980.
460. Lopez, M. I. and J. E. Sicre, 1988, J. Phys. Chem., 92, 563-564.

461. Lopez, M. I. and J. E. Sicre, 1990, J. Phys. Chem., 94, 3860-3863.
462. Lucazeau, G. and C. Sandorfy, 1970, J. Mol. Spectrosc., 35, 214-231.
463. Lyman, J. and R. Holland, 1988, J. Phys. Chem., 92, 7232-7241.
464. MacLeod, H., G. P. Smith and D. M. Golden, 1988, J. Geophys. Res., 93, 3813-3823.
465. Magneron, I., A. Mellouki, G. Le Bras, G. K. Moortgat, A. Horowitz and K. Wirtz, 2005, J. Phys. Chem. A, 109, 4552-4561.
466. Magneron, I., R. Thévenet, A. Mellouki, G. Le Bras, G. K. Moortgat and K. Wirtz, 2002, J. Phys. Chem. A, 106, 2526-2537.
467. Magnotta, F. and H. S. Johnston, 1980, Geophys. Res. Lett., 7, 769-772.
468. Majer, J. R. and J. P. Simons. Photochemical Processes in Halogenated Compounds. In *Advances in Photochemistry*; Interscience, 1964; Vol. 2; pp 137-181.
469. Malicet, J., J. Brion and D. Daumont, 1989, Chem. Phys. Lett., 158, 293-296.
470. Malicet, J., D. Daumont, J. Charbonnier, C. Parisse, A. Chakir and J. Brion, 1995, J. Atm. Chem, 21, 263-273.
471. Maloney, K. K. and H. B. Palmer, 1973, Int. J. Chem. Kinet., 5, 1023-1037.
472. Man, S.-Q., W. M. Kwok, D. L. Phillips and A. E. Johnson, 1996, J. Chem. Phys., 105, 5842-5857.
473. Mandelman, M. and R. W. Nicholls, 1977, J. Quant. Spectrosc. Radiat. Trans., 17, 483-491.
474. Margitan, J. J., 1983, J. Phys. Chem., 87, 674-679.
475. Margitan, J. J. and R. T. Watson, 1982, J. Phys. Chem., 86, 3819-3824.
476. Maric, D. and J. P. Burrows, 1999, J. Quant. Spectrosc. Radiat. Transfer, 62, 345-369.
477. Maric, D., J. P. Burrows, R. Meller and G. K. Moortgat, 1993, J. Photochem. Photobiol. A Chem., 70, 205-214.
478. Maric, D., J. P. Burrows and G. K. Moortgat, 1994, J. Photochem. Photobiol A: Chem., 83, 179-192.
479. Maric, D., J. N. Crowley and J. P. Burrows, 1997, J. Phys. Chem., 101, 2561-2567.
480. Maricq, M. M., personal communication to JPL subcommittee.
481. Maricq, M. M. and J. J. Szente, 1992, J. Phys. Chem., 96, 4925-4930.
482. Maricq, M. M. and J. J. Szente, 1994, J. Phys. Chem., 98, 2078-2082.
483. Maricq, M. M. and J. J. Szente, 1995, J. Phys. Chem., 99, 4554-4557.
484. Maricq, M. M. and J. J. Szente, 1996, J. Phys. Chem., 100, 4507-4513.
485. Maricq, M. M. and T. J. Wallington, 1992, J. Phys. Chem., 96, 982-986.
486. Marinelli, W. J. and H. S. Johnston, 1982, Chem. Phys. Lett., 93, 127-132.
487. Marinelli, W. J., D. M. Swanson and H. S. Johnston, 1982, J. Chem. Phys., 76, 2864-2870.
488. Marling, L., 1977, J. Chem. Phys., 66, 4200-4225.
489. Marston, G., I. C. Walker, N. J. Mason, J. M. Gingell, H. Zhao, K. L. Brown, F. Motte-Tollet, J. Delwiche and M. R. F. Siggel, 1998, J. Phys. B: Atom. Mol. Phys., 31, 3387-3405.
490. Martin, H. and R. Gareis, 1956, Z. Elektrochemie, 60, 959-964.
491. Martin, R. M. and J. E. Willard, 1964, J. Chem. Phys., 40, 2999-3007.
492. Martinez, R. D., A. A. Buitrago, N. W. Howell, C. H. Hearn and J. A. Joens, 1992, Atmos. Environ., 26A, 785-792.
493. Mashnin, T. S., A. V. Cheryshev and L. N. Krasnoperov, 1993, Chem. Phys. Lett., 207, 105-109.
494. Matchuk, N. M., V. I. Tupikov, A. I. Malkova and S. Y. Pshezhetskii, 1976, Opt. Spektrosk. (Opt. Spectrosc.), 40, 14-18 (17-19).
495. Mathieson, L. and A. L. G. Rees, 1956, J. Chem. Phys., 25, 753-761.
496. Matsumi, Y., F. J. Comes, G. Hancock, A. Hofzumahaus, A. J. Hynes, M. Kawasaki and A. R. Ravishankara, 2002, J. Geophys. Res., in press.
497. Matsumi, Y., P. K. Das and M. Kawasaki, 1990, J. Chem. Phys., 92, 1696-1701.
498. Matsumi, Y., P. K. Das and M. Kawasaki, 1992, J. Chem. Phys., 97, 5261.
499. Matsumi, Y., K. Tonokura, M. Kawasaki and T. Ibuki, 1990, J. Chem. Phys., 93, 7981-7985.
500. Mauersberger, K., J. Barnes, D. Hanson and J. Morton, 1986, Geophys. Res. Lett., 13, 671-673.
501. Mauersberger, K., D. Hanson, J. Barnes and J. Morton, 1987, J. Geophys. Res., 92, 8480-8482.
502. Mauldin, R. L., III, J. B. Burkholder and A. R. Ravishankara, 1992, J. Phys. Chem., 96, 2582-2588.
503. Mazely, T. L., R. R. Friedl and S. P. Sander, 1995, J. Phys. Chem., 99, 8162-8169.
504. Mazely, T. L., R. R. Friedl and S. P. Sander, 1997, J. Phys. Chem., 101, 7090-7097.
505. McAdam, K., B. Veyret and R. Lesclaux, 1987, Chem. Phys. Lett., 133, 39-44.
506. McElcheran, D. E., M. H. J. Wijnen and E. W. R. Steacie, 1958, Can. J. Chem., 36, 321-339.
507. McGivern, W. S., R. Li, P. Zou and S. W. North, 1999, J. Chem. Phys., 111, 5771-5779.
508. McGrath, M. P., K. C. Clemitshaw, F. S. Rowland and W. J. Hehre, 1988, Geophys. Res. Lett., 15, 883-886.
509. McGrath, M. P., K. C. Clemitshaw, F. S. Rowland and W. J. Hehre, 1990, J. Phys. Chem., 94, 6126-6132.
510. McMillan, V., personal communication.
511. McPeters, R. D. and A. M. Bass, 1982, Geophys. Res. Lett., 9, 227-230.
512. McQuigg, R. D. and J. G. Calvert, 1969, J. Am. Chem. Soc., 91, 1590-1599.

513. Meller, R., personal communication to NASA Data Panel.
514. Meller, R., D. Boglu and G. K. Moortgat. "UV spectra of several halogenated carbonyl compounds and FTIR studies of the degradation of CF_3COCl, HCFC-123 and HFC-143a"; Kinetics and Mechanisms for the Reactions of Halogenated Organic Compounds in the Troposphere. STEP-HALOCSIDE/AFEAS WORKSHOP, 1991, Dublin, Ireland.
515. Meller, R. and G. K. Moortgat, 1995, J. Photochem. Photobio. A: Chem., 86, 15-25.
516. Meller, R. and G. K. Moortgat, 1997, J. Photochem. Photobiol. A: Chem., 108, 105-116.
517. Meller, R. and G. K. Moortgat, 2000, J. Geophys. Res. D, 105, 7089-7101.
518. Meller, R., W. Raber, J. N. Crowley, M. E. Jenkin and G. K. Moortgat, 1991, J. Photochem. Photobiol., 62, 163-171.
519. Mellouki, A. and Y. Mu, 2003, J. Photochem. Photobiol. A: Chem., 157, 295-300.
520. Mentall, J. E., E. P. Gentieu, M. Krauss and D. Neumann, 1971, J. Chem. Phys., 55, 5471-5479.
521. Mérienne, M.-F., A. Jenouvrier, B. Coquart and J. P. Lux, 1997, J. Atmos. Chem., 27, 219-232.
522. Mérienne, M. F., B. Coquart and A. Jenouvrier, 1990, Planet. Space Sci., 38, 617-625.
523. Mérienne, M. F., A. Jenouvrier and B. Coquart, 1995, J. Atm. Chem, 20, 281-297.
524. Meyrahn, H. Bildungswege und Analytik des Peroxyacetylnitrats (PAN) in der Atmosphäre, PhD-Thesis, Johann-Gutenberg-Universität, 1984.
525. Meyrahn, H., G. K. Moortgat and P. Warneck, 1981, J. Photochem., 17, 138.
526. Meyrahn, H., J. Pauly, W. Schneider and P. Warneck, 1986, J. Atmos. Chem., 4, 277-291.
527. Mihalcea, R. M., D. S. Baer and R. K. Hanson, 1996, Appl. Optics, 35, 4059-4064.
528. Miller, C. E., S. L. Nickolaisen, J. S. Francisco and S. P. Sander, 1997, J. Chem. Phys., 107, 2300-2307.
529. Minaev, B. F., 1999, J. Phys. Chem. A, 103, 7294-7309.
530. Minschwaner, K., G. P. Anderson, L. A. Hall and K. Yoshino, 1992, J. Geophys. Res., 97, 10103-10108.
531. Minschwaner, K. and D. E. Siskind, 1993, J. Geophys. Res., 98, 20401-20412.
532. Minton, T. K., C. M. Nelson, T. A. Moore and M. Okumura, 1992, Science, 258, 1342-1345.
533. Mishalanie, E. A., J. C. Rutkowski, R. S. Hutte and J. W. Birks, 1986, J. Phys. Chem., 90, 5578-5584.
534. Mitchell, D. N., R. P. Wayne, P. J. Allen, R. P. Harrison and R. J. Twin, 1980, J. Chem. Soc. Faraday Trans. 2, 76, 785-793.
535. Mo, Y., K. Tonokura, Y. Matsumi, M. Kawasaki, T. Sato, T. Arikawa, P. T. A. Reilly, Y. Xie, Y. Yang, Y. Huang and R. J. Gordon, 1992, J. Chem. Phys., 97, 4815-4826.
536. Molina, L. T. and M. J. Molina, 1977, Geophys. Res. Lett., 4, 83-86.
537. Molina, L. T. and M. J. Molina, 1978, J. Phys. Chem., 82, 2410-2414.
538. Molina, L. T. and M. J. Molina, 1979, J. Photochem., 11, 139-144.
539. Molina, L. T. and M. J. Molina, 1981, J. Photochem., 15, 97-108.
540. Molina, L. T. and M. J. Molina. "Chemistry of fluorine in the stratosphere"; 182nd American Chemical Society National Meeting, 1982, New York.
541. Molina, L. T. and M. J. Molina, 1983, J. Phys. Chem., 87, 1306-1308.
542. Molina, L. T. and M. J. Molina, 1986, J. Geophys. Res., 91, 14501-14508.
543. Molina, L. T. and M. J. Molina, 1987, J. Phys. Chem., 91 433-436.
544. Molina, L. T. and M. J. Molina, 1996, Geophys. Res. Lett., 23, 563-565.
545. Molina, L. T., M. J. Molina and F. S. Rowland, 1982, J. Phys. Chem., 86, 2672-2676.
546. Molina, L. T., S. D. Schinke and M. J. Molina, 1977, Geophys. Res. Lett., 4, 580-582.
547. Molina, M. J. and G. Arguello, 1979, Geophys. Res. Lett., 6, 953-955.
548. Molina, M. J., A. J. Colussi, L. T. Molina, R. N. Schindler and T. L. Tso, 1990, Chem. Phys. Lett., 173, 310-315.
549. Molina, M. J., T. Ishiwata and L. T. Molina, 1980, J. Phys. Chem., 84, 821-826.
550. Moore, T. A., M. Okumura and T. K. Minton, 1997, J. Phys. Chem., 1-7, 3337-3338.
551. Moore, T. A., M. Okumura, J. W. Seale and T. K. Minton, 1999, J. Phys. Chem. A, 103, 1692-1695.
552. Moore, T. A., M. Okumura, M. Tagawa and T. K. Minton, 1995, Faraday Discuss, 100, 295-307.
553. Moortgat, G. K., 2001, Pure Appl. Chem., 73, 487-490.
554. Moortgat, G. K. "RADICAL: Evaluation of Radical Sources in Atmospheric Chemistry through Chamber and Laboratory Studies," ENVA-CT97-0419, EUR 20254 EN, 2002.
555. Moortgat, G. K., W. Klippel, K. H. MÖbus, W. Seiler and P. Warneck FAA-EE-80-47, Federal Aviation Administration, Washington, DC 1980.
556. Moortgat, G. K., R. Meller and W. Schneider. Temperature dependence (256-296K) of the absorption cross-sections of bromoform in the wavelength range 285-360 nm. In *The Tropospheric Chemistry of Ozone in the Polar Regions*; H. Niki and K. H. Becker, Eds.; Springer-Verlag: Berlin, 1993; pp 359-369.
557. Moortgat, G. K., W. Seiler and P. Warneck, 1983, J. Chem. Phys., 78, 1185-1190.
558. Moortgat, G. K., F. Slemr, W. Seiler and P. Warneck, 1978, Chem. Phys. Lett., 54, 444-447.
559. Moortgat, G. K., B. Veyret and R. Lesclaux, 1989, J. Phys. Chem., 93, 2362-2368.
560. Moortgat, G. K. and P. Warneck, 1979, J. Chem. Phys., 70, 3639-3651.

561. Morel, O., R. Simonaitis and J. Heicklen, 1980, Chem. Phys. Lett., 73, 38-42.
562. Mössinger, J. C., D. M. Rowley and R. A. Cox, 2002, Atmos. Chem. Phys., 2, 227-234.
563. Mossinger, J. C., D. E. Shallcross and R. A. Cox, 1998, J. Chem. Soc. Faraday Trans., 94, 1391-1396.
564. Motte-Tollet, F., M.-P. Ska, G. M. Marston, I. C. Walker, M. R. F. Siggel, J. M. Gingell, L. Kaminski, K. L. Brown and N. J. Mason, 1997, Chem. Phys. Lett., 275, 298-306.
565. Müller, H. S. P. and H. Willner, 1992, Ber. Bunsenges. Phys. Chem., 96, 427-431.
566. Munk, J., P. Pagsberg, E. Ratajczak and A. Sillesen, 1986, J. Phys. Chem. , 90, 2752-2757.
567. Murtagh, D. P., 1988, Planet. Space Sci., 36, 819-828.
568. Myer, J. A. and J. A. R. Samson, 1970, J. Chem. Phys., 52, 266-271.
569. Myer, J. A. and J. A. R. Samson, 1970, J. Chem. Phys., 52, 716-718.
570. Myers, T. L., N. R. Forde, B. Hu, D. C. Kitchen and L. J. Butler, 1997, J. Chem. Phys., 81, 5361-5373.
571. Nakayama, T., M. T. Kitamura and K. Watanabe, 1959, J. Chem. Phys., 30, 1180-1186.
572. Nayak, A. K., T. J. Buckley, M. J. Kurylo and A. Fahr, 1996, J. Geophys. Res., 101, 9055-9062.
573. Nayak, A. K., M. J. Kurylo and A. Fahr, 1995, J. Geophys. Res, 100, 11185-11189.
574. Nee, J. B., 1991, J. Quant. Spectrosc. Radiat. Transfer, 46, 55.
575. Nee, J. B., M. Suto and L. C. Lee, 1985, J. Phys. B: Atom. Mol. Phys., 18, L293-L294.
576. Nee, J. B., M. Suto and L. C. Lee, 1986, J. Chem. Phys., 85, 4919-4924.
577. Nee, J. B., M. Suto and L. C. Lee, 1986, J. Chem. Phys., 85, 719-724.
578. Nelson, C. M., T. A. Moore and M. Okumura, 1994, J. Chem. Phys., 100, 8055-8064.
579. Nelson, C. M., T. A. Moore, M. Okumura and T. K. Minton, 1996, Chem. Phys, 2248, 287-307.
580. Nelson, H. H. and H. S. Johnston, 1981, J. Phys. Chem., 85, 3891-3896.
581. Ni, C.-K. and G. W. Flynn, 1993, Chem. Phys. Lett., 210, 333-339.
582. Nickolaisen, S. L., C. E. Miller, S. P. Sander, M. R. Hand, I. H. Williams and J. S. Francisco, 1996, J. Chem. Phys., 104, 2857.
583. Nickolaisen, S. L., S. P. Sander and R. R. Friedl, 1996, J. Phys. Chem., 100, 10165-10178.
584. Nicolet, M., 1981, Planet. Space Sci., 29, 951-974.
585. Nicolet, M. and R. Kennes, 1989, Planet. Space Sci., 37, 459-491.
586. Nicovich, J. M. and P. H. Wine, 1988, J. Geophys. Res., 93, 2417.
587. Nishida, S., K. Takahashi, Y. Matsumi, N. Taniguchi and S. Hayashida, 2004, J. Phys. Chem. A., 108, 2451-2456.
588. Nizkorodov, S. A., S. P. Sander and L. R. Brown, 2004, J. Phys. Chem. A, 108, 4864-4872.
589. Nölle, A., H. Heydtmann, R. Meller and G. K. Moortgat, 1993, Geophys. Res. Lett., 20, 707-710.
590. Nölle, A., H. Heydtmann, R. Meller, W. Schneider and G. K. Moortgat, 1992, Geophys. Res. Lett., 19, 281-284.
591. Nölle, A., C. Krumscheid and H. Heydtmann, 1999, Chem. Phys. Lett., 299, 561-565.
592. Ny, T.-Z. and S.-P. Choong, 1933, Chinese J. Phys., 1, 38-54.
593. Ogilvie, J. F., 1971, Trans. Faraday Soc., 67, 2205-2215.
594. Ogorzalek Loo, R., H.-P. Haerri, G. E. Hall and P. L. Houston, 1989, J. Chem. Phys., 90, 4222-4236.
595. Oh, D., W. Sisk, A. Young and H. Johnston, 1986, J. Chem. Phys., 85, 7146-7158.
596. Okabe, H., 1977, J. Chem. Phys., 66, 2058-2062.
597. Okabe, H. In *Photochemistry of Small Molecules*; John Wiley and Sons Inc.: New York, 1978; pp 217.
598. Okabe, H., 1980, J. Chem. Phys., 72, 6642-6650.
599. Okabe, H., 1981, J. Chem. Phys., 75, 2772-2778.
600. Okabe, H., 1983, J. Chem. Phys., 78, 1312-1317.
601. Orkin, V. L., R. E. Huie and M. J. Kurylo, 1997, J. Phys. Chem. A, 101, 9118-9124.
602. Orkin, V. L. and E. E. Kasimovskaya, 1995, J. Atm. Chem, 21, 1-11.
603. Orkin, V. L., V. G. Khamaganov, A. G. Guschin, R. E. Huie and M. J. Kurylo, 1997, J. Phys. Chem. A, 101, 174-178.
604. Orkin, V. L., F. Louis, R. E. Huie and M. J. Kurylo, 2002, J. Phys. Chem. A, 106, 10195-10199.
605. Orlando, J. J. and J. B. Burkholder, 1995, J. Phys. Chem., 99, 1143-1150.
606. Orlando, J. J., J. B. Burkholder, A. M. R. P. Bopegedera and C. J. Howard, 1991, J. Mol. Spectrosc., 145, 278-289.
607. Orlando, J. J., J. B. Burkholder, S. A. McKeen and A. R. Ravishankara, 1991, J. Geophys. Res., 96, 5013-5023.
608. Orlando, J. J. and G. S. Tyndall, 2001, Int. J. Chem. Kinet., 33, 149-156.
609. Orlando, J. J. and G. S. Tyndall, 2003, J. Photochem. Photobiol. A: Photochem., 157, 161-166.
610. Orlando, J. J., G. S. Tyndall, J.-M. Fracheboud, E. G. Estupiñan, S. Haberkorn and A. Zimmer, 1999, Atmos. Environ., 33, 1621-1629.
611. Orlando, J. J., G. S. Tyndall, G. K. Moortgat and J. G. Calvert, 1993, J. Phys. Chem., 97, 10996-11000.
612. Orphal, J. "A Critical Review of the Absorption Cross-Sections of O_3 and NO_2 in the 240-790 nm Region, Part 1, Ozone," ESA Technical Note MO-TN-ESA-GO-0302, European Space Agency, ESA-ESTEC, Noordwijk, 2002.

613. Orphal, J. "A Critical Review of the Absorption Cross-Sections of O_3 and NO_2 in the 240-790 nm Region, Part 2, Nitrogen Dioxide," ESA Technical Note MO-TN-ESA-GO-0302, European Space Agency, ESA-ESTEC, Noordwijk, 2002.
614. Orphal, J., 2003, J. Photochem. Photobiol., A 157, 185-209.
615. Orphal, J., S. Dreher, S. Voigt, J. P. Burrows, R. Jost and A. Delon, 1998, J. Chem. Phys., 109, 10217-10221.
616. Orphal, J., C. E. Fellows and J.-M. Flaud, 2003, J. Geophys. Res., 108 (D3), 4077.
617. Osbourne, B. A., G. Marston, L. Kaminski, N. C. Jones, J. M. Gingell, N. J. Mason, I. C. Walker, J. Delwiche and M.-J. Hubin-Franskin, 2000, J. Quant. Spectrosc. Radiat. Transfer, 64, 67-74.
618. Pagsberg, P., E. Bjergbakke, E. Ratajczak and A. Sillesen, 1997, Chem. Phys. Lett., 272, 383-390.
619. Pagsberg, P., A. Sillesen, J. T. Jodowski and E. Ratajczak, 1996, Chem. Phys. Lett., 249, 358-364.
620. Pagsberg, P. B., E. Ratajczak, A. Sillesen and J. T. Jodkowski, 1987, Chem. Phys. Lett., 141, 88-94.
621. Paraskevopoulos, G. and R. J. Cvetanovic, 1969, J. Am. Chem. Soc., 91, 7572.
622. Park, J., Y. Lee and G. W. Flynn, 1991, Chem. Phys. Lett., 186, 441-449.
623. Parkes, D. A., 1977, Int. J. Chem. Kinet., 9, 451-469.
624. Parkes, D. A., D. M. Paul, C. P. Quinn and R. C. Robson, 1973, Chem. Phys. Lett., 23, 425-429.
625. Parmenter, C. S., 1964, J. Chem. Phys., 41, 658-665.
626. Passchier, A. A., J. D. Christian and N. W. Gregory, 1967, J. Phys. Chem., 71, 937-942.
627. Paukert, T. T. and H. S. Johnston, 1972, J. Chem. Phys., 56, 2824-2838.
628. Paur, R. J. and A. M. Bass. In *Atmospheric Ozone*; C. S. Zerefos and A. Ghazi, Eds., 1985; pp 610-616.
629. Pence, W., S. Baughum and S. Leone, 1981, J. Phys. Chem., 85, 3844-3851.
630. Permien, T., R. Vogt and R. N. Schindler. Mechanisms of Gas Phase-Liquid Phase Chemical Transformations. In *Air Pollution Report #17*; R. A. Cox, Ed.; Environmental Research Program of the CEC: Brussels, 1988.
631. Petersen, A. B. and I. W. M. Smith, 1978, Chem. Phys., 30, 407-413.
632. Peterson, K. A. and J. S. Francisco, 2002, J. Chem. Phys., 117, 6103-6107.
633. Pfister, R. and R. J. Huber, 2002, personal communication.
634. Phillips, D. L., A. B. Myers and J. J. Valentini, 1992, J. Phys. Chem., 96, 2039-2044.
635. Pilling, M. J. and M. J. C. Smith, 1985, J. Phys. Chem., 89, 4713-4720.
636. Platt, U., D. Perner, G. W. Harris, A. M. Winer and J. N. Pitts Jr., 1980, Nature, 285, 312-314.
637. Plenge, J., R. Flesch, S. Kühl, B. Vogel, R. Müller, F. Stroh and E. Rühl, 2004, J. Phys. Chem. A, 108, 4859-4863.
638. Plum, C. N., E. Sanhueza, R. Atkinson, W. P. L. Carter and J. N. J. Pitts, 1983, Environ. Sci. Technol., 17, 479-484.
639. Pope, F. D., C. A. Smith, N. M. R. Ashfold and A. J. Orr-Ewing, 2005, Phys. Chem. Chem. Phys., 7, 79-84.
640. Pope, F. D., C. A. Smith, P. R. Davis, D. E. Shallcross, M. N. R. Ashfold and A. J. Orr-Ewing, 2005, J. Chem. Soc., Faraday Disc, 130/4, 1-14.
641. Porret, D. and C. F. Goodeve, 1937, Trans. Faraday Soc., 33, 690-693.
642. Porret, D. and C. F. Goodeve, 1938, Proc. Roy. Soc. London A, 165, 31-42.
643. Porter, G., Z. G. Szabo and M. G. Townsend, 1962, Proc. Roy. Soc. London, A 270, 493-500.
644. Prahlad, V. and V. Kumar, 1995, J. Quant. Spectrosc. Radiat. Transfer, 54, 945-955.
645. Preston, K. F. and R. F. Barr, 1971, J. Chem. Phys., 54, 3347-3348.
646. Raber, W. H. and G. K. Moortgat. Photooxidation of selected carbonyl compounds in air: methyl ethyl ketone, methyl vinyl ketone, methacrolein, and methylglyoxal. In *Progress and Problems in Atmospheric Chemistry*; J. Barker, Ed.; World Scientific Publ. Co.: Singapore, 1996; pp 318-373.
647. Rabinowitch, E. and W. C. Wood, 1936, Trans. Faraday Soc., 32, 540-546.
648. Rahn, T., H. Zhang, M. Wahlen and G. A. Blake, 1998, Geophys. Res. Lett., 25, 4489-4492.
649. Rattigan, O., E. Lutman, R. L. Jones and R. A. Cox, 1992, Ber. Bunsenges. Phys. Chem., 96, 399-404.
650. Rattigan, O., E. Lutman, R. L. Jones, R. A. Cox, K. Clemitshaw and J. Williams, 1992, J. Photochem. Photobiol. A: Chem., 69, 125-126.
651. Rattigan, O. V., R. L. Jones and R. A. Cox, 1994, Chem. Phys. Lett., 230, 121-126.
652. Rattigan, O. V., D. J. Lary, R. L. Jones and R. A. Cox, 1996, J. Geophys. Res., 101, 23021-23033.
653. Rattigan, O. V., D. M. Rowley, O. Wild, R. L. Jones and R. A. Cox, 1994, J. Chem. Soc. Faraday Trans., 90, 1819-1829.
654. Rattigan, O. V., D. E. Shallcross and R. A. Cox, 1997, J. Chem. Soc. Soc. Faraday Trans., 93, 2839-2846.
655. Rattigan, O. V., O. Wild and R. A. Cox, 1998, J. Photochem. Photobiol. A: Chem., 112, 1-7.
656. Rattigan, O. V., O. Wild, R. L. Jones and R. A. Cox, 1993, J. Photochem. Photobiol. A: Chem., 73, 1-9.
657. Ravishankara, A. R., 1995, Faraday Discuss, 100, 335-336.
658. Ravishankara, A. R. and R. L. Mauldin, 1986, J. Geophys. Res., 91, 8709-8712.
659. Ravishankara, A. R., S. Solomon, A. A. Turnipseed and R. F. Warren, 1993, Science, 259, 194-199.
660. Ravishankara, A. R. and P. H. Wine, 1983, Chem. Phys. Lett., 101, 73-78.
661. Ravishankara, A. R., P. H. Wine and A. O. Langford, 1979, Chem. Phys. Lett., 63, 479-484.

662. Ravishankara, A. R., P. H. Wine, C. A. Smith, P. E. Barbone and A. Torabi, 1986, J. Geophys. Res., 91, 5355-5360.
663. Rebbert, R. E. and P. Ausloos, 1976/1977, J. Photochem., 6, 265-276.
664. Rebbert, R. E. and P. J. Ausloos, 1975, J. Photochem., 4, 419-434.
665. Rebbert, R. E., S. G. Lias and P. Ausloos, 1973, Int. J. Chem. Kinet., 5, 893-908.
666. Rebbert, R. E., S. G. Lias and P. Ausloos, 1978, J. Photochem., 8, 17-27.
667. Regan, P. M., D. Ascenzi, A. Brown, G. G. Balint-Kurti and A. J. Orr-Ewing, 2000, J. Chem. Phys., 112, 10259-10268.
668. Regan, P. M., S. R. Langford, D. Ascenzi, P. A. Cook, A. J. Orr-Ewing and M. N. R. Ashfold, 1999, Phys. Chem. Chem. Phys., 1, 3247-3251.
669. Regan, P. M., S. R. Langford, A. J. Orr-Ewing and M. N. R. Ashfold, 1999, J. Chem. Phys., 110, 281-288.
670. Reid, S. A., J. T. Brandon and H. Reisler, 1993, J. Phys. Chem., 97, 540-543.
671. Ribaud, M. G., 1919, Ann. Phys., 12, 107-226.
672. Rigaud, P., B. Leroy, G. Le Bras, G. Poulet, J. L. Jourdain and J. Combourieu, 1977, Chem. Phys. Lett., 46, 161-163.
673. Robbins, D. E., 1976, Geophys. Res. Lett., 3, 213-216. See also Erratum, GRL, 1976, Vol. 3, p. 757.
674. Robbins, D. E. and R. S. Stolarski, 1976, Geophys. Rev. Lett., 3, 603-606.
675. Röckmann, T. J., C. A. M. Brenninkmeijer, M. Wollenhaupt, J. N. Crowley and P. J. Crutzen, 2000, Geophys. Res. Lett., 27, 1399-1402.
676. Röckmann, T. J., J. Kaiser, C. A. M. Brenninkmeijer, J. N. Crowley, R. Borchers, W. A. Brand and P. J. Crutzen, 2001, J. Geophys. Res., 106, 10,403-10,410.
677. Roehl, C. M., D. Bauer and G. K. Moortgat, 1996, J. Phys. Chem., 100, 4038-4047.
678. Roehl, C. M., J. B. Burkholder, G. K. Moortgat, A. R. Ravishankara and P. J. Crutzen, 1997, J. Geophys. Res., 102, 12819-12829.
679. Roehl, C. M., T. L. Mazely, R. R. Friedl, Y. M. Li, J. S. Francisco and S. P. Sander, 2001, J. Phys. Chem. A, 105, 1592-1598.
680. Roehl, C. M., S. A. Nizkorodov, H. Zhang, G. A. Blake and P. O. Wennberg, 2002, J. Phys. Chem., A, 106, 3766-3772.
681. Roehl, C. M., J. J. Orlando and J. G. Calvert, 1992, J. Photochem. Photobiol. A: Chem., 69, 1-5.
682. Roehl, C. M., J. J. Orlando, G. S. Tyndall, R. E. Shetter, G. J. Vasquez, C. A. Cantrell and J. G. Calvert, 1994, J. Phys. Chem., 98, 7837-7843.
683. Rogers, J. D., 1990, J . Phys. Chem., 94, 4011-4015.
684. Romand, J., 1949, Ann. Phys. (Paris), 4, 529-590.
685. Romand, J. and J. Mayence, 1949, Compt. Rend. Acad. Sci. Paris, 228, 998-1000.
686. Romand, J. and B. Vodar, 1948, Compt. Rend. Acad. Sci. Paris, 226, 238-240.
687. Röth, E. P., R. Ruhnke, G. Moortgat, R. Meller and W. Schneider "UV/VIS-Absorption Cross Sections and Quantum Yields for Use in Photochemistry and Atmospheric Modeling," Forschungszentrum Jülich Publication, Part 1 : Inorganic Substances (jül-3340), Part 2: Organic Substances (jül-3341), 1997.
688. Rowland, F. S. and M. J. Molina, 1975, Rev. Geophys. Space Phys., 13, 1-35.
689. Rowland, F. S., J. E. Spencer and M. J. Molina, 1976, J. Phys. Chem., 80, 2711-2713.
690. Rowley, D. M., M. H. Harwood, R. A. Freshwater and R. L. Jones, 1996, J. Phys. Chem., 100, 3020-3029.
691. Rowley, D. M., J. C. Mössinger, R. A. Cox and R. L. Jones, 1999, J. Atmos. Chem., 34, 137-151.
692. Roxlo, C. and A. Mandl, 1980, J. Appl. Phys., 51, 2969-2972.
693. Ruhl, E., A. Jefferson and V. Vaida, 1990, J. Phys. Chem., 94, 2990-2994.
694. Russell, B. R., L. O. Edwards and J. W. Raymonda, 1973, J. Am. Chem. Soc., 95, 2129-2133.
695. Safary, E., 1954, Ann. Phys. (Paris), 9, 203-254.
696. Safary, E., J. Romand and B. Vodar, 1951, J. Chem. Phys., 19, 379-380.
697. Saiz-Lopez, A., R. W. Saunders, D. M. Joseph, S. H. Ashworth and J. M. C. Plane, 2004, Atmos. Chem. Phys., 4, 1443-1450.
698. Salawitch, R. J., P. O. Wennberg, G. C. Toon, B. Sen and J.-F. Blavier, 2002, Geophys. Res. Lett., 29, 10.1029/2002GL015006, 9-1 - 9-4.
699. Salomon, D., A. W. Kirk and E. Tschuikow-Roux, 1977, J. Photochem., 7, 345-353.
700. Sander, S. P., 1986, J. Phys. Chem., 90, 4135-4142.
701. Sander, S. P., 1986, J. Phys. Chem., 90, 2194-2199.
702. Sander, S. P. and R. R. Friedl, 1989, J. Phys. Chem., 93, 4764-4771.
703. Sander, S. P., R. R. Friedl, W. B. DeMore, D. M. Golden, M. J. Kurylo, R. F. Hampson, R. E. Huie, G. K. Moortgat, A. R. Ravishankara, C. E. Kolb and M. J. Molina "Chemical Kinetics and Photochemical Data for Use in Stratospheric Modeling, Evaluation Number 13," JPL Publication 00-3, Jet Propulsion Laboratory, California Institute of Technology, Pasadena, CA, 2000.
704. Sander, S. P., M. Peterson, R. T. Watson and R. Patrick, 1982, J. Phys. Chem., 86, 1236-1240.
705. Sander, S. P. and R. T. Watson, 1981, J. Phys. Chem., 85, 2960-2964.
706. Sandorfy, C., 1976, Atmos. Environ., 10, 343-351.

707. Sauvageau, P., J. Doucet, R. Gilbert and C. Sandorfy, 1974, J. Chem. Phys., 61, 391-395.
708. Sauvageau, P., R. Gilbert, P. P. Berlow and C. Sandorfy, 1973, J. Chem. Phys., 59, 762-765.
709. Schiffman, A., D. D. Nelson, Jr. and D. J. Nesbitt, 1993, J. Chem. Phys., 98, 6935-6946.
710. Schindler, R., M. Liesner, S. Schmidt, U. Kirschner and T. Benter, 1997, J. Photochem. Photobiol. A: Chem., 107, 9-19.
711. Schmidt, S., T. Benter and R. N. Schindler, 1998, Chem. Phys. Lett., 282, 292-298.
712. Schmitt, G. and F. J. Comes, 1980, J. Photochem., 14, 107-123.
713. Schmitt, G. and F. J. Comes, 1987, J. Photochem. Photobiol. A, 41, 13-30.
714. Schneider, W., G. K. Moortgat, J. P. Burrows and G. Tyndall, 1987, J. Photochem. Photobiol., 40, 195-217.
715. Schneider, W. F., T. J. Wallington, K. Minschwaner and E. A. Stahlberg, 1995, Environ. Sci. Technol., 29, 247-250.
716. Schott, G. and N. Davidson, 1958, J. Amer. Chem. Soc., 80, 1841-1853.
717. Seccombe, D. P., R. Y. L. Chim, R. P. Tucket, H. W. Jochims and H. Baumgaertel, 2001, J. Chem. Phys., 114, 4058-4073.
718. Seccombe, D. P., R. P. Tuckett, H. Baumgärtel and H. W. Jochims, 1999, Phys. Chem. Chem. Phys., 1, 773-782.
719. Seery, D. J. and D. Britton, 1964, J. Phys. Chem., 68, 2263-2266.
720. Seki, K. and H. Okabe, 1992, J. Phys. Chem., 96, 3345-3349.
721. Sellevåg, S. R., T. Kelly, H. Sidebottom and C. J. Nielsen, 2004, Phys. Chem. Chem. Phys., 6, 1243-1252.
722. Selwyn, G., J. Podolske and H. S. Johnston, 1977, Geophys. Res. Lett., 4, 427-430.
723. Selwyn, G. S. and H. S. Johnston, 1981, J. Chem. Phys., 74, 3791-3803.
724. Senapati, D. and P. K. Das, 2004, Chem.Phys. Lett., 393, 535-538.
725. Senapati, D., K. Kavita and P. K. Das, 2002, J. Phys. Chem. A, 106, 8479-8482.
726. Senum, G. I., Y.-N. Lee and J. S. Gaffney, 1984, J. Phys. Chem., 88, 1269-1270.
727. Shardanand and A. D. P. Rao, 1977, J. Quant. Spectrosc. Radiat. Transfer, 17, 433-439.
728. Sharpe, S., B. Hartnett, H. S. Sethi and D. S. Sethi, 1987, J. Photochem., 38, 1-13.
729. Sidebottom, H. W., J. M. Tedder and J. C. Walton, 1969, Trans. Faraday Soc., 65, 755-762.
730. Silvente, E., R. C. Richter, M. Zheng, E. S. Saltzman and A. J. Hynes, 1997, Chem. Phys. Lett., 264, 309-315.
731. Simon, F.-G., W. Schneider and G. K. Moortgat, 1990, Int. J. Chem. Kinet., 22, 791-813.
732. Simon, F. G., W. Schneider, G. K. Moortgat and J. P. Burrows, 1990, J. Photochem. Photobiol., A55, 1-23.
733. Simon, P. C., D. Gillotay, N. Vanlaethem-Meurée and J. Wisemberg, 1988, Annales Geophysicae, 6, 239-248.
734. Simon, P. C., D. Gillotay, N. Vanlaethem-Meurée and J. Wisemberg, 1988, J. Atmos. Chem., 7, 107-135.
735. Simonaitis, R., R. I. Greenberg and J. Heicklen, 1972, Int. J. Chem. Kinet., 4, 497-512.
736. Simons, J. W., R. J. Paur, H. A. Webster III and E. J. Blair, 1973, J. Phys. Chem., 59, 1203-1208.
737. Singer, R. J., J. N. Crowley, J. P. Burrows, W. Schneider and G. K. Moortgat, 1989, J. Photochem. Photobiol., 48, 17-32.
738. Singleton, D. L., G. Paraskevopoulos and R. S. Irwin, 1987, J. Photochem., 37, 209-216.
739. Singleton, D. L., G. Paraskevopoulos and R. S. Irwin, 1989, Res. Chem. Intermediates, 12, 1-12.
740. Singleton, D. L., G. Paraskevopoulos and R. S. Irwin, 1990, J. Phys. Chem., 94, 695-699.
741. Skorokhodov, V., Y. Sato, K. Suto, Y. Matsumi and M. Kawasaki, 1996, J. Phys. Chem., 100, 12321-12328.
742. Smith, F.-G., F. M. G. Tablas, L. T. Molina and M. J. Molina, 2001, J. Phys. Chem. A, 105, 8658-8664.
743. Smith, G. D., L. T. Molina and M. J. Molina, 2000, J. Phys.Chem. A, 104, 8916-8921.
744. Smith, G. D., L. T. Molina and M. J. Molina, 2002, J. Phys. Chem. A, 106, 1233-1240.
745. Smith, W. S., C. C. Chou and F. S. Rowland, 1977, Geophys. Res. Lett., 4, 517-519.
746. Soller, R., J. M. Nicovich and P. H. Wine, 2002, J. Phys. Chem. A, 106, 8378-8385.
747. Solomon, S., J. B. Burkholder, A. R. Ravishankara and R. R. Garcia, 1994, J. Geophys. Res., 99, 20929-20935.
748. Spencer, J. E. and F. S. Rowland, 1978, J. Phys. Chem., 82, 7-10.
749. Staffelbach, T. A., J. J. Orlando, G. S. Tyndall and J. G. Calvert, 1995, J. Geophys. Res., 100, 14189-14198.
750. Stanton, J. F., C. M. L. Rittby, R. J. Bartlett and D. W. Toohey, 1991, J. Phys. Chem., 95, 2107-2110.
751. Steinfeld, J. I., S. M. Adler-Golden and J. W. Gallagher, 1987, J. Phys. Chem. Ref. Data, 16, 911-951.
752. Stephens, E. R., 1969, Adv. Environ. Sci. Technol., 1, 119-146.
753. Stickel, R. E., A. J. Hynes, J. D. Bradshaw, W. L. Chameides and D. D. Davis, 1988, J. Phys. Chem., 92, 1862-1864.
754. Stief, L. J., W. A. Payne and R. B. Klemm, 1975, J. Chem. Phys., 62, 4000-4008.
755. Stockwell, W. R. and J. G. Calvert, 1978, J. Photochem., 8, 193-203.
756. Stutz, J., E. S. Kim, U. Platt, P. Bruno, C. Perrino and A. Febo, 2000, J. Geophys. Res., 105, 14585-14592.

757. Sulzer, P. and K. Wieland, 1952, Helv. Phys. Acta, 25, 653-676.
758. Suto, M. and L. C. Lee, 1984, J. Chem. Phys., 81, 1294-1297.
759. Suto, M. and L. C. Lee, 1985, J. Geophys. Res., 90, 13037-13040.
760. Swanson, D., B. Kan and H. S. Johnston, 1984, J. Phys. Chem., 88, 3115-3118.
761. Tadic, J., G. K. Moortgat and K. Wirtz, 2005, J. Photochem. Photobiol. A: Chem., 177, 116-124.
762. Takahashi, K., Y. Matsumi and M. Kawasaki, 1996, J. Phys. Chem., 100, 4084-4089.
763. Taketani, F., K. Takahashi and Y. Matsumi, 2005, J. Phys. Chem. A, 109, 2855-2860.
764. Talukdar, R., A. Mellouki, T. Gierczak, J. B. Burkholder, S. A. McKeen and A. R. Ravishankara, 1991, J. Phys. Chem., 95, 5815-5821.
765. Talukdar, R., A. Mellouki, T. Gierczak, J. B. Burkholder, S. A. McKeen and A. R. Ravishankara, 1991, Science, 252, 693-695.
766. Talukdar, R. K., J. B. Burkholder, A.-M. Schmoltner, J. M. Roberts, R. Wilson and A. R. Ravishankara, 1995, J. Geophys. Res., 100, 14163-14173.
767. Talukdar, R. K., M. K. Gilles, F. Battin-Leclerc, A. R. Ravishankara, J.-M. Fracheboud, J. J. Orlando and G. S. Tyndall, 1997, Geophys. Res. Lett., 24, 1091-1094.
768. Talukdar, R. K., M. Hunter, R. F. Warren, J. B. Burkholder and A. R. Ravishankara, 1996, Chem. Phys. Lett., 262, 669-674.
769. Talukdar, R. K., C. A. Longfellow, M. K. Gilles and A. R. Ravishankara, 1998, Geophys. Res. lett., 25, 143-146.
770. Talukdar, R. K., A. Mellouki, J. B. Burkholder, M. K. Gilles, G. Le Bras and A. R. Ravishankara, 2001, J. Phys. Chem. A, 105, 5188-5196.
771. Talukdar, R. K., G. L. Vashjiani and A. R. Ravishankara, 1992, J. Chem. Phys., 96, 8194-8201.
772. Tanaka, Y., E. C. Y. Inn and K. Watanabe, 1953, J, Chem. Phys., 21, 1651-1653.
773. Tanaka, Y., M. Kawasaki, Y. Matsumi, H. Fujiwara, T. Ishiwata, L. J. Rogers, R. N. Dixon and M. N. R. Ashfold, 1998, J. Chem. Phys., 109, 1315-1325.
774. Tang, K. Y., P. W. Fairchild and E. K. C. Lee, 1979, J. Phys. Chem., 83, 569-573.
775. Tellinghuisen, J., 1973, J. Chem. Phys., 58, 2821-2834.
776. Tellinghuisen, J., 2003, J. Phys. Chem. A, 107, 753-775.
777. Thelen, M.-A., P. Felder and J. R. Huber, 1993, Chem. Phys. Lett., 213, 275-281.
778. Thompson, B. A., P. Harteck and J. Reeves, R. R., 1963, J. Geophys. Res., 68, 6431-6436.
779. Toniolo, A., G. Granucci, S. Inglese and M. Persico, 2001, Phys. Chem. Chem. Phys., 3, 4266-4279.
780. Toniolo, A., M. Persico and D. Pitea, 2000, J. Phys. Chem. A, 104, 7278-7283.
781. Tonokura, K., Y. Matsumi, M. Kawasaki, H. L. Kim, S. Yabushita, S. Fujimura and K. Saito, 1993, J. Chem. Phys., 99, 3461-3467.
782. Tonokura, K., Y. Matsumi, M. Kawasaki, S. Tasaki and R. Bersohn, 1992, J. Chem. Phys., 97, 8210-8215.
783. Troe, J., 2000, Z. Phys. Chem., 214, 573-581.
784. Trolier, M., R. L. Mauldin, III and A. R. Ravishankara, 1990, J. Phys. Chem., 94, 4896-4907.
785. Trolier, M. and J. R. Wiesenfeld, 1988, J. Geophys. Res., 93, 7119-7124.
786. Turatti, F., D. W. T. Griffith, S. R. Wilson, M. B. Esler, T. Rahn, H. Zhang and G. A. Blake, 2000, Geophys. Res. Lett., 27, 2489-2492.
787. Turco, R. P., 1975, Geophys. Surveys, 2, 153-192.
788. Turnipseed, A. A., M. K. Gilles, J. B. Burkholder and A. R. Ravishankara, 1995, Chem. Phys. Lett., 242, 427-434.
789. Turnipseed, A. A., G. L. Vaghjiani, J. E. Thompson and A. R. Ravishankara, 1992, J. Chem. Phys., 96, 5887-5895.
790. Tyndall, G. S., R. A. Cox, C. Granier, R. Lesclaux, G. K. Moortgat, M. J. Pilling, A. R. Ravishankara and T. J. Wallington, 2001, J. Geophys. Res., 106, 12157-12182.
791. Tyndall, G. S., C. S. Kegley-Owen, J. J. Orlando and J. G. Calvert, 1997, J. Chem. Soc. Faraday Trans., 93, 2675-2682.
792. Tyndall, G. S., K. M. Stedman, W. Schneider, J. P. Burrows and G. K. Moortgat, 1987, J. Photochem., 36, 133-139.
793. Tzeng, W. B., Y. R. Lee and S. M. Lin, 1994, Chem. Phys. Lett., 227, 467-471.
794. Uma, S. and P. K. Das, 1994, Can. J. Chem., 72, 865-869.
795. Uma, S. and P. K. Das, 1995, Chem. Phys. Lett., 241, 335-338.
796. Uma, S. and P. K. Das, 1996, J. Chem. Phys., 104, 4470-4474.
797. Uthman, A. P., P. J. Demlein, T. D. Allston, M. C. Withiam, M. J. McClements and G. A. Takacs, 1978, J. Phys. Chem., 82, 2252-2257.
798. Vaghjiani, G., 1993, J. Chem. Phys., 99, 5936-5943.
799. Vaghjiani, G. L. and A. R. Ravishankara, 1989, J. Geophys. Res., 94, 3487-3492.
800. Vaghjiani, G. L. and A. R. Ravishankara, 1990, J. Chem. Phys., 92, 996-1003.
801. Vaghjiani, G. L., A. A. Turnipseed, R. F. Warren and A. R. Ravishankara, 1992, J. Chem. Phys., 96, 5878.
802. Vaida, V., S. Solomon, E. C. Richards, E. Ruhl and A. Jefferson, 1989, Nature, 342, 405-408.

803. Van den Bergh, H. and J. Troe, 1976, J. Chem. Phys., 64, 736-742.
804. Vandaele, A. C., C. Hermans, S. Fally, M. Carleer, R. Colin, M.-F. Mérienne, A. Jenouvrier and B. Coquart, 2002, J. Geophys. Res., D 107, 4384.
805. Vandaele, A. C., C. Hermans, S. Fally, M. Carleer and M.-F. Merienne, 2003, J. Quant. Spectrosc. Radiat. Transfer, 76, 373-391.
806. Vandaele, A. C., C. Hermans, P. C. Simon, M. Van Roozendael, J. M. Guilmot, M. Carleer and R. Colin, 1966, J. Atmos. Chem., 25, 289-305.
807. Vandaele, A. C., D. Hermans, P. C. Simon, M. Carleer, R. Colin, S. Fally, M.-F. Meriénne, A. Jenouvrier and B. Coquart, 1998, J. Quant. Spectrosc. Radiat. Transfer, 59, 171-184.
808. Vanlaethem-Meurée, N., J. Wisemberg and P. C. Simon, 1978, Bull. Acad. Roy. Belgique Cl. Sci., 64, 31.
809. Vanlaethem-Meurée, N., J. Wisemberg and P. C. Simon, 1978, Bull. Acad. Roy. Belgique Cl. Sci., 64, 42.
810. Vanlaethem-Meurée, N., J. Wisemberg and P. C. Simon, 1979, Geophys. Res. Lett., 6, 451-454.
811. Vassy, A. and E. Vassy, 1948, J. Chem. Phys., 16, 1163-1164.
812. Vasudev, R., 1990, Geophys. Res. Lett., 17, 2153-2155.
813. Vatsa, R. K., A. Kumar, P. D. Naik, K. V. S. Rama Rao and J. P. Mittal, 1993, Chem. Phys. Lett., 207, 75-80.
814. Vatsa, R. K. and H.-R. Volpp, 2001, Chem. Phys. Lett., 340, 289-295.
815. Vésine, E. and A. Mellouki, 1997, J. Chim. Phys. Physico-Chim. Biol., 94, 1634-1641.
816. Vesley, G. F. and P. A. Leermakers, 1964, J. Phys. Chem., 68, 2364-2366.
817. Vetter, R., T. Ritschel and L. Zulicke, 2003, J. Phys. Chem., A, 107, 1405-1412.
818. Vigroux, E., 1953, Ann. Phys., 8, 709-762.
819. Vigroux, E., 1967, C. R. Acad. Sc. Paris, 264, 1290-1291.
820. Vigroux, E., 1969, Ann. Geophys., 25, 169-172.
821. Villenave, E., I. Morozov and R. Lesclaux, 2000, J. Phys. Chem. A, 104, 9933-9940.
822. Vogt, K. and J. Koenigsberger, 1923, Z. Physik, 13, 292-310.
823. Vogt, R. and R. N. Schindler. Air Pollution Report 34, 1990; pp 167-171.
824. Vogt, R. and R. N. Schindler, 1992, J. Photochem. Photobiol. A: Chem., 66, 133-140.
825. Voigt, S., J. Orphal, K. Bogumil and J. P. Burrows, 2001, J. Photochem. Photobiol. A, 143, 1-9.
826. Voigt, S., J. Orphal and J. P. Burrows, 2002, J. Photochem. Photobiol. A: Chem., 149, 1-7.
827. Volkamer, R., P. Spietz, J. P. Burrows and U. Platt, 2005, J. Photochem. Photobiol. A: Chem., 172, 35-36.
828. von Hessberg, P., J. Kaiser, M. B. Enghoff, C. A. McLinden, S. L. Sorensen, T. Rockmann and M. S. Johnson, 2004, Atmos. Chem. Phys., 4, 1237-1253.
829. Wahner, A., A. R. Ravishankara, S. P. Sander and R. R. Friedl, 1988, Chem. Phys. Lett., 152, 507-512.
830. Wahner, A., G. S. Tyndall and A. R. Ravishankara, 1987, J. Phys. Chem., 91, 2734-2738.
831. Wallington, T. J., P. Dagaut and M. J. Kurylo, 1988, J. Photochem. Photobiol. A: Chemistry, 42, 173-185.
832. Wallington, T. J., P. Dagaut and M. J. Kurylo, 1992, Chem. Rev., 92, 667-710.
833. Wallington, T. J., M. M. Mariq, T. Ellerman and O. J. Nielsen, 1992, J. Phys. Chem., 96, 982-986.
834. Walton, J. C., 1972, J. Chem. Soc. Farad. Trans., 68, 1559-1565.
835. Wang, L. and J. Zhang, 2000, Environ. Sci. Technol., 34, 4221-4227.
836. Wangberg, I., T. Etzkorn, I. Barnes, U. Platt and K. H. Becker, 1997, J. Phys. Chem. A, 101, 9694-9698.
837. Wannenmacher, E. A. J., P. Felder and R. J. Huber, 1991, J. Chem. Phys., 95, 986-997.
838. Warneck, P., 2001, Atmos. Environ., 35, 5773-5777.
839. Watson, R. T., 1977, J. Phys. Chem. Ref. Data, 6, 871-917.
840. Wayne, R. P., I. Barnes, J. P. Burrows, C. E. Canosa-Mas, J. Hjorth, G. Le Bras, G. K. Moortgat, D. Perner, G. Poulet, G. Restelli and H. Sidebottom, 1991, Atmos. Environ., 25A, 1-203.
841. Wayne, R. P., G. Poulet, P. Biggs, J. P. Burrows, R. A. Cox, P. J. Crutzen, G. D. Hayman, M. E. Jenkin, G. Le Bras, G. K. Moorgat, U. Platt and R. N. Schindler, 1995, Atmos. Environ., 29, 2675-2881.
842. Weaver, J., J. Meagher and J. Heicklen, 1976, J. Photochem., 6, 111-126.
843. Wen, W. Y. and R. M. Noyes, 1972, J. Phys. Chem., 76, 1017-1018.
844. Wennberg, P. O., J. W. Brault, T. F. Hanisco, R. J. Salawitch and G. H. Mount, 1997, J. Geophys. Res., D102, 8887-8898.
845. Wennberg, P. O., R. J. Salawitch, D. J. Donaldson, T. F. Hanisco, E. J. Lanzendorf, K. K. Perkins, S. A. Lloyd, V. Vaida, R. S. Gao, E. J. Hintsa, R. C. Cohen, W. H. Swartz, T. L. Kusterer and D. E. Anderson, 1999, Geophys. Res. Lett., 26, 1373-1376.
846. Wheeler, M. D., S. M. Newman, T. Ishiwata, M. Kawasaki and A. J. Orr-Ewing, 1998, Chem. Phys. Lett., 285, 346-351.
847. Wijnen, M. H., 1961, J. Am. Chem. Soc., 83, 3014-3017.
848. Wilmouth, D. M., T. F. Hanisco, N. M. Donahue and J. G. Anderson, 1999, J. Phys. Chem A, 103, 8935-8945.
849. Wine, P. H., A. R. Ravishankara, D. L. Philen, D. D. Davis and R. T. Watson, 1977, Chem. Phys. Lett., 50, 101-106.

850. Winterhalter, R., N. R. Jensen, I. Magneron, K. Wirtz, A. Mellouki, Y. Mu, J. Tadic, A. Horowitz, G. K. Moortgat and J. Hjorth. "Proceedings of the EUROTRAC-2 Symposium 2000", 2001, Springer, Berlin.
851. WMO *Atmospheric Ozone: 1985*; National Aeronautics and Space Administration: Geneva, 1986.
852. Wollenhaupt, M., S. A. Carl, A. Horowitz and J. N. Crowley, 2000, J. Phys. Chem., A, 104, 2695-2705.
853. Wrede, E., S. Laubach, S. Schulenburg, A. Brown, E. R. Wouters, A. J. Orr-Ewing and N. M. R. Ashfold, 2001, J. Chem. Phys., 114, 2629-2646.
854. Xu, D., J. S. Francisco, J. Huang and W. M. Jackson, 2002, J. Chem. Phys., 117, 2578-2585.
855. Yamamoto, S. and R. A. Back, 1985, Can. J. Chem., 63, 549-554.
856. Yao, F., I. Wilson and H. Johnston, 1982, J. Phys. Chem., 86, 3611-3615.
857. Yokelson, R. J., J. Burkholder, R. W. Fox and A. R. Ravishankara, 1997, J. Phys. Chem. A, 101, 6667-6678.
858. Yokelson, R. J., J. B. Burkholder, R. W. Fox, R. K. Talukdar and A. R. Ravishankara, 1994, J. Phys. Chem., 98, 13144-13150.
859. Yoshino, K., A. S. C. Cheung, J. R. Esmond, W. H. Parkinson, D. E. Freeman, S. L. Guberman, A. Jenouvrier, B. Coquart and M. F. Merienne, 1988, Planet. Space Sci., 36, 1469-1475.
860. Yoshino, K., J. R. Esmond, A. S.-C. Cheung, D. E. Freeman and W. H. Parkinson, 1992, Planet. Space Sci., 40, 185-192.
861. Yoshino, K., J. R. Esmond, A. S. C. Cheung, D. E. Freeman and W. H. Parkinson, 1990, J. Geophys. Res., 95, 11743.
862. Yoshino, K., J. R. Esmond, D. E. Freeman and W. H. Parkinson, 1993, J. Geophys. Res., 98, 5205-5211.
863. Yoshino, K., J. R. Esmond and W. H. Parkinson, 1997, Chem. Phys., 221, 169-174.
864. Yoshino, K., D. E. Freeman, J. R. Esmond, R. S. Friedman and W. H. Parkinson, 1988, Planet. Space Sci., 36, 1201-1210.
865. Yoshino, K., D. E. Freeman, J. R. Esmond, R. S. Friedman and W. H. Parkinson, 1989, Planet. Space Sci., 37, 419-426.
866. Yoshino, K., D. E. Freeman, J. R. Esmond and W. H. Parkinson, 1987, Planet. Space Sci., 35, 1067-1075.
867. Yoshino, K., D. E. Freeman, J. R. Esmond and W. H. Parkinson, 1988, Planet. Space Sci., 36, 395-398.
868. Yoshino, K., D. E. Freeman and W. H. Parkinson, 1984, Planet. Space Sci., 32, 1219-1222.
869. Yoshino, K., D. E. Freeman and W. H. Parkinson, 1984, J. Phys. Chem. Ref. Data, 13, 207-227.
870. Yoshino, K., D. F. Freeman, J. R. Esmond and W. H. Parkinson, 1983, Planet. Space Sci., 31, 339-353
871. Yujing, M. and A. Mellouki, 2000, J. Photochem. Photobiol. A: Chem., 134, 31-36.
872. Yung, Y. L. and C. E. Miller, 1997, Science, 278, 1778-1780.
873. Zaraga, F., N. S. Nogar and C. B. Moore, 1976, J. Mol. Spectrosc., 63, 564-571.
874. Zelikoff, M. and L. M. Aschenbrand, 1954, J. Chem. Phys., 22 1685-1687.
875. Zelikoff, M., K. Watanabe and E. C. Y. Inn, 1953, J. Chem. Phys., 21, 1643-1647.
876. Zetzsch, C. In *Proceedings of the International Ozone Symposium 1988*; R. Bojkov and P. Fabian, Eds.; Deepak: Hampton, VA, 1989.
877. Zhang, H., C. M. Roehl, S. P. Sander and P. O. Wennberg, 2000, J. Geophys. Res., D 105, 14593-14598.
878. Zhang, H., C. M. Roehl, S. P. Sander and P. O. Wennberg, 2000, J. Geophys. Res., 105, 14593-14598.
879. Zhang, H., P. O. Wennberg, V. H. Wu and G. A. Blake, 2000, Geophys. Res. Lett., 27, 2481-2484.
880. Zhang, J., M. Dulligan and C. Wittig, 1997, J. Chem. Phys., 107, 1403-1405.
881. Zhang, L., W. Fuss and K. L. Kompa, 1990, Chem. Phys., 144, 289-297.
882. Zhu, L. and G. Johnston, 1995, J. Phys. Chem., 99, 15114-15119.
883. Zhu, L., D. Kellis and C.-F. Ding, 1996, Chem. Phys. Lett., 257, 487-491.
884. Zou, P., W. S. McGivern and S. W. North, 2000, Phys. Chem. Chem. Phys., 2, 3785-3790.
885. Zou, P., W. S. McGivern, O. Sokhabi, A. G. Suits and S. W. North, 2000, J. Chem. Phys., 113, 7149-7157.
886. Zou, P., J. Park, B. A. Schmitz, T. Nguyen and S. W. North, 2002, J. Phys. Chem. A, 106, 1004-1010.